Characterization of TDP-43-related de novo proteins in ALS/FTD

Sahba Seddighi
St. John's College | University of Oxford

A thesis submitted to the University of Oxford for the Degree of
DOCTOR OF PHILOSOPHY

Co-supervised by:

Michael E Ward, MD, PhD
National Institute of Neurological Disorders & Stroke, NIH

Cornelia van Duijn, PhD
Nuffield Department of Population Health, Oxford

Abstract

Mislocalization of the DNA/RNA-binding protein TDP-43, characterized by its nuclear loss and cytosolic accumulation, is the predominate pathology in amyotrophic lateral sclerosis (ALS) and occurs in up to 50% of frontotemporal dementia (FTD) cases. TDP-43 plays a major role in splicing regulation, and its loss from the nucleus leads to the erroneous expression of intronic sequences, called cryptic exons. Cryptic exons are non-conserved sequences that often result in degradation of affected transcripts, with potential deleterious consequences for cellular function. The aim of my dissertation work was to address whether certain cryptic exon-harboring transcripts could generate de novo proteins in settings of TDP-43 deficiency. I first discuss the development of a proteogenomic informatic pipeline, leveraging parallel transcriptomic and proteomic data from TDP-43-depleted human iPSC-derived neurons to identify 65 putative cryptic peptides from 12 transcripts. The cryptic exons identified in TDP-43-depleted human iPSC-derived neurons were highly predictive of dysregulated splicing in postmortem brain tissue from patients with TDP-43 proteinopathy, thus validating the physiological relevance of our in vitro model. I then demonstrate the orthogonal validation of cryptic peptides identified by proteogenomics using antibody- and targeted proteomics-based assays in TDP-43-depleted iPSC-derived neurons. I next show that expression of cryptic exon sequences can alter the interactome of affected proteins, thereby likely affecting their function. Finally, using an ultra-sensitive target proteomics approach, I demonstrate that at least 18 de novo peptides across 13 genes are unequivocally present in the CSF of individuals with ALS/FTD spectrum disorders. The discovery of cryptic exon translation suggests potential new mechanisms of disease pathogenesis downstream of TDP-43 dysfunction in ALS/FTD and provides a novel strategy for the development of assays to monitor TDP-43 function in living individuals.

Declarations

I confirm that the work presented in this thesis is my own. Any information derived from other sources has been acknowledged as so in the text. The contents of this thesis have not been previously submitted for a degree, diploma, or other qualification at the University of Oxford or any other institution of learning.

Acknowledgements

I would first like to thank my PhD co-supervisors, Michael Ward and Cornelia van Duijn. I owe a debt of gratitude to Michael for teaching me how to carve new spaces of inquiry in neuroscience and for his patience, enthusiasm, encouragement, and guidance that allowed me to accomplish this work. I am also indebted to Cornelia for affording me the opportunity to develop as a "big data" scientist and for introducing me to the rich field of molecular epidemiology. I would like to thank every member of the Ward and van Duijn research groups and collaborators for sharing their expertise, enthusiasm, and invaluable time with me during the last few years – in particular, Andy Qi and Anna-Leigh Brown, who were instrumental in developing this work. I must also thank the NIH-Oxford/Cambridge Scholars Program, Johns Hopkins School of Medicine MSTP, and the International Biomedical Research Alliance for the funding and administrative support to pursue my academic goals across disciplinary and national boundaries throughout these four years. My deep appreciation also goes to all those who selflessly donated samples to advance research on neurodegenerative diseases – without them, much of this work would not have been possible. And, finally, a heartfelt *thank you* to my family, friends, and friends-turned-family for their love, support, encouragement, and understanding that has made this journey possible and so enjoyable.

Commonly used abbreviations

AA – Amino Acid

AD – Alzheimer's disease

ALS – Amyotrophic lateral sclerosis

APMS – Affinity purification mass spectrometry

AUC – Area under the curve

BP – Base pair

CE – Cryptic exon

CRISPR – Clustered Regularly Interspaced Short Palindromic Repeats

CRISPRi – CRISPR-interference

DDA – Data-dependent acquisition

DIA – Data-independent acquisition

FTD – Frontotemporal dementia

FUS – Fused in sarcoma

GO – Gene ontology

GWAS – Genome-wide association study

hnRNP – Heteronuclear ribonucleoprotein

i3N – iPSC-derived neuron

iPSC – Induced pluripotent stem cell

KD – Knockdown

LFC – Log-fold change

NMD – Nonsense-mediated mRNA decay

NT – Nucleotide

PRM – Parallel reaction monitoring

PSI – Percent spliced in

STMN2 – Stathmin2

TARDBP – Transactive response DNA/RNA-binding protein

TDP-43 – Transactive response DNA binding protein 43 kDa

Publications produced during the PhD

Seddighi S.*, Yue A.Q.*, Brown, A.L.*, Wilkins O.G., Bereda C., Belair C., Zhang Y., Prudencio M., Keuss M.J.,Khandeshi A., Pickles, S., Kargbo-Hill S.E., Hawrot J., Ramos D.M, Yuan H., Roberts J., Sacramento E.K, Shah S.I., Nalls M.A, Colon-Mercado J., Reyes J.F., Ryan V.H., Nelson M.P., Cook C, Li Z., Screven L., Kwan J.Y., Mehta M.R., Zanovello M., Halleger M., Shantaraman A., Ping L., Koike Y., Oskarsson B., Staff N., Duong D.M., Ahmed A., Secrier M., Ule J., Jacobson S., Reich D.S., Rohrer J., Malaspina A., Dickson D.W., Glass J.D., Ori A., Seyfried N.T., Maragkakis M., Petrucelli L., Fratta P., Ward M.E.. Mis-spliced transcripts generate de novo proteins in TDP-43-related ALS/FTD. ***Science Translational Medicine***. Jan 2024.

Seddighi S., Cookson M.R., Ward M.E. Human Induced Pluripotent Stem Cell Models of Genetic Contribution to Neurodegenerative Disease. ***Nature Reviews Neuroscience.*** (*solicited - in preparation*).

Pasquini L, Pereira F.L., **Seddighi S**., Zeng Y., Wei Y., Illán-Gala I., Vatsavayai S.C., Friedberg A., Lee A.J., Brown J.A., Spina S., Grinberg L.T., Sirkis D.W., Bonham L.W., Yokoyama J.S., Boxer A.L, Kramer J.H, Rosen H.J, Humphrey J., Gitler A.D., Miller B.L., Pollard K.S., Ward M.E., Seeley W.W. FTLD targets brain regions expressing recently evolved genes. ***MedRxiv***. Sep 2023.

Diaz-Torres S., He W., Thorp J., **Seddighi S.**, Mullany S., IGGC International Glaucoma Genetics Consortium, Hammond C.J., Hysi P.G., Pasquale L.R., Khawaja A.P., Hewitt A.W, Craig J.E., Mackey D.A., Wiggs J.L., van Duijn C., Lupton M.K., Ong J.S., MacGregor S., Gharahkhani P. Disentangling the genetic overlap and causal relationships between primary open-angle glaucoma, brain morphology and four major

neurodegenerative disorders. ***Lancet EBioMed.*** June 2023.

Reilly L.*, **Seddighi S.***, Singleton A.B., Cookson M.R., Ward M.E. Qi Y.A. Variant biomarker discovery using mass spectrometry-based proteogenomics. ***Frontiers in Aging***. April 2023.

Brown A.L.*, Wilkins O.G.*, Keuss M.J*., Hill S.E.*, Zanovello M., Lee W.C., Bampton A., Lee F.C.Y, Masino L., Qi Y.A., Bryce SmithS., Gatt A., Hallegger M., Fagegaltier D., Phatnani H.; NYGC ALS Consortium, Newcombe J., Gustavsson E.K., **Seddighi S.**, Reyes J.F., Coon S.L., Ramos D., Schiavo G., Fisher E.M.C., Raj T., Secrier M., Lashley T., Ule J., Buratti E., Humphrey J., Ward M.E., Fratta P. TDP-43 loss and ALS-risk SNPs drive mis-splicing and depletion of UNC13A. ***Nature.*** Feb 2022. PMID: 35197628.

Contents

Figures

Tables

CHAPTER 1: TDP-43 proteinopathies

1.1 Introduction to TDP-43 and TDP-43 proteinopathy

TAR DNA/RNA-binding protein-43 (TDP-43), encoded by the *TARDBP* gene, is an evolutionarily conserved and ubiquitously expressed nucleic acid-binding protein belonging to the heterogeneous nuclear ribonucleoprotein (hnRNP) family (Prasad et al., 2019). TDP-43 was initially identified in a screen for proteins that bind to and regulate human immunodeficiency virus type 1 (HIV-1) expression(Ou et al., 1995). Since the discovery of TDP-43 as a suppressor of *HIV-1* gene expression, subsequent studies have demonstrated pivotal roles for TDP-43 across a broad range of cellular processes, including transcriptional regulation; messenger RNA (mRNA) splicing, stability, and transportation; and translational regulation (Prasad et al., 2019).

In 2006, TDP-43 was identified as the major component of ubiquitinated cytoplasmic inclusions deposited in the spinal motor neurons of individuals with amyotrophic lateral sclerosis (ALS) and the cortical neurons of individuals with frontotemporal lobar degeneration (FTLD, now known as FTLD-TDP) (Neumann et al., 2006). Several autosomal dominant mutations in *TARDBP*, the gene encoding TDP-43, were subsequently linked to ALS and FTLD-TDP phenotypes (Pesiridis et al., 2009), further supporting a pathological link between TDP-43 dysfunction and disease. Interestingly, most individuals with ALS and FTLD-TDP do not harbor any *TARDBP* mutations, yet approximately 97% of ALS cases and 45% of FTLD cases are characterized by TDP-43 pathology on autopsy, suggesting that multiple pathogenic disease mechanisms converge on TDP-43 proteinopathy (De Boer et al., 2021).

Following the discovery of TDP-43 pathology in ALS and FTLD, TDP-43 inclusions were documented across a spectrum of neurodegenerative conditions in rapid succession, including Alzheimer's disease (AD) (Meneses et al., 2021), dementia with lewy bodies (DLB) (Arai et al., 2009), chronic traumatic encephalopathy (C. Yang et al., 2020), and, most recently, the pathological entity known as limbic-predominant age-related TDP-43 encephalopathy (LATE) that typically impacts adults over the age of 80 (Nelson et al., 2019). Diseases linked to TDP-43 deposition are now collectively termed "TDP-43 proteinopathies." While TDP-43 pathology is a primary event in ALS and FTLD-TDP, it appears to be a secondary event in other neurodegenerative disorders, and its involvement in the onset and progression of polyproteinopathies remains poorly understood. Unraveling the mechanisms by which TDP-43 mediates neurodegeneration could provide a common entry point to develop more effective diagnostics and therapeutics for a range of thus far intractable neurodegenerative conditions.

1.1.1 Amyotrophic lateral sclerosis

Amyotrophic lateral sclerosis (ALS) is a rapidly fatal neuromuscular disease characterized by progressive loss of motor neurons in the cerebral cortex and spinal cord, but with increasingly recognized extra-motor manifestations (Masrori & Van Damme, 2020). It currently affects an estimated 40,000 individuals in Europe (Chiò et al., 2013), with a global incidence of 1.75 per 100,000 person-years (Logroscino et al., 2022). The progressive loss of neurons in the motor cortex, brain stem, and spinal cord of patients with ALS results in weakness, muscle wasting and, ultimately, paralysis and death from respiratory failure (Masrori & Van Damme, 2020). There is currently no cure for ALS, and approved therapies only modestly extend survival

time, which is typically limited to 2-3 years following symptom-onset (Masrori & Van Damme, 2020; Mead et al., 2023).

ALS is an age-related disease, with a peak incidence in those aged 70-74 years (Huisman et al., 2011). The average age of onset is typically lower for individuals with familial ALS (fALS, 40-60 years old), compared to those with sporadic ALS (sALS, 58-63 years old) (Logroscino et al., 2010). Approximately 10% of ALS cases are familial and follow an autosomal dominant inheritance pattern, while the remaining 90% are classified as sporadic, with only partially understood, heterogeneous etiology (Masrori & Van Damme, 2020). The most common genetic cause of ALS is a hexanucleotide repeat expansion in the non-coding region of the *C9orf72* gene, accounting for approximately 40% of fALS cases and present in about 10% of sALS cases (Smeyers et al., 2021; Umoh et al., 2016). The *C9ORF72* expansion mutation is most common in North American and European populations and is rarely found in Asian populations (Chen et al., 2016; Ogachi et al., 2012; Tsai et al., 2012; Zou et al., 2013). A single founder effect originating in Finland is speculated to underlie this regional variance (Pliner et al., 2014; Smith et al., 2013). Beyond *C9orf72* mutations, an additional 20% of familial cases are caused by mutations in the superoxide dismutase 1 (*SOD1*) gene. *SOD1* mutations are the most common genetic cause of fALS in Asian populations (Mejzini et al., 2019). Finally, an estimated 1-5% of familial ALS cases are linked to mutations in the *TARDBP* or the fused in sarcoma (*FUS*) genes (Chen et al., 2013), with mutations in other genes being relatively uncommon (Mejzini et al., 2019). Heritability studies suggest that around 40-60% of the variance in susceptibility to sALS can be attributed to genetic factors (Al-Chalabi et al., 2010; Ryan et al., 2019; Wingo et al., 2011).

The pathogenesis of ALS is likely multifactorial, involving complex interactions between genetic mutations, environmental factors, and the disruption of vital molecular pathways

(Kiernan et al., 2011; van Es et al., 2017; Vucic et al., 2020). Known environmental risk factors include head injury, smoking, and physical activity – though these factors are believed to exert relatively small effects (van Es et al., 2017). Cellular and molecular contributors, such as mitochondrial dysfunction, glutamate excitotoxicity, oxidative stress, and glutamate excitotoxicity, have also been identified (Le Gall et al., 2020).

On autopsy, ALS is characterized by degeneration and loss of neurons in the motor cortex and the anterior horn of the spinal cord and axonal loss in the lateral columns of the spinal cord (Saberi et al., 2015). Other pathological features include reactive astrogliosis, vacuolization – empty spaces surrounding neurons – and spongiosis – small holes rendering a sponge-like appearance (Saberi et al., 2015).

Approximately 97% of ALS cases are characterized by TDP-43 positive cytoplasmic inclusions (Tan et al., 2017), and a small portion present with aggregates of SOD1 (~2%) or FUS (<1%) protein (Kwiatkowski et al., 2009; S. C. Ling et al., 2013; Vance et al., 2009). TDP-43 cytoplasmic inclusions are not only observed in neurons, but also present in glia. The three predominant cell-type specific patterns of TDP-43 proteinopathy in ALS are: (1) mixed neuronal and glial (59% of cases), (2) glial (22% of cases), and (3) neuronal (7% of cases) (De Boer et al., 2021; Williams et al., 2017). TDP-43 pathologic burden in extra-motor regions is associated with cognitive impairment in ALS. Indeed, as many as half of those diagnosed with ALS also exhibit behavioral and language changes that are typical of FTD, and an estimated 5-25% of cases are formally diagnosed with FTD (Saxon et al., 2017; Strong et al., 2017).

1.1.2 Frontotemporal dementia

FTLD is the neuropathological description that underlies the clinical spectrum of frontotmeporal dementia (FTD). FTD is a clinically heterogeneous neurocognitive disease characterized by changes in behavior, executive function, and/or language proficiency (Warren et al., 2013). It is the second most common cause of early-onset dementia after AD in individuals under the age of 65 and affects an estimated 15-22 per 100,000 persons (Knopman & Roberts, 2011). There is currently no cure for FTD, and the average survival time varies by subtype of disease, ranging from 3 to 12 years from symptom-onset (Roberson et al., 2005).

As with ALS, age is a major risk factor for FTD. The mean age at presentation is 58, with a peak incidence in those aged 60-69 (Onyike & Diehl-Schmid, 2013).Approximately 40% of FTD cases have a positive family history (Seltman & Matthews, 2012). The most commonly associated genes are *C9orf72*, microtubules associated protein tau (*MAPT*), and granulin (*GRN*) (Borroni et al., 2018; Guven et al., 2016; Onyike & Diehl-Schmid, 2013). More broadly, FTD-associated genes can be categorized by their role in three key cellular process 1) protein homeostasis, encompassing mutations in *CHMP2B* (Guven et al., 2016), *OPTN* (Maruyama et al., 2010), *UBQLN2* (Deng et al., 2011), *SQSTM1* (Fecto et al., 2011), and *TBK1* (Cirulli et al., 2015; Freischmidt et al., 2015)*;* 2) microtubule dynamics, encompassing mutations in *MAPT* (Hutton et al., 1998), *DCTN1* (Puls et al., 2003), *CHCHD10* (Bannwarth et al., 2014), *TUBA4A* (Smith et al., 2014), and *KIF5A* (Nicolas et al., 2018); and RNA regulation and stability, encompassing mutations in *TARDBP* (Borroni et al., 2009)*, FUS* (Kwiatkowski et al., 2009; Vance et al., 2009)*, ATXN2* (Elden et al., 2010), *TAF15* (Ticozzi et al., 2011), *hnRNPA1* and *hnRNPA2B1* (H. J. Kim et al., 2013), *MATR3* (H. J. Kim et al., 2013), *SFPQ* (Thomas-Jinu et al., 2017), and *TIA1* (Mackenzie et al., 2017). There is a significant genetic overlap between FTD and ALS. Indeed, disruptions in protein homeostasis, microtubule dynamics, and RNA

regulation are central mechanisms implicated in both forms of neurodegeneration (Abramazon et al., 2020; Butti et al., 2018; Clark et al., 2016; Medinas et al., 2017).

FTLD is characterized by prominent atrophy of the frontal and temporal lobes, accompanied microscopically by gliosis and spongy changes around degenerating neurons (Kersaitis et al., 2004; Schofield et al., 2005). FTLD is a pathologically heterogeneous disease and thus subtyped according to the major protein constituent of neuronal and glial inclusions and their distribution (Broe et al., 2003; Josephs et al., 2011). The three key pathological subtypes of FTLD are: (1) FTLD-tau, accounting for approximately 35%–50% of cases and typically associated with specific clinical syndromes, such as progressive supranuclear palsy and corticobasal syndrome (Burrell et al., 2016); (2) FTLD-FUS, which accounts for approximately 10% of cases and is associated with behavioral variant FTD (bvFTD). BvFTD typically presents with psychiatric features and severe disinhibition, but no significant motor or language deficits (De Boer et al., 2021); and (3) FTLD-TDP-43, the most common subtype, representing up to 50% of all FTD cases (Tan et al., 2017). FTLD-TDP is further subdivided into four key pathological subtypes. FTLD-TDP type A is characterized by round cytoplasmic TDP-43 inclusions and short dystrophic neurites, mainly in neocortical layer 2; type B by cytoplasmic inclusions found across all cortical layers (Mackenzie, I. R. et al., 2011); type C by long, dystrophic neurites found in upper cortical layers; and type D by lentiform cytoplasmic inclusions and short, dystrophic neurites, predominantly in the hippocampal region (Mackenzie, I. R. et al., 2011). Type A often presents as progressive non-fluent aphasia, bvFTD, or FTD-ALS (Hofmann et al., 2019; Mackenzie, I. R. et al., 2011); type B as bvFTD or FTD-ALS (Burrell, J. R. et al., 2016; Hofmann et al., 2019; Mackenzie, I. R. et al., 2011); type C as semantic variant primary progressive aphasia and, less commonly, bvFTD (Elahi and

Miller, 2017; Mackenzie, Ian RA et al., 2011); and type D, a rare subtype, is associated with *VCP* mutations causing early-onset Paget disease of bone and frontotemporal dementia (IBMPFD) and FTD with extrapyramidal motor features (Kawakami et al., 2019; Neumann et al., 2022).

Due to the striking concordance in the genetic and pathological features of ALS and FTD, approximately 30-40% of individuals with FTD also experience signs of lower motor neuron dysfunction, and roughly 15% are formally diagnosed with ALS (Burrell et al., 2016). Given the extensive overlap in the genetic, neuropathological, and clinical features of ALS and FTD, they are thought to exist on a common disease continuum, named ALS-FTD spectrum disorder (ALS/FTD) (Burrell et al., 2016).

1.1.3 TDP-43 polyproteinopathies

In the past decade, TDP-43 positive inclusions have been reported in an expanding range of neurodegenerative diseases. This includes the most common neurodegenerative disorder, AD. Though AD is pathologically defined by cardinal neurofibrillary tangles and amyloid plaques (Deture & Dickson, 2019), concomitant TDP-43 pathology is also documented in approximately 57% of AD cases (Meneses et al., 2021). The extent of TDP-43 pathology in AD cases appears to correlate with the severity of hippocampal atrophy and cognitive impairment, suggesting that TDP-43 co-pathology may exacerbate AD progression (Meneses et al., 2021). A genetic link between APOE4, the most common risk factor for AD, and the stage and burden of TDP-43 pathology has also been reported (Meneses et al., 2021; H. S. Yang et al., 2018).

Additional diseases with evidence of TDP-43 co-pathology include tauopathies, such as chronic traumatic encephalopathy (H. S. Yang et al., 2018), alpha-synucleinopathies, such as DLB (Arai et al., 2009) and Guam parkinsonism-dementia (Hasegawa et al., 2007), and Huntington's disease (Hasegawa et al., 2007). In each case, TDP-43 deposition localizes to disease-affected brain regions, and its contributions to disease onset and progression in TDP-43 polyproteinopathies remains to be fully understood. However, the expanding clinical continuum of TDP-43 proteinopathies suggests a key role for TDP-43 in neurodegeneration and underscores a need to better understand the pathogenic mechanisms of TDP-43 dysregulation.

1.1.4 An unmet need for TDP-43 biomarkers

Despite the importance of TDP-43 in ALS/FTD pathophysiology and its involvement across multiple other neurodegenerative diseases, there is currently no way to detect or monitor TDP-43 pathology in living individuals. This poses a major challenge to the design of clinical trials targeting aggregated TDP-43 or aiming to rectify the downstream effects of impaired TDP-43 function (Hayes & Kalab, 2022). A TDP-43 biomarker could more effectively identify those who are likely to benefit from TDP-43-directed therapies, particularly in pathologically heterogeneous conditions, such as FTD, and neurodegenerative diseases with concomitant TDP-43 pathology.

Biomarkers of TDP-43 dysfunction could also serve as outcome measures in clinical trials. A key challenge in developing effective therapies for FTD lies in the variability of clinical presentations of disease, which typically is not predictive of pathology or molecular subtypes (Roberson et al., 2006). Dominant symptoms can include language deficits, behavioral changes,

and/or motor problems (Olney et al., 2017). The disease course is also highly variable, with some patients experiencing rapid decline, while others progress much more slowly (Kipps et al., 2010; Moore et al., 2020). The diversity of clinical presentations and rate of progression in FTD, together with its relatively rare prevalence, challenge the design of clinical trials relying on historical clinical outcome measures (Knopman et al., 2008; Irwin et al., 2015). While radiographic (structural MRI) and fluid biomarkers (eg, neurofilament) provide measures of disease progression (Elahi et al., 2017; Gendron et al., 2017; Meet et al., 2016), these outcome measures are not specific to pathological subtypes, and are indirect measurements of disease-relevant changes. Splicing dysregulation, on the other hand, is a direct result of TDP-43 loss-of-function and could provide a functional biomarker to monitor TDP-43 function and therapeutic responses in a longitudinal manner during trials.

Furthermore, emerging evidence indicates that TDP-43 nuclear loss of function is an early-disease phenomenon that precedes the formation of identifiable cytosolic aggregates and occurs prior to symptom onset in ALS (Guise et al., 2024; Iguchi et al., 2013; Spence H, 2024; Vatsavayai et al., 2016; C. Yang et al., 2014). The notion that TDP-43 nuclear dysfunction is an early disease event was initially demonstrated by a case in which a 74-year-old female underwent temporal lobe resection for epilepsy five years prior to developing symptoms of FTD (Vatasavayai et al., 2016). Retrospective analysis of the archival tissue revealed loss of nuclear TDP-43 in some neurons without any cytoplasmic TDP-43 inclusions, despite the presence of florid TDP-43 inclusions at autopsy eight years after symptom onset (Vatasavayai et al., 2016). Furthermore, using an aptamer-based detection strategy to examine postmortem brain samples from a larger cohort of ALS cases and controls, Spence and colleagues recently demonstrated that TDP-43 nuclear loss is an early event that precedes cytoplasmic inclusions and the clinical

inflection point in ALS (Spence et al., 2024). As such, biomarkers of TDP-43 dysfunction could enable detection of disease at an early stage of cellular dysfunction, when therapies are most likely to be efficacious.

1.2 Structure and function of TDP-43

TDP-43 protein structure

TDP-43 is a highly conserved, 414 amino acid-long hnRNP encoded by the *TARDBP* gene on chromosome 1 (1.p36.22) (Chen-Plotkin et al., 2010). The protein structure is composed of an N-terminal region, nuclear localization signal (NLS), two RNA recognition motifs (RRM1 and RRM2), nuclear export signal (NES), and a C-terminal region containing a prion-like glutamine/asparagine-rich domain and a glycine-rich region (**Fig. 1.1**) (Bright et al., 2021; Chen-Plotkin et al., 2010; Jiang et al., 2016; Kuo et al., 2014; Lukavsky et al., 2013; Mompeán et al., 2016; Qin et al., 2014).

Interactions of the N-terminal domain facilitate TDP-43 self-assembly, which is necessary for many of its physiological functions (Jiang et al., 2017). Furthermore, TDP-43 homodimerization has been shown to improve solubility and protect against the formation of TDP-43 cytoplasmic inclusions (Jiang et al., 2017; Prasad et al., 2019). However, a growing body of evidence also suggests that NTD self-assembly may also be involved in TDP-43 aggregation

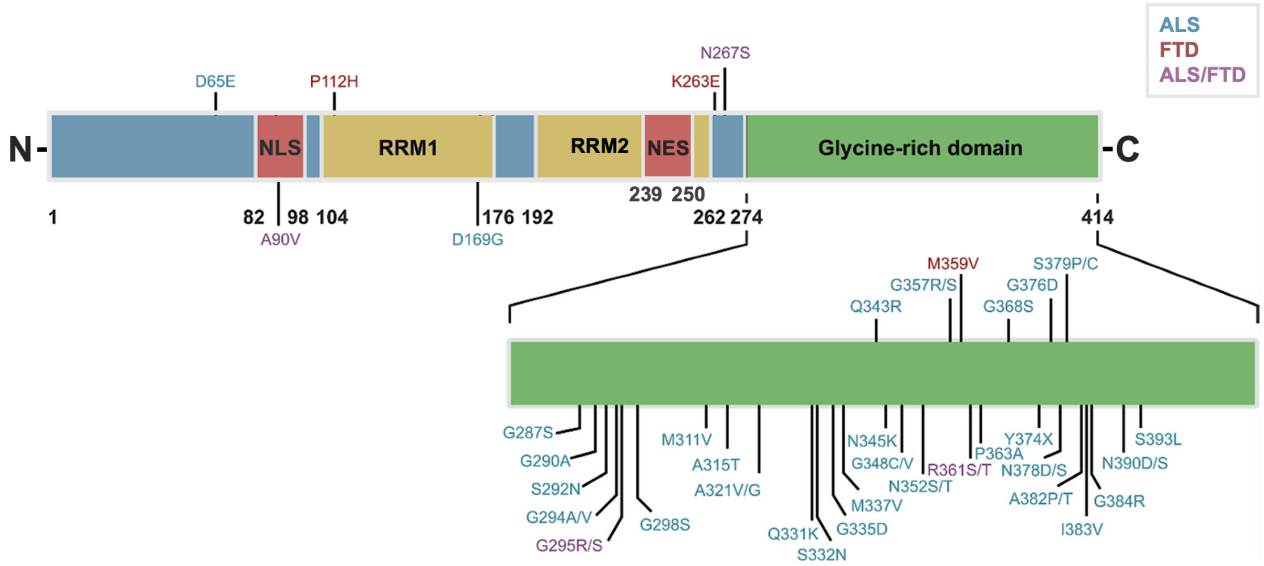

Figure 1.1. Structural features of TDP-43. TDP-43 is composed of an N-terminal domain, nuclear localization signal (NLS), two DNA/RNA- binding domains (RRM1 and RRM2), nuclear export signal (NES), and a glycine-rich C-terminal domain, where the majority of pathogenic *TARDBP* mutations identified for ALS and FTD lie. Text colors indicate the phenotype associated with a given mutation (blue = ALS, red = FTD, purple= ALS/FTD). Figure adapted from (Bright et al., 2021).

(Afroz et al., 2017; Shiina et al., 2010; Tsoi et al., 2017; Y. J. Zhang et al., 2013).

The TDP-43 RNA-recognition motifs, RRM1 and RRM2, are both highly conserved and essential for its interactions with RNA/DNA molecules to regulate transcription, pre-mRNA splicing, and mRNA stabilization and transport (De Boer et al., 2021). RRM1 underlies TDP-43's affinity for UG-rich regions, while RRM2 enhances its RNA-binding capacity (Ayala et al., 2011; S. C. Ling et al., 2013).

The glycine-rich C-terminal domain is a disordered and poorly conserved region that regulates the solubility and intrinsic aggregation of TDP-43, allowing for the formation of membraneless biomolecular condensates in a process known as liquid-liquid phase separation

(LLPS) (Schmidt et al., 2019). LLPS occurs physiologically and in response to cellular stress, enabling recruitment of TDP-43 to stress granules that play a vital role in maintaining cellular health (Schmidt et al., 2019). Defects in the dynamics of LLPS formation and disassembly may lead to aggregation, as supported by the large number of disease-causing mutations in this region (**Fig. 1.1**) (Versluys et al., 2022). The C-terminal domain additionally mediates the interactions of TDP-43 with other members of the hnRNP family to regulate splicing, thus representing another avenue for pathogenesis (Buratti et al., 2005; D'Ambrogio et al., 2009).

While TDP-43 predominantly localizes to the nucleus, it shuttles to and from the cytoplasm to exert its physiological functions. The nucleocytoplasmic shuttling of TDP-43 is mediated by the NES and NLS (Winton et al., 2008). TDP-43 nuclear export occurs via passive diffusion (Duan et al., 2022), while its nuclear import occurs via active transport, namely through interactions of the TDP-43 NLS with importins alpha and beta (Ayala et al., 2008; Nishimura et al., 2010).

Physiological functions of TDP-43

In the cytoplasm, TDP-43 plays an essential role in RNA transport, stability, and translation (Prasad et al., 2019). In neurons, RNA trafficking across compartments is necessary for regulating spatial translation (Das et al., 2019). TDP-43 forms cytoplasmic granules with RNA molecules, which are then transported across neurons for targeted delivery of mRNAs to distal compartments (Kiebler & Bassell, 2006; Krichevsky & Kosik, 2001). This process is disrupted by ALS causal mutations, further supporting the significance of TDP-43-mediated RNA trafficking in disease (Alami et al., 2014). TDP-43 also regulates RNA stability by binding

to the 3' untranslated regions (3'UTRs) of mRNAs. This activity has been shown to enhance RNA stability of some genes, such as *NEFL*, *G3BP,* and *HDAC6* (Fiesel et al., 2010; Sidibé et al., 2021; Strong et al., 2007), while contributing to destabilization of others, such as *VEGF* and *GRN* (Colombrita et al., 2012). Finally, TDP-43 regulates RNA translation by interacting with translation and elongation factors, as well as ribosomal subunits in the cytoplasm (Freibaum et al., 2010; S. H. Kim et al., 2010; Nagano et al., 2020; Neelagandan et al., 2019).

Within the nuclear compartment, TDP-43 functions as a key regulator of RNA processing, typically by binding to "UG"-rich dinucleotide repeats of pre-mRNAs (J. P. Ling et al., 2015). The role of TDP-43 as regulator of alternative splicing was first described in the context of the cystic fibrosis gene *CFTR*, where the binding of TDP-43 to UG-rich motifs leads to skipping of exon 9 and the production of an inactive CFTR protein (Buratti et al., 2001). Since then, a number of other alternative splicing targets of TDP-43, such as *POLDIP3*, *PFKP*, and *SORT1*, have also been characterized (Buratti et al., 2001; Fiesel et al., 2010; Klim et al., 2019; J. P. Ling et al., 2015; S. C. Ling et al., 2013; Tollervey et al., 2011). In addition to regulating the alternative splicing of canonical exons, TDP-43 plays a key role in the repression of intronic sequences during RNA splicing (J. P. Ling et al., 2015). TDP-43 also regulates RNA stability by controlling sites of polyadenylation (Murphy et al., 2021; Rot et al., 2017). Lastly, TDP-43 participates in miRNA processing and the regulation of long non-coding RNAs, which modulate gene expression, transcription, and translation (Ederle & Dormann, 2017).

1.3 TDP-43 pathology: gain or loss of function?

TDP-43 proteinopathy involves both its nuclear depletion and its cytoplasmic aggregation. It is likely that both loss of normal function and toxic gain of function mechanisms are involved in TDP-43-mediated neurodegeneration (Lee et al., 2012).

One possibility for a toxic-gain-of-function mechanism is the ribostasis hypothesis, which posits that TDP-43 over-abundance in the cytoplasm results in the formation of dense aggregates that lead to mRNA sequestration, therby inhibiting their translation (Bjork et al., 2022). Indeed, overexpression of TDP-43 within the cytoplasmic compartment leads to a reduction in protein synthesis (Charif et al., 2020; Russo et al., 2017). Protein synthesis deficits have also been well documented in ALS/FTD patient tissues (Lehmkuhl & Zarnescu, 2018), including through a recent single-cell proteomic analysis of ALS motor neurons, demonstrating dysregulation of translation factors in affected cells (Guise et al., 2024; J. P. Ling et al., 2015).

While the loss-of-function consequences of TDP-43 proteinopathy are likely complex given its multifaceted roles across a range of cellular processes, elucidating the contributions of pathological splicing has been a key area of focus in the field. When TDP-43 is lost from the nucleus, intronic sequences are erroneously de-repressed and incorporated into mRNAs, resulting in the expression of so-called "cryptic exons" (J. P. Ling et al., 2015). The transcriptional targets of TDP-43-related splicing repression are highly species and cell-type specific (Humphrey et al., 2017; Jeong et al., 2017) and often result in the degradation of affected transcripts by nonsense-mediated decay (Humphrey et al., 2017; Jeong et al., 2017; J. P. Ling et al., 2015; Mehta et al., 2023) (**Fig. 1.2**). Other novel RNA isoforms are also observed in the context of TDP-43 loss of function, including 3' or 5' extensions of annotated exons, exon skip events, and premature polyadenylation. While often considered aberrant events that lead to transcript and protein destabilization, TDP-43-related splicing changes could conceivably also carry

normal functions in the cell. This is exemplified by a recently discovered cryptic exon that is essential for sex determination in mice (Miyawaki et al., 2020) and by cryptic exons that control synaptic protein expression levels following seizure (Eom et al., 2013).

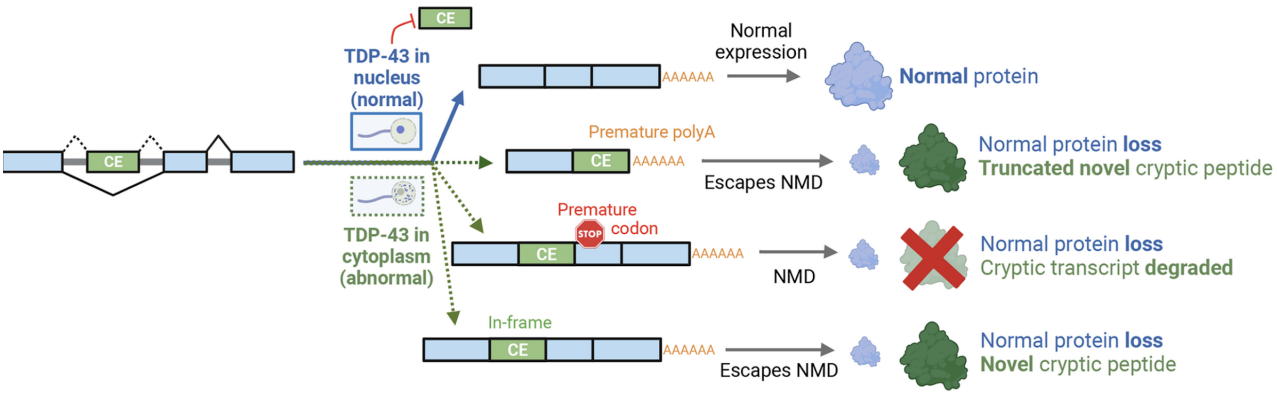

Figure 1.2. Consequences of TDP-43-related splicing dysregulation. Nuclear loss of TDP-43 causes de-repression of cryptic exons. Most cryptic exons introduce a premature termination codon or polyA signal, resulting in degradation of affected transcripts and proteins. However, certain cryptic exons may be in-frame and could generate stable polypeptides. Figure adapted from (Mehta et al., 2023).

The pathogenic contributions of cryptic exons have been a topic of active investigation since the discovery of a TDP-43-related cryptic exon in the *STMN2* gene – now recognized as a hallmark of TDP-43-related neurodegeneration (Klim et al., 2019; Melamed et al., 2019). This gene encodes a microtubule-associated protein that is necessary for axonal growth and repair. Using TDP-43 KD cellular models, in 2019, two teams independently demonstrated that the *STMN2* cryptic exon contains a stop codon and polyadenylation site and results in a dramatic reduction in the *STMN2* transcript and protein levels. The *STMN2* cryptic exon is also found in the brain and spinal cord of individuals with ALS/FTLD-TDP and in postmortem neurons that displayed TDP-43 pathology (Brown et al., 2022; E. Y. Liu et al., 2019; Melamed et al., 2019; Prudencio et al., 2020). Furthermore, they showed that motor neurons lacking TDP-43 were

unable to regenerate after axotomy, but that axonal regrowth could be rescued by restoration of normal STMN2 protein levels, thus demonstrating a critical role for STMN2 in the maintenance of motor neurons (Klim et al., 2019; Melamed et al., 2019). Following the discovery of TDP-43 loss as a key player in ALS, the hunt for additional disease-implicated cryptic exons quickly ensued.

Using TDP-43-depleted cellular models, we and others subsequently found that the ALS and FTD-associated risk variants in *UNC13A* impair TDP-43's ability to bind *UNC13A* transcripts (Brown et al., 2022; Ma et al., 2022). The compromised binding of TDP-43 protein to *UNC13A* transcripts leads to CE de-repression, resulting in destabilization and loss of *UNC13A*, a crucial synaptic gene. Homozygous risk allele carriers were also found to have a dose-response increase in *UNC13A* cryptic exon-harboring transcripts compared to heterozygous and non-carriers. These findings provide a mechanistic explanation for the association between *UNC13A* risk variants, one of the strongest risk loci for ALS, and disease onset and progression in ALS/FTD-TDP (Brown et al., 2022).

These recent fundamental discoveries underscore a need to better understand the mechanisms by which TDP-43 loss of function mediates neurodegeneration. Recent advances in human induced pluripotent stem cell (iPSC) technology and genome engineering approaches provide an opportunity to further examine the consequences of TDP-43 dysfunction in disease-relevant cell types and, crucially, to distinguish disease causal mechanisms from epiphenomena. The next chapter outlines how iPSCs can be leveraged to uncover the biological derangements that drive neurodegenerative diseases and provides a discussion of the current challenges and future directions for iPSC-based studies of neurodegeneration.

CHAPTER 2: Human induced pluripotent stem cell models of neurodegenerative disease

2.1 Overview

A major advance in understanding risk of age-related neurodegenerative diseases has come from human genetics, encompassing both monogenic familial forms and oligogenic or sporadic diseases. However, understanding the biology of genetic variation, and hence inferring causal mechanisms, remains challenging. This is true for both coding and non-coding variants, and particularly for the latter, where effect on disease risk is relatively small. Here, I develop the argument that human iPSCs represent an appropriate platform for inferring biological mechanisms associated with neurodegeneration. I outline how iPSCs can be used to model both stronger effects of single variants in familial genes and to evaluate the effects of more modest risk factor variants, either alone or in combination. Finally, I discuss the current limitations of iPSC-based models and suggest approaches to overcome these challenges.

2.2 From classical genetics to modern genomics

Genetic factors play a major role in the etiopathogenesis of both monogenic and sporadic neurodegenerative disorders. Over the last several decades, human genetic studies of densely affected families have uncovered most of the highly-penetrant, rare genetic alterations

that cause mendelian forms of neurodegenerative diseases. In parallel, genome-wide association studies (GWAS) have identified many low-penetrant, common mutations that modulate the risk of complex, sporadic neurodegenerative diseases. Rapid advancements in long-read sequencing technology now enable precise characterization of structural risk variants that were refractory to conventional short-read sequencing-based methods. With a vast and rapidly expanding list of disease-associated genetic variants, the next challenge lies in interpreting these associations in a biological context. Resolving the contribution of genetic variants to the onset and progression of neurodegenerative diseases is of prime interest to both targeted drug discovery and precision medicine-based initiatives in neurology.

2.3 Using iPSCs to identify causal variants and polygenic interactions

Characterization of disease-associated variants should ideally be performed in model systems that faithfully recapitulate human disease processes. Since the discovery of methods to generate iPSCs (Takahashi et al., 2007), tremendous progress has been made in the cellular modeling of inaccessible human central nervous system (CNS) cell types, such as neurons, astrocytes, and microglia. iPSC-derived cell lines from patients and non-diseased "control" individuals have been widely used to study the mechanisms of neurodegenerative disorders.

Despite the tremendous potential of iPSCs, the genetic background of donors can exert a significant influence on iPSC cell phenotypes and represents a major caveat in cellular modeling of neurodegenerative diseases (Volpato & Webber, 2020). Based on systematic generation, genotyping, and phenotyping of over 700 iPSC lines from healthy donors, the Human Induced Pluripotent Stem Cells Initiative found that 5-46% of variability in iPSC phenotypes, including

cellular morphology and differentiation capacity, was driven primarily by inter-individual differences (Kilpinen et al., 2017). Several additional studies have found that iPSC lines from the same donor exhibit greater similarity to each other than to iPSC lines from different donors, based on either gene expression (Carcamo-Orive et al., 2017; Thomas et al., 2015) or methylation signatures (Burrows et al., 2016). Moreover, iPSC lines can exhibit substantial heterogeneity in differentiation potentials – even across iPSC clones from a single individual – making it difficult to disentangle disease-associated phenotypes from differentiation artifacts.

One strategy to overcome this limitation is to generate a large panel of iPSC lines from multiple donors, but this often requires complex experimental workflows and specialized equipment, which limits the adoption of this approach by standard academic laboratories. To address this challenge, several collaborative efforts have emerged to generate iPSCs and accompanying data resources from a large collection of donor lines for the research community. For instance, Answer ALS has generated and deeply characterized over 1,000 iPSC lines from ALS patients and matched controls to enable new insights on common and divergent clinical-molecular features of ALS (Baxi et al., 2022).

Even when well-powered and carefully conducted, studies comparing non–isogenic disease and control lines can fail to reveal disease-associated phenotypes. For example, a large transcriptomic analysis of motor neurons differentiated from 341 ALS and 92 healthy control participants from the Answer ALS project found both cell composition and sex to be major sources of variability between cell lines derived from different donors (Workman et al., 2023). Variability of differentiation potential across lines contributed to the majority of observed transcriptomic changes, potentially masking disease pathways (Workman et al., 2023).

Technological advances in genome editing, most notably the development of highly efficient CRISPR/Cas9 technology, now affords the ability to generate isogenic iPSC controls. This typically involves either correcting disease-associated variants in patient-derived iPSC lines or introducing mutations in well-characterized iPSCs from unaffected controls. While isogenic modeling strategies minimize sources of variability and enable more direct comparisons in the same genetic background, off-target mutations and chromosomal abnormalities can arise during the editing and expansion process and should be assessed by proper quality control measures (Rayner et al., 2019; Workman et al., 2023). Another critical challenge of this approach lies in the identification of the functionally relevant mutation. Inferences of causality are generally easier for more penetrant variants that compellingly segregate with disease, yet even presumed monogenic disease genes have been found to harbor multiple potentially causal variants.

Cellular modeling of complex, sporadic neurodegenerative diseases faces similar challenges in the identification of causal genes and variants from association loci. Most GWAS-identified variants for sporadic neurodegenerative disorders lie in non-coding regions and can impact gene expression via either cis (proximal)- or trans (distal)-acting mechanisms (Altshuler et al., 2008; Hindorff et al., 2009). One default approach has been to map variants to the nearest gene, but relying exclusively on physical proximity can be misleading (Altshuler et al., 2008). Pinpointing causal variants from association signals is also challenged by the fact that multiple variants from a haplotype can hitchhike the same tag SNP (Dickson et al., 2010).

In recent years, a suite of statistical inference methods has been developed for functional gene and variant prioritization from association loci and gene-to-function mapping to aid in the interpretation of GWAS signals (Uffelmann et al., 2021). While significant progress has been made, the utility of these tools remains limited by inconsistent predictive accuracies and cross-

platform disagreement (Klein et al., 2020; Kvon et al., 2014). Furthermore, multiple independent and interacting variants may collectively underlie an association signal, leading to the manifestation of risk-associated haplotypes, rather than independent driver mutations. One such example is the Parkinson's disease risk haplotype on chromosome 12, which harbors multiple coding variants in the Leucine-rich repeat kinase 2 (*LRRK2*), as well as non-coding variants upstream to *LRRK2* that are associated with familial and sporadic forms of the disease (Cookson, 2010; Nalls et al., 2019; Reed et al., 2019). Similarly, two common haplotypes at the Transmembrane protein-106B (*TMEM106B*) locus are associated with the risk of numerous neurodegenerative diseases, including frontotemporal lobar degeneration, Alzheimer's disease, and limbic-predominant age-related TDP-43 encephalopathy (Ren et al., 2018). In the case of Alzheimer's disease, variants in both Poliovirus receptor-related 2 (*PVRL2*) and apolipoprotein C1 (*APOC1*) have been found to interact with the *APOE* risk allele (Zhou et al., 2019).

For these reasons, in contrast to monogenic neurodegenerative diseases that are primarily driven by a single gene and best modeled by isogenic controls, complex, polygenic diseases are typically best modeled by iPSC lines derived from patients and age/sex-matched controls. In the future, pooled editing and phenotyping may enable better modeling of complex disease. Massively parallel reporter assays and CRISPR-based pooled screens can be employed to characterize noncoding genetic risk variants at-scale (Cooper et al., 2022). The feasibility of combining base editing screens with pathway-wide readouts to systemically map the genetic determinants of disease pathways has been previously demonstrated (Coelho et al., 2023). Large-scale efforts to establish and characterize iPSC lines, often with accompanying foundational multi-omic datasets, are also underway and will help overcome current limitations in sporadic disease modeling (Roberts et al., 2017; Skarnes et al., 2021).

Even for monogenic causes of neurodegeneration, the sheer number of likely causal variants has proven difficult to model by traditional academic labs. For example, since the microtubule associated protein tau (*MAPT*) gene was first identified as a cause of monogenic frontotemporal dementia (FTD) in 1998 (Hutton et al., 1998), more than 50 potentially causal *MAPT* mutations have been reported in FTLD-Tau cohorts worldwide (Cruts et al., 2012). Similarly, following the discovery of TAR DNA-binding protein (*TARDBP*) mutations as a primary cause of amyotrophic lateral sclerosis (ALS) (Kabashi et al., 2008; Sreedharan et al., 2008), more than 50 *TARDBP* mutations have been identified in patients with sporadic and familial ALS (Suk & Rousseaux, 2020).

To address this issue, numerous consortia have emerged to generate iPSC lines and accompanying foundational datasets for various neurodegenerative disease subtypes. For example, the Tau Consortium Stem Cell Group has generated and clinically characterized over 30 iPSC lines from *MAPT* mutation carriers, non-carrier family members, and autopsy-confirmed progressive supra nuclear palsy (PSP) for the research community (Karch et al., 2019). The Huntington's disease (HD) iPSC consortium provides a resource of 14 well-characterized iPSC lines from early and late-onset HD patients and matched controls (Mattis et al., 2012). As a part of the ROS and MAP cohorts, 16 iPSC lines from richly phenotyped patients with late-onset Alzheimer's disease were generated and found to have similar expression profiles to corresponding donor brains (Lagomarsino et al., 2021). Despite these heroic efforts, the inherent variability of iPSC lines, coupled with the heterogeneity of polygenic disease, requires larger sample sizes to fully uncover the biological derangements that drive neurodegeneration across disease subtypes. The iPSC Neurodegenerative Disease Initiative (iNDI) is a genome engineering initiative led by the NIH Center for Alzheimer's and Related

Dementias to generate isogenic genome-edited iPSC lines and deep phenotypic datasets for more than 100 mutations associated with Alzheimer's disease and related dementias (Ramos et al., 2021). As an extension of iNDI, PD ASAP was recently conceived to include isogenic iPSC lines harboring an expanded list of Parkinson's disease-specific variants, as well as patient-derived iPSC lines and mutation-corrected isogenic controls (Schekman & Rile, 2019).

2.3 Evaluating the cell-type specific effects of genetic variants

The vast majority of non-coding variants overlap with regulatory genomic regions, which often operate in a cell-type-specific manner (Dimas et al., 2009; Maurano et al., 2012; Schaub et al., 2012). Considering the bioactive context of variants is therefore an essential component of disease modeling. Expression profiling provides a means to predict the relative sensitivity of different cell types to a given variant. However, variants may also have cell-type specific effects that are independent of baseline expression profiles. For example, the *LRRK2* non-coding variant is bioactive in microglia, while the expression is just as high in excitatory neurons in the cortex (Langston et al., 2022). Conversely, the *LRRK2*-p.R1441H mutation is bioactive in neurons, where it causes impairments in the axonal transport of autophagosomes (Dou et al., 2023). iPSCs provide a suitable platform for direct comparisons of variant effects within and across diverse cell types differentiated from the same donor line.

Furthermore, the development of methods to generate a broader repertoire of iPSC-derived cellular subtype models will enable dissection of the molecular mechanisms of selective cell vulnerability – a widely acknowledged, but poorly understood, feature of many neurodegenerative disorders (Fu et al., 2018). The value of this approach has been demonstrated

by numerous studies. For example, using stem cell-derived motor neuron subtypes, An and colleagues discovered key proteostatic differences across motor neuron sub-populations that contribute to selective vulnerability in ALS (An et al., 2019). Moreover, a study of iPSC-derived substantia nigra and ventral tegmental area-like dopaminergic neurons demonstrated the selective sensitivity of substantia nigra-like cell subpopulations to mitochondrial toxins (Oosterveen et al., 2021). Differences in α-Syn pathology has also been identified in familial PD patient-derived midbrain dopaminergic neurons when compared to pathology observed in cortical projection neurons (Oosterveen et al., 2021). While the mechanisms of selective cellular and regional vulnerability have been challenging to dissect (Fu et al., 2018), the ongoing development of new iPSC differentiation protocols (Tsunemoto et al., 2018) is providing critically important tools for unraveling this fundamental disease feature that remains largely unexplored.

2.5 Advancements in high-throughput variant phenotyping

The classic approach to disease modeling has largely adhered to the study of one gene, using one set of assays, in one cell type at a time. While this approach can provide deep mechanistic insights into the molecular perturbation of interest, its inherent lack of scalability poses a significant challenge in the ability to compare gene and variant effects across diverse cell types, modalities, and laboratories. Recent advances in multi-omics methods now enable high-throughput interrogation of cellular effects across different modalities and cell types. However, the two key cellular screening approaches, array-based and pooled phenotyping, each have their own virtues and drawbacks. As such, the selection of a suitable phenotyping strategy should be

guided by several key experimental considerations (Al'Khafaji et al., 2023; Bennett et al., 2023; Datlinger et al., 2017; Feldman et al., 2019; Y. Li et al., 2021; Smullen et al., 2023; Yu et al., 2007), summarized in **Box 1**.

Box 1 Considerations for selecting a variant phenotyping strategy

Array-based phenotyping

Arrayed phenotyping is a historically useful method for high-content studies of a single genotype per well, allowing for direct genotype-phenotype correlations for validation studies.

Advantages

- Can be conducted in standard laboratory settings
- Can accommodate multi-omics readouts
- Well-suited for studies of both cell-autonomous and non-cell-autonomous effects

Limitations

- Limited scalability and labor-intensive, particularly in parallel culture setups
- Prone to well-position artifacts that result in pseudophenotypes
- Randomization is challenging without robotic platforms

Pooled phenotyping

Pooled phenotyping arrangements combine several genetic perturbations within a single well, offering high-throughput capabilities that are well suited for discovery applications. This approach can accommodate simultaneous characterization of isogenic sets or iPSCs from different patient lines in a single experiment. Barcoding technology, combined with single cell sequencing or optical pooled *in situ* sequencing, enables demultiplexing of isogneic sets, while iPSCs from different patient lines can be demixed by algorithms that target single nucleotide polymorphisms (SNPs).

Advantages

- Efficient and scalable
- Cost-effective
- Employs standard laboratory equipment (eg, single cell transcriptomic readouts, optical pooled readouts)
- No positional artifacts
- Suitable for phenotyping more complex models, such as multi-cell 2D culture, organoids, and in vivo xenotransplantation models

Limitations

- Library preparation can be time-consuming
- Requires deconvolution algorithms to map readouts
- Certain readouts, such as long-read single cell sequencing and single cell proteomics, are only available for array-based screening or require advanced technologies for pooled applications

Some methodologies are restricted to bulk lysates, enabling aggregate assessments across cell populations, while ignoring heterogeneity within cell populations (Y. Li et al., 2021). A growing suite of single-cell techniques, including single-cell proteomics (Bennett et al., 2023; Mund et al., 2022) and long-read single-cell sequencing for splicing annotations (Al'Khafaji et al., 2023), are on the horizon to enable a more nuanced understanding of heterogeneity within and across cell types. While bulk techniques have cost advantages, pooled phenotyping strategies, which combine multiple genetic perturbations in a single experiment and use single-cell techniques to parse phenotypic data, are increasingly employed to illuminate new biology at unprecedented resolution.

2.6 Limitations & opportunities in iPSC-based neurodegenerative disease modeling

Although iPSC-based disease modeling holds enormous potential in uncovering novel mechanisms and therapeutic targets for neurodegenerative disorders, several key limitations remain to be addressed to unlock the full potential of this technology.

In pursuit of solutions for achieving desired cell fate specification and mitigating heterogeneity in differentiation potentials, numerous methods for directed differentiation of iPSC lines by inducible transcription factors have been developed. This approach both reduces variability in differentiation efficiencies and shortens the time for cell conversion. For instance, a single transcription factor-based protocol effectively converts human iPSCs into functional neurons with nearly 100% purity in less than two weeks (Y. Zhang et al., 2013). Inducible transcription factors can equally be used to direct differentiation of non-neuronal cells (Dräger

et al., 2022). Several recent studies have sought to systematically explore the landscape of transcription factors that mediate cellular programming in an effort to enhance cell fate engineering efforts. The Human TFome is one such initiative, in which a library of 1,564 transcription factor genes and 1,732 transcription factor splice isoforms were screened in human iPSC lines to assess the ability of individual transcription factors in inducing differentiation into neurons, fibroblasts, oligodendrocytes and vascular endothelial-like cells (Ng et al., 2021). Systematic CRISPR-based activation of endogenous transcription factors has also proven useful in identifying regulators of neuronal-fate specification (Y. Liu et al., 2018). The application of unbiased discovery strategies, combining forward genetic approaches with single cell readouts, will likely help to further refine cellular phenotypes. To complement these efforts, several groups have developed computational tools to predict the fidelity of various cell fate conversion approaches and provide insights on ways to enhance existing cellular engineering protocols (Cahan et al., 2014; D'Alessio et al., 2015).

While strategies for cell fate (re-)programming to minimize sources of variability continue to rapidly evolve, achieving aging-related phenotypes in pluripotent-derived lineages remains a major challenge in the cellular modeling of late-onset neurodegenerative disorders. Various strategies have been developed to induce aging-related features in iPSC-derived cell lines, based on varying definitions of aging. One approach involves the overexpression of progerin, a truncated form of the nuclear protein lamin A that is associated with premature aging. This has been shown to induce multiple aging-associated features, including dopamine associated-phenotypes such as intracellular accumulation of neuromelanin, to better recapitulate late-onset Parkinson's disease phenotypes (Miller et al., 2013). However, it is unclear to what extent progerin expression faithfully tackles the complexity of biological aging. Another

approach for achieving phenotypic maturation in CNS lineages involves the use of inducible transcription factors to directly reprogram aged somatic cells while bypassing pluripotent stem cell stages (Maroof et al., 2013); however, this approach faces key challenges arising from variability in differentiation efficiencies that can affect the uniformity of resulting cell populations and, at present, can only be applied to model a limited set of cell types. In the future, the application of forward genetic strategies to systematically identify chemical or genetic needs for de-rejuvination of iPSC-derived models could provide a promising strategy to overcome current limitations in capturing the interface of aging and disease.

Furthermore, while traditional two-dimensional cell cultures represent an attractive paradigm for the precise manipulation and phenotyping of cell types, they do not capture the complexity and interactions present in the natural, three-dimensional environment of the human brain. This limitation has led to the development of models that can more accurately replicate in vivo conditions. For example, co-culture methods, in which multiple cell types are grown together, were developed to more effectively capture cell-cell and cell-matrix interactions in the CNS (Paschos et al., 2015). To recapitulate the architecture of complex neuronal tissue and provide a more representative model of in vivo physiology than two-dimensional cell cultures, three-dimensional iPSC derived structures known as organoids have been developed (Sato et al., 2009). In the context of neurodegenerative diseases, patient iPSC-derived cerebral organoids expressing tau-V337M have been used to identify events preceding neurodegeneration in FTD and to test potential targets for therapeutic intervention (Bowles et al., 2021). The value of brain organoid models of AD for high-throughput screening of drugs has also been demonstrated (Park et al., 2021).

Despite these significant advances, organoids lack the vascularization, immune system, and microenvironment that exist in vivo. To address these limitations, xenotransplantation models, which involve the transplantation of human iPSCs in murine models, have emerged as an in vivo alternative to traditional stem cell modeling approaches. The feasibility of engrafting iPSC-derived organoids into mouse brains was recently demonstrated (Mansour et al., 2018). Humanized microglia xenotransplantation models have also been developed for applications in the study of AD (Fattorelli et al., 2021). These examples highlight the potential of xenotransplantation models in addressing existing bottlenecks in translational research. Indeed, several antisense oligonucleotide (ASO) therapies are currently under development for neurodegenerative disorders that may benefit from such models. For example, ASO-based targeting of FUS was recently found to be a promising therapeutic strategy in ALS/FTD mouse models (Korobeynikov et al., 2022) and approved for compassionate use by the FDA in under one year. Blocking the STMN2 cryptic exon splice site has also been shown to rescue phenotypes in TDP-43 'opathies, including ALS/FTD, and represents an attractive target for ASO development (Baughn et al., 2023). Nonetheless, the swift deployment of ASO therapies for terminal diseases necessitates a careful balance between providing potential benefits and minimizing harm to patients. Xenotransplantation models serve as a crucial bridge in this context by enabling a more comprehensive understanding of drug effects in an in vivo setting, prior to first-in-human clinical trials. Moreover, the application of CRISPR therapeutics targeting uniquely human genes and variants, with tools such as base or prime editing, is an additional area of rapid development for gene therapy in the context of neurodegenerative diseases. A recent report demonstrating that RNA-targeting CRISPR therapeutics can eliminate cytotoxic CAG repeats (Morelli et al., 2023) showcases the potential of precision gene editing

approaches in addressing the core mechanisms of neurodegenerative disorders. As this area of investigation continues to flourish, the integration of xenotransplantation models holds great promise in determining the efficacy and safety of CRISPR therapeutic interventions prior to human trials. However, it is important to acknowledge that the immunosuppressive strategies that are often employed to enhance engraftment in xenotransplantation models represent a key challenge when investigating neurodegenerative disorders that are associated with autoimmune dysregulation. As such, findings derived from such models may not fully capture the mechanisms of disease progression or the role of immune responses, thus limiting their translational relevance until these challenges are more effectively addressed (Vadori et al., 2015). In the meantime, the research applications of iPSC-based disease modeling have the potential to identify novel disease mechanisms and therapeutic targets to be further validated for a range of currently intractable neurodegenerative conditions.

CHAPTER 3: Materials & methods

Statement of prior publication

The content in this chapter was modified from Sahba Seddighi *et al.*, Mis-spliced transcripts generate de novo proteins in TDP-43–related ALS/FTD. *Sci. Transl. Med.*16, eadg7162 (2024). Reprinted with permission from AAAS.

3.1 Overview of thesis aims and methods

The objective of my dissertation was to characterize the downstream consequences of TDP-43-related splicing dysregulation in iPSC-derived neurons and determine whether mis-spliced transcripts could generate de novo protein products in settings of TDP-43 loss. I started by developing a neuronal cryptic exon catalog, based on total RNA-sequencing and differential splicing analyses on human iPSC–derived neurons with TDP-43 depleted by CRISPRi. I then used an unbiased proteogenomic strategy, integrating parallel RNA-seq and shotgun proteomics in the TDP-43–depleted human iPSC–derived neurons, to identify de novo peptides that map to cryptic exon coordinates. Next, we cross-referenced these predicted CEs against datasets from ALS/FTD postmortem brain tissue to test the fidelity of our in vitro model in predicting TDP-43 pathology in human brains. We used Western blot and targeted proteomics to validate the presence of de novo peptides in TDP-43–depleted human iPSC–derived neurons. Using affinity purification mass spectrometry, I then examined the impact of de novo peptides on the biology

of the proteins in which they were expressed. Lastly, we developed a novel targeted proteomics assay to unequivocally demonstrate the presence of de novo "cryptic" peptides in CSF samples from patients with ALS/FTD spectrum disorders.

3.2 Transcriptomic studies of human iPSC-derived neurons and postmortem brain tissue

3.2.1 CRISPRi knockdown experiments

Cell culture maintenance

Human iPSCs were grown as previously described (Fernandopulle et al., 2018; Pantazis et al., 2022). Briefly, cells were grown on Matrigel (Corning # 354277)-coated cell culture plates in Essential 8 media (ThermoFisher Scientific # A1517001). Cells were dissociated by incubation with Accutase (Life Technologies # A1110501) for 5 minutes at 37°C and pelleted by centrifugation at 200 x g for 5 minutes. Cell pellets were washed with PBS and pelleted again by centrifugation at 200 x g for 5 minutes. Final pellets were resuspended in E8 supplemented with the ROCK inhibitor Y-27632 (Selleckchem # S1049) to promote adherence and survival and plated onto Matrigel-coated cell culture plates. Media was changed every 1-2 days and Y-27632 was removed from cell culture media when cells formed colonies of > 20 cells.

CRISPRi-mediated gene knockdown in human iPSCs

CRISPRi knockdown experiments were performed in the i11w-mNC line, a derivative of the previously described WTC11 line (Brown et al., 2022; Martin, 2011; Tian et al., 2019). This line stable expresses CAG-dCas9-BFP-KRAB at the CLYBL safe harbor locus and a tetracycline-inducible mNGN2 transgene at the AAVS1 locus. sgRNAs targeting TARDBP, FUS, or a non-targeting control sgRNA were delivered to iPSCs via lentiviral transduction. iPSCs were split and treated with lentivirus by resuspension of the final cell pellet in PBS containing lentivirus (day -4). Cells were incubated in PBS-lentivirus for 5 min and added dropwise to cell culture plates containing E8 + 10 μM Y-27632 media. 24 hours post- transduction (day -3), cells were washed with PBS and fresh E8 media was added (without Y- 27632). On day -2, cells were dissociated and replated in E8 media containing 10 μM Y-27632 and 10ug/ml puromycin to select for cells that were successfully transduced with the sgRNA lentivirus. On day -1, cells were washed with PBS to remove debris, and fresh E8 + puromycin (10μg/ml final concentration) was added to the cells. On day 0, cells were visually inspected and >95% BFP+, suggesting >95% of cells expressed sgRNA. Cells were replated using the above method and plated into Neuronal Induction Media containing Knockout DMEM/F12 media (Life Technologies # 12660012), N2 supplement (Life Technologies # 17502048), 1× GlutaMAX (ThermoFisher Scientific # 35050061), 1× MEM Non-essential Amino Acids (Thermofisher Scientific # 11140050), 10 μM Y-27632 and 2 μg/ml doxycycline (Clontech # 631311). On day 1 and day 2, media was changed, and fresh Neuronal Induction Media was added, excluding Y- 27632. On day 3, cells were dissociated and replated using the above method, and replated into poly-L-ornithine (0.1 mg/ml; Sigma # P3655-10MG)-coated cell culture plates at a density of 1.5 million cells per well of a 6-well plate. From day 3 until the end of the experiment (day 17), cells were cultured in

Neuronal Maturation Media: BrainPhys Neuronal Medium (StemCell Technologies # 05790), 1x B27 Plus Supplement (ThermoFisher Scientific # A3582801), 10 ng/ml BDNF (PeproTech # 450-02), 10 ng/ml GDNF (PeproTech # 450-10) 10 ng/ml NT-3 (PeproTech # 450-03), 1 µg/ml mouse laminin (Sigma # L2020-1MG), and 2 µg/ml doxycycline (Clontech # 631311). Half media changes were done every 3-4 days until collection at day 17.

sgRNA cloning

sgRNAs targeting *TARDBP*, *FUS*, or a non-targeting control sgRNA were cloned into the CROP-seq vector (Addgene # 127965) and driven by the mouse U6 promoter. This vector contains EF1a promoter driving puromycin resistance and BFP expression. The CROP-seq vector was cut via restriction digest using BstXI and BlpI, and a double stranded DNA oligo with appropriate sticky end overhangs were ligated into the cut vector using DNA Ligation Kit, Mighty Mix (Takara # 6023). To generate DNA oligos with appropriate overhangs, "top" and "bottom" ssDNA oligos containing the sgRNA sequence and compatible overhangs were annealed (see sequences below):

	sgRNA sequence	Top oligo (5'->3')	Bottom oligo (5'->3')
TARDBP sgRNA1	GGGAAGTCAGCCGTGAGACC	TTGGGGAAGTCAGCCGTGAGAC CGTTTAAGAGC	TTAGCTCTTAAACGGTCTCACG GCTGACTTCCCCAACAAG
FUS sgRNA1	GGGCCTCAAACGGTAGGTAA	TTGGGGCCTCAAACGGTAGGTA AGTTTAAGAGC	TTAGCTCTTAAACTTACCTACCG TTTGAGGCCCCAACAAG
Non-targeting sgRNA (NT_02194)	GGCCGTGGGCAACACTGTAT	TTGGGCCGTGGGCAACACTGTA TGTTTAAGAGC	TTAGCTCTTAAACATACAGTGT TGCCCACGGCCCAACAAG
Non-targeting sgRNA (NT_00976)	GAAGTTACTCTACAAAACAG	TTGGAAGTTACTCTACAAAACAG GTTTAAGAGC	TTAGCTCTTAAACCTGTTTTGTA GAGTAACTTCCAACAAG
Non-targeting sgRNA (NT_02724)	GAATATGTGCGTGCATGAAG	TTGGAATATGTGCGTGCATGAA GGTTTAAGAGC	TTAGCTCTTAAACCTTCATGCAC GCACATATTCCAACAAG

Lentivirus generation

Lentivirus was prepared by transfection of early passage Lenti-X 293T cells (Takara # 632180) with the sgRNA plasmid using lipofectamine 3000 using manufacturer's recommended protocol. LentiX cells were cultured in DMEM, high glucose, GlutaMAXTM Supplement (Thermo Fisher Scientific # 10566024) supplemented with 10% FBS (Thermo Fisher Scientific # A3160402). 24 hours after transfection, cells were washed with PBS and replaced with fresh media containing 1x ViralBoost (ALSTEM # VB100). Media was collected 96 hours after transfection and lentivirus was concentrated using Lenti-X concentrator (Takara Bio # 631231) using manufacturer's protocol. Lentivirus was resuspended in PBS in 1/10 of the original cell culture dish volume, aliquoted, and stored at -80°C until use.

3.2.2 Short-read RNA sequencing, differential gene expression, and splicing analysis

On day 17 of differentiation, cells were washed with PBS and lysed directly in cell culture plates with 300ul of Tri-reagent (Zymo Research # R2050-1-200). RNA was extracted from day 17 neurons using Direct-zol RNA Miniprep Kit (Zymo Research # R2051) following manufacturer's protocol, including optional DNase treatment step. RNA was quantified using a Qubit Fluorometer. Libraries were prepared using NEBNext Ultra II Directional RNA Library Prep Kit for Illumina (NEB # E7760L) with the NEBNext Poly(A) mRNA Magnetic Isolation

Module (NEB # E7490L). Libraries were indexed, pooled, and sequenced (2 x 150bp) on a Novaseq 6000 using v1.5 reagents.

Paired-end fastq.gz files were trimmed for sequencing adapters using cutadapt v2.5 (Martin, 2011) and quality checked using FastQC v0.11.6 (Andrews, 2010), followed by splice aware alignment against GRCh38.p13.genome.fa using STAR v2.7.3a (Dobin et al., 2013). Differential expression analysis was done using StringTie2 (Kovaka et al., 2019) and DESeq2 (Love et al., 2014). We ran MAJIQ (v2.1) (Vaquero-Garcia et al., 2016) on aligned BAM files to perform differential splicing analysis. We set a threshold of 10% difference in percent spliced in (ΔΨ) for calling a significant change between groups. We then used custom R scripts to parse the output of the deltaPSI module to obtain the PSI (Ψ) and the probability of change for each junction. We defined cryptic splicing as junctions with PSI less than 5% in control samples, a ΔΨ of more than 10%. Junctions were annotated according to the gene annotations from gencode.v37.annotation.gtf. Our splicing pipeline is implemented using Snakemake version 5.5.4 (Mölder et al., 2021) (https://github.com/frattalab/splicing). Finally, we developed a novel pipeline to visualize and automatically categorize each mis-spliced junction from MAJIQ as cryptic exon, exon skip, likely intron retention, or canonical junction (https://github.com/NIH-CARD/proteogenomic- pipeline).

3.2.3 Informatic pipeline for categorization and visualization of differential splicing events

Junction type categorization

Given a 6 column .csv file consisting of splice events (col1:chr#, col2:start, col3:end, col4:strand, col5:gene_name and col6:gene_id), we built a pipeline to automatically categorize each splice event as cryptic exon, exon skip, likely intron retention, or canonical junction, and to provide visual representations of each mis-splicing event in the form of sashimi plots.

The first step in deciding the type of a splicing event is the identification of the transcript this event arises from. We used a 3-layered approach for identifying the biologically relevant transcript for each splicing event: 1) Principal isoforms from the BAM file of all KD samples (using StringTie2), 2) APPRIS principal isoforms 1 and 3) the transcript (from EnsDB V103) with maximum number of exons and longest transcript in terms of its size (number of BPs). Using this approach, transcripts for all splicing events are identified and sashimi plots for all splicing events are generated.

Based on a comparison of the genomic coordinates of each event with the genomic coordinates of the exons of the principal Tx, an event is declared as exon skip (complete overlap between exonic boundaries), cryptic exon, intron retention, or canonical junction.

Events in which genomic coordinates completely overlap with two non-consecutive exons of the principal Tx are declared as exon skip events. The pipeline also differentiates between simple exon-skip events (where the event's genomic coordinates overlap with non-consecutive exons, such as 1 and 3 (net exon number difference of 2)), and multi-exon-skip events (where net exon number difference is > 2). Events for which one of the genomic coordinates overlap with an exon in the principal Tx, while the other lies in the intronic region, are categorized as cryptic events. For these events, we identify genomic coordinates of the upstream and downstream exon and involved intronic region.

Furthermore, in order to classify whether a cryptic event is ce_inclusion, ce_extension, or IR, bed files for all BAM files for all KD samples are created. These bed files are needed to calculate coverage bed files for each probable cryptic exon. For each probable cryptic exon, a coverage bed file containing the average number of reads from all KD samples for the entire intron range of interest is calculated.

Sashimi plot visualization of junctions

In order to identify genomic coordinates of a probable cryptic event, its coverage bed file is scanned from the intronic genomic coordinate of the LSV to the opposite exon. If the read coverage drops to 40% along the way, this event is classified as a CE_inclusion (cassette cryptic exon). If the coverage never drops to zero, this event is classified as CE_extension. If the coverage never drops to zero across the entire intron, then this event is classified as a probable intron retention (IR) event. Category-wise sashimi plots are also generated for user-verification.

3.2.4 Long-read sequencing and data processing

Prior library preparation, RNA integrity was assessed using Qubit™ RNA IQ assay kit (ThermoFisher, Q33221). 50 ng total RNAs were used to prepare cDNA-PCR libraries following manufacturer's protocol (SQK-PCS109, Oxford Nanopore Technologies (ONT)). Sequence-specific cDNA-PCR sequencing was adapted from the ONT protocol (ss-cdna-pcr-sequencing_sqk-pcs109-CPSS_9087_v109_revO_14Aug2019-promethion). Briefly, 500 ng total RNAs were reverse-transcribed at 50°C using the Maxima H Minus Reverse Transcriptase

(ThermoFisher Scientific, EP0751) in the presence of 2 pmoles of each custom sequence-specific primer (Supplementary Table S2C). The corresponding cDNA was purified with 0.5 volume of Agencourt RNAClean XP beads (Beckman, A63987) and washed with 100 µl Small Fragment Buffer (SFB). cDNA was eluted in 12 µl H2O and amplified by PCR for 15 cycles (95°C 30"; 95°C 15", 62°C 15", 65°C 8'30", x15; 65°C, 6') using the LongAmp Taq Master mix (NEB, M0287). PCR-cDNA libraries were purified using 0.5 volume of Agencourt RNAClean XP beads, washed with 100 µl Small Fragment Buffer (SFB) and eluted in 12 µl of elution buffer. Final libraries were quantified using Qubit 1X dsDNA High Sensitivity (HS) assay kit (ThermoFisher Scientific, Q33231) and analyzed on a BioAnalyzer (High Sensitivity DNA kit, Agilent, 5067-4626). Libraries were loaded onto R9.4.1 flow cells (ONT, FLO-PRO002) and ran on a Promethion device (ONT, PRO-SEQ024).

Nanopore direct RNA sequencing data were basecalled using Guppy (v3.4.5). Reads were first aligned against ribosomal sequences obtained from SILVA (Quast et al., 2013). Non-ribosomal reads were subsequently mapped to the human genome (hg38) using minimap2 (version 2.17) (H. Li, 2018) with parameters -a -x splice -k 12 -u b --secondary=no. Basecalled reads were also separately aligned against the human transcriptome (Ensembl version 92) using -a -x map-ont -k 12 -u f -- secondary=no. Transcript identification and quantification was performed with Bambu at maximum sensitivity with parameters NDR=1, min.txScore.singleExon = 0, remove.subsetTx = TRUE, min.readCount = 2, min.readFractionByGene = 0, min.txScore.multiExon = 0, min.exonDistance = 0, min.primarySecondaryDist = 0, txScoreBaseline = 0. Only reads overlapping genes with splicing changes identified from Illumina sequencing were used.

3.2.5 Splicing analysis of postmortem brain tissue

FACS-sorted frontal cortex neuronal nuclei were obtained from the Gene Expression Ombius (GEO) GSE126543 and aligned, as per (Brown et al., 2022). Briefly, samples were quality trimmed using Fastp aligned to the GRCh38 genome using STAR (v2.7.0f) (Brown et al., 2022) with gene models from GENCODE v31. Our alignment pipeline is implemented in Snakemake version 5.5.443 and available at: https://github.com/frattalab/rna_seq_snakemake. STAR's splice junction output tables were then clustered and converted into PSI metrics using Dasper (D. Zhang et al., 2021). As splicing tools can be prone to one-off errors for exact splice junction coordinates, the 340 bona fide splicing events from MAJIQ were manually curated against the splice junctions output by STAR to confirm the absence or presence of the event in the FACs-sorted nuclei.

Our analysis of postmortem brain tissue from NYGC contains 472 neurological tissue samples from 286 individuals from the NYGC ALS dataset, including non-neurological disease controls, FTLD, ALS, FTD with ALS (ALS-FTLD), or ALS with suspected Alzheimer's disease (ALS- AD). Patients with FTD were classified according to a pathologist's diagnosis of FTD with TDP- 43 inclusions (FTLD-TDP), or those with FUS or Tau aggregates. ALS samples were divided into the following subcategories using the available Consortium metadata: ALS with or without reported SOD1 or FUS mutations. ALS-TDP was categorized as all non-SOD1 or FUS ALS samples, but postmortem TDP-43 inclusions pathology was not systematically measured in ALS samples. Sample processing, library preparation, and RNA-seq quality control are described previously (Prudencio et al., 2020; Tam et al., 2019). RNA was extracted from flash-frozen postmortem tissue using TRIzol (Thermo Fisher Scientific) chloroform and 500 ng of the total

RNA was used to create libraries for RNA-Seq with the KAPA Stranded RNA-Seq Kit with RiboErase (KAPA Biosystems) for ribosomal RNA depletion. The libraries had an average insert size of 375 bp and y were sequenced either on an Illumina HiSeq 2500 (125 bp paired end) or an Illumina NovaSeq (100 bp paired end). The samples had a median sequencing depth of 42 million read pairs with a range of 16 to 167 million read pairs.

All samples underwent the same processing, which included adapter trimming with Trimmomatic and alignment to the GRCh38 genome with STAR (2.7.2a) (Dobin et al., 2013) with indexes from GENCODE v30. Quality control was conducted thoroughly to validate sex and tissue type of sample using SAMtools (Brown et al., 2022; H. Li et al., 2009) and Picard Tools (Broad Institute, GitHub Repository: https://broadinstitute.github.io/picard/. A modified form of our splice junction parsing pipeline (Brown et al., 2022) was used to find read counts in the NYGC dataset for the 340 bona fide splicing events from MAJIQ. We extracted all junctions from the NYGC samples which overlapped the 340 bona fide splice events and manually curated them to ensure that no splice junctions were missed due to one-off errors on exact splice coordinates. For each splice junction, to calculate the area under the curve (AUC) for classification performance between TDP-43-proteinopathy and non-TDP-43 proteinopathy samples, the read count for each splice junction was first library-sized normalized and then converted to z-scores across samples. Meta-scores were created as sum of the z-scores across either all cryptic junctions, only those junctions which have a positive predictive value above 0.6, or predictive junctions excluding *STMN2*. AUC scores were calculated in R version 4.2.1, using the *pROC* package (Prudencio et al., 2017; Robin et al., 2011).

3.2.6 qRT-PCR studies of cryptic exons in postmortem brain tissue

Frontal cortex tissues from individuals with neuropathologically confirmed FTLD-TDP and those without neuropathological features were provided by the Mayo Clinic Florida Brain Bank. Written informed consent was provided by all participants or their family members, and all protocols were approved by the Mayo Clinic Institution Review Board and Ethics Committee. Sample size was determined based on the availability of tissue in our brain bank. Quantification of the cryptic transcript variants was carried out using complementary DNA (cDNA) resulting from 500 ng of RNA (RNA integrity, RIN ≥ 7.0) that was available from a previous study (Prudencio et al., 2017). CRISPRi- iPSC-derived neuron (i3877 N) cDNA was generated from our previous publication (Prudencio et al., 2020), in which TDP-43 is downregulated to about 50%. Quantitative real-time PCRs (qRT-PCR) were conducted using SYBR GreenER qPCR SuperMix (Invitrogen) for all samples in triplicates. qRT-PCR were run in a QuantStudioTM 7 Flex Real-Time PCR System (Applied Biosystems). Relative quantification was determined using the ΔΔCt method and normalized to the endogenous controls *GAPDH* and *RPLP0*. Primer efficiency was verified for each cryptic exon variants prior running the qRT-PCRs. See Supplementary Table S3F for primers. To compare *tSTMN2* RNA between controls and FTLD-TDP cases, unpaired Mann-Whitney tests were performed. To compare *tSTMN2* RNA between iPSC-derived neurons treated with

control sgRNA (sgControl) and the two different sgRNAs against *TARDBP* (sgTARDBP-1 and siTARDBP-8), we used one-way ANOVA. All statistical analyses were done using GraphPad Prism 9 (GraphPad Software). For each figure the type of analysis used, and the number of subjects is indicated in the figure and/or legend.

3.3 Proteogenomic detection of cryptic peptides in human iPSC-derived neurons

3.3.1 Ribosome profiling

Previously published ribosome profiling libraries (Brown et al., 2022) were re-sequenced at higher depth following depletion using a Cas9-based protocol (Wilkins & Ule, 2021). Reads were processed as previously described (Brown et al., 2022). Briefly, for unbiased analysis of differential ribosome footprint enrichment in introns, following demultiplexing with Ultraplex v1.2.4, reads were first pre-mapped to list of common contaminant ncRNA sequences using Bowtie2 v2.3.5.1, then the remaining reads were mapped to the human genome (hg38 using Gencode V29 as reference) using STAR_2.6.1a_08- 27 (Dobin et al., 2013), followed by deduplication with UMI-Tools v1.0.1. Reads of the expected length (27-31 nt) which aligned uniquely to intronic regions, without overlap to any exons, were identified using an R script ('search for intron translation.R'). The number of such footprints for each intron was calculated in each sample, then DESeq2 (Love et al., 2014) was used to analyze whether there were

significantly changed densities of footprints on each intron (thus analogous to typical RNA-seq analysis with DESeq2, but treating each intron as a distinct 'gene').

For analysis of periodicity, reads were first processed using the standard pipeline described above (removing common ncRNA contaminants and PCR duplicates, and ensuring that all RFPs aligned uniquely to the genome), then FASTQs containing only uniquely aligned reads were extracted from the deduplicated genomic BAM files. The extracted FASTQs were then re- aligned to a fasta file containing just the coding sequences for the list of transcripts encoding CEs that were predicted to be translated; the first base of each RFP was ignored (as this is often mismatched due to non-templated nucleotide addition during reverse transcription) and the rest of the footprint was required to match perfectly, through the use of harsh mismatch penalties (-- norc --no-unal --very-sensitive -N 1 --mp 10000 --np 10000 --rdg 10000 --rfg 10000 -a) with Bowtie2 (Langmead & Salzberg, 2012). The length and sub-codon position of reads aligning to CEs was then calculated. Equivalent analysis but using alignment with Bowtie2 to annotated transcripts was also performed, and the results were compared. All pipelines and code used are deposited at Zenodo (DOI 10.5281/zenodo.10479046).

3.3.2 De novo peptide sequence prediction

All MAJIQ derived cryptic splice junctions were annotated by Dasper (D. Zhang et al., 2021) to separate junctions by whether they were novel acceptor, novel donor, or novel exon skipping events. Cryptic exons are those were either the donor, acceptor, or both ends of the junction is novel, whereas skipptic events are novel exon skips. In order to find the exonic regions created by these novel splice junctions, we used all exons defined in the Gencode v31,

and all of the potential exonic regions defined by two different transcript assembly tools, Scallop (Shao & Kingsford, 2017)and Stringtie2 (Kovaka et al., 2019). We filtered out false positive exonic regions by mapping the number of splice junctions that ended on both the 5' and 3' ends of the exonic region and those with less than 10 splice junctions on both ends across all TDP-KD samples were filtered out as being potential false positives. We mapped all novel exonic regions back to those which overlapped cryptic junctions. In order to build the possible open reading frames, we first determined which of the known transcripts overlapped with the cryptic events and could be used as 'backbone transcripts'. We then filtered out transcripts which were not expressed, with a liberal mean expression cut-off of 1 transcript per million across all samples, determined by SALMON (Shao & Kingsford, 2017). We then inserted the novel cryptic event into each of the expressed backbone transcripts and used the genomic regions to extract the nucleotide sequences. For each nucleotide sequence, we translated into the amino acid sequence, and extracted all possible open reading frames (ORF) between every methionine and every stop codon.

3.3.3 Data-dependent acquisition (DDA) mass spectrometry

Sample preparation

For the iPSC-derived neurons grown and differentiated in 6-well plates, neurons were washed with ice-cold phosphate-buffered saline (PBS) three times before adding 150 ul of lysis buffer with high percentage of detergents, consisting of 50 mM Tris-HCl pH 8, 50 mM NaCl, 1% v/v SDS, 1% v/v Triton X-100, 1% v/v NP-40, 1% v/v Tween 20, 1% v/v glycerol, 1%

sodium deoxycholate (w/v), 5 mM EDTA pH 8, 5 mM dithiothreitol, 5 KU benzonase and protease inhibitors. Cell lysates were collected and incubated at 65°C for 30 min, followed by addition of 10mM iodoacetamide and 30 min incubation in the dark. The automated protein digestion was performed as previously described (Reilly et al., 2021). Briefly, the protein input of each sample was normalized to 20 ug and was captured by the hydrophilic beads on an automated KingFisher APEX robot. The final concentration of tryptic peptides from iPSC-derived neurons was normalized to 0.2 ug/ul using peptide measurement on a NanoDrop. We injected 5 ul of total peptides for proteomic analyses.

Liquid chromatography and mass spectrometry analyses

For the data-dependent acquisition (DDA) liquid chromatography and tandem mass spectrometry (LC-MS/MS) analyses, peptides were first separated on an Ultimate 3000 nano-LC system coupled with a 50cm column (75 μm I.D., 2 μm C18 particle) and were injected to a high-resolution Orbitrap Eclipse MS (Thermo Scientific). A 120 min effective LC gradient 2-35% liquid phase B was used. Liquid phase A was 5% DMSO in 0.1% formic acid (FA) water, and liquid phase B was 5% DMSO in 0.1% FA acetonitrile. The full (MS1) scan was conducted 375-1400 m/z at 120k-resolution. The dynamic exclusion was set to 45 s excluding the ion after 1 time detection. The fragment (MS2) scan was set to cycle time 3 s, isolation window 1.6 m/z, HCD collision energy 30%, and the fragments were detected in linear ion trap at rapid scan rate with auto maximum injection time.

Database search and statistical analyses

For DDA-based discovery proteomics, we used PEAKS studio (v10.6) with a customized database containing uniport-human proteome reference (UP000005640) and open reading frames (ORFs*)* in silico translated from mis-spliced junctions identified by total RNA sequencing. Trypsin was chosen as the digestion enzyme (allowing semi-tryptic digestion), mass error tolerance was set to 15 ppm, and 3 mis-cleavages were allowed. The statistical analysis was conducted in R studio (v4.3), the simple two-side t-test was used for comparison, and p-values were adjusted for multiple-comparisons using Benjamini-Hochberg procedure. The differential expression analysis was carried out in Spectronaut (v16) (Martinez-Val et al., 2021), where log fold changes and q-value were generated for volcano plot analysis.

3.3.4 Data-independent acquisition (DIA) mass spectrometry

Sample preparation

Cell pellets of five control and five TDP-43 knockdown (KD) samples were collected in 2ml Eppendorf tubes and snap-frozen in liquid nitrogen. On preparation for MS, samples were thawed on ice before adding 200 µl lysis buffer (2% SDS, 100 mM HEPES, pH8, 50 mM DTT). Samples were then vortexed (five times) prior to sonication (Bioruptor Plus) for 10 cycles (30 s ON/60 s OFF) at high setting, at 20°C. Reduction (15 min, 45°C) was followed by alkylation with 20 mM iodoacetamide (IAA) for 30 min at room temperature in the dark. Protein amounts were quantified by EZQ™ (Invitrogen) and 200µg of protein from each sample were taken along for digestion. Proteins were precipitated overnight at −20°C after addition of a 4×

volume of ice-cold acetone. The following day, the samples were centrifuged at 20,800 *g* for 30 min at 4°C and the supernatant carefully removed. Pellets were washed twice with 1 ml ice-cold 80% (v/v) acetone in water then centrifuged at 20,800 *g* at 4°C. They were then allowed to air-dry before addition of 100 µl of digestion buffer (1M Guanidine, 100 mM HEPES, 100mM HEPES, pH8), followed by sonication (as above) and addition of LysC (Wako) at 1:100 (w/w) enzyme:protein for 4 h at 37°C with shaking (Eppendorf ThermoMixer®C, thermoblock for 1.5 ml tubes, at 1,000 rpm for 1 h, then 650 rpm). Samples were then diluted 1:1 with Milli-Q water, and trypsin (Promega) added at the same enzyme to protein ratio. Samples were further digested overnight at 37°C with shaking (650 rpm). The following day, digests were acidified by the addition of TFA to a final concentration of 2% (v/v) and then desalted with Waters Oasis® HLB µElution Plate 30 µm (Waters Corporation, Milford, MA, USA) in the presence of a slow vacuum. In this process, the columns were conditioned with 3 × 100 µl solvent B (80% (v/v) acetonitrile; 0.05% (v/v) formic acid) and equilibrated with 3 × 100 µl solvent A (0.05% (v/v) formic acid in Milli-Q water). The samples were loaded, washed 3 times with 100 µl solvent A, and then eluted into 0.2-ml PCR tubes with 50 µl solvent B. The eluates were dried down with the speed vacuum centrifuge and dissolved at a concentration of 1 µg/µl in reconstitution buffer (5% (v/v) acetonitrile, 0.1% (v/v) formic acid in Milli-Q water). Samples were spiked with iRT peptides (Biognosys, Switzerland) and analyzed as described below.

Liquid chromatography and mass spectrometry

Peptides were separated in trap/elute mode using the nanoAcquity MClass Ultra-High Performance Liquid Chromatography system (Waters, Waters Corporation, Milford, MA, USA)

equipped with a trapping (nanoAcquity Symmetry C18, 5 µm, 180 µm × 20 mm) and an analytical column (nanoAcquity BEH C18, 1.7 µm, 75 µm × 250 mm). Solvent A was water and 0.1% formic acid, solvent B was acetonitrile, and 0.1% formic acid. 1 µl of the sample (~1 µg on column) was loaded with a constant flow of solvent A at 5 µl/min onto the trapping column. The trapping time was 6 min. Peptides were eluted via the analytical column with a constant 0.3 µl/min flow. During the elution, the percentage of solvent B increased in a nonlinear fashion from 0–40% in 120 min. The total run time was 145 min, including equilibration and conditioning. The LC was coupled to an Orbitrap Exploris 480 (Thermo Fisher Scientific, Bremen, Germany) using the Proxeon nanospray source. The peptides were introduced into the mass spectrometer via a Pico-Tip Emitter 360-µm outer diameter × 20-µm inner diameter, 10-µm tip (New Objective) heated at 300 °C, and a spray voltage of 2.2 kV was applied. The capillary temperature was set at 300°C. The radiofrequency ion funnel was set to 30%. For DIA data acquisition, full-scan mass spectrometry (MS) spectra with a mass range of 350–1650 m/z were acquired in profile mode in the Orbitrap with a resolution of 120,000 FWHM. The default charge state was set to 3+. The filling time was set at a maximum of 60 ms with a limitation of 3×10^6 ions. DIA scans were acquired with 40 mass window segments of different widths across the MS1 mass range. Higher collisional dissociation fragmentation (stepped normalized collision energy; 25, 27.5, and 30%) was applied, and MS/MS spectra were acquired with a resolution of 30,000 FWHM with a fixed first mass of 200 m/z after accumulation of 3×10^6 ions or after filling time of 35 ms (whichever occurred first). Data were acquired in profile mode. For data acquisition and processing of the raw data Xcalibur 4.3 (Thermo) and Tune version 2.0 were used.

Database search and statistical analysis

Direct DIA search was performed against a human FASTA database (SwissProt, release 2016_01) (Bairoch & Apweiler, 2000) and a list of common contaminants using Pulsar engine in Spectronaut Professional+ (version 14.9, Biognosys AG, Schlieren, Switzerland) (Martinez-Val et al., 2021). The following modifications were included in the search: Carbamidomethyl (C) (Fixed) and Oxidation (M)/Acetyl (Protein N-term; Variable). A maximum of 2 missed cleavages for trypsin were allowed. The identifications were filtered to satisfy FDR of 1% on peptide and protein quantification. Precursor matching, protein inference, and quantification were performed in Spectronaut using default settings. The contrast table (differential expression analysis) was then exported to perform further data visualization (i.e., volcano plot) using R/Bioconductor.

3.4. Orthogonal validation of cryptic peptides in human iPSC-derived neurons

3.4.1 Western blot

iPSC-derived neurons pellets were lysed in Co-IP buffer (50 mM Tris–HCl, pH 7.4, 300 mM NaCl, 1% Triton X-100, 5 mM EDTA) plus both protease and phosphatase inhibitors, sonicated on ice, and then centrifuged at 16,000 × g for 20 min. Supernatants were saved as cell lysates. The protein concentration of lysates was determined by BCA assay, and samples were

then subjected to Western blot analysis. Equal amounts of protein were loaded into 10-well 3-8% Tris-Acetate (MYO18A, MYO18A-CE), or 10-well 10% Tris-Glycine gels (HDGFL2, HDGFL2-CE, TDP-43, FUS and GAPDH) (ThermoFisher). After transferring proteins to membranes, membranes were blocked with 5% nonfat dry milk in Tris-buffer saline (TBS) plus 0.1% Tween 20 (TBST) for 1 h, then incubated with anti-rabbit MYO18A-CE antibody (1:500), anti-rabbit MYO18A antibody (1:500, ThermoFisher, PA5-76549), anti-rabbit HDGFL2-CE antibody (1:500), anti-rabbit HDGFL2 antibody (1:1000, Proteintech, 15134-1-AP), anti-rabbit TDP-43 antibody (1:1000, Proteintech, 12892-1-AP), anti-mouse FUS antibody (1:500, Santa Cruz Biotechnology, SC- 47711) or anti-mouse GAPDH antibody (1:5000, Meridian Life Science, H86504M) overnight at 4°C. Membranes were washed in TBST and incubated with donkey anti-rabbit or anti-mouse IgG antibodies conjugated to horseradish peroxidase (1:5000; Jackson ImmunoResearch) for 1 h at room temperature. Protein expression was visualized by enhanced chemiluminescence treatment and exposure to Amersham ImageQuant 800. MYO18A-CE antibody to detect the cryptic sequence in MYO18A was generated by Labcorp by immunizing rabbits with a peptide including the complete 20 residue neoepitope (VKEEDKTLPKPGSPGKEEGA). HDGFL2-CE antibody to detect the cryptic sequence in HDGFL2 was generated by Labcorp by immunizing rabbits with a peptide including the 16 residue neoepitope (RLHESERVRKQERERD).

3.4.2 Meso Scale Discovery assay

HDGFL2 cryptic protein quantification in TDP-43–depleted human iPSC–derived neuron lysates was carried out using an MSD-based sandwich immunoassay. Briefly, TDP-43–

depleted human iPSC–derived neuron lysates were diluted in TBS. Serial dilutions of TDP-43–depleted human iPSC–derived neuron lysates (0, 0.5, 1, 2, 4, and 8 μg) were tested in duplicate wells. The wild-type HDGFL2 antibody at a concentration of 4 μg/ml (Proteintech, #15134-1-AP) was used as the capture antibody. The Sulfo-tagged–HDGFL2-CE antibody at a concentration of 4 μg/ml was used as the detection antibody. Response values corresponding to the intensity of emitted light on electrochemical stimulation of the assay plate using the MSD QUICKPLEX SQ120 were acquired.

3.4.3 Immunofluorescence staining

The iPSC-derived neuron dCas9-BFP-KRAB iPSC were transduced with lentivirus expressing TDP-43 sgRNA for 3 days, and then selected by addition of puromycin (1 μg/ml, P8833-100MG, Sigma-Aldrich). To differentiate iPSC-derived neuron dCas9-BFP-KRAB iPSCs expressing TDP-43 sgRNA into neurons, iPSCs were dissociated using Accutase (#AT-104, Innovative Cell Technologies, Inc), and then seeded on dishes coated with Matrigel (354230, Corning) in differentiation media [Knock-out DMEM/F12 (12660012, Thermo Fisher Scientific) with 1 × NEAA (11140-050, Thermo Fisher Scientific), 1 × GlutaMAX (35050-061, Thermo Fisher Scientific), 2 μg/ml doxycycline (D9891- 5G, Sigma-Aldrich), and 10 uM Thiazovivin]. Media was changed daily, and Thiazovivin was removed after first media change. Three days after differentiation, cells were dissociated using Accutase, and then seeded on poly-L-ornithine (P4957-50Ml, Sigma-Aldrich)-coated glass coverslips in 24-well plate at a density of 2 × 104 cells/well in maturation medium [50% Knock- out DMEM/F12 (12660012, Thermo Fisher Scientific), 50% NeurobasalTM-A Medium (10888- 022, Thermo Fisher Scientific), 0.5 ×

B-27 supplement (A3582801, Thermo Fisher Scientific), 0.5 × N2 (17502048, Thermo Fisher Scientific), 0.5 × GlutaMAX, 1 × NEAA, 1 μg/ml mouse laminin (23017-015, Fisher Scientific), 10 ng/ml BDNF (300-104P, Gemini Bio Products), 10 ng/ml NT3 (300-175P, Gemini Bio Products), and 2 μg/ml doxycycline]. Fourteen days later, the neurons were fixed with 4% paraformaldehyde. The fixed neurons were permeabilized with 0.5% Triton X-100 for 10 min and blocked with 10% normal goat serum in PBS for 1 h, then incubated with the anti-rabbit HDGFL2-CE antibody (1:500) and anti-mouse TDP-43 antibody (1:500, H00023435-M01, Novus) overnight at 4°C. After washing, sections or cells were incubated with corresponding Alexa Fluor 488-conjugated donkey anti-rabbit antibody (1:500, Molecular Probes) and Alexa Fluor 568-conjugated donkey anti-mouse antibody (1:500, Molecular Probes) for 2 h. Normal goat serum (1%) in PBS was used to dilute the primary and secondary antibodies. Hoechst 33258 (1 μg/ml, H3569, Thermo Fisher Scientific) was used to stain cellular nuclei. Images were obtained on a Zeiss LSM 980 laser scanning confocal microscope.

3.4.4 TDP-43-GFP rescue experiments

Green fluorescent protein (GFP)-TDP-43 inducible cell lines were previously generated as previously described (Hallegger et al., 2021). Briefly, Flp-In HEK293 was transfected with siRNA against TARDBP for 72 hours. In the rescue experiments, 24 hours before the collection of cells and protein lysates, the medium was replaced with Dulbecco's modified Eagle's medium with doxycycline to induce the siRNA-resistant N-terminally GFP-tagged TDP-43.

3.4.5 Parallel reaction monitoring-based targeted proteomics

Sample preparation

For the iPSC-derived neurons grown and differentiated in 6-well plates, neurons were washed with ice-cold phosphate-buffered saline (PBS) three times before adding 150 ul of lysis buffer with high percentage of detergents, consisting of 50 mM Tris-HCl pH 8, 50 mM NaCl, 1% v/v SDS, 1% v/v Triton X-100, 1% v/v NP-40, 1% v/v Tween 20, 1% v/v glycerol, 1% sodium deoxycholate (w/v), 5 mM EDTA pH 8, 5 mM dithiothreitol, 5 KU benzonase and protease inhibitors. Cell lysates were collected and incubated at 65°C for 30 min, followed by addition of 10mM iodoacetamide and 30 min incubation in the dark. The automated protein digestion was performed as previously described (Reilly et al., 2021). Briefly, the protein input of each sample was normalized to 20 ug and was captured by the hydrophilic beads on an automated KingFisher APEX robot. The final concentration of tryptic peptides from iPSC-derived neurons was normalized to 0.2 ug/ul using peptide measurement on a NanoDrop. We injected 5 ul of total peptides for proteomic analyses.

Liquid chromatography and mass spectrometry analyses

For parallel reaction monitoring (PRM) liquid chromatography and tandem mass spectrometry (LC-MS/MS) analyses, peptides were first separated on an Ultimate 3000 nano-LC system coupled with a 50cm column (75 µm I.D., 2 µm C18 particle) and were injected to a high-resolution Orbitrap Eclipse MS (Thermo Scientific). A 60 min effective LC gradient 2-35% liquid phase B was used. The MS1 scan was conducted 350-2000 m/z at 120k-resolution. The

MS2 was conducted based on mass list table generated by Skyline using orbitrap with a 30k resolution and 3 s loop control.

Database search and statistical analyses

For targeted proteomics, MS raw files of PRM were directly loaded to Skyline (daily version) (MacLean et al., 2010) for quantification and visualization. Only common y-ions identified in both light and heavy peptides were used for quantification and dot product estimation. The light peptide intensity was normalized by its heavy labeled counterpart. The dot product (dotp) was calculated using Skyline (daily version) to measure the spectral similarity between the transition peak areas and the theoretical spectra. Statistical analyses were done using Mann-Whitney *U* test in GraphPad Prism 9 (GraphPad Software).

3.5 Assessing the impact of cryptic peptides on the biology of proteins

3.5.1 Protein structure prediction

To assess the potential impact of the inclusion of an additional coding exon to HDGFL2 (Q7Z4V5) and MYO18A (Q92614) protein structures, we exploited Alphafold2 (10.1038/s41586-021-03819-2) using the monomer settings. The input sequences for the two proteins were computed by adding the cryptic peptide sequences to the canonical sequences from UniProt. The resulting structure files were visualized on https://molstar.org/viewer/.

3.5.2 Immunoprecipitation and on-bead digestion

Immunoprecipitation (Co-IP) of HDGFL2-WT and HDGFL2-CE studies were performed as previously described (Y.-J. Zhang et al., 2016). In brief, HEK293T cells were transfected with vector, HDGFL2-WT or HDGFL2-CE plasmids. Forty-eight hours post-transfection, the cell pellets were collected and then lysed in Co-IP buffer (50 mM Tris–HCl, pH 7.4, 300 mM NaCl, 1% Triton X-100, 5 mM EDTA) containing protease and phosphatase inhibitors. After sonication on ice, the lysates were centrifuged at 16,000 × g for 20 min and the protein concentration of the resulting supernatants was determined by Bicinchoninic acid assay (BCA) (23225, Thermo Fisher Scientific). Supernatants containing 500 µg of protein from cells expressing vector, HDGFL2-WT or HDGFL2-CE were pre-cleared with 15 µl Protein G Dynabeads (10003D, Thermo Fisher Scientific), and then incubated with a mouse monoclonal Flag antibody (2 µl, Sigma, F1804- 200UG) overnight at 4°C with gentle shaking. The antigen-antibody immuno-complex was captured by 20 µl Protein G Dynabeads for 4 h, and then the beads were separated using a magnetic tube stand. After washing twice with Co-IP buffer, three times with chilled PBS and once with 50 mM ammonium bicarbonate (ABC) (Sigma, Cat# A6141), the beads were subjected to on-bead digestion with 100 µl 20 µg/ml trypsin (Promega, Cat # V5073) on a Thermomixer at 1200 rpm and 37°C for 16 hrs. The next morning, the supernatants were separated from the beads and mixed with 10 µL of 5% Trifluoroacetic acid (ThermoScientific, Cat # 28904) in a chemical safety hood to acidify the samples, which were then frozen at -30°C prior to mass spec.

3.5.3 Affinity purification mass spectrometry

Each 10-cm dish of cells was washed three times with ice-cold phosphate-buffered saline (PBS; Lonza Cat. #17-516F) and lysed with 0.5 mL of ice-cold lysis buffer containing 50 mM TrisHCL, pH 8, 150 mM NaCl, 0.1% TritonX-100, and 1x protease inhibitor cocktail (Roche SKU 5892791001). Each dish was rocked for 15 min at 4°C before collecting cell lysates and centrifuging at 20,000g for 15 min at 4°C. The remaining lysate supernatants were collected. Antibodies for the appropriate control or experimental condition were added to each sample and rotated overnight at 4°C for 16 hours. Sample protein concentrations were evaluated using a detergent compatible protein assay (DCA) (Bio-Rad, Hercules, CA, Cat. #5000111) and normalized to 0.4 μg/μL. Automated affinity purification was then performed for 4 hours on a KingFisher Flex Purification System (Thermo Scientific) at 4°C. Eluates were transferred to a ThermoMixer and incubated at 37°C for 16 hours. Peptides were then dried using a SpeedVac vacuum concentrator (Thermo Scientific) and reconstituted in 2% acetonitrile and 0.4% trifluoroacetic acid (TFA). The peptide concentrations were evaluated on a Denovix DS-11 FX Spectrophotometer/Fluorometer (peptide mode, acquisition wavelength 215 nm, E 0.1% (mg/mL), correction factor of 25.99) and normalized to 0.1 μg/μL. Analysis of 5 μL of each normalized peptide sample was conducted via LC-MS/MS. Precursor matching, protein inference, and quantification were performed in Spectronaut using the DirectDIA workflow in default settings. Differential abundance analysis was carried out in the Spectronaut software 16.2, generating log fold changes and q-values by using a two-sided t-test and Benjamini-Hochberg adjustment for multiple comparisons. R software version 4.2.3 was used to data visualization.

3.5.4 STRING analysis

GO analysis was performed on significantly enriched HDGFL2-interacting proteins (*P*adj < 0.05), compared with control IgG pull-downs, or HDGFL2-interacting proteins that were significantly changed in their interactions depending on TDP-43 knockdown (*P*adj < 0.05). GO term analysis was performed in ShinyGo v0.76.3 (Ge et al., 2020). String analysis was performed using String v11.5 (Szklarczyk et al., 2019), and resulting networks were downloaded and visualized using Cytoscape (v3.9.1) (Shannon et al., 2003).

3.6 Detection of cryptic peptides in ALS/FTD CSF

3.6.1 ALS CSF TMT-MS proteomics

Sample preparation

Briefly, 150 µl of CSF from each of the 24 individual CSF samples from the Emory ALS Center biobank was incubated with 200 µl of High Select Top14 Abundant Protein Depletion Resin (Thermo Fisher Scientific, A36372) at room temperature in centrifuge columns (Thermo Fisher Scientific, A89868) essentially as previously described (Higginbotham et al., 2020). After 15 min of rotation, the samples were centrifuged at 1000*g* for 2 min. Sample flow-throughs were reduced and alkylated with 5 µl of 0.5 M tris-2(-carboxyethyl)-phosphine and 25 µl of 0.4 M chloroacetamide at 90°C for 10 min, followed by water bath sonication for 15 min. The samples

were dried by speed vacuum (Labconco), then resolved in 150ul of 6M urea buffer [6 M urea and 75 mM sodium phosphate (pH 8.5)]. Protein concentration was assessed by bicinchoninic acid (BCA) method according to the manufacturer's protocol (Thermo Fisher Scientific). Immunodepleted CSF (125 µl) from all samples was digested with lysyl endopeptidase (LysC) and trypsin. Briefly, LysC (5 µg; Wako) was used for overnight digestion at room temperature. Samples were then diluted to 1 M urea with 50 mM ammonium bicarbonate (ABC). An equal amount (5 µg) of trypsin (Promega) was added, and the samples were subsequently incubated for 12 hours. The digested peptide solutions were acidified to a final concentration of 1% formic acid (FA) and 0.1% trifluoroacetic acid (TFA), followed by desalting with 30 mg of HLB C18 columns (Waters) as described previously (Higginbotham et al., 2020). The peptides were subsequently eluted in 1 ml of 50% acetonitrile (ACN). To normalize protein quantification across batches, 150 µl of aliquots from all 24 CSF samples were combined to generate a pooled sample, which was then aliquoted into 3 global internal standards (GIS) with 850 µl each. All individual samples and the pooled standards were dried by speed vacuum (Labconco).

All 24 samples and 3 GIS samples were divided into three batches, labeled using an 11-plex TMT kit (Thermo Fisher Scientific, lot no.RF234620), and derivatized as previously described *(63)*. See the Supplementary Table S6A for sample to batch arrangement. Nine of the 11 TMT channels were used for labeling: 127N, 128N, 128C, 129N, 129C, 130N, 130C, 131N, and 131C. Briefly, 5 mg of each TMT reagent was dissolved in 256 µl of anhydrous ACN. Each CSF peptide digest was resuspended in 50 µl of 100 mM triethylammonium bicarbonate (TEAB) buffer, and 20.5 µl of TMT reagent solution was subsequently added. After 1 hour, the reaction was quenched with 4 µl of 5% hydroxylamine (Thermo Fisher Scientific, 90115) for 15 min. After labeling, the peptide solutions were combined according to the batch arrangement.

Each TMT batch was desalted with 100 mg of Sep-Pak C18 columns (Waters) and dried by speed vacuum (Labconco).

To enhance the depth of the discovery CSF proteome, these TMT labeled samples were subjected to high-pH fractionation as previously described (Higginbotham et al., 2020). TMT-labeled peptides (~220 μg) from each discovery sample were dissolved in 100 μl of loading buffer [1 mM ammonium formate in 2% (v/v) ACN], injected completely with an autosampler, and fractionated using a ZORBAX 300Extend-C18 column (2.1 mm by 150 mm, 3.5 μm; Agilent Technologies) on an Agilent 1100 HPLC (high-performance liquid chromatography) system monitored at 280 nm. A total of 96 fractions were collected over a 60-min gradient of 100% mobile phase A [4.5 mM ammonium formate (pH 10) in 2% (v/v) ACN] from 0 to 2 min, 0 to 12% mobile phase B [4.5 mM ammonium formate (pH 10) in 90% (v/v) ACN] from 2 to 8 min, 12 to 40% mobile phase B from 8 to 36 min, 40 to 44% mobile phase B from 36 to 40 min, 44 to 60% mobile phase B from 40 to 45 min, and 60% mobile phase B until completion with a flow rate of 0.4 ml/min. The 96 fractions were collected with an even time distribution and pooled into 24 fractions. All fractions were dried down by vacuum centrifugation in a speedvac.

Mass spectrometry analysis

Each fraction was brought up in 10 ul of loading buffer (0.1% FA and 0.03 % TFA) and 2 ul was loaded onto an in-house packed analytical column (75um x 50 cm packed with 1.9um Dr. Maisch ReproSil-Pur C18 beads). Elution was carried out across 100 mins at a flow rate of 250nl/min using an EasyNlc 1200 (ThermoFisher). The gradient went from 1% B (0.1% FA in ACN) to 40% B. Mass spectra were collected on a Orbitrap Fusion Lumos mass spectrometer.

The mass spectrometer was set to collect at top speed with a cycle time of 3 seconds. Full scans were collected with a range of 375-1500 m/z, 120k resolution, an AGC of 40000 and a maximum injection time of 50ms. Tandem scans were collected at 50k resolution with an isolation window of 1.2 m/z, collision energy of 36%, an AGC target of 50k and a max injection time of 86ms.

3.6.2 ALS CSF 2D-LC-MS/MS proteomics

Sample preparation

A pooled sample was made by mixing 28 ALS CSF samples from the Emory ALS Center biobank with equal volume. The pooled sample (800ul) was reduced and alkylated with 16 µl of 0.5 M tris-2(-carboxyethyl)-phosphine and 80 µl of 0.4 M chloroacetamide at 90°C for 10 min, followed by water bath sonication for 10 min. The sample was diluted with 896 µl of 8 M urea buffer [8 M urea and 100 mM NaHPO4 (pH 8.5)] to a final concentration of 4 M urea. LysC (300 mAU) was used for overnight digestion at room temperature. 120 µg of trypsin (Promega) was added after the sample was diluted to 1 M urea with 50 mM ammonium bicarbonate (ABC). The digestion was carried out for another 12 hours at room temperature. The digested peptide solution was acidified to a final concentration of 1% formic acid (FA) and 0.1% trifluoroacetic acid (TFA) (Johnson et al., 2020; Quast et al., 2013), followed by desalting with 2 of 30 mg of HLB C18 columns (Waters) as described previously (Johnson et al., 2020). The peptides were subsequently eluted in 2 ml of 50% acetonitrile (ACN) then dried by speed vacuum (Labconco).

High-pH fractionation

Dried samples were re-suspended in high pH loading buffer (0.07% vol/vol NH4OH, 0.045% vol/vol FA, 2% vol/vol ACN) and loaded onto a Water's BEH (2.1mm x 150 mm with 1.7 μm beads). A Thermo Vanquish UPLC system was used to carry out the fractionation. Solvent A consisted of 0.0175% (vol/vol) NH4OH, 0.01125% (vol/vol) FA, and 2% (vol/vol) ACN; solvent B consisted of 0.0175% (vol/vol) NH4OH, 0.01125% (vol/vol) FA, and 90% (vol/vol) ACN. The sample elution was performed over a 25 min gradient with a flow rate of 0.6 mL/min with a gradient from 0 to 50% B. A total of 192 individual fractions were collected, consolidated down to 96 fractions and dried by speed vacuum (Labconco).

Mass spectrometry analysis

Each of the 96 high-pH peptide fractions was resuspended in loading buffer (15ul of 0.1% FA, 0.03% TFA, 1% ACN), and 3ul were separated on a Water's CSH C18 column (1.7um C18 150um x 15 cm) by an Easy-nLC 1200 system (Thermo Fisher Scientific) and monitored on an Orbitrap Fusion mass spectrometer (Thermo Fisher Scientific). Elution was performed over a 45 min gradient at a rate of 1250 nl/min with Buffer B ranging from 1% to 99% (Buffer A: 0.1% FA in water, Buffer B: 80% ACN in water and 0.1% FA). The mass spectrometer was set to acquire data in top speed mode with 3 s cycles. Full MS scans were collected at a resolution of 120,000 (300-1500 m/z range, 4 × 10e5 AGC, 50 ms maximum ion time). All HCD MS/MS spectra were acquired at a resolution of 15,000 (0.7 m/z isolation width, 35% collision energy, 54 ms maximum ion time). Dynamic exclusion was set to exclude previously sequenced peaks

for 20 s within a 10 ppm isolation window. Only charge states from 2+ to 5+ were chosen for tandem MS/MS.

3.6.3 Data-independent acquisition (DIA)-based targeted proteomics

ALS CSF DIA proteomics sample preparation

CSF samples were collected through the Neurological Disease Biorepository and Biomarker Initiative at the Mayo Clinic's campus in Jacksonville, Florida (IRB #13-004314 and IRB# 11-002986). Our cohort of cases consisted of nine males and six females (Caucasian, and not of Hispanic ethnicity), with a median age at CSF collection of 64 years (range: 50 to 78) and a median age of ALS onset of 59 years (range: 49 to 79 years).

We depleted the top 14 most abundant proteins in 100 ul CSF from each patient using a rapid 10min incubation with High-Select depletion resin (Thermo Scientific). The proteins in depleted CSF were extracted and denatured by the same 4X lysis buffer used for iPSC-derived neuron lysate, consisting of 50 mM Tris-HCl pH 8, 50 mM NaCl, 1% v/v SDS, 1% v/v Triton X-100, 1% v/v NP-40, 1% v/v Tween 20, 1% v/v glycerol, 1% sodium deoxycholate (w/v), 5 mM EDTA pH 8, 5 mM dithiothreitol, 5 KU benzonase and protease inhibitors.

Lysates were collected and incubated at 65°C for 30 min, followed by addition of 10mM iodoacetamide and 30 min incubation in the dark. The automated protein digestion was performed as previously described (Reilly et al., 2021). Briefly, the protein input of each sample was normalized to 20 ug and captured by the hydrophilic beads on an automated KingFisher APEX robot. The final concentration of tryptic peptides from CSF was normalized to 0.2 ug/ul

using peptide measurement on a NanoDrop. We injected 5 ul of total peptides for proteomic analyses.

Liquid chromatography and mass spectrometry analyses

For the data-independent acquisition (DIA) liquid chromatography and tandem mass spectrometry (LC-MS/MS) analyses of CSF samples, peptides were first separated on an Ultimate 3000 nano-LC system coupled with a 50cm column (75 μm I.D., 2 μm C18 particle) and were injected to a high-resolution Orbitrap Eclipse MS (Thermo Scientific). A 90 min effective LC gradient 2-35% liquid phase B was used. The MS1 scan was conducted 390-1010 m/z at 120k- resolution. For MS2 scan, we used an isolation window at 8 m/z in a range of 400-1000 m/z with 30% HCD collision energy. The fragments were detected in the Orbitrap with a 30k resolution and 3 s loop control.

Addition of heavy isotope-labeled peptides

The standard peptides were 8-15-mers (i.e., amino acid residues in length) identified in discovery proteomics or predicted by PeptideRank (http://wlab.ethz.ch/peptiderank/) where trypsin was chosen as the protease. To make their heavy isotopic labeled counterparts, we labeled their lysine (i.e., $^{13}C6^{13}N2$, Lys8) or arginine (i.e., $^{13}C6^{13}N4$, Arg10) at C-terminus, except the semi-tryptic peptides, which were labeled at the closest lysine or arginine to C-terminus. The heavy labeled peptides were reconstituted to 0.05 to 1pmol/ul based on their signal abundance in mass spectrometry compared against their light counterparts (endogenous peptides) and

pooled. The iRT standards (Biognosys) and pooled heavy standards were spiked into the digested peptides at 1:10 ratio for targeted proteomics.

Database search and statistical analysis

For the DIA proteomics database search, direct DIA-library was used in Spectronaut (v16) (Martinez-Val et al., 2021) with a customized database containing uniport-human proteome reference (UP000005640) and open reading frames (ORFs*)* in silico translated from mis-spliced junctions identified by total RNA sequencing. Trypsin was chosen as the digestion enzyme (allowing semi-tryptic digestion), mass error tolerance was set to 15ppm, and 3 mis-cleavages were allowed. For targeted proteomics, MS raw DIA files were directly loaded to Skyline (daily version) (MacLean et al., 2010) for quantification and visualization. Only common y-ions identified in both light and heavy peptides were used for quantification and dot product estimation. The light peptide intensity was normalized by its heavy labeled counterpart. The dot product (dotp) was calculated using Skyline (daily version) to measure the spectral similarity between the transition peak areas and the theoretical spectra. The statistical analysis was conducted in R studio (v4.3), the simple two-side t-test was used for comparison, and p-values were adjusted for multiple-comparisons using Benjamini-Hochberg procedure. The differentiation expression analysis was carried out in Spectronaut (v16) (Martinez-Val et al., 2021)*,* where log fold changes and q-value were generated for volcano plot analysis.

3.7 Statistical analyses

Graphs were generated using GraphPad Prism version 9.3.1. Data are displayed as means ± SEM; individual data points are also shown. Statistical testing was performed using GraphPad Prism version 9.3.1 and R statistical programming language. Shapiro-Wilk test was used to assess normality. *P* values for normally distributed datasets were determined by unpaired *t* test, with Benjamini-Hochberg adjustment for multiple comparisons. For non-normally distributed data, nonparametric analysis was carried out using the Mann-Whitney test or one-way analysis of variance (ANOVA). $P < 0.05$ was considered significant for two-tailed tests, whereas $P < 0.1$ was considered significant for one-tailed tests. The number of biological replicates and details of statistical analyses are provided in the figure legends.

CHAPTER 4: TDP-43–depleted human iPSC–derived neurons express cryptic exons that generate de novo proteins

Statement of prior publication and co-author contributions

- The content in this chapter was modified from Sahba Seddighi *et al.*, Mis-spliced transcripts generate de novo proteins in TDP-43–related ALS/FTD. *Sci. Transl. Med.*16, eadg7162 (2024). Reprinted with permission from AAAS.
- Co-author contributions: The TDP-43 knockdown strategy was developed by Sarah Kargbo-Hill and Daniel Ramos. Ribosome sequencing data were provided by Oscar Wilkins. Long-read sequencing data were provided by Cedric Belair. Validation analyses in postmortem brain datasets were performed by Anna-Leigh Brown. Cryptic exon qRTPCR data were provided by Mercedes Prudencio.

4.1 Introduction

As introduced in Chapter 1, cytoplasmic TDP-43 inclusions occur in the brains and spinal cords of approximately 97% of amyotrophic lateral sclerosis (ALS), 45% of frontotemporal dementia (FTD), and 57% of Alzheimer's disease (AD) cases (Meneses et al., 2021; Neumann et al., 2009). TDP-43 mislocalization involves both its clearance from the nucleus and the formation of cytosolic aggregates (Halliday et al., 2012; Meneses et al., 2021; Neumann et al., 2009), and both of these events appear to play causal roles in disease pathogenesis. Nuclear clearance of TDP-43 can occur before symptom onset and precedes the

formation of cytosolic aggregates (Iguchi et al., 2013; Vatsavayai et al., 2016; C. Yang et al., 2014), suggesting that loss of normal TDP-43 function is an early disease mechanism.

TDP-43 has two RNA recognition motifs and directly regulates RNA metabolism by acting as a potent splicing repressor. When TDP-43 splicing repression is lost, the erroneous inclusion of intronic sequences called cryptic exons (CEs) occurs (J. P. Ling et al., 2015). Because CEs are non-conserved intronic sequences, they often introduce frameshifts, premature stop codons, or premature polyadenylation sequences. Such splicing errors can reduce the expression of affected transcripts via nonsense-mediated decay (NMD) or other RNA degradation pathways (Humphrey et al., 2017; Mehta et al., 2023). In turn, the expression of proteins derived from these transcripts often declines in parallel. One such example is the well-characterized CE in *stathmin-2* (*STMN2*), which causes loss of STMN2 mRNA and protein in the cortex and spinal cord of patients with ALS or with frontotemporal lobar degeneration (FTLD; a subset of FTD) (Klim et al., 2019; Melamed et al., 2019; Prudencio et al., 2020). We and others recently found that TDP-43 also normally represses a CE in *UNC13A*, a critical synaptic gene (Brown et al., 2022; Ma et al., 2022). ALS-linked and FTD-linked risk variants in *UNC13A* reduce the affinity of TDP-43 for *UNC13A* transcripts, thereby promoting CE expression and UNC13A loss in neurons with TDP-43 insufficiency (Brown et al., 2022). These two examples demonstrate that mis-splicing due to TDP-43 mislocalization can reduce the expression of critical downstream genes, likely affecting neuronal biology during disease.

TDP-43 loss causes widespread CE expression and other related pathological splicing events that affect hundreds of transcripts (Klim et al., 2019; J. P. Ling et al., 2015; Melamed et al., 2019). Certain genes exhibit reduced expression after CE inclusion, but it is also possible that de novo proteins could be synthesized from CE transcripts. Expression of de novo proteins

downstream of TDP-43 loss of function could have several important ramifications. Translation of CEs could alter the functions of proteins or induce toxic gain of function with pathophysiological implications. Alternatively, de novo proteins could trigger an autoimmune response, akin to previous observations in autoimmune encephalitis and cancer (Macdonald et al., 2017; Prüss, 2021).

In this chapter, I aim to address whether certain CEs generate de novo proteins in TDP-43-deficient human iPSC-derived neurons. We used a CRISPR-interference (CRISPRi)-based strategy to knockdown TDP-43 expression in human iPSC-derived neurons. Through RNA-sequencing and splicing analyses of these cells, we then developed a compendium of neuronal cryptic exons. Applying a proteogenomic strategy, integrating parallel RNA-sequencing and proteomic data from TDP-43-depleted human iPSC-derived neurons, allowed us to identify putative cryptic peptides that arise from mis-spliced CE junctions. Finally, we cross-referenced the predicted CEs, including those that generated protein products, against datasets from ALS/FTD postmortem brain tissue, allowing us to examine the fidelity of our iPSC-neuron model in capturing human disease-relevant events.

4.2 Results

Ribosomes bind to intronic regions of mis-spliced transcripts in TDP-43–deficient human iPSC–derived neurons

Ribo-seq provides a map of the position and density of ribosomes on individual mRNAs and a proxy for protein translation. If TDP-43–deficient human iPSC–derived neurons translate CEs into de novo proteins (**Fig. 4.1A**), then we reasoned that Ribo-seq may reveal ribosome-bound CEs. Using short-read total RNA sequencing (RNA-seq) in TDP-43–depleted human iPSC–derived glutamatergic neurons (**fig. 4.2, A and B**), we identified 340 cryptic splicing events across 233 genes out of a total of 498 alternative splicing events (**Fig. 4.1B, fig. 4.2C, and table S4A**). These splicing events included previously identified targets of TDP-43–related splicing repression, such as CEs in *STMN2* and *UNC13A* (Brown et al., 2022; Klim et al., 2019). The majority (70%) of cryptic splicing events were cassette exons, with the remainder comprising exon extension (12%), intron retention (9%), and exon skipping (9%) (**fig. 4.2, C and D, table S4A, and Appendix I**).

We then queried Ribo-seq data from TDP-43–depleted human iPSC–derived neurons (Brown et al., 2022) for evidence of changes in ribosome binding within all intronic regions upon TDP-43 knockdown. We identified 30 genes featuring introns with significantly increased footprints in the TDP-43 knockdown Ribo-seq dataset ($P_{adj} < 0.1$; **table S4B**). When we cross-referenced these sequences with cryptic splicing events identified in Figure 4.1B, we found that more than half of these were CE-containing genes (**Fig. 4.1C**). By contrast, only five genes had introns with significant decreases in ribosome footprints ($P_{adj} < 0.1$), and none was annotated as containing CEs (**table S4B**). Next, we selected CEs predicted to generate in-frame peptides and investigated the periodicity of their ribosome footprints. These showed periodicity that was similar to what we observed in annotated exons, suggesting that the signal in CEs was derived from translating ribosomes (**Fig. 4.1D**). Overall, TDP-43–depleted human iPSC–derived

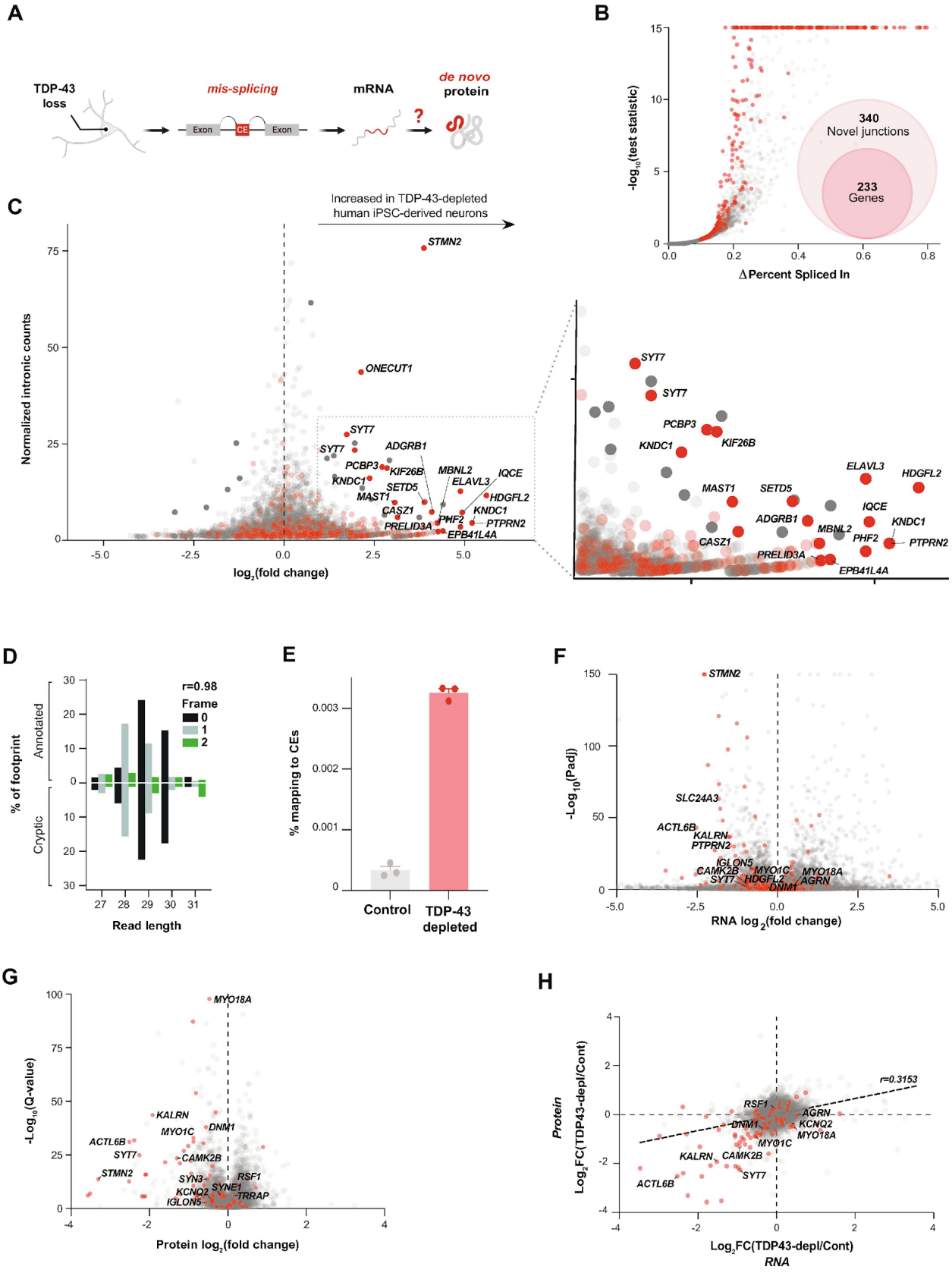
A
TDP-43 loss
mis-splicing
mRNA
de novo protein
Exon
CE
Exon
B
-log10(test statistic)
340 Novel junctions
233 Genes
ΔPercent Spliced In
C
Increased in TDP-43-depleted human iPSC-derived neurons
Normalized intronic counts
log2(fold change)
STMN2
ONECUT1
SYT7
ADGRB1
PCBP3
KIF26B
KNDC1
MBNL2
ELAVL3
IQCE
SETD5
MAST1
HDGFL2
CASZ1
PHF2
PRELID3A
EPB41L4A
PTPRN2
D
% of footprint
Annotated
Cryptic
r=0.98
Frame
0
1
2
Read length
E
% mapping to CEs
Control
TDP-43 depleted
F
-Log10(Padj)
RNA log2(fold change)
SLC24A3
ACTL6B
KALRN
PTPRN2
IGLON5
CAMK2B
MYO1C
SYT7
HDGFL2
DNM1
MYO18A
AGRN
G
-Log10(Q-value)
Protein log2(fold change)
MYO18A
KALRN
MYO1C
DNM1
ACTL6B
SYT7
CAMK2B
STMN2
SYN3
RSF1
KCNQ2
SYNE1
TRRAP
IGLON5
H
Protein
Log2FC(TDP43-depl/Cont)
RNA
r=0.3153
RSF1
AGRN
DNM1
KCNQ2
MYO18A
MYO1C
KALRN
CAMK2B
SYT7
ACTL6B

Figure 4.1. Transcriptional and proteomic analysis of TDP-43–depleted human iPSC–derived neurons. (A) Overview of CE RNA and potential de novo protein production due to pathological mis-splicing in TDP-43–depleted human iPSC–derived neurons. **(B)** Shown is differential splicing in TDP-43–depleted human iPSC–derived neurons compared with human iPSC–derived control neurons expressing normal amounts of TDP-43. CE genes are shown in red. **(C)** Differential ribosome footprint density of intronic mRNA is shown for TDP-43–depleted human iPSC–derived neurons compared with human iPSC–derived control neurons. CE genes are shown in red. **(D)** Shown is the percentage abundance of each footprint type, defined by length and sub-codon position, for annotated coding sequences (positive *Y* axis) and a subset of high-confidence CEs, which are predicted to be translated (negative *Y* axis). Pearson's correlation between the values for annotated and cryptic transcripts is shown. Data are from one TDP-43–depleted human iPSC–derived neuronal cell line. **(E)** Shown is the percentage of footprints aligning to the subset of CEs used in (C) for three TDP-43–depleted and three control human iPSC–derived neuronal samples. **(F)** Differential transcript abundance was quantified in TDP-43–depleted and control human iPSC–derived neurons using total short-read RNA-seq. CE genes are shown in red. **(G)** Differential protein abundance in TDP-43–depleted and control human iPSC–derived neurons was quantified using mass spectrometry proteomics. CE genes are shown in red**. (H)** Quantification of mRNA (RNA-seq) and protein by data-independent acquisition (DIA) proteomics of TDP-43–depleted and control human iPSC–derived neurons is shown. CEs are shown in red.

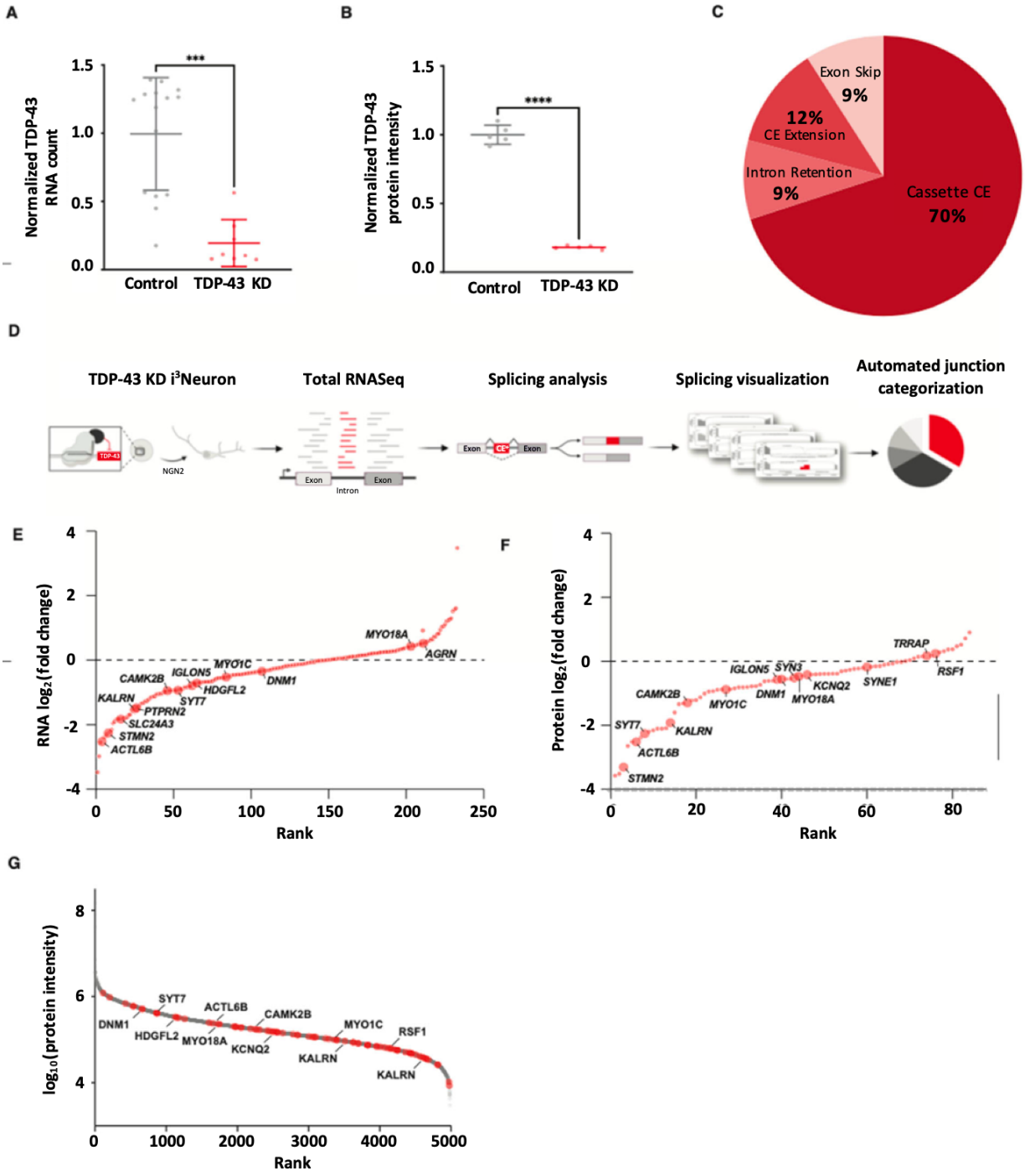

Figure 4.2. TDP-43 downregulation in iPSC-derived neurons causes mis-splicing and loss of associated transcript and protein products. (A) Differential TDP-43 transcript abundance in control and TDP-43 KD iPSC neurons, quantified using total short-read RNAseq. P-value shown from Mann-Whitney u-test. *** $p \leq 0.0005$. These differences reflect the changes shown in companion Figure 1. **(B)** Differential TDP-43 protein abundance in control and TDP-43 KD iPSC-derived neurons, quantified using DIA total proteomics. P-value

shown from one-way t-test. **** p<0.0001; Shapiro-Wilk Test for Normality, p>0.05 (ns). These differences reflect the changes shown in companion Figure 1. **(C)** Mis-spliced junction types in TDP-43 KD iPSC-derived neurons **(D)** Proteogenomic workflow to identify and characterize TDP-43 related mis-spliced junctions in iPSC-derived neurons **(E)** Rank plot of LFC in cryptic exon RNA abundance in control vs TDP-43 KD iPSC-derived neurons **(F)** Rank plot of LFC in cryptic exon parent protein abundance in control vs TDP-43 KD iPSC-derived neurons **(G)** Rank plot of baseline protein abundance in iPSC-derived neurons. Parent proteins of cryptic exon-harboring genes are shown in red.

neurons had roughly nine times more ribosome footprints within CEs than did control human iPSC–derived neurons with normal amounts of TDP-43 **(Fig. 4.1E**).

Using total RNA-seq and proteomics, we characterized the impact of neuronal TDP-43 loss on CE gene expression at the transcript and protein level (**Fig. 4.1F to H; fig. 4.2, E to G; and table S4, C and D**). Consistent with prior observations that CEs can reduce mRNA stability (Brown et al., 2022; Klim et al., 2019; Ma et al., 2022; Melamed et al., 2019; Prudencio et al., 2020), 37% of CE gene transcripts were reduced in TDP-43–depleted human iPSC–derived neurons (**Fig. 4.1F**). We found evidence of additional instability of mis-spliced genes at the protein level, where 80% of proteins from CE genes displayed decreased expression (**Fig. 4.1G**). Analysis of the transcript and peptide abundance of CE-harboring genes at the same time point revealed that whereas some genes (e.g., *SYT7* and *KALRN*) contained out-of-frame CEs and had unstable transcript and protein products, others (e.g., *DNM1* and *MYO18A*) contained in-frame CEs and remained highly expressed (**Fig. 4.1 H**). Collectively, these data show that whereas CEs often reduce the expression of CE genes, certain CEs and other abnormally spliced transcripts do not affect expression and might be translated into de novo proteins.

TDP-43-related cryptic exons generate de novo proteins in human iPSC–derived neurons

To identify potential CE-associated de novo proteins at a large scale, we developed an unbiased proteogenomic pipeline that combined proteomics and transcriptomics to identify new peptides (**Fig. 4.3A**). Using RNA-seq data from TDP-43–depleted human iPSC–derived neurons, the pipeline returned in-frame amino acid sequences from mis-spliced junctions, henceforth referred to as cryptic peptides. We then added these in silico translated protein sequences of CEs to a standard human proteome reference, allowing us to search for trypsin-digested cryptic peptides in shotgun proteomic datasets from TDP-43–depleted human iPSC–derived neurons (**Appendix II**). This pipeline identified 65 putative trypsin-digested cryptic peptides across 12 genes in TDP-43–depleted human iPSC–derived neurons (**Fig. 4.3B and table S2, E and F**), consistent with the possibility that certain CEs are translated into proteins.

More than half of the identified cryptic peptides were predicted to be in frame – and therefore would not cause a premature stop codon – when mapped to short-read RNA-seq of pathologically spliced transcripts (**Fig. 4.3B**). One such example is a 46–amino acid, in-frame cryptic peptide in hepatoma-derived growth factor-related protein 2 (HDGFL2) that mapped to

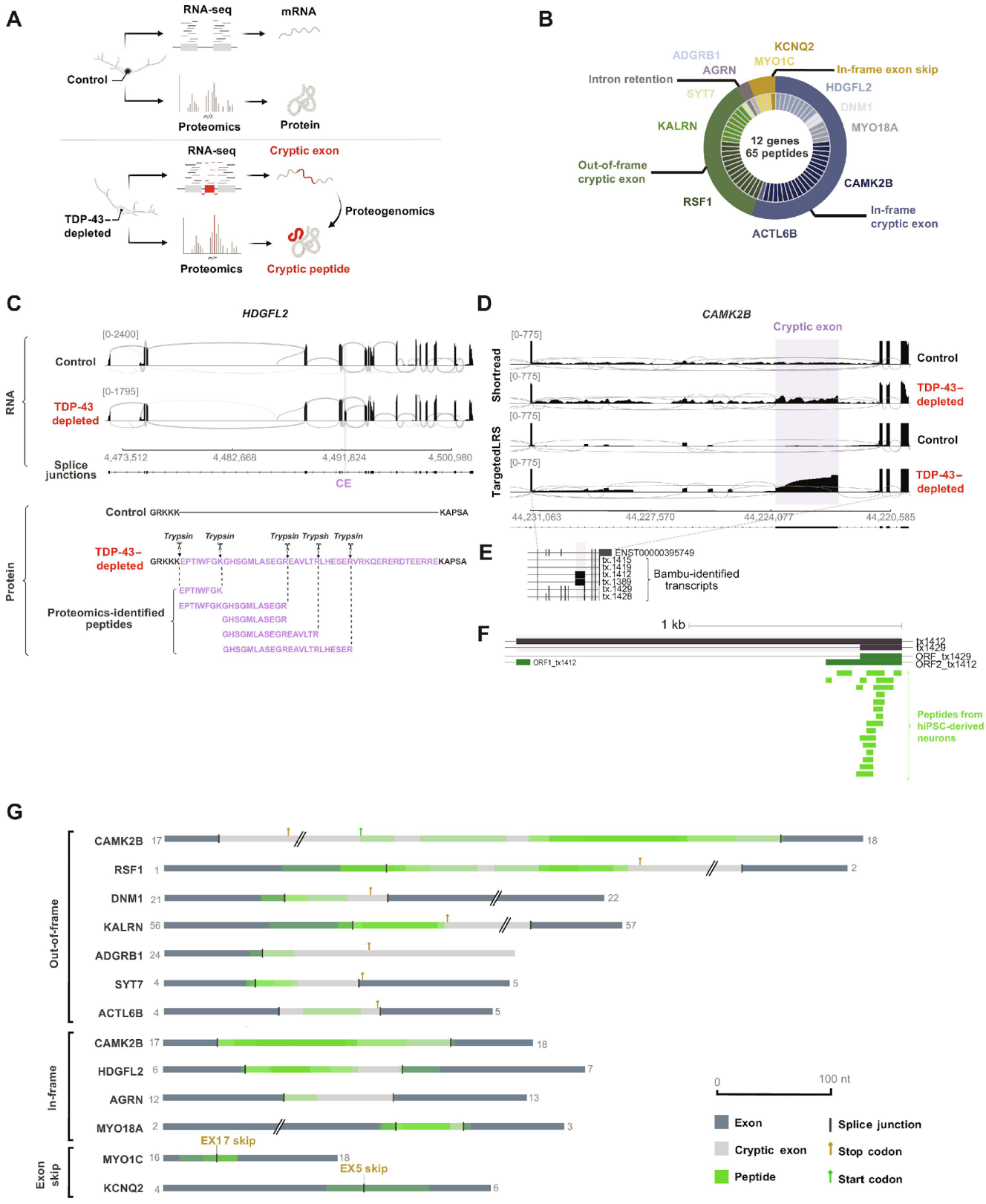
A
RNA-seq
mRNA
Control
Proteomics
Protein
RNA-seq
Cryptic exon
TDP-43–
depleted
Proteogenomics
Proteomics
Cryptic peptide
B
ADGRB1
KCNQ2
MYO1C
AGRN
In-frame exon skip
Intron retention
SYT7
HDGFL2
DNM1
KALRN
MYO18A
12 genes
65 peptides
Out-of-frame
cryptic exon
CAMK2B
RSF1
In-frame
cryptic exon
ACTL6B
C
HDGFL2
RNA
[0-2400]
Control
[0-1795]
TDP-43
depleted
Splice
junctions
4,473,512
4,482,668
4,491,824
4,500,980
CE
Protein
Control GRKKK KAPSA
Trypsin
TDP-43–
depleted
GRKKKEPTIWFGKGHSGMLASEGREAVLTRLHESERVRKQERERDTEERREKAPSA
Proteomics-identified
peptides
EPTIWFGK
EPTIWFGKGHSGMLASEGR
GHSGMLASEGR
GHSGMLASEGREAVLTR
GHSGMLASEGREAVLTRLHESER
D
CAMK2B
Cryptic exon
Shortread
[0-775]
Control
TDP-43–
depleted
TargetedLRS
Control
TDP-43–
depleted
44,231,063
44,227,570
44,224,077
44,220,585
E
ENST00000395749
tx:1415
tx:1419
tx:1412
tx:1369
tx:1429
tx:1428
Bambu-identified
transcripts
F
1 kb
tx1412
tx1429
ORF1_tx1412
ORF_tx1429
ORF2_tx1412
Peptides from
hiPSC-derived
neurons
G
Out-of-frame
CAMK2B 17 18
RSF1 1 2
DNM1 21 22
KALRN 56 57
ADGRB1 24
SYT7 4 5
ACTL6B 4 5
In-frame
CAMK2B 17 18
HDGFL2 6 7
AGRN 12 13
MYO18A 2 3
EX17 skip
Exon
skip
MYO1C 16 18
EX5 skip
KCNQ2 4 6
0
100 nt
Exon
Cryptic exon
Peptide
Splice junction
Stop codon
Start codon

Figure 4.3. Formation of de novo cryptic peptides from mis-spliced transcripts in TDP-43–depleted human iPSC–derived neurons. (A) Proteogenomic pipeline used to identify de novo cryptic peptides caused by RNA mis-splicing in TDP-43–depleted human iPSC–derived neurons. **(B)** Proteogenomic analysis of TDP-43–depleted human iPSC–derived neurons identified 65 putative trypsin-digested cryptic peptides across 12 genes. The outer circle of the pie chart represents genes. The inner circle represents the number of putative trypsin-digested cryptic peptides that were identified for each gene. **(C)** Representative sashimi plots showing the inclusion of an in-frame CE (purple) in HDGFL2 transcripts in TDP-43–depleted human iPSC–derived neurons. The amino acid sequence of the putative translation of this CE is shown below the sashimi plot, with trypsin cleavage sites and proteogenomic-identified cryptic peptides annotated. **(D)** Representative sashimi plots comparing Illumina short-read RNA-seq versus Nanopore long-read sequencing of the *CAMK2B* transcript in control and TDP-43–depleted human iPSC–derived neurons. The CE expressed in TDP-43–depleted human iPSC–derived neurons is highlighted in purple. **(E)** Precise mapping of *CAMK2B* exon junctions and splice isoforms of transcripts in TDP-43–depleted human iPSC–derived neurons using Nanopore long-read sequencing. **(F)** Tryptic-cryptic peptides (green) identified using the proteogenomic pipeline are mapped to an in-frame CE in *CAMK2B* identified using Nanopore long-read sequencing. **(G)** Graphical representation of proteogenomic-identified cryptic peptides mapped to transcripts from Nanopore long-read sequencing. Two genes, *MYO1C* and *KCNQ2*, contained an in-frame exon skipping event upon TDP-43 loss. Four genes, *HDGFL2*, *AGRN*, *MYO18A*, and *CAMK2B*, contained in-frame CEs. An out-of-frame *CAMK2B* CE was also identified. Canonical upstream and downstream exons are in dark gray. CEs are in light gray. Cryptic peptide locations are overlaid in green.

a CE in intron 6 (**Fig. 4.3C and fig. 4.4A**). We detected five distinct trypsin-cleaved peptides for HDGFL2 in TDP-43–depleted human iPSC–derived neurons **(Fig. 4.3C)**. Twenty-three trypsin-cleaved cryptic peptides mapped to out-of-frame CEs in *RSF1*, *KALRN*, and *SYT7* (**table S4A**). On the basis of the frame of these out-of-frame cryptic peptides, the parent transcripts were predicted to harbor a premature stop codon in the downstream exon. Two additional trypsin-cleaved cryptic peptides mapped to retained introns, whereas four were due to exon skipping (**Fig. 4.3B**).

Short-read RNA-seq relies on informatic approaches to stitch together individual reads into full-length transcripts. Errors in predicted full-length sequences can arise when multiple

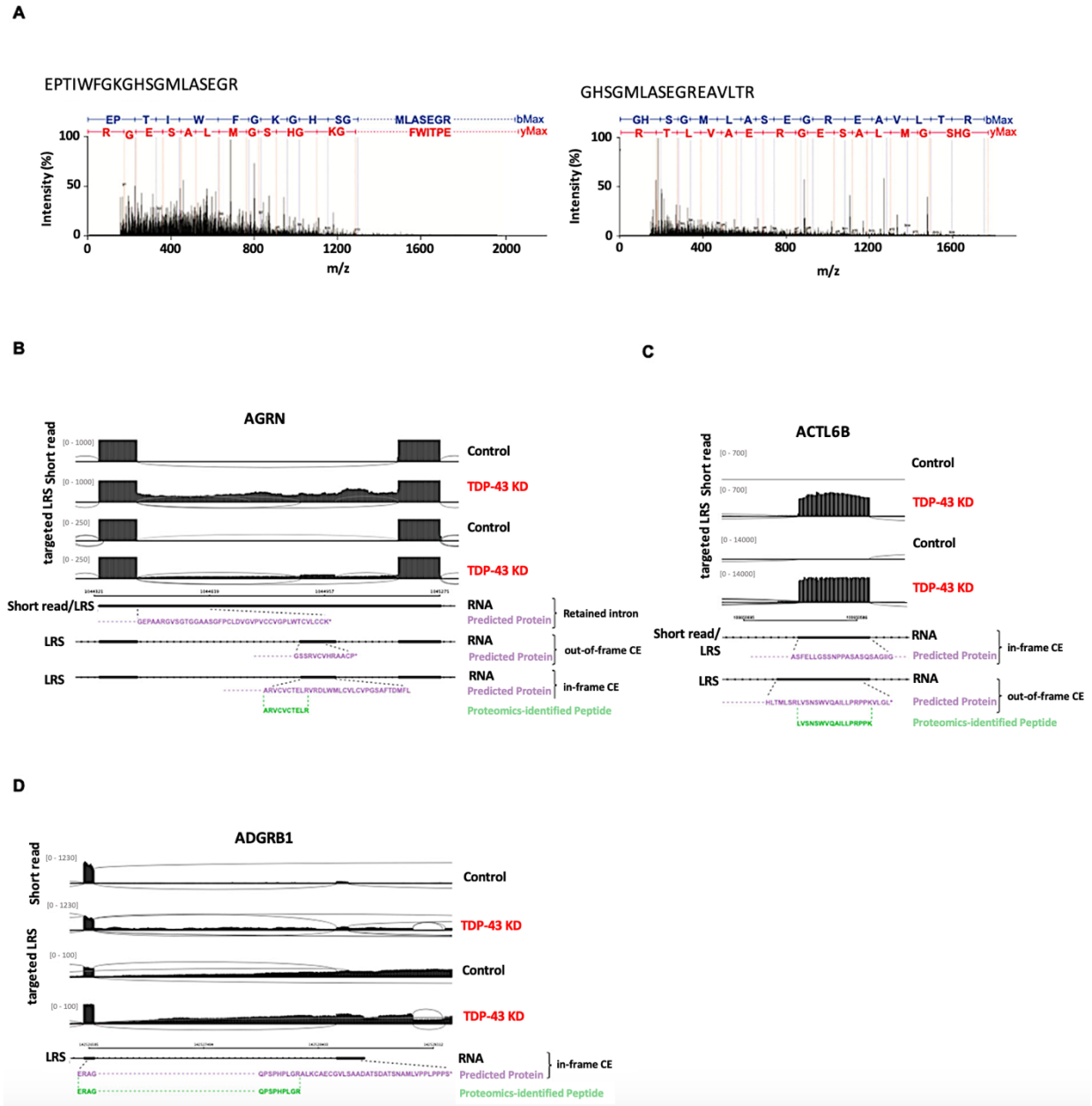

Figure 4.4. Identification of full-length transcripts expressing cryptic peptides with Nanopore long-read sequencing. (A) MS/MS spectra of two cryptic peptides that map to the HDGFL2 cryptic exon, identified using label-free DIA mass spectrometry. **(B-D)** Representative sashimi plots comparing Illumina short-read RNAseq and Nanopore long-read RNAseq for *AGRN* (B), *ACTL6B* (C) and *ADGRB1* (D) transcripts in control and TDP43-KD iPSC-derived neurons. The corresponding transcripts (black) identified by Nanopore long-read sequencing, their predicted amino-acid sequences (purple), and cryptic peptides (green) are shown. Transcripts were identified with bambu.

transcript isoforms are coexpressed, particularly in settings of pathological splicing. To unequivocally determine the frame of translation for each cryptic peptide, we performed Nanopore long-read sequencing of control and TDP-43–depleted human iPSC–derived neurons (**Fig. 4.3, D to G; fig. 4.4, B to D; and table S4G**). Mapping all putative cryptic peptides against long-read data from which we could extract the frame, we confirmed four genes (i.e., *HDGFL2*, *AGRN*, *MYO18A*, and *CAMK2B*) with in-frame CEs and two genes (i.e., *MYO1C* and *KCNQ2*) with in-frame exon skipping events in TDP-43–depleted human iPSC–derived neurons (**Fig. 4.3G**). An example of an in-frame cryptic peptide from *CAMK2B* is shown in Fig. 4.3 (D to F), demonstrating the improved fidelity of long-read sequencing over short-read sequencing in mapping cryptic peptides to complex, pathologically spliced transcripts.

TDP-43-depleted human iPSC–derived neurons predict mis-splicing in postmortem brain tissue from patients with ALS/FTD

Previously, TDP-43–depleted human iPSC neurons successfully predicted individual CEs that were later validated in patients with ALS/FTD (Brown et al., 2022; Klim et al., 2019; Melamed et al., 2019). Most of the putative cryptic peptides that we observed mapped to CEs that have not been previously described. We therefore tested the fidelity of our TDP-43–depleted human iPSC–derived neuron model in the global prediction of ALS/FTD-associated CEs using three separate approaches. First, we cross-referenced CEs found in TDP-43–depleted human iPSC–derived neurons against a published RNA-seq dataset of fluorescence-activated cell sorting (FACS)–sorted neuronal nuclei from postmortem cortex samples from patients with

ALS/FTD (E. Y. Liu et al., 2019). Of the 340 cryptic splice junctions that we identified in TDP-43–depleted human iPSC–derived neurons, 230 were detected in FACS-sorted neuronal nuclei from postmortem cortical samples. Some cryptic splice junctions were highly expressed in both TDP-43–positive and TDP-43–negative nuclei, possibly reflecting the cell-type-specific nature of TDP-43–dependent splicing events; it is possible that some events designated as "cryptic" in our iPSC-derived neuron model are part of other unannotated isoforms that may be basally expressed in other tissue or cell types. For example, our previous analysis of the *UNC13B* frameshift exon revealed that the same exon could either lead to an NMD transcript or, when included in another transcript, form a truncated *UNC13B* isoform. This truncated *UNC13B* isoform was wildly expressed in bulk post-mortem tissue but was not detected in any of the cell lines explored (Brown et al., 2022). Of the 230 junctions, 122 were enriched in nuclei lacking TDP-43. Neuronal nuclei from ALS/FTD postmortem cortex samples clustered according to TDP-43 nuclear presence, rather than by patient demographics (**Fig. 4.5A and table S4, H and I**). Using dimensionality reduction analysis of all 230 CEs predicted by TDP-43–depleted human iPSC–derived neurons and detected in FACS-sorted postmortem cortical neuronal nuclei, we found that TDP-43–positive and TDP-43–negative nuclei could be separated on the basis of the first principal component, accounting for 47% of the variability in the dataset (**Fig. 4.5B**). These data indicate that many cryptic splicing events observed in TDP-43–depleted human iPSC–derived neurons also occur in TDP-43–negative cortical neuronal nuclei derived from ALS/FTD patient brain tissue.

Second, we tested whether cryptic splicing predicted by our TDP-43–depleted human iPSC–derived neuron data could identify cases with TDP-43 pathology in postmortem cortical

brain samples. We analyzed bulk RNA-seq datasets from the New York Genome Center (NYGC), comprising 168 frontal and temporal cortex samples from 82 non-neurological disease controls, 20 FTLD–non-TDP cases, and 66 FTLD-TDP cases and 304 motor cortex samples from 49 non-neurological disease controls, 11 ALS non-TDP cases, and 244 ALS-TDP cases. Despite the anticipated low expression and degradation of many CEs by NMD, and the limits of bulk RNA-seq in which only a small proportion of cells have TDP-43 pathology, we detected 298 of the 340 pathologically spliced junctions with at least one spliced read across all the

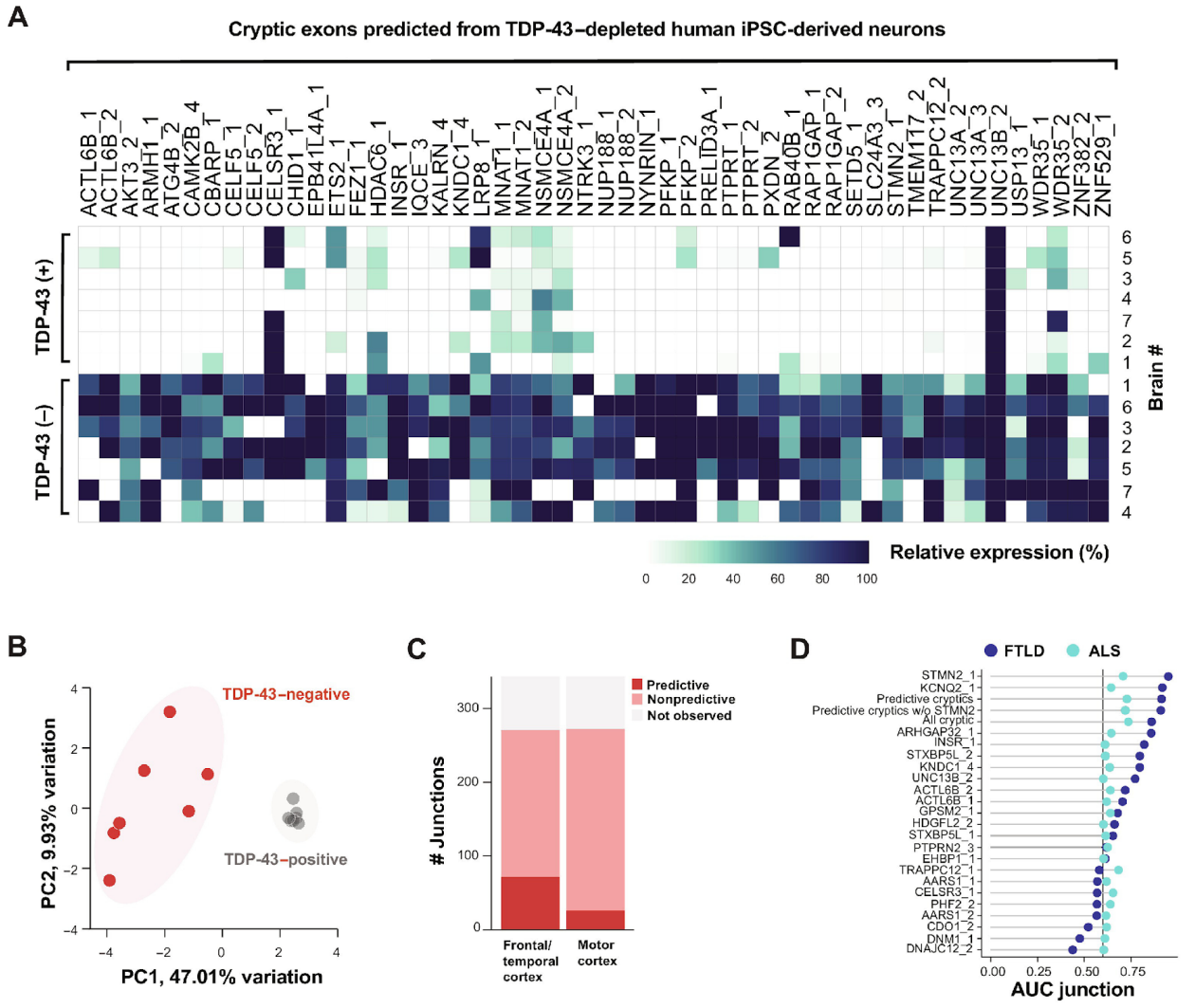
A
Cryptic exons predicted from TDP-43–depleted human iPSC-derived neurons
ACTL6B_1
ACTL6B_2
AKT3_2
ARMH1_1
ATG4B_2
CAMK2B_4
CBARP_1
CELF5_1
CELF5_2
CELSR3_1
CHID1_1
EPB41L4A_1
ETS2_1
FEZ1_1
HDAC6_1
INSR_1
IQCE_3
KALRN_4
KNDC1_4
LRP8_1
MNAT1_1
MNAT1_2
NSMCE4A_1
NSMCE4A_2
NTRK3_1
NUP188_1
NUP188_2
NYNRIN_1
PFKP_1
PFKP_2
PRELID3A_1
PTPRT_1
PTPRT_2
PXDN_2
RAB40B_1
RAP1GAP_1
RAP1GAP_2
SETD5_1
SLC24A3_3
STMN2_1
TMEM117_2
TRAPPC12_2
UNC13A_2
UNC13A_3
UNC13B_2
USP13_1
WDR35_1
WDR35_2
ZNF382_2
ZNF529_1
TDP-43 (+)
TDP-43 (–)
6
5
3
4
7
2
1
1
6
3
2
5
7
4
Brain #
Relative expression (%)
0
20
40
60
80
100
B
TDP-43–negative
TDP-43–positive
PC2, 9.93% variation
PC1, 47.01% variation
C
Predictive
Nonpredictive
Not observed
Junctions
Frontal/ temporal cortex
Motor cortex
D
FTLD
ALS
STMN2_1
KCNQ2_1
Predictive cryptics
Predictive cryptics w/o STMN2
All cryptic
ARHGAP32_1
INSR_1
STXBP5L_2
KNDC1_4
UNC13B_2
ACTL6B_2
ACTL6B_1
GPSM2_1
HDGFL2_2
STXBP5L_1
PTPRN2_3
EHBP1_1
TRAPPC12_1
AARS1_1
CELSR3_1
PHF2_2
AARS1_2
CDO1_2
DNM1_1
DNAJC12_2
AUC junction
E
CAMK2B
CDK7
ARHGAP32
ACTL6B
MYO18A
HDGFL2
DNM1
SYT7
Cryptic RNA (ΔΔct x 10⁻³)
Control
FTLD-TDP

Figure. 4.5. TDP-43 cryptic exons in TDP-43–depleted human iPSC–derived neurons predict TDP-43 pathology in postmortem brain tissue. (A) Heatmap showing the relative abundance of CEs predicted from TDP-43–depleted human iPSC–derived neurons in FACS-sorted TDP-43–positive and TDP-43–negative neuronal nuclei preparations from postmortem ALS/FTD cortical samples (n = 7) (*17*). The "percent spliced in" (PSI) value represents the ratio of transcripts that include a splicing event versus the total number of transcripts. We defined enriched junctions as those with PSI in TDP-43–negative nuclei greater than twice the PSI in TDP-43–positive nuclei (mean TDP-43–negative PSI > 0.10). The top 50 most expressed cryptic splice junctions in TDP-43–negative nuclei, compared with TDP-43–positive nuclei, are shown, and cases were organized by unsupervised hierarchical clustering based on CE PSI. **(B)** Principal components analysis (PCA) on PSI of 230 predicted TDP-43 CEs in TDP-43–positive and TDP-43–negative neuronal nuclei from ALS/FTD postmortem cortical samples. **(C)** Bar plot showing the number of predicted CEs detected in bulk RNA-seq of ALS/FTD postmortem brain tissue samples from the NYGC biobank. CEs were classified by whether they were observed in postmortem brain tissue and were detected/nonpredictive or detected/predictive of TDP-43 pathology versus non–TDP-43 pathology. **(D)** AUC is shown for predicted CEs that identified TDP-43 pathology in FTLD frontal/temporal cortex and ALS motor cortex postmortem tissue from patients with ALS/FTLD patients. Meta-expression scores for all CEs, only predictive exons (AUC > = 0.6), and predictive exons excluding *STMN2* expression are shown. **(E)** Shown is quantitative RT-PCR–based validation of eight CEs in an independent set of postmortem frontal cortex brain samples from patients with FTLD-TDP (n = 89) and age-matched controls with non-neurological disease (n = 27). Data are presented as means ± SEM. P values are from the Mann-Whitney test: $^{*}P < 0.05$ and $^{****}P \leq 0.0001$.

samples (**Fig. 4.5C and table S4, H and I**). Next, we tested whether CE expression could predict cases with TDP-43 proteinopathy. Many CE junctions identified in TDP-43–depleted human iPSC–derived neurons had positive prediction power in the FTLD (Johnson et al., 2020) and ALS postmortem samples (Moisse, Mepham, et al., 2009)(**Fig. 4.5C and table S4, H and J to L**). We then generated meta-scores by combining expression data from individual or multiple cryptic junctions. We created three different meta-scores: one using the expression of all cryptic events, one using only those junctions with a high predictive power [area under the curve (AUC) > = 0.6], and one with all predictive cryptic junctions excluding the *STMN2* junction. In the

FTLD and ALS postmortem samples, *STMN2*, *KCNQ2*, and all predictive cryptic junctions had the highest power to distinguish cases from controls (**Fig. 4.5D and table S4, H, K, and L**).

Third, we used quantitative polymerase chain reaction with reverse transcription (RT-qPCR) to assess CE expression in an independent cohort of 89 FTLD-TDP postmortem cortex samples versus 27 healthy control cortex samples focusing on eight transcripts associated with potential cryptic peptide expression (**table S4M**). We observed substantially higher expression of each of these CEs in patients with FTLD compared with controls (**Fig. 4.5E, fig. 4.6A**). Thus, we validated our TDP-43–depleted human iPSC–derived neuron data in three independent human datasets.

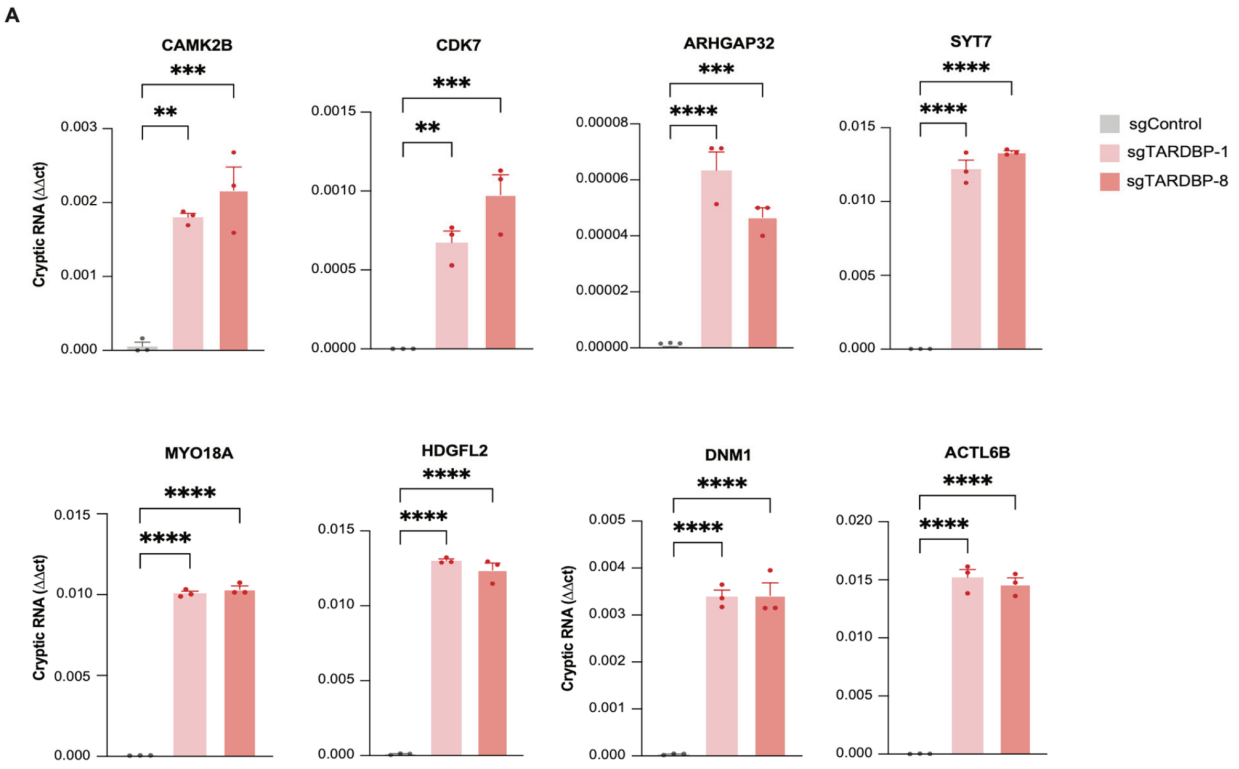

Figure 4.6. Validation of cryptic RNA enrichment in TDP-43 deficient iPSC-derived neurons. (A) qRT-PCR analyses of RNA from iPSC-derived neurons treated with control sgRNA (sgControl) or two different guides against *TARDBP* (sgTARDBP-1, sgTARDBP-8), which lead to ~50% reduction in *TARDBP* RNA and TDP-43 protein expression. Data are presented as mean +/- SEM. *P*-values shown are from one-way ANOVA: *$p \leq 0.05$, **$p \leq 0.005$, ***$p \leq 0.0005$; ****$p \leq 0.0001$

4.3 Discussion

In this chapter, I demonstrate that loss of nuclear TDP-43 causes widespread pathological splicing in iPSC-derived neurons and present a carefully annotated neuronal cryptic exon catalog as a resource for the scientific community. While the majority (~80%) of mis-spliced junctions in TDP-43-depleted iPSC-derived neurons were cryptic splicing events, intron retention and exon skipping events were also evident. Cross-referencing this list of mis-spliced

junctions against two independent datasets from postmortem ALS/FTD brain tissue demonstrated the fidelity of our in vitro model in predicting pathological splicing that occurs in patient brains. I then show indirect evidence of cryptic exon translation from ribosome sequencing in TDP-43-deficient iPSC-derived neurons. This provided the rationale for the development of an unbiased proteogenomic pipeline to enable direct detection of cryptic peptides in iPSC-derived neurons at a large scale. This approach successfully identified 65 putative cryptic peptides across 12 unique genes in TDP-43-depleted human iPSC-derived neurons.

Our data suggest that only a small fraction of CE-harboring transcripts produce stable polypeptides, whereas most undergo degradation at the RNA or protein level. Of 154 CE-harboring genes, only 27 contained in-frame insertions, which are less likely to trigger RNA degradation pathways, such as NMD. Additional quality control pathways, such as ubiquitin-proteasome system, chaperone mediated autophagy, and macroautophagy, may regulate the degradation of misfolded proteins translated from CEs (Ciechanover & Kwon, 2015).

In the FTLD and ALS postmortem samples, the *STMN2* CE had the highest power to distinguish cases from controls. Despite high ribosome occupancy of *STMN2* intronic sequences, no STMN2 de novo peptides were identified in our proteomic studies, suggesting that any proteins produced from the *STMN2* CE are highly unstable or poorly detectable by mass spectrometry. On the other hand, transcripts and proteins that remain stably expressed with cryptic exon inclusion may be ideal targets for peptide and/or RNA-based TDP-43 biomarker development.

One major limitation inherent to our short-read sequencing approach is the potential uncertainty that arises during the mapping of short strands of RNA (typically, fragments of 50-

300 base pairs) to the reference annotation in reconstructing full-length transcripts (Slatko et al., 2018). This can challenge the identification of novel splice isoforms, particularly in settings where multiple transcript isoforms are co-expressed. Long-read sequencing platforms provide a technical advantage by generating reads of 10 kb or longer to directly sequence full-length transcripts (Slatko et al., 2018; Wang et al., 2021). To accurately map putative cryptic peptides to mRNA transcripts, we thus generated a database of long-read sequences in control and TDP-43–depleted human iPSC–derived neurons to confirm our proteogenomic findings. While informatic methods to analyze long-read data for splicing abnormalities at-scale are still in development, this dataset enabled us to unequivocally determine the frame of translation for each cryptic peptide and to identify novel transcript isoforms that were missed by short-read sequencing.

Our reliance on bulk RNA-sequencing data from postmortem brain tissue for validation studies also limits the interpretation of our findings. Bulk RNA-sequencing datasets represent a heterogeneous mixture of cells, of which only a small fraction harbor TDP-43 pathology. Single-cell RNA-sequencing of postmortem tissue could enable more refined studies of human disease-relevant cryptic exons. This possibility was recently demonstrated in study by Gittings and colleagues, where single-nuclei RNA sequencing of postmortem brain tissue from patients with ALS-FTD spectrum disease demonstrated that TDP-43-related cryptic exons were most highly expressed in Von Economo neurons (VENs) (Gittings et al., 2023). VENs are found in the human anterior cingulate cortex and frontoinsular cortex and exhibit selective vulnerability in FTLD (Gami-Patel et al., 2019). While their study only referenced 66 cryptic exons, our expanded dataset of neuronal CEs could enable re-analyses of their single-cell datasets to provide further insights on human disease-relevant cryptic exons.

Relatedly, previous studies have demonstrated that the targets of TDP-43-related splicing repression vary by species and cell type (Jeong et al., 2017). Our analyses of postmortem brain tissue from ALS/FTD brains were limited to cryptic exons from iPSC-derived cortical-like neurons. Thus, it is possible that TDP-43-related mis-spliced junctions occurring in other disease-affected cell types were missed. Future studies to characterize TDP-43-related CEs across other disease-relevant cell types could provide a more nuanced understanding of the heterogeneous mechanisms of TDP-43 pathology. The expanded list of disease-relevant CEs could additionally aid in the development of TDP-43 biomarkers to monitor disease activity across affected cell types.

Lastly, whether there exists a relationship between the degree of TDP-43 pathology and cryptic exon emergence remains to be determined. Studies examining cryptic exons across various TDP-43 knockdown levels could enable novel insights on the identity of cryptic exons that may emerge at different stages of disease. This could then be validated using postmortem brain RNA-sequencing data from ALS/FTD patients with varying stages of disease.

In summary, the cryptic exon compendium provided in this chapter, together with emerging efforts to characterize CE-harboring transcripts across different cell types and disease states, could be leveraged toward the development of mRNA and protein-based diagnostics and may provide critical insights on the pathogenic mechanisms of TDP-43 dysfunction in ALS/FTD.

CHAPTER 5: Expression of cryptic exons alters protein interactomes

Statement of prior publication and co-author contributions

- The content in this chapter was modified from Sahba Seddighi *et al.*, Mis-spliced transcripts generate de novo proteins in TDP-43–related ALS/FTD. *Sci. Transl. Med.*16, eadg7162 (2024). Reprinted with permission from AAAS.
- Co-author contributions: Western blot and immunoassay experiments were performed by Yong-Jie Zhang and Matthew Keuss. TDP-43 rescue experiments were performed by Puja Mehta. The targeted proteomics strategy was developed jointly with Andy Qi. Affinity purification mass spectrometry data were provided by Colleen Bereda, Jessica Roberts, and Yong-Jie Zhang for analysis.

5.1 Introduction

In the previous chapter, I discussed the development of a proteogenomic pipeline to identify TDP-43-related de novo proteins at a large scale in human iPSC-derived neurons. Our informatic predictions were based on data from short-read RNA-seq and shotgun proteomics – two methods with important caveats that warrant further validation. As discussed in the last chapter, predicting full-length sequences from short-read RNA-seq data can lead to errors that compromise splicing detection, particularly for genes with multiple isoforms (Alkan et al., 2011). This challenges our protegenomic informatic predictions, which are predicated on the accurate determination of CE coordinates to generate biologically relevant, in-frame amino acid

sequences. In addition, while shotgun mass spectrometry has become the method of choice for large-scale discovery proteomics studies, the results are based on the statistical alignment of peptide fragmentation patterns against reference databases and require further validation (Serang et al., 2012). Matching of experimental data against reference datasets can be challenged by factors such as the peptide length, uniqueness of the amino acid sequence, post-translational modifications – including those that arise during the sample preparation process – the proteolytic enzyme of choice, and the lingering danger of false discovery arising from thousands of possible peptide-spectrum comparisons (Nesvizhskii & Aebersold, 2005).

Given these nuances in the interpretation of proteogenomic data, this chapter focuses on the validation of our findings using two orthogonal approaches: first, an antibody-based strategy and, second, an ultra-sensitive, targeted proteomics approach. The development of antibodies, while widely considered a gold-standard method for accurate protein identification, is a labor-intensive and costly endeavor. An alternative and more scalable approach is provided by a form of targeted proteomics known as parallel reaction monitoring (PRM). In PRM analyses, heavy isotope-labeled synthetic peptides are spiked into samples, serving as an internal standard to enhance the accuracy and sensitivity of mass spectrometry-based analyses by comparing endogenous signals against those of the internal standard (Rauniyar, 2015). Using these approaches to validate the expression of cryptic peptides, we then asked whether the incorporation of cryptic exons could alter the binding partners, and thereby likely the function, of cryptic exon-harboring proteins.

5.2 Results

Cryptic peptides can be orthogonally validated

To validate the existence of a de novo protein sequence identified by proteogenomics, we assayed HDGFL2, a protein only modestly reduced in expression in TDP-43–depleted human iPSC–derived neurons (**table S4D**) and predicted to express an in-frame cryptic peptide (**Figs. 4.3C and 5.1A**). A commercially available polyclonal antibody against canonical HDGFL2 detected a single band on Western blot at the predicted molecular weight in control neurons (**Fig. 5.1B**). However, this antibody detected an additional higher molecular weight protein in TDP-43–depleted human iPSC–derived neurons and TDP-43–depleted SH-SY5Y cells, matching the predicted molecular weight of HDGFL2 expressing a CE (HDGFL2-CE) (**Fig. 5.1, B and C; fig. 5.2, A and B**). We developed an antibody specific to the HDGFL2 cryptic peptide (**Fig. 5.1, A and B**) and used a MesoScale Discovery (MSD)–based sandwich immunoassay to accurately quantify this cryptic peptide in TDP-43–depleted human iPSC–derived neurons (**fig. 5.2C**). We used immunofluorescence staining to confirm that the expression of the HDGFL2-CE peptide was restricted to cells with loss of nuclear TDP-43 expression (**Fig. 5.1D**). We next used small interfering RNAs (siRNAs) to knock down TDP-43 in human embryonic kidney (HEK) 293 cells harboring a doxycycline-inducible, siRNA-resistant green fluorescent protein (GFP)–TDP-43 transgene (*20*). Induction of siRNA-resistant GFP–TDP-43 prevented HDGFL2 cryptic-peptide production, confirming that the expression of the cryptic protein was due to TDP-43 loss of function (**fig. 5.2, D and E, table S5A**).

We developed an additional antibody against an in-frame cryptic peptide in MYO18A (**fig. 5.3, A and B**). Using this antibody in a Western blot assay, we detected a protein of the

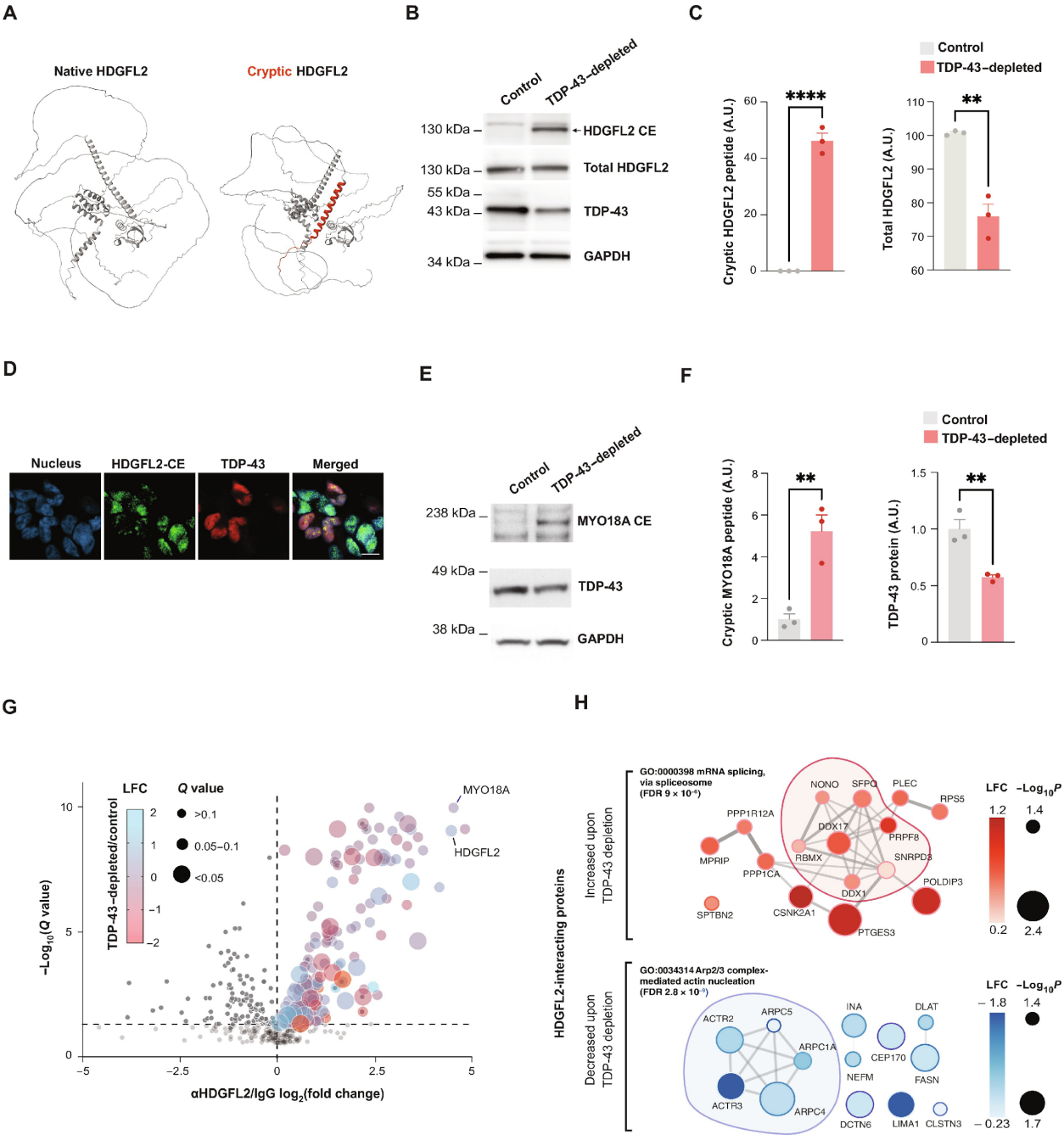

Figure 5.1. Cryptic peptides in TDP-43–depleted human iPSC–derived neurons alter the protein interactome. (A) Predicted structure of HDGFL2 (using AlphaFold), annotated with the predicted cryptic peptide induced by TDP-43 depletion highlighted in red. **(B)** Antibody-based detection of an HDGFL2 cryptic peptide in TDP-43–depleted human iPSC–derived neurons. Representative Western blot shows a band of the expected molecular weight of HDGFL2-CE specifically in TDP-43–depleted but not control human iPSC–derived neurons. **(C)** Quantification of HDGFL2-CE and total HDGFL2 in Western blot from (B) ($n = 3$, two-sample t test, $^{**}P < 0.01$ and $^{****}P < 0.0001$; Shapiro-Wilk test for normality, $P > 0.05$ not significant). **(D)**

Immunofluorescence staining highlights the selective expression of the HDGFL2 cryptic peptide in TDP-43–depleted human iPSC–derived neurons (scale bar,10 μm). **(E)** Antibody-based detection of a MYO18A cryptic peptide in TDP-43–depleted human iPSC–derived neurons. Representative Western blot shows a band of the expected molecular weight of the MYO18A-CE specifically in TDP-43–depleted human iPSC–derived neurons. **(F)** Quantification of MYO18A-CE and TDP-43 protein expression ($n = 3$, two-sample t test, $^{**}P < 0.01$; Shapiro-Wilk test for normality, $P > 0.05$ not significant). **(G)** Affinity purification mass spectrometry analysis of HDGFL2 protein-protein interactions in TDP-43–depleted and control human iPSC–derived neurons. A volcano plot of co-immunoprecipitated proteins using anti-HDGFL2 antibody versus control IgG is shown. The dot color reflects log fold change (LFC) in TDP-43–depleted versus control human iPSC–derived neurons, and the dot size reflects the adjusted P value (q value). **(H)** STRING diagram of proteins whose interactions with HDGFL2 were significantly altered by TDP-43–depleted versus control human iPSC–derived neurons ($P_{adj} < 0.05$). The dot color reflects LFC in TDP-43–depleted versus control human iPSC–derived neurons.

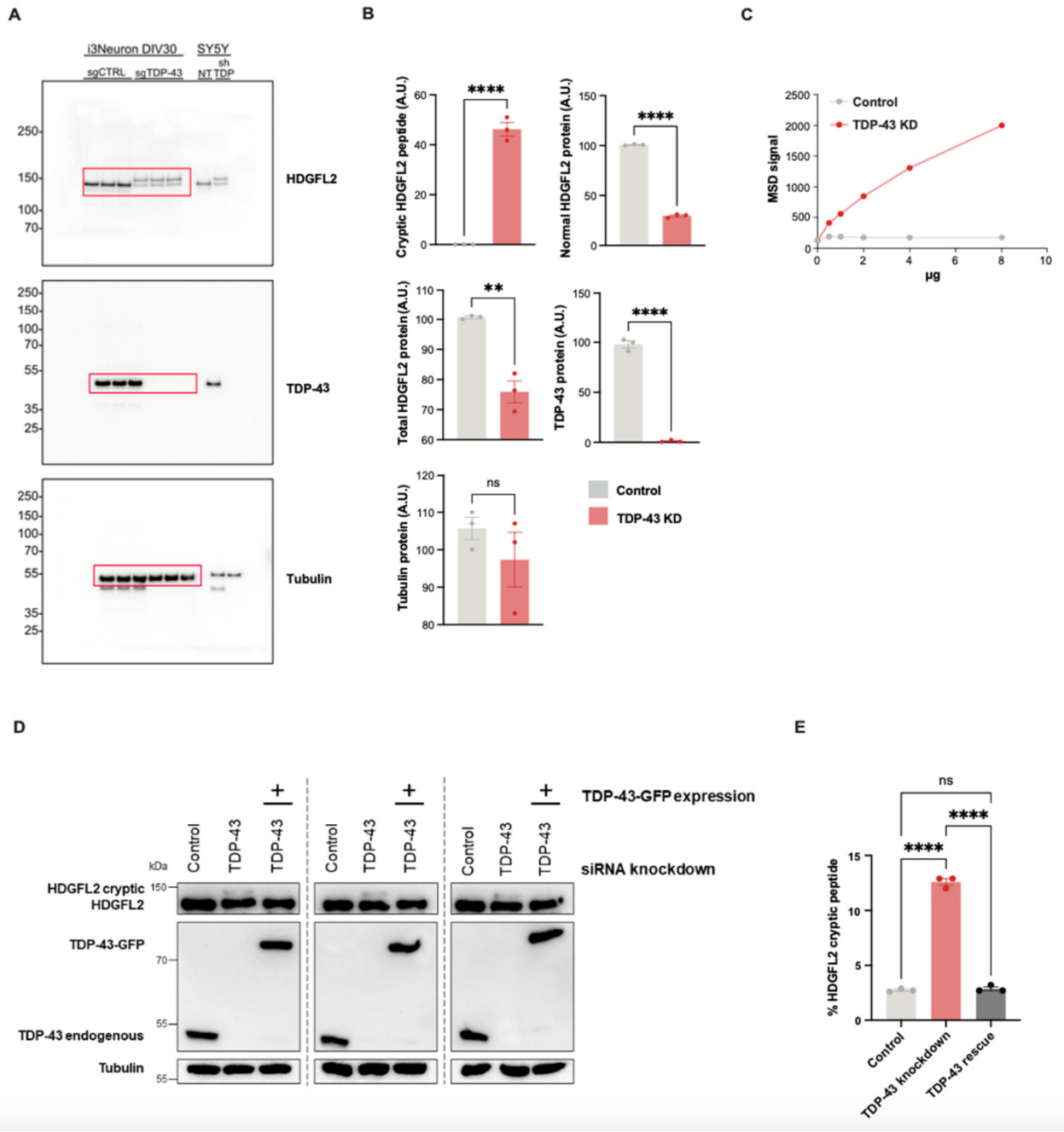

Figure 5.2. TDP-43 loss results in HDGFL2 cryptic peptide expression. (A) Antibody-based detection of the HDGFL2 cryptic peptide in TDP-43 depleted iPSC-derived neurons and SH-SY5Y cells. Representative western blot showing a band of the expected (higher) molecular weight of HDGFL2-CE specifically in TDP-43 depleted iPSC-derived neurons and SH-SY5Y cells **(B)** Quantification of cryptic HDGFL2, normal HDGFL2, total HDGFL2, TDP-43, and tubulin in iPSC-derived neurons (red boxes in (A)). Data are represented as mean +/- SEM. *P*-values shown are from unpaired t-test: **p*≤0.05, ***p*≤0.005, *****p*≤0.0001, ns=not significant; Shapiro–Wilk Test for Normality, *p*>0.05 (ns). **(C)** An MSD assay pairing an anti-

HDGFL2 antibody and a wild-type anti-HDGFL2 antibody specifically detects endogenous HDGFL2-CE produced in TDP-43 depleted iPSC-derived neurons and not wild-type HDGFL2 in control iPSC-derived neurons. **(D)** Representative western blots showing that an HDGFL2 CE band appears upon siRNA-induced TDP-43 KD in HEK293 cells and disappears 24 hours following expression of siRNA-resistant GFP-tagged TDP-43. The CE band is a slightly higher molecular weight than the normal (and more highly-abundant) HDGFL2 band. **(E)** Quantification of the HDGFL2 cryptic peptide in control, TDP-43 KD, and TDP-43 rescue HEK293 cells. Data are represented as mean +/- SEM. *P*-values shown are from One-Way ANOVA test: ****$p \leq 0.0001$, ns= not significant; Shapiro– Wilk Test for Normality, $p>0.05$ (ns).

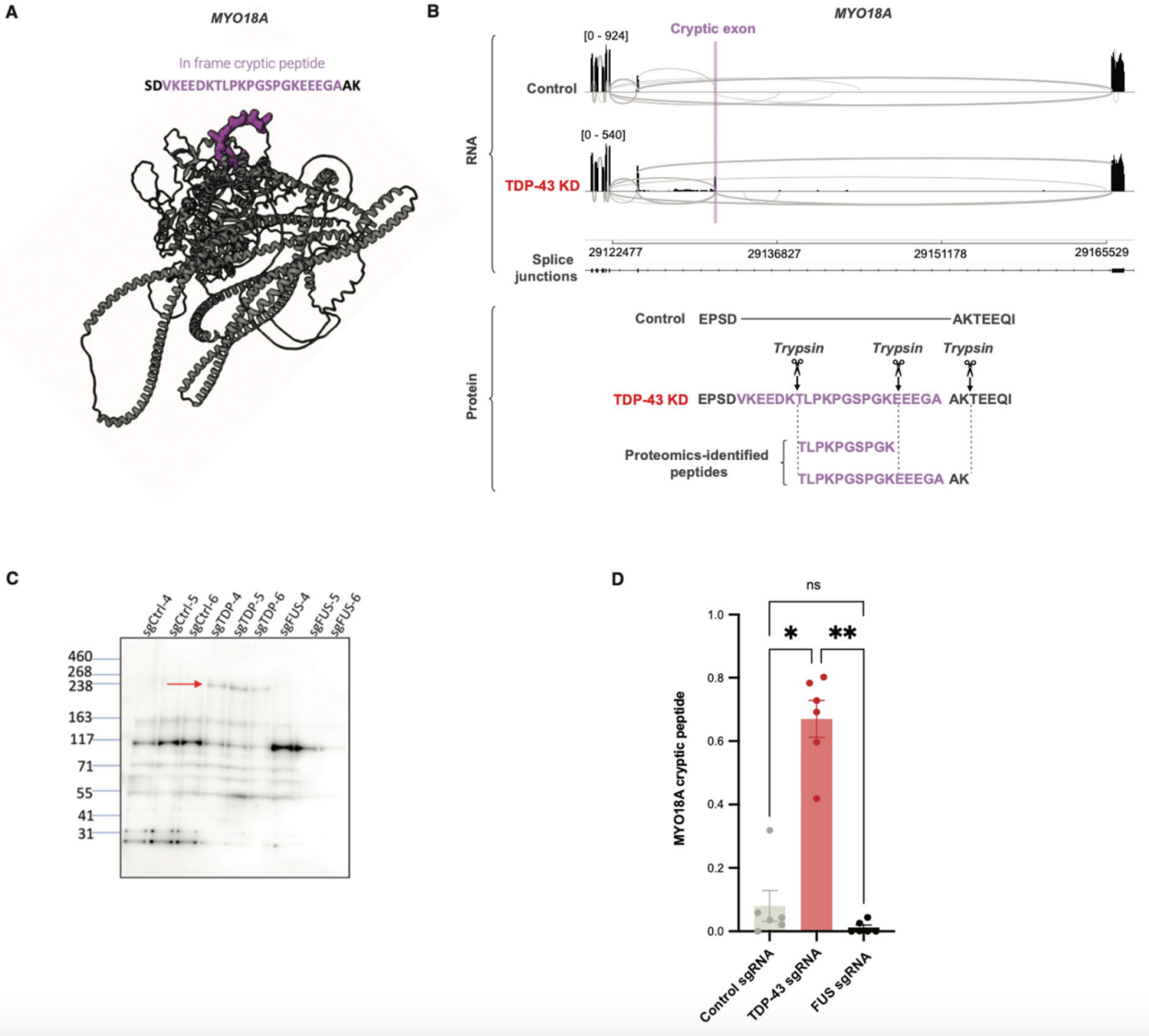

Figure 5.3. TDP-43 loss causes formation of a MYO18A cryptic peptide. (A) Predicted structure of MYO18A (AlphaFold) harboring the predicted translated cryptic exon (purple) induced by TDP-43 depletion, which resides on the protein surface. A polyclonal antibody was raised against this translated MYO18A cryptic exon. **(B)** TDP-43 loss causes formation of a cryptic exon in MYO18A (sashimi plot shown, top), with a predicted in-frame cryptic exon (purple). Two cryptic peptides, detected by proteogenomics, map to this in-frame cryptic exon (bottom). **(C)** Representative western blot using an antibody against the MYO18A cryptic peptide, showing a band of the expected molecular weight of MYO18A-CE (red arrow) specifically in TDP-43 depleted, but not control or FUS depleted, iPSC-derived neurons. **(D)** Quantification of the MYO18A cryptic peptide in control, TDP-43 KD, and FUS KD iPSC-derived neurons. Data are represented as mean +/- SEM. *P*-values shown are from one-way Kruskal-Wallis test: $*p \leq 0.05$, $**p \leq 0.005$, ns = not significant.

anticipated molecular weight of MYO18A expressing a CE (MYO18A-CE) in TDP-43–depleted human iPSC–derived neurons but not in control human iPSC–derived neurons or those depleted of fused in sarcoma (FUS), an ALS/FTD-associated RNA binding protein that does not cause loss of TDP-43 function (**Fig. 5.1, E and F; fig. 5.3, C and D**). These data validate our predictions that some CEs are translated into de novo proteins expressed highly enough to be detected by standard immunoassays and are specific to loss of TDP-43 function.

Inclusion of cryptic exon sequences can alter the interactome of affected proteins

We reasoned that the inclusion of a 46–amino acid cryptic peptide in HDGFL2 – a protein thought to regulate chromatin and DNA repair in non-neuronal cells (Baude et al., 2015) – might alter its interacting partners and thus its biology. We performed affinity purification mass spectrometry of HDGFL2 in control and TDP-43–depleted human iPSC–derived neurons, using an anti-HDGFL2 antibody to immunoprecipitate HDGFL2 and its associated proteins. We identified 178 HDGFL2-interacting proteins that were significantly enriched in anti-HDGFL2 antibodies compared to control immunoglobulin G (IgG) pull-down assays ($P_{adj} < 0.05$; **Fig. 5.1G and table S5, B and C**). Gene Ontology (GO) term analysis of HDGFL2-interacting proteins in neurons revealed strong enrichments in the ribosome, spliceosome, actin, and neurodegeneration-related pathways (**fig. 5.4, A and B**). Unexpectedly, MYO18A was a top interacting protein of HDGFL2, clustering with other actin-regulating HDGFL2 interactors (**fig. 5.4C**). We then analyzed how TDP-43 loss—which causes expression of HDGFL-CE—altered the HDGFL2 interactome. Sixteen proteins increased their relative interactions with HDGFL2 upon TDP-43 loss, a large fraction of which regulate mRNA

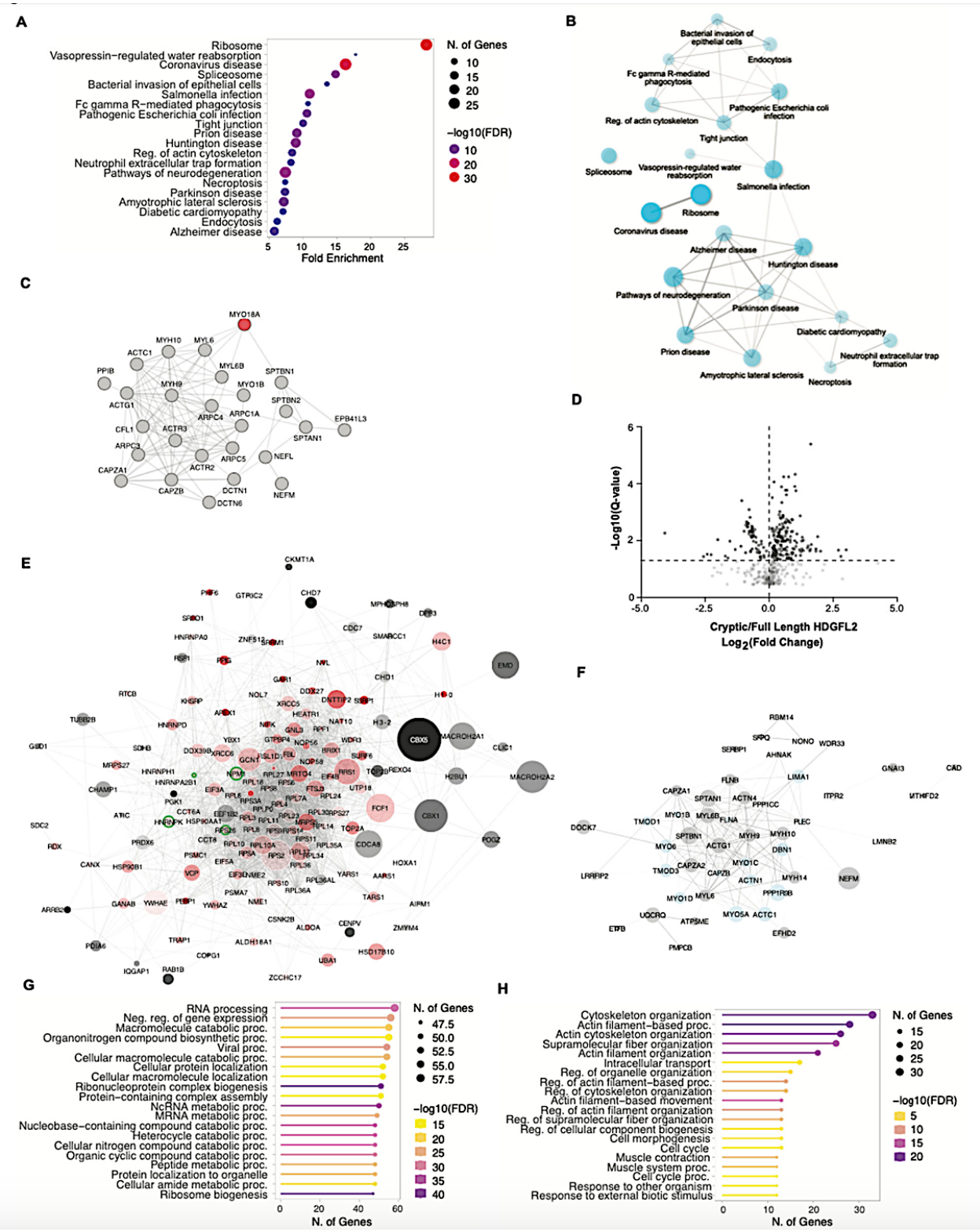

Figure 5.4. Cryptic exon inclusion alters the interacting partners of affected proteins. (A) KEGG pathway analysis of HDGFL2 interacting proteins in iPSC-derived neurons that were identified via DIA APMS (anti-HDGFL2 vs control IgG pulldown). **(B)** Graph representation of

HDGFL2- interacting proteins associated with the KEGG pathways identified in (A). **(C)** STRING diagram of the subset of HDGFL2 interacting proteins associated with MYO18A interactions and cytoskeleton regulation. **(D)** Affinity purification mass spectrometry analysis of HDGFL2 protein-protein interactions of CE-HDGFL2-myc-flag or FL-HDGFL2-myc-flag in HEK-293 cells. Volcano plot of co-immunoprecipitated proteins with anti-flag antibody in CE-HDGFL2- myc-flag versus FL-HDGFL2-myc-flag is shown. **(E)** STRING diagram of proteins with increased interactions in CE-HDGFL2-myc-flag, as compared to FL-HDGFL2-myc-flag, HEK- 293 cells. Dot color intensity reflects LFC of CE/FL-HDGFL2-myc-flag, and dot size reflects the adjusted inverse -log10 *p*-value. Proteins involved in RNA-binding (GO: 0003723 - "RNA- binding") are shown in red, and proteins involved in splicing (GO: 0033119 - "negative regulation of RNA splicing") are outlined in green. **(F)** STRING diagram of proteins with decreased interactions in CE-HDGFL2-myc-flag, as compared to FL-HDGFL2-myc-falg, HEK-293 cells. Dot color intensity reflects LFC in FL-HDGFL2-myc-falg HEK-293 cells, and dot size reflects the adjusted *p*-value. Proteins involved in actin organization (GO: 0007015 - "Actin filament organization") are shown in blue. **(G)** GO biological process enrichment analysis of HDGFL2 interacting proteins with increased interactions in CE-HDGFL2-myc-falg versus FL-HDGFL2-myc-flag HEK-293 cells. **(H)** GO biological process enrichment analysis of HDGFL2 interacting proteins with decreased interactions in CE-HDGFL2-myc-flag versus FL-HDGFL2-myc-flag HEK-293 cells.

splicing, chromatin remodeling, and DNA repair (**Fig. 5.1, G and H**). In contrast, 13 proteins decreased their relative interactions with HDGFL2 upon TDP-43 loss. Most of these proteins play roles in cytoskeleton organization, with five comprising core regulators of Arp2/3 actin nucleation (**Fig. 5.1H**). We next directly tested whether the interactomes of CE-HDGFL2 and full-length native HDGFL2 (FL-HDGFL2) differed by expressing CE-HDGFL2-myc-flag or FL-HDGFL2-myc-flag in HEK293 cells followed by affinity purification mass spectrometry using an anti-flag antibody. We observed substantial differences in the interactomes of CE-HDGFL2-myc-flag and FL-HDGFL2-myc-flag (**fig. 5.4, D to G, and table S5, D and E**). CE-HDGFL2 displayed increased interactions with RNA binding proteins, including a small number of splicing-regulating proteins, consistent with our observation from endogenous HDGFL2 pull-down assays of TDP-43–depleted human iPSC–derived neurons (**fig. 5.4, E and G**). As

expected, CE-HDGFL2 had reduced interactions with proteins that regulated the actin cytoskeleton (**fig. 5.4, F and H**). These observations demonstrate that the inclusion of CE sequences in a translated protein can alter its protein-protein interactome downstream of TDP-43 loss of function.

Targeted proteomics enables scalable validation of cryptic peptides

Because antibody development against new peptides is a time- and resource-intensive endeavor, we developed a targeted mass spectrometry–based approach to validate and measure additional cryptic peptides predicted by proteogenomics. By co-injecting endogenous cryptic peptides and a panel of their stable isotope (SIL) heavy peptide standards coupled with parallel reaction monitoring (PRM) mass spectrometry proteomics, we quantified dozens of peptides in a single sample run (**Fig. 5.5A**). We designed PRM assays for the 65 cryptic peptides predicted by our proteogenomic pipeline (**table S5F**). Of these, we successfully quantified 12 endogenous trypsin-digested cryptic peptides across four genes in TDP-43–depleted human iPSC–derived neurons (**Fig. 5.5, B to D, and fig. 5.6A**) that were precisely co-eluted with their SIL counterparts (**Fig. 5.5B and fig. 5.6A**) and displayed nearly identical fragmentation spectra to the corresponding heavy peptides (**Fig. 5.5C and fig. 5.6A**). The spectral plot and corresponding mass spectra for an *SYT7* cryptic peptide are shown in Fig. 5.2 (B and C); peptides from *CAMK2B*, *MYO18A*, and *RSF1* could also be detected (**fig. 5.6A**). Consistent with CE mRNA expression, we found that cryptic peptides from all four genes were highly increased in TDP-43–depleted human iPSC–derived neurons, with almost no expression in control human iPSC–derived neurons (**Fig. 5.5E, table S5G**). These experiments suggest that

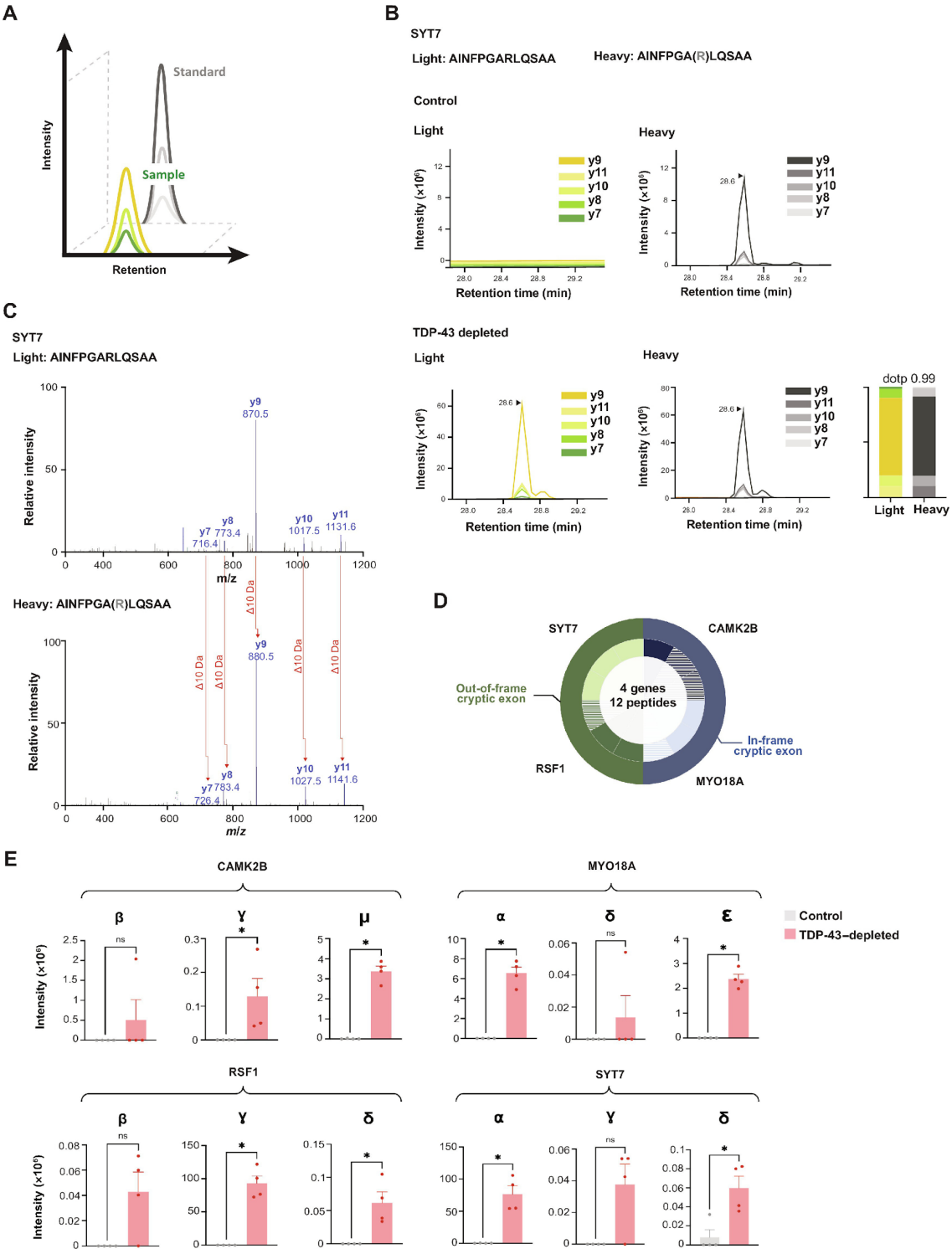

Figure 5.5. Scalable cryptic peptide validation in TDP-43–depleted human iPSC–derived neurons by targeted proteomics. (A) Schematic of PRM-MS. Co-elution of SIL peptides allows for sensitive measurement of corresponding endogenous peptides. **(B)** PRM-MS assay using a synthetic SIL peptide internal standard identifies a cryptic peptide in SYT7 in TDP-43–depleted

but not in control human iPSC–derived neurons. The spectral plot of heavy standards and light (endogenous) y ions from an SYT7 cryptic peptide is shown, with accompanying dot product (dotp), which indicates the correlation between the peptide fragment-ion peak areas and theoretical spectra. **(C)** Corresponding mass spectra of endogenous and heavy peptide standards of the SYT7 cryptic peptide in TDP-43–depleted human iPSC–derived neurons. **(D)** The detection of 12 trypsin-digested cryptic peptides across four genes using single-shot PRM assays in TDP-43–depleted human iPSC–derived neuronal lysates is shown. The outer circle represents the gene, and the inner circle represents the number of cryptic peptides detected by PRM per gene. Hatched color signifies the successful detection of one to two y ions; solid color signifies the detection of three or more y ions. **(E)** Quantification of cryptic peptide expression in TDP-43–depleted and control human iPSC–derived neurons using PRM assays. $n = 4$ replicates per sample. Mann-Whitney *U* test. $*P < 0.05$, ns, not significant.

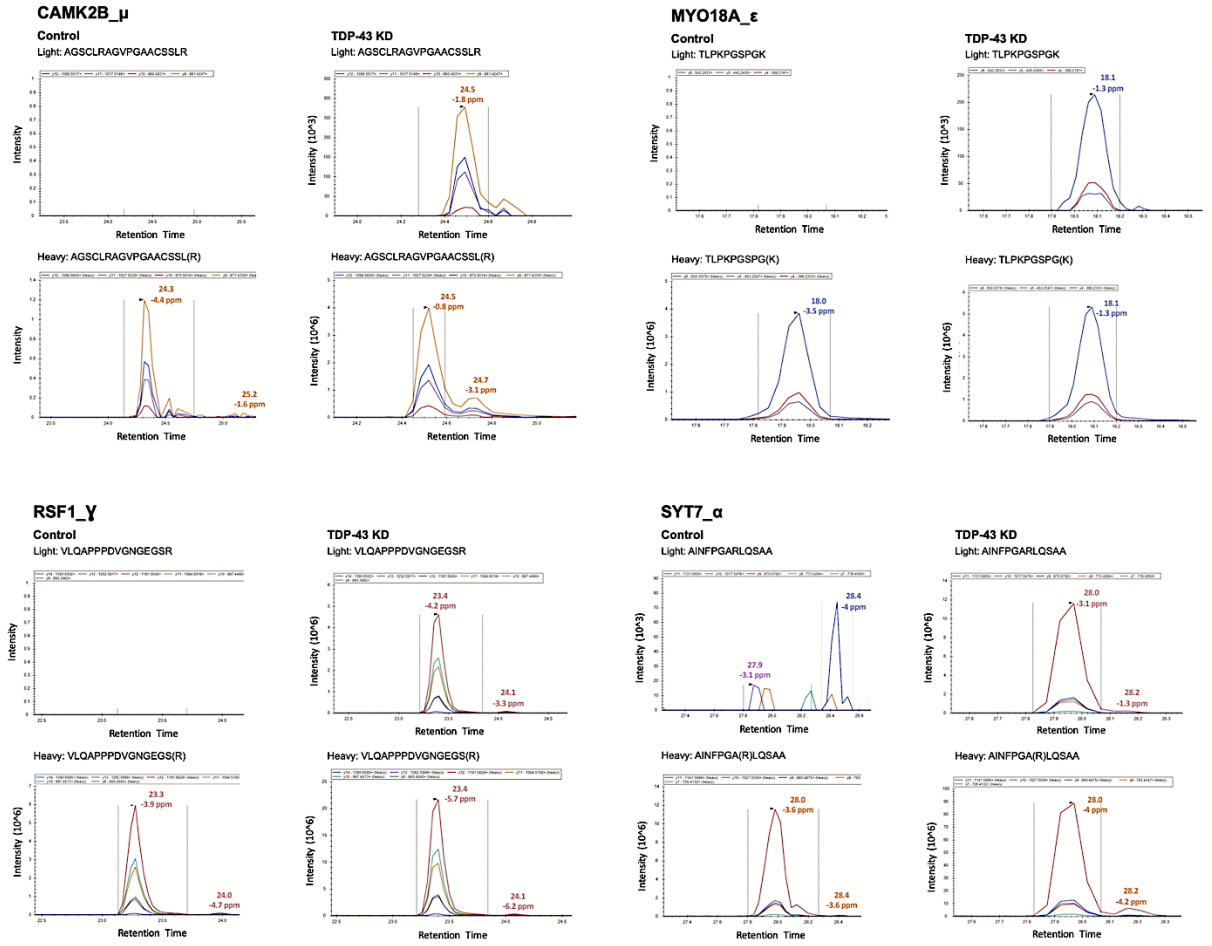

Fig. 5.6. Cryptic peptide validation in TDP-43 deficient iPSC-derived neurons via targeted proteomics. (A) Spectral plot of heavy standards and light (endogenous) ions for 4 representative cryptic peptides in TDP-43 KD and control iPSC-derived neurons. Y-axis shows intensity value; x-axis shows retention time.

multiple genes express cryptic peptides in the setting of functional TDP-43 loss and demonstrate that proteomics can detect and measure the expression of cryptic peptides in complex biological samples.

5.3 Discussion

In this chapter, I first discuss the orthogonal validation of a de novo protein resulting from cryptic splicing of HDGFL2. An antibody developed against the cryptic peptide sequence confirmed the expression of the HDGFL2-CE peptide in TDP-43-depleted human iPSC-derived neurons. I next show that overexpression of GFP-TDP-43 in TDP-43-depleted cells prevented generation of the HDGFL2 cryptic peptide, confirming that cryptic protein expression is a consequence of TDP-43 loss of function. I then discuss the development of an additional antibody against the MYO18A cryptic peptide sequence, which confirmed that expression of the CE protein was specific to TDP-43 loss in iPSC-derived neurons, and not present upon knockdown of another ALS-related gene, *FUS*. Next, designing a targeted mass spectrometry assay to detect 12 CE peptides across four genes in iPSC-derived neurons provided a scalable strategy for orthogonal validation of hits from our proteogeonomic informatic pipeline. Finally, using affinity purification mass spectrometry, I demonstrate that CE peptide expression can, indeed, alter the interacting partners of proteins downstream of TDP-43 loss of function.

These findings are relevant to ALS/FTD pathophysiology. In addition to the well-described loss-of-function mechanisms downstream of cryptic splicing, new possibilities of altered protein function should now be considered. We found that TDP-43 loss increased HDGFL2 interaction with splicing regulators, while decreasing its interaction with other protein networks, such as those that regulate actin dynamics. This suggests both the gain and the loss of function of HDGFL2 occur as a direct consequence of CE expression. Although these observations hint at the possibility that TDP-43 loss of function may alter the biology of functionally interrelated proteins, further studies are needed to address whether CE-harboring proteins play a direct role in disease pathogenesis or are an epiphenomenon. Quantifying

parameters such as actin filament turnover rates, microtubule growth dynamics, and neurite outgrowth rates in cells expressing native HDGFL2 versus CE-HDGFL2 could enable direct assessment of the impact of CE expression on cytoskeletal dynamics. The cytoskeleton not only provides cells with structural support, but also facilitates the transport of cargo across long axonal distances to enable proper synaptic function (Hirokawa, 1993). Indeed, genes that affect cytoskeletal dynamics are essential for motor neuron health and survival, and several have been previously implicated as risk loci for ALS, including *TUBA4A, ALS2*, *PFN1*, and *KIF5A* (Castellanos-Montiel et al., 2020; X. Liu & Henty-Ridilla, 2022).

In addition to TDP-43 loss of function, cytoplasmic aggregation of TDP-43 is a known driver of toxic gain of function that can induce cell death and may exacerbate functional TDP-43 loss by modulating its capacity to regulate RNA biology (Barmada et al., 2010; Gasset-Rosa et al., 2019; Yu et al., 2021). Because transient mislocalization and formation of aggregate-like inclusions of TDP-43 occur in settings of cell stress (e.g., after axotomy or oxidative stress), our findings also imply that CE expression downstream of TDP-43 mislocalization could play a regulatory role in settings outside of disease pathophysiology (Lee et al., 2012; Moisse, Mepham, et al., 2009; Moisse, Volkening, et al., 2009). As an intriguing next step, inducing cellular stress (eg, via axotomy), followed by RNA-sequencing and splicing analyses could enable characterization of changes in CE expression upon stress induction to determine whether CE expression could be involved in settings beyond disease pathophysiology.

We additionally found that HDGFL2 interacts with two other targets of TDP-43–related splicing regulation: MYO18A, a CE-harboring member of the actin regulatory network, and POLDIP3, which exhibits exon skipping in settings of TDP-43 loss. Whether functional relationships exist between genes that form CEs upon TDP-43 mislocalization will need to be

explored. A comparison of cytoskeletal dynamics upon knockdown of HDGFL2 and MYO18A, both individually and simultaneously, should provide further insights on any existing functional relationships between HDGFL2 and MYO18A.

Furthermore, prior studies have shown that nuclear TDP-43 dysfunction compromises DNA repair mechanisms, resulting in genomic instability (Mitra et al., 2019; Konopka et al., 2020). Interestingly, HDGFL2 and POLDIP3 are both implicated in the response to DNA damage (Baude et al., 2015; Singh et al., 2022). These facts, together with the observed increase in interactions between HDGFL2 and POLDIP3 upon TDP-43 loss in neurons, could suggest a compensatory response to TDP-43 loss. Conversely, the increased protein-protein interaction could indicate an increased propensity for aggregation upon CE expression. Filter trap assays designed to capture insoluble protein aggregates (Chhipi-Shrestha et al., 2022) could provide further insights on this intriguing possibility. Emerging single-protein resolution spatial proteomics methods (Unterauer et al., 2023) could also be leveraged to explore whether CE expression results in the aggregation and sequestration of proteins in subcellular compartments, thereby possibly affecting their functions.

CHAPTER 6: Cryptic peptides are present in human CSF

Statement of prior publication and co-author contributions

- The content in this chapter was modified from Sahba Seddighi *et al.*, Mis-spliced transcripts generate de novo proteins in TDP-43–related ALS/FTD. *Sci. Transl. Med.*16, eadg7162 (2024). Reprinted with permission from AAAS.
- Co-author contributions: ALS CSF TMT-proteomics datasets were provided by Lingyang Ping and Duc Duong. The targeted proteomic strategy was developed jointly with Andy Qi.

6.1 Introduction

Currently, there are no methods that enable the identification of living patients with TDP-43 pathology, nor any means to monitor responses to TDP-43-directed therapies that are in development for ALS/FTD spectrum disorders. Approximately 20 to 50% of patients with AD – and 75% of patients with severe AD – also have TDP-43 co-pathology and may represent an additional patient subpopulation that could benefit from drugs targeting pathogenic TDP-43 (Amador-Ortiz et al., 2007; Josephs et al., 2014; Uryu et al., 2008). Identification of imaging-based techniques to detect TDP-43 or its pathological forms has proven challenging. Antibody-based strategies to monitor the abundance and biochemical properties (e.g., phosphorylation and solubility) of TDP-43 have been attempted, but the interpretability and theragnostic utility of these assays in clinical settings are uncertain. A critical unmet need to develop molecular

readouts of TDP-43 pathology therefore exists, both to guide disease stratification and to enable better deployment of TDP-43–directed therapies. Given that mis-splicing is a direct consequence of TDP-43 dysfunction, assays that monitor cryptic peptides in biospecimens could be useful for monitoring therapeutic responses.

As an initial step towards this goal, we asked whether patients with ALS/FTD spectrum disorders associated with TDP-43 mislocalization express cryptic peptides. In this chapter, I discuss the development of a targeted mass spectrometry-based method to unequivocally demonstrate the presence of TDP-43-related cryptic peptides in the CSF of ALS/ FTD patients.

6.2 Results

Cryptic exon parent proteins are found in ALS CSF

Because most CE genes encode intracellular proteins, it was unclear whether proteins encoded by these genes were present in clinically relevant biofluids, such as CSF. We compared a shotgun proteomics dataset from ALS CSF samples and our CE dataset from TDP-43–depleted human iPSC–derived neurons (**table S6A**). Canonical proteins from 47 CE genes were present in ALS CSF samples, including several that expressed cryptic peptides in TDP-43–depleted human iPSC–derived neurons (**Fig. 6.1, A and B, and table S6C**). We searched two additional ALS CSF proteomics datasets from independent patient cohorts and identified four additional CE genes with canonical proteins expressed in human CSF (**Fig. 6.1B; fig. 6.2, A**

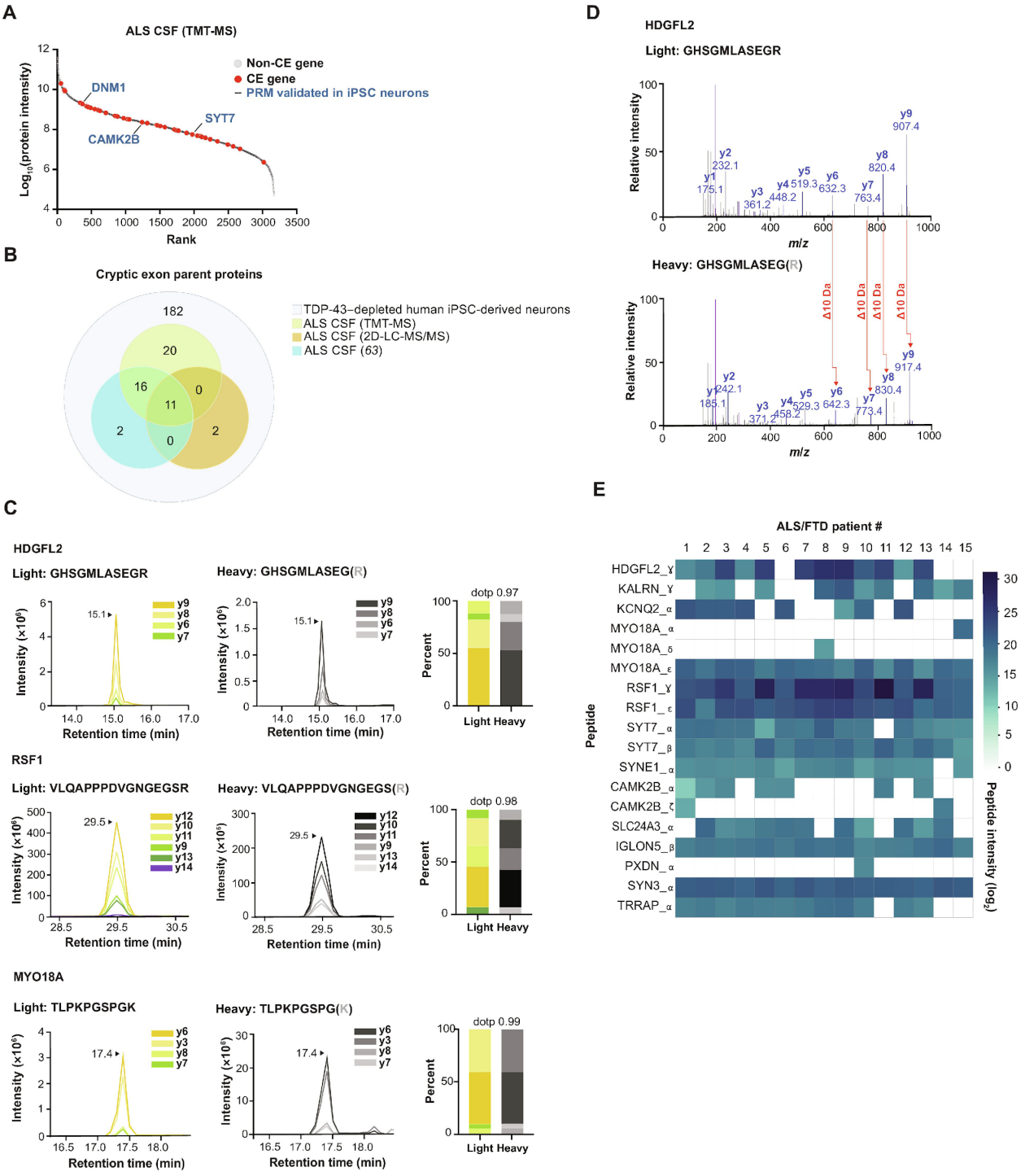

Figure 6.1. Cryptic peptides are present in CSF samples from patients with ALS. (A) Rank plot of proteins detected in CSF samples from 24 patients with ALS. Forty-seven CE genes that were predicted in TDP-43–depleted human iPSC–derived neurons are shown in red. PRM-validated cryptic peptides expressing genes (from human iPSC–derived neuron studies) are annotated in blue text. **(B)** Euler diagram of three CSF proteomics datasets versus CEs predicted in TDP-43–depleted human iPSC–derived neurons. **(C)** Representative spectra of three heavy

(standard) and light (endogenous) cryptic peptides detected in CSF from patients with ALS/FTD spectrum disorders (n = 13 ALS, n = 1 ALS/FTD, n = 1 ALS/mild cognitive impairment). Also shown is the dotp, which indicates the correlation between the peptide fragment-ion peak areas and theoretical spectra. The spectra for 15 additional cryptic peptides in ALS/FTD CSF samples are shown in fig. 6.3A. **(D)** MS/MS spectrum of a cryptic peptide in HDGFL2 that corresponds to the reference peptide (top) and endogenous peptide (bottom) detected in ALS/FTD CSF samples. **(E)** Heatmap of AUC intensities of 18 cryptic peptides from 13 different proteins in CSF samples from 15 patients with ALS/FTD.

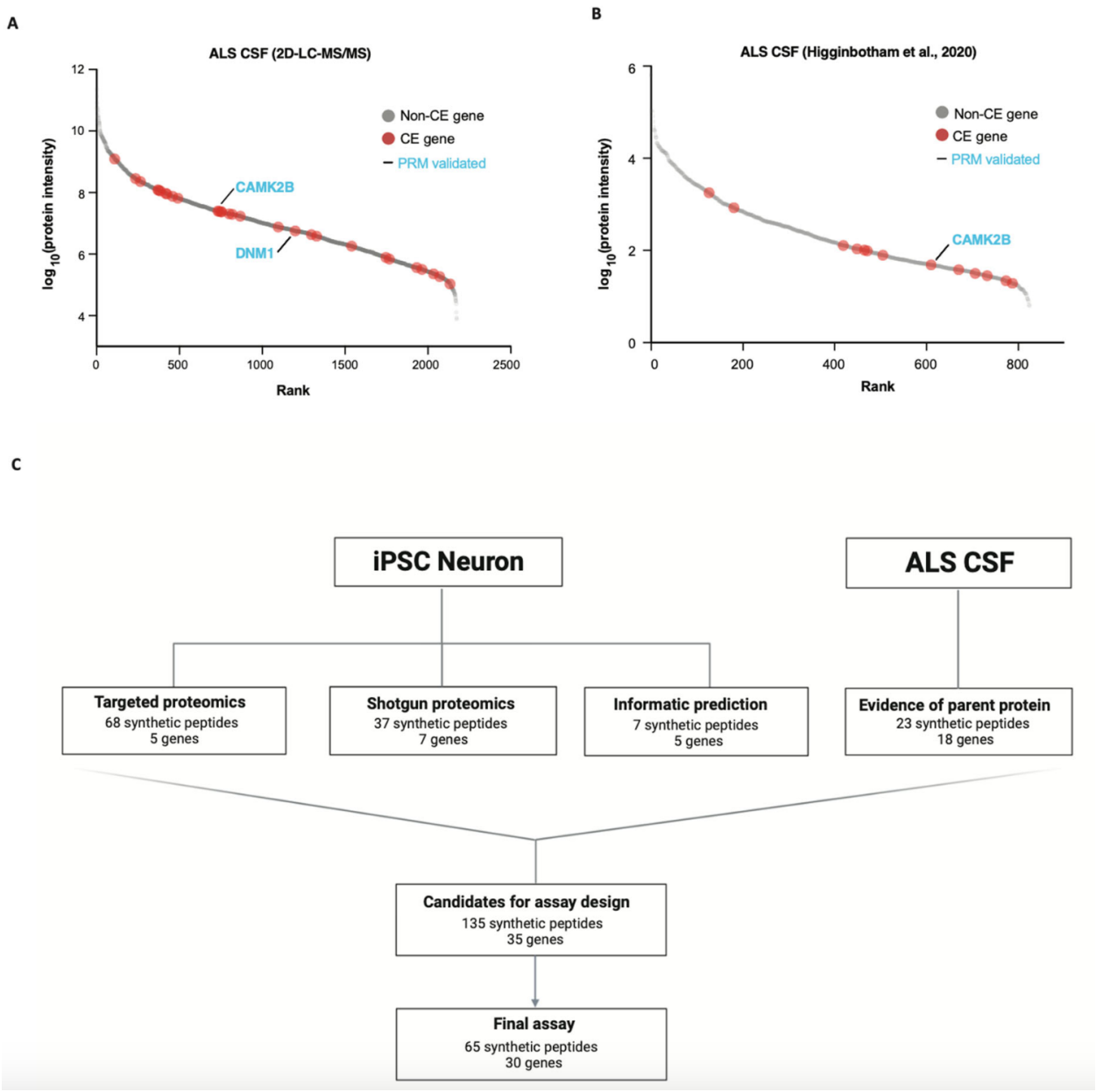

Fig. 6.2. Design of targeted proteomics assay for cryptic peptide detection in ALS/FTD CSF. (A-B) Rank plot of proteins detected in CSF from patients with ALS from an internal (A) and previously published (B) dataset. Parent proteins of iPSC-derived neuron-predicted cryptic exon genes are shown in red. **(C)** Selection process for heavy isotope-labeled peptides for use in targeted proteomics assay.

and B; and table S6, B to F). These observations provided a rationale for developing assays that could detect cryptic peptide variants of these proteins in ALS/ FTD CSF samples.

Cryptic peptides can be detected in the CSF of patients with ALS/FTD spectrum disorders

We augmented our previous list of SIL peptide standards with these additional candidates and used data-independent acquisition (DIA) proteomics to co-measure 65 endogenous and heavy peptide standards in ALS/FTD patient CSF in a single mass spectrometry run (**fig. 6.2C and table S4H**). We successfully detected 18 tryptic peptides across 13 genes that mapped to CEs in the CSF of patients with ALS/FTD spectrum disorders (**Fig. 6.1, C to E; fig. 6.3A; and table S6, G to I**). These endogenous tryptic-cryptic peptides co-eluted with their heavy peptide standards (**Fig. 6.1C and fig. 6.3A**) and had matching mass spectra (**Fig. 6.1D**). We monitored the expression of these peptides in CSF from 15 patients with ALS/FTD. Most peptides were unequivocally observed in multiple patients, with 10 peptides across eight genes detectable in >80% of patients (**Fig. 6.1E and table S6, H and I**). Cryptic peptides were also detected in healthy control individuals, but variation across mass spectrometry runs and limited sample sizes precluded quantitative comparison between control individuals and patients with ALS/FTD (**table S6J**). These data indicate that, as in TDP-43–depleted human iPSC–derived neurons, CEs are expressed and translated in the CNS of patients with ALS/FTD.

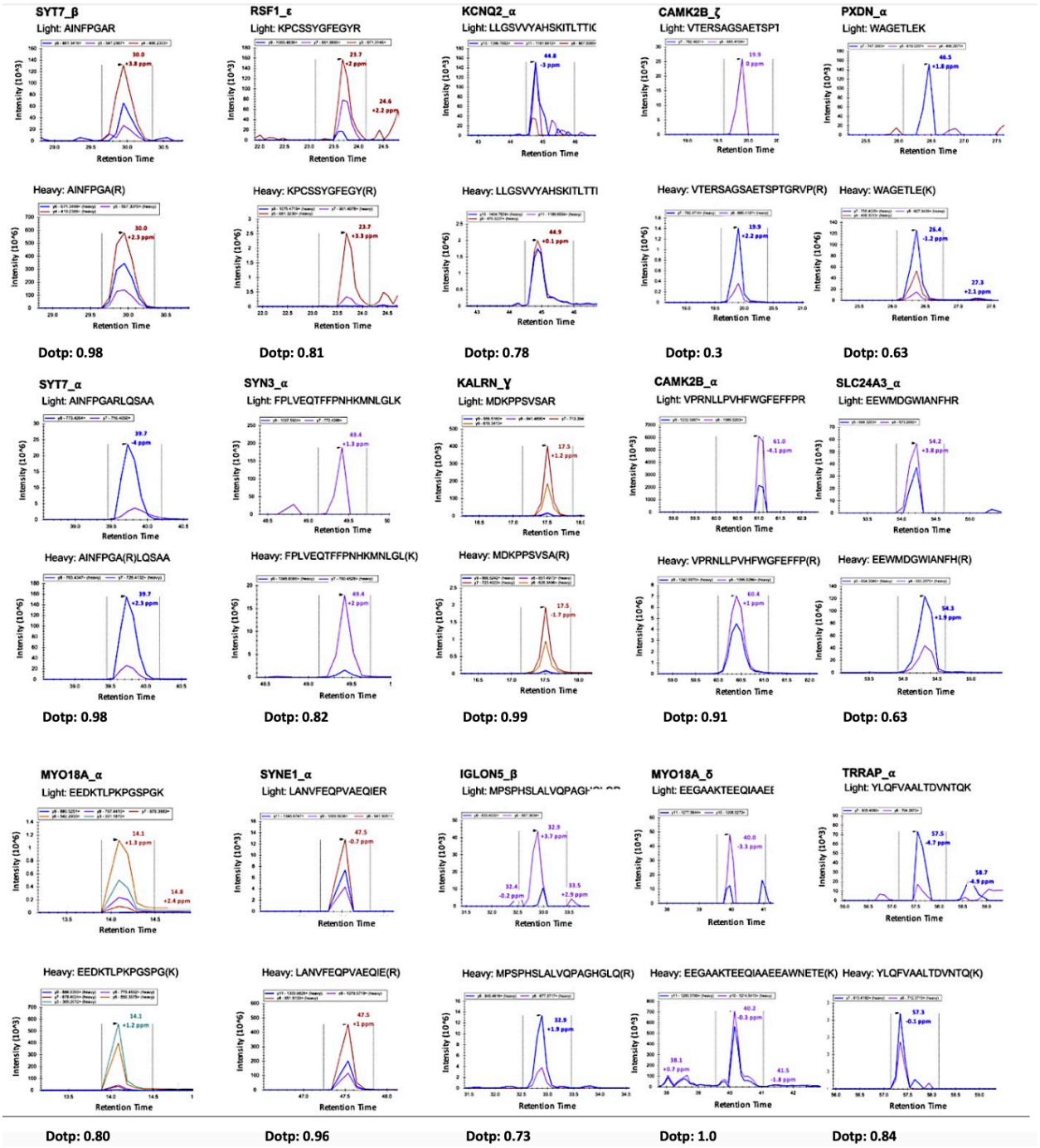

Fig. 6.3. Detection of cryptic peptides in ALS/FTD CSF. (A) Spectral plot of heavy standards and light (endogenous) ions for cryptic peptides in representative ALS/FTD CSF samples. Peptides with three or more fragment ions are considered high-confident; any peptide with fewer than three fragment ions should be interpreted with caution. Y-axis shows intensity; x-axis shows retention time.

6.3 Discussion

In this chapter, I detail the development of a targeted proteomics assay that enabled detection of de novo proteins in CSF samples from patients with ALS/FTD spectrum disorders. Since most CE genes encode intracellular proteins, it was initially unclear whether their protein products could be present in clinically relevant biofluids. Cross-referencing our CE dataset from TDP-43–depleted human iPSC–derived neurons against three independent shotgun proteomics datasets from ALS CSF samples revealed multiple CE genes with canonical proteins that are present in human CSF, thus providing a rationale for the development of an assay to detect cryptic peptide variants in clinically relevant biofluids. By applying a novel DIA-targeted mass spectrometry proteomic strategy, we successfully established that at least 18 cryptic peptides across 13 genes are unambiguously present in the CSF of patients with ALS/FTD spectrum disorders. These findings demonstrate that certain CEs are indeed translated in the CNS of patients with TDP-43 proteinopathy and provide a potential strategy to monitor TDP-43 dysfunction in living individuals.

Our study of patient biofluid samples has important limitations. We were unable to conclusively determine whether cryptic peptides are expressed more highly in cases compared to healthy controls and therefore cannot conclude that these peptides are specific for diseases involving TDP-43 pathology. Our mass spectrometry assays were designed to enable specific detection of target peptides in both cultured cells and human CSF; however, in their current form, they are only semi-quantitative when applied to human CSF and subject to technical artifacts when analyzing the absolute abundance of peptides in biofluid samples with high dynamic ranges and low peptide abundances. Future development of more sensitive,

quantitative proteomic and antibody-based assays will enable reliable comparisons of cryptic peptide abundances across patients with ALS/FTD and non-disease controls, as well as across different patient populations, such as those with AD, dementia with Lewy bodies, and Parkinson's disease with coexistent TDP-43 pathology.

Furthermore, our detection method began with depletion of the top 14 contaminants in CSF. While immunodepletion of highly abundant proteins from biological fluids facilitates detection of low-abundant proteins by mass spectrometry (Roche et al., 2009), the possibility of unwanted interactions between the bait and cryptic proteins – either directly or by associating with target proteins – must also be considered. Indeed, it has been previously demonstrated that the abundance of many candidate biomarkers of neurological diseases is strongly affected by depletion methods (Günther et al., 2015). The depletion of the top 14 contaminants also introduces additional technical variability to sample preparation. SRM assays are the gold standard for absolute protein quantification and enable target peptides to be measured without immunodepletion, but the development and optimization of such assays are laborious and specialized.

Certain cryptic peptides were also detected in healthy control individuals. However, perceived "healthy" controls could harbor early TDP-43 pathology. Approximately 20 to 50% of all AD cases exhibit concomitant TDP-43 pathology before the onset of overt symptoms (Amador-Ortiz et al., 2007; Meneses et al., 2021). In addition, there are no clearly defined antemortem pathological markers of limbic predominant age-related TDP-43 encephalopathy (LATE). The current lack of a definitive antemortem TDP-43 assay therefore poses a major challenge in the interpretation of our findings from control samples. These challenges underscore a need for careful selection of control populations in future studies. One potential

approach to overcome this limitation is to use antemortem CSF samples from individuals with postmortem immunohistochemical assessment for the presence of TDP-43 aggregates. This could also provide a more carefully selected disease population for the study of TDP-43 proteinopathy, particularly in the context of pathologically heterogeneous diseases and TDP-43 poly-proteinopathies. Genetic markers, such as *C9orf72* repeat expansion, can be used to predict the presence of TDP-43 aggregates or suggest their absence in the setting of rare genetic markers, such as *FUS* and *SOD1* mutations. As a pure tauopathy, progressive supranuclear palsy may represent a superior control population to age-matched "healthy" individuals.

Furthermore, a proper comparison of cryptic peptide abundances across different individuals and neurodegenerative diseases was beyond the technical capabilities of our current assay. Due to the relative insensitivity and technical variability of our assay, such comparisons using the current assay would be premature, as it could result in both false positives and/or false negatives. Moreover, whether the identity or levels of cryptic peptides could correspond to disease severity or endophenotypes remains to be addressed. The development of improved mass-spectrometry proteomic assays, including targeted triple-quad mass spectrometry assays and immuno-affinity-mass-spectrometry assays, will enable such comparisons in the future.

Given the new datasets presented in this chapter, our hope is that multiple efforts to develop either mass spectrometry– or antibody-based methods – for absolute quantification of cryptic peptides can ensue in parallel.

CHAPTER 7: Concluding remarks and future perspectives

Statement of prior publication

Some contents in this chapter were modified from Sahba Seddighi *et al.*, Mis-spliced transcripts generate de novo proteins in TDP-43–related ALS/FTD. *Sci. Transl. Med.*16, eadg7162 (2024). Reprinted with permission from AAAS.

7.1 Thesis summary

In **Chapter 1**, I introduce TDP-43 as the major disease-associated protein in ALS and FTLD-TDP and review the literature surrounding TDP-43 as a co-pathology in other neurodegenerative disorders, highlighting a critical unmet for biomarkers to detect and monitor TDP-43 pathology in living individuals. I then review the structure of TDP-43 and its relation to the protein's physiological functions. Finally, I discuss how both loss and gain-of-function of TDP-43 can drive neurodegenerative processes, ending with a discussion of recent seminal discoveries surrounding cryptic exon biology that underscore a need to more fully characterize the role of TDP-43 dysfunction in disease.

In **Chapter 2**, I review advances in iPSC technology that can be leveraged toward the identification of novel molecular mechanisms and therapeutic targets for neurodegenerative diseases. I outline the contributions of human genetic studies and describe how iPSC models can provide an opportunity to examine whether a given molecular disturbance has a causal role in disease. Finally, I discuss the promises and limitations of rejuvenated iPSCs,

transdifferentiation strategies, and the use of simplex versus complex cellular models for unraveling the molecular drivers of neurodegenerative disease.

Chapter 3 provides an overview of the materials and methods in the context of my thesis aims. Broadly, the goal of my thesis was to examine the downstream consequences of splicing dysregulation in the context of TDP-43 depletion and determine whether mis-spliced transcripts generate de novo protein products. My studies began with an in-depth analysis of mis-splicing events in TDP-43-depleted iPSC neurons (**Methods 3.2**), which allowed for the design of a proteogenomic strategy to detect de novo protein sequences arising from mis-spliced junctions in TDP-43-depleted human iPSC-derived neurons (**Methods 3.3**). We then validated our proteogenomic findings using sensitive antibody and targeted proteomics-based strategies (**Methods 3.4**). Next, we asked whether cryptic peptides could impact the interactome, and thereby likely the function, of proteins (**Methods 3.5**) via affinity purification mass-spectrometry. Finally, we designed a novel targeted proteomics assay to detect TDP-43-related cryptic peptides in the CSF of individuals with ALS/FTD (**Methods 3.6**).

In **Chapter 4**, I discuss the development of a proteogenomic pipeline to detect de novo peptides from mis-spliced junctions in TDP-43-depleted human iPSC-derived neurons. I first used RNA sequencing data from TDP-43-depleted iPSC neurons to develop a catalog of TDP-43-related cryptic exons in neurons. While most cryptic exons are expected to undergo degradation by non-sense mediated decay, we found that some introns had bound ribosomes in TDP-43-depleted iPSC-derived neurons, suggesting that certain cryptic exons could be translated. We next asked whether we could find direct evidence of cryptic exon translation in TDP-43-depleted iPSC-derived neurons. To this end, we developed an informatic pipeline to predict in-frame amino acid sequences from mis-spliced transcripts. Cross-referencing these in

silico predictions against our experimental proteomics data from TDP-43 depleted iPSC neurons revealed 65 putative cryptic peptides across 12 unique genes. Finally, we validated the physiological relevance of our in vitro model by demonstrating that the mis-spliced junctions from our iPSC studies could reliably predict pathological splicing events in the brains of individuals with ALS/FTD patients.

In **Chapter 5**, I describe the orthogonal validation of putative de novo peptides and examine the effects of cryptic exon expression on the interactome of proteins. We first developed an antibody against the cryptic peptide in HDGFL2 and used an immunofluorescence staining strategy to detect this cryptic peptide and an MSD immunoassay to accurately quantify its abundance in TDP-43-depleted iPSC-derived neurons. We then developed a second antibody against the cryptic peptide in MYO18A, which was used to confirm the expression of the CE in TDP-43-depleted iPSC-derived neurons by Western blot. Finally, we asked whether the HDGFL2 cryptic peptide could alter its interacting partners, as an initial step in exploring the impact of cryptic exons on protein biology. Using our in-house HDGFL2 cryptic peptide antibody for affinity purification mass spectrometry analysis, we found that 16 proteins increased their interactions and 13 proteins decreased their interactions with HDGFL2 upon TDP-43 loss, suggesting that cryptic exons can alter the interactome of proteins, with potential gain and loss-of-function mechanisms that merit further study. Finally, we developed a targeted proteomics-based strategy to scalably validate 12 cryptic peptides across four genes in TDP-43-depleted iPSC-derived neurons.

Finally, in **Chapter 6**, I discuss the development and application of a novel targeted proteomics assay for the detection of cryptic peptides in CSF samples from ALS/FTD patients. We first augmented our list of cryptic peptides from iPSC neuron studies by identifying cryptic

exon-harboring genes with canonical proteins that are expressed in the CSF of patients with ALS. Then, we developed heavy peptide standards against all candidate de novo proteins, enabling us to co-measure 65 putative cryptic proteins in ALS/FTD patient CSF samples in a single mass spectrometry run. This enabled successful detection of 18 cryptic peptides across 13 genes in the CSF of patients with ALS/FTD, thereby establishing that cryptic exons are indeed translated in the CNS of patients with ALS/FTD.

7.2 Ongoing work and future directions

7.2.1 TDP-43 biomarker assay development

Biomarkers for early diagnosis, disease subtype stratification, and response to treatments are vitally important for both patient care and the improved design of clinical trials. While fluid biomarkers of neurodegeneration, such as serum neurofilament light chain, CSF phosphorylated neurofilament heavy chain, and urinary p75ECD (Rossi et al., 2018; Shepheard et al., 2017; Verde et al., 2019), are available, there are currently no specific biomarkers of ALS/FTD or TDP-43 proteinopathy.

An ideal functional TDP-43 biomarker should have high sensitivity and specificity, linear correlation with disease activity, and remain stably expressed throughout the day (Hansson, 2021). The development of sufficiently sensitive and reliable assays to enable clinical-grade quantification of TDP-43 function in living patients is therefore likely to be a multi-year effort, akin to the developmental history of assays that reliably quantify neurofilament, amyloid-beta,

and tau in CSF. While developing a clinical-grade assay for TDP-43 dysfunction was beyond the scope of my thesis, the value of this work was to provide an extended list of candidate biomarkers for additional testing towards the development of quantitative biomarker assays. In the future, targeted mass spectrometry–based approaches could be optimal for developing ultra-sensitive bioassays for clinical application. An example of this is SRM, wherein synthetic stable isotope-labeled peptides are used as internal standards to enable the quantification of trace analytes (Picotti & Aebersold, 2012). Antibody-based approaches may also prove useful in the detection of cryptic peptides. Recently, an antibody-based MSD assay targeting the same HDGFL2-CE neoepitope that we detected in our targeted mass spectrometry-based studies was developed by Irwin and colleagues and applied to CSF samples from controls and ALS cases (Irwin et al., 2024). Their study shows that the HDGFL2 cryptic peptide can be detected in both controls and ALS cases, including presymptomatic *C9orf72* ALS mutation carriers (Irwin et al., 2024) and that a quantitative assay allows discrimination between the two groups. Our work does not develop quantitative assays, but provides evidence for multiple cryptic peptides. When analyzing our preliminary mass spectrometry data from controls, cryptic peptide – similar to the differential abundance shown in Irwin et al., 2024 – can be detected. Data from controls and FTD-ALS samples for the 18 peptides that were detected in ALS CSF is provided in Table S6J. While variation across mass spectrometry runs and limited sample sizes preclude quantitative comparisons between control and disease subjects in this early stage of assay development, the value of this dataset is to provide an extended list of candidate biomarkers for additional testing by us and others towards developing quantitative biomarker assays. To enable optimal detection of ultra-low abundant cryptic peptides in human biofluid samples with high dynamic ranges, a

combinatorial approach, involving antibody-based enrichment followed by targeted proteomics, could be ideal.

A closely related strategy may involve leveraging high-sensitivity antibodies or aptamers against native proteins expressing cryptic peptides. Such tools could subsequently enable SIMOA assays that can measure analytes at the single-molecule level (Rissin et al., 2010). New methods to enrich brain-derived exosomes in plasma and paired single-molecule detection strategies (e.g., SMAC) are being developed and open exciting possibilities for noninvasive disease profiling in the blood (Mao et al., 2021).

The demonstration of HDGFL2 cryptic neoepitope expression in the CSF and blood of pre-symptomatic *C9orf72* ALS mutation carriers (Irwin et al., 2024) raises key questions about the temporal presentation of cryptic peptides during the course of disease. Irwin and colleagues propose that HDGFL2-CE peptide levels may peak before symptom onset and decrease with disease progression, possibly as a result of cell death before symptom onset. Further work is needed to examine the longitudinal trajectories of cryptic peptides, beyond the first few years of clinical disease, and any association that may exist with phenoconversion and disease progression.

Ultimately, a multi-analyte panel for cryptic peptides may increase sensitivity and could represent an effective diagnostic strategy. This is consistent with our findings of improved disease predictability in postmortem brain tissue upon consideration of multiple CEs over any single mis-spliced junction (except for *STMN2* CE, which cannot yet be detected at the protein level). The characterization of a broader repertoire of bona fide cryptic peptides elicited by TDP-43 loss in disease-relevant cell types will provide an expanded list of putative biomarker candidates for biomarker studies.

Beyond peptide-based biomarkers, the possibility of cryptic exon RNA-based biomarkers should also be considered. The proof of concept for RNA-based cryptic exon biomarkers has already been demonstrated for the *STMN2* cryptic exon, which can reliably discriminate between individuals with FTD-TDP, progressive supranuclear palsy, and healthy controls on RNA-sequencing of postmortem frontal cortex tissue (Gate et al., 2021). As discussed in Chapter 4, we have now characterized a much longer list of cryptic exon junctions with positive predictive power for TDP-43 pathology in postmortem brain samples from individuals with FTLD-TDP and ALS. These datasets could be leveraged in the development of novel RNA-based biomarkers. However, a major challenge in developing cryptic exon-based biomarkers is that most cryptic exon-harboring transcripts are expected to undergo degradation by NMD and do not remain stably expressed. Furthermore, if transcript levels are low, a highly sensitive detection strategy would be needed. Ultra-sensitive, single-molecule detection strategies, such as SMAC, may prove useful in such applications.

Importantly, the successful development of a clinical-grade biomarker assay hinges on the appropriate selection of control groups. Future studies should compare cryptic peptide abundances not only across patients with ALS/FTD and non-disease controls, but also across other TDP-43 proteinopathies, such as LATE, and diseases with co-existent TDP-43 pathology, including AD and DLB.

The current lack of a definitive antemortem TDP-43 assay poses a challenge in the selection of controls. Increasing evidence indicates that nuclear TDP-43 dysfunction may represent an early pathological event preceding clinical symptom onset in TDP-43 proteinopathies (Vatsavayai et al., 2016, Spence et al., 2024). Given the expanding clinical continuum of TDP-43 proteinoapthies across a range of neurodegenerative conditions,

including AD (Amador-Ortiz et al., 2007; Boer et al., 2020; Josephs et al., 2014), it is conceivable that some "healthy," presymptomatic controls could in fact harbor early TDP-43 pathology. In addition, limbic predominant age-related TDP-43 encephalopathy (LATE) can only be detected postmortem. Nonetheless, genetic markers, such as *C9orf72* repeat expansion, can be used to predict the presence of TDP-43 aggregates or suggest their absence in the presence of other genetic markers of disease, such as *FUS* and *SOD1* mutations. Since the frequency of TDP-43 pathology increases with age, younger individuals might be an ideal control group. These challenges underscore the importance of carefully selecting control populations for future studies.

If successful, the development of a TDP-43 functional biomarker could be transformative to the field of ALS/FTD and related TDP-43 proteinopathies. Currently available neurofilament markers are broadly reflective of neurodegeneration and non-specific to TDP-43 dysfunction, thus limiting their utility as measures of target engagement in clinical trials. With new therapies on the horizon, cryptic peptide biomarkers could provide a functional readout for treatment responses at a mechanistic level, with critical applications in trials targeting TDP-43 dysfunction. Furthermore, since TDP-43 dysfunction appears to take place during the presymptomatic phase of disease, cryptic peptide biomarkers could enable earlier diagnosis and clinical trial enrollment during an optimal therapeutic window.

In the future, the development of more sensitive, quantitative assays and will enable more extensive longitudinal studies aimed at characterizing the dynamic nature of cryptic peptides (including HDGLF2), their correlation with neurofilament markers and phenoconversion, as well as any associations that may exist with disease endophenotypes across the ALS-FTD spectrum. Importantly, the impact of TDP-43 biomarkers extends well beyond

ALS and FTD, as TDP-43 biomarkers could additionally be employed to discriminate mixed-etiology TDP-43 polyproteinopathies from more 'pure' pathologies that may benefit from different therapeutic strategies. Ultimately, cryptic peptide biomarkers could enable early diagnosis and provide a functional readout for treatment responses, allowing for more effective clinical trials to intervene at a much earlier stages of disease.

7.2.2 Cryptic peptide gain and loss-of-function mechanisms

The discovery of cryptic peptides downstream of nuclear TDP-43 dysfunction raises important questions regarding their involvement in disease pathogenesis. The loss-of-function mechanisms of cryptic splicing have been well described. It is now well known that cryptic exon-mediated loss of the STMN2 protein is a key contributor to ALS pathogenesis (Guerra San Juan et al., 2022; Klim et al., 2019; Krus et al., 2022; López-Erauskin et al., 2024; Melamed et al., 2019) and that cryptic exon-splicing of *UNC13A* modifies diseases progression in ALS and FTD (Brown et al., 2022). These findings are in line with our observation that most proteins from CE genes display reduced expression levels in the setting of TDP-43 loss. Our data further demonstrate the loss-of-function consequences of cryptic exons at the protein level by demonstrating that HDGFL2 CE expression results in decreased HDGFL2 interactions with proteins that regulate actin dynamics.

In addition to the loss of functional protein, the possibility of gain-of-function toxicity should also be considered. Our finding that HDGFL2 CE expression leads to increased interactions of HDGFL2 with 16 different proteins suggests possible gain-of-function effects. It is also plausible that cryptic peptides, either independently or in conjunction with TDP-43

aggregates, disrupt protein homeostasis and lead to impaired neuronal function. Future studies of candidate proteins will be essential to delineate the specific cellular pathways perturbed by cryptic peptides and to assess their impact on neuronal function and viability. Ultimately, an enhanced understanding of the determinants of cryptic peptide-mediated cytotoxicity may offer novel therapeutic strategies for mitigating their deleterious effects.

7.2.3 Possible autoimmune implications of cryptic peptides

The discovery of cryptic exon translation also provides a rationale for future evaluation of the potential role of cryptic peptides in autoimmune dysregulation in neurodegenerative disorders. It is conceivable that cryptic peptides could be presented by MHCs for recognition by cytotoxic T cells. Infiltration of cytotoxic CD8+ T cells has been previously reported in the brain and spinal cord of patients with ALS (Engelhardt et al., 1993; Graves et al., 2004; Rodrigues Lima-Junior et al., 2021). The possibility that cryptic peptides could elicit the expression of autoantibodies warrants further consideration. Neo-antigens are now well described for other neurodegenerative disorders, including Lewy body dementia and Parkinson's disease, and suggest the possibility of searching for T cell or antibody-based responses against such antigens (Gate et al., 2021; Sulzer et al., 2017). Retrospective analysis of stored serum samples recently led to the seminal discovery of Epstein-Barr virus as the viral etiology of multiple sclerosis (Bjornevik et al., 2022; Lanz et al., 2022). Similar approaches may be fruitful for the study of CE-related autoantibodies in ALS and other TDP-43 proteinopathies.

7.3 Closing Remarks

In summary, this body of work demonstrates that loss of nuclear TDP-43 leads to the generation of de novo cryptic proteins in cellular models of disease and in the CNS of patients with ALS and FTD. These findings should guide new discoveries on the role of cryptic peptides in TDP-43 proteinopathies and provide a strategy for the development of clinical-grade assays to measure TDP-43 function in patient CSF.

References

Afroz, T., Hock, E. M., Ernst, P., Foglieni, C., Jambeau, M., Gilhespy, L. A. B., Laferriere, F., Maniecka, Z., Plückthun, A., Mittl, P., Paganetti, P., Allain, F. H. T., & Polymenidou, M. (2017). Functional and dynamic polymerization of the ALS-linked protein TDP-43 antagonizes its pathologic aggregation. *Nature Communications*, *8*(1). https://doi.org/10.1038/s41467-017-00062-0

Alami, N. H., Smith, R. B., Carrasco, M. A., Williams, L. A., Winborn, C. S., Han, S. S. W., Kiskinis, E., Winborn, B., Freibaum, B. D., Kanagaraj, A., Clare, A. J., Badders, N. M., Bilican, B., Chaum, E., Chandran, S., Shaw, C. E., Eggan, K. C., Maniatis, T., & Taylor, J. P. (2014). Axonal Transport of TDP-43 mRNA Granules Is Impaired by ALS-Causing Mutations. *Neuron*, *81*(3). https://doi.org/10.1016/j.neuron.2013.12.018

Al-Chalabi, A., Fang, F., Hanby, M. F., Leigh, P. N., Shaw, C. E., Ye, W., & Rijsdijk, F. (2010). An estimate of amyotrophic lateral sclerosis heritability using twin data. *Journal of Neurology, Neurosurgery and Psychiatry*, *81*(12). https://doi.org/10.1136/jnnp.2010.207464

Alkan, C., Sajjadian, S., & Eichler, E. E. (2011). Limitations of next-generation genome sequence assembly. In *Nature Methods* (Vol. 8, Issue 1). https://doi.org/10.1038/nmeth.1527

Al'Khafaji, A. M., Smith, J. T., Garimella, K. V., Babadi, M., Popic, V., Sade-Feldman, M., Gatzen, M., Sarkizova, S., Schwartz, M. A., Blaum, E. M., Day, A., Costello, M., Bowers, T., Gabriel, S., Banks, E., Philippakis, A. A., Boland, G. M., Blainey, P. C., & Hacohen, N. (2023). High-throughput RNA isoform sequencing using programmed cDNA concatenation. *Nature Biotechnology*. https://doi.org/10.1038/s41587-023-01815-7

Altshuler, D., Daly, M. J., & Lander, E. S. (2008). Genetic mapping in human disease. In *Science* (Vol. 322, Issue 5903). https://doi.org/10.1126/science.1156409

Amador-Ortiz, C., Lin, W. L., Ahmed, Z., Personett, D., Davies, P., Duara, R., Graff-Radford, N. R., Hutton, M. L., & Dickson, D. W. (2007). TDP-43 immunoreactivity in hippocampal sclerosis and Alzheimer's disease. *Annals of Neurology*. https://doi.org/10.1002/ana.21154

An, D., Fujiki, R., Iannitelli, D. E., Smerdon, J. W., Maity, S., Rose, M. F., Gelber, A., Wanaselja, E. K., Yagudayeva, I., Lee, J. Y., Vogel, C., Wichterle, H., Engle, E. C., & Mazzoni, E. O. (2019). Stem cell-derived cranial and spinal motor neurons reveal proteostatic differences between ALS resistant and sensitive motor neurons. *ELife*, *8*. https://doi.org/10.7554/eLife.44423

Andrews, S. (2010). FastQC - A quality control tool for high throughput sequence data. http://www.bioinformatics.babraham.ac.uk/projects/fastqc/. *Babraham Bioinformatics*.

Arai, T., Mackenzie, I. R. A., Hasegawa, M., Nonoka, T., Niizato, K., Tsuchiya, K., Iritani, S., Onaya, M., & Akiyama, H. (2009). Phosphorylated TDP-43 in Alzheimer's disease and dementia with Lewy bodies. *Acta Neuropathologica*, *117*(2). https://doi.org/10.1007/s00401-008-0480-1

Ayala, Y. M., De Conti, L., Avendaño-Vázquez, S. E., Dhir, A., Romano, M., D'Ambrogio, A., Tollervey, J., Ule, J., Baralle, M., Buratti, E., & Baralle, F. E. (2011). TDP-43 regulates its mRNA levels through a negative feedback loop. *EMBO Journal*, *30*(2). https://doi.org/10.1038/emboj.2010.310

Ayala, Y. M., Zago, P., D'Ambrogio, A., Xu, Y. F., Petrucelli, L., Buratti, E., & Baralle, F. E. (2008). Structural determinants of the cellular localization and shuttling of TDP-43. *Journal of Cell Science*, *121*(22). https://doi.org/10.1242/jcs.038950

Bairoch, A., & Apweiler, R. (2000). The SWISS-PROT protein sequence database and its supplement TrEMBL in 2000. In *Nucleic Acids Research*. https://doi.org/10.1093/nar/28.1.45

Bannwarth, S., Ait-El-Mkadem, S., Chaussenot, A., Genin, E. C., Lacas-Gervais, S., Fragaki, K., Berg-Alonso, L., Kageyama, Y., Serre, V., Moore, D. G., Verschueren, A., Rouzier, C., Le Ber, I.,

Augé, G., Cochaud, C., Lespinasse, F., N'guyen, K., De Septenville, A., Brice, A., … Paquis-Flucklinger, V. (2014). A mitochondrial origin for frontotemporal dementia and amyotrophic lateral sclerosis through CHCHD10 involvement. *Brain*, *137*(8). https://doi.org/10.1093/brain/awu138

Barmada, S. J., Skibinski, G., Korb, E., Rao, E. J., Wu, J. Y., & Finkbeiner, S. (2010). Cytoplasmic Mislocalization of TDP-43 Is Toxic to Neurons and Enhanced by a Mutation Associated with Familial Amyotrophic Lateral Sclerosis. *The Journal of Neuroscience*, *30*(2), 639 LP – 649. https://doi.org/10.1523/JNEUROSCI.4988-09.2010

Baude, A., Aaes, T. L., Zhai, B., Al-Nakouzi, N., Oo, H. Z., Daugaard, M., Rohde, M., & Jäättelä, M. (2015). Hepatoma-derived growth factor-related protein 2 promotes DNA repair by homologous recombination. *Nucleic Acids Research*. https://doi.org/10.1093/nar/gkv1526

Baughn, M. W., Melamed, Z., López-Erauskin, J., Beccari, M. S., Ling, K., Zuberi, A., Presa, M., Gonzalo-Gil, E., Maimon, R., Vazquez-Sanchez, S., Chaturvedi, S., Bravo-Hernández, M., Taupin, V., Moore, S., Artates, J. W., Acks, E., Sandra Ndayambaje, I., Agra de Almeida Quadros, A. R., Jafar-Nejad, P., … Cleveland, D. W. (2023). Mechanism of STMN2 cryptic splice-polyadenylation and its correction for TDP-43 proteinopathies. *Science*, *379*(6637). https://doi.org/10.1126/science.abq5622

Baxi, E. G., Thompson, T., Li, J., Kaye, J. A., Lim, R. G., Wu, J., Ramamoorthy, D., Lima, L., Vaibhav, V., Matlock, A., Frank, A., Coyne, A. N., Landin, B., Ornelas, L., Mosmiller, E., Thrower, S., Farr, S. M., Panther, L., Gomez, E., … Rothstein, J. D. (2022). Answer ALS, a large-scale resource for sporadic and familial ALS combining clinical and multi-omics data from induced pluripotent cell lines. *Nature Neuroscience*, *25*(2). https://doi.org/10.1038/s41593-021-01006-0

Bennett, H. M., Stephenson, W., Rose, C. M., & Darmanis, S. (2023). Single-cell proteomics enabled by next-generation sequencing or mass spectrometry. In *Nature Methods* (Vol. 20, Issue 3). https://doi.org/10.1038/s41592-023-01791-5

Bjork, R. T., Mortimore, N. P., Loganathan, S., & Zarnescu, D. C. (2022). Dysregulation of Translation in TDP-43 Proteinopathies: Deficits in the RNA Supply Chain and Local Protein Production. In *Frontiers in Neuroscience* (Vol. 16). https://doi.org/10.3389/fnins.2022.840357

Bjornevik, K., Cortese, M., Healy, B. C., Kuhle, J., Mina, M. J., Leng, Y., Elledge, S. J., Niebuhr, D. W., Scher, A. I., Munger, K. L., & Ascherio, A. (2022). Longitudinal analysis reveals high prevalence of Epstein-Barr virus associated with multiple sclerosis. *Science*. https://doi.org/10.1126/science.abj8222

Borroni, B., Benussi, A., Premi, E., Alberici, A., Marcello, E., Gardoni, F., Di Luca, M., & Padovani, A. (2018). Biological, Neuroimaging, and Neurophysiological Markers in Frontotemporal Dementia: Three Faces of the Same Coin. In *Journal of Alzheimer's Disease* (Vol. 62, Issue 3). https://doi.org/10.3233/JAD-170584

Borroni, B., Bonvicini, C., Alberici, A., Buratti, E., Agosti, C., Archetti, S., Papetti, A., Stuani, C., Di Luca, M., Gennarelli, M., & Padovani, A. (2009). Mutation within TARDBP leads to Frontotemporal Dementia without motor neuron disease. *Human Mutation*, *30*(11), E974–E983. https://doi.org/https://doi.org/10.1002/humu.21100

Bowles, K. R., Silva, M. C., Whitney, K., Bertucci, T., Berlind, J. E., Lai, J. D., Garza, J. C., Boles, N. C., Mahali, S., Strang, K. H., Marsh, J. A., Chen, C., Pugh, D. A., Liu, Y., Gordon, R. E., Goderie, S. K., Chowdhury, R., Lotz, S., Lane, K., … Temple, S. (2021). ELAVL4, splicing, and glutamatergic dysfunction precede neuron loss in MAPT mutation cerebral organoids. *Cell*, *184*(17). https://doi.org/10.1016/j.cell.2021.07.003

Breevoort, S., Gibson, S., Figueroa, K., Bromberg, M., & Pulst, S. (2022). Expanding Clinical Spectrum of *C9ORF72*-Related Disorders and Promising Therapeutic Strategies: A Review. *Neurology Genetics*, *8*(3), e670. https://doi.org/10.1212/nxg.0000000000000670

Bright, F., Chan, G., van Hummel, A., Ittner, L. M., & Ke, Y. D. (2021). Tdp-43 and inflammation: Implications for amyotrophic lateral sclerosis and frontotemporal dementia. In *International Journal of Molecular Sciences* (Vol. 22, Issue 15). https://doi.org/10.3390/ijms22157781

Broe, M., Hodges, J. R., Schofield, E., Shepherd, C. E., Kril, J. J., & Halliday, G. M. (2003). Staging disease severity in pathologically confirmed cases of frontotemporal dementia. *Neurology*, *60*(6). https://doi.org/10.1212/01.WNL.0000052685.09194.39

Brown, A.-L., Wilkins, O. G., Keuss, M. J., Hill, S. E., Zanovello, M., Lee, W. C., Bampton, A., Lee, F. C. Y., Masino, L., Qi, Y. A., Bryce-Smith, S., Gatt, A., Hallegger, M., Fagegaltier, D., Phatnani, H., Phatnani, H., Kwan, J., Sareen, D., Broach, J. R., … Consortium, N. A. L. S. (2022). TDP-43 loss and ALS-risk SNPs drive mis-splicing and depletion of UNC13A. *Nature*, *603*(7899), 131–137. https://doi.org/10.1038/s41586-022-04436-3

Buratti, E., Brindisi, A., Giombi, M., Tisminetzky, S., Ayala, Y. M., & Baralle, F. E. (2005). TDP-43 binds heterogeneous nuclear ribonucleoprotein A/B through its C-terminal tail: An important region for the inhibition of cystic fibrosis transmembrane conductance regulator exon 9 splicing. *Journal of Biological Chemistry*, *280*(45). https://doi.org/10.1074/jbc.M505557200

Butti, Z., & Patten, S. A. (2019). RNA Dysregulation in Amyotrophic Lateral Sclerosis. *Frontiers in Genetics*, *9*. https://doi.org/10.3389/fgene.2018.00712

Buratti, E., Dörk, T., Zuccato, E., Pagani, F., Romano, M., & Baralle, F. E. (2001). Nuclear factor TDP-43 and SR proteins promote in vitro and in vivo CFTR exon 9 skipping. *EMBO Journal*, *20*(7). https://doi.org/10.1093/emboj/20.7.1774

Burrell, J. R., Halliday, G. M., Kril, J. J., Ittner, L. M., Götz, J., Kiernan, M. C., & Hodges, J. R. (2016). The frontotemporal dementia-motor neuron disease continuum. In *The Lancet* (Vol. 388, Issue 10047). https://doi.org/10.1016/S0140-6736(16)00737-6

Burrows, C. K., Banovich, N. E., Pavlovic, B. J., Patterson, K., Gallego Romero, I., Pritchard, J. K., & Gilad, Y. (2016). Genetic Variation, Not Cell Type of Origin, Underlies the Majority of Identifiable Regulatory Differences in iPSCs. *PLoS Genetics*, *12*(1). https://doi.org/10.1371/journal.pgen.1005793

Cahan, P., Li, H., Morris, S. A., Lummertz Da Rocha, E., Daley, G. Q., & Collins, J. J. (2014). CellNet: Network biology applied to stem cell engineering. *Cell*, *158*(4). https://doi.org/10.1016/j.cell.2014.07.020

Carcamo-Orive, I., Hoffman, G. E., Cundiff, P., Beckmann, N. D., D'Souza, S. L., Knowles, J. W., Patel, A., Papatsenko, D., Abbasi, F., Reaven, G. M., Whalen, S., Lee, P., Shahbazi, M., Henrion, M. Y. R., Zhu, K., Wang, S., Roussos, P., Schadt, E. E., Pandey, G., … Lemischka, I. (2017). Analysis of Transcriptional Variability in a Large Human iPSC Library Reveals Genetic and Non-genetic Determinants of Heterogeneity. *Cell Stem Cell*, *20*(4). https://doi.org/10.1016/j.stem.2016.11.005

Castellanos-Montiel, M. J., Chaineau, M., & Durcan, T. M. (2020). The Neglected Genes of ALS: Cytoskeletal Dynamics Impact Synaptic Degeneration in ALS. In *Frontiers in Cellular Neuroscience* (Vol. 14). https://doi.org/10.3389/fncel.2020.594975

Charif, S. E., Luchelli, L., Vila, A., Blaustein, M., & Igaz, L. M. (2020). Cytoplasmic Expression of the ALS/FTD-Related Protein TDP-43 Decreases Global Translation Both in vitro and in vivo. *Frontiers in Cellular Neuroscience*, *14*. https://doi.org/10.3389/fncel.2020.594561

Chen, S., Sayana, P., Zhang, X., & Le, W. (2013). Genetics of amyotrophic lateral sclerosis: An update. In *Molecular Neurodegeneration* (Vol. 8, Issue 1). https://doi.org/10.1186/1750-1326-8-28

Chen-Plotkin, A. S., Lee, V. M. Y., & Trojanowski, J. Q. (2010). TAR DNA-binding protein 43 in neurodegenerative disease. In *Nature Reviews Neurology* (Vol. 6, Issue 4). https://doi.org/10.1038/nrneurol.2010.18

Chen, Y., Lin, Z., Chen, X., Cao, B., Wei, Q., Ou, R., Zhao, B., Song, W., Wu, Y., Shang, H.-F. (2016). Large C9orf72 repeat expansions are seen in Chinese patients with sporadic amyotrophic lateral sclerosis. *Neurobiology of Aging*, *38*, 217.e15–217.e22. https://doi.org/10.1016/j.neurobiolaging.2015.11.016

Chhipi-Shrestha, J. K., Yoshida, M., & Iwasaki, S. (2022). Filter trapping protocol to detect aggregated proteins in human cell lines. *STAR Protocols*, *3*(3). https://doi.org/10.1016/j.xpro.2022.101571

Chiò, A., Logroscino, G., Traynor, B. J., Collins, J., Simeone, J. C., Goldstein, L. A., & White, L. A. (2013). Global epidemiology of amyotrophic lateral sclerosis: A systematic review of the published literature. In *Neuroepidemiology* (Vol. 41, Issue 2). https://doi.org/10.1159/000351153

Ciechanover, A., & Kwon, Y. T. (2015). Degradation of misfolded proteins in neurodegenerative diseases: therapeutic targets and strategies. In *Experimental and Molecular Medicine* (Vol. 47, Issue 3). https://doi.org/10.1038/EMM.2014.117

Cirulli, E. T., Lasseigne, B. N., Petrovski, S., Sapp, P. C., Dion, P. A., Leblond, C. S., Couthouis, J., Lu, Y. F., Wang, Q., Krueger, B. J., Ren, Z., Keebler, J., Han, Y., Levy, S. E., Boone, B. E.,

Wimbish, J. R., Waite, L. L., Jones, A. L., Carulli, J. P., … Muñoz-Blanco, J. L. (2015). Exome sequencing in amyotrophic lateral sclerosis identifies risk genes and pathways. *Science*, *347*(6229). https://doi.org/10.1126/science.aaa3650

Clark, J. A., Yeaman, E. J., Blizzard, C. A., Chuckowree, J. A., & Dickson, T. C. (2016). A Case for Microtubule Vulnerability in Amyotrophic Lateral Sclerosis: Altered Dynamics During Disease. *Frontiers in Cellular Neuroscience*, *10*. https://doi.org/10.3389/fncel.2016.00204

Coelho, M. A., Cooper, S., Strauss, M. E., Karakoc, E., Bhosle, S., Gonçalves, E., Picco, G., Burgold, T., Cattaneo, C. M., Veninga, V., Consonni, S., Dinçer, C., Vieira, S. F., Gibson, F., Barthorpe, S., Hardy, C., Rein, J., Thomas, M., Marioni, J., … Garnett, M. J. (2023). Base editing screens map mutations affecting interferon-γ signaling in cancer. *Cancer Cell*, *41*(2). https://doi.org/10.1016/j.ccell.2022.12.009

Colombrita, C., Onesto, E., Megiorni, F., Pizzuti, A., Baralle, F. E., Buratti, E., Silani, V., & Ratti, A. (2012). TDP-43 and FUS RNA-binding proteins bind distinct sets of cytoplasmic messenger RNAs and differently regulate their post-transcriptional fate in motoneuron-like cells. *Journal of Biological Chemistry*, *287*(19). https://doi.org/10.1074/jbc.M111.333450

Cookson, M. R. (2010). The role of leucine-rich repeat kinase 2 (LRRK2) in Parkinson's disease. In *Nature Reviews Neuroscience* (Vol. 11, Issue 12). https://doi.org/10.1038/nrn2935

Cooper, Y. A., Guo, Q., & Geschwind, D. H. (2022). Multiplexed functional genomic assays to decipher the noncoding genome. In *Human Molecular Genetics* (Vol. 31, Issue R1). https://doi.org/10.1093/hmg/ddac194

Cruts, M., Theuns, J., & Van Broeckhoven, C. (2012). Locus-specific mutation databases for neurodegenerative brain diseases. *Human Mutation*, *33*(9). https://doi.org/10.1002/humu.22117

D'Alessio, A. C., Fan, Z. P., Wert, K. J., Baranov, P., Cohen, M. A., Saini, J. S., Cohick, E., Charniga, C., Dadon, D., Hannett, N. M., Young, M. J., Temple, S., Jaenisch, R., Lee, T. I., & Young, R. A. (2015). A systematic approach to identify candidate transcription factors that control cell identity. *Stem Cell Reports*, *5*(5). https://doi.org/10.1016/j.stemcr.2015.09.016

D'Ambrogio, A., Buratti, E., Stuani, C., Guarnaccia, C., Romano, M., Ayala, Y. M., & Baralle, F. E. (2009). Functional mapping of the interaction between TDP-43 and hnRNP A2 in vivo. *Nucleic Acids Research*, *37*(12). https://doi.org/10.1093/nar/gkp342

Das, S., Singer, R. H., & Yoon, Y. J. (2019). The travels of mRNAs in neurons: do they know where they are going? In *Current Opinion in Neurobiology* (Vol. 57). https://doi.org/10.1016/j.conb.2019.01.016

Datlinger, P., Rendeiro, A. F., Schmidl, C., Krausgruber, T., Traxler, P., Klughammer, J., Schuster, L. C., Kuchler, A., Alpar, D., & Bock, C. (2017). Pooled CRISPR screening with single-cell transcriptome readout. *Nature Methods*, *14*(3). https://doi.org/10.1038/nmeth.4177

Day, S., Roberts, S., Launder, N. H., Goh, A. M. Y., Draper, B., Bahar-Fuchs, A., Loi, S.M, Laver, K., Withall, A., Cations, M. (2022). Age of Symptom Onset and Longitudinal Course of Sporadic Alzheimer's Disease, Frontotemporal Dementia, and Vascular Dementia: A Systematic Review and Meta-Analysis. *Journal of Alzheimer's Disease*, *85*(4), 1819–1833. https://doi.org/10.3233/jad-215360

De Boer, E. M. J., Orie, V. K., Williams, T., Baker, M. R., De Oliveira, H. M., Polvikoski, T., Silsby, M., Menon, P., Van Den Bos, M., Halliday, G. M., Van Den Berg, L. H., Van Den Bosch, L., Van Damme, P., Kiernan, M., Van Es, M. A., & Vucic, S. (2021). TDP-43 proteinopathies: A

new wave of neurodegenerative diseases. In *Journal of Neurology, Neurosurgery and Psychiatry* (Vol. 92, Issue 1). https://doi.org/10.1136/jnnp-2020-322983

Deng, H. X., Chen, W., Hong, S. T., Boycott, K. M., Gorrie, G. H., Siddique, N., Yang, Y., Fecto, F., Shi, Y., Zhai, H., Jiang, H., Hirano, M., Rampersaud, E., Jansen, G. H., Donkervoort, S., Bigio, E. H., Brooks, B. R., Ajroud, K., Sufit, R. L., … Siddique, T. (2011). Mutations in UBQLN2 cause dominant X-linked juvenile and adult-onset ALS and ALS/dementia. *Nature*, *477*(7363). https://doi.org/10.1038/nature10353

Deture, M. A., & Dickson, D. W. (2019). The neuropathological diagnosis of Alzheimer's disease. In *Molecular Neurodegeneration* (Vol. 14, Issue 1). https://doi.org/10.1186/s13024-019-0333-5

Dickson, S. P., Wang, K., Krantz, I., Hakonarson, H., & Goldstein, D. B. (2010). Rare Variants Create Synthetic Genome-Wide Associations. *PLoS Biology*, *8*(1). https://doi.org/10.1371/journal.pbio.1000294

Dimas, A. S., Deutsch, S., Stranger, B. E., Montgomery, S. B., Borel, C., Attar-Cohen, H., Ingle, C., Beazley, C., Arcelus, M. G., Sekowska, M., Gagnebin, M., Nisbett, J., Deloukas, P., Dermitzakis, E. T., & Antonarakis, S. E. (2009). Common regulatory variation impacts gene expression in a cell type-dependent manner. *Science*, *325*(5945). https://doi.org/10.1126/science.1174148

Dobin, A., Davis, C. A., Schlesinger, F., Drenkow, J., Zaleski, C., Jha, S., Batut, P., Chaisson, M., & Gingeras, T. R. (2013). STAR: Ultrafast universal RNA-seq aligner. *Bioinformatics*. https://doi.org/10.1093/bioinformatics/bts635

Dou, D., Smith, E. M., Evans, C. S., Boecker, C. A., & Holzbaur, E. L. F. (2023). Regulatory imbalance between LRRK2 kinase, PPM1H phosphatase, and ARF6 GTPase disrupts the axonal transport of autophagosomes. *Cell Reports*, *42*(5). https://doi.org/10.1016/j.celrep.2023.112448

Dräger, N. M., Sattler, S. M., Huang, C. T. L., Teter, O. M., Leng, K., Hashemi, S. H., Hong, J., Aviles, G., Clelland, C. D., Zhan, L., Udeochu, J. C., Kodama, L., Singleton, A. B., Nalls, M. A., Ichida, J., Ward, M. E., Faghri, F., Gan, L., & Kampmann, M. (2022). A CRISPRi/a platform in human iPSC-derived microglia uncovers regulators of disease states. *Nature Neuroscience*, *25*(9). https://doi.org/10.1038/s41593-022-01131-4

Duan, L., Zaepfel, B. L., Aksenova, V., Dasso, M., Rothstein, J. D., Kalab, P., & Hayes, L. R. (2022). Nuclear RNA binding regulates TDP-43 nuclear localization and passive nuclear export. *Cell Reports*, *40*(3). https://doi.org/10.1016/j.celrep.2022.111106

Ederle, H., & Dormann, D. (2017). TDP-43 and FUS en route from the nucleus to the cytoplasm. In *FEBS Letters* (Vol. 591, Issue 11). https://doi.org/10.1002/1873-3468.12646

Elahi, F. M., Marx, G., Cobigo, Y., Staffaroni, A. M., Kornak, J., Tosun, D., Boxer, A. L., Kramer, J. H., Miller, B. L., Rosen, H. J. (2017). Longitudinal white matter change in frontotemporal dementia subtypes and sporadic late onset Alzheimer's disease. *NeuroImage: Clinical*, *16*, 595–603. https://doi.org/10.1016/j.nicl.2017.09.007

Elden, A. C., Kim, H. J., Hart, M. P., Chen-Plotkin, A. S., Johnson, B. S., Fang, X., Armakola, M., Geser, F., Greene, R., Lu, M. M., Padmanabhan, A., Clay-Falcone, D., McCluskey, L., Elman, L., Juhr, D., Gruber, P. J., Rüb, U., Auburger, G., Trojanowski, J. Q., … Gitler, A. D. (2010). Ataxin-2 intermediate-length polyglutamine expansions are associated with increased risk for ALS. *Nature*, *466*(7310). https://doi.org/10.1038/nature09320

Engelhardt, J. I., Tajti, J., & Appel, S. H. (1993). Lymphocytic Infiltrates in the Spinal Cord in Amyotrophic Lateral Sclerosis. *Archives of Neurology*. https://doi.org/10.1001/archneur.1993.00540010026013

Fattorelli, N., Martinez-Muriana, A., Wolfs, L., Geric, I., De Strooper, B., & Mancuso, R. (2021). Stem-cell-derived human microglia transplanted into mouse brain to study human disease. *Nature Protocols*, *16*(2). https://doi.org/10.1038/s41596-020-00447-4

Fecto, F., Yan, J., Vemula, S. P., Liu, E., Yang, Y., Chen, W., Zheng, J. G., Shi, Y., Siddique, N., Arrat, H., Donkervoort, S., Ajroud-Driss, S., Sufit, R. L., Heller, S. L., Deng, H. X., & Siddique, T. (2011). SQSTM1 mutations in familial and sporadic amyotrophic lateral sclerosis. *Archives of Neurology*, *68*(11). https://doi.org/10.1001/archneurol.2011.250

Feldman, D., Singh, A., Schmid-Burgk, J. L., Carlson, R. J., Mezger, A., Garrity, A. J., Zhang, F., & Blainey, P. C. (2019). Optical Pooled Screens in Human Cells. *Cell*. https://doi.org/10.1016/j.cell.2019.09.016

Fernandopulle, M. S., Prestil, R., Grunseich, C., Wang, C., Gan, L., & Ward, M. E. (2018). Transcription Factor–Mediated Differentiation of Human iPSCs into Neurons. *Current Protocols in Cell Biology*. https://doi.org/10.1002/cpcb.51

Fiesel, F. C., Voigt, A., Weber, S. S., Van Den Haute, C., Waldenmaier, A., Görner, K., Walter, M., Marlene, A. L., Kern, J. V., Rasse, T. M., Schmidt, T., Springer, W., Kirchner, R., Bonin, M., Neumann, M., Baekelandt, V., Alunni-Fabbroni, M., Schulz, J. B., & Kahle, P. J. (2010). Knockdown of transactive response DNA-binding protein (TDP-43) downregulates histone deacetylase 6. *EMBO Journal*, *29*(1). https://doi.org/10.1038/emboj.2009.324

Eom, T., Zhang, C., Wang, H., Lay, K., Fak, J., Noebels, J. L., & Darnell, R. B. (2013). NOVA-dependent regulation of cryptic NMD exons controls synaptic protein levels after seizure. *ELife*, *2*. https://doi.org/10.7554/elife.00178

Freibaum, B. D., Chitta, R. K., High, A. A., & Taylor, J. P. (2010). Global analysis of TDP-43 interacting proteins reveals strong association with RNA splicing and translation machinery. *Journal of Proteome Research*, *9*(2). https://doi.org/10.1021/pr901076y

Freischmidt, A., Wieland, T., Richter, B., Ruf, W., Schaeffer, V., Müller, K., Marroquin, N., Nordin, F., Hübers, A., Weydt, P., Pinto, S., Press, R., Millecamps, S., Molko, N., Bernard, E., Desnuelle, C., Soriani, M. H., Dorst, J., Graf, E., … Weishaupt, J. H. (2015). Haploinsufficiency of TBK1 causes familial ALS and fronto-temporal dementia. *Nature Neuroscience*, *18*(5). https://doi.org/10.1038/nn.4000

Fu, H., Hardy, J., & Duff, K. E. (2018). Selective vulnerability in neurodegenerative diseases. In *Nature Neuroscience* (Vol. 21, Issue 10). https://doi.org/10.1038/s41593-018-0221-2

Gami-Patel, P., van Dijken, I., van Swieten, J. C., Pijnenburg, Y. A. L., Rozemuller, A. J. M., Hoozemans, J. J. M., & Dijkstra, A. A. (2019). Von Economo neurons are part of a larger neuronal population that are selectively vulnerable in C9orf72 frontotemporal dementia. In *Neuropathology and Applied Neurobiology* (Vol. 45, Issue 7). https://doi.org/10.1111/nan.12558

Gasset-Rosa, F., Lu, S., Yu, H., Chen, C., Melamed, Z., Guo, L., Shorter, J., Da Cruz, S., & Cleveland, D. W. (2019). Cytoplasmic TDP-43 De-mixing Independent of Stress Granules Drives Inhibition of Nuclear Import, Loss of Nuclear TDP-43, and Cell Death. *Neuron*, *102*(2), 339-357.e7. https://doi.org/10.1016/j.neuron.2019.02.038

Gate, D., Tapp, E., Leventhal, O., Shahid, M., Nonninger, T. J., Yang, A. C., Strempfl, K., Unger, M. S., Fehlmann, T., Oh, H., Channappa, D., Henderson, V. W., Keller, A., Aigner, L., Galasko, D. R., Davis, M. M., Poston, K. L., & Wyss-Coray, T. (2021). CD4+ T cells contribute to neurodegeneration in Lewy body dementia. *Science*. https://doi.org/10.1126/science.abf7266

Gendron, T. F., Daughrity, L. M., Heckman, M. G., Diehl, N. N., Wuu, J., Miller, T. M., Pastor, P., Trojanowski, J. Q., Grossman, M., Berry, J. D., Hu, W. T., Ratti, A., Banatar, M., Silani, V., Glass, J. D., Floeter, M. K., Jeromin, A., Boylan, K. B., Petrucelli, L. (2017). Phosphorylated neurofilament heavy chain: A biomarker of survival for *C9ORF 72* -associated amyotrophic lateral sclerosis. *Annals of Neurology*, *82*(1), 139–146. https://doi.org/10.1002/ana.24980

Ge, S. X., Jung, D., Jung, D., & Yao, R. (2020). ShinyGO: A graphical gene-set enrichment tool for animals and plants. *Bioinformatics*. https://doi.org/10.1093/bioinformatics/btz931

Gittings, L. M., Alsop, E. B., Antone, J., Singer, M., Whitsett, T. G., Sattler, R., & Van Keuren-Jensen, K. (2023). Cryptic exon detection and transcriptomic changes revealed in single-nuclei RNA sequencing of C9ORF72 patients spanning the ALS-FTD spectrum. *Acta Neuropathologica*, *146*(3). https://doi.org/10.1007/s00401-023-02599-5

Graves, M. C., Fiala, M., Dinglasan, L. A. V., Liu, N. Q., Sayre, J., Chiappelli, F., van Kooten, C., & Vinters, H. V. (2004). Inflammation in amyotrophic lateral sclerosis spinal cord and brain is mediated by activated macrophages, mast cells and t cells. *Amyotrophic Lateral Sclerosis and Other Motor Neuron Disorders*. https://doi.org/10.1080/14660820410020286

Guerra San Juan, I., Nash, L. A., Smith, K. S., Leyton-Jaimes, M. F., Qian, M., Klim, J. R., Limone, F., Dorr, A. B., Couto, A., Pintacuda, G., Joseph, B. J., Whisenant, D. E., Noble, C., Melnik, V., Potter, D., Holmes, A., Burberry, A., Verhage, M., & Eggan, K. (2022). Loss of mouse Stmn2 function causes motor neuropathy. *Neuron*, *110*(10). https://doi.org/10.1016/j.neuron.2022.02.011

Guise, A. J., Misal, S. A., Carson, R., Chu, J. H., Boekweg, H., Van Der Watt, D., Welsh, N. C., Truong, T., Liang, Y., Xu, S., Benedetto, G., Gagnon, J., Payne, S. H., Plowey, E. D., & Kelly, R. T. (2024). TDP-43-stratified single-cell proteomics of postmortem human spinal motor neurons

reveals protein dynamics in amyotrophic lateral sclerosis. *Cell Reports*, *43*(1). https://doi.org/10.1016/j.celrep.2023.113636

Günther, R., Krause, E., Schümann, M., Blasig, I. E., & Haseloff, R. F. (2015). Depletion of highly abundant proteins from human cerebrospinal fluid: A cautionary note. In *Molecular Neurodegeneration* (Vol. 10, Issue 1). https://doi.org/10.1186/s13024-015-0050-7

Guven, G., Lohmann, E., Bras, J., Gibbs, J. R., Gurvit, H., Bilgic, B., Hanagasi, H., Rizzu, P., Heutink, P., Emre, M., Erginel-Unaltuna, N., Just, W., Hardy, J., Singleton, A., & Guerreiro, R. (2016). Mutation frequency of the major frontotemporal dementia genes, MAPT, GRN and C9ORF72 in a Turkish cohort of dementia patients. *PLoS ONE*, *11*(9). https://doi.org/10.1371/journal.pone.0162592

Hallegger, M., Chakrabarti, A. M., Lee, F. C. Y., Lee, B. L., Amalietti, A. G., Odeh, H. M., Copley, K. E., Rubien, J. D., Portz, B., Kuret, K., Huppertz, I., Rau, F., Patani, R., Fawzi, N. L., Shorter, J., Luscombe, N. M., & Ule, J. (2021). TDP-43 condensation properties specify its RNA-binding and regulatory repertoire. *Cell*. https://doi.org/10.1016/j.cell.2021.07.018

Halliday, G., Bigio, E. H., Cairns, N. J., Neumann, M., MacKenzie, I. R. A., & Mann, D. M. A. (2012). Mechanisms of disease in frontotemporal lobar degeneration: Gain of function versus loss of function effects. In *Acta Neuropathologica*. https://doi.org/10.1007/s00401-012-1030-4

Hansson, O. (2021). Biomarkers for neurodegenerative diseases. In *Nature Medicine* (Vol. 27, Issue 6). https://doi.org/10.1038/s41591-021-01382-x

Hasegawa, M., Arai, T., Akiyama, H., Nonaka, T., Mori, H., Hashimoto, T., Yamazaki, M., & Oyanagi, K. (2007). TDP-43 is deposited in the Guam parkinsonism-dementia complex brains. *Brain*, *130*(5). https://doi.org/10.1093/brain/awm065

Hayes, L. R., & Kalab, P. (2022). Emerging Therapies and Novel Targets for TDP-43 Proteinopathy in ALS/FTD. In *Neurotherapeutics* (Vol. 19, Issue 4). https://doi.org/10.1007/s13311-022-01260-5

Higginbotham, L., Ping, L., Dammer, E. B., Duong, D. M., Zhou, M., Gearing, M., Hurst, C., Glass, J. D., Factor, S. A., Johnson, E. C. B., Hajjar, I., Lah, J. J., Levey, A. I., & Seyfried, N. T. (2020). Integrated proteomics reveals brain-based cerebrospinal fluid biomarkers in asymptomatic and symptomatic Alzheimer's disease. *Science Advances*. https://doi.org/10.1126/sciadv.aaz9360

Hindorff, L. A., Sethupathy, P., Junkins, H. A., Ramos, E. M., Mehta, J. P., Collins, F. S., & Manolio, T. A. (2009). Potential etiologic and functional implications of genome-wide association loci for human diseases and traits. *Proceedings of the National Academy of Sciences of the United States of America*, *106*(23). https://doi.org/10.1073/pnas.0903103106

Hirokawa, N. (1993). Axonal transport and the cytoskeleton. *Current Opinion in Neurobiology*, *3*(5). https://doi.org/10.1016/0959-4388(93)90144-N

Huisman, M. H. B., De Jong, S. W., Van Doormaal, P. T. C., Weinreich, S. S., Schelhaas, H. J., Van Der Kooi, A. J., De Visser, M., Veldink, J. H., & Van Den Berg, L. H. (2011). Population based epidemiology of amyotrophic lateral sclerosis using capture-recapture methodology. *Journal of Neurology, Neurosurgery and Psychiatry*, *82*(10). https://doi.org/10.1136/jnnp.2011.244939

Humphrey, J., Emmett, W., Fratta, P., Isaacs, A. M., & Plagnol, V. (2017). Quantitative analysis of cryptic splicing associated with TDP-43 depletion. *BMC Medical Genomics*. https://doi.org/10.1186/s12920-017-0274-1

Hutton, M., Lendon, C. L., Rizzu, P., Baker, M., Froelich, S., Houlden, H. H., Pickering-Brown, S., Chakraverty, S., Isaacs, A., Grover, A., Hackett, J., Adamson, J., Lincoln, S., Dickson, D., Davies, P., Petersen, R. C., Stevena, M., De Graaff, E., Wauters, E., … Heutink, P. (1998).

Association of missense and 5'-splice-site mutations in tau with the inherited dementia FTDP-17. *Nature*, *393*(6686). https://doi.org/10.1038/31508

Iguchi, Y., Katsuno, M., Niwa, J. I., Takagi, S., Ishigaki, S., Ikenaka, K., Kawai, K., Watanabe, H., Yamanaka, K., Takahashi, R., Misawa, H., Sasaki, S., Tanaka, F., & Sobue, G. (2013). Loss of TDP-43 causes age-dependent progressive motor neuron degeneration. *Brain*. https://doi.org/10.1093/brain/awt029

Irwin, D. J., Cairns, N. J., Grossman, M., McMillan, C. T., Lee, E. B., Van Deerlin, V. M., Lee, V. M-Y, Trojanowski, J. Q. (2014). Frontotemporal lobar degeneration: defining phenotypic diversity through personalized medicine. *Acta Neuropathologica*, *129*(4), 469–491. https://doi.org/10.1007/s00401-014-1380-1

Irwin, K. E., Jasin, P., Braunstein, K. E., Sinha, I. R., Garret, M. A., Bowden, K. D., Chang, K., Troncoso, J. C., Moghekar, A., Oh, E. S., Raitcheva, D., Bartlett, D., Miller, T., Berry, J. D., Traynor, B. J., Ling, J. P., & Wong, P. C. (2024). A fluid biomarker reveals loss of TDP-43 splicing repression in presymptomatic ALS–FTD. *Nature Medicine*, *30*(2). https://doi.org/10.1038/s41591-023-02788-5

Jeong, Y. H., Ling, J. P., Lin, S. Z., Donde, A. N., Braunstein, K. E., Majounie, E., Traynor, B. J., LaClair, K. D., Lloyd, T. E., & Wong, P. C. (2017). Tdp-43 cryptic exons are highly variable between cell types. *Molecular Neurodegeneration*. https://doi.org/10.1186/s13024-016-0144-x

Jiang, L. L., Xue, W., Hong, J. Y., Zhang, J. T., Li, M. J., Yu, S. N., He, J. H., & Hu, H. Y. (2017). The N-terminal dimerization is required for TDP-43 splicing activity. *Scientific Reports*, *7*(1). https://doi.org/10.1038/s41598-017-06263-3

Jiang, L. L., Zhao, J., Yin, X. F., He, W. T., Yang, H., Che, M. X., & Hu, H. Y. (2016). Two mutations G335D and Q343R within the amyloidogenic core region of TDP-43 influence its aggregation and inclusion formation. *Scientific Reports*, *6*. https://doi.org/10.1038/srep23928

Johnson, E. C. B., Dammer, E. B., Duong, D. M., Ping, L., Zhou, M., Yin, L., Higginbotham, L. A., Guajardo, A., White, B., Troncoso, J. C., Thambisetty, M., Montine, T. J., Lee, E. B., Trojanowski, J. Q., Beach, T. G., Reiman, E. M., Haroutunian, V., Wang, M., Schadt, E., … Seyfried, N. T. (2020). Large-scale proteomic analysis of Alzheimer's disease brain and cerebrospinal fluid reveals early changes in energy metabolism associated with microglia and astrocyte activation. *Nature Medicine*, *26*(5), 769–780. https://doi.org/10.1038/s41591-020-0815-6

Josephs, K. A., Hodges, J. R., Snowden, J. S., MacKenzie, I. R., Neumann, M., Mann, D. M., & Dickson, D. W. (2011). Neuropathological background of phenotypical variability in frontotemporal dementia. In *Acta Neuropathologica* (Vol. 122, Issue 2). https://doi.org/10.1007/s00401-011-0839-6

Josephs, K. A., Murray, M. E., Whitwell, J. L., Parisi, J. E., Petrucelli, L., Jack, C. R., Petersen, R. C., & Dickson, D. W. (2014). Staging TDP-43 pathology in Alzheimer's disease. *Acta Neuropathologica*. https://doi.org/10.1007/s00401-013-1211-9

Kabashi, E., Valdmanis, P. N., Dion, P., Spiegelman, D., McConkey, B. J., Velde, C. Vande, Bouchard, J. P., Lacomblez, L., Pochigaeva, K., Salachas, F., Pradat, P. F., Camu, W., Meininger, V., Dupre, N., & Rouleau, G. A. (2008). TARDBP mutations in individuals with sporadic and familial amyotrophic lateral sclerosis. *Nature Genetics*, *40*(5). https://doi.org/10.1038/ng.132

Karch, C. M., Kao, A. W., Karydas, A., Onanuga, K., Martinez, R., Argouarch, A., Wang, C., Huang, C., Sohn, P. D., Bowles, K. R., Spina, S., Silva, M. C., Marsh, J. A., Hsu, S., Pugh, D. A.,

Ghoshal, N., Norton, J., Huang, Y., Lee, S. E., … Kampmann, M. (2019). A Comprehensive Resource for Induced Pluripotent Stem Cells from Patients with Primary Tauopathies. *Stem Cell Reports*, *13*(5). https://doi.org/10.1016/j.stemcr.2019.09.006

Kawakami, I., Arai, T., & Hasegawa, M. (2019). The basis of clinicopathological heterogeneity in TDP-43 proteinopathy. *Acta Neuropathologica*, *138*(5), 751–770. https://doi.org/10.1007/s00401-019-02077-x

Kersaitis, C., Halliday, G. M., & Kril, J. J. (2004). Regional and cellular pathology in frontotemporal dementia: Relationship to stage of disease in cases with and without Pick bodies. *Acta Neuropathologica*, *108*(6). https://doi.org/10.1007/s00401-004-0917-0

Kiebler, M. A., & Bassell, G. J. (2006). Neuronal RNA Granules: Movers and Makers. In *Neuron* (Vol. 51, Issue 6). https://doi.org/10.1016/j.neuron.2006.08.021

Kiernan, M. C., Vucic, S., Cheah, B. C., Turner, M. R., Eisen, A., Hardiman, O., Burrell, J. R., & Zoing, M. C. (2011). Amyotrophic lateral sclerosis. *The Lancet*, *377*(9769). https://doi.org/10.1016/S0140-6736(10)61156-7

Kilpinen, H., Goncalves, A., Leha, A., Afzal, V., Alasoo, K., Ashford, S., Bala, S., Bensaddek, D., Casale, F. P., Culley, O. J., Danecek, P., Faulconbridge, A., Harrison, P. W., Kathuria, A., McCarthy, D., McCarthy, S. A., Meleckyte, R., Memari, Y., Moens, N., … Gaffney, D. J. (2017). Common genetic variation drives molecular heterogeneity in human iPSCs. *Nature*, *546*(7658). https://doi.org/10.1038/nature22403

Kim, H. J., Kim, N. C., Wang, Y. D., Scarborough, E. A., Moore, J., Diaz, Z., MacLea, K. S., Freibaum, B., Li, S., Molliex, A., Kanagaraj, A. P., Carter, R., Boylan, K. B., Wojtas, A. M., Rademakers, R., Pinkus, J. L., Greenberg, S. A., Trojanowski, J. Q., Traynor, B. J., … Taylor, J.

P. (2013). Mutations in prion-like domains in hnRNPA2B1 and hnRNPA1 cause multisystem proteinopathy and ALS. *Nature*, *495*(7442). https://doi.org/10.1038/nature11922

Kim, S. H., Shanware, N. P., Bowler, M. J., & Tibbetts, R. S. (2010). Amyotrophic lateral sclerosis-associated proteins TDP-43 and FUS/TLS function in a common biochemical complex to co-regulate HDAC6 mRNA. *Journal of Biological Chemistry*, *285*(44). https://doi.org/10.1074/jbc.M110.154831

Kipps, C. M., Hodges, J. R., & Hornberger, M. (2010). Nonprogressive behavioural frontotemporal dementia: recent developments and clinical implications of the "bvFTD phenocopy syndrome." *Current Opinion in Neurology*, *23*(6), 628–632. https://doi.org/10.1097/wco.0b013e3283404309

Klein, J. C., Agarwal, V., Inoue, F., Keith, A., Martin, B., Kircher, M., Ahituv, N., & Shendure, J. (2020). A systematic evaluation of the design and context dependencies of massively parallel reporter assays. *Nature Methods*, *17*(11). https://doi.org/10.1038/s41592-020-0965-y

Klim, J. R., Williams, L. A., Limone, F., Guerra San Juan, I., Davis-Dusenbery, B. N., Mordes, D. A., Burberry, A., Steinbaugh, M. J., Gamage, K. K., Kirchner, R., Moccia, R., Cassel, S. H., Chen, K., Wainger, B. J., Woolf, C. J., & Eggan, K. (2019). ALS-implicated protein TDP-43 sustains levels of STMN2, a mediator of motor neuron growth and repair. *Nature Neuroscience*. https://doi.org/10.1038/s41593-018-0300-4

Knopman, D. S., Kramer, J. H., Boeve, B. F., Caselli, R. J., Graff-Radford, N. R., Mendez, M. F., Miller, B. L., Mercaldo, N. (2008). Development of methodology for conducting clinical trials in frontotemporal lobar degeneration. *Brain*, *131*(11), 2957–2968. https://doi.org/10.1093/brain/awn234

Knopman, D. S., & Roberts, R. O. (2011). Estimating the number of persons with frontotemporal lobar degeneration in the US population. *Journal of Molecular Neuroscience*, *45*(3). https://doi.org/10.1007/s12031-011-9538-y

Korobeynikov, V. A., Lyashchenko, A. K., Blanco-Redondo, B., Jafar-Nejad, P., & Shneider, N. A. (2022). Antisense oligonucleotide silencing of FUS expression as a therapeutic approach in amyotrophic lateral sclerosis. *Nature Medicine*, *28*(1). https://doi.org/10.1038/s41591-021-01615-z

Kovaka, S., Zimin, A. V., Pertea, G. M., Razaghi, R., Salzberg, S. L., & Pertea, M. (2019). Transcriptome assembly from long-read RNA-seq alignments with StringTie2. *Genome Biology*. https://doi.org/10.1186/s13059-019-1910-1

Krichevsky, A. M., & Kosik, K. S. (2001). Neuronal RNA granules: A link between RNA localization and stimulation-dependent translation. *Neuron*, *32*(4). https://doi.org/10.1016/S0896-6273(01)00508-6

Krus, K. L., Strickland, A., Yamada, Y., Devault, L., Schmidt, R. E., Bloom, A. J., Milbrandt, J., & DiAntonio, A. (2022). Loss of Stathmin-2, a hallmark of TDP-43-associated ALS, causes motor neuropathy. *Cell Reports*, *39*(13). https://doi.org/10.1016/j.celrep.2022.111001

Kuo, P. H., Chiang, C. H., Wang, Y. T., Doudeva, L. G., & Yuan, H. S. (2014). The crystal structure of TDP-43 RRM1-DNA complex reveals the specific recognition for UG- and TG-rich nucleic acids. *Nucleic Acids Research*, *42*(7). https://doi.org/10.1093/nar/gkt1407

Kvon, E. Z., Kazmar, T., Stampfel, G., Yáñez-Cuna, J. O., Pagani, M., Schernhuber, K., Dickson, B. J., & Stark, A. (2014). Genome-scale functional characterization of Drosophila developmental enhancers in vivo. *Nature*, *512*(1). https://doi.org/10.1038/nature13395

Kwiatkowski, T. J., Bosco, D. A., LeClerc, A. L., Tamrazian, E., Vanderburg, C. R., Russ, C., Davis, A., Gilchrist, J., Kasarskis, E. J., Munsat, T., Valdmanis, P., Rouleau, G. A., Hosler, B. A., Cortelli, P., De Jong, P. J., Yoshinaga, Y., Haines, J. L., Pericak-Vance, M. A., Yan, J., … Brown, R. H. (2009). Mutations in the FUS/TLS gene on chromosome 16 cause familial amyotrophic lateral sclerosis. *Science*, *323*(5918). https://doi.org/10.1126/science.1166066

Lagomarsino, V. N., Pearse, R. V., Liu, L., Hsieh, Y. C., Fernandez, M. A., Vinton, E. A., Paull, D., Felsky, D., Tasaki, S., Gaiteri, C., Vardarajan, B., Lee, H., Muratore, C. R., Benoit, C. R., Chou, V., Fancher, S. B., He, A., Merchant, J. P., Duong, D. M., … Young-Pearse, T. L. (2021). Stem cell-derived neurons reflect features of protein networks, neuropathology, and cognitive outcome of their aged human donors. *Neuron*, *109*(21). https://doi.org/10.1016/j.neuron.2021.08.003

Langmead, B., & Salzberg, S. L. (2012). Fast gapped-read alignment with Bowtie 2. *Nature Methods*. https://doi.org/10.1038/nmeth.1923

Langston, R. G., Beilina, A., Reed, X., Kaganovich, A., Singleton, A. B., Blauwendraat, C., Gibbs, J. R., & Cookson, M. R. (2022). Association of a common genetic variant with Parkinson's disease is mediated by microglia. *Science Translational Medicine*, *14*(655), eabp8869. https://doi.org/10.1126/scitranslmed.abp8869

Lanz, T. V., Brewer, R. C., Ho, P. P., Moon, J. S., Jude, K. M., Fernandez, D., Fernandes, R. A., Gomez, A. M., Nadj, G. S., Bartley, C. M., Schubert, R. D., Hawes, I. A., Vazquez, S. E., Iyer, M., Zuchero, J. B., Teegen, B., Dunn, J. E., Lock, C. B., Kipp, L. B., … Robinson, W. H. (2022). Clonally expanded B cells in multiple sclerosis bind EBV EBNA1 and GlialCAM. *Nature*. https://doi.org/10.1038/s41586-022-04432-7

Le Gall, L., Anakor, E., Connolly, O., Vijayakumar, U. G., Duddy, W. J., & Duguez, S. (2020). Molecular and cellular mechanisms affected in als. In *Journal of Personalized Medicine* (Vol. 10, Issue 3). https://doi.org/10.3390/jpm10030101

Lee, E. B., Lee, V. M. Y., & Trojanowski, J. Q. (2012). Gains or losses: Molecular mechanisms of TDP43-mediated neurodegeneration. In *Nature Reviews Neuroscience*. https://doi.org/10.1038/nrn3121

Lehmkuhl, E. M., & Zarnescu, D. C. (2018). Lost in translation: Evidence for protein synthesis deficits in ALS/FTD and related neurodegenerative diseases. In *Advances in Neurobiology* (Vol. 20). https://doi.org/10.1007/978-3-319-89689-2_11

Li, H. (2018). Minimap2: Pairwise alignment for nucleotide sequences. *Bioinformatics*. https://doi.org/10.1093/bioinformatics/bty191

Li, H., Handsaker, B., Wysoker, A., Fennell, T., Ruan, J., Homer, N., Marth, G., Abecasis, G., & Durbin, R. (2009). The Sequence Alignment/Map format and SAMtools. *Bioinformatics*. https://doi.org/10.1093/bioinformatics/btp352

Li, Y., Ma, L., Wu, D., & Chen, G. (2021). Advances in bulk and single-cell multi-omics approaches for systems biology and precision medicine. *Briefings in Bioinformatics*, *22*(5). https://doi.org/10.1093/bib/bbab024

Ling, J. P., Pletnikova, O., Troncoso, J. C., & Wong, P. C. (2015). TDP-43 repression of nonconserved cryptic exons is compromised in ALS-FTD. *Science*. https://doi.org/10.1126/science.aab0983

Ling, S. C., Polymenidou, M., & Cleveland, D. W. (2013). Converging mechanisms in als and FTD: Disrupted RNA and protein homeostasis. In *Neuron*. https://doi.org/10.1016/j.neuron.2013.07.033

Liu, E. Y., Russ, J., Cali, C. P., Phan, J. M., Amlie-Wolf, A., & Lee, E. B. (2019). Loss of Nuclear TDP-43 Is Associated with Decondensation of LINE Retrotransposons. *Cell Reports*. https://doi.org/10.1016/j.celrep.2019.04.003

Liu, X., & Henty-Ridilla, J. L. (2022). Multiple roles for the cytoskeleton in ALS. *Experimental Neurology*, *355*. https://doi.org/10.1016/j.expneurol.2022.114143

Liu, Y., Yu, C., Daley, T. P., Wang, F., Cao, W. S., Bhate, S., Lin, X., Still, C., Liu, H., Zhao, D., Wang, H., Xie, X. S., Ding, S., Wong, W. H., Wernig, M., & Qi, L. S. (2018). CRISPR Activation Screens Systematically Identify Factors that Drive Neuronal Fate and Reprogramming. *Cell Stem Cell*, *23*(5). https://doi.org/10.1016/j.stem.2018.09.003

Logroscino, G., Traynor, B. J., Hardiman, O., Chió, A., Mitchell, D., Swingler, R. J., Millul, A., Benn, E., & Beghi, E. (2010). Incidence of amyotrophic lateral sclerosis in Europe. *Journal of Neurology, Neurosurgery and Psychiatry*, *81*(4). https://doi.org/10.1136/jnnp.2009.183525

Logroscino, G., Urso, D., & Tortelli, R. (2022). The challenge of amyotrophic lateral sclerosis descriptive epidemiology: to estimate low incidence rates across complex phenotypes in different geographic areas. *Current Opinion in Neurology*, *35*(5). https://doi.org/10.1097/WCO.0000000000001097

López-Erauskin, J., Bravo-Hernandez, M., Presa, M., Baughn, M. W., Melamed, Z., Beccari, M. S., Agra de Almeida Quadros, A. R., Arnold-Garcia, O., Zuberi, A., Ling, K., Platoshyn, O., Niño-Jara, E., Ndayambaje, I. S., McAlonis-Downes, M., Cabrera, L., Artates, J. W., Ryan, J., Hermann, A., Ravits, J., … Lagier-Tourenne, C. (2024). Stathmin-2 loss leads to neurofilament-dependent axonal collapse driving motor and sensory denervation. *Nature Neuroscience*, *27*(1). https://doi.org/10.1038/s41593-023-01496-0

Love, M. I., Huber, W., & Anders, S. (2014). Moderated estimation of fold change and dispersion for RNA-seq data with DESeq2. *Genome Biology*. https://doi.org/10.1186/s13059-014-0550-8

Lukavsky, P. J., Daujotyte, D., Tollervey, J. R., Ule, J., Stuani, C., Buratti, E., Baralle, F. E., Damberger, F. F., & Allain, F. H. T. (2013). Molecular basis of UG-rich RNA recognition by the human splicing factor TDP-43. *Nature Structural and Molecular Biology*, *20*(12). https://doi.org/10.1038/nsmb.2698

Ma, X. R., Prudencio, M., Koike, Y., Vatsavayai, S. C., Kim, G., Harbinski, F., Briner, A., Rodriguez, C. M., Guo, C., Akiyama, T., Schmidt, H. B., Cummings, B. B., Wyatt, D. W., Kurylo, K., Miller, G., Mekhoubad, S., Sallee, N., Mekonnen, G., Ganser, L., … Gitler, A. D. (2022). TDP-43 represses cryptic exon inclusion in the FTD–ALS gene UNC13A. *Nature*. https://doi.org/10.1038/s41586-022-04424-7

Macdonald, I. K., Parsy-Kowalska, C. B., & Chapman, C. J. (2017). Autoantibodies: Opportunities for Early Cancer Detection. In *Trends in Cancer*. https://doi.org/10.1016/j.trecan.2017.02.003

Mackenzie, I. R., Nicholson, A. M., Sarkar, M., Messing, J., Purice, M. D., Pottier, C., Annu, K., Baker, M., Perkerson, R. B., Kurti, A., Matchett, B. J., Mittag, T., Temirov, J., Hsiung, G. Y. R., Krieger, C., Murray, M. E., Kato, M., Fryer, J. D., Petrucelli, L., … Rademakers, R. (2017). TIA1 Mutations in Amyotrophic Lateral Sclerosis and Frontotemporal Dementia Promote Phase Separation and Alter Stress Granule Dynamics. *Neuron*, *95*(4). https://doi.org/10.1016/j.neuron.2017.07.025

MacLean, B., Tomazela, D. M., Shulman, N., Chambers, M., Finney, G. L., Frewen, B., Kern, R., Tabb, D. L., Liebler, D. C., & MacCoss, M. J. (2010). Skyline: An open source document editor for creating and analyzing targeted proteomics experiments. *Bioinformatics*. https://doi.org/10.1093/bioinformatics/btq054

Mansour, A. A., Gonçalves, J. T., Bloyd, C. W., Li, H., Fernandes, S., Quang, D., Johnston, S., Parylak, S. L., Jin, X., & Gage, F. H. (2018). An in vivo model of functional and vascularized human brain organoids. *Nature Biotechnology*, *36*(5). https://doi.org/10.1038/nbt.4127

Mao, C. P., Wang, S. C., Su, Y. P., Tseng, S. H., He, L., Wu, A. A., Roden, R. B. S., Xiao, J., & Hung, C. F. (2021). Protein detection in blood with single-molecule imaging. *Science Advances*. https://doi.org/10.1126/sciadv.abg6522

Maroof, A. M., Keros, S., Tyson, J. A., Ying, S. W., Ganat, Y. M., Merkle, F. T., Liu, B., Goulburn, A., Stanley, E. G., Elefanty, A. G., Widmer, H. R., Eggan, K., Goldstein, P. A., Anderson, S. A., & Studer, L. (2013). Directed differentiation and functional maturation of cortical interneurons from human embryonic stem cells. *Cell Stem Cell*, *12*(5). https://doi.org/10.1016/j.stem.2013.04.008

Martin, M. (2011). Cutadapt removes adapter sequences from high-throughput sequencing reads. *EMBnet.Journal*. https://doi.org/10.14806/ej.17.1.200

Martinez-Val, A., Bekker-Jensen, D. B., Hogrebe, A., & Olsen, J. V. (2021). Data Processing and Analysis for DIA-Based Phosphoproteomics Using Spectronaut. In *Methods in Molecular Biology*. https://doi.org/10.1007/978-1-0716-1641-3_6

Maruyama, H., Morino, H., Ito, H., Izumi, Y., Kato, H., Watanabe, Y., Kinoshita, Y., Kamada, M., Nodera, H., Suzuki, H., Komure, O., Matsuura, S., Kobatake, K., Morimoto, N., Abe, K., Suzuki, N., Aoki, M., Kawata, A., Hirai, T., … Kawakami, H. (2010). Mutations of optineurin in amyotrophic lateral sclerosis. *Nature*, *465*(7295). https://doi.org/10.1038/nature08971

Masrori, P., & Van Damme, P. (2020). Amyotrophic lateral sclerosis: a clinical review. In *European Journal of Neurology* (Vol. 27, Issue 10). https://doi.org/10.1111/ene.14393

Mattis, V. B., Svendsen, S. P., Ebert, A., Svendsen, C. N., King, A. R., Casale, M., Winokur, S. T., Batugedara, G., Vawter, M., Donovan, P. J., Lock, L. F., Thompson, L. M., Zhu, Y., Fossale, E., Atwal, R. S., Gillis, T., Mysore, J., Li, J. H., Seong, I., … Arjomand, J. (2012). Induced pluripotent stem cells from patients with huntington's disease show CAG repeat expansion associated phenotypes. *Cell Stem Cell*, *11*(2). https://doi.org/10.1016/j.stem.2012.04.027

Maurano, M. T., Humbert, R., Rynes, E., Thurman, R. E., Haugen, E., Wang, H., Reynolds, A. P., Sandstrom, R., Qu, H., Brody, J., Shafer, A., Neri, F., Lee, K., Kutyavin, T., Stehling-Sun, S., Johnson, A. K., Canfield, T. K., Giste, E., Diegel, M., … Stamatoyannopoulos, J. A. (2012). Systematic localization of common disease-associated variation in regulatory DNA. *Science*, *337*(6099). https://doi.org/10.1126/science.1222794

Mead, R. J., Shan, N., Reiser, H. J., Marshall, F., & Shaw, P. J. (2023). Amyotrophic lateral sclerosis: a neurodegenerative disorder poised for successful therapeutic translation. In *Nature Reviews Drug Discovery* (Vol. 22, Issue 3). https://doi.org/10.1038/s41573-022-00612-2

Medinas, D. B., Valenzuela, V., & Hetz, C. (2017). Proteostasis disturbance in amyotrophic lateral sclerosis. *Human Molecular Genetics*, *26*(R2), R91–R104. https://doi.org/10.1093/hmg/ddx274

Meeter, L. H., Dopper, E. G., Jiskoot, L. C., Sanchez-Valle, R., Graff, C., Benussi, L., … Öijerstedt, L. (2016). Neurofilament light chain: a biomarker for genetic frontotemporal dementia. *Annals of Clinical and Translational Neurology*, *3*(8), 623–636. https://doi.org/10.1002/acn3.325

Mehta, P. R., Brown, A.-L., Ward, M. E., & Fratta, P. (2023). The era of cryptic exons: implications for ALS-FTD. *Molecular Neurodegeneration*, *18*(1), 16. https://doi.org/10.1186/s13024-023-00608-5

Mejzini, R., Flynn, L. L., Pitout, I. L., Fletcher, S., Wilton, S. D., & Akkari, P. A. (2019). ALS Genetics, Mechanisms, and Therapeutics: Where Are We Now? *Frontiers in Neuroscience*, *13*. https://doi.org/10.3389/fnins.2019.01310

Melamed, Z., López-Erauskin, J., Baughn, M. W., Zhang, O., Drenner, K., Sun, Y., Freyermuth, F., McMahon, M. A., Beccari, M. S., Artates, J. W., Ohkubo, T., Rodriguez, M., Lin, N., Wu, D., Bennett, C. F., Rigo, F., Da Cruz, S., Ravits, J., Lagier-Tourenne, C., & Cleveland, D. W. (2019). Premature polyadenylation-mediated loss of stathmin-2 is a hallmark of TDP-43-dependent neurodegeneration. *Nature Neuroscience*. https://doi.org/10.1038/s41593-018-0293-z

Meneses, A., Koga, S., O'Leary, J., Dickson, D. W., Bu, G., & Zhao, N. (2021). TDP-43 Pathology in Alzheimer's Disease. In *Molecular Neurodegeneration*. https://doi.org/10.1186/s13024-021-00503-x

Miller, J. D., Ganat, Y. M., Kishinevsky, S., Bowman, R. L., Liu, B., Tu, E. Y., Mandal, P. K., Vera, E., Shim, J. W., Kriks, S., Taldone, T., Fusaki, N., Tomishima, M. J., Krainc, D., Milner, T. A., Rossi, D. J., & Studer, L. (2013). Human iPSC-based modeling of late-onset disease via progerin-induced aging. *Cell Stem Cell*, *13*(6). https://doi.org/10.1016/j.stem.2013.11.006

Miyawaki, S., Kuroki, S., Maeda, R., Okashita, N., Koopman, P., & Tachibana, M. (2020). The mouse Sry locus harbors a cryptic exon that is essential for male sex determination. *Science*, *370*(6512), 121–124. https://doi.org/10.1126/science.abb6430

Moisse, K., Mepham, J., Volkening, K., Welch, I., Hill, T., & Strong, M. J. (2009). Cytosolic TDP-43 expression following axotomy is associated with caspase 3 activation in NFL-/- mice: Support for a role for TDP-43 in the physiological response to neuronal injury. *Brain Research*. https://doi.org/10.1016/j.brainres.2009.07.023

Moisse, K., Volkening, K., Leystra-Lantz, C., Welch, I., Hill, T., & Strong, M. J. (2009). Divergent patterns of cytosolic TDP-43 and neuronal progranulin expression following axotomy:

Implications for TDP-43 in the physiological response to neuronal injury. *Brain Research*. https://doi.org/10.1016/j.brainres.2008.10.021

Mölder, F., Jablonski, K. P., Letcher, B., Hall, M. B., Tomkins-Tinch, C. H., Sochat, V., Forster, J., Lee, S., Twardziok, S. O., Kanitz, A., Wilm, A., Holtgrewe, M., Rahmann, S., Nahnsen, S., & Köster, J. (2021). Sustainable data analysis with Snakemake. *F1000Research*. https://doi.org/10.12688/f1000research.29032.1

Mompeán, M., Romano, V., Pantoja-Uceda, D., Stuani, C., Baralle, F. E., Buratti, E., & Laurents, D. V. (2016). The TDP-43 N-terminal domain structure at high resolution. *The FEBS Journal*, *283*(7). https://doi.org/10.1111/febs.13651

Morelli, K. H., Wu, Q., Gosztyla, M. L., Liu, H., Yao, M., Zhang, C., Chen, J., Marina, R. J., Lee, K., Jones, K. L., Huang, M. Y., Li, A., Smith-Geater, C., Thompson, L. M., Duan, W., & Yeo, G. W. (2023). An RNA-targeting CRISPR–Cas13d system alleviates disease-related phenotypes in Huntington's disease models. *Nature Neuroscience*, *26*(1). https://doi.org/10.1038/s41593-022-01207-1

Mund, A., Coscia, F., Kriston, A., Hollandi, R., Kovács, F., Brunner, A. D., Migh, E., Schweizer, L., Santos, A., Bzorek, M., Naimy, S., Rahbek-Gjerdrum, L. M., Dyring-Andersen, B., Bulkescher, J., Lukas, C., Eckert, M. A., Lengyel, E., Gnann, C., Lundberg, E., … Mann, M. (2022). Deep Visual Proteomics defines single-cell identity and heterogeneity. *Nature Biotechnology*, *40*(8). https://doi.org/10.1038/s41587-022-01302-5

Murphy, M. R., Doymaz, A., & Kleiman, F. E. (2021). Poly(A) tail dynamics: Measuring polyadenylation, deadenylation and poly(A) tail length. In *Methods in Enzymology* (Vol. 655). https://doi.org/10.1016/bs.mie.2021.04.005

Nagano, S., Jinno, J., Abdelhamid, R. F., Jin, Y., Shibata, M., Watanabe, S., Hirokawa, S., Nishizawa, M., Sakimura, K., Onodera, O., Okada, H., Okada, T., Saito, Y., Takahashi-Fujigasaki, J., Murayama, S., Wakatsuki, S., Mochizuki, H., & Araki, T. (2020). TDP-43 transports ribosomal protein mRNA to regulate axonal local translation in neuronal axons. *Acta Neuropathologica*, *140*(5). https://doi.org/10.1007/s00401-020-02205-y

Nalls, M. A., Blauwendraat, C., Vallerga, C. L., Heilbron, K., Bandres-Ciga, S., Chang, D., Tan, M., Kia, D. A., Noyce, A. J., Xue, A., Bras, J., Young, E., von Coelln, R., Simón-Sánchez, J., Schulte, C., Sharma, M., Krohn, L., Pihlstrøm, L., Siitonen, A., … Zhang, F. (2019). Identification of novel risk loci, causal insights, and heritable risk for Parkinson's disease: a meta-analysis of genome-wide association studies. *The Lancet Neurology*, *18*(12). https://doi.org/10.1016/S1474-4422(19)30320-5

Neelagandan, N., Gonnella, G., Dang, S., Janiesch, P. C., Miller, K. K., Küchler, K., Marques, R. F., Indenbirken, D., Alawi, M., Grundhoff, A., Kurtz, S., & Duncan, K. E. (2019). TDP-43 enhances translation of specific mRNAs linked to neurodegenerative disease. *Nucleic Acids Research*, *47*(1). https://doi.org/10.1093/nar/gky972

Nelson, P. T., Dickson, D. W., Trojanowski, J. Q., Jack, C. R., Boyle, P. A., Arfanakis, K., Rademakers, R., Alafuzoff, I., Attems, J., Brayne, C., Coyle-Gilchrist, I. T. S., Chui, H. C., Fardo, D. W., Flanagan, M. E., Halliday, G., Hokkanen, S. R. K., Hunter, S., Jicha, G. A., Katsumata, Y., … Schneider, J. A. (2019). Limbic-predominant age-related TDP-43 encephalopathy (LATE): Consensus working group report. In *Brain* (Vol. 142, Issue 6). https://doi.org/10.1093/brain/awz099

Nesvizhskii, A. I., & Aebersold, R. (2005). Interpretation of shotgun proteomic data: The protein inference problem. In *Molecular and Cellular Proteomics* (Vol. 4, Issue 10). https://doi.org/10.1074/mcp.R500012-MCP200

Neumann, M., Sampathu, D. M., Kwong, L. K., Truax, A. C., Micsenyi, M. C., Chou, T. T., Bruce, J., Schuck, T., Grossman, M., Clark, C. M., McCluskey, L. F., Miller, B. L., Masliah, E., Mackenzie, I. R., Feldman, H., Feiden, W., Kretzschmar, H. A., Trojanowski, J. Q., & Lee, V. M. Y. (2006). Ubiquitinated TDP-43 in frontotemporal lobar degeneration and amyotrophic lateral sclerosis. *Science*, *314*(5796). https://doi.org/10.1126/science.1134108

Neumann, M. (2022). *FTLD-TDP pathological subtypes: clinical and mechanistic significance. Adv Exp Med Biol, 1281*, 201-217. https://www.ncbi.nlm.nih.gov/pmc/articles/PMC8183578/

Neumann, M. (2007). TDP-43 proteinopathies: a new class of proteinopathies. *Future Neurology*, *2*(5), 549–557. https://doi.org/10.2217/14796708.2.5.549

Neumann, M., Tolnay, M., & Mackenzie, I. R. A. (2009). The molecular basis of frontotemporal dementia. *Expert Reviews in Molecular Medicine*, *11*, e23.

Ng, A. H. M., Khoshakhlagh, P., Rojo Arias, J. E., Pasquini, G., Wang, K., Swiersy, A., Shipman, S. L., Appleton, E., Kiaee, K., Kohman, R. E., Vernet, A., Dysart, M., Leeper, K., Saylor, W., Huang, J. Y., Graveline, A., Taipale, J., Hill, D. E., Vidal, M., … Church, G. M. (2021). A comprehensive library of human transcription factors for cell fate engineering. *Nature Biotechnology*, *39*(4). https://doi.org/10.1038/s41587-020-0742-6

Nicolas, A., Kenna, K., Renton, A. E., Ticozzi, N., Faghri, F., Chia, R., Dominov, J. A., Kenna, B. J., Nalls, M. A., Keagle, P., Rivera, A. M., van Rheenen, W., Murphy, N. A., van Vugt, J. J. F. A., Geiger, J. T., van der Spek, R., Pliner, H. A., Shankaracharya, Smith, B. N., … Traynor, B. J.

(2018). Genome-wide Analyses Identify KIF5A as a Novel ALS Gene. *Neuron*, *97*(6). https://doi.org/10.1016/j.neuron.2018.02.027

Nishimura, A. L., Upunski, V., Troakes, C., Kathe, C., Fratta, P., Howell, M., Gallo, J. M., Hortobágyi, T., Shaw, C. E., & Rogelj, B. (2010). Nuclear import impairment causes cytoplasmic trans-activation response DNA-binding protein accumulation and is associated with frontotemporal lobar degeneration. *Brain*, *133*(6). https://doi.org/10.1093/brain/awq111

Ogaki, K., Li, Y., Atsuta, N., Tomiyama, H., Funayama, M., Watanabe, H., … Sobue, G. (2012). Analysis of C9orf72 repeat expansion in 563 Japanese patients with amyotrophic lateral sclerosis. *Neurobiology of Aging*, *33*(10), 2527.e11–2527.e16. https://doi.org/10.1016/j.neurobiolaging.2012.05.011

Onyike, C. U., & Diehl-Schmid, J. (2013). The epidemiology of frontotemporal dementia. *International Review of Psychiatry*, *25*(2). https://doi.org/10.3109/09540261.2013.776523

Oosterveen, T., Garção, P., Moles-Garcia, E., Soleilhavoup, C., Travaglio, M., Sheraz, S., Peltrini, R., Patrick, K., Labas, V., Combes-Soia, L., Marklund, U., Hohenstein, P., & Panman, L. (2021). Pluripotent stem cell derived dopaminergic subpopulations model the selective neuron degeneration in Parkinson's disease. *Stem Cell Reports*, *16*(11). https://doi.org/10.1016/j.stemcr.2021.09.014

Ou, S. H., Wu, F., Harrich, D., García-Martínez, L. F., & Gaynor, R. B. (1995). Cloning and characterization of a novel cellular protein, TDP-43, that binds to human immunodeficiency virus type 1 TAR DNA sequence motifs. *Journal of Virology*, *69*(6). https://doi.org/10.1128/jvi.69.6.3584-3596.1995

Pantazis, C. B., Yang, A., Lara, E., McDonough, J. A., Blauwendraat, C., Peng, L., Oguro, H., Kanaujiya, J., Zou, J., Sebesta, D., Pratt, G., Cross, E., Blockwick, J., Buxton, P., Kinner-Bibeau,

L., Medura, C., Tompkins, C., Hughes, S., Santiana, M., … Merkle, F. T. (2022). A reference human induced pluripotent stem cell line for large-scale collaborative studies. *Cell Stem Cell*, *29*(12), 1685-1702.e22. https://doi.org/https://doi.org/10.1016/j.stem.2022.11.004

Park, J. C., Jang, S. Y., Lee, D., Lee, J., Kang, U., Chang, H., Kim, H. J., Han, S. H., Seo, J., Choi, M., Lee, D. Y., Byun, M. S., Yi, D., Cho, K. H., & Mook-Jung, I. (2021). A logical network-based drug-screening platform for Alzheimer's disease representing pathological features of human brain organoids. *Nature Communications*, *12*(1). https://doi.org/10.1038/s41467-020-20440-5

Paschos, N. K., Brown, W. E., Eswaramoorthy, R., Hu, J. C., & Athanasiou, K. A. (2015). Advances in tissue engineering through stem cell-based co-culture. In *Journal of Tissue Engineering and Regenerative Medicine* (Vol. 9, Issue 5). https://doi.org/10.1002/term.1870

Pesiridis, G. S., Lee, V. M. Y., & Trojanowski, J. Q. (2009). Mutations in TDP-43 link glycine-rich domain functions to amyotrophic lateral sclerosis. *Human Molecular Genetics*, *18*(R2). https://doi.org/10.1093/hmg/ddp303

Picotti, P., & Aebersold, R. (2012). Selected reaction monitoring-based proteomics: Workflows, potential, pitfalls and future directions. In *Nature Methods*. https://doi.org/10.1038/nmeth.2015

Pliner, H. A., Mann, D. M., & Traynor, B. J. (2014). Searching for Grendel: origin and global spread of the C9ORF72 repeat expansion. *Acta Neuropathologica*, *127*(3), 391–396. https://doi.org/10.1007/s00401-014-1250-x

Prasad, A., Bharathi, V., Sivalingam, V., Girdhar, A., & Patel, B. K. (2019). Molecular mechanisms of TDP-43 misfolding and pathology in amyotrophic lateral sclerosis. In *Frontiers in Molecular Neuroscience*. https://doi.org/10.3389/fnmol.2019.00025

Prudencio, M., Gonzales, P. K., Cook, C. N., Gendron, T. F., Daughrity, L. M., Song, Y., Ebbert, M. T. W., van Blitterswijk, M., Zhang, Y. J., Jansen-West, K., Baker, M. C., DeTure, M.,

Rademakers, R., Boylan, K. B., Dickson, D. W., Petrucelli, L., & Link, C. D. (2017). Repetitive element transcripts are elevated in the brain of C9orf72 ALS/FTLD patients. *Human Molecular Genetics*. https://doi.org/10.1093/hmg/ddx233

Prudencio, M., Humphrey, J., Pickles, S., Brown, A.-L., Hill, S. E., Kachergus, J., Shi, J., Heckman, M., Spiegel, M., Cook, C., Song, Y., Yue, M., Daughrity, L., Carlomagno, Y., Jansen-West, K., Fernandez De Castro, C., DeTure, M., Koga, S., Wang, Y.-C., … Petrucelli, L. (2020). Truncated stathmin-2 is a marker of TDP-43 pathology in frontotemporal dementia. *Journal of Clinical Investigation*. https://doi.org/10.1172/jci139741

Prüss, H. (2021). Autoantibodies in neurological disease. In *Nature Reviews Immunology*. https://doi.org/10.1038/s41577-021-00543-w

Puls, I., Jonnakuty, C., LaMonte, B. H., Holzbaur, E. L. F., Tokito, M., Mann, E., Floeter, M. K., Bidus, K., Drayna, D., Oh, S. J., Brown, R. H., Ludlow, C. L., & Fischbeck, K. H. (2003). Mutant dynactin in motor neuron disease. *Nature Genetics*, *33*(4). https://doi.org/10.1038/ng1123

Qin, H., Lim, L. Z., Wei, Y., & Song, J. (2014). TDP-43 N terminus encodes a novel ubiquitin-like fold and its unfolded form in equilibrium that can be shifted by binding to ssDNA. *Proceedings of the National Academy of Sciences of the United States of America*, *111*(52). https://doi.org/10.1073/pnas.1413994112

Quast, C., Pruesse, E., Yilmaz, P., Gerken, J., Schweer, T., Yarza, P., Peplies, J., & Glöckner, F. O. (2013). The SILVA ribosomal RNA gene database project: Improved data processing and web-based tools. *Nucleic Acids Research*. https://doi.org/10.1093/nar/gks1219

Ramos, D. M., Skarnes, W. C., Singleton, A. B., Cookson, M. R., & Ward, M. E. (2021). Tackling neurodegenerative diseases with genomic engineering: A new stem cell initiative from the NIH. *Neuron*, *109*(7). https://doi.org/10.1016/j.neuron.2021.03.022

Rauniyar, N. (2015). Parallel reaction monitoring: A targeted experiment performed using high resolution and high mass accuracy mass spectrometry. In *International Journal of Molecular Sciences* (Vol. 16, Issue 12). https://doi.org/10.3390/ijms161226120

Rayner, E., Durin, M.-A., Thomas, R., Moralli, D., O'Cathail, S. M., Tomlinson, I., Green, C. M., & Lewis, A. (2019). CRISPR-Cas9 Causes Chromosomal Instability and Rearrangements in Cancer Cell Lines, Detectable by Cytogenetic Methods. *The CRISPR Journal*, *2*(6). https://doi.org/10.1089/crispr.2019.0006

Reed, X., Bandrés-Ciga, S., Blauwendraat, C., & Cookson, M. R. (2019). The role of monogenic genes in idiopathic Parkinson's disease. In *Neurobiology of Disease* (Vol. 124). https://doi.org/10.1016/j.nbd.2018.11.012

Reilly, L., Peng, L., Lara, E., Ramos, D., Fernandopulle, M., Pantazis, C. B., Stadler, J., Santiana, M., Dadu, A., Iben, J., Faghri, F., Nalls, M. A., Coon, S. L., Narayan, P., Singleton, A. B., Cookson, M. R., Ward, M. E., & Qi, Y. A. (2021). A fully automated FAIMS-DIA proteomic pipeline for high-throughput characterization of iPSC-derived neurons. *BioRxiv*, 2021.11.24.469921. https://doi.org/10.1101/2021.11.24.469921

Ren, Y., Van Blitterswijk, M., Allen, M., Carrasquillo, M. M., Reddy, J. S., Wang, X., Beach, T. G., Dickson, D. W., Ertekin-Taner, N., Asmann, Y. W., & Rademakers, R. (2018). TMEM106B haplotypes have distinct gene expression patterns in aged brain. *Molecular Neurodegeneration*, *13*(1). https://doi.org/10.1186/s13024-018-0268-2

Rissin, D. M., Kan, C. W., Campbell, T. G., Howes, S. C., Fournier, D. R., Song, L., Piech, T., Patel, P. P., Chang, L., Rivnak, A. J., Ferrell, E. P., Randall, J. D., Provuncher, G. K., Walt, D. R., & Duffy, D. C. (2010). Single-molecule enzyme-linked immunosorbent assay detects serum proteins at subfemtomolar concentrations. *Nature Biotechnology*. https://doi.org/10.1038/nbt.1641

Roberson, E. D. (2006). Frontotemporal dementia. *Curr Neurol Neurosci Rep* , *6*(6), 481–489.

Smith, B. N., Newhouse, S., Shatunov, A., Vance, C., Topp, S., Johnson, L., … Sapp, P. C. (2013). The C9ORF72 expansion mutation is a common cause of ALS+/−FTD in Europe and has a single founder. *European Journal of Human Genetics*, *21*(1), 102–108. https://doi.org/10.1038/ejhg.2012.98

Roberson, E. D., Hesse, J. H., Rose, K. D., Slama, H., Johnson, J. K., Yaffe, K., Forman, M. S., Miller, C. A., Trojanowski, J. Q., Kramer, J. H., & Miller, B. L. (2005). Frontotemporal dementia progresses to death faster than Alzheimer disease. *Neurology*, *65*(5). https://doi.org/10.1212/01.wnl.0000173837.82820.9f

Roberts, B., Haupt, A., Tucker, A., Grancharova, T., Arakaki, J., Fuqua, M. A., Nelson, A., Hookway, C., Ludmann, S. A., Mueller, I. A., Yang, R., Horwitz, R., Rafelski, S. M., & Gunawardane, R. N. (2017). Systematic gene tagging using CRISPR/Cas9 in human stem cells to illuminate cell organization. *Molecular Biology of the Cell*, *28*(21). https://doi.org/10.1091/mbc.E17-03-0209

Robin, X., Turck, N., Hainard, A., Tiberti, N., Lisacek, F., Sanchez, J. C., & Müller, M. (2011). pROC: An open-source package for R and S+ to analyze and compare ROC curves. *BMC Bioinformatics*. https://doi.org/10.1186/1471-2105-12-77

Roche, S., Tiers, L., Provansal, M., Seveno, M., Piva, M. T., Jouin, P., & Lehmann, S. (2009). Depletion of one, six, twelve or twenty major blood proteins before proteomic analysis: The more the better? *Journal of Proteomics*, *72*(6). https://doi.org/10.1016/j.jprot.2009.03.008

Rodrigues Lima-Junior, J., Sulzer, D., Lindestam Arlehamn, C. S., & Sette, A. (2021). The role of immune-mediated alterations and disorders in ALS disease. In *Human Immunology*. https://doi.org/10.1016/j.humimm.2021.01.017

Rossi, D., Volanti, P., Brambilla, L., Colletti, T., Spataro, R., & La Bella, V. (2018). CSF neurofilament proteins as diagnostic and prognostic biomarkers for amyotrophic lateral sclerosis. *Journal of Neurology*, *265*(3). https://doi.org/10.1007/s00415-017-8730-6

Rot, G., Wang, Z., Huppertz, I., Modic, M., Lenče, T., Hallegger, M., Haberman, N., Curk, T., von Mering, C., & Ule, J. (2017). High-Resolution RNA Maps Suggest Common Principles of Splicing and Polyadenylation Regulation by TDP-43. *Cell Reports*, *19*(5). https://doi.org/10.1016/j.celrep.2017.04.028

Russo, A., Scardigli, R., Regina, F. La, Murray, M. E., Romano, N., Dickson, D. W., Wolozin, B., Cattaneo, A., & Ceci, M. (2017). Increased cytoplasmic TDP-43 reduces global protein synthesis by interacting with Rack1 on polyribosomes. *Human Molecular Genetics*, *26*(8). https://doi.org/10.1093/hmg/ddx035

Ryan, M., Heverin, M., McLaughlin, R. L., & Hardiman, O. (2019). Lifetime Risk and Heritability of Amyotrophic Lateral Sclerosis. *JAMA Neurology*, *76*(11). https://doi.org/10.1001/jamaneurol.2019.2044

Saberi, S., Stauffer, J. E., Schulte, D. J., & Ravits, J. (2015). Neuropathology of Amyotrophic Lateral Sclerosis and Its Variants. In *Neurologic Clinics* (Vol. 33, Issue 4). https://doi.org/10.1016/j.ncl.2015.07.012

Sato, T., Vries, R. G., Snippert, H. J., Van De Wetering, M., Barker, N., Stange, D. E., Van Es, J. H., Abo, A., Kujala, P., Peters, P. J., & Clevers, H. (2009). Single Lgr5 stem cells build crypt-villus structures in vitro without a mesenchymal niche. *Nature*, *459*(7244). https://doi.org/10.1038/nature07935

Saxon, J. A., Thompson, J. C., Jones, M., Harris, J. M., Richardson, A. M. T., Langheinrich, T., Neary, D., Mann, D. M. A., & Snowden, J. S. (2017). Examining the language and behavioural profile in FTD and ALS-FTD. *Journal of Neurology, Neurosurgery and Psychiatry*, *88*(8). https://doi.org/10.1136/jnnp-2017-315667

Schaub, M. A., Boyle, A. P., Kundaje, A., Batzoglou, S., & Snyder, M. (2012). Linking disease associations with regulatory information in the human genome. *Genome Research*, *22*(9). https://doi.org/10.1101/gr.136127.111

Schekman, R., & Rile, E. A. (2019). Coordinating a new approach to basic research into parkinson's disease. *ELife*, *8*. https://doi.org/10.7554/eLife.51167

Schmidt, H. B., Barreau, A., & Rohatgi, R. (2019). Phase separation-deficient TDP43 remains functional in splicing. *Nature Communications*, *10*(1). https://doi.org/10.1038/s41467-019-12740-2

Schofield, E. C., Caine, D., Kril, J. J., Cordato, N. J., & Halliday, G. M. (2005). Staging disease severity in movement disorder tauopathies: Brain atrophy separates progressive supranuclear palsy from corticobasal degeneration. *Movement Disorders*, *20*(1). https://doi.org/10.1002/mds.20286

Seltman, R. E., & Matthews, B. R. (2012). Frontotemporal lobar degeneration: Epidemiology, pathology, diagnosis and management. In *CNS Drugs* (Vol. 26, Issue 10). https://doi.org/10.2165/11640070-000000000-00000

Serang, O., Moruz, L., Hoopmann, M. R., & Käll, L. (2012). Recognizing uncertainty increases robustness and reproducibility of mass spectrometry-based protein inferences. In *Journal of Proteome Research* (Vol. 11, Issue 12). https://doi.org/10.1021/pr300426s

Shannon, P., Markiel, A., Ozier, O., Baliga, N. S., Wang, J. T., Ramage, D., Amin, N., Schwikowski, B., & Ideker, T. (2003). Cytoscape: A software Environment for integrated models of biomolecular interaction networks. *Genome Research*. https://doi.org/10.1101/gr.1239303

Shao, M., & Kingsford, C. (2017). accurate assembly of transcripts through phase-preserving graph decomposition. *Nature Biotechnology*. https://doi.org/10.1038/nbt.4020

Shepheard, S. R., Wuu, J., Cardoso, M., Wiklendt, L., Dinning, P. G., Chataway, T., Schultz, D., Benatar, M., & Rogers, M. L. (2017). Urinary p75ECD: A prognostic, disease progression, and pharmacodynamic biomarker in ALS. *Neurology*, *88*(12). https://doi.org/10.1212/WNL.0000000000003741

Shiina, Y., Arima, K., Tabunoki, H., & Satoh, J. I. (2010). TDP-43 dimerizes in human cells in culture. *Cellular and Molecular Neurobiology*, *30*(4). https://doi.org/10.1007/s10571-009-9489-9

Sidibé, H., Khalfallah, Y., Xiao, S., Gómez, N. B., Fakim, H., Tank, E. M. H., Di Tomasso, G., Bareke, E., Aulas, A., McKeever, P. M., Melamed, Z., Destroimaisons, L., Deshaies, J. E., Zinman, L., Parker, J. A., Legault, P., Tétreault, M., Barmada, S. J., Robertson, J., & Vande Velde, C. (2021). TDP-43 stabilizes G3BP1 mRNA: Relevance to amyotrophic lateral sclerosis/frontotemporal dementia. *Brain*, *144*(11). https://doi.org/10.1093/brain/awab217

Singh, M., Zhang, S., Perez, A. M., Lee, E. Y. C., Lee, M. Y. W. T., & Zhang, D. (2022). POLDIP3: At the Crossroad of RNA and DNA Metabolism. In *Genes* (Vol. 13, Issue 11). https://doi.org/10.3390/genes13111921

Skarnes, W. C., Ning, G., Giansiracusa, S., Cruz, A. S., Blauwendraat, C., Saavedra, B., Holden, K., Cookson, M. R., Ward, M. E., & McDonough, J. A. (2021). Controlling homology-directed repair outcomes in human stem cells with dCas9. *BioRxiv*.

Slatko, B. E., Gardner, A. F., & Ausubel, F. M. (2018). Overview of Next-Generation Sequencing Technologies. *Current Protocols in Molecular Biology*, *122*(1). https://doi.org/10.1002/cpmb.59

Smeyers, J., Banchi, E. G., & Latouche, M. (2021). C9ORF72: What It Is, What It Does, and Why It Matters. In *Frontiers in Cellular Neuroscience* (Vol. 15). https://doi.org/10.3389/fncel.2021.661447

Smith, B. N., Ticozzi, N., Fallini, C., Gkazi, A. S., Topp, S., Kenna, K. P., Scotter, E. L., Kost, J., Keagle, P., Miller, J. W., Calini, D., Vance, C., Danielson, E. W., Troakes, C., Tiloca, C., Al-Sarraj, S., Lewis, E. A., King, A., Colombrita, C., … Bertolin, C. (2014). Exome-wide rare variant analysis identifies TUBA4A mutations associated with familial ALS. *Neuron*, *84*(2). https://doi.org/10.1016/j.neuron.2014.09.027

Smullen, M., Olson, M. N., Reichert, J. M., Dawes, P., Murray, L. F., Baer, C. E., Wang, Q., Readhead, B., Church, G. M., Lim, E. T., & Chan, Y. (2023). Reliable multiplex generation of pooled induced pluripotent stem cells. *Cell Reports Methods*, *3*(9). https://doi.org/10.1016/j.crmeth.2023.100570

Spence, H., Waldron, F. M., Saleeb, R. S., Brown, A.-L., Rifai, O. M., Gilodi, M., … Gregory, J. M. (2024). RNA aptamer reveals nuclear TDP-43 pathology is an early aggregation event that coincides with STMN-2 cryptic splicing and precedes clinical manifestation in ALS. *Acta Neuropathologica*, *147*(1). https://pubmed.ncbi.nlm.nih.gov/32116499/

Spence H, W. F. S. R. B. A. R. O. G. M. R. F. R. K. M. G. W. D. O. J. P. A. F. P. S. N. T. G. Z. E. H. M. G. J. (2024). RNA aptamer reveals nuclear TDP-43 pathology is an early aggregation

event that coincides with STMN-2 cryptic splicing and precedes clinical manifestation in ALS. *Acta Neuropathol*, *147*(1).

Sreedharan, J., Blair, I. P., Tripathi, V. B., Hu, X., Vance, C., Rogelj, B., Ackerley, S., Durnall, J. C., Williams, K. L., Buratti, E., Baralle, F., De Belleroche, J., Mitchell, J. D., Leigh, P. N., Al-Chalabi, A., Miller, C. C., Nicholson, G., & Shaw, C. E. (2008). TDP-43 mutations in familial and sporadic amyotrophic lateral sclerosis. *Science*, *319*(5870). https://doi.org/10.1126/science.1154584

Strong, M. J., Abrahams, S., Goldstein, L. H., Woolley, S., Mclaughlin, P., Snowden, J., Mioshi, E., Roberts-South, A., Benatar, M., HortobáGyi, T., Rosenfeld, J., Silani, V., Ince, P. G., & Turner, M. R. (2017). Amyotrophic lateral sclerosis - frontotemporal spectrum disorder (ALS-FTSD): Revised diagnostic criteria. *Amyotrophic Lateral Sclerosis and Frontotemporal Degeneration*, *18*(3–4). https://doi.org/10.1080/21678421.2016.1267768

Strong, M. J., Volkening, K., Hammond, R., Yang, W., Strong, W., Leystra-Lantz, C., & Shoesmith, C. (2007). TDP43 is a human low molecular weight neurofilament (hNFL) mRNA-binding protein. *Molecular and Cellular Neuroscience*, *35*(2). https://doi.org/10.1016/j.mcn.2007.03.007

Suk, T. R., & Rousseaux, M. W. C. (2020). The role of TDP-43 mislocalization in amyotrophic lateral sclerosis. In *Molecular Neurodegeneration* (Vol. 15, Issue 1). https://doi.org/10.1186/s13024-020-00397-1

Sulzer, D., Alcalay, R. N., Garretti, F., Cote, L., Kanter, E., Agin-Liebes, J., Liong, C., McMurtrey, C., Hildebrand, W. H., Mao, X., Dawson, V. L., Dawson, T. M., Oseroff, C., Pham, J., Sidney, J., Dillon, M. B., Carpenter, C., Weiskopf, D., Phillips, E., … Sette, A. (2017). T cells from patients with Parkinson's disease recognize α-synuclein peptides. *Nature*. https://doi.org/10.1038/nature22815

Szklarczyk, D., Gable, A. L., Lyon, D., Junge, A., Wyder, S., Huerta-Cepas, J., Simonovic, M., Doncheva, N. T., Morris, J. H., Bork, P., Jensen, L. J., & Von Mering, C. (2019). STRING v11: Protein-protein association networks with increased coverage, supporting functional discovery in genome-wide experimental datasets. *Nucleic Acids Research*. https://doi.org/10.1093/nar/gky1131

Takahashi, K., Tanabe, K., Ohnuki, M., Narita, M., Ichisaka, T., Tomoda, K., & Yamanaka, S. (2007). Induction of Pluripotent Stem Cells from Adult Human Fibroblasts by Defined Factors. *Cell*, *131*(5). https://doi.org/10.1016/j.cell.2007.11.019

Tam, O. H., Rozhkov, N. V., Shaw, R., Kim, D., Hubbard, I., Fennessey, S., Propp, N., Phatnani, H., Kwan, J., Sareen, D., Broach, J. R., Simmons, Z., Arcila-Londono, X., Lee, E. B., Van Deerlin, V. M., Shneider, N. A., Fraenkel, E., Ostrow, L. W., Baas, F., … Gale Hammell, M. (2019). Postmortem Cortex Samples Identify Distinct Molecular Subtypes of ALS: Retrotransposon Activation, Oxidative Stress, and Activated Glia. *Cell Reports*. https://doi.org/10.1016/j.celrep.2019.09.066

Tan, R. H., Ke, Y. D., Ittner, L. M., & Halliday, G. M. (2017). ALS/FTLD: experimental models and reality. In *Acta Neuropathologica* (Vol. 133, Issue 2). https://doi.org/10.1007/s00401-016-1666-6

The Overlapping Genetics of Amyotrophic Lateral Sclerosis and Frontotemporal Dementia. (2020). *Front Neurosci, 14:42.* https://www.ncbi.nlm.nih.gov/pmc/articles/PMC7012787/

Thomas, S. M., Kagan, C., Pavlovic, B. J., Burnett, J., Patterson, K., Pritchard, J. K., & Gilad, Y. (2015). Reprogramming LCLs to iPSCs Results in Recovery of Donor-Specific Gene Expression Signature. *PLoS Genetics*, *11*(5). https://doi.org/10.1371/journal.pgen.1005216

Thomas-Jinu, S., Gordon, P. M., Fielding, T., Taylor, R., Smith, B. N., Snowden, V., Blanc, E., Vance, C., Topp, S., Wong, C. H., Bielen, H., Williams, K. L., McCann, E. P., Nicholson, G. A.,

Pan-Vazquez, A., Fox, A. H., Bond, C. S., Talbot, W. S., Blair, I. P., … Houart, C. (2017). Non-nuclear Pool of Splicing Factor SFPQ Regulates Axonal Transcripts Required for Normal Motor Development. *Neuron*, *94*(2). https://doi.org/10.1016/j.neuron.2017.03.026

Tian, R., Gachechiladze, M. A., Ludwig, C. H., Laurie, M. T., Hong, J. Y., Nathaniel, D., Prabhu, A. V., Fernandopulle, M. S., Patel, R., Abshari, M., Ward, M. E., & Kampmann, M. (2019). CRISPR Interference-Based Platform for Multimodal Genetic Screens in Human iPSC-Derived Neurons. *Neuron*. https://doi.org/10.1016/j.neuron.2019.07.014

Ticozzi, N., Vance, C., LeClerc, A. L., Keagle, P., Glass, J. D., McKenna-Yasek, D., Sapp, P. C., Silani, V., Bosco, D. A., Shaw, C. E., Brown, R. H., & Landers, J. E. (2011). Mutational analysis reveals the FUS homolog TAF15 as a candidate gene for familial amyotrophic lateral sclerosis. *American Journal of Medical Genetics, Part B: Neuropsychiatric Genetics*, *156*(3). https://doi.org/10.1002/ajmg.b.31158

Tollervey, J. R., Curk, T., Rogelj, B., Briese, M., Cereda, M., Kayikci, M., König, J., Hortobágyi, T., Nishimura, A. L., Župunski, V., Patani, R., Chandran, S., Rot, G., Zupan, B., Shaw, C. E., & Ule, J. (2011). Characterizing the RNA targets and position-dependent splicing regulation by TDP-43. *Nature Neuroscience*, *14*(4). https://doi.org/10.1038/nn.2778

Tsai, C.-P., Soong, B.-W., Tu, P.-H., Lin, K.-P., Fuh, J.-L., Tsai, P.-C., … Lee, Y.-C. (2012). A hexanucleotide repeat expansion in C9ORF72 causes familial and sporadic ALS in Taiwan. *Neurobiology of Aging*, *33*(9), 2232.e11–2232.e18. https://doi.org/10.1016/j.neurobiolaging.2012.05.002

Tsoi, P. S., Choi, K. J., Leonard, P. G., Sizovs, A., Moosa, M. M., MacKenzie, K. R., Ferreon, J. C., & Ferreon, A. C. M. (2017). The N-Terminal Domain of ALS-Linked TDP-43 Assembles without

Misfolding. *Angewandte Chemie - International Edition*, *56*(41). https://doi.org/10.1002/anie.201706769

Tsunemoto, R., Lee, S., Szucs, A., Chubukov, P., Sokolova, I., Blanchard, J. W., Eade, K. T., Bruggemann, J., Wu, C., Torkamani, A., Sanna, P. P., & Baldwin, K. K. (2018). Diverse reprogramming codes for neuronal identity. *Nature*, *557*(7705). https://doi.org/10.1038/s41586-018-0103-5

Uffelmann, E., Huang, Q. Q., Munung, N. S., de Vries, J., Okada, Y., Martin, A. R., Martin, H. C., Lappalainen, T., & Posthuma, D. (2021). Genome-wide association studies. In *Nature Reviews Methods Primers* (Vol. 1, Issue 1). https://doi.org/10.1038/s43586-021-00056-9

Umoh, M. E., Fournier, C., Li, Y., Polak, M., Shaw, L., Landers, J. E., Hu, W., Gearing, M., & Glass, J. D. (2016). Comparative analysis of C9orf72 and sporadic disease in an ALS clinic population. *Neurology*, *87*(10). https://doi.org/10.1212/WNL.0000000000003067

Unterauer, E. M., Boushehri, S. S., Jevdokimenko, K., Masullo, L. A., Ganji, M., Sograte-Idrissi, S., Kowalewski, R., Strauss, S., Reinhardt, S. C. M., Perovic, A., Marr, C., Opazo, F., Fornasiero, E. F., & Jungmann, R. (2023). Spatial proteomics in neurons at single-protein resolution. *BioRxiv*.

Uryu, K., Nakashima-Yasuda, H., Forman, M. S., Kwong, L. K., Clark, C. M., Grossman, M., Miller, B. L., Kretzschmar, H. A., Lee, V. M. Y., Trojanowski, J. Q., & Neumann, M. (2008). Concomitant TAR-DNA-binding protein 43 pathology is present in Alzheimer disease and corticobasal degeneration but not in other tauopathies. *Journal of Neuropathology and Experimental Neurology*. https://doi.org/10.1097/NEN.0b013e31817713b5

Vadori, M., Aron Badin, R., Hantraye, P., & Cozzi, E. (2015). Current status of neuronal cell xenotransplantation. *International Journal of Surgery (London, England)*, *23*(Pt B), 267–272. https://doi.org/10.1016/j.ijsu.2015.09.052

Van Es, M. A., Hardiman, O., Chio, A., Al-Chalabi, A., Pasterkamp, R. J., Veldink, J. H., & van den Berg, L. H. (2017). Amyotrophic lateral sclerosis. In *The Lancet* (Vol. 390, Issue 10107). https://doi.org/10.1016/S0140-6736(17)31287-4

Vance, C., Rogelj, B., Hortobágyi, T., De Vos, K. J., Nishimura, A. L., Sreedharan, J., Hu, X., Smith, B., Ruddy, D., Wright, P., Ganesalingam, J., Williams, K. L., Tripathi, V., Al-Saraj, S., Al-Chalabi, A., Leigh, P. N., Blair, I. P., Nicholson, G., De Belleroche, J., … Shaw, C. E. (2009). Mutations in FUS, an RNA processing protein, cause familial amyotrophic lateral sclerosis type 6. *Science*, *323*(5918). https://doi.org/10.1126/science.1165942

Vaquero-Garcia, J., Barrera, A., Gazzara, M. R., Gonzalez-Vallinas, J., Lahens, N. F., Hogenesch, J. B., Lynch, K. W., & Barash, Y. (2016). A new view of transcriptome complexity and regulation through the lens of local splicing variations. *ELife*. https://doi.org/10.7554/eLife.11752

Vatsavayai, S. C., Yoon, S. J., Gardner, R. C., Gendron, T. F., Vargas, J. N. S., Trujillo, A., Pribadi, M., Phillips, J. J., Gaus, S. E., Hixson, J. D., Garcia, P. A., Rabinovici, G. D., Coppola, G., Geschwind, D. H., Petrucelli, L., Miller, B. L., & Seeley, W. W. (2016). Timing and significance of pathological features in C9orf72 expansion-associated frontotemporal dementia. *Brain*. https://doi.org/10.1093/brain/aww250

Verde, F., Steinacker, P., Weishaupt, J. H., Kassubek, J., Oeckl, P., Halbgebauer, S., Tumani, H., Von Arnim, C. A. F., Dorst, J., Feneberg, E., Mayer, B., Müller, H. P., Gorges, M., Rosenbohm, A., Volk, A. E., Silani, V., Ludolph, A. C., & Otto, M. (2019). Neurofilament light chain in serum for the diagnosis of amyotrophic lateral sclerosis. *Journal of Neurology, Neurosurgery and Psychiatry*, *90*(2). https://doi.org/10.1136/jnnp-2018-318704

Versluys, L., Ervilha Pereira, P., Schuermans, N., De Paepe, B., De Bleecker, J. L., Bogaert, E., & Dermaut, B. (2022). Expanding the TDP-43 Proteinopathy Pathway From Neurons to Muscle:

Physiological and Pathophysiological Functions. In *Frontiers in Neuroscience* (Vol. 16). https://doi.org/10.3389/fnins.2022.815765

Volpato, V., & Webber, C. (2020). Addressing variability in iPSC-derived models of human disease: Guidelines to promote reproducibility. In *DMM Disease Models and Mechanisms* (Vol. 13, Issue 1). https://doi.org/10.1242/dmm.042317

Vucic, S., Higashihara, M., Sobue, G., Atsuta, N., Doi, Y., Kuwabara, S., Kim, S. H., Kim, I., Oh, K. W., Park, J., Kim, E. M., Talman, P., Menon, P., & Kiernan, M. C. (2020). ALS is a multistep process in South Korean, Japanese, and Australian patients. *Neurology*, *94*(15). https://doi.org/10.1212/WNL.0000000000009015

Wang, Y., Zhao, Y., Bollas, A., Wang, Y., & Au, K. F. (2021). Nanopore sequencing technology, bioinformatics and applications. In *Nature Biotechnology* (Vol. 39, Issue 11). https://doi.org/10.1038/s41587-021-01108-x

Warren, J. D., Rohrer, J. D., & Rossor, M. N. (2013). Clinical review. Frontotemporal dementia. *BMJ (Clinical Research Ed.)*, *347*. https://doi.org/10.1136/bmj.f4827

Wilkins, O. G., & Ule, J. (2021). Ribocutter: Cas9-mediated rRNA depletion from multiplexed Ribo-seq libraries. *BioRxiv*.

Williams, S. M., Khan, G., Harris, B. T., Ravits, J., & Sierks, M. R. (2017). TDP-43 protein variants as biomarkers in amyotrophic lateral sclerosis. *BMC Neuroscience*, *18*(1). https://doi.org/10.1186/s12868-017-0334-7

Wingo, T. S., Cutler, D. J., Yarab, N., Kelly, C. M., & Glass, J. D. (2011). The heritability of amyotrophic lateral sclerosis in a clinically ascertained United States research registry. *PLoS ONE*, *6*(11). https://doi.org/10.1371/journal.pone.0027985

Winton, M. J., Igaz, L. M., Wong, M. M., Kwong, L. K., Trojanowski, J. Q., & Lee, V. M. Y. (2008). Disturbance of nuclear and cytoplasmic TAR DNA-binding protein (TDP-43) induces disease-like redistribution, sequestration, and aggregate formation. *Journal of Biological Chemistry*, *283*(19). https://doi.org/10.1074/jbc.M800342200

Workman, M. J., Lim, R. G., Wu, J., Frank, A., Ornelas, L., Panther, L., Galvez, E., Perez, D., Meepe, I., Lei, S., Valencia, V., Gomez, E., Liu, C., Moran, R., Pinedo, L., Tsitkov, S., Ho, R., Kaye, J. A., Thompson, T., … Svendsen, C. N. (2023). Large-scale differentiation of iPSC-derived motor neurons from ALS and control subjects. *Neuron*. https://doi.org/10.1016/j.neuron.2023.01.010

Yang, C., Nag, S., Xing, G., Aggarwal, N. T., & Schneider, J. A. (2020). A Clinicopathological Report of a 93-Year-Old Former Street Boxer With Coexistence of Chronic Traumatic Encephalopathy, Alzheimer's Disease, Dementia With Lewy Bodies, and Hippocampal Sclerosis With TDP-43 Pathology. *Frontiers in Neurology*, *11*. https://doi.org/10.3389/fneur.2020.00042

Yang, C., Wang, H., Qiao, T., Yang, B., Aliaga, L., Qiu, L., Tan, W., Salameh, J., McKenna-Yasek, D. M., Smith, T., Peng, L., Moore, M. J., Brown, R. H., Cai, H., & Xu, Z. (2014). Partial loss of TDP-43 function causes phenotypes of amyotrophic lateral sclerosis. *Proceedings of the National Academy of Sciences of the United States of America*. https://doi.org/10.1073/pnas.1322641111

Yang, H. S., Yu, L., White, C. C., Chibnik, L. B., Chhatwal, J. P., Sperling, R. A., Bennett, D. A., Schneider, J. A., & De Jager, P. L. (2018). Evaluation of TDP-43 proteinopathy and hippocampal sclerosis in relation to APOE ε4 haplotype status: a community-based cohort study. *The Lancet Neurology*, *17*(9). https://doi.org/10.1016/S1474-4422(18)30251-5

Yu, H., Lu, S., Gasior, K., Singh, D., Vazquez-Sanchez, S., Tapia, O., Toprani, D., Beccari, M. S., Yates, J. R., Da Cruz, S., Newby, J. M., Lafarga, M., Gladfelter, A. S., Villa, E., & Cleveland, D.

W. (2021). HSP70 chaperones RNA-free TDP-43 into anisotropic intranuclear liquid spherical shells. *Science*, *371*(6529), eabb4309. https://doi.org/10.1126/science.abb4309

Yu, H., Nguyen, K., Royce, T., Qian, J., Nelson, K., Snyder, M., & Gerstein, M. (2007). Positional artifacts in microarrays: Experimental verification and construction of COP, an automated detection tool. *Nucleic Acids Research*, *35*(2). https://doi.org/10.1093/nar/gkl871

Zhang, D., Reynolds, R. H., Garcia-Ruiz, S., Gustavsson, E. K., Sethi, S., Aguti, S., Barbosa, I. A., Collier, J. J., Houlden, H., McFarland, R., Muntoni, F., Oláhová, M., Poulton, J., Simpson, M., Pitceathly, R. D. S., Taylor, R. W., Zhou, H., Deshpande, C., Botia, J. A., … Ryten, M. (2021). Detection of pathogenic splicing events from RNA-sequencing data using dasper. *BioRxiv*.

Zhang, Y. J., Caulfield, T., Xu, Y. F., Gendron, T. F., Hubbard, J., Stetler, C., Sasaguri, H., Whitelaw, E. C., Cai, S., Lee, W. C., & Petrucelli, L. (2013). The dual functions of the extreme N-terminus of TDP-43 in regulating its biological activity and inclusion formation. *Human Molecular Genetics*, *22*(15). https://doi.org/10.1093/hmg/ddt166

Zhang, Y., Pak, C. H., Han, Y., Ahlenius, H., Zhang, Z., Chanda, S., Marro, S., Patzke, C., Acuna, C., Covy, J., Xu, W., Yang, N., Danko, T., Chen, L., Wernig, M., & Südhof, T. C. (2013). Rapid single-step induction of functional neurons from human pluripotent stem cells. *Neuron*, *78*(5). https://doi.org/10.1016/j.neuron.2013.05.029

Zhang, Y.-J., Gendron, T. F., Grima, J. C., Sasaguri, H., Jansen-West, K., Xu, Y.-F., Katzman, R. B., Gass, J., Murray, M. E., Shinohara, M., Lin, W.-L., Garrett, A., Stankowski, J. N., Daughrity, L., Tong, J., Perkerson, E. A., Yue, M., Chew, J., Castanedes-Casey, M., … Petrucelli, L. (2016). C9ORF72 poly(GA) aggregates sequester and impair HR23 and nucleocytoplasmic transport proteins. *Nature Neuroscience*, *19*(5), 668–677. https://doi.org/10.1038/nn.4272

Zhou, X., Chen, Y., Mok, K. Y., Kwok, T. C. Y., Mok, V. C. T., Guo, Q., Ip, F. C., Chen, Y., Mullapudi, N., Weiner, M. W., Aisen, P., Petersen, R., Jack, C. R., Jagust, W., Trojanowski, J. Q., Toga, A. W., Beckett, L., Green, R. C., Saykin, A. J., … Ip, N. Y. (2019). Non-coding variability at the APOE locus contributes to the Alzheimer's risk. *Nature Communications*. https://doi.org/10.1038/s41467-019-10945-z

Zou, Z.-Y., Li, X.-G., Liu, M.-S., & Cui, L.-Y. (2013). Screening for C9orf72 repeat expansions in Chinese amyotrophic lateral sclerosis patients. *Neurobiology of Aging*, *34*(6), 1710.e5–1710.e6. https://doi.org/10.1016/j.neurobiolaging.2012.11.018

Appendix

I. Sashimi plots of mis-spliced junctions in TDP-43 KD iPSC-derived neurons

All sashimi plots can be accessed at: https://shorturl.at/efqTY

II. Custom database of de novo peptides

This file can be accessed at: https://shorturl.at/efqTY

III. Supplementary tables

Table S4A. Differentially spliced junctions in TDP-43 KD vs control iPSC-derived neurons

Gene	Chr	Start	End	DeltaPSI	Ctrl_e_psi	FDR
AGRN	chr1	1022462	1031785	0.10201744	0.008	1.70E-05
CASZ1	chr1	10661399	10665082	0.14002582	0.021	2.20E-09
GPSM2	chr1	108896431	108896864	0.60788599	0.003	1.19E-11
ELAPOR1	chr1	109197654	109198573	0.19745964	0.008	2.41E-21
ELAPOR1	chr1	109197654	109198573	0.29132517	0.011	6.78E-22
RP1-283E3.8	chr1	1709640	1719358	0.110452	0.015	7.96E-07
IGSF21	chr1	18228010	18281081	0.21993653	0	9.16E-23
IGSF21	chr1	18281170	18291866	0.25522244	0	1.50E-20
KIF17	chr1	20686126	20690188	0.10485114	0.04	4.95E-05
RAP1GAP	chr1	21598502	21598723	0.13838634	0	7.77E-11
RAP1GAP	chr1	21598820	21599494	0.11599216	0.001	5.01E-08
AKT3	chr1	243512426	243523309	0.12915862	0.001	1.52E-09
AKT3	chr1	243527864	243545510	0.13565721	0	5.76E-10
KIF26B	chr1	245419745	245464259	0.15552974	0	1.45E-15

DLGAP3	chr1	34907437	34929069	0.10604489	0.005	4.42E-07
DLGAP3	chr1	34929068	34929451	0.12466593	0	3.26E-09
TFAP2E	chr1	35588552	35589019	0.17442474	0	4.14E-13
TFAP2E	chr1	35589133	35589930	0.59325466	0.001	1.08E-08
RP5-864K19.4	chr1	38860240	38873441	0.12397327	0.02	0.00013269
MACF1	chr1	39159020	39231182	0.10594002	0.035	1.51E-08
ARMH1	chr1	44704173	44723219	0.35584659	0.005	1.21E-20
LRP8	chr1	53274820	53275631	0.10353321	0.026	1.79E-09
USP24	chr1	55078651	55081322	0.14823146	0.001	8.24E-19
USP24	chr1	55078651	55081322	0.20704279	0.002	7.15E-23
NPHP4	chr1	5888611	5890867	0.11483287	0.006	2.93E-06
CAMTA1	chr1	7249626	7411597	0.11741599	0.018	1.14E-09
KCNIP2	chr10	101829199	101831072	0.1427095	0.007	3.10E-11
KCNIP2	chr10	101831167	101839753	0.6057256	0.022	1.80E-08
KCNIP2	chr10	101831167	101839753	0.22125692	0.003	4.82E-21

PSD	chr10	102417121	102417940	0.24260187	0	9.92E-21
PSD	chr10	102418046	102418701	0.36524426	0	7.25E-20
ACTR1A	chr10	102472981	102480536	0.23146292	0.001	3.52E-11
NSMCE4A	chr10	121971069	121973523	0.15629087	0.02	3.25E-23
NSMCE4A	chr10	121973599	121974004	0.15409331	0.008	1.89E-16
KNDC1	chr10	133160569	133161067	0.15132585	0.011	2.51E-11
KNDC1	chr10	133160569	133161085	0.34730585	0.011	1.06E-20
KNDC1	chr10	133166939	133167381	0.28052864	0.001	3.87E-20
KNDC1	chr10	133207351	133208723	0.20895768	0	3.51E-21
KNDC1	chr10	133209925	133210610	0.46987856	0.047	2.44E-15
RP11-108K14.8	chr10	133389747	133390907	0.62264209	0.007	2.71E-07
PAOX	chr10	133389747	133390907	0.67167744	0.008	0.00011861
PAOX	chr10	133391098	133391312	0.43518766	0.006	1.15E-18
RP11-108K14.8	chr10	133391098	133391312	0.43518766	0.006	1.15E-18
ADARB2	chr10	1363917	1376116	0.19796532	0	6.13E-23

ADARB2	chr10	1376218	1379074	0.28774659	0.001	5.69E-22
ADARB2	chr10	1645966	1737051	0.28870059	0.005	5.91E-22
PFKP	chr10	3099352	3099557	0.41050698	0.001	1.49E-18
PFKP	chr10	3099819	3101365	0.56179152	0	2.62E-10
RP11-291L22.9	chr10	38435253	38437090	0.25598087	0.044	3.66E-10
DNAJC12	chr10	67823392	67835392	0.10776019	0.03	2.20E-09
DNAJC12	chr10	67835525	67837934	0.17352953	0.042	4.21E-12
TTC12	chr11	113329808	113329920	0.1000877	0.047	7.34E-05
HYOU1	chr11	119055571	119056070	0.11627151	0.032	5.67E-12
HYOU1	chr11	119055571	119056070	0.10144476	0.027	6.35E-06
UBASH3B	chr11	122656210	122744155	0.36557237	0	3.45E-20
FEZ1	chr11	125489822	125495836	0.224643	0.021	1.00E-22
ARHGAP32	chr11	128992046	128998319	0.77590911	0.005	0.00019527
TSPAN18	chr11	44920000	44925716	0.12758012	0.036	1.10E-05
MADD	chr11	47325032	47328658	0.19994872	0.001	2.71E-21
MADD	chr11	47325032	47328658	0.18717283	0.001	1.66E-21

VWCE	chr11	61271760	61273117	0.2214468	0.001	5.73E-12
SYT7	chr11	61547308	61547530	0.63289508	0	0.00193208
SYT7	chr11	61547308	61547530	0.77644012	0.006	0.00231785
SYT7	chr11	61547620	61551384	0.51012121	0	1.73E-12
ESRRA	chr11	64305736	64313951	0.10100018	0.027	7.18E-06
NADSYN1	chr11	71485324	71485542	0.1337929	0	3.16E-13
NADSYN1	chr11	71503303	71505511	0.10455826	0.029	6.31E-05
UVRAG	chr11	76008867	76012927	0.18331161	0.046	6.92E-10
RSF1	chr11	77813783	77820528	0.21188086	0	4.12E-21
RSF1	chr11	77813787	77820528	0.19485624	0	2.18E-21
DENND2B	chr11	8750725	8776192	0.13605046	0	3.38E-09
CHID1	chr11	900980	902148	0.1809722	0.008	4.72E-23
DTX1	chr12	113058451	113093162	0.10521014	0.031	4.91E-06
MED13L	chr12	116022601	116054245	0.16821299	0	3.88E-23
MED13L	chr12	116054357	116096669	0.10283074	0	6.12E-06
RNFT2	chr12	116779348	116788636	0.17178585	0	4.08E-13
RFLNA	chr12	124149791	124195458	0.13378668	0.036	2.21E-06

EP400	chr12	131992230	132005077	0.30170056	0.001	1.06E-19
EP400	chr12	131992230	132005077	0.46503431	0.003	6.01E-15
EP400	chr12	131995013	132005076	0.10446116	0.007	5.25E-05
CACNA1C	chr12	2680575	2682550	0.16666428	0.021	1.46E-11
KIF21A	chr12	39370261	39386971	0.10014134	0.001	6.50E-06
TMEM117	chr12	43836196	43836744	0.46796016	0.001	7.98E-18
TMEM117	chr12	43836901	43844624	0.4277822	0.001	3.00E-19
GALNT8	chr12	4761143	4763952	0.20552986	0.041	9.83E-12
RP11-234B24.6	chr12	4761143	4763952	0.22797211	0.043	1.31E-13
RP11-234B24.6	chr12	4761143	4763952	0.20552986	0.041	9.83E-12
GALNT8	chr12	4761143	4763952	0.22797211	0.043	1.31E-13
ITGA7	chr12	55685288	55686202	0.35270549	0	1.56E-20
ITGA7	chr12	55686314	55687971	0.31417434	0	2.00E-21
CEP290	chr12	88086789	88087780	0.47332978	0.005	1.88E-16
CEP290	chr12	88118743	88119021	0.14997054	0.039	1.54E-06
CEP290	chr12	88119150	88120114	0.14018523	0.049	4.48E-06

XPO4	chr13	20799339	20800113	0.1485895	0.034	7.84E-07
LMO7	chr13	75804541	75809154	0.1156669 5	0.021	1.77E-05
MBNL2	chr13	97334440	97338647	0.2127986	0.001	6.86E-18
EVL	chr14	10013315 9	100135905	0.2383581 7	0.035	0.000312 91
NYNRIN	chr14	24412691	24412997	0.6077010 2	0.037	4.05E-06
G2E3	chr14	30559272	30563746	0.2441413 7	0	1.06E-20
MNAT1	chr14	60809016	60811985	0.1329406 1	0.036	2.64E-05
MNAT1	chr14	60812127	60817918	0.3708825 8	0.002	6.53E-20
MNAT1	chr14	60817949	60818722	0.1723057 7	0	1.67E-12
LIN52	chr14	74101238	74114006	0.1399588 4	0.028	3.58E-11
TGFB3	chr14	75959345	75960814	0.3790974 3	0.004	3.90E-20
SEMA6D	chr15	47412472	47469226	0.2246659 6	0	1.01E-22
SEMA6D	chr15	47469299	47470474	0.1417150 3	0	2.05E-23
ONECUT1	chr15	52777690	52788780	0.4424563 3	0.001	5.59E-17
ONECUT1	chr15	52780742	52788780	0.1043584 1	0.006	1.53E-06
FAM81A	chr15	59439064	59458550	0.1394899 3	0.002	1.92E-07

RP11-106M3.5	chr15	72271288	72287236	0.17425608	0.039	0.00033976
LOXL1-AS1	chr15	73920038	73926240	0.11152068	0.035	1.67E-05
ISLR2	chr15	74130665	74131207	0.16166647	0.008	7.04E-22
ISL2	chr15	76336941	76340276	0.29456367	0.016	7.57E-22
ISL2	chr15	76336941	76340276	0.37433026	0.024	6.39E-18
ISL2	chr15	76337967	76340276	0.10403449	0.017	7.46E-06
LINGO1	chr15	77641025	77677089	0.1035751	0	6.92E-09
LINGO1	chr15	77735053	77756560	0.10834601	0.001	5.04E-11
LINGO1	chr15	77756719	77795939	0.10331298	0.001	9.92E-10
NTRK3	chr15	88256486	88256605	0.55460462	0.035	9.75E-14
ATF7IP2	chr16	10386122	10414574	0.20721944	0.024	9.55E-09
PKD1	chr16	2094211	2094888	0.16210234	0.036	2.19E-12
CORO7	chr16	4367442	4387986	0.14849071	0.004	1.22E-13
CORO7-PAM16	chr16	4367442	4387986	0.14849071	0.004	1.22E-13
ZNF423	chr16	49638874	49640443	0.23840622	0.001	1.35E-22
ADCY7	chr16	50246203	50246881	0.12534976	0.001	2.53E-07

NKD1	chr16	50608360	50620845	0.63272229	0.001	6.39E-09
NKD1	chr16	50620949	50621602	0.71534426	0.001	0.00019225
NKD1	chr16	50621709	50625224	0.12352274	0.026	4.73E-05
CNOT1	chr16	58538915	58539520	0.14368331	0.01	7.57E-10
ZDHHC1	chr16	67401065	67416171	0.18564966	0.02	3.63E-07
ZDHHC1	chr16	67401068	67416171	0.15685106	0.029	3.09E-05
AARS1	chr16	70271972	70272796	0.27389405	0	3.43E-22
AARS1	chr16	70272882	70276486	0.1574127	0	3.12E-23
MTSS2	chr16	70665541	70666339	0.1412846	0.021	1.61E-07
NECAB2	chr16	83990630	83993528	0.39494945	0.001	5.28E-17
NECAB2	chr16	83993614	83994302	0.43664312	0.002	1.14E-16
USP10	chr16	84733503	84735056	0.17941583	0.002	4.59E-23
USP10	chr16	84735173	84740309	0.20139652	0.002	6.52E-23
MYO1C	chr17	1472228	1474812	0.27039511	0.011	3.07E-22
MYO1C	chr17	1472228	1474812	0.22911364	0.009	1.10E-22
PHF12	chr17	28915448	28917285	0.1106265	0.013	1.93E-09
MYO18A	chr17	29131442	29165942	0.31211152	0.001	2.18E-21

MRPL45P2	chr17	47486884	47490166	0.11111997	0.029	4.52E-06
ITGA3	chr17	50081193	50081310	0.1113601	0.025	9.06E-11
KIAA0753	chr17	6579864	6580932	0.40511149	0.004	1.22E-16
KIAA0753	chr17	6580975	6589779	0.2324394	0.001	1.18E-22
TTYH2	chr17	74252014	74252234	0.17745494	0.043	6.67E-06
USP36	chr17	78836372	78836897	0.21211933	0.007	4.00E-21
USP36	chr17	78836976	78838587	0.10344042	0.003	5.39E-06
SLC26A11	chr17	80223337	80224082	0.12169174	0	5.64E-07
CEP131	chr17	81207239	81208144	0.15145468	0	1.96E-12
CEP131	chr17	81208356	81208928	0.12571493	0	5.61E-09
NPLOC4	chr17	81559416	81563921	0.10329145	0.005	9.27E-08
CCDC57	chr17	82134194	82157748	0.10159879	0.045	4.00E-05
RAB40B	chr17	82664556	82696389	0.25720329	0.027	2.12E-22
PRELID3A	chr18	12429436	12430178	0.35293231	0	1.33E-18
PRELID3A	chr18	12430292	12431150	0.63040703	0	2.57E-06
DLGAP1	chr18	4147667	4151180	0.58222685	0	3.85E-09

CBLN2	chr18	72542326	72542982	0.12330287	0.04	2.03E-05
ELAVL3	chr19	11458611	11463496	0.19803154	0	2.49E-21
ELAVL3	chr19	11463662	11466172	0.16212937	0	3.57E-23
CBARP	chr19	1235342	1235501	0.40459257	0.019	1.44E-18
MAST1	chr19	12841066	12842139	0.27510947	0	3.23E-20
MAST1	chr19	12842178	12843529	0.12104681	0	5.97E-09
ADGRL1	chr19	14176669	14177531	0.1168359	0	8.53E-13
SLC1A6	chr19	14972917	14976761	0.10275676	0.024	7.41E-07
SLC1A6	chr19	14972917	14979000	0.19567796	0.001	1.02E-14
MYO9B	chr19	17203004	17203147	0.10883188	0.003	1.09E-05
UNC13A	chr19	17623216	17623542	0.10517066	0.024	2.69E-06
UNC13A	chr19	17641556	17642414	0.41008159	0	2.88E-17
UNC13A	chr19	17642541	17642845	0.40328169	0	1.56E-18
ZNF826P	chr19	20409956	20424786	0.47939052	0.011	9.97E-16
SPPL2B	chr19	2337333	2337443	0.11014832	0.027	3.19E-11
CELF5	chr19	3278111	3278208	0.25819554	0.048	1.57E-20

CELF5	chr19	3278316	3281199	0.5546003 7	0	6.32E-12
GRAMD1A	chr19	35000486	35001098	0.3121741 4	0.007	2.00E-21
GRAMD1A	chr19	35001244	35009119	0.2972813 6	0.015	7.34E-20
ZNF529	chr19	36572392	36573043	0.5651037 9	0.011	2.31E-10
ZNF382	chr19	36605446	36607552	0.2115052 1	0.019	8.57E-16
ZNF382	chr19	36605521	36607552	0.2075510 1	0.002	3.52E-21
ZNF527	chr19	37374045	37374158	0.1641040 6	0.035	2.98E-05
SIPA1L3	chr19	37907358	38008096	0.2572517 1	0.004	2.12E-22
LRFN1	chr19	39316136	39316734	0.1040031 2	0	3.93E-06
LRFN1	chr19	39316786	39318325	0.1478726 2	0.013	1.54E-07
POU2F2	chr19	42122576	42130343	0.2539922	0	1.95E-22
POU2F2	chr19	42130499	42160332	0.4347620 7	0	1.90E-17
LIPE-AS1	chr19	42397224	42420328	0.1077391 9	0	4.36E-06
HDGFL2	chr19	4491835	4492015	0.4652560 3	0	5.68E-15
HDGFL2	chr19	4492152	4493703	0.5836017 7	0	9.56E-09
IGLON5	chr19	51320670	51322064	0.1437864 4	0	2.19E-23

LLNLR-271E8.1	chr19	58583172	58585763	0.2279081	0.039	6.16E-21
LLNLR-271E8.1	chr19	58583172	58585763	0.31087647	0.045	1.36E-19
CENPBD1P1	chr19	58583176	58585763	0.11671561	0.035	7.26E-06
LLNLR-271E8.1	chr19	58585793	58586155	0.15416016	0.037	3.03E-07
INSR	chr19	7169831	7170537	0.45946804	0.004	6.37E-17
FBN3	chr19	8083372	8084235	0.79724752	0.001	0.00019761
FBN3	chr19	8084411	8085363	0.67156531	0	0.0001795
FBN3	chr19	8117589	8118351	0.14531891	0	6.76E-09
FBN3	chr19	8118452	8118897	0.28155885	0	4.34E-22
FBN3	chr19	8118456	8118897	0.35172294	0.001	1.34E-20
CERS4	chr19	8210862	8240486	0.10631865	0.003	1.06E-08
RGPD4	chr2	107872928	107878621	0.22583298	0.002	1.96E-17
GREB1	chr2	11580832	11588746	0.16100815	0.007	3.51E-23
GREB1	chr2	11580832	11588746	0.12229079	0.007	4.29E-15
PXDN	chr2	1649675	1650800	0.45933052	0.004	5.44E-14

PXDN	chr2	1650886	1653628	0.41178807	0.002	1.59E-18
METTL8	chr2	171392197	171433026	0.22840492	0.007	1.20E-11
WDR35	chr2	19975663	19977925	0.57573756	0.029	1.02E-10
WDR35	chr2	19978167	19978751	0.19571622	0.001	1.35E-10
SPEG	chr2	219464608	219465596	0.25096341	0	1.42E-20
FKBP1B	chr2	24054192	24060814	0.10283246	0.04	5.96E-06
ATG4B	chr2	241668685	241668875	0.23380556	0	7.40E-21
ATG4B	chr2	241668985	241670726	0.40019405	0	1.18E-18
TRAPPC12	chr2	3457693	3457795	0.56839574	0.033	2.68E-09
TRAPPC12	chr2	3458515	3460263	0.64343794	0.002	0.00088066
EML6	chr2	54928751	54947858	0.12579675	0.03	2.03E-06
KIAA1841	chr2	61088468	61090479	0.10520088	0.01	2.23E-06
EHBP1	chr2	62831158	62859169	0.11260888	0.033	2.89E-08
EHBP1	chr2	62831158	62859169	0.10691324	0.028	1.31E-09
CNGA3	chr2	98370076	98375922	0.19715939	0.01	6.05E-23
CNGA3	chr2	98376036	98377687	0.1982927	0.004	6.16E-23

SLC24A3	chr20	19681991	19683910	0.24840425	0.007	1.70E-22
SLC24A3	chr20	19681991	19683913	0.31696957	0.019	2.56E-21
SLC24A3	chr20	19683960	19684176	0.50121925	0.023	2.73E-14
RIN2	chr20	19965024	19968392	0.12518881	0.005	1.12E-07
RALGAPA2	chr20	20472956	20490914	0.32963098	0	4.48E-21
RALGAPA2	chr20	20491001	20495117	0.23906554	0	1.37E-22
C20orf194	chr20	3343731	3344641	0.30231788	0	8.70E-22
C20orf194	chr20	3344699	3348525	0.36918506	0	2.90E-18
PTPRT	chr20	42098552	42099129	0.28317897	0	1.79E-19
PTPRT	chr20	42099289	42102124	0.18409015	0	2.80E-09
RP1-138B7.8	chr20	43515415	43528657	0.18326065	0.006	3.65E-09
L3MBTL1	chr20	43515415	43528657	0.17906095	0.006	6.30E-09
RP1-138B7.8	chr20	43515415	43528657	0.19571758	0.007	4.30E-11
L3MBTL1	chr20	43515415	43528657	0.18310147	0.006	2.71E-10
PREX1	chr20	48737497	48745025	0.12496403	0.049	0.0002002
PEDS1	chr20	50129690	50143502	0.1044851	0.017	9.61E-06

NPEPL1	chr20	58694592	58694812	0.2608456	0	2.08E-20
STX16-NPEPL1	chr20	58694592	58694812	0.2608456	0	2.08E-20
RP5-967N21.13	chr20	6015490	6026171	0.10782541	0.01	7.88E-08
CRLS1	chr20	6015490	6026171	0.10391623	0.01	4.96E-07
CDH4	chr20	61254937	61545630	0.24338004	0	1.51E-22
KCNQ2	chr20	63439708	63444659	0.33597561	0.001	6.40E-21
KCNQ2	chr20	63439708	63444659	0.33334517	0.001	2.90E-21
RP4-583P15.15	chr20	63709164	63732003	0.15241488	0	2.96E-23
ZGPAT	chr20	63709164	63732003	0.15241488	0	2.96E-23
ETS2	chr21	38806808	38810035	0.19088366	0.038	4.24E-13
ADARB1	chr21	45181517	45182584	0.26784376	0.04	2.40E-20
PCBP3	chr21	45755452	45788298	0.13773011	0.009	3.47E-07
DIP2A	chr21	46556091	46556403	0.10788935	0.039	9.07E-06
BCL2L13	chr22	17702386	17722274	0.20697416	0.003	7.10E-23
GNB1L	chr22	19821375	19823987	0.40604927	0	1.02E-18
GNB1L	chr22	19824077	19854443	0.25026028	0	1.78E-22

SYN3	chr22	32672017	32864915	0.25513432	0.001	1.99E-22
STXBP5L	chr3	120908416	120909571	0.27188511	0.013	1.04E-20
STXBP5L	chr3	120908428	120909571	0.28730061	0	5.14E-22
KALRN	chr3	124664330	124666449	0.13233173	0	1.37E-11
KALRN	chr3	124700033	124700977	0.31811779	0.005	3.19E-21
KALRN	chr3	124700033	124701093	0.41495698	0.007	7.82E-18
KALRN	chr3	124701255	124702038	0.72706334	0.009	0.00019308
IFT122	chr3	129483682	129483926	0.29231192	0	6.74E-22
IFT122	chr3	129484024	129488257	0.15628372	0	1.03E-10
NUP210	chr3	13366091	13375504	0.20798359	0.025	7.25E-23
NUP210	chr3	13366091	13375504	0.28429816	0.035	4.87E-22
GRIP2	chr3	14507700	14511165	0.12505371	0.017	1.95E-07
GRIP2	chr3	14507700	14511165	0.13164723	0.021	9.33E-08
GRIP2	chr3	14511479	14511586	0.10300268	0.034	0.00014944
USP13	chr3	179701179	179706934	0.36952995	0.033	1.69E-20

MAP6D1	chr3	183818111	183820100	0.1179176	0.015	2.10E-06
RP11-449K6.5	chr3	183818111	183820100	0.38635164	0.042	1.63E-11
MAP6D1	chr3	183818111	183822316	0.14753123	0.005	2.66E-08
RP11-449K6.5	chr3	183818111	183822316	0.488311	0.013	3.33E-17
ETV5	chr3	186104572	186105305	0.38326046	0.003	3.11E-19
CELSR3	chr3	48650289	48650480	0.15272407	0.033	2.41E-09
FRMD4B	chr3	69302436	69306406	0.46955152	0.012	6.79E-16
FRMD4B	chr3	69310517	69311263	0.6022738	0.017	2.31E-10
SHQ1	chr3	72750836	72762906	0.19625136	0.001	5.96E-23
SHQ1	chr3	72763014	72792916	0.25977979	0.001	2.24E-22
SETD5	chr3	9468615	9470459	0.26622414	0.001	2.39E-20
NOP14-AS1	chr4	2942327	2946872	0.11162941	0.006	0.00012813
NOP14-AS1	chr4	2942327	2946872	0.2277325	0.029	3.60E-06
LINC02506	chr4	32157136	32157956	0.1043251	0.005	4.78E-09
ZNF141	chr4	343908	372664	0.11224899	0.031	5.28E-07
SCFD2	chr4	53143787	53145333	0.10612385	0	1.26E-06
SDAD1	chr4	75982037	75984832	0.11466947	0	2.42E-09

SEPTIN11	chr4	77030970	77032457	0.17572004	0.001	1.19E-21
SEPTIN11	chr4	77032553	77034497	0.10039284	0.001	6.32E-05
PRKG2	chr4	81110611	81110808	0.20293451	0.031	9.21E-09
TMEM175	chr4	932540	951207	0.30588864	0	1.45E-21
TMEM175	chr4	932540	951207	0.20598228	0	6.96E-23
EPB41L4A	chr5	112266330	112267210	0.69694427	0	0.00019262
EPB41L4A	chr5	112267284	112275326	0.76741657	0.001	0.00019463
CDO1	chr5	115813258	115813898	0.3032244	0.011	1.16E-21
CDO1	chr5	115813954	115816228	0.15567009	0.003	6.39E-22
CYFIP2	chr5	157328050	157330161	0.15213701	0.021	2.93E-13
KCNIP1	chr5	170353964	170451777	0.40170346	0.001	8.88E-20
KCNIP1	chr5	170504633	170669499	0.20213722	0.012	6.53E-23
KCNIP1	chr5	170669660	170718758	0.2107832	0.021	7.67E-23
RANBP17	chr5	171265847	171271151	0.19722005	0.005	6.07E-23
AACSP1	chr5	178776276	178785269	0.27975798	0.003	3.96E-22

CPLANE1	chr5	37122489	37124745	0.13526232	0.014	1.83E-06
ARL¬¨,Ä†15.00	chr5	54171928	54242070	0.17376387	0.003	4.24E-23
CDK7	chr5	69261458	69262205	0.11938707	0	1.23E-07
MTRR	chr5	7878322	7885701	0.18630018	0	5.12E-23
MTRR	chr5	7878322	7885701	0.21684753	0	8.61E-23
RHOBTB3	chr5	95816627	95823836	0.35682994	0.002	1.01E-15
LIN28B	chr6	104941013	104950460	0.17277486	0.032	1.03E-06
SYNE1	chr6	152244656	152247823	0.21108036	0	7.67E-23
SYNE1	chr6	152247944	152249161	0.20298407	0	6.63E-23
RNASET2	chr6	166952548	166955484	0.11026844	0.036	3.37E-05
TCTE1	chr6	44280390	44285964	0.113625	0.022	3.20E-05
BCKDHB	chr6	80127624	80128599	0.164318	0.017	6.03E-08
BCKDHB	chr6	80169030	80169811	0.13898936	0.035	1.60E-06
HULC	chr6	8558643	8779887	0.57690742	0.029	1.08E-14
ACTL6B	chr7	100650135	100650575	0.63648517	0.001	1.84E-05
ACTL6B	chr7	100650643	100655019	0.44098672	0	3.29E-16

CTTNBP2	chr7	117861316	117862098	0.1278058 3	0.008	9.07E-08
PTPRZ1	chr7	122031559	122034095	0.1211032 5	0.049	3.54E-05
PTPRZ1	chr7	122044568	122047674	0.1033522 4	0.048	6.85E-05
WASL	chr7	123684580	123692347	0.4183759 9	0	1.90E-16
WASL	chr7	123684580	123692347	0.4001247 5	0	5.36E-17
WASL	chr7	123684581	123688997	0.1748114 3	0.039	1.70E-06
PTPRN2	chr7	157682937	157690552	0.2039075 6	0.047	7.16E-23
PTPRN2	chr7	158040550	158081298	0.2484090 6	0	1.69E-22
PTPRN2	chr7	158100856	158110829	0.1140360 1	0.013	1.20E-08
IQCE	chr7	2559217	2562526	0.1435641 8	0.005	1.56E-15
IQCE	chr7	2559217	2564878	0.5216947	0.001	7.23E-12
IQCE	chr7	2565071	2567116	0.7912062 4	0	0.000196 93
CAMK2B	chr7	44220901	44222117	0.2259337 4	0.001	5.89E-21
CAMK2B	chr7	44230633	44231005	0.2720168	0.04	2.92E-20
CAMK2B	chr7	44254607	44258490	0.3519495 6	0	1.51E-20
CAMK2B	chr7	44258610	44258872	0.2978803 3	0	8.75E-22

ADCY1	chr7	45622743	45625299	0.39528687	0	6.91E-19
ADCY1	chr7	45625377	45648670	0.21067252	0	7.64E-23
ADCY1	chr7	45625430	45648670	0.12955252	0	2.09E-09
SEPTIN7P2	chr7	45728313	45735607	0.21312839	0.007	7.99E-23
SEPTIN7P2	chr7	45735670	45736787	0.14372243	0.003	3.88E-15
FOXK1	chr7	4737421	4740838	0.20018472	0.001	8.25E-16
ICA1	chr7	8141817	8141969	0.20754045	0.034	6.92E-10
ICA1	chr7	8142055	8143875	0.23876116	0.042	4.93E-13
SEMA3D	chr7	85181287	85186677	0.1142958	0.042	0.00022644
TRRAP	chr7	98881250	98881695	0.21377741	0	8.10E-23
ADCY8	chr8	130904042	130908924	0.53602247	0.002	3.39E-16
ZFAT	chr8	134637712	134645005	0.22777299	0.001	2.70E-16
ADGRB1	chr8	142531271	142533295	0.1339546	0.004	9.70E-17
CSGALNACT1	chr8	19408695	19409237	0.13816754	0.042	0.0001402
ATP6V1B2	chr8	20225819	20226059	0.55537245	0.001	1.41E-13

ATP6V1B2	chr8	20226166	20226439	0.55239553	0.001	8.56E-14
RBPMS	chr8	30556794	30558887	0.15998712	0.042	8.89E-06
STMN2	chr8	79611214	79616822	0.47192062	0	1.70E-13
INTS8	chr8	94832174	94834300	0.11167393	0	1.61E-07
ZNF462	chr9	106863356	106865981	0.13423451	0.005	3.75E-07
DNM1	chr9	128250940	128253047	0.20764226	0.001	7.20E-23
DNM1	chr9	128250940	128253047	0.16739566	0.001	9.62E-22
RP11-101E3.5	chr9	128952846	128956141	0.60698277	0	3.41E-08
NUP188	chr9	128952846	128956141	0.60698277	0	3.41E-08
RP11-101E3.5	chr9	128956174	128956350	0.35686778	0	1.10E-20
NUP188	chr9	128956174	128956350	0.35686778	0	1.10E-20
LINC01503	chr9	129336988	129337785	0.58234197	0.001	2.83E-08
LINC01503	chr9	129337959	129338792	0.49036674	0	1.72E-14
LINC00963	chr9	129498511	129503323	0.14181842	0.028	1.26E-17
STKLD1	chr9	133379122	133395600	0.14052411	0.002	1.92E-07

UNC13B	chr9	35313989	35364545	0.31139714	0.024	1.77E-21
UNC13B	chr9	35364567	35366947	0.1147629	0.006	1.93E-07
FRG1HP	chr9	41015187	41032833	0.10117145	0.044	0.00042275
AK3	chr9	4724376	4740936	0.11586448	0.023	0.00012728
DAPK1	chr9	87499139	87506820	0.20046276	0.033	6.36E-23
DAPK1	chr9	87537793	87604954	0.20247615	0.001	6.62E-23
PTPRD	chr9	9018735	9127165	0.49148511	0.016	9.90E-15
PTPRD	chr9	9127206	9183304	0.45840863	0.015	7.36E-16
PHF2	chr9	93660560	93661348	0.51966048	0	2.66E-12
PHF2	chr9	93661646	93662906	0.22926569	0.017	5.30E-21
RAI2	chrX	17839105	17861098	0.16822157	0.001	6.23E-11
GTPBP6	chrX	315020	316914	0.12874219	0.04	5.01E-06
HDAC6	chrX	48818109	48820106	0.13233782	0.002	2.81E-12
TBL1X	chrX	9689246	9691579	0.10566927	0.002	9.59E-06

Table S4B. Differential ribosomal profiling in TDP-43 KD vs control iPSC-derived neurons

gene_name	intron_id	baseMean	log2FoldChange	lfcSE	padj
AARS1	ENST00000261772_17	4.504	4.206	1.309	0.129
ADARB1	ENST00000360697_7	2.321	0.097	0.912	0.999
ADARB1	ENST00000360697_3	4.243	2.539	0.918	0.293
ADARB2	ENST00000381312_9	41.683	-0.089	0.571	0.999
ADARB2	ENST00000381312_3	2.531	-0.695	0.834	0.999
ADARB2	ENST00000381312_7	2.356	-0.640	0.843	0.999
ADCY1	ENST00000297323_3	2.045	-0.021	0.955	0.999
ADCY8	ENST00000286355_6	2.088	1.849	1.138	0.942
ADCY8	ENST00000286355_11	3.335	3.683	1.241	0.186
ADCY8	ENST00000286355_7	2.459	-2.581	1.017	0.469
ADGRB1	ENST00000517894_24	7.389	4.093	1.074	0.022
ADGRL1	ENST00000340736_19	3.170	-0.171	0.732	0.999

ADGRL1	ENST00000340736_23	2.032	1.283	1.174	0.999
ADGRL1	ENST00000340736_5	1.844	0.190	1.043	0.999
AGRN	ENST00000379370_33	2.502	-0.534	0.853	0.999
AGRN	ENST00000379370_2	14.569	0.109	0.543	0.999
AGRN	ENST00000379370_3	6.951	1.641	0.584	0.263
AK3	ENST00000381809_4	10.491	0.926	0.469	0.834
AKT3	ENST00000263826_2	3.689	1.352	0.755	0.902
AKT3	ENST00000263826_12	2.917	1.018	0.829	0.999
AKT3	ENST00000263826_8	1.917	0.948	1.204	0.999
ARHGAP32	ENST00000310343_11	3.517	3.867	1.252	0.153
ARL15	ENST00000504924_1	3.082	0.233	0.816	0.999
ATG4B	ENST00000404914_10	4.195	2.521	0.964	0.406
BCL2L13	ENST00000618481_1	2.161	0.317	0.907	0.999
C20orf194	ENST00000252032_28	3.301	-0.203	0.707	0.999
C20orf194	ENST00000252032_27	3.638	0.621	1.015	0.999
CACNA1C	ENST00000347598_3	6.010	0.579	0.534	0.999
CACNA1C	ENST00000347598_30	2.527	-0.164	0.794	0.999
CAMK2B	ENST00000395749_4	5.486	2.494	0.803	0.153
CAMK2B	ENST00000395749_5	2.212	0.868	0.891	0.999
CAMK2B	ENST00000395749_11	5.806	-0.177	0.527	0.999
CAMTA1	ENST00000303635_6	6.342	1.044	0.596	0.919
CAMTA1	ENST00000303635_7	1.975	-0.051	0.984	0.999
CAMTA1	ENST00000303635_11	9.489	-0.361	0.418	0.999
CAMTA1	ENST00000303635_3	7.939	-0.111	0.462	0.999
CAMTA1	ENST00000303635_4	5.102	-0.035	0.614	0.999
CAMTA1	ENST00000303635_5	8.107	0.157	0.544	0.999
CASZ1	ENST00000377022_18	1.857	0.581	1.230	0.999
CASZ1	ENST00000377022_16	6.058	3.142	0.946	0.099
CASZ1	ENST00000377022_19	1.687	0.950	1.170	0.999
CASZ1	ENST00000377022_20	4.329	0.330	0.650	0.999
CASZ1	ENST00000377022_17	1.986	2.865	1.310	0.703
CBARP	ENST00000590083_8	3.184	1.048	0.956	0.999

CDH4	ENST00000614565_2	25.169	-0.042	0.318	0.999
CDH4	ENST00000614565_1	4.086	-1.741	0.723	0.565
CDO1	ENST00000250535_4	2.763	0.571	0.907	0.999
CELF5	ENST00000292672_1	7.892	2.816	0.854	0.102
CELF5	ENST00000292672_5	3.191	1.474	0.834	0.914
CNGA3	ENST00000393504_1	5.170	0.647	0.577	0.999
CNGA3	ENST00000393504_5	2.346	-0.807	0.825	0.999
CORO7	ENST00000251166_19	1.844	-0.373	0.969	0.999
CSGALNACT1	ENST00000454498_2	1.683	-0.052	1.014	0.999
CSGALNACT1	ENST00000454498_7	4.209	0.862	0.675	0.999
CTTNBP2	ENST00000160373_22	3.477	3.850	1.287	0.178
CYFIP2	ENST00000616178_30	2.143	-1.871	1.012	0.902
CYFIP2	ENST00000616178_1	1.871	0.191	1.029	0.999
CYFIP2	ENST00000616178_31	5.354	0.737	0.696	0.999
CYFIP2	ENST00000616178_20	1.762	3.859	1.291	0.178
DAPK1	ENST00000408954_2	6.776	1.876	0.617	0.162
DAPK1	ENST00000408954_3	2.587	0.051	0.811	0.999
DLGAP1	ENST00000315677_8	1.673	-0.614	1.032	0.999
DLGAP1	ENST00000315677_6	1.682	-0.602	1.014	0.999
DLGAP1	ENST00000315677_12	5.705	0.163	0.545	0.999
DLGAP1	ENST00000315677_11	5.635	1.668	0.783	0.731
DLGAP3	ENST00000373347_11	3.542	2.979	1.092	0.313
DNM1	ENST00000372923_10	2.952	-0.654	0.771	0.999
DNM1	ENST00000372923_14	3.899	-0.288	0.662	0.999
DTX1	ENST00000257600_2	3.187	0.551	0.759	0.999
EHBP1	ENST00000263991_11	2.260	-0.596	1.273	0.999
ELAVL3	ENST00000359227_4	12.759	4.881	1.035	0.001
ELAVL3	ENST00000359227_6	1.974	0.998	1.071	0.999
ELAVL3	ENST00000359227_3	2.085	-2.874	1.417	0.797
EP400	ENST00000389562_44	1.997	1.293	1.269	0.999
EPB41L4A	ENST00000621003_19	2.489	4.395	1.264	0.063
EPB41L4A	ENST00000621003_21	2.013	1.838	1.130	0.942

EPB41L4A	ENST00000621003_22	2.806	1.759	1.096	0.950
ETS2	ENST00000360214_2	1.638	-0.847	1.045	0.999
ETV5	ENST00000306376_2	1.968	0.915	1.108	0.999
EVL	ENST00000392920_8	2.600	0.749	0.816	0.999
EVL	ENST00000392920_3	2.123	-0.106	0.902	0.999
FEZ1	ENST00000278919_8	2.131	-0.984	1.640	0.999
FOXK1	ENST00000328914_1	2.908	2.582	1.121	0.622
FRMD4B	ENST00000398540_20	2.221	4.245	1.286	0.102
G2E3	ENST00000206595_1	1.683	3.844	1.548	0.515
GNB1L	ENST00000329517_6	1.846	0.768	1.070	0.999
GRAMD1A	ENST00000317991_1	2.553	-0.879	0.867	0.999
GREB1	ENST00000381486_10	1.916	0.910	1.076	0.999
GREB1	ENST00000381486_7	2.546	2.392	1.239	0.856
HDGFL2	ENST00000616600_6	11.659	5.605	1.202	0.001
ICA1	ENST00000402384_8	1.916	0.910	1.076	0.999
IGLON5	ENST00000270642_1	4.331	2.054	0.803	0.461
IGSF21	ENST00000251296_3	1.946	1.064	1.101	0.999
IGSF21	ENST00000251296_2	2.497	1.552	0.958	0.946
INSR	ENST00000302850_20	2.743	-0.008	1.082	0.999
IQCE	ENST00000476665_1	7.267	4.931	1.219	0.011
ISLR2	ENST00000361742_1	19.028	0.087	0.362	0.999
ISLR2	ENST00000361742_2	3.224	2.183	1.002	0.704
KALRN	ENST00000240874_1	10.313	-0.015	0.441	0.999
KCNIP1	ENST00000434108_1	16.915	0.212	0.379	0.999
KCNIP2	ENST00000461105_9	1.832	0.760	1.062	0.999
KCNQ2	ENST00000359125_16	2.564	0.975	0.922	0.999
KCNQ2	ENST00000359125_7	9.865	0.730	0.470	0.991
KCNQ2	ENST00000359125_2	1.998	-0.154	1.103	0.999
KIAA0753	ENST00000361413_1	5.959	0.664	0.567	0.999
KIF21A	ENST00000361418_26	1.821	0.810	1.286	0.999
KIF21A	ENST00000361418_37	4.437	2.148	0.939	0.639
KIF26B	ENST00000407071_2	11.345	0.277	0.542	0.999

KIF26B	ENST00000407071_5	1.872	0.024	0.952	0.999
KIF26B	ENST00000407071_4	18.757	2.851	0.468	0.000
KNDC1	ENST00000304613_3	3.720	-1.603	0.818	0.840
KNDC1	ENST00000304613_1	16.174	2.368	0.455	0.000
KNDC1	ENST00000304613_20	4.557	5.213	1.234	0.007
LINGO1	ENST00000355300_1	1.869	0.303	1.047	0.999
LRP8	ENST00000306052_17	2.928	-0.770	0.870	0.999
LRP8	ENST00000306052_14	2.635	1.752	0.957	0.902
MACF1	ENST00000361689_52	8.976	0.004	0.588	0.999
MACF1	ENST00000361689_1	7.784	-0.056	0.513	0.999
MAST1	ENST00000251472_3	9.852	3.061	0.691	0.003
MAST1	ENST00000251472_17	4.078	-0.059	0.708	0.999
MAST1	ENST00000251472_1	4.229	2.010	0.862	0.622
MAST1	ENST00000251472_12	2.053	0.745	0.910	0.999
MBNL2	ENST00000376673_3	4.549	4.250	1.234	0.069
MED13L	ENST00000281928_29	2.640	-0.781	1.108	0.999
METTL8	ENST00000612742_9	1.667	2.701	2.021	0.991
MNAT1	ENST00000261245_7	1.867	0.801	1.386	0.999
MTSS2	ENST00000338779_4	4.365	1.354	0.724	0.899
MYO18A	ENST00000527372_40	1.654	0.483	1.386	0.999
NPEPL1	ENST00000356091_3	2.189	4.142	1.285	0.128
NPEPL1	ENST00000356091_6	2.200	1.394	0.980	0.991
NUP188	ENST00000372577_24	1.711	-1.423	1.070	0.991
NUP210	ENST00000254508_20	7.514	1.282	0.542	0.597
ONECUT1	ENST00000305901_1	43.650	2.133	0.261	0.000
PCBP3	ENST00000400314_11	3.464	-1.225	0.867	0.991
PCBP3	ENST00000400314_2	19.010	2.718	0.461	0.000
PCBP3	ENST00000400314_1	4.108	1.005	0.688	0.991
PCBP3	ENST00000400314_9	1.797	-0.564	1.002	0.999
PCBP3	ENST00000400314_3	3.203	-0.315	0.763	0.999
PFKP	ENST00000381125_1	4.661	-0.735	0.713	0.999
PFKP	ENST00000381125_16	4.591	-0.070	0.595	0.999

PHF12	ENST00000332830_13	1.745	0.137	0.973	0.999
PHF12	ENST00000332830_8	3.333	2.213	1.091	0.797
PHF2	ENST00000359246_12	3.529	4.887	1.260	0.018
PHF2	ENST00000359246_1	2.792	-0.833	0.750	0.999
PRELID3A	ENST00000440960_1	2.257	0.155	0.967	0.999
PRELID3A	ENST00000440960_6	2.319	4.268	1.267	0.088
PREX1	ENST00000371941_37	1.807	3.941	1.555	0.470
PREX1	ENST00000371941_39	2.037	2.102	1.324	0.973
PRKG2	ENST00000264399_18	3.424	0.446	0.702	0.999
PRKG2	ENST00000264399_5	5.566	2.195	0.735	0.178
PSD	ENST00000020673_12	11.913	0.346	0.630	0.999
PSD	ENST00000020673_7	10.677	-0.167	0.510	0.999
PSD	ENST00000020673_16	4.292	4.073	1.239	0.104
PTPRD	ENST00000381196_2	1.731	-1.181	1.091	0.999
PTPRD	ENST00000381196_41	4.345	-0.198	0.622	0.999
PTPRD	ENST00000381196_36	4.697	0.804	0.639	0.999
PTPRD	ENST00000381196_34	1.854	1.603	1.195	0.991
PTPRD	ENST00000381196_35	17.324	0.021	0.363	0.999
PTPRD	ENST00000381196_37	4.915	0.538	0.584	0.999
PTPRD	ENST00000381196_38	3.077	0.680	0.865	0.999
PTPRD	ENST00000381196_39	4.607	1.189	0.673	0.914
PTPRD	ENST00000381196_32	1.663	-0.710	1.584	0.999
PTPRD	ENST00000381196_11	1.734	-2.086	1.246	0.939
PTPRN2	ENST00000389418_21	16.781	0.488	0.356	0.991
PTPRN2	ENST00000389418_12	11.747	-0.059	0.388	0.999
PTPRN2	ENST00000389418_13	2.226	1.486	1.092	0.991
PTPRN2	ENST00000389418_8	3.265	-0.136	1.193	0.999
PTPRN2	ENST00000389418_6	4.188	-0.543	0.775	0.999
PTPRN2	ENST00000389418_9	3.272	0.451	0.823	0.999
PTPRN2	ENST00000389418_14	4.508	5.205	1.226	0.007
PTPRN2	ENST00000389418_22	13.148	0.022	0.413	0.999
PTPRN2	ENST00000389418_20	11.699	0.958	0.416	0.622

PTPRN2	ENST00000389418_2	3.476	1.174	0.814	0.991
PTPRN2	ENST00000389418_1	4.888	0.406	0.998	0.999
PTPRN2	ENST00000389418_3	3.743	0.105	1.055	0.999
PTPRN2	ENST00000389418_11	19.876	-0.853	0.347	0.525
PTPRT	ENST00000373198_25	2.169	-0.583	1.488	0.999
PTPRT	ENST00000373198_31	7.394	-0.671	0.479	0.991
PTPRT	ENST00000373198_26	2.264	-1.068	0.903	0.999
PXDN	ENST00000252804_7	2.653	3.418	1.339	0.463
PXDN	ENST00000252804_22	3.537	0.250	0.999	0.999
RAB40B	ENST00000571995_5	2.131	0.605	0.936	0.999
RAI2	ENST00000545871_2	2.354	3.053	1.381	0.690
RAI2	ENST00000545871_1	1.999	1.927	1.486	0.999
RALGAPA2	ENST00000202677_3	1.862	0.097	1.562	0.999
RANBP17	ENST00000523189_14	4.400	-1.062	0.620	0.922
RIN2	ENST00000255006_2	3.807	-0.268	0.648	0.999
RNFT2	ENST00000257575_7	3.512	1.037	0.784	0.992
RNFT2	ENST00000257575_5	3.186	-1.162	0.769	0.991
RSF1	ENST00000308488_15	3.185	0.721	0.791	0.999
SCFD2	ENST00000401642_5	1.728	-0.318	1.123	0.999
SCFD2	ENST00000401642_4	2.850	0.062	1.280	0.999
SEMA6D	ENST00000316364_1	4.260	-0.303	0.652	0.999
SEPTIN11	ENST00000510515_11	1.965	2.969	1.289	0.622
SEPTIN11	ENST00000510515_1	3.299	-1.136	1.034	0.999
SETD5	ENST00000402198_1	2.588	-0.004	0.824	0.999
SETD5	ENST00000402198_18	9.928	3.884	0.864	0.003
SETD5	ENST00000402198_3	2.284	1.275	1.040	0.999
SIPA1L3	ENST00000222345_1	4.399	-0.282	0.623	0.999
SIPA1L3	ENST00000222345_2	1.985	0.563	1.032	0.999
SLC24A3	ENST00000328041_2	3.727	0.081	0.652	0.999
STMN2	ENST00000518111_1	75.711	3.891	0.380	0.000
SYN3	ENST00000358763_7	1.637	0.895	1.079	0.999
SYN3	ENST00000358763_8	8.819	0.156	0.797	0.999

SYN3	ENST00000358763_10	4.068	-0.988	0.675	0.991
SYN3	ENST00000358763_11	1.977	-0.961	1.858	0.999
SYN3	ENST00000358763_13	9.330	-0.308	0.511	0.999
SYT7	ENST00000540677_4	4.164	1.654	0.846	0.841
SYT7	ENST00000540677_9	4.871	1.085	0.658	0.942
SYT7	ENST00000540677_7	23.395	1.956	0.342	0.000
SYT7	ENST00000540677_6	27.460	1.735	0.327	0.000
TCTE1	ENST00000371505_3	2.303	-1.069	0.897	0.999
TMEM117	ENST00000266534_3	1.692	0.933	1.120	0.999
TMEM175	ENST00000264771_10	4.387	0.977	0.662	0.991
TRAPPC12	ENST00000324266_7	2.318	3.173	1.341	0.597
TRAPPC12	ENST00000324266_6	2.456	0.104	0.956	0.999
TRAPPC12	ENST00000324266_2	1.848	-1.775	1.294	0.991
TRAPPC12	ENST00000324266_9	11.612	0.472	0.417	0.999
TRAPPC12	ENST00000324266_8	3.359	0.425	0.791	0.999
TRRAP	ENST00000359863_1	1.846	-0.598	1.124	0.999
TSPAN18	ENST00000340160_1	3.409	0.441	0.724	0.999
TSPAN18	ENST00000340160_4	1.909	1.879	1.157	0.942
UBASH3B	ENST00000284273_1	5.345	0.143	0.555	0.999
UNC13B	ENST00000619578_1	1.899	-2.074	1.104	0.896
USP13	ENST00000263966_19	12.951	-0.183	0.780	0.999
ZGPAT	ENST00000328969_2	1.660	2.717	1.413	0.856
ZNF423	ENST00000561648_5	2.333	1.504	0.982	0.991
ZNF423	ENST00000561648_3	2.896	1.877	1.031	0.902
ZNF462	ENST00000277225_1	23.451	1.005	0.315	0.134

Table S4C. Differential transcript abundance in TDP-43 KD vs control iPSC-derived neurons

gene_name	baseMean	log2FoldChange	lfcSE	stat	pvalue	padj
STMN2	748018.798	-2.256	0.064	-35.420	8.31E-275	5.16E-271
ATG4B	26919.977	-2.291	0.077	-29.865	5.58E-196	1.43E-192
ADCY1	49242.682	-1.831	0.077	-23.756	9.52E-125	1.15E-121
CDO1	12462.537	-1.264	0.054	-23.255	1.27E-119	1.41E-116
RNFT2	7786.980	-0.939	0.042	-22.259	9.21E-110	8.89E-107
PRELID3A	1604.846	-1.544	0.072	-21.374	2.32E-101	2.02E-98
PTPRT	15939.469	-2.157	0.107	-20.161	2.17E-90	1.63E-87
IGSF21	7657.346	-1.820	0.098	-18.561	6.62E-77	3.42E-74
NUP188	18920.865	-1.025	0.056	-18.333	4.48E-75	2.21E-72
SLC24A3	5215.706	-1.821	0.106	-17.228	1.64E-66	6.19E-64
TRAPPC12	10217.193	-1.779	0.109	-16.281	1.36E-59	4.60E-57
PTPRZ1	1947.131	1.297	0.083	15.618	5.51E-55	1.64E-52

ETV5	9544.176	-0.695	0.045	-15.487	4.27E-54	1.23E-51
EML6	5574.172	0.599	0.040	15.091	1.86E-51	5.01E-49
CDH4	18239.485	-1.705	0.113	-15.062	2.86E-51	7.63E-49
RBPMS	1169.879	1.053	0.073	14.485	1.52E-47	3.63E-45
ACTL6B	22952.687	-2.522	0.177	-14.262	3.76E-46	8.46E-44
KALRN	35771.872	-1.519	0.115	-13.186	1.05E-39	1.87E-37
CDK7	3357.708	-1.470	0.112	-13.174	1.24E-39	2.17E-37
KCNIP1	14780.786	-0.398	0.033	-12.127	7.63E-34	1.04E-31
WASL	12278.299	-1.042	0.086	-12.069	1.54E-33	2.07E-31
PTPRN2	27484.772	-1.475	0.123	-11.994	3.81E-33	5.09E-31
MAST1	82385.645	-1.349	0.113	-11.953	6.28E-33	8.25E-31
UBASH3B	8588.058	-1.950	0.170	-11.457	2.18E-30	2.53E-28
LOXL1-AS1	844.333	0.943	0.084	11.230	2.91E-29	3.15E-27
AKT3	21489.902	-0.972	0.087	-11.185	4.85E-29	5.19E-27
CBARP	16289.732	-1.309	0.124	-10.591	3.29E-26	3.03E-24
FBN3	4343.504	-1.771	0.172	-10.282	8.46E-25	7.22E-23
MNAT1	2185.433	-1.825	0.189	-9.667	4.15E-22	3.13E-20
NPEPL1	3594.458	-1.265	0.132	-9.566	1.11E-21	8.27E-20
DENND2B	4909.061	0.488	0.051	9.557	1.22E-21	8.98E-20
STXBP5L	6015.393	-1.534	0.167	-9.203	3.48E-20	2.33E-18
TTC12	1791.837	0.443	0.049	9.029	1.74E-19	1.10E-17
TGFB3	1926.791	0.404	0.047	8.514	1.67E-17	8.89E-16
TMEM117	2102.689	-0.667	0.079	-8.397	4.59E-17	2.34E-15
IGLON5	69220.639	-0.781	0.093	-8.378	5.40E-17	2.72E-15
NECAB2	6111.727	-0.804	0.096	-8.335	7.74E-17	3.86E-15
ELAVL3	48465.357	-2.379	0.293	-8.119	4.69E-16	2.18E-14
SLC26A11	8282.559	-0.685	0.085	-8.102	5.40E-16	2.49E-14
CHID1	7384.707	-1.900	0.240	-7.925	2.27E-15	9.81E-14
PFKP	2652.373	-3.473	0.438	-7.924	2.29E-15	9.88E-14
CELF5	33677.722	-1.405	0.185	-7.606	2.83E-14	1.12E-12
ADCY8	1288.354	-0.714	0.097	-7.341	2.12E-13	7.74E-12
BCKDHB	2489.646	-0.702	0.096	-7.288	3.15E-13	1.13E-11

ZFAT	3159.965	0.410	0.056	7.288	3.14E-13	1.13E-11
KIAA0753	1054.723	-2.546	0.358	-7.118	1.10E-12	3.73E-11
MACF1	5629.783	1.612	0.227	7.100	1.24E-12	4.19E-11
ONECUT1	2791.347	1.263	0.178	7.097	1.27E-12	4.26E-11
CYFIP2	103222.465	-1.060	0.150	-7.057	1.70E-12	5.64E-11
TBL1X	3802.771	0.456	0.065	6.990	2.76E-12	8.97E-11
PEDS1	12954.366	0.250	0.036	6.975	3.05E-12	9.90E-11
CEP290	15455.455	-0.980	0.144	-6.786	1.15E-11	3.54E-10
PXDN	27122.923	-1.120	0.167	-6.708	1.97E-11	5.88E-10
FRMD4B	78.708	3.477	0.520	6.682	2.35E-11	6.95E-10
INSR	12880.928	-0.942	0.142	-6.641	3.12E-11	9.11E-10
MYO1C	8123.941	-0.522	0.080	-6.554	5.59E-11	1.60E-09
TFAP2E	346.336	1.230	0.194	6.349	2.17E-10	5.72E-09
ACTR1A	46696.668	-2.976	0.473	-6.287	3.23E-10	8.36E-09
USP13	5831.558	-1.215	0.197	-6.157	7.39E-10	1.84E-08
ETS2	14217.454	-0.649	0.107	-6.073	1.26E-09	3.00E-08
NSMCE4A	4349.834	-0.940	0.156	-6.025	1.69E-09	3.97E-08
SPEG	2850.117	1.211	0.202	5.996	2.02E-09	4.68E-08
ITGA7	5612.301	-0.724	0.122	-5.947	2.74E-09	6.21E-08
CENPBD1P1	16282.193	-0.446	0.076	-5.902	3.58E-09	8.00E-08
UNC13A	42383.737	-1.141	0.197	-5.786	7.20E-09	1.54E-07
ICA1	4358.071	-0.660	0.115	-5.757	8.57E-09	1.82E-07
NPLOC4	24060.196	-0.562	0.099	-5.661	1.51E-08	3.07E-07
CORO7	18354.997	-0.934	0.165	-5.651	1.60E-08	3.25E-07
C20orf194	21110.279	-1.846	0.336	-5.501	3.78E-08	7.26E-07
DNAJC12	5343.974	-0.670	0.124	-5.400	6.68E-08	1.23E-06
PAOX	727.728	-0.900	0.168	-5.367	7.99E-08	1.46E-06
ZDHHC1	1656.237	0.518	0.097	5.357	8.45E-08	1.53E-06
UVRAG	15413.868	-0.271	0.051	-5.334	9.60E-08	1.73E-06
UNC13B	40972.149	-0.833	0.158	-5.291	1.22E-07	2.15E-06
SHQ1	2365.140	-0.942	0.188	-5.016	5.28E-07	8.38E-06
SCFD2	4847.372	0.158	0.032	4.969	6.72E-07	1.04E-05

DLGAP1	5585.763	-0.935	0.190	-4.933	8.08E-07	1.23E-05
ISL2	3327.489	-1.164	0.239	-4.879	1.06E-06	1.58E-05
GPSM2	1896.890	0.651	0.136	4.771	1.83E-06	2.61E-05
NYNRIN	13539.545	-0.420	0.090	-4.643	3.43E-06	4.59E-05
NUP210	12476.804	-1.036	0.228	-4.536	5.72E-06	7.33E-05
MTSS2	5239.670	-2.219	0.490	-4.533	5.83E-06	7.46E-05
RNASET2	2014.124	0.261	0.058	4.502	6.74E-06	8.53E-05
SEMA6D	22437.811	-0.311	0.070	-4.416	1.00E-05	0.00012288
ZNF826P	1253.271	-0.457	0.104	-4.393	1.12E-05	0.00013507
LLNLR-271E8.1	513.947	1.560	0.359	4.351	1.36E-05	0.00016068
LIN28B	7674.224	-0.457	0.106	-4.318	1.57E-05	0.00018375
PRKG2	2511.337	-0.663	0.155	-4.272	1.93E-05	0.00022262
POU2F2	236.815	0.739	0.177	4.184	2.86E-05	0.0003149
ISLR2	51232.576	1.110	0.271	4.090	4.31E-05	0.00045729
CAMK2B	12799.222	-0.944	0.237	-3.989	6.65E-05	0.00067492
MAP6D1	357.197	1.516	0.383	3.954	7.69E-05	0.00076772
KNDC1	8158.136	-0.594	0.150	-3.947	7.91E-05	0.00078761
CBLN2	1277.566	0.488	0.124	3.946	7.95E-05	0.00079125
PHF2	6816.799	-2.389	0.613	-3.896	9.76E-05	0.00094737
KIF21A	45905.119	-1.051	0.279	-3.775	0.00016024	0.00146509
HDGFL2	21550.488	-0.713	0.199	-3.590	0.0003306	0.00278232
GRAMD1A	36196.639	-0.549	0.153	-3.578	0.00034657	0.00290464
MADD	16672.103	-1.683	0.471	-3.572	0.00035455	0.00296323
ADARB2	7003.718	-1.330	0.376	-3.541	0.00039797	0.00327888
ITGA3	10953.227	-0.427	0.121	-3.539	0.00040168	0.00330444

PHF12	19679.751	-0.151	0.043	-3.508	0.0004512 7	0.00365979
SLC1A6	13647.551	0.376	0.108	3.471	0.0005194 4	0.00412791
RIN2	7666.004	-0.306	0.090	-3.394	0.0006883 5	0.00526113
USP10	20073.923	-0.378	0.117	-3.234	0.0012195 2	0.00858901
CASZ1	13157.889	0.506	0.163	3.105	0.0019053 8	0.01248492
ADARB1	16915.797	0.321	0.105	3.064	0.0021832 9	0.01401645
WDR35	5067.068	-0.244	0.082	-2.989	0.0027969 7	0.01717953
FEZ1	43307.444	-0.834	0.286	-2.914	0.0035705	0.02099012
LIPE-AS1	651.816	0.294	0.102	2.889	0.0038641 9	0.02236651
ELAPOR1	3401.481	-0.552	0.191	-2.884	0.0039233 1	0.02265743
XPO4	8348.545	-0.308	0.108	-2.849	0.0043895	0.0249063
KIF17	728.190	-0.441	0.155	-2.847	0.0044075 6	0.02498268
SIPA1L3	8885.219	0.257	0.091	2.818	0.0048362 6	0.0269005
METTL8	3182.090	0.216	0.077	2.791	0.0052494 5	0.02883714
SEPTIN11	27130.616	-0.910	0.339	-2.679	0.0073745 6	0.03798612
SYT7	22747.314	-0.929	0.350	-2.654	0.0079533	0.04038806
LINC01503	687.450	0.263	0.102	2.583	0.0098028 3	0.04795398

MYO9B	1220.602	0.609	0.245	2.485	0.0129714 1	0.05988894
LRP8	36728.224	-0.122	0.049	-2.479	0.0131732 2	0.06057621
IFT122	4655.993	-0.406	0.165	-2.458	0.0139850 1	0.06352293
NPHP4	5711.836	0.279	0.114	2.444	0.0145435 2	0.06533511
PCBP3	8297.039	-0.391	0.161	-2.427	0.0152254 4	0.0675755
EVL	121397.408	0.272	0.114	2.380	0.0173014	0.07467724
GNB1L	2477.680	-0.253	0.109	-2.323	0.0201682 8	0.0841504
CACNA1C	8414.637	0.170	0.074	2.311	0.0208454 5	0.08635057
ATP6V1B2	56752.027	-1.794	0.793	-2.264	0.0235631 1	0.09479543
FKBP1B	15216.939	-0.126	0.056	-2.256	0.0240793 7	0.09634629
MTRR	5302.630	-0.498	0.221	-2.252	0.0243276 7	0.09710739
LINC02506	1897.013	-0.807	0.359	-2.249	0.0245069 1	0.09764351
LIN52	5148.979	-0.683	0.307	-2.227	0.0259224 7	0.10189203
MED13L	24827.597	0.208	0.093	2.221	0.0263174 8	0.10297909
ZNF462	15116.973	0.736	0.333	2.209	0.0271417 1	0.10552034
RALGAPA2	2781.994	-0.671	0.306	-2.195	0.0281307 8	0.10830012

DAPK1	37301.214	-0.105	0.048	-2.183	0.0290134 7	0.11079563
CEP131	7421.492	-0.366	0.170	-2.153	0.0312974 2	0.11743356
SETD5	10191.712	-0.619	0.299	-2.070	0.0384563 4	0.13680813
ESRRA	2128.343	-0.368	0.179	-2.056	0.0398252 5	0.14065356
RAP1GAP	3023.420	-0.490	0.253	-1.940	0.0523544 9	0.17161581
AGRN	87540.485	0.521	0.268	1.939	0.0524958	0.17194934
ARMH1	711.783	0.263	0.137	1.923	0.0544701 3	0.17660091
NOP14-AS1	4932.041	-0.230	0.122	-1.887	0.0592083 3	0.18738455
CELSR3	6014.818	1.034	0.551	1.877	0.0605184 3	0.19046303
STKLD1	596.725	0.153	0.082	1.873	0.0610934	0.19176923
FOXK1	16078.577	0.114	0.062	1.838	0.0660715 2	0.20274405
NKD1	5421.756	0.112	0.061	1.823	0.0683553 1	0.20780032
IQCE	17065.450	-0.445	0.245	-1.819	0.0689776 1	0.20913633
ZNF529	5224.836	-0.163	0.091	-1.796	0.0724582 7	0.21656385
HYOU1	23282.195	-0.179	0.100	-1.789	0.0736292	0.2190833
DTX1	14953.229	-0.356	0.200	-1.778	0.0753688 7	0.22270473
GTPBP6	6141.099	-0.231	0.131	-1.767	0.0772331 8	0.2265656

GTPBP6	6141.099	-0.231	0.131	-1.767	0.07723318	0.2265656
USP24	12491.993	-0.885	0.505	-1.752	0.07977894	0.23184322
SEMA3D	6055.096	-0.385	0.223	-1.727	0.08413077	0.24099376
GRIP2	742.110	-0.327	0.191	-1.717	0.08605216	0.24475374
DNM1	52505.854	-0.346	0.204	-1.699	0.08932627	0.25110254
RP5-864K19.4	275.339	-0.407	0.240	-1.696	0.0899551	0.25214457
AK3	4731.829	-0.555	0.328	-1.693	0.09054282	0.25330197
G2E3	5620.044	-0.247	0.153	-1.616	0.1061779	0.28218679
CRLS1	7814.761	-0.151	0.094	-1.599	0.1098382	0.28852773
CAMTA1	10033.849	0.216	0.136	1.586	0.11273368	0.29298219
CNOT1	6984.071	-0.531	0.349	-1.522	0.12791594	0.31820865
KIAA1841	7245.988	-0.327	0.217	-1.512	0.13065375	0.32247262
SPPL2B	7086.501	0.202	0.138	1.465	0.14292636	0.34251132
FAM81A	1349.185	0.111	0.076	1.465	0.14300299	0.34258456
CCDC57	401.746	0.281	0.194	1.450	0.14699518	0.34868741
PSD	7867.162	0.557	0.392	1.424	0.15458095	0.36040974
SDAD1	6983.078	-0.350	0.256	-1.368	0.17133696	0.38537708
ZNF382	670.268	0.651	0.480	1.356	0.1750865	0.39100103

LRFN1	17106.970	0.167	0.124	1.343	0.1792138 7	0.39670202
TCTE1	30.472	-0.843	0.637	-1.323	0.1857008 6	0.4056805
HULC	2217.076	0.054	0.042	1.304	0.1922054 9	0.41449523
LMO7	539.834	0.242	0.193	1.256	0.2092355 4	0.43689402
BCL2L13	7486.066	0.191	0.152	1.254	0.2097051 9	0.4374334
TTYH2	686.760	0.808	0.646	1.251	0.2109778 9	0.43907683
CTTNBP2	11124.166	0.138	0.111	1.246	0.2126258 2	0.44132319
RP1-283E3.8	1372.205	0.832	0.679	1.226	0.2200416 2	0.45079599
CNGA3	2297.741	-0.266	0.222	-1.197	0.2311252 6	0.465409
RAI2	2203.212	0.158	0.140	1.131	0.2580446 7	0.49764613
NTRK3	3890.385	0.531	0.482	1.101	0.2708964 5	0.51200477
LINC00963	5352.854	0.236	0.214	1.101	0.2710940 2	0.51217775
RP11-291L22.9	328.654	0.142	0.135	1.048	0.2946256 6	0.53836789
TRRAP	9856.883	-0.515	0.499	-1.033	0.3017274 3	0.54526438
DIP2A	8800.318	-0.293	0.295	-0.990	0.3219366 7	0.56624849
CPLANE1	2346.536	0.326	0.329	0.990	0.3219821 1	0.5663055

MYO18A	15399.792	0.430	0.441	0.974	0.3300829	0.57446179
AARS1	49070.141	-0.178	0.190	-0.935	0.34957407	0.59374185
ARHGAP32	5128.970	0.284	0.319	0.890	0.37373239	0.6169359
KCNQ2	56941.529	0.388	0.455	0.852	0.39440196	0.63664134
NADSYN1	2143.048	0.350	0.435	0.806	0.42017071	0.65976638
KIF26B	17946.615	-0.181	0.225	-0.802	0.42228742	0.66168307
PKD1	33780.081	-0.442	0.553	-0.800	0.42359501	0.66264438
PTPRD	1837.689	-0.542	0.703	-0.770	0.44111026	0.67695046
GALNT8	388.010	-0.455	0.592	-0.768	0.44242326	0.67804263
RGPD4	1726.534	0.090	0.120	0.748	0.45474512	0.68868466
SYN3	374.791	0.348	0.468	0.742	0.45801553	0.69122598
SEPTIN7P2	868.951	0.199	0.281	0.708	0.4790127	0.70810305
L3MBTL1	2498.151	0.117	0.169	0.696	0.48620834	0.71313985
ADGRL1	31059.889	0.224	0.336	0.667	0.50476512	0.72712533
RP11-106M3.5	42.033	-1.126	1.713	-0.658	0.51082903	0.73130112
TMEM175	2775.133	-0.099	0.152	-0.648	0.51724079	0.73656221
HDAC6	6347.652	-0.202	0.318	-0.635	0.52530106	0.74209995

VWCE	2054.919	0.059	0.096	0.616	0.5379684 7	0.75050392
DLGAP3	14871.912	-0.139	0.228	-0.610	0.5421539 8	0.75335701
INTS8	3044.115	-0.116	0.206	-0.563	0.5732077 3	0.77528383
CSGALNACT 1	2106.842	0.447	0.819	0.546	0.5851404 1	0.78333109
EP400	1440.442	-0.165	0.305	-0.542	0.5875168	0.78464937
FRG1HP	70.551	-0.130	0.242	-0.536	0.5922451 9	0.7878659
ZNF141	7216.618	0.059	0.113	0.524	0.6005922 9	0.79379275
ZNF527	3484.060	0.039	0.093	0.424	0.6713969 1	0.83898878
RSF1	35245.262	-0.061	0.145	-0.417	0.6767365	0.84248529
ATF7IP2	1019.705	0.041	0.102	0.401	0.6884138 9	0.84917046
ZGPAT	1516.011	-0.058	0.162	-0.358	0.7203291 6	0.86709752
ZNF423	17793.004	0.074	0.239	0.312	0.755112	0.88694276
MRPL45P2	330.503	0.077	0.269	0.287	0.7740697 3	0.89728099
RHOBTB3	18974.667	-0.024	0.086	-0.276	0.7827743 7	0.90164127
SYNE1	1387.453	0.106	0.389	0.273	0.7850760 9	0.90280883
ADGRB1	27875.397	-0.050	0.236	-0.213	0.8314419 2	0.92427676
RAB40B	4123.760	-0.018	0.097	-0.190	0.8491627	0.93276358
RANBP17	1199.619	0.035	0.188	0.184	0.8536413 1	0.93498965

LINGO1	74436.598	-0.021	0.135	-0.157	0.8753182	0.9455989
CERS4	1219.434	-0.073	0.474	-0.154	0.8779594	0.94658787
USP36	3335.039	0.026	0.196	0.131	0.8954166	0.95457767
ADCY7	5617.638	0.047	0.373	0.127	0.8992446	0.95681143
GREB1	2318.298	0.069	0.587	0.118	0.9062467	0.95995853
RFLNA	3595.717	0.010	0.088	0.110	0.9121915	0.96230039
PREX1	13180.529	0.010	0.092	0.107	0.9149062	0.96352479
MBNL2	89.820	-0.078	0.789	-0.099	0.9211096	0.96652367
EHBP1	15394.730	-0.009	0.149	-0.059	0.9526793	0.98021248
KCNIP2	1747.616	-0.019	0.362	-0.052	0.9582853	0.9824928
EPB41L4A	5561.332	0.015	0.681	0.023	0.9819176	0.99284615
AACSP1	111.199	-0.007	0.521	-0.013	0.9894156	0.99588605
TSPAN18	10481.852	0.000	0.366	-0.001	0.9991027	0.99967773

Table S4D. Differential protein abundance in TDP-43 KD vs control iPSC-derived neurons

gene_name	UniprotID	AVG.Log2.Ratio	Pvalue	Qvalue	NegLog10_Qvalue
AARS1	P49588	-0.555	3.42E-89	4.83E-87	86.316
ACTL6B	O94805	-2.515	6.62E-33	9.45E-32	31.024
ACTR1A	P61163	-0.876	5.13E-33	7.58E-32	31.120
ADARB1	P78563	0.521	2.22E-15	7.16E-15	14.145
AGRN	O00468	-0.015	0.65972224	0.18329627	0.737
AK3	Q9UIJ7	-0.399	3.22E-21	1.82E-20	19.741
AKT3	Q9Y243	-2.155	3.15E-06	3.03E-06	5.519
ARHGAP32	A7KAX9	0.371	0.26240486	0.08492955	1.071
ARL15	Q9NXU5	-0.387	0.00165493	0.00093787	3.028
ATG4B	Q9Y4P1	-0.785	8.30E-06	7.37E-06	5.133
ATP6V1B2	P21281	-0.071	1.81E-06	1.82E-06	5.740
BCL2L13	Q9BXK5	-0.173	1.38E-05	1.17E-05	4.932
CAMK2B	Q13554	-1.295	4.28E-25	3.33E-24	23.477
CASZ1	Q86V15	0.718	1.38E-10	2.56E-10	9.592

CBARP	Q8N350	-2.641	1.28E-09	2.07E-09	8.685
CDK7	P50613	-0.609	5.58E-06	5.12E-06	5.291
CELF5	Q8N6W0	-3.519	8.97E-08	1.11E-07	6.954
CELSR3	Q9NYQ7	-0.383	1.97E-07	2.31E-07	6.637
CHID1	Q9BWS9	-2.517	9.23E-14	2.49E-13	12.604
CNOT1	A5YKK6	-0.211	1.12E-12	2.61E-12	11.583
CORO7	P57737	-1.121	1.33E-28	1.30E-27	26.886
CTTNBP2	Q8WZ74	-0.287	0.39022268	0.1182493	0.927
CYFIP2	Q96F07	-0.812	2.69E-56	1.42E-54	53.847
DAPK1	P53355	-0.808	2.43E-08	3.28E-08	7.484
DNAJC12	Q9UKB3	-1.336	2.04E-05	1.69E-05	4.773
DNM1	Q05193	-0.557	4.98E-40	1.15E-38	37.939
EHBP1	Q8NDI1	-0.144	4.10E-08	5.33E-08	7.274
ELAVL3	Q14576	-2.388	1.09E-33	1.77E-32	31.752
EP400	Q96L91	0.012	0.06039209	0.0237308	1.625
EVL	Q9UI08	0.185	0.0018632	0.00104563	2.981
FEZ1	Q99689	-0.411	0.00555422	0.00281367	2.551
FKBP1B	P68106	0.148	0.00918537	0.00442987	2.354
FOXK1	P85037	-0.267	0.41484152	0.12443286	0.905
GRAMD1A	Q96CP6	-0.882	1.29E-11	2.66E-11	10.575
GREB1	Q4ZG55	0.290	0.00893022	0.00432053	2.364
GTPBP6	O43824	-0.548	1.51E-09	2.41E-09	8.619
HDAC6	Q9UBN7	-1.596	3.92E-23	2.61E-22	21.584
HDGFL2	Q7Z4V5	0.380	3.91E-14	1.09E-13	12.964
HYOU1	Q9Y4L1	-0.308	4.44E-47	1.61E-45	44.793
IGLON5	A6NGN9	-0.565	0.00330812	0.00176526	2.753
ISLR2	Q6UXK2	-0.626	3.00E-32	4.14E-31	30.383
ITGA3	P26006	-0.840	8.43E-05	6.13E-05	4.212
ITGA7	Q13683	-0.802	2.38E-07	2.75E-07	6.561
KALRN	O60229	-1.920	7.35E-46	2.33E-44	43.632
KCNQ2	O43526	-0.414	6.19E-05	4.61E-05	4.337
KIF21A	Q7Z4S6	-0.891	4.11E-90	6.52E-88	87.186

LIN28B	Q6ZN17	-0.016	0.75279038	0.20393425	0.691
LINGO1	Q96FE5	-0.613	8.95E-12	1.88E-11	10.725
MACF1	Q9UPN3	0.038	0.05517988	0.02189435	1.660
MADD	Q8WXG6	-2.081	3.65E-17	1.41E-16	15.852
MAST1	Q9Y2H9	-0.403	0.00050361	0.00031678	3.499
MYO18A	Q92614	-0.470	4.69E-101	1.49E-98	97.827
MYO1C	O00159	-0.879	5.90E-35	1.03E-33	32.988
NECAB2	Q7Z6G3	-1.209	2.07E-07	2.42E-07	6.617
NPEPL1	Q8NDH3	-2.103	2.15E-06	2.13E-06	5.671
NPLOC4	Q8TAT6	-0.225	1.72E-07	2.04E-07	6.689
NUP188	Q5SRE5	-1.221	1.46E-22	9.44E-22	21.025
NUP210	Q8TEM1	-0.457	8.78E-17	3.29E-16	15.483
PCBP3	P57721	-0.775	1.08E-06	1.14E-06	5.944
PFKP	Q01813	-2.188	1.86E-06	1.86E-06	5.730
PHF2	O75151	0.318	0.00129778	0.00075674	3.121
PREX1	Q8TCU6	-0.239	6.61E-12	1.41E-11	10.850
PRKG2	Q13237	-0.944	9.37E-24	6.47E-23	22.189
PTPRD	P23468	0.087	0.16369834	0.05678692	1.246
RAP1GAP	P47736	-0.733	2.73E-14	7.70E-14	13.113
RSF1	Q96T23	0.246	4.52E-12	9.77E-12	11.010
SCFD2	Q8WU76	-0.388	2.02E-06	2.01E-06	5.697
SEMA6D	Q8NFY4	-0.152	0.47853428	0.14055008	0.852
SEPTIN11	Q9NVA2	-0.083	0.00878384	0.00425944	2.371
STMN2	Q93045	-3.304	8.46E-15	2.55E-14	13.594
SYN3	O14994	-0.516	7.08E-15	2.14E-14	13.669
SYNE1	Q8NF91	-0.178	5.43E-07	5.96E-07	6.225
SYT7	O43581	-2.255	1.61E-26	1.36E-25	24.867
TRAPPC12	Q8WVT3	-3.569	9.36E-07	9.93E-07	6.003
TRRAP	Q9Y4A5	0.175	6.92E-07	7.52E-07	6.124
UBASH3B	Q8TF42	-1.316	0.00083003	0.00050054	3.301
UNC13A	Q9UPW8	0.141	0.00024363	0.00016251	3.789
UNC13B	O14795	-1.011	5.95E-31	7.41E-30	29.130

USP10	Q14694	-0.111	1.80E-06	1.82E-06	5.741
USP24	Q9UPU5	-0.930	1.32E-17	5.28E-17	16.278
WASL	O00401	-2.105	4.41E-17	1.69E-16	15.773
XPO4	Q9C0E2	-0.383	0.00012135	8.54E-05	4.068
ZNF423	Q2M1K9	0.472	0.60404648	0.17089308	0.767
ZNF462	Q96JM2	0.901	1.94E-30	2.32E-29	28.634

Table S4E. Shotgun proteomics database search results

Peptide	Gene	ppm	m.z	RT	10Log P	Median intensity	Log10 .intensity
ACLLVKMVSCR	CAMK2B	3.300	611.828	87.820	9.070	73791.000	4.868
ACLLVKMVSCRAGSCLRAGVPGAACSSLR	CAMK2B	4.400	960.495	102.280	16.880	246425.000	5.392
AGSCLRAGVPGAACSSLR	CAMK2B	-1.300	838.419	84.720	10.090	135530.000	5.132
AGSCLRAGVPGAACSSLRVTER	CAMK2B	5.600	721.041	118.570	10.950	246410.000	5.392
AGVPGAACSSLR	CAMK2B	4.800	544.781	25.560	22.130	200880.000	5.303
AGVPGAACSSLRVTER	CAMK2B	-6.700	525.272	31.890	16.350	855280.000	5.932
AGVPGAACSSLRVTERSAGSAETSPTGR	CAMK2B	-2.300	892.439	115.140	25.640	99146.000	4.996
AGVPGAACSSLRVTERSAGSAETSPTGRVPR	CAMK2B	-7.200	1009.841	87.620	14.850	577740.000	5.762
AINFPGARLQSAACR	SYT7	13.700	787.925	95.720	6.110	473470.000	5.675
APPGVPRPAPPVR	DNM1	-2.000	655.887	31.590	7.990	283990.000	5.453

APPGVPRPAPPVRVNCHVDFVLSFR	DNM1	-5.500	1364.225	111.500	10.930	0.000	N/A
ARVCVCTELR	AGRN	-3.600	575.295	54.350	15.670	2327500.000	6.367
EEDKTLPKPGSPGK	MYO18A	-0.400	494.931	26.010	12.740	1092300.000	6.038
EKAPSASDSDSK	HDGFL2	-12.900	611.275	52.000	13.950	725210.000	5.860
EPSDVKEEDK	MYO18A	-5.000	588.270	31.380	5.230	278950.000	5.446
EPSDVKEEDKTLPKPGSPGK	MYO18A	-10.900	1069.541	72.860	11.410	227280.000	5.357
EPTIWFGK	HDGFL2	13.500	489.265	26.070	9.200	3820250.000	6.582
EPTIWFGKGHSGMLASEGR	HDGFL2	1.300	687.340	15.240	20.490	49390.000	4.694
ERAGQPSPHPLGR	ADGRB1	9.600	467.921	13.210	7.040	166990.000	5.223
EVATQFK	MYO1C	2.600	411.723	23.950	9.880	569310.000	5.755
GAGGGSSPK	RSF1	-1.900	717.351	57.230	5.520	62810.000	4.798
GAGGGSSPKLNHSNEPQHK	RSF1	-2.500	951.462	68.730	11.360	96348.000	4.984
GAGGGSSPKLNHSNEPQHKIPGK	RSF1	1.900	575.050	58.230	9.940	12765000.000	7.106
GHSGMLASEGR	HDGFL2	1.800	551.260	24.780	7.460	5329000.000	6.727
GHSGMLASEGREAVLTR	HDGFL2	-8.900	885.939	72.310	30.340	229045.000	5.360
GHSGMLASEGREAVLTRLHESER	HDGFL2	-7.300	841.414	91.920	16.460	0.000	N/A
GHSGMLASEGREAVLTRLHESERVR	HDGFL2	-8.800	1389.203	112.780	8.450	0.000	N/A
KEPTIWFGKGHSGMLASEGR	HDGFL2	-12.700	730.028	67.480	14.540	768100.000	5.885
KGHSGMLASEGR	HDGFL2	-0.700	410.540	20.460	15.580	581270.000	5.764

KNSLLWEFRPQTGCMYVAVGGSTHSK	CAMK2B	-0.200	966.143	75.030	6.350	0.000	N/A
KNTRGAGGGSSPK	RSF1	2.200	608.823	65.260	17.700	4227450.000	6.626
KPCSSYGFEGYR	RSF1	4.800	697.315	22.100	7.750	3302267.000	6.519
LCSGKPEGTGSR	KALRN	5.000	596.296	66.430	25.210	1897200.000	6.278
LCSGKPEGTGSRVS	KALRN	10.600	689.349	66.410	8.640	5566400.000	6.746
LLGSVVYAHSKITLTTIGYGDKYPQTWNGR	KCNQ2	-7.300	1113.581	110.200	5.940	876080.000	5.943
LLLLTHYCSLSPR	RSF1	-8.600	758.415	109.900	6.210	37045.000	4.569
LPEYEFKMDKPPSVSAR	KALRN	-12.400	997.494	68.670	20.540	0.000	N/A
LPEYEFKMDKPPSVSARLCSGKPEGTGSR	KALRN	5.200	792.401	98.920	10.290	76095.000	4.881
LVSNSWVQAILLPRPPK	ACTL6B	-11.900	640.040	146.130	5.130	22393.000	4.350
MDKPPSVSAR	KALRN	-4.500	544.278	26.970	28.680	735710.000	5.867
MDKPPSVSARLCSGKPEGTGSR	KALRN	8.500	754.050	75.080	14.530	100170.000	5.001
MDKPPSVSARLCSGKPEGTGSRVS	KALRN	4.200	816.081	109.360	12.290	16727.000	4.223
MSLHSSPGDR	CAMK2B	-11.700	543.746	29.830	9.280	3346300.000	6.525
MVSCRAGSCLR	CAMK2B	11.500	591.788	60.080	5.760	0.000	N/A

MVSCRAGSCLRAGVPGAACSSLR	CAMK2B	-0.200	751.366	93.410	19.020	6727.000	3.828
MVSCRAGSCLRAGVPGAACSSLRVTER	CAMK2B	5.000	913.125	118.410	9.820	111200.000	5.046
NLKEVATQFK	MYO1C	0.000	589.332	32.720	26.200	763800.000	5.883
NNDLLFRNLKEVATQFK	MYO1C	1.600	684.042	113.040	9.690	1804590.000	6.256
NTRGAGGGSSPK	RSF1	0.200	544.774	29.630	14.690	46743.500	4.670
NTRGAGGGSSPKLNHSNEPQHK	RSF1	-6.600	758.369	64.300	13.410	22728.000	4.357
NTRGAGGGSSPKLNHSNEPQHKIPGK	RSF1	9.500	890.135	85.410	7.590	989860.000	5.996
REPSDVKEEDK	MYO18A	0.400	666.324	28.980	6.970	1679960.000	6.225
SAGSAETSPTGR	CAMK2B	2.600	560.765	32.880	20.920	1268500.000	6.103
SAGSAETSPTGRVPR	CAMK2B	-4.300	736.873	37.660	17.370	1057850.000	6.024
SAGSAETSPTGRVPRNLLPVHFWGFEFFPR	CAMK2B	-9.800	1120.563	114.180	5.890	64707.000	4.811
TNYFEKPLLLVCIAR	CAMK2B	3.600	594.000	83.690	9.780	51853.000	4.715
VLQAPPPDVGNGEGSR	RSF1	4.000	796.908	108.930	18.190	2373000.000	6.375
VLQAPPPDVGNGEGSRGGR	RSF1	-6.400	931.971	72.690	17.340	113510.000	5.055
VLQAPPPDVGNGEGSRGGRCCGSVIR	RSF1	-12.300	861.083	64.710	17.030	957840.000	5.981

VLQAPPPDVGNGEGSRGGRCCGSVIRR	RSF1	-4.800	913.122	87.030	9.350	632380.000	5.801
VSASNPWGISLPSEPSEFVRLPEYEFK	KALRN	2.300	1022.516	116.330	17.270	44046.000	4.644
VTERSAGSAETSPTGR	CAMK2B	5.700	803.400	97.940	13.570	349710.000	5.544
VTERSAGSAETSPTGRVPR	CAMK2B	4.400	979.510	120.090	11.630	4530.800	3.656
VTERSAGSAETSPTGRVPRNLLPVHFWGFEFFPR	CAMK2B	-4.600	1282.321	110.560	5.100	0.000	N/A
YGPLLDLPELPFPELERVLQAPPPDVGNGEGSRGGR	RSF1	-9.900	1281.318	106.080	6.220	373860.000	5.573

Table S4F. Amino acid sequence of putative cryptic peptides across 12 genes

gene_name	peptide
ACTL6B	LVSNSWVQAILLPRPPK
ADGRB1	ERAGQPSPHPLGR
AGRN	ARVCVCTELR
CAMK2B	AGVPGAACSSLRVTERSAGSAETSPTGR
CAMK2B	AGVPGAACSSLR
CAMK2B	SAGSAETSPTGR
CAMK2B	MVSCRAGSCLRAGVPGAACSSLR
CAMK2B	SAGSAETSPTGRVPR
CAMK2B	ACLLVKMVSCRAGSCLRAGVPGAACSSLR
CAMK2B	AGVPGAACSSLRVTER
CAMK2B	AGVPGAACSSLRVTERSAGSAETSPTGRVPR
CAMK2B	VTERSAGSAETSPTGR
CAMK2B	VTERSAGSAETSPTGRVPR
CAMK2B	AGSCLRAGVPGAACSSLRVTER
CAMK2B	AGSCLRAGVPGAACSSLR
CAMK2B	MVSCRAGSCLRAGVPGAACSSLRVTER
CAMK2B	TNYFEKPLLLVCIAR
CAMK2B	MSLHSSPGDR
CAMK2B	ACLLVKMVSCR
CAMK2B	KNSLLWEFRPQTGCMYVAVGGSTHSK
CAMK2B	SAGSAETSPTGRVPRNLLPVHFWGFEFFPR
CAMK2B	MVSCRAGSCLR
CAMK2B	VTERSAGSAETSPTGRVPRNLLPVHFWGFEFFPR
DNM1	APPGVPRPAPPVRVNCHVDFVLSFR
DNM1	APPGVPRPAPPVR
HDGFL2	GHSGMLASEGREAVLTR
HDGFL2	EPTIWFGKGHSGMLASEGR
HDGFL2	GHSGMLASEGREAVLTRLHESER

HDGFL2	KGHSGMLASEGR
HDGFL2	KEPTIWFGKGHSGMLASEGR
HDGFL2	EKAPSASDSDSK
HDGFL2	EPTIWFGK
HDGFL2	GHSGMLASEGREAVLTRLHESERVR
HDGFL2	GHSGMLASEGR
KALRN	MDKPPSVSAR
KALRN	LCSGKPEGTGSR
KALRN	LPEYEFKMDKPPSVSAR
KALRN	VSASNPWGISLPSEPSEFVRLPEYEFK
KALRN	MDKPPSVSARLCSGKPEGTGSR
KALRN	MDKPPSVSARLCSGKPEGTGSRVS
KALRN	LPEYEFKMDKPPSVSARLCSGKPEGTGSR
KALRN	LCSGKPEGTGSRVS
KCNQ2	LLGSVVYAHSKITLTTIGYGDKYPQTWNGR
MYO18A	EEDKTLPKPGSPGK
MYO18A	EPSDVKEEDKTLPKPGSPGK
MYO18A	REPSDVKEEDK
MYO18A	EPSDVKEEDK
MYO1C	NLKEVATQFK
MYO1C	EVATQFK
MYO1C	NNDLLFRNLKEVATQFK
RSF1	VLQAPPPDVGNGEGSR
RSF1	KNTRGAGGGSSPK
RSF1	VLQAPPPDVGNGEGSRGGR
RSF1	VLQAPPPDVGNGEGSRGGRCCGSVIR
RSF1	NTRGAGGGSSPK
RSF1	NTRGAGGGSSPKLNHSNEPQHK
RSF1	GAGGGSSPKLNHSNEPQHK
RSF1	GAGGGSSPKLNHSNEPQHKIPGK
RSF1	VLQAPPPDVGNGEGSRGGRCCGSVIRR
RSF1	KPCSSYGFEGYR

RSF1	NTRGAGGGSSPKLNHSNEPQHKIPGK
RSF1	YGPLLDLPELPFPELERVLQAPPPDVGNGEGSRGG R
RSF1	LLLLTHYCSLSPR
RSF1	GAGGGSSPK
SYT7	AINFPGARLQSAACR

Table S4F. Amino acid sequence of putative cryptic peptides across 12 genes

gene_name	peptide
ACTL6B	LVSNSWVQAILLPRPPK
ADGRB1	ERAGQPSPHPLGR
AGRN	ARVCVCTELR
CAMK2B	AGVPGAACSSLRVTERSAGSAETSPTGR
CAMK2B	AGVPGAACSSLR
CAMK2B	SAGSAETSPTGR
CAMK2B	MVSCRAGSCLRAGVPGAACSSLR
CAMK2B	SAGSAETSPTGRVPR
CAMK2B	ACLLVKMVSCRAGSCLRAGVPGAACSSLR
CAMK2B	AGVPGAACSSLRVTER
CAMK2B	AGVPGAACSSLRVTERSAGSAETSPTGRVPR
CAMK2B	VTERSAGSAETSPTGR
CAMK2B	VTERSAGSAETSPTGRVPR
CAMK2B	AGSCLRAGVPGAACSSLRVTER
CAMK2B	AGSCLRAGVPGAACSSLR
CAMK2B	MVSCRAGSCLRAGVPGAACSSLRVTER
CAMK2B	TNYFEKPLLLVCIAR
CAMK2B	MSLHSSPGDR
CAMK2B	ACLLVKMVSCR
CAMK2B	KNSLLWEFRPQTGCMYVAVGGSTHSK
CAMK2B	SAGSAETSPTGRVPRNLLPVHFWGFEFFPR
CAMK2B	MVSCRAGSCLR
CAMK2B	VTERSAGSAETSPTGRVPRNLLPVHFWGFEFFPR
DNM1	APPGVPRPAPPVRVNCHVDFVLSFR
DNM1	APPGVPRPAPPVR
HDGFL2	GHSGMLASEGREAVLTR
HDGFL2	EPTIWFGKGHSGMLASEGR

HDGFL2	GHSGMLASEGREAVLTRLHESER
HDGFL2	KGHSGMLASEGR
HDGFL2	KEPTIWFGKGHSGMLASEGR
HDGFL2	EKAPSASDSDSK
HDGFL2	EPTIWFGK
HDGFL2	GHSGMLASEGREAVLTRLHESERVR
HDGFL2	GHSGMLASEGR
KALRN	MDKPPSVSAR
KALRN	LCSGKPEGTGSR
KALRN	LPEYEFKMDKPPSVSAR
KALRN	VSASNPWGISLPSEPSEFVRLPEYEFK
KALRN	MDKPPSVSARLCSGKPEGTGSR
KALRN	MDKPPSVSARLCSGKPEGTGSRVS
KALRN	LPEYEFKMDKPPSVSARLCSGKPEGTGSR
KALRN	LCSGKPEGTGSRVS
KCNQ2	LLGSVVYAHSKITLTTIGYGDKYPQTWNGR
MYO18A	EEDKTLPKPGSPGK
MYO18A	EPSDVKEEDKTLPKPGSPGK
MYO18A	REPSDVKEEDK
MYO18A	EPSDVKEEDK
MYO1C	NLKEVATQFK
MYO1C	EVATQFK
MYO1C	NNDLLFRNLKEVATQFK
RSF1	VLQAPPPDVGNGEGSR
RSF1	KNTRGAGGGSSPK
RSF1	VLQAPPPDVGNGEGSRGGR
RSF1	VLQAPPPDVGNGEGSRGGRCCGSVIR
RSF1	NTRGAGGGSSPK
RSF1	NTRGAGGGSSPKLNHSNEPQHK
RSF1	GAGGGSSPKLNHSNEPQHK
RSF1	GAGGGSSPKLNHSNEPQHKIPGK
RSF1	VLQAPPPDVGNGEGSRGGRCCGSVIRR

RSF1	KPCSSYGFEGYR
RSF1	NTRGAGGGSSPKLNHSNEPQHKIPGK
RSF1	YGPLLDLPELPFPELERVLQAPPPDVGNGEGSRGGR
RSF1	LLLLTHYCSLSPR
RSF1	GAGGGSSPK
SYT7	AINFPGARLQSAACR

Table S4G. List of targeted long-read sequencing primers

Gene	Sequence (5'-Oxford Nanopore primer - [sequence-specific] -3')
ACTL6B	ACTTGCCTGTCGCTCTATCTTCACATTTTTACTTCTTTCAACCCAGA
HDGFL2	ACTTGCCTGTCGCTCTATCTTCCATGTTGGTTGGAAATCACAGA
KALRN	ACTTGCCTGTCGCTCTATCTTCAGATGGCTACGTCCCTTGGTTC
AGRN	ACTTGCCTGTCGCTCTATCTTCGAACCTGTGTCAAACCTGAG
PXDN	ACTTGCCTGTCGCTCTATCTTCACAGCAGACAAACTCTGAGGAG
CAMK2B	ACTTGCCTGTCGCTCTATCTTCTCCAAACACCAACTCTGTCCGGCGA
ADGRB1	ACTTGCCTGTCGCTCTATCTTCCTCGGTCTGGAGGTCGATGATG
ADGRL1	ACTTGCCTGTCGCTCTATCTTCTCAGACCTCGGTCTGGAGGTCGAT
SIPA1L3	ACTTGCCTGTCGCTCTATCTTCGATGGGTCATCTTGGTCACACC
SEMA6D	ACTTGCCTGTCGCTCTATCTTCCCACATGGGAATAGCACACTTG
LINGO1	ACTTGCCTGTCGCTCTATCTTCGGAAGGACTGGAGAGTGAGCAG
SYT7	ACTTGCCTGTCGCTCTATCTTCGCGTTGTGCATAAAGTGGTGAG
CHID1	ACTTGCCTGTCGCTCTATCTTCTCACTCACTCCATGGCTTAGAA
LRFN1	ACTTGCCTGTCGCTCTATCTTCTCACACGGTACTCTCCAGCATC
TRRAP	ACTTGCCTGTCGCTCTATCTTCTATAAGGAACGAGGCAGGGAGA
KIF21A	ACTTGCCTGTCGCTCTATCTTCGCCTAGTAAGTACAGGACAACA
SYN3	ACTTGCCTGTCGCTCTATCTTCACCAAGGCTGAGAAGGAAGATG
SEPTIN11	ACTTGCCTGTCGCTCTATCTTCCTTGGCTTGCCAGGCTTTATGT
ELAVL3	ACTTGCCTGTCGCTCTATCTTCCTTGTGCTGTTTGCTGGTCTTG
UNC13A	ACTTGCCTGTCGCTCTATCTTCCGCGTGTCCGACTTGAGCTTCA

Table S4H. Lookup table of mis-spliced junctions and corresponding symbols

Symbol	Majiq_junction	fixed_junction
AACSP1_1	chr5:178776276-178785269	chr5:178776276-178785269
AARS1_1	chr16:70272882-70276486	chr16:70272882-70276486
AARS1_2	chr16:70271972-70272796	chr16:70271972-70272796
ACTL6B_1	chr7:100650643-100655019	chr7:100650643-100655019
ACTL6B_2	chr7:100650135-100650575	chr7:100650135-100650575
ACTR1A_1	chr10:102472981-102480536	chr10:102472981-102480536
ADARB1_1	chr21:45181517-45182584	chr21:45181516-45182585
ADARB2_1	chr10:1376218-1379074	chr10:1376218-1379074
ADARB2_2	chr10:1363917-1376116	chr10:1363917-1376116
ADARB2_3	chr10:1645966-1737051	chr10:1645966-1737051
ADCY1_1	chr7:45622743-45625299	chr7:45622743-45625299
ADCY1_2	chr7:45625377-45648670	chr7:45625377-45648670
ADCY1_3	chr7:45625430-45648670	chr7:45625430-45648670
ADCY7_1	chr16:50246203-50246881	chr16:50246203-50246881
ADCY8_1	chr8:130904042-130908924	chr8:130904042-130908924
ADGRB1_1	chr8:142531271-142533295	chr8:142531271-142533295
ADGRL1_1	chr19:14176669-14177531	chr19:14176669-14177531
AGRN_1	chr1:1022462-1031785	chr1:1022462-1031785
AK3_1	chr9:4724376-4740936	chr9:4724375-4740937
AKT3_1	chr1:243527864-243545510	chr1:243527864-243545510
AKT3_2	chr1:243512426-243523309	chr1:243512426-243523309
ARHGAP32_1	chr11:128992046-128998319	chr11:128992046-128998319
ARL15_1	chr5:54171928-54242070	chr5:54171928-54242070
ARMH1_1	chr1:44704173-44723219	chr1:44704173-44723219
ATF7IP2_1	chr16:10386122-10414574	chr16:10386122-10414574
ATG4B_1	chr2:241668685-241668875	chr2:241668685-241668875

ATG4B_2	chr2:241668985-241670726	chr2:241668985-241670726
ATP6V1B2_1	chr8:20225819-20226059	chr8:20225819-20226059
ATP6V1B2_2	chr8:20226166-20226439	chr8:20226166-20226439
BCKDHB_1	chr6:80169030-80169811	chr6:80169030-80169811
BCKDHB_2	chr6:80127624-80128599	chr6:80127624-80128599
BCL2L13_1	chr22:17702386-17722274	chr22:17702386-17722274
C20orf194_1	chr20:3344699-3348525	chr20:3344699-3348525
C20orf194_2	chr20:3343731-3344641	chr20:3343731-3344641
CACNA1C_1	chr12:2680575-2682550	chr12:2680575-2682550
CAMK2B_1	chr7:44258610-44258872	chr7:44258610-44258872
CAMK2B_2	chr7:44254607-44258490	chr7:44254607-44258490
CAMK2B_3	chr7:44230633-44231005	chr7:44230632-44231006
CAMK2B_4	chr7:44220901-44222117	chr7:44220901-44222117
CAMTA1_1	chr1:7249626-7411597	chr1:7249626-7411597
CASZ1_1	chr1:10661399-10665082	chr1:10661399-10665082
CBARP_1	chr19:1235342-1235501	chr19:1235342-1235501
CBLN2_1	chr18:72542326-72542982	chr18:72542326-72542982
CCDC57_1	chr17:82134194-82157748	chr17:82134194-82157748
CDH4_1	chr20:61254937-61545630	chr20:61254937-61545630
CDK7_1	chr5:69261458-69262205	chr5:69261458-69262205
CDO1_1	chr5:115813258-115813898	chr5:115813258-115813898
CDO1_2	chr5:115813954-115816228	chr5:115813954-115816228
CELF5_1	chr19:3278111-3278208	chr19:3278110-3278213
CELF5_2	chr19:3278316-3281199	chr19:3278316-3281199
CELSR3_1	chr3:48650289-48650480	chr3:48650289-48650480
CENPBD1P1_1	chr19:58583176-58585763	chr19:58583176-58585763
CEP131_1	chr17:81208356-81208928	chr17:81208356-81208928
CEP131_2	chr17:81207239-81208144	chr17:81207239-81208144
CEP290_1	chr12:88118743-88119021	chr12:88118743-88119021
CEP290_2	chr12:88119150-88120114	chr12:88119150-88120114
CEP290_3	chr12:88086789-88087780	chr12:88086789-88087780
CERS4_1	chr19:8210862-8240486	chr19:8210862-8240486

CHID1_1	chr11:900980-902148	chr11:900980-902148
CNGA3_1	chr2:98370076-98375922	chr2:98370076-98375922
CNGA3_2	chr2:98376036-98377687	chr2:98376036-98377687
CNOT1_1	chr16:58538915-58539520	chr16:58538914-58539521
CORO7_1	chr16:4367442-4387986	chr16:4367442-4387986
CPLANE1_1	chr5:37122489-37124745	chr5:37122488-37124014
CRLS1_1	chr20:6015490-6026171	chr20:6015490-6026171
CSGALNACT1_1	chr8:19408695-19409237	chr8:19408694-19409238
CTTNBP2_1	chr7:117861316-117862098	chr7:117861316-117862098
CYFIP2_1	chr5:157328050-157330161	chr5:157328049-157330162
DAPK1_1	chr9:87499139-87506820	chr9:87499139-87506820
DAPK1_2	chr9:87537793-87604954	chr9:87537793-87604954
DENND2B_1	chr11:8750725-8776192	chr11:8750725-8776192
DIP2A_1	chr21:46556091-46556403	chr21:46556091-46556403
DLGAP1_1	chr18:4147667-4151180	chr18:4147667-4151180
DLGAP3_1	chr1:34929068-34929451	chr1:34929068-34929451
DLGAP3_2	chr1:34907437-34929069	chr1:34907437-34929069
DNAJC12_1	chr10:67835525-67837934	chr10:67835525-67837934
DNAJC12_2	chr10:67823392-67835392	chr10:67823392-67835392
DNM1_1	chr9:128250940-128253047	chr9:128250940-128253047
DTX1_1	chr12:113058451-113093162	chr12:113058451-113093162
EHBP1_1	chr2:62831158-62859169	chr2:62831158-62859169
ELAPOR1_1	chr1:109197654-109198573	chr1:109197654-109198573
ELAVL3_1	chr19:11463662-11466172	chr19:11463662-11466172
ELAVL3_2	chr19:11458611-11463496	chr19:11458611-11463496
EML6_1	chr2:54928751-54947858	chr2:54928751-54947858
EP400_1	chr12:131995013-132005076	chr12:131995013-132005076
EP400_2	chr12:131992230-132005077	chr12:131992230-132005077
EPB41L4A_1	chr5:112267284-112275326	chr5:112267284-112275326
EPB41L4A_2	chr5:112266330-112267210	chr5:112266330-112267210
ESRRA_1	chr11:64305736-64313951	chr11:64305736-64313951

ETS2_1	chr21:38806808-38810035	chr21:38806808-38810035
ETV5_1	chr3:186104572-186105305	chr3:186104572-186105305
EVL_1	chr14:100133159-100135905	chr14:100133159-100135905
FAM81A_1	chr15:59439064-59458550	chr15:59439064-59458550
FBN3_1	chr19:8084411-8085363	chr19:8084411-8085363
FBN3_2	chr19:8083372-8084235	chr19:8083372-8084235
FBN3_3	chr19:8117589-8118351	chr19:8117589-8118351
FBN3_4	chr19:8118452-8118897	chr19:8118452-8118897
FBN3_5	chr19:8118456-8118897	chr19:8118456-8118897
FEZ1_1	chr11:125489822-125495836	chr11:125489822-125495836
FKBP1B_1	chr2:24054192-24060814	chr2:24054192-24060814
FOXK1_1	chr7:4737421-4740838	chr7:4737421-4740838
FRG1HP_1	chr9:41015187-41032833	chr9:41015186-41032834
FRMD4B_1	chr3:69310517-69311263	chr3:69310517-69311263
FRMD4B_2	chr3:69302436-69306406	chr3:69302435-69305629
G2E3_1	chr14:30559272-30563746	chr14:30559272-30563746
GALNT8_1	chr12:4761143-4763952	chr12:4761143-4763952
GNB1L_1	chr22:19824077-19854443	chr22:19824077-19854443
GNB1L_2	chr22:19821375-19823987	chr22:19821375-19824019
GPSM2_1	chr1:108896431-108896864	chr1:108896431-108896864
GRAMD1A_1	chr19:35001244-35009119	chr19:35001244-35009119
GRAMD1A_2	chr19:35000486-35001098	chr19:35000486-35001098
GREB1_1	chr2:11580832-11588746	chr2:11580832-11588746
GRIP2_1	chr3:14507700-14511165	chr3:14507700-14511165
GRIP2_2	chr3:14511479-14511586	chr3:14511479-14511586
GTPBP6_1	chrX:315020-316914	chrX:315020-316914
HDAC6_1	chrX:48818109-48820106	chrX:48818109-48820106
HDGFL2_1	chr19:4491835-4492015	chr19:4491835-4492015
HDGFL2_2	chr19:4492152-4493703	chr19:4492152-4493703
HULC_1	chr6:8558643-8779887	chr6:8558643-8779887
HYOU1_1	chr11:119055571-119056070	chr11:119055571-119056070
ICA1_1	chr7:8141817-8141969	chr7:8141817-8141969

ICA1_2	chr7:8142055-8143875	chr7:8142055-8143875
IFT122_1	chr3:129483682-129483926	chr3:129483682-129483926
IFT122_2	chr3:129484024-129488257	chr3:129484024-129488257
IGLON5_1	chr19:51320670-51322064	chr19:51320670-51322064
IGSF21_1	chr1:18228010-18281081	chr1:18228010-18281081
IGSF21_2	chr1:18281170-18291866	chr1:18281170-18291866
INSR_1	chr19:7169831-7170537	chr19:7169831-7170537
INTS8_1	chr8:94832174-94834300	chr8:94832174-94834300
IQCE_1	chr7:2559217-2562526	chr7:2559217-2562526
IQCE_2	chr7:2559217-2564878	chr7:2559217-2564878
IQCE_3	chr7:2565071-2567116	chr7:2565071-2567116
ISL2_1	chr15:76337967-76340276	chr15:76337967-76340276
ISL2_2	chr15:76336941-76340276	chr15:76336941-76340276
ISLR2_1	chr15:74130665-74131207	chr15:74130665-74131207
ITGA3_1	chr17:50081193-50081310	chr17:50081193-50081310
ITGA7_1	chr12:55685288-55686202	chr12:55685288-55686202
ITGA7_2	chr12:55686314-55687971	chr12:55686314-55687971
KALRN_1	chr3:124700033-124700977	chr3:124700033-124700977
KALRN_2	chr3:124700033-124701093	chr3:124700033-124701093
KALRN_3	chr3:124664330-124666449	chr3:124664330-124666449
KALRN_4	chr3:124701255-124702038	chr3:124701255-124702038
KCNIP1_1	chr5:170504633-170669499	chr5:170504633-170669499
KCNIP1_2	chr5:170669660-170718758	chr5:170669660-170718758
KCNIP1_3	chr5:170353964-170451777	chr5:170353964-170451777
KCNIP2_1	chr10:101829199-101831072	chr10:101829199-101831072
KCNIP2_2	chr10:101831167-101839753	chr10:101831167-101839753
KCNQ2_1	chr20:63439708-63444659	chr20:63439708-63444659
KIAA0753_1	chr17:6580975-6589779	chr17:6580975-6589779
KIAA0753_2	chr17:6579864-6580932	chr17:6579864-6580932
KIAA1841_1	chr2:61088468-61090479	chr2:61088468-61090479
KIF17_1	chr1:20686126-20690188	chr1:20686126-20690188
KIF21A_1	chr12:39370261-39386971	chr12:39370261-39386971

KIF26B_1	chr1:245419745-245464259	chr1:245419745-245464259
KNDC1_1	chr10:133160569-133161067	chr10:133160569-133161067
KNDC1_2	chr10:133160569-133161085	chr10:133160569-133161085
KNDC1_3	chr10:133207351-133208723	chr10:133207351-133208723
KNDC1_4	chr10:133166939-133167381	chr10:133166939-133167381
KNDC1_5	chr10:133209925-133210610	chr10:133209924-133210611
L3MBTL1_1	chr20:43515415-43528657	chr20:43515415-43528657
LIN28B_1	chr6:104941013-104950460	chr6:104941013-104950460
LIN52_1	chr14:74101238-74114006	chr14:74101238-74114006
LINC00963_1	chr9:129498511-129503323	chr9:129498511-129503323
LINC01503_1	chr9:129336988-129337785	chr9:129336988-129337785
LINC01503_2	chr9:129337959-129338792	chr9:129337959-129338792
LINC02506_1	chr4:32157136-32157956	chr4:32157136-32157956
LINGO1_1	chr15:77641025-77677089	chr15:77641025-77677089
LINGO1_2	chr15:77756719-77795939	chr15:77756719-77795939
LINGO1_3	chr15:77735053-77756560	chr15:77735053-77756560
LIPE-AS1_1	chr19:42397224-42420328	chr19:42397224-42420328
LLNLR-271E8.1_1	chr19:58583172-58585763	chr19:58583172-58585763
LLNLR-271E8.1_2	chr19:58585793-58586155	chr19:58585793-58586155
LMO7_1	chr13:75804541-75809154	chr13:75804541-75809154
LOXL1-AS1_1	chr15:73920038-73926240	chr15:73920038-73926240
LRFN1_1	chr19:39316786-39318325	chr19:39316786-39318326
LRFN1_2	chr19:39316136-39316734	chr19:39316136-39316734
LRP8_1	chr1:53274820-53275631	chr1:53274820-53275631
MACF1_1	chr1:39159020-39231182	chr1:39159020-39231182
MADD_1	chr11:47325032-47328658	chr11:47325032-47328658
MAP6D1_1	chr3:183818111-183820100	chr3:183818111-183820100
MAP6D1_2	chr3:183818111-183822316	chr3:183818111-183822316
MAST1_1	chr19:12842178-12843529	chr19:12842178-12843529
MAST1_2	chr19:12841066-12842139	chr19:12841066-12842139

MBNL2_1	chr13:97334440-97338647	chr13:97334440-97338647
MED13L_1	chr12:116054357-116096669	chr12:116054357-116096669
MED13L_2	chr12:116022601-116054245	chr12:116022601-116054245
METTL8_1	chr2:171392197-171433026	chr2:171392197-171433026
MNAT1_1	chr14:60812127-60817918	chr14:60812127-60817918
MNAT1_2	chr14:60817949-60818722	chr14:60817949-60818722
MNAT1_3	chr14:60809016-60811985	chr14:60809016-60811985
MRPL45P2_1	chr17:47486884-47490166	chr17:47486884-47490166
MTRR_1	chr5:7878322-7885701	chr5:7878322-7885701
MTSS2_1	chr16:70665541-70666339	chr16:70665540-70666340
MYO18A_1	chr17:29131442-29165942	chr17:29131442-29165942
MYO1C_1	chr17:1472228-1474812	chr17:1472228-1474812
MYO9B_1	chr19:17203004-17203147	chr19:17203004-17203147
NADSYN1_1	chr11:71503303-71505511	chr11:71503303-71505511
NADSYN1_2	chr11:71485324-71485542	chr11:71485212-71485542
NECAB2_1	chr16:83993614-83994302	chr16:83993614-83994302
NECAB2_2	chr16:83990630-83993528	chr16:83990630-83993528
NKD1_1	chr16:50608360-50620845	chr16:50608360-50620845
NKD1_2	chr16:50620949-50621602	chr16:50620949-50621602
NKD1_3	chr16:50621709-50625224	chr16:50621709-50625224
NOP14-AS1_1	chr4:2942327-2946872	chr4:2942326-2944073
NPEPL1_1	chr20:58694592-58694812	chr20:58694592-58694812
NPHP4_1	chr1:5888611-5890867	chr1:5888611-5890867
NPLOC4_1	chr17:81559416-81563921	chr17:81559416-81563921
NSMCE4A_1	chr10:121973599-121974004	chr10:121973599-121974004
NSMCE4A_2	chr10:121971069-121973523	chr10:121971069-121973523
NTRK3_1	chr15:88256486-88256605	chr15:88256486-88256605
NUP188_1	chr9:128952846-128956141	chr9:128952846-128956141
NUP188_2	chr9:128956174-128956350	chr9:128956174-128956350
NUP210_1	chr3:13366091-13375504	chr3:13366091-13375504
NYNRIN_1	chr14:24412691-24412997	chr14:24412691-24412997
ONECUT1_1	chr15:52777690-52788780	chr15:52777690-52788780

ONECUT1_2	chr15:52780742-52788780	chr15:52780742-52788780
PAOX_1	chr10:133391098-133391312	chr10:133391098-133391312
PAOX_2	chr10:133389747-133390907	chr10:133389747-133390907
PCBP3_1	chr21:45755452-45788298	chr21:45755452-45788298
PEDS1_1	chr20:50129690-50143502	chr20:50129690-50143502
PFKP_1	chr10:3099352-3099557	chr10:3099352-3099557
PFKP_2	chr10:3099819-3101365	chr10:3099819-3101365
PHF12_1	chr17:28915448-28917285	chr17:28915448-28917285
PHF2_1	chr9:93661646-93662906	chr9:93661646-93662907
PHF2_2	chr9:93660560-93661348	chr9:93660560-93661348
PKD1_1	chr16:2094211-2094888	chr16:2094211-2094888
POU2F2_1	chr19:42130499-42160332	chr19:42130499-42160332
POU2F2_2	chr19:42122576-42130343	chr19:42122576-42130343
PRELID3A_1	chr18:12429436-12430178	chr18:12429436-12430178
PRELID3A_2	chr18:12430292-12431150	chr18:12430292-12431150
PREX1_1	chr20:48737497-48745025	chr20:48737497-48745025
PRKG2_1	chr4:81110611-81110808	chr4:81110611-81110808
PSD_1	chr10:102417121-102417940	chr10:102417121-102417940
PSD_2	chr10:102418046-102418701	chr10:102418046-102418701
PTPRD_1	chr9:9127206-9183304	chr9:9127206-9183304
PTPRD_2	chr9:9018735-9127165	chr9:9018735-9127165
PTPRN2_1	chr7:158040550-158081298	chr7:158040550-158081298
PTPRN2_2	chr7:158100856-158110829	chr7:158100856-158110829
PTPRN2_3	chr7:157682937-157690552	chr7:157682937-157690552
PTPRT_1	chr20:42099289-42102124	chr20:42099289-42102124
PTPRT_2	chr20:42098552-42099129	chr20:42098552-42099129
PTPRZ1_1	chr7:122031559-122034095	chr7:122031559-122034095
PTPRZ1_2	chr7:122044568-122047674	chr7:122044568-122047674
PXDN_1	chr2:1650886-1653628	chr2:1650886-1653628
PXDN_2	chr2:1649675-1650800	chr2:1649675-1650800
RAB40B_1	chr17:82664556-82696389	chr17:82664556-82696389
RAI2_1	chrX:17839105-17861098	chrX:17839105-17861098

RALGAPA2_1	chr20:20491001-20495117	chr20:20491001-20495117
RALGAPA2_2	chr20:20472956-20490914	chr20:20472956-20490914
RANBP17_1	chr5:171265847-171271151	chr5:171265847-171271151
RAP1GAP_1	chr1:21598820-21599494	chr1:21598820-21599494
RAP1GAP_2	chr1:21598502-21598723	chr1:21598502-21598723
RBPMS_1	chr8:30556794-30558887	chr8:30556794-30558887
RFLNA_1	chr12:124149791-124195458	chr12:124149791-124195458
RGPD4_1	chr2:107872928-107878621	chr2:107872928-107878621
RHOBTB3_1	chr5:95816627-95823836	chr5:95816627-95823836
RIN2_1	chr20:19965024-19968392	chr20:19965024-19968392
RNASET2_1	chr6:166952548-166955484	chr6:166952548-166955484
RNFT2_1	chr12:116779348-116788636	chr12:116779348-116788636
RP1-283E3.8_1	chr1:1709640-1719358	chr1:1709640-1719358
RP11-106M3.5_1	chr15:72271288-72287236	chr15:72271287-72287237
RP11-291L22.9_1	chr10:38435253-38437090	chr10:38435253-38437090
RP5-864K19.4_1	chr1:38860240-38873441	chr1:38860240-38873441
RSF1_1	chr11:77813783-77820528	chr11:77813783-77820528
RSF1_2	chr11:77813787-77820528	chr11:77813787-77820528
SCFD2_1	chr4:53143787-53145333	chr4:53143787-53145333
SDAD1_1	chr4:75982037-75984832	chr4:75982037-75984832
SEMA3D_1	chr7:85181287-85186677	chr7:85181286-85186678
SEMA6D_1	chr15:47412472-47469226	chr15:47412472-47469226
SEMA6D_2	chr15:47469299-47470474	chr15:47469299-47470474
SEPTIN11_1	chr4:77030970-77032457	chr4:77030970-77032457
SEPTIN11_2	chr4:77032553-77034497	chr4:77032553-77034497
SEPTIN7P2_1	chr7:45735670-45736787	chr7:45735670-45736787
SEPTIN7P2_2	chr7:45728313-45735607	chr7:45728313-45735607
SETD5_1	chr3:9468615-9470459	chr3:9468615-9470459
SHQ1_1	chr3:72763014-72792916	chr3:72763014-72792916
SHQ1_2	chr3:72750836-72762906	chr3:72750836-72762906
SIPA1L3_1	chr19:37907358-38008096	chr19:37907358-38008096
SLC1A6_1	chr19:14972917-14976761	chr19:14972917-14976761

SLC1A6_2	chr19:14972917-14979000	chr19:14972917-14979000
SLC24A3_1	chr20:19681991-19683910	chr20:19681991-19683910
SLC24A3_2	chr20:19681991-19683913	chr20:19681991-19683913
SLC24A3_3	chr20:19683960-19684176	chr20:19683960-19684176
SLC26A11_1	chr17:80223337-80224082	chr17:80223337-80224082
SPEG_1	chr2:219464608-219465596	chr2:219464608-219465596
SPPL2B_1	chr19:2337333-2337443	chr19:2337333-2337443
STKLD1_1	chr9:133379122-133395600	chr9:133379122-133395600
STMN2_1	chr8:79611214-79616822	chr8:79611214-79616822
STXBP5L_1	chr3:120908416-120909571	chr3:120908416-120909571
STXBP5L_2	chr3:120908428-120909571	chr3:120908428-120909571
SYN3_1	chr22:32672017-32864915	chr22:32672017-32864915
SYNE1_1	chr6:152247944-152249161	chr6:152247944-152249161
SYNE1_2	chr6:152244656-152247823	chr6:152244656-152247823
SYT7_1	chr11:61547620-61551384	chr11:61547620-61551384
SYT7_2	chr11:61547308-61547530	chr11:61547308-61547530
TBL1X_1	chrX:9689246-9691579	chrX:9689246-9691579
TCTE1_1	chr6:44280390-44285964	chr6:44280390-44285964
TFAP2E_1	chr1:35588552-35589019	chr1:35588552-35589019
TFAP2E_2	chr1:35589133-35589930	chr1:35589133-35589930
TGFB3_1	chr14:75959345-75960814	chr14:75959345-75960814
TMEM117_1	chr12:43836196-43836744	chr12:43836196-43836744
TMEM117_2	chr12:43836901-43844624	chr12:43836901-43844624
TMEM175_1	chr4:932540-951207	chr4:932540-951207
TRAPPC12_1	chr2:3457693-3457795	chr2:3457693-3457795
TRAPPC12_2	chr2:3458515-3460263	chr2:3458515-3460263
TRRAP_1	chr7:98881250-98881695	chr7:98881250-98881695
TSPAN18_1	chr11:44920000-44925716	chr11:44919999-44925717
TTC12_1	chr11:113329808-113329920	chr11:113329808-113329920
TTYH2_1	chr17:74252014-74252234	chr17:74252014-74252234
UBASH3B_1	chr11:122656210-122744155	chr11:122656210-122744155
UNC13A_1	chr19:17623216-17623542	chr19:17623216-17623542

UNC13A_2	chr19:17642541-17642845	chr19:17642541-17642845
UNC13A_3	chr19:17641556-17642414	chr19:17641556-17642414
UNC13B_1	chr9:35313989-35364545	chr9:35313989-35364545
UNC13B_2	chr9:35364567-35366947	chr9:35364567-35366947
USP10_1	chr16:84733503-84735056	chr16:84733503-84735056
USP10_2	chr16:84735173-84740309	chr16:84735173-84740309
USP13_1	chr3:179701179-179706934	chr3:179701179-179706934
USP24_1	chr1:55078651-55081322	chr1:55078651-55081322
USP36_1	chr17:78836976-78838587	chr17:78836976-78838587
USP36_2	chr17:78836372-78836897	chr17:78836372-78836897
UVRAG_1	chr11:76008867-76012927	chr11:76008867-76012927
VWCE_1	chr11:61271760-61273117	chr11:61271760-61273117
WASL_1	chr7:123684581-123688997	chr7:123684580-123688997
WASL_2	chr7:123684580-123692347	chr7:123684580-123692347
WDR35_1	chr2:19978167-19978751	chr2:19978167-19978751
WDR35_2	chr2:19975663-19977925	chr2:19975663-19977925
XPO4_1	chr13:20799339-20800113	chr13:20799339-20800113
ZDHHC1_1	chr16:67401068-67416171	chr16:67401068-67416171
ZDHHC1_2	chr16:67401065-67416171	chr16:67401065-67416171
ZFAT_1	chr8:134637712-134645005	chr8:134637712-134645005
ZGPAT_1	chr20:63709164-63732003	chr20:63709164-63732003
ZNF141_1	chr4:343908-372664	chr4:343908-372664
ZNF382_1	chr19:36605446-36607552	chr19:36605446-36607552
ZNF382_2	chr19:36605521-36607552	chr19:36605521-36607552
ZNF423_1	chr16:49638874-49640443	chr16:49638874-49640443
ZNF462_1	chr9:106863356-106865981	chr9:106863356-106865981
ZNF527_1	chr19:37374045-37374158	chr19:37374045-37374158
ZNF529_1	chr19:36572392-36573043	chr19:36572392-36573043
ZNF826P_1	chr19:20409956-20424786	chr19:20409956-20424786

Table S4I. Percent spliced in (PSI) values of iPSC neuron-predicted cryptic exons in FACS sorted TDP-43 positive and negative neuronal nuclei from postmortem ALS/FTD cortex

Symbol	TDP-43_positive_nuclei							TDP-43_negative_nuclei						
	ftd_als_s2	ftd_als_s6	ftd_als_s7	ftd_s1	ftd_s3	ftd_s4	ftd_s5	ftd_als_s2	ftd_als_s6	ftd_s5	ftd_s4	ftd_s3	ftd_s1	ftd_als_s7
AARS1_1	0.00	0.00	0.00	0.00	0.00	0.00	0.00	0.08	0.00	0.00	0.00	0.00	0.00	0.00
AARS1_2	0.00	0.00	0.00	0.00	0.00	0.00	0.00	0.08	0.03	0.00	0.00	0.11	0.00	0.00
ACTL6B_1	0.00	0.00	0.00	0.00	0.00	0.00	0.10	0.00	1.00	0.00	0.00	0.67	0.75	1.00
ACTL6B_2	0.00	0.00	0.00	0.00	0.00	0.00	0.18	1.00	1.00	0.00	1.00	0.82	1.00	0.00
ACTR1A_1	0.00	0.00	0.00	0.00	0.00	0.00	0.00	0.00	0.00	0.00	0.00	0.00	0.25	0.00
ADCY1_1	0.00	0.00	0.00	0.06	0.00	0.00	0.00	0.57	0.42	0.25	0.27	0.50	0.21	0.00
ADCY1_2	0.00	0.00	0.00	0.03	0.00	0.00	0.03	0.50	0.14	0.18	0.31	0.45	0.27	0.00
ADCY8_1	0.00	0.00	0.00	0.00	0.00	0.00	0.00	0.57	0.57	0.50	0.53	0.00	0.00	0.00
ADGRL1_1	0.00	0.00	0.00	0.00	0.00	0.00	0.01	0.04	0.00	0.02	0.00	0.02	0.03	0.00
AGRN_1	0.00	0.00	0.00	1.00	0.00	0.00	0.00	0.00	0.00	0.00	0.00	0.00	0.00	0.00
AKT3_1	0.00	0.00	0.00	0.00	0.00	0.00	0.00	0.16	0.10	0.05	0.00	0.21	0.10	0.00
AKT3_2	0.01	0.00	0.00	0.00	0.00	0.00	0.00	0.70	0.65	0.44	0.55	0.52	0.42	0.60
ARHGAP32_1	0.02	0.01	0.00	0.04	0.00	0.04	0.01	0.33	0.39	0.51	0.00	0.22	0.58	0.47
ARL15_1	0.00	0.00	0.00	0.00	0.00	0.00	0.00	0.00	0.50	0.27	0.00	0.00	0.00	0.00
ARMH1_1	0.00	0.00	0.00	0.00	0.00	0.00	0.00	1.00	1.00	0.00	1.00	0.67	1.00	1.00
ATF7IP2_1	0.00	0.00	0.00	0.00	0.00	0.00	0.50	0.22	0.33	0.00	0.33	0.33	0.00	0.00

ATG4B_1	0.00	0.00	0.00	0.00	0.00	0.00	0.00	0.31	0.33	0.19	0.30	0.32	0.10	0.80
ATG4B_2	0.00	0.00	0.00	0.00	0.00	0.00	0.00	0.73	1.00	0.70	0.00	1.00	0.67	0.00
ATP6V1B2_1	0.00	0.00	0.00	0.00	0.00	0.00	0.00	0.33	0.00	0.00	0.50	0.00	0.00	0.00
ATP6V1B2_2	0.00	0.00	0.00	0.00	0.00	0.00	0.00	0.33	0.00	0.00	0.00	0.00	0.00	0.00
BCKDHB_1	0.00	0.67	0.00	0.00	0.00	0.00	0.17	0.17	0.86	0.00	0.00	0.50	0.00	0.00
BCKDHB_2	0.22	0.45	0.00	0.00	0.00	0.11	0.50	0.00	0.33	0.40	0.00	0.00	0.00	0.00
BCL2L13_1	0.00	0.00	0.00	0.00	0.00	0.00	0.00	0.00	0.18	0.00	0.00	0.00	0.00	0.00
C20orf194_1	0.00	0.00	0.00	0.00	0.00	0.00	0.00	0.31	0.00	1.00	0.00	0.00	0.00	0.00
C20orf194_2	0.00	0.00	0.00	0.00	0.00	0.00	0.00	0.56	0.00	0.00	0.00	0.00	0.00	0.00
CACNA1C_1	0.08	0.00	0.00	0.06	0.10	0.00	0.00	0.00	0.00	0.00	0.02	0.00	0.02	0.00
CAMK2B_1	0.00	0.00	0.00	0.00	0.00	0.00	0.00	0.28	0.18	0.60	0.00	0.09	0.57	0.00
CAMK2B_2	0.00	0.00	0.00	0.00	0.00	0.00	0.00	0.31	0.18	0.46	0.27	0.17	0.50	0.00
CAMK2B_3	0.00	0.00	0.00	0.00	0.00	0.00	0.00	0.00	0.00	0.00	0.00	0.09	0.00	0.00
CAMK2B_4	0.00	0.00	0.00	0.03	0.00	0.00	0.01	0.75	0.53	0.81	0.37	0.81	0.83	0.56
CBARP_1	0.00	0.00	0.00	0.25	0.00	0.00	0.00	0.50	0.50	1.00	0.50	0.75	1.00	0.00
CBLN2_1	0.00	0.00	0.00	0.00	0.00	0.00	0.00	0.67	0.00	0.00	0.00	0.00	0.00	0.00
CCDC57_1	0.00	0.05	0.00	0.00	0.00	0.00	0.24	0.00	0.00	0.00	0.11	0.13	0.11	0.23
CDK7_1	0.00	0.00	0.00	0.00	0.00	0.00	0.00	0.91	0.75	0.67	0.00	0.70	0.00	0.00
CDO1_1	0.14	0.00	0.00	0.00	0.00	0.00	0.00	0.74	0.59	0.29	0.11	1.00	0.19	0.00
CDO1_2	0.17	0.00	0.00	0.00	0.00	0.00	0.00	0.00	0.00	0.00	0.00	0.50	0.07	0.00
CELF5_1	0.00	0.00	0.00	0.00	0.00	0.00	0.06	0.92	1.00	1.00	0.05	0.40	0.71	0.00
CELF5_2	0.00	0.00	0.00	0.00	0.00	0.00	0.00	1.00	1.00	0.75	0.51	0.00	0.80	0.00
CELSR3_1	1.00	1.00	1.00	1.00	0.00	0.00	1.00	1.00	1.00	1.00	0.00	0.00	1.00	0.00

CEP290_1	0.31	0.08	0.67	0.10	0.00	0.06	0.07	0.24	0.15	0.03	0.05	0.04	0.05	0.00
CEP290_2	0.19	0.09	0.09	0.06	0.00	0.00	0.02	0.19	0.20	0.02	0.00	0.04	0.00	0.00
CEP290_3	0.00	0.00	0.00	0.01	0.00	0.00	0.01	0.83	0.72	0.20	0.14	0.63	0.13	0.09
CHID1_1	0.00	0.11	0.00	0.00	0.33	0.00	0.00	1.00	0.75	1.00	0.00	0.80	1.00	0.00
CORO7_1	0.00	0.00	0.00	0.00	0.00	0.00	0.00	0.00	0.25	1.00	0.00	0.00	0.67	0.00
CPLANE1_1	0.00	0.00	0.00	0.00	0.00	0.00	0.00	0.00	0.00	0.00	0.00	0.01	0.00	0.00
CSGALNACT1_1	0.13	0.00	0.00	0.00	0.00	0.00	0.00	0.29	0.00	0.00	0.00	0.00	0.00	0.00
CTTNBP2_1	0.00	0.00	0.00	0.00	0.15	0.00	0.00	0.54	0.53	0.21	0.61	0.32	0.50	0.00
CYFIP2_1	0.00	0.00	0.00	0.00	0.00	0.00	0.00	0.07	0.01	0.00	0.02	0.00	0.00	0.00
DAPK1_1	0.02	0.02	0.00	0.03	0.02	0.10	0.00	0.02	0.04	0.03	0.00	0.02	0.01	0.00
DAPK1_2	0.00	0.00	0.00	0.00	0.00	0.00	0.00	0.00	0.00	0.00	0.00	0.00	0.04	0.00
DIP2A_1	0.00	0.00	0.00	0.17	0.00	0.00	0.00	0.00	0.00	0.00	0.00	0.00	0.50	0.00
DLGAP1_1	0.00	0.00	0.00	0.00	0.00	0.00	0.00	0.01	0.06	0.02	0.00	0.01	0.00	0.00
DLGAP3_2	0.00	0.00	0.00	0.50	0.00	0.00	0.00	0.00	0.00	0.00	0.00	0.00	0.00	0.00
DNM1_1	0.00	0.00	0.00	0.00	0.00	0.00	0.00	0.29	0.00	0.00	0.00	0.00	0.00	0.00
EHBP1_1	0.00	0.01	0.00	0.01	0.00	0.00	0.01	0.01	0.00	0.00	0.03	0.00	0.00	0.00
ELAPOR1_1	0.07	0.00	0.00	0.09	0.00	0.00	0.04	0.38	0.50	0.25	1.00	0.71	0.00	0.00
ELAVL3_1	0.00	0.00	0.00	0.00	0.00	0.00	0.00	0.00	0.00	0.00	0.00	0.00	0.05	0.00
ELAVL3_2	0.00	0.00	0.00	0.00	0.00	0.00	0.00	0.10	0.05	0.00	0.00	0.00	0.18	0.00
EML6_1	0.00	0.00	0.00	0.25	0.00	0.00	0.15	0.00	0.67	0.00	0.00	0.00	0.00	0.00
EP400_2	0.00	0.00	0.00	0.00	0.00	0.00	0.00	0.05	0.13	0.00	0.00	0.09	0.00	0.00
EPB41L4A_1	0.00	0.00	0.00	0.00	0.00	0.00	0.00	1.00	1.00	0.50	0.00	1.00	0.00	0.00

EPB41L4A_2	0.00	0.00	0.00	0.00	0.00	0.00	0.00	1.00	1.00	0.50	0.00	0.00	0.00	0.00
ETS2_1	0.17	0.50	0.00	0.00	0.00	0.00	0.50	0.96	0.96	0.85	0.90	0.97	0.92	0.91
EVL_1	0.00	0.00	0.00	0.00	0.00	0.00	0.01	0.00	0.02	0.02	0.00	0.00	0.00	0.00
FAM81A_1	0.00	0.00	0.00	0.00	0.00	0.00	1.00	0.10	0.03	0.18	0.00	0.21	0.45	0.00
FEZ1_1	0.00	0.00	0.00	0.00	0.06	0.05	0.06	0.75	0.71	0.33	0.11	0.50	0.32	0.71
FOXK1_1	0.00	0.00	0.00	0.00	0.00	0.00	0.00	0.00	0.00	0.00	0.00	0.02	0.00	0.00
FRMD4B_1	0.00	0.00	0.00	1.00	0.00	0.00	0.00	0.00	0.40	0.00	1.00	0.00	1.00	0.00
G2E3_1	0.00	0.00	0.00	0.00	0.00	0.00	0.00	0.00	0.00	0.00	0.00	0.13	0.00	0.00
GPSM2_1	0.00	0.00	0.00	0.00	0.00	0.00	0.00	0.00	0.00	0.25	0.00	0.00	0.00	0.00
GRIP2_2	1.00	0.50	0.00	0.60	0.00	1.00	1.00	0.00	0.00	0.00	0.00	0.00	1.00	0.00
HDAC6_1	0.56	0.11	0.00	0.50	0.23	0.00	0.25	0.44	0.50	0.00	0.10	0.50	0.86	1.00
ICA1_1	0.08	0.07	0.00	0.00	0.04	0.12	0.00	0.48	0.45	0.29	0.86	0.36	0.00	0.00
ICA1_2	0.02	0.09	0.00	0.00	0.00	0.14	0.00	0.49	0.37	0.08	0.75	0.23	0.00	0.00
IFT122_1	0.00	0.00	0.00	0.00	0.00	0.00	0.00	0.75	0.60	0.00	0.00	0.40	0.00	0.00
IFT122_2	0.00	0.00	0.00	0.00	0.00	0.00	0.00	0.17	0.00	0.00	0.00	0.00	0.00	0.00
IGSF21_1	0.00	0.00	0.00	0.00	0.00	0.00	0.00	0.15	0.15	0.00	0.00	0.21	0.20	0.00
IGSF21_2	0.00	0.00	0.00	0.00	0.00	0.00	0.00	0.11	0.23	0.00	0.03	0.38	0.00	0.00
INSR_1	0.00	0.00	0.00	0.00	0.00	0.00	0.00	1.00	1.00	1.00	0.13	1.00	0.86	0.63
INTS8_1	0.00	0.00	0.00	0.00	0.00	0.00	0.00	0.00	0.00	0.00	0.00	0.00	0.21	0.00
IQCE_2	0.00	0.00	0.00	0.00	0.00	0.00	0.00	0.00	0.00	0.09	0.00	0.17	0.33	0.00
IQCE_3	0.00	0.00	0.00	0.00	0.00	0.00	0.00	0.00	0.83	1.00	1.00	0.88	0.50	1.00
ISLR2_1	0.00	0.00	0.00	0.00	0.00	0.00	0.00	1.00	0.00	0.50	1.00	0.00	0.00	0.00
ITGA3_1	0.00	0.00	0.00	0.00	0.00	0.00	0.00	0.00	0.18	0.00	0.07	0.25	0.00	0.00

ITGA7_1	0.00	0.00	0.00	0.00	0.00	0.00	0.00	0.00	0.00	0.00	0.00	1.00	0.00	0.00
ITGA7_2	0.00	0.00	0.00	0.00	0.00	0.00	0.00	0.50	0.00	0.25	0.00	0.00	0.00	0.00
KALRN_1	0.00	0.00	0.00	0.00	0.00	0.00	0.01	0.17	0.13	0.21	0.16	0.10	0.13	0.10
KALRN_2	0.00	0.00	0.00	0.01	0.00	0.00	0.01	0.16	0.20	0.70	0.22	0.71	0.51	0.64
KALRN_4	0.00	0.00	0.01	0.01	0.00	0.00	0.03	0.33	0.36	0.94	0.68	0.99	0.72	0.86
KCNIP1_1	0.00	0.00	0.00	0.00	0.00	0.00	0.00	1.00	0.00	0.00	0.00	0.00	0.00	0.00
KCNIP1_2	0.00	0.00	0.00	0.00	0.00	0.00	0.00	0.00	0.00	0.00	0.47	0.00	1.00	0.00
KCNIP2_1	0.00	0.00	0.00	0.00	0.00	0.00	0.00	0.25	0.14	1.00	0.00	0.00	0.71	0.00
KCNIP2_2	0.00	0.00	0.00	0.00	0.00	0.00	0.00	0.00	0.00	0.00	0.00	0.00	0.50	0.00
KCNQ2_1	0.00	0.00	0.00	0.02	0.00	0.00	0.00	0.28	0.27	0.29	0.22	0.23	0.38	0.00
KIAA0753_1	0.00	0.00	0.00	0.00	0.00	0.00	0.00	0.75	0.30	0.00	0.00	0.25	0.00	0.00
KIAA0753_2	0.00	0.00	0.00	0.00	0.00	0.00	0.00	1.00	0.36	0.00	0.00	0.00	0.00	0.00
KIAA1841_1	0.00	0.00	0.00	0.00	0.13	0.00	0.00	0.00	0.25	0.00	0.08	0.13	0.00	0.00
KIF17_1	0.00	0.00	0.00	0.00	0.00	0.00	0.00	0.20	0.00	0.00	0.00	0.00	0.00	0.00
KIF21A_1	0.00	0.00	0.00	0.00	0.00	0.00	0.04	0.10	0.15	0.00	0.00	0.00	0.00	0.00
KNDC1_2	0.00	0.00	0.00	0.00	0.00	0.00	0.00	0.17	0.00	0.67	0.00	0.20	0.00	0.00
KNDC1_4	0.22	0.00	0.00	0.00	0.00	0.00	0.25	1.00	0.56	1.00	0.00	1.00	1.00	0.00
L3MBTL1_1	0.00	0.00	0.00	0.00	0.00	0.00	0.00	0.25	0.00	0.00	0.00	0.00	0.00	0.00
LIN52_1	0.00	0.00	0.00	0.00	0.00	0.00	0.00	0.00	0.00	0.00	0.00	0.25	0.00	0.00
LINC00963_1	0.00	0.00	0.00	0.00	0.00	0.00	0.00	1.00	0.00	0.00	0.00	0.00	0.00	0.00
LINC01503_1	0.00	0.00	0.00	0.00	0.00	0.00	1.00	0.00	0.00	0.00	0.00	1.00	0.00	0.00
LINC01503_2	0.00	0.00	0.00	0.00	0.00	0.00	0.00	0.00	0.00	1.00	0.00	0.00	0.00	0.00
LINGO1_1	0.00	0.00	0.00	0.00	0.00	0.00	0.00	0.23	0.03	0.13	0.00	0.14	0.04	0.00

LLNLR-271E8.1_1	0.00	0.00	0.00	0.25	0.00	0.00	0.00	0.00	0.29	0.00	0.00	0.00	0.00	0.00
LLNLR-271E8.1_2	0.00	0.00	0.00	0.33	0.00	0.00	0.00	0.33	0.50	0.00	0.00	0.00	0.00	0.00
LMO7_1	0.00	0.00	0.00	0.00	0.00	0.00	0.02	0.00	0.00	0.00	0.17	0.00	0.01	0.00
LRFN1_1	0.00	0.00	0.00	0.00	0.00	0.00	0.00	0.00	1.00	0.00	0.00	0.00	0.00	0.00
LRFN1_2	0.00	0.00	0.00	0.00	0.00	0.00	0.00	0.00	1.00	0.00	0.44	0.00	0.00	0.00
LRP8_1	0.00	0.83	0.00	0.50	0.00	0.43	1.00	0.50	1.00	0.63	0.13	0.75	0.33	0.14
MADD_1	0.00	0.00	0.00	0.00	0.00	0.00	0.00	0.00	0.00	0.00	0.09	0.00	0.00	0.00
MAP6D1_1	0.00	0.00	0.00	0.00	0.00	0.00	0.00	1.00	1.00	0.00	0.00	0.50	0.33	0.00
MAP6D1_2	0.00	0.00	0.50	0.00	0.00	0.00	0.00	0.00	0.00	0.00	0.00	0.00	0.00	0.44
MBNL2_1	0.00	0.00	0.00	0.00	0.00	0.00	0.00	0.01	0.00	0.00	0.00	0.00	0.00	0.00
MED13L_1	0.00	0.00	0.06	0.00	0.00	0.00	0.00	0.00	0.00	0.44	0.22	0.00	0.00	0.00
MED13L_2	0.00	0.00	0.00	0.00	0.00	0.00	0.00	0.00	0.10	0.17	0.00	0.00	0.00	0.00
METTL8_1	0.00	0.00	0.00	0.00	0.00	0.00	0.00	0.00	1.00	1.00	0.60	0.33	0.00	0.00
MNAT1_1	0.24	0.15	0.21	0.00	0.09	0.02	0.03	0.81	0.87	0.83	0.47	0.80	0.79	1.00
MNAT1_2	0.23	0.19	0.05	0.00	0.09	0.09	0.03	0.82	0.83	0.81	0.70	0.77	0.74	1.00
MRPL45P2_1	0.00	0.00	0.00	0.00	0.25	0.38	0.00	0.20	0.17	0.00	0.90	0.50	0.00	0.00
MTRR_1	0.00	0.00	0.00	0.00	0.00	0.00	0.00	0.03	0.00	0.00	0.00	0.00	0.00	0.12
MTSS2_1	0.14	0.05	0.00	0.00	0.00	0.00	0.07	0.00	0.00	0.12	0.00	0.00	0.05	0.00
MYO18A_1	0.00	0.00	0.00	0.00	0.00	0.00	0.00	0.57	0.88	0.67	0.00	0.67	0.33	0.00
NADSYN1_1	0.00	0.00	0.00	0.00	0.07	0.30	0.13	0.19	0.13	0.13	0.00	0.31	0.18	0.35
NADSYN1_2	0.00	0.00	0.00	0.00	0.00	0.00	0.10	0.69	0.64	0.00	0.79	0.40	0.00	0.00

NECAB2_1	0.00	0.00	0.00	0.00	0.00	0.00	0.00	0.14	0.00	0.09	0.00	0.00	0.71	0.50
NECAB2_2	0.00	0.00	0.00	0.00	0.00	0.00	0.00	0.00	0.00	0.17	0.00	0.10	0.71	0.50
NOP14-AS1_1	0.60	0.00	0.00	0.33	1.00	0.00	0.00	0.25	1.00	0.80	0.00	0.50	0.50	0.00
NPEPL1_1	0.00	0.00	0.00	0.00	0.00	0.00	0.00	0.00	0.00	0.00	0.00	0.25	0.00	0.00
NPLOC4_1	0.00	0.00	0.00	0.00	0.00	0.00	0.00	0.29	0.10	0.75	0.00	0.00	0.00	0.00
NSMCE4A_1	0.40	0.27	0.41	0.00	0.07	0.56	0.17	0.77	1.00	0.95	1.00	0.88	0.65	0.00
NSMCE4A_2	0.44	0.10	0.03	0.15	0.24	0.42	0.12	0.43	0.65	0.88	1.00	0.86	0.53	0.00
NTRK3_1	0.33	0.00	0.00	0.00	0.00	0.00	0.00	0.80	0.00	0.89	0.00	0.56	1.00	1.00
NUP188_1	0.00	0.00	0.00	0.00	0.00	0.00	0.00	0.92	1.00	0.67	0.60	0.80	0.00	0.00
NUP188_2	0.00	0.00	0.00	0.00	0.00	0.00	0.00	0.93	1.00	0.80	0.67	0.83	0.40	0.00
NUP210_1	0.00	0.00	0.00	0.00	0.00	0.00	0.00	0.00	0.00	0.00	0.00	0.14	0.00	0.00
NYNRIN_1	0.00	0.00	0.00	0.00	0.00	0.00	0.00	0.00	1.00	1.00	1.00	1.00	1.00	0.00
PAOX_1	0.00	0.00	0.00	0.00	0.00	0.00	0.00	1.00	0.00	0.00	0.00	0.50	0.00	0.00
PCBP3_1	1.00	0.00	0.00	0.00	0.00	0.00	0.20	0.00	0.00	1.00	0.00	1.00	1.00	0.00
PEDS1_1	0.00	0.00	0.00	0.00	0.00	0.00	0.10	0.09	0.05	0.00	0.15	0.17	0.11	0.00
PFKP_1	0.00	0.00	0.00	0.00	0.00	0.00	0.00	1.00	1.00	1.00	1.00	1.00	0.92	0.00
PFKP_2	0.00	0.17	0.00	0.00	0.00	0.00	0.27	1.00	1.00	1.00	1.00	1.00	1.00	1.00
PHF12_1	0.00	0.00	0.09	0.00	0.04	0.00	0.01	0.02	0.13	0.04	0.06	0.22	0.03	0.00
POU2F2_1	0.00	0.00	0.00	0.00	0.00	0.00	0.00	0.07	0.00	0.06	0.00	0.00	0.50	0.00
POU2F2_2	0.00	0.00	0.00	0.00	0.00	0.00	0.00	0.17	0.05	0.06	0.00	0.00	0.00	0.00
PRELID3A_1	0.00	0.00	0.00	0.00	0.00	0.00	0.00	1.00	0.00	0.57	0.00	1.00	1.00	0.00
PRELID3A_2	0.00	0.00	0.00	0.00	0.00	0.00	0.00	0.75	0.00	0.00	0.00	1.00	0.00	0.00
PSD_2	0.00	0.00	0.00	0.00	0.00	0.00	0.00	0.00	0.25	0.00	0.00	0.00	0.00	0.00

PTPRD_1	0.03	0.02	0.21	0.00	0.00	0.00	0.00	0.03	0.02	0.07	0.06	0.13	0.08	0.14
PTPRD_2	0.00	0.00	0.00	0.00	0.00	0.00	0.00	0.08	0.04	0.08	0.00	0.12	0.10	0.00
PTPRN2_2	0.01	0.00	0.00	0.00	0.00	0.00	0.00	0.06	0.04	0.00	0.01	0.00	0.00	0.00
PTPRN2_3	0.00	0.00	0.00	0.00	0.00	0.00	0.00	0.00	0.00	0.00	0.00	0.00	0.03	0.00
PTPRT_1	0.00	0.00	0.00	0.04	0.00	0.00	0.03	1.00	0.94	0.97	0.38	1.00	0.94	1.00
PTPRT_2	0.00	0.00	0.00	0.00	0.00	0.00	0.03	1.00	0.67	0.90	0.23	1.00	0.67	0.00
PTPRZ1_1	0.07	0.13	0.33	0.75	0.00	0.00	0.83	0.00	0.50	0.43	0.56	0.20	0.00	0.33
PTPRZ1_2	0.00	0.06	0.00	0.00	0.00	0.45	0.13	0.00	0.00	0.12	0.00	0.18	0.00	0.00
PXDN_1	0.00	0.00	0.00	0.00	0.00	0.00	0.00	0.94	0.80	0.00	0.00	0.67	0.00	0.00
PXDN_2	0.00	0.00	0.00	0.00	0.00	0.00	0.33	1.00	0.85	1.00	0.00	0.87	0.75	1.00
RAB40B_1	0.00	1.00	0.00	0.25	0.00	0.00	0.00	0.40	0.78	0.91	0.67	0.38	0.25	0.00
RALGAPA2_1	0.00	0.00	0.00	0.00	0.00	0.00	0.00	0.50	0.25	0.00	0.00	0.67	0.18	0.00
RALGAPA2_2	0.00	0.00	0.00	0.00	0.00	0.00	0.00	0.50	0.67	0.13	0.00	0.86	0.27	0.00
RANBP17_1	0.00	0.00	0.00	0.00	0.00	0.00	0.00	0.14	0.00	0.00	0.00	0.00	0.00	0.00
RAP1GAP_1	0.00	0.00	0.00	0.03	0.00	0.00	0.00	1.00	0.83	0.69	0.74	0.88	0.22	1.00
RAP1GAP_2	0.00	0.00	0.00	0.03	0.00	0.00	0.00	1.00	0.70	0.69	0.63	0.82	0.42	0.83
RFLNA_1	0.00	0.00	0.00	0.00	0.00	0.00	0.00	0.00	0.40	0.00	0.00	0.00	0.00	0.00
RNASET2_1	0.80	0.00	0.00	0.00	0.00	0.00	0.00	0.00	0.00	0.00	0.00	0.00	0.00	0.00
RNFT2_1	0.00	0.00	0.00	0.00	0.00	0.00	0.00	0.50	0.00	0.00	0.00	0.00	0.00	0.00
RP1-283E3.8_1	0.00	0.00	0.00	0.01	0.00	0.00	0.00	0.00	0.04	0.00	0.00	0.00	0.02	0.00
RP11-291L22.9_1	0.00	0.00	0.00	0.00	0.86	1.00	1.00	1.00	0.00	0.00	1.00	1.00	0.00	0.00
RSF1_1	0.00	0.00	0.00	0.00	0.00	0.00	0.00	0.03	0.00	0.13	0.00	0.14	0.00	0.00

RSF1_2	0.00	0.00	0.00	0.00	0.00	0.00	0.00	0.00	0.08	0.08	0.00	0.00	0.00	0.00
SDAD1_1	0.00	0.00	0.00	0.00	0.00	0.00	0.00	0.00	0.06	0.00	0.00	0.00	0.00	0.00
SEMA3D_1	0.00	0.00	0.00	0.00	0.00	0.00	0.00	0.50	0.00	0.00	0.00	0.00	0.00	0.00
SEMA6D_2	0.00	0.00	0.00	0.15	0.00	0.00	0.00	0.00	0.00	0.15	0.00	0.00	0.00	0.00
SEPTIN11_1	0.00	0.00	0.00	0.00	0.00	0.00	0.00	0.11	0.00	0.09	0.23	0.13	0.00	0.00
SEPTIN11_2	0.00	0.00	0.00	0.00	0.00	0.00	0.00	0.13	0.00	0.00	1.00	0.00	0.00	0.00
SEPTIN7P2_1	0.01	0.00	0.01	0.08	0.00	0.00	0.00	0.61	0.59	0.30	0.14	0.61	0.27	0.36
SEPTIN7P2_2	0.00	0.00	0.00	0.00	0.00	0.00	0.00	0.23	0.21	0.07	0.00	0.32	0.03	0.09
SETD5_1	0.00	0.00	0.00	0.00	0.00	0.00	0.00	0.53	0.76	0.50	0.13	0.81	0.49	0.53
SHQ1_1	0.00	0.00	0.00	0.00	0.00	0.00	0.00	0.00	0.00	1.00	0.00	1.00	0.00	0.00
SHQ1_2	0.00	0.00	0.00	0.00	0.00	0.00	0.00	0.00	0.00	0.00	0.00	0.00	1.00	0.00
SLC1A6_1	0.00	0.00	0.00	0.00	0.00	0.00	0.00	0.00	0.00	0.00	1.00	0.00	0.33	0.00
SLC24A3_2	0.00	0.00	0.00	0.00	0.00	0.00	0.00	0.00	1.00	0.00	1.00	0.00	1.00	0.00
SLC24A3_3	0.00	0.00	0.00	0.00	0.00	0.00	0.00	0.00	1.00	0.00	1.00	1.00	1.00	0.00
STKLD1_1	0.00	0.00	0.00	0.00	0.00	0.00	0.00	0.00	0.00	0.14	0.00	0.00	0.00	0.00
STMN2_1	0.00	0.00	0.00	0.00	0.01	0.02	0.03	0.84	0.70	0.75	0.60	0.77	0.47	0.42
STXBP5L_1	0.07	0.00	0.00	0.00	0.00	0.00	0.03	0.31	0.41	0.27	0.11	0.33	0.30	1.00
STXBP5L_2	0.02	0.00	0.00	0.00	0.00	0.00	0.00	0.37	0.20	0.23	0.78	0.42	0.30	0.00
SYNE1_1	0.00	0.00	0.00	0.00	0.00	0.00	0.00	0.00	0.02	0.00	0.00	0.00	0.00	0.00
SYNE1_2	0.00	0.00	0.00	0.00	0.00	0.00	0.00	0.00	0.01	0.00	0.00	0.01	0.00	0.00
SYT7_1	0.00	0.00	0.00	0.00	0.00	0.00	0.00	0.13	0.11	0.03	0.24	0.19	0.15	0.20
SYT7_2	0.00	0.00	0.00	0.00	0.00	0.00	0.00	0.18	0.17	0.21	0.23	0.11	0.11	0.30
TCTE1_1	0.00	0.00	0.00	0.00	0.00	0.02	0.00	0.00	0.00	0.00	0.00	0.00	0.00	0.00

TGFB3_1	0.00	0.00	0.00	0.00	0.00	0.00	0.00	1.00	1.00	1.00	0.00	0.00	0.00	0.00
TMEM117_2	0.00	0.00	0.00	0.00	0.00	0.00	0.00	1.00	0.50	0.71	0.00	0.44	0.50	0.00
TMEM175_1	0.00	0.00	0.00	0.00	0.00	0.00	0.00	0.13	0.06	0.09	0.00	0.00	0.00	0.00
TRAPPC12_1	0.00	0.25	0.00	0.00	0.00	0.00	0.05	0.86	0.30	0.17	0.00	0.79	0.00	1.00
TRAPPC12_2	0.06	0.00	0.00	0.00	0.00	0.00	0.05	0.92	1.00	0.62	1.00	1.00	0.50	1.00
TRRAP_1	0.00	0.00	0.00	0.01	0.00	0.00	0.00	0.28	0.38	0.05	0.25	0.37	0.02	0.05
TTC12_1	0.00	0.40	0.00	0.00	0.00	0.00	0.00	0.80	0.16	0.00	1.00	1.00	0.00	0.00
TTYH2_1	0.00	0.60	0.00	0.00	0.00	0.00	0.00	0.00	0.00	0.00	0.00	0.00	0.00	0.00
UBASH3B_1	0.00	0.00	0.00	0.00	0.00	0.00	0.00	0.00	0.00	0.00	0.00	0.00	1.00	0.00
UNC13A_2	0.00	0.00	0.00	0.00	0.00	0.00	0.01	0.87	0.79	0.25	0.12	0.95	0.16	0.19
UNC13A_3	0.02	0.00	0.00	0.01	0.01	0.00	0.03	0.98	0.95	0.56	0.24	1.00	0.40	0.75
UNC13B_1	0.18	0.23	0.91	0.69	0.07	0.13	0.00	0.35	0.19	0.44	0.00	0.48	0.00	0.00
UNC13B_2	1.00	1.00	1.00	1.00	1.00	1.00	1.00	1.00	1.00	1.00	1.00	1.00	1.00	1.00
USP10_1	0.00	0.00	0.00	0.00	0.00	0.00	0.00	0.00	0.00	0.00	0.00	0.00	0.11	0.00
USP10_2	0.00	0.00	0.00	0.00	0.00	0.00	0.00	0.00	0.00	0.00	0.00	0.00	0.00	0.50
USP13_1	0.00	0.00	0.00	0.00	0.19	0.00	0.00	0.60	0.69	0.56	0.00	0.14	0.33	1.00
USP24_1	0.00	0.00	0.00	0.00	0.00	0.00	0.00	0.00	0.00	0.00	0.00	0.00	0.13	0.00
USP36_1	0.00	0.00	0.00	0.00	0.17	0.00	0.00	0.00	0.00	0.00	0.00	0.11	0.00	0.00
USP36_2	0.00	0.00	0.00	0.00	0.17	0.00	0.00	0.16	0.03	0.20	0.00	0.00	0.13	0.00
UVRAG_1	0.08	0.08	0.00	0.09	0.04	0.27	0.07	0.00	0.03	0.04	0.12	0.06	0.05	0.00
WASL_1	0.00	0.00	0.00	0.00	0.00	0.00	0.00	0.00	0.00	0.43	0.00	0.00	0.40	0.00
WASL_2	0.00	0.00	0.00	0.00	0.00	0.00	0.00	0.86	0.60	0.00	0.00	0.00	0.00	0.00
WDR35_1	0.02	0.00	0.00	0.05	0.00	0.00	0.25	0.94	0.88	0.94	0.75	1.00	1.00	1.00

WDR35_2	0.10	0.23	0.89	0.29	0.41	0.00	0.35	0.94	0.94	0.94	0.94	1.00	1.00	1.00
XPO4_1	0.00	0.19	0.00	0.00	0.00	0.00	0.00	0.17	0.00	0.00	0.00	0.00	0.00	0.00
ZFAT_1	0.00	0.00	0.00	0.00	0.00	0.00	0.00	0.00	0.00	0.00	0.00	0.00	0.43	0.00
ZGPAT_1	0.00	0.00	0.00	0.00	0.00	0.00	0.00	0.40	0.00	0.00	0.00	0.00	0.00	0.00
ZNF141_1	0.00	0.03	0.00	0.00	0.00	0.00	0.01	0.00	0.00	0.00	0.00	0.00	0.03	0.00
ZNF382_1	0.00	0.05	1.00	0.00	0.00	0.00	0.00	0.19	0.20	0.41	0.06	0.00	0.17	0.00
ZNF382_2	0.00	0.00	0.00	0.00	0.09	0.00	0.00	0.19	0.60	0.12	0.94	0.00	0.33	1.00
ZNF423_1	0.00	0.00	0.00	0.00	0.00	0.00	0.00	0.00	1.00	0.00	0.00	0.25	0.00	0.00
ZNF527_1	1.00	0.00	0.00	0.00	0.00	0.00	0.00	0.00	0.00	0.00	0.00	0.00	1.00	0.00
ZNF529_1	0.00	0.00	0.00	0.33	0.00	0.00	0.00	0.92	0.80	0.89	1.00	1.00	0.00	1.00
ZNF826P_1	0.00	0.00	0.00	1.00	0.00	0.00	0.00	0.00	0.00	0.00	0.00	0.00	0.00	0.00

Table S4J. Trait file for postmortem bulk RNAseq dataset (NYGC)

donor_id	disease	tissue	pathology	sex	age	onset	motor_onset
NEUEL133AK6	ALS	Motor_Cortex	TDP-path	Female	60	59	Limb
NEUYV496XLP	ALS-FTD	Motor_Cortex	TDP-path	Male	71	70	Bulbar
NEUZU200WEQ	ALS	Motor_Cortex	TDP-path	Male	62	55	Bulbar
NEUME287RK2	ALS-FTD	Motor_Cortex	TDP-path	Female	67	65	Bulbar
NEUEC006FND	ALS	Motor_Cortex	TDP-path	Female	62	58	Limb
NEUKM699KKH	ALS-FTD	Motor_Cortex	TDP-path	Female	69	67	Bulbar
NEUWX086DGZ	ALS	Motor_Cortex	TDP-path	Female	70	67	Bulbar
NEUJZ255ZC5	ALS	Motor_Cortex	TDP-path	Male	68	67	Limb
NEUHC282LVJ	Control	Motor_Cortex	non-TDP path	Female	90		Not Applicable
NEUYB686REL	ALS	Motor_Cortex	TDP-path	Male	74	73	Axial and Limb
NEUJR139GPF	ALS	Motor_Cortex	TDP-path	Male	69	58	Limb
NEUNW210GCW	ALS	Motor_Cortex	TDP-path	Male	53		Unknown
NEUEL133AK6	ALS	Motor_Cortex	TDP-path	Female	60	59	Limb
NEUYV496XLP	ALS-FTD	Motor_Cortex	TDP-path	Male	71	70	Bulbar
NEUZU200WEQ	ALS	Motor_Cortex	TDP-path	Male	62	55	Bulbar
NEUME287RK2	ALS-FTD	Motor_Cortex	TDP-path	Female	67	65	Bulbar
NEUEC006FND	ALS	Motor_Cortex	TDP-path	Female	62	58	Limb
NEUKM699KKH	ALS-FTD	Motor_Cortex	TDP-path	Female	69	67	Bulbar
NEUWX086DGZ	ALS	Motor_Cortex	TDP-path	Female	70	67	Bulbar

NEUJZ255ZC5	ALS	Motor_Cortex	TDP-path	Male	68	67	Limb
NEUHC282LVJ	Control	Motor_Cortex	non-TDP path	Female	90		Not Applicable
NEUYB686REL	ALS	Motor_Cortex	TDP-path	Male	74	73	Axial and Limb
NEUGA773REC	ALS	Motor_Cortex	TDP-path	Male	49	48	Limb
NEUNW210GCW	ALS	Motor_Cortex	TDP-path	Male	53		Unknown
JHU38	ALS	Motor_Cortex	TDP-path	Female	34	33	Limb
JHU51	ALS	Motor_Cortex	TDP-path	Male	65	63	Limb
NEURJ387PPV	ALS	Motor_Cortex	TDP-path	Female	68	64	Limb
NEUFT454ZFP	ALS	Motor_Cortex	TDP-path	Male	56	53	Bulbar
NEUMP035RP4	ALS	Motor_Cortex	TDP-path	Male	69	57	Bulbar
NEUDM397JGD	ALS	Motor_Cortex	TDP-path	Female	71	70	Bulbar
NEUHD481VCL	Control	Motor_Cortex	non-TDP path	Female	54		Not Applicable
NEUDR086ZDQ	ALS	Motor_Cortex	TDP-path	Female	71	69	Limb
NEUDG361GA9	ALS	Motor_Cortex	TDP-path	Female	72	70	Bulbar
NEUFT454ZFP	ALS	Motor_Cortex	TDP-path	Male	56	53	Bulbar
NEUMP035RP4	ALS	Motor_Cortex	TDP-path	Male	69	57	Bulbar
NEUDM397JGD	ALS	Motor_Cortex	TDP-path	Female	71	70	Bulbar
NEUHD481VCL	Control	Motor_Cortex	non-TDP path	Female	54		Not Applicable
NEUDR086ZDQ	ALS	Motor_Cortex	TDP-path	Female	71	69	Limb
NEUDG361GA9	ALS	Motor_Cortex	TDP-path	Female	72	70	Bulbar
NEUYY221HZA	ALS	Motor_Cortex	TDP-path	Male	65	59	Limb
NEUUE532LFF	ALS	Motor_Cortex	TDP-path	Male	74	70	Limb
NEUCV649UJK	ALS	Motor_Cortex	TDP-path	Male	80	79	Limb

NEURK749WFB	ALS	Motor_Cortex	TDP-path	Female	65	58	Limb
NEUPK732LNT	ALS	Motor_Cortex	TDP-path	Female	76	72	Limb
NEUCW292DYJ	ALS	Motor_Cortex	TDP-path	Female	67	56	Bulbar
NEUYY221HZA	ALS	Motor_Cortex	TDP-path	Male	65	59	Limb
NEUUE532LFF	ALS	Motor_Cortex	TDP-path	Male	74	70	Limb
NEUNL548ZBN	ALS-FTD	Motor_Cortex	TDP-path	Male	60	59	Limb
NEULH901PYF	ALS	Motor_Cortex	TDP-path	Male	59	58	Limb
NEUXT258BD4	ALS	Motor_Cortex	TDP-path	Female	65	65	Limb
NEUEF397VVN	ALS-AD	Motor_Cortex	TDP-path	Female	76	74	Limb
NEUEF397VVN	ALS-AD	Motor_Cortex	TDP-path	Female	76	74	Limb
NEUWZ373ZHA	ALS	Motor_Cortex	TDP-path	Female	69	65	Limb
NEUWZ373ZHA	ALS	Motor_Cortex	TDP-path	Female	69	65	Limb
NEUTL441LZ7	ALS	Motor_Cortex	TDP-path	Male	67	63	Limb
NEUTL441LZ7	ALS	Motor_Cortex	TDP-path	Male	67	63	Limb
NEUVZ387WGH	ALS-AD	Motor_Cortex	TDP-path	Female	66	63	Axial
NEUAT369TG5	ALS	Motor_Cortex	TDP-path	Female	81	79	Bulbar
NEUAT369TG5	ALS	Motor_Cortex	TDP-path	Female	81	79	Bulbar
NEUAV667LJK	ALS	Motor_Cortex	TDP-path	Male	85	79	Limb
NEUAV667LJK	ALS	Motor_Cortex	TDP-path	Male	85	79	Limb
NEUNW244GF0	ALS	Motor_Cortex	TDP-path	Female	61	57	Limb
NEUNW244GF0	ALS	Motor_Cortex	TDP-path	Female	61	57	Limb
NEUTP019MY9	ALS	Motor_Cortex	TDP-path	Female	61	60	Unknown
NEUTP019MY9	ALS	Motor_Cortex	TDP-path	Female	61	60	Unknown

NEUGV399KJW	ALS	Motor_Cortex	TDP-path	Female	63	61	Limb
NEUGV399KJW	ALS	Motor_Cortex	TDP-path	Female	63	61	Limb
NEUZX073BDK	ALS	Motor_Cortex	TDP-path	Female	68	59	Limb
NEUZX073BDK	ALS	Motor_Cortex	TDP-path	Female	68	59	Limb
NEUKY135CV6	ALS-AD	Motor_Cortex	TDP-path	Male	74	70	Unknown
NEUKY135CV6	ALS-AD	Motor_Cortex	TDP-path	Male	74	70	Unknown
NEUYX020CB0	ALS-AD	Motor_Cortex	TDP-path	Male	67	64	Limb
NEUYX020CB0	ALS-AD	Motor_Cortex	TDP-path	Male	67	64	Limb
NEUMT947ALA	ALS	Motor_Cortex	TDP-path	Male	74		Unknown
NEUMT947ALA	ALS	Motor_Cortex	TDP-path	Male	74		Unknown
NEUWP285RM6	ALS-AD	Motor_Cortex	TDP-path	Female	60	57	Limb
NEUWP285RM6	ALS-AD	Motor_Cortex	TDP-path	Female	60	57	Limb
NEUDT233ZZ1	ALS	Motor_Cortex	TDP-path	Male	39	35	Unknown
NEUDT233ZZ1	ALS	Motor_Cortex	TDP-path	Male	39	35	Unknown
NEUDG727NTW	ALS	Motor_Cortex	TDP-path	Female	63	60	Bulbar and Limb
NEUDG727NTW	ALS	Motor_Cortex	TDP-path	Female	63	60	Bulbar and Limb
NEUTB398FC9	ALS	Motor_Cortex	TDP-path	Male	83	81	Unknown
NEUTB398FC9	ALS	Motor_Cortex	TDP-path	Male	83	81	Unknown
NEUEF856BLV	ALS	Motor_Cortex	TDP-path	Female	61	60	Limb
NEUEF856BLV	ALS	Motor_Cortex	TDP-path	Female	61	60	Limb
NEUCG551GV1	Control	Motor_Cortex	non-TDP path	Female	57		Not Applicable

NEUGY741GH8	Control	Motor_Cortex	non-TDP path	Male	59		Not Applicable
NEUGY741GH8	Control	Motor_Cortex	non-TDP path	Male	59		Not Applicable
NEUFF179PPT	ALS	Motor_Cortex	TDP-path	Male	59	50	Limb
NEUFF179PPT	ALS	Motor_Cortex	TDP-path	Male	59	50	Limb
JHU73	ALS	Motor_Cortex	TDP-path	Female	70	67	Limb
JHU73	ALS	Motor_Cortex	TDP-path	Female	70	67	Limb
JHU74	ALS	Motor_Cortex	non-TDP path	Male	47	46	Bulbar
JHU74	ALS	Motor_Cortex	non-TDP path	Male	47	46	Bulbar
JHU79	ALS	Motor_Cortex	TDP-path	Male	82	80	Bulbar
JHU79	ALS	Motor_Cortex	TDP-path	Male	82	80	Bulbar
JHU82	ALS	Motor_Cortex	TDP-path	Male	66	63	Limb
JHU82	ALS	Motor_Cortex	TDP-path	Male	66	63	Limb
JHU83	ALS	Motor_Cortex	non-TDP path	Male	50	44	Limb
JHU83	ALS	Motor_Cortex	non-TDP path	Male	50	44	Limb
NEUGY575NUQ	ALS	Motor_Cortex	TDP-path	Male	69	67	Limb
NEUGY575NUQ	ALS	Motor_Cortex	TDP-path	Male	69	67	Limb
NEUHA141EEC	Control	Motor_Cortex	non-TDP path	Male	72		Not Applicable
NEUDA151YMK	Control	Motor_Cortex	non-TDP path	Female	37		Not Applicable
NEUDA151YMK	Control	Motor_Cortex	non-TDP path	Female	37		Not Applicable
NEUJB238MJR	Control	Motor_Cortex	non-TDP path	Male	50		Not Applicable
NEUZB953VCD	ALS	Motor_Cortex	TDP-path	Female	68	67	Limb
NEUZB953VCD	ALS	Motor_Cortex	TDP-path	Female	68	67	Limb
NEUAP156PM4	ALS	Motor_Cortex	TDP-path	Female	69	65	Bulbar

NEUAP156PM4	ALS	Motor_Cortex	TDP-path	Female	69	65	Bulbar
NEUUW911LWA	ALS-FTD	Motor_Cortex	TDP-path	Male	59	57	Bulbar
NEUUW911LWA	ALS-FTD	Motor_Cortex	TDP-path	Male	59	57	Bulbar
NEUEH612JPA	ALS-AD	Motor_Cortex	TDP-path	Female	71	69	Bulbar
NEUEH612JPA	ALS-AD	Motor_Cortex	TDP-path	Female	71	69	Bulbar
NEURX991BWB	ALS	Motor_Cortex	TDP-path	Female	59	57	Axial and Bulbar
NEURX991BWB	ALS	Motor_Cortex	TDP-path	Female	59	57	Axial and Bulbar
NEUNL974RU6	ALS	Motor_Cortex	TDP-path	Male	53	50	Limb
NEUMK638LUX	ALS	Motor_Cortex	TDP-path	Male	72	69	Limb
NEUMK638LUX	ALS	Motor_Cortex	TDP-path	Male	72	69	Limb
JHU75	ALS	Motor_Cortex	TDP-path	Female	58	54	Limb
JHU77	ALS	Motor_Cortex	TDP-path	Male	76	73	Limb
NEUZV622ZHF	ALS	Motor_Cortex	TDP-path	Male	68	67	Limb
NEUZV622ZHF	ALS	Motor_Cortex	TDP-path	Male	68	67	Limb
NEUWG523WRV	ALS	Motor_Cortex	TDP-path	Male	38	36	Limb
NEUHX090PGV	Control	Motor_Cortex	non-TDP path	Male	72		Not Applicable
NEUUT049NND	Control	Motor_Cortex	non-TDP path	Female	71		Not Applicable
NEUUT049NND	Control	Motor_Cortex	non-TDP path	Female	71		Not Applicable
NEUTP414KZ2	Control	Motor_Cortex	non-TDP path	Female	52		Not Applicable
NEUTP414KZ2	Control	Motor_Cortex	non-TDP path	Female	52		Not Applicable
NEUML172BXK	Control	Motor_Cortex	non-TDP path	Female	70		Not Applicable
NEUML172BXK	Control	Motor_Cortex	non-TDP path	Female	70		Not Applicable
NEUXY076JMB	ALS	Motor_Cortex	TDP-path	Female	72	70	Bulbar

NEUXY076JMB	ALS	Motor_Cortex	TDP-path	Female	72	70	Bulbar
NEUEG442LDR	Control	Motor_Cortex	non-TDP path	Male	22		Not Applicable
NEUEG442LDR	Control	Motor_Cortex	non-TDP path	Male	22		Not Applicable
NEUEA633EN5	ALS	Motor_Cortex	TDP-path	Female	71	69	Bulbar
NEUEA633EN5	ALS	Motor_Cortex	TDP-path	Female	71	69	Bulbar
NEUWL993GU2	ALS	Motor_Cortex	TDP-path	Male	69	61	Limb
NEUWL993GU2	ALS	Motor_Cortex	TDP-path	Male	69	61	Limb
NEUZK186ZK4	ALS	Motor_Cortex	TDP-path	Female	54	50	Limb
NEUZK186ZK4	ALS	Motor_Cortex	TDP-path	Female	54	50	Limb
NEULN488RD5	ALS	Motor_Cortex	TDP-path	Male	69	67	Bulbar and Limb
NEULN488RD5	ALS	Motor_Cortex	TDP-path	Male	69	67	Bulbar and Limb
NEUAY067UTB	ALS	Motor_Cortex	TDP-path	Female	67	64	Limb
NEUAY067UTB	ALS	Motor_Cortex	TDP-path	Female	67	64	Limb
NEUGK141CFH	ALS	Motor_Cortex	TDP-path	Female	78	75	Limb
NEUGK141CFH	ALS	Motor_Cortex	TDP-path	Female	78	75	Limb
NEUEP010ZFE	Control	Motor_Cortex	non-TDP path	Male	51		Not Applicable
NEUEP010ZFE	Control	Motor_Cortex	non-TDP path	Male	51		Not Applicable
NEUGJ583BEE	Control	Motor_Cortex	non-TDP path	Male	70		Not Applicable
NEUGJ583BEE	Control	Motor_Cortex	non-TDP path	Male	70		Not Applicable
NEULH417FZJ	ALS	Motor_Cortex	TDP-path	Male	60	53	Limb
NEULH417FZJ	ALS	Motor_Cortex	TDP-path	Male	60	53	Limb

NEUAL503EPH	ALS-FTD	Motor_Cortex	TDP-path	Male	72	71	Axial
NEUAL503EPH	ALS-FTD	Motor_Cortex	TDP-path	Male	72	71	Axial
NEUXW599BNC	Control	Motor_Cortex	non-TDP path	Female	74		Not Applicable
NEUXW599BNC	Control	Motor_Cortex	non-TDP path	Female	74		Not Applicable
NEUBB078VEG	ALS	Motor_Cortex	TDP-path	Female	51	46	Bulbar
NEUBB078VEG	ALS	Motor_Cortex	TDP-path	Female	51	46	Bulbar
NEUWD570BTK	Control	Motor_Cortex	non-TDP path	Male	68		Not Applicable
NEUWD570BTK	Control	Motor_Cortex	non-TDP path	Male	68		Not Applicable
NEUJL308UBK	ALS	Motor_Cortex	TDP-path	Female	59	52	Limb
NEUMY028JH4	ALS	Motor_Cortex	TDP-path	Female	54	50	Limb
NEUMY028JH4	ALS	Motor_Cortex	TDP-path	Female	54	50	Limb
NEUXR145UBL	ALS-FTD	Motor_Cortex	TDP-path	Male	66	66	Bulbar
NEUKN209FNW	ALS	Motor_Cortex	non-TDP path	Male	48	47	Limb
NEUUF289NRL	ALS	Motor_Cortex	TDP-path	Male	72	68	Axial and Limb
NEUUF289NRL	ALS	Motor_Cortex	TDP-path	Male	72	68	Axial and Limb
NEUPU334DL1	ALS	Motor_Cortex	TDP-path	Female	66	65	Bulbar
NEUKD974CXJ	ALS	Motor_Cortex	TDP-path	Female	56	54	Bulbar
NEUEB569WFU	ALS	Motor_Cortex	TDP-path	Male	64	57	Bulbar
NEUEB569WFU	ALS	Motor_Cortex	TDP-path	Male	64	57	Bulbar
NEUGU437VNF	ALS	Motor_Cortex	TDP-path	Female	66	61	Limb
NEUGU437VNF	ALS	Motor_Cortex	TDP-path	Female	66	61	Limb
NEUAG831KFQ	ALS	Motor_Cortex	TDP-path	Male	66	61	Bulbar and Limb

NEUAG831KFQ	ALS	Motor_Cortex	TDP-path	Male	66	61	Bulbar and Limb
NEUWX051HMF	ALS-FTD	Motor_Cortex	TDP-path	Male	55	45	Axial and Bulbar
NEUWX051HMF	ALS-FTD	Motor_Cortex	TDP-path	Male	55	45	Axial and Bulbar
NEUNY116EZW	ALS-AD	Motor_Cortex	TDP-path	Female	68	64	Bulbar
NEUNY116EZW	ALS-AD	Motor_Cortex	TDP-path	Female	68	64	Bulbar
NEUHM340FBZ	ALS	Motor_Cortex	TDP-path	Male	80	79	Limb
NEUHM340FBZ	ALS	Motor_Cortex	TDP-path	Male	80	79	Limb
NEUGD887RT1	ALS	Motor_Cortex	non-TDP path	Female	32	29	Limb
NEUGD887RT1	ALS	Motor_Cortex	non-TDP path	Female	32	29	Limb
NEUXZ213MVF	ALS	Motor_Cortex	TDP-path	Male	54	50	Bulbar
NEUXZ213MVF	ALS	Motor_Cortex	TDP-path	Male	54	50	Bulbar
NEUFV843EVC	ALS	Motor_Cortex	TDP-path	Female	65	64	Limb
NEUFV843EVC	ALS	Motor_Cortex	TDP-path	Female	65	64	Limb
NEURJ886YZU	ALS	Motor_Cortex	TDP-path	Male	64	61	Limb
NEURJ886YZU	ALS	Motor_Cortex	TDP-path	Male	64	61	Limb
NEUTD254HL0	ALS	Motor_Cortex	TDP-path	Male	48	44	Limb
NEUTD254HL0	ALS	Motor_Cortex	TDP-path	Male	48	44	Limb
NEUXN530DK8	ALS	Motor_Cortex	TDP-path	Male	53	49	Bulbar
NEUXN530DK8	ALS	Motor_Cortex	TDP-path	Male	53	49	Bulbar
NEUPM864FBE	ALS	Motor_Cortex	TDP-path	Male	67	65	Bulbar and Limb
NEUKV592NUT	ALS	Motor_Cortex	non-TDP path	Female	45	42	Limb

NEUKV592NUT	ALS	Motor_Cortex	non-TDP path	Female	45	42	Limb
NEUWG326WUJ	ALS	Motor_Cortex	TDP-path	Male	67	66	Limb
NEUWG326WUJ	ALS	Motor_Cortex	TDP-path	Male	67	66	Limb
NEUKZ727YY5	ALS	Motor_Cortex	TDP-path	Male	70	68	Limb
NEUKZ727YY5	ALS	Motor_Cortex	TDP-path	Male	70	68	Limb
NEULP959LBP	ALS	Motor_Cortex	TDP-path	Male	59	53	Limb
NEULP959LBP	ALS	Motor_Cortex	TDP-path	Male	59	53	Limb
NEULT268RM4	ALS-FTD	Motor_Cortex	TDP-path	Male	73	72	Limb
NEUZX847VWV-NEUWR459TCY	ALS-FTD	Motor_Cortex	TDP-path	Male	57	55	Axial
NEUZX847VWV-NEUWR459TCY	ALS-FTD	Motor_Cortex	TDP-path	Male	57	55	Axial
NEUHM399CBL	ALS	Motor_Cortex	TDP-path	Male	68	65	Limb
NEURN516YR8	ALS	Motor_Cortex	TDP-path	Female	58	57	Limb
NEURN516YR8	ALS	Motor_Cortex	TDP-path	Female	58	57	Limb
NEUKJ257ZPG	ALS	Motor_Cortex	TDP-path	Male	67	66	Limb
NEUKJ257ZPG	ALS	Motor_Cortex	TDP-path	Male	67	66	Limb
NEUKG838WER	ALS	Motor_Cortex	TDP-path	Male	60	58	Bulbar
NEUKG838WER	ALS	Motor_Cortex	TDP-path	Male	60	58	Bulbar
NEUGL022MN2	ALS	Motor_Cortex	TDP-path	Female	55	52	Bulbar
NEUGL022MN2	ALS	Motor_Cortex	TDP-path	Female	55	52	Bulbar
NEUTC651YRK	ALS	Motor_Cortex	TDP-path	Male	78	76	Limb
NEUZK363UAQ	ALS-FTD	Motor_Cortex	TDP-path	Female	73	72	Bulbar

NEUZK363UAQ	ALS-FTD	Motor_Cortex	TDP-path	Female	73	72	Bulbar
NEUBE992ZD1	ALS	Motor_Cortex	TDP-path	Male	68	65	Generalized
NEUBE992ZD1	ALS	Motor_Cortex	TDP-path	Male	68	65	Generalized
NEULA285XJ0	ALS	Motor_Cortex	TDP-path	Male	67	65	Limb
NEULA285XJ0	ALS	Motor_Cortex	TDP-path	Male	67	65	Limb
NEUEE362LGE	ALS	Motor_Cortex	TDP-path	Female	69	66	Limb
NEUEE362LGE	ALS	Motor_Cortex	TDP-path	Female	69	66	Limb
NEUUY552RBK	ALS-FTD	Motor_Cortex	TDP-path	Female	61	58	Limb
NEUUY552RBK	ALS-FTD	Motor_Cortex	TDP-path	Female	61	58	Limb
NEUDT709YHN	ALS	Motor_Cortex	TDP-path	Female	68	63	Limb
NEUXD265LJ8	ALS-FTD	Motor_Cortex	TDP-path	Male	72	67	Limb
NEUXD265LJ8	ALS-FTD	Motor_Cortex	TDP-path	Male	72	67	Limb
18-228-63	ALS	Motor_Cortex	TDP-path	Male	78	76	Bulbar
18-227-15	ALS	Motor_Cortex	TDP-path	Female	61	58	Limb
16-223-17	ALS	Motor_Cortex	TDP-path	Female	78	77	Bulbar
15-217-60	ALS-FTD	Motor_Cortex	TDP-path	Female	80	78	Bulbar
15-211-72	ALS	Motor_Cortex	TDP-path	Male	50	40	Limb
15-207-34	ALS-FTD	Motor_Cortex	TDP-path	Female	77	76	Limb
14-200-25	ALS	Motor_Cortex	TDP-path	Male	68	56	Bulbar
14-198-02	ALS	Motor_Cortex	TDP-path	Female	66	63	Bulbar
13-194-74	ALS	Motor_Cortex	TDP-path	Male	73	71	Bulbar
13-193-72	ALS-FTD	Motor_Cortex	TDP-path	Female	68	67	Bulbar
13-192-54	ALS	Motor_Cortex	TDP-path	Male	63	62	Limb

13-190-33	ALS	Motor_Cortex	TDP-path	Male	43	41	Limb
90-065-49	ALS	Motor_Cortex	TDP-path	Male	61	58	Limb
91-077-47	ALS	Motor_Cortex	TDP-path	Male	51	49	Limb
91-078-52	ALS	Motor_Cortex	TDP-path	Male	50	49	Limb
93-098-25	ALS	Motor_Cortex	TDP-path	Female	67	66	Limb
94-100-17	ALS	Motor_Cortex	TDP-path	Female	66	64	Bulbar
94-105-45	ALS	Motor_Cortex	TDP-path	Male	53	51	Bulbar
97-125-35	ALS	Motor_Cortex	TDP-path	Male	73	72	Limb
97-126-29	ALS	Motor_Cortex	non-TDP path	Female	40	38	Limb
98-132-80	ALS	Motor_Cortex	non-TDP path	Female	40	38	Limb
02-148-00	ALS	Motor_Cortex	TDP-path	Female	60	58	Limb
04-152-76	ALS-FTD	Motor_Cortex	TDP-path	Female	75	73	Bulbar
06-159-51	ALS	Motor_Cortex	TDP-path	Male	66	63	Limb
10-167-35	ALS	Motor_Cortex	TDP-path	Male	68	65	Limb
10-169-12	ALS	Motor_Cortex	TDP-path	Female	61	59	Limb
11-178-56	ALS	Motor_Cortex	TDP-path	Female	64	61	Limb
13-189-06	ALS-FTD	Motor_Cortex	TDP-path	Female	64	59	Limb
13-191-47	ALS-FTD	Motor_Cortex	TDP-path	Male	53	50	Limb
13-195-03	ALS	Motor_Cortex	TDP-path	Male	78	77	Limb
13-196-12	ALS	Motor_Cortex	TDP-path	Male	68	61	Limb
14-199-05	ALS	Motor_Cortex	TDP-path	Male	68	67	Limb
14-201-94	ALS	Motor_Cortex	TDP-path	Male	60	59	Limb
14-202-10	ALS	Motor_Cortex	TDP-path	Female	68	64	Limb

14-203-19	ALS-FTD	Motor_Cortex	TDP-path	Male	69	65	Limb
14-204-56	ALS	Motor_Cortex	TDP-path	Female	61	60	Limb
15-205-18	ALS	Motor_Cortex	TDP-path	Male	78	77	Limb
15-209-43	ALS	Motor_Cortex	TDP-path	Male	59	50	Limb
15-210-54	ALS	Motor_Cortex	TDP-path	Female	56	55	Limb
15-212-81	ALS	Motor_Cortex	TDP-path	Male	60	58	Bulbar
15-213-15	ALS	Motor_Cortex	TDP-path	Female	65	63	Limb
15-214-17	ALS	Motor_Cortex	TDP-path	Female	62		Limb
15-216-56	ALS	Motor_Cortex	TDP-path	Male	40	37	Bulbar
16-219-14	ALS	Motor_Cortex	TDP-path	Female	66	63	Bulbar
16-220-23	ALS-AD	Motor_Cortex	TDP-path	Male	68	67	Limb
16-221-38	ALS	Motor_Cortex	TDP-path	Male	71		Limb
16-222-00	ALS	Motor_Cortex	TDP-path	Female	74	71	Bulbar
16-224-35	ALS	Motor_Cortex	TDP-path	Male	73	69	Bulbar
16-225-87	ALS-FTD	Motor_Cortex	TDP-path	Male	69	66	Limb
17-225-99	Control	Motor_Cortex	non-TDP path	Female	64		Not Applicable
17-226-00	ALS	Motor_Cortex	TDP-path	Female	65	65	Limb
18-229-70	ALS	Motor_Cortex	TDP-path	Female	70	66	Bulbar
91-CTRL-86	Control	Motor_Cortex	non-TDP path	Male	59		Not Applicable
91-CTRL-25	Control	Motor_Cortex	non-TDP path	Male	39		Not Applicable
95-CTRL-76	Control	Motor_Cortex	non-TDP path	Female	76		Not Applicable
98-CTRL-10	Control	Motor_Cortex	non-TDP path	Male	60		Not Applicable
98-CTRL-59	Control	Motor_Cortex	non-TDP path	Male	44		Not Applicable

99-CTRL-58	Control	Motor_Cortex	non-TDP path	Male	48		Not Applicable
00-CTRL-97	Control	Motor_Cortex	non-TDP path	Male	31		Not Applicable
11-CTRL-20	Control	Motor_Cortex	non-TDP path	Male	72		Not Applicable
NEUGV102NYT	Control	Motor_Cortex	non-TDP path	Female	63		Not Applicable
NEULV114EY9	ALS	Motor_Cortex	TDP-path	Male	55	52	Limb
NEULV114EY9	ALS	Motor_Cortex	TDP-path	Male	55	52	Limb
MSSM-JC-8	Control	Motor_Cortex	non-TDP path	Female	65		Not Applicable
MSSM-JC-8	Control	Motor_Cortex	non-TDP path	Female	65		Not Applicable
MSSM-JC-24	Control	Motor_Cortex	non-TDP path	Male	68		Not Applicable
MSSM-JC-24	Control	Motor_Cortex	non-TDP path	Male	68		Not Applicable
MSSM-JC-30	Control	Motor_Cortex	non-TDP path	Male	59		Not Applicable
MSSM-JC-30	Control	Motor_Cortex	non-TDP path	Male	59		Not Applicable
MSSM-JC-41	Control	Motor_Cortex	non-TDP path	Female	88		Not Applicable
MSSM-JC-46	Control	Motor_Cortex	non-TDP path	Male	57		Not Applicable
MSSM-JC-46	Control	Motor_Cortex	non-TDP path	Male	57		Not Applicable
MSSM-JC-53	Control	Motor_Cortex	non-TDP path	Female	60		Not Applicable
MSSM-JC-53	Control	Motor_Cortex	non-TDP path	Female	60		Not Applicable
NEUYT145HVC	ALS	Motor_Cortex	TDP-path	Male	40		Unknown
NEUHC282LVJ	Control	Frontal_Cortex	non-TDP path	Female	90		Not Applicable
NEUHD481VCL	Control	Frontal_Cortex	non-TDP path	Female	54		Not Applicable
GWF14-01	FTD	Frontal_Cortex	TDP-path	Female	72		Not Applicable
NEUCG551GV1	Control	Frontal_Cortex	non-TDP path	Female	57		Not Applicable
NEUGY741GH8	Control	Frontal_Cortex	non-TDP path	Male	59		Not Applicable

PF-UCL-1	Control	Frontal_Cortex	non-TDP path	Male	89	Not Applicable
PF-UCL-1	Control	Temporal_Cortex	non-TDP path	Male	89	Not Applicable
PF-UCL-3	Control	Frontal_Cortex	non-TDP path	Male	68	Not Applicable
PF-UCL-5	Control	Frontal_Cortex	non-TDP path	Male	81	Not Applicable
PF-UCL-5	Control	Temporal_Cortex	non-TDP path	Male	81	Not Applicable
PF-UCL-7	Control	Temporal_Cortex	non-TDP path	Male	68	Not Applicable
PF-UCL-9	Control	Frontal_Cortex	non-TDP path	Female	90	Not Applicable
PF-UCL-9	Control	Temporal_Cortex	non-TDP path	Female	90	Not Applicable
PF-UCL-15	Control	Frontal_Cortex	non-TDP path	Male	79	Not Applicable
PF-UCL-15	Control	Temporal_Cortex	non-TDP path	Male	79	Not Applicable
PF-UCL-17	Control	Frontal_Cortex	non-TDP path	Male	81	Not Applicable
PF-UCL-17	Control	Temporal_Cortex	non-TDP path	Male	81	Not Applicable
PF-UCL-21	Control	Frontal_Cortex	non-TDP path	Male	71	Not Applicable
PF-UCL-21	Control	Temporal_Cortex	non-TDP path	Male	71	Not Applicable
PF-UCL-23	Control	Temporal_Cortex	non-TDP path	Male	77	Not Applicable
PF-UCL-27	Control	Temporal_Cortex	non-TDP path	Male	74	Not Applicable
PF-UCL-35	Control	Temporal_Cortex	non-TDP path	Female	77	Not Applicable
PF-UCL-39	Control	Temporal_Cortex	non-TDP path	Male	60	Not Applicable
PF-UCL-43	Control	Frontal_Cortex	non-TDP path	Male	67	Not Applicable
PF-UCL-43	Control	Temporal_Cortex	non-TDP path	Male	67	Not Applicable
PF-UCL-45	Control	Frontal_Cortex	non-TDP path	Female	75	Not Applicable
PF-UCL-47	Control	Frontal_Cortex	non-TDP path	Male	45	Not Applicable
PF-UCL-47	Control	Temporal_Cortex	non-TDP path	Male	45	Not Applicable

PF-UCL-49	Control	Frontal_Cortex	non-TDP path	Female	66	Not Applicable
PF-UCL-53	Control	Temporal_Cortex	non-TDP path	Male	63	Not Applicable
PF-UCL-57	Control	Frontal_Cortex	non-TDP path	Male	54	Not Applicable
PF-UCL-57	Control	Temporal_Cortex	non-TDP path	Male	54	Not Applicable
PF-UCL-59	Control	Frontal_Cortex	non-TDP path	Female	64	Not Applicable
PF-UCL-59	Control	Temporal_Cortex	non-TDP path	Female	64	Not Applicable
PF-UCL-61	Control	Frontal_Cortex	non-TDP path	Female	52	Not Applicable
PF-UCL-61	Control	Temporal_Cortex	non-TDP path	Female	52	Not Applicable
PF-UCL-63	Control	Frontal_Cortex	non-TDP path	Female	74	Not Applicable
PF-UCL-63	Control	Temporal_Cortex	non-TDP path	Female	74	Not Applicable
PF-UCL-65	FTD	Frontal_Cortex	TDP-path	Female	79	Not Applicable
PF-UCL-65	FTD	Temporal_Cortex	TDP-path	Female	79	Not Applicable
PF-UCL-66	FTD	Frontal_Cortex	TDP-path	Female	87	Not Applicable
PF-UCL-67	FTD	Frontal_Cortex	TDP-path	Female	68	Not Applicable
PF-UCL-67	FTD	Temporal_Cortex	TDP-path	Female	68	Not Applicable
PF-UCL-68	FTD	Frontal_Cortex	TDP-path	Male	53	Not Applicable
PF-UCL-68	FTD	Temporal_Cortex	TDP-path	Male	53	Not Applicable
PF-UCL-69	FTD	Frontal_Cortex	TDP-path	Male	61	Not Applicable
PF-UCL-69	FTD	Temporal_Cortex	TDP-path	Male	61	Not Applicable
PF-UCL-70	FTD	Frontal_Cortex	TDP-path	Male	62	Not Applicable
PF-UCL-70	FTD	Temporal_Cortex	TDP-path	Male	62	Not Applicable
PF-UCL-71	FTD	Frontal_Cortex	TDP-path	Male	72	Not Applicable
PF-UCL-71	FTD	Temporal_Cortex	TDP-path	Male	72	Not Applicable

PF-UCL-72	FTD	Frontal_Cortex	TDP-path	Female	63	Not Applicable
PF-UCL-73	FTD	Frontal_Cortex	TDP-path	Male	55	Not Applicable
PF-UCL-73	FTD	Temporal_Cortex	TDP-path	Male	55	Not Applicable
PF-UCL-74	FTD	Frontal_Cortex	TDP-path	Female	71	Not Applicable
PF-UCL-75	FTD	Frontal_Cortex	TDP-path	Male	72	Not Applicable
PF-UCL-75	FTD	Temporal_Cortex	TDP-path	Male	72	Not Applicable
PF-UCL-76	FTD	Frontal_Cortex	TDP-path	Male	61	Not Applicable
PF-UCL-76	FTD	Temporal_Cortex	TDP-path	Male	61	Not Applicable
PF-UCL-77	FTD	Frontal_Cortex	TDP-path	Male	71	Not Applicable
PF-UCL-77	FTD	Temporal_Cortex	TDP-path	Male	71	Not Applicable
PF-UCL-78	FTD	Frontal_Cortex	TDP-path	Male	69	Not Applicable
PF-UCL-78	FTD	Temporal_Cortex	TDP-path	Male	69	Not Applicable
PF-UCL-79	FTD	Frontal_Cortex	TDP-path	Female	67	Unknown
PF-UCL-79	FTD	Temporal_Cortex	TDP-path	Female	67	Unknown
PF-UCL-80	FTD	Temporal_Cortex	TDP-path	Female	83	Not Applicable
PF-UCL-81	FTD	Frontal_Cortex	TDP-path	Female	73	Not Applicable
PF-UCL-81	FTD	Temporal_Cortex	TDP-path	Female	73	Not Applicable
PF-UCL-82	FTD	Frontal_Cortex	TDP-path	Female	73	Not Applicable
PF-UCL-82	FTD	Temporal_Cortex	TDP-path	Female	73	Not Applicable
PF-UCL-83	FTD	Frontal_Cortex	TDP-path	Male	78	Not Applicable
PF-UCL-83	FTD	Temporal_Cortex	TDP-path	Male	78	Not Applicable
PF-UCL-84	FTD	Frontal_Cortex	TDP-path	Male	74	Not Applicable
PF-UCL-84	FTD	Temporal_Cortex	TDP-path	Male	74	Not Applicable

PF-UCL-85	FTD	Frontal_Cortex	TDP-path	Male	65	Not Applicable
PF-UCL-85	FTD	Temporal_Cortex	TDP-path	Male	65	Not Applicable
PF-UCL-86	FTD	Frontal_Cortex	TDP-path	Male	66	Not Applicable
PF-UCL-87	FTD	Frontal_Cortex	TDP-path	Male	67	Not Applicable
PF-UCL-87	FTD	Temporal_Cortex	TDP-path	Male	67	Not Applicable
PF-UCL-88	FTD	Frontal_Cortex	TDP-path	Female	80	Not Applicable
PF-UCL-88	FTD	Temporal_Cortex	TDP-path	Female	80	Not Applicable
PF-UCL-89	FTD	Frontal_Cortex	TDP-path	Female	72	Not Applicable
PF-UCL-89	FTD	Temporal_Cortex	TDP-path	Female	72	Not Applicable
PF-UCL-126	FTD	Frontal_Cortex	TDP-path	Male	76	Not Applicable
PF-UCL-91	FTD	Frontal_Cortex	TDP-path	Female	67	Unknown
PF-UCL-91	FTD	Temporal_Cortex	TDP-path	Female	67	Unknown
PF-UCL-92	FTD	Frontal_Cortex	TDP-path	Female	74	Not Applicable
PF-UCL-92	FTD	Temporal_Cortex	TDP-path	Female	74	Not Applicable
PF-UCL-93	FTD	Temporal_Cortex	TDP-path	Male	60	Not Applicable
PF-UCL-94	FTD	Frontal_Cortex	TDP-path	Male	68	Not Applicable
PF-UCL-94	FTD	Temporal_Cortex	TDP-path	Male	68	Not Applicable
PF-UCL-95	FTD	Frontal_Cortex	TDP-path	Male	45	Not Applicable
PF-UCL-95	FTD	Temporal_Cortex	TDP-path	Male	45	Not Applicable
PF-UCL-97	FTD	Frontal_Cortex	TDP-path	Female	67	Not Applicable
PF-UCL-97	FTD	Temporal_Cortex	TDP-path	Female	67	Not Applicable
PF-UCL-98	FTD	Frontal_Cortex	TDP-path	Female	62	Not Applicable
PF-UCL-98	FTD	Temporal_Cortex	TDP-path	Female	62	Not Applicable

PF-UCL-99	FTD	Frontal_Cortex	TDP-path	Male	71	Not Applicable
PF-UCL-99	FTD	Temporal_Cortex	TDP-path	Male	71	Not Applicable
PF-UCL-100	FTD	Frontal_Cortex	TDP-path	Female	66	Not Applicable
PF-UCL-100	FTD	Temporal_Cortex	TDP-path	Female	66	Not Applicable
PF-UCL-101	FTD	Frontal_Cortex	TDP-path	Male	70	Not Applicable
PF-UCL-101	FTD	Temporal_Cortex	TDP-path	Male	70	Not Applicable
PF-UCL-103	FTD	Frontal_Cortex	non-TDP path	Male	75	Not Applicable
PF-UCL-104	FTD	Frontal_Cortex	non-TDP path	Male	66	Not Applicable
PF-UCL-104	FTD	Temporal_Cortex	non-TDP path	Male	66	Not Applicable
PF-UCL-106	FTD	Frontal_Cortex	non-TDP path	Male	66	Not Applicable
PF-UCL-106	FTD	Temporal_Cortex	non-TDP path	Male	66	Not Applicable
PF-UCL-107	FTD	Frontal_Cortex	non-TDP path	Male	74	Not Applicable
PF-UCL-107	FTD	Temporal_Cortex	non-TDP path	Male	74	Not Applicable
PF-UCL-108	FTD	Frontal_Cortex	non-TDP path	Female	68	Not Applicable
PF-UCL-109	FTD	Frontal_Cortex	non-TDP path	Male	51	Not Applicable
PF-UCL-109	FTD	Temporal_Cortex	non-TDP path	Male	51	Not Applicable
PF-UCL-110	FTD	Frontal_Cortex	non-TDP path	Male	67	Not Applicable
PF-UCL-110	FTD	Temporal_Cortex	non-TDP path	Male	67	Not Applicable
PF-UCL-111	FTD	Frontal_Cortex	non-TDP path	Female	56	Not Applicable
PF-UCL-111	FTD	Temporal_Cortex	non-TDP path	Female	56	Not Applicable
PF-UCL-112	FTD	Frontal_Cortex	non-TDP path	Female	43	Not Applicable
PF-UCL-113	FTD	Frontal_Cortex	non-TDP path	Male	45	Not Applicable
PF-UCL-113	FTD	Temporal_Cortex	non-TDP path	Male	45	Not Applicable

PF-UCL-114	FTD	Frontal_Cortex	non-TDP path	Female		Not Applicable
PF-UCL-115	FTD	Frontal_Cortex	non-TDP path	Female	72	Not Applicable
PF-UCL-115	FTD	Temporal_Cortex	non-TDP path	Female	72	Not Applicable
PF-UCL-116	Control	Temporal_Cortex	non-TDP path	Male	88	Not Applicable
PF-UCL-117	Control	Frontal_Cortex	non-TDP path	Female	80	Not Applicable
PF-UCL-118	Control	Frontal_Cortex	non-TDP path	Female	79	Not Applicable
PF-UCL-118	Control	Temporal_Cortex	non-TDP path	Female	79	Not Applicable
PF-UCL-119	Control	Frontal_Cortex	non-TDP path	Female	90	Not Applicable
PF-UCL-119	Control	Temporal_Cortex	non-TDP path	Female	90	Not Applicable
PF-UCL-120	Control	Frontal_Cortex	non-TDP path	Female	86	Not Applicable
PF-UCL-121	Control	Frontal_Cortex	non-TDP path	Female	83	Not Applicable
PF-UCL-121	Control	Temporal_Cortex	non-TDP path	Female	83	Not Applicable
PF-UCL-122	Control	Frontal_Cortex	non-TDP path	Male	69	Not Applicable
PF-UCL-122	Control	Temporal_Cortex	non-TDP path	Male	69	Not Applicable
PF-UCL-123	Control	Frontal_Cortex	non-TDP path	Female	68	Not Applicable
PF-UCL-123	Control	Temporal_Cortex	non-TDP path	Female	68	Not Applicable
PF-UCL-124	Control	Frontal_Cortex	non-TDP path	Male	38	Not Applicable
PF-UCL-124	Control	Temporal_Cortex	non-TDP path	Male	38	Not Applicable
PF-UCL-125	Control	Frontal_Cortex	non-TDP path	Female	71	Not Applicable
PF-UCL-125	Control	Temporal_Cortex	non-TDP path	Female	71	Not Applicable
NEUEP010ZFE	Control	Frontal_Cortex	non-TDP path	Male	51	Not Applicable
NEUGJ583BEE	Control	Frontal_Cortex	non-TDP path	Male	70	Not Applicable
NEUHX090PGV	Control	Frontal_Cortex	non-TDP path	Male	72	Not Applicable

NEUUT049NND	Control	Frontal_Cortex	non-TDP path	Female	71	Not Applicable
NEUTP414KZ2	Control	Frontal_Cortex	non-TDP path	Female	52	Not Applicable
NEUML172BXK	Control	Frontal_Cortex	non-TDP path	Female	70	Not Applicable
NEUEG442LDR	Control	Frontal_Cortex	non-TDP path	Male	22	Not Applicable
NEUDA151YMK	Control	Frontal_Cortex	non-TDP path	Female	37	Not Applicable
NEUJB238MJR	Control	Frontal_Cortex	non-TDP path	Male	50	Not Applicable
NEUXW599BNC	Control	Frontal_Cortex	non-TDP path	Female	74	Not Applicable
NEUWD570BTK	Control	Frontal_Cortex	non-TDP path	Male	68	Not Applicable
17-225-99	Control	Frontal_Cortex	non-TDP path	Female	64	Not Applicable
91-CTRL-81	Control	Frontal_Cortex	non-TDP path	Male	58	Not Applicable
92-CTRL-25	Control	Frontal_Cortex	non-TDP path	Male	62	Not Applicable
94-CTRL-04	Control	Frontal_Cortex	non-TDP path	Male	79	Not Applicable
98-CTRL-10	Control	Frontal_Cortex	non-TDP path	Male	60	Not Applicable
98-CTRL-59	Control	Frontal_Cortex	non-TDP path	Male	44	Not Applicable
00-CTRL-97	Control	Frontal_Cortex	non-TDP path	Male	31	Not Applicable
10-CTRL-83	Control	Frontal_Cortex	non-TDP path	Male	70	Not Applicable
11-CTRL-20	Control	Frontal_Cortex	non-TDP path	Male	72	Not Applicable
11-CTRL-43	Control	Frontal_Cortex	non-TDP path	Female	25	Not Applicable
NEUGV102NYT	Control	Frontal_Cortex	non-TDP path	Female	63	Not Applicable
MSSM-JC-8	Control	Frontal_Cortex	non-TDP path	Female	65	Not Applicable
MSSM-JC-24	Control	Frontal_Cortex	non-TDP path	Male	68	Not Applicable
MSSM-JC-25	Control	Frontal_Cortex	non-TDP path	Male	55	Not Applicable
MSSM-JC-30	Control	Frontal_Cortex	non-TDP path	Male	59	Not Applicable

MSSM-JC-42	Control	Frontal_Cortex	non-TDP path	Female	59	Not Applicable
MSSM-JC-46	Control	Frontal_Cortex	non-TDP path	Male	57	Not Applicable

Table S4K. AUC of iPSC neuron-predicted cryptic exons in postmortem bulk RNAseq from FTLD temporal cortex

Symbol	auc
KIF17_1	0.4573678
ELAPOR1_1	0.60145573
PFKP_2	0.84803922
DNAJC12_2	0.43805704
DNAJC12_1	0.49049317
KCNIP2_1	0.59759358
NSMCE4A_2	0.57471777
NSMCE4A_1	0.61437909
KNDC1_4	0.7966429
KNDC1_5	0.51426025
CHID1_1	0.66146762
UVRAG_1	0.54367201
FEZ1_1	0.64653892
ARHGAP32_1	0.85784314
CACNA1C_1	0.61690434
CEP290_1	0.48351159
CEP290_2	0.57234106
RFLNA_1	0.48707665
XPO4_1	0.45112894
LMO7_1	0.57664884
MNAT1_1	0.62225193
MNAT1_2	0.60665478
FAM81A_1	0.545306
NECAB2_2	0.45187166
NECAB2_1	0.48499703
MRPL45P2_1	0.52005348
CCDC57_1	0.55466429

CBLN2_1	0.64691028
SPPL2B_1	0.52881759
TRAPPC12_1	0.58110517
TRAPPC12_2	0.73722519
GREB1_1	0.45083185
FKBP1B_1	0.57226679
KIAA1841_1	0.51589424
EHBP1_1	0.61244801
ETS2_1	0.59031491
PCBP3_1	0.5375817
GRIP2_2	0.66042781
CELSR3_1	0.56907308
USP13_1	0.55243613
MAP6D1_1	0.51463161
CDO1_2	0.52168746
KCNIP1_1	0.45885324
KCNIP1_2	0.5375817
BCKDHB_2	0.53542781
BCKDHB_1	0.55882353
RNASET2_1	0.43166964
ICA1_1	0.5815508
ICA1_2	0.61705288
CTTNBP2_1	0.52762923
PTPRZ1_2	0.51381462
PTPRN2_3	0.61890969
UNC13B_1	0.67543078
UNC13B_2	0.77220737
HDAC6_1	0.5802139
PFKP_1	0.83674985
RP11-291L22.9_1	0.5103981
KNDC1_2	0.81543375
TTC12_1	0.46286393

MED13L_2	0.47162805
ATF7IP2_1	0.50579323
USP10_1	0.47756982
USP10_2	0.49747475
RAB40B_1	0.60338681
ZNF826P_1	0.5063874
ZNF529_1	0.55919489
PEDS1_1	0.53579917
SETD5_1	0.71286393
KALRN_4	0.69385027
ZNF141_1	0.47950089
CDO1_1	0.57256387
TCTE1_1	0.4280303
IQCE_3	0.57598039
CAMK2B_4	0.73128342
CAMK2B_3	0.52562389
PTPRN2_1	0.50430778
PTPRN2_2	0.4701426
DAPK1_1	0.58593286
DNM1_1	0.4760101
RAP1GAP_2	0.83571004
RAP1GAP_1	0.87017231
MACF1_1	0.52510398
GPSM2_1	0.67869875
PSD_2	0.52272727
KNDC1_1	0.56535948
DENND2B_1	0.47727273
ITGA7_1	0.64393939
CEP290_3	0.57635175
EP400_2	0.58481878
NYNRIN_1	0.55488711
LIN52_1	0.55926916

EVL_1	0.48529412
ISLR2_1	0.55466429
CNOT1_1	0.51515152
PHF12_1	0.54278075
TTYH2_1	0.51648841
CBARP_1	0.82011289
CELF5_2	0.80622401
HDGFL2_1	0.63636364
HDGFL2_2	0.66176471
INSR_1	0.82011289
ELAVL3_2	0.64393939
ELAVL3_1	0.63970588
UNC13A_3	0.79545455
ZNF382_1	0.53060012
POU2F2_2	0.5381016
LLNLR-271E8.1_2	0.53446227
WDR35_2	0.60056447
CRLS1_1	0.54582591
SLC24A3_2	0.50601604
KCNQ2_1	0.91755793
DIP2A_1	0.6489899
STXBP5L_1	0.65359477
STXBP5L_2	0.79723708
TMEM175_1	0.66822638
HULC_1	0.51782531
IQCE_1	0.51901367
IQCE_2	0.60308972
FOXK1_1	0.54010695
SEPTIN7P2_1	0.61125966
ACTL6B_2	0.71895425
WASL_2	0.5711527
STMN2_1	0.9520202

USP24_1	0.58303625
DTX1_1	0.47311349
ZNF423_1	0.49405823
MYO1C_1	0.51671123
CERS4_1	0.5221331
ZNF382_2	0.52911468
SLC24A3_1	0.51841949
SLC24A3_3	0.5439691
NUP210_1	0.46226976
SEPTIN11_1	0.49212715
RBPMS_1	0.62091503
NADSYN1_1	0.53594771
ITGA3_1	0.47987225
NPLOC4_1	0.58949792
SLC1A6_1	0.51841949
GRAMD1A_1	0.51218063
SIPA1L3_1	0.54864825
PAOX_1	0.6036839
PXDN_2	0.55258467
FRMD4B_1	0.58615567
DLGAP3_2	0.62254902
MAP6D1_2	0.55243613
LINC00963_1	0.42825312
CORO7_1	0.70112894
MYO9B_1	0.55830362
WDR35_1	0.54337493
PRKG2_1	0.48351159
EPB41L4A_2	0.54352347
EPB41L4A_1	0.5557041
MED13L_1	0.48841355
ZNF527_1	0.47756982
LLNLR-271E8.1_1	0.52124183

BCL2L13_1	0.48440285
ADGRB1_1	0.49019608
HYOU1_1	0.46939988
TGFB3_1	0.60457516
ADCY7_1	0.49019608
AKT3_1	0.51128936
AGRN_1	0.62462864
RSF1_2	0.59729649
L3MBTL1_1	0.57107843
PAOX_2	0.69979204
KIF21A_1	0.50519905
LINGO1_2	0.49554367
RAI2_1	0.49264706
SEMA6D_2	0.48796791
MYO18A_1	0.59180036
SEPTIN11_2	0.5135918
SYT7_1	0.64795009
USP36_2	0.57768865
SCFD2_1	0.49019608
LOXL1-AS1_1	0.56142305
ZDHHC1_1	0.51099228
USP36_1	0.49673203
EML6_1	0.47504456
KALRN_1	0.57308378
ACTL6B_1	0.70447118
CDK7_1	0.55369875
CENPBD1P1_1	0.49346405
METTL8_1	0.49316696
GRIP2_1	0.53334819
AKT3_2	0.62849079
KIAA0753_2	0.55124777
CAMK2B_2	0.75824421

PTPRD_1	0.49160725
C20orf194_2	0.51292335
RANBP17_1	0.50274807
ADCY8_1	0.52807487
MBNL2_1	0.49792038
PTPRD_2	0.49309269
MADD_1	0.49509804
LINGO1_3	0.50995247
POU2F2_1	0.50274807
PREX1_1	0.49777184
ADARB1_1	0.49777184
KCNIP2_2	0.57687166
SYT7_2	0.66718657
FRMD4B_2	0.55050505
ARMH1_1	0.54099822
AARS1_2	0.56714201
SEPTIN7P2_2	0.53988414
RIN2_1	0.50274807
CAMK2B_1	0.81105169
FBN3_5	0.49509804
PXDN_1	0.52881759
IGSF21_1	0.57575758
TFAP2E_2	0.52272727
G2E3_1	0.53030303
CELF5_1	0.78030303
UNC13A_2	0.68181818
LRFN1_2	0.52272727
LRFN1_1	0.52272727
ATG4B_1	0.68181818
ATG4B_2	0.75
NPEPL1_1	0.51515152
IFT122_1	0.54545455

ADCY1_1	0.68939394
ETV5_1	0.51515152
ZDHHC1_2	0.53669043
ADGRL1_1	0.68181818
ADCY1_2	0.68181818
LINGO1_1	0.63636364
VWCE_1	0.51789958
GRAMD1A_2	0.52540107
TMEM117_1	0.63636364
TMEM117_2	0.59090909
ITGA7_2	0.57924837
DLGAP1_1	0.57575758
ADCY1_3	0.52272727
PTPRT_2	0.53787879
SHQ1_1	0.5103981
KALRN_2	0.6825609
IFT122_2	0.52272727
MTRR_1	0.54545455
TRRAP_1	0.59848485
STKLD1_1	0.50757576
TFAP2E_1	0.50757576
AARS1_1	0.57011289
PHF2_2	0.56818182
NUP188_2	0.57575758
KIAA0753_1	0.57026144
LINC01503_1	0.52272727
LINC01503_2	0.50757576
NADSYN1_2	0.52272727
SYNE1_1	0.54545455
NUP188_1	0.53030303
ADARB2_2	0.50757576
NTRK3_1	0.54842543

PRELID3A_1	0.58333333
FBN3_2	0.50757576
ZGPAT_1	0.53787879
SYNE1_2	0.51515152
IGSF21_2	0.53787879
PRELID3A_2	0.56818182
C20orf194_1	0.5530303
WASL_1	0.53787879
DAPK1_2	0.51515152
INTS8_1	0.51515152
RSF1_1	0.56818182
ADARB2_1	0.53030303
ISL2_1	0.50274807
SLC26A11_1	0.5085413
LINC02506_1	0.51515152
MAST1_2	0.50757576
MAST1_1	0.50757576
PTPRT_1	0.54545455
AK3_1	0.50757576
TSPAN18_1	0.49762329
GNB1L_2	0.50757576
GNB1L_1	0.50757576
CYFIP2_1	0.50757576
NKD1_1	0.51515152
KALRN_3	0.51515152
CNGA3_2	0.51322044
RALGAPA2_2	0.51515152
CEP131_2	0.50757576
SLC1A6_2	0.51515152
PSD_1	0.50274807
GALNT8_1	0.49762329
TBL1X_1	0.49509804

CNGA3_1	0.49019608
PHF2_1	0.49509804
All cryptic	0.86111111
Predictive cryptics	0.91963755
Predictive cryptics w/o STMN2	0.91696376

Table S4L. AUC of iPSC neuron-predicted cryptic exons in postmortem bulk RNAseq from ALS motor cortex

Symbol	auc
DLGAP3_2	0.5101776
ELAPOR1_1	0.58722678
PFKP_1	0.49163251
DNAJC12_2	0.6039959
DNAJC12_1	0.58394809
KCNIP2_1	0.50423497
NSMCE4A_2	0.51731557
NSMCE4A_1	0.54665301
KNDC1_2	0.56659836
CHID1_1	0.51086066
UVRAG_1	0.59275956
TTC12_1	0.59665301
HYOU1_1	0.48958333
FEZ1_1	0.5931694
ARHGAP32_1	0.64429645
RFLNA_1	0.49241803
EP400_2	0.57117486
LMO7_1	0.53944672
MNAT1_1	0.5635929
MNAT1_2	0.5273224
LIN52_1	0.49460383
PHF12_1	0.5817623
MRPL45P2_1	0.48709016
CBLN2_1	0.48568989
CBARP_1	0.56212432
SPPL2B_1	0.53531421
TRAPPC12_1	0.68312842

GREB1_1	0.51113388
WDR35_2	0.51734973
FKBP1B_1	0.57756148
EHBP1_1	0.60321038
METTL8_1	0.52103825
ETS2_1	0.51325137
PCBP3_1	0.44935109
BCL2L13_1	0.54446721
NUP210_1	0.49040301
GRIP2_2	0.55573771
CELSR3_1	0.65409836
STXBP5L_1	0.6147541
USP13_1	0.49665301
MAP6D1_1	0.54429645
MAP6D1_2	0.53131831
CDO1_1	0.59569672
KCNIP1_2	0.54357924
HULC_1	0.51284153
BCKDHB_2	0.51557377
BCKDHB_1	0.5948429
ICA1_1	0.50368853
ICA1_2	0.53480191
ACTL6B_2	0.63941257
ACTL6B_1	0.62001366
CTTNBP2_1	0.55259563
PTPRZ1_2	0.46229508
PTPRN2_3	0.62588798
UNC13B_1	0.52749317
UNC13B_2	0.60187842
DNM1_1	0.61038251
HDAC6_1	0.4710724
KIF17_1	0.42599044

AKT3_2	0.56994536
PFKP_2	0.58722678
RP11-291L22.9_1	0.52817623
CACNA1C_1	0.55737705
XPO4_1	0.53244536
G2E3_1	0.51434426
NECAB2_1	0.52964481
RAB40B_1	0.55010246
DLGAP1_1	0.53483607
SLC1A6_1	0.50840164
CRLS1_1	0.52223361
PTPRT_1	0.51434426
SETD5_1	0.54610656
STXBP5L_2	0.61325137
KALRN_4	0.56950137
CDO1_2	0.61963798
WASL_2	0.59467213
DAPK1_1	0.50901639
AGRN_1	0.48644126
IGSF21_2	0.53483607
RAP1GAP_2	0.57848361
RAP1GAP_1	0.5545082
GPSM2_1	0.63934426
AKT3_1	0.56557377
KNDC1_4	0.63603142
NADSYN1_1	0.44818989
RSF1_2	0.50443989
KIF21A_1	0.57243853
TMEM117_1	0.55122951
TMEM117_2	0.54713115
TGFB3_1	0.55075137
FAM81A_1	0.52988388

AARS1_1	0.61885246
MYO18A_1	0.52602459
TTYH2_1	0.55771858
CELF5_2	0.56967213
HDGFL2_1	0.55942623
INSR_1	0.61099727
ELAVL3_2	0.56352459
ADGRL1_1	0.53688525
UNC13A_3	0.56967213
UNC13A_2	0.54918033
ZNF382_2	0.55696721
TRAPPC12_2	0.56014344
WDR35_1	0.57021858
ATG4B_1	0.52663934
C20orf194_2	0.5204918
C20orf194_1	0.51840847
SLC24A3_2	0.53189891
SLC24A3_3	0.5130123
L3MBTL1_1	0.4965847
KCNQ2_1	0.64330601
DIP2A_1	0.51010929
SHQ1_2	0.50819672
KALRN_2	0.56181694
SYNE1_1	0.50389344
RNASET2_1	0.52247268
CAMK2B_4	0.57028689
CAMK2B_2	0.56762295
CAMK2B_1	0.55416667
TRRAP_1	0.54713115
STMN2_1	0.70819672
PTPRD_1	0.53302596
NUP188_1	0.52254098

NUP188_2	0.53278689
USP24_1	0.54419399
KNDC1_1	0.51273907
KNDC1_5	0.45778689
PAOX_2	0.54754098
ITGA7_1	0.53814891
CEP290_3	0.54361339
NYNRIN_1	0.49699454
LINGO1_1	0.52663934
ATF7IP2_1	0.53203552
SLC26A11_1	0.5
CELF5_1	0.55160519
HDGFL2_2	0.60249317
CERS4_1	0.53736339
POU2F2_2	0.49931694
LLNLR-271E8.1_1	0.52120902
LLNLR-271E8.1_2	0.48852459
PTPRT_2	0.5204918
ZNF141_1	0.47247268
TMEM175_1	0.53333333
EPB41L4A_2	0.54801913
EPB41L4A_1	0.55327869
IQCE_2	0.52230191
FOXK1_1	0.50819672
ADCY1_1	0.55532787
ADCY1_2	0.56147541
ADCY1_3	0.50614754
SEPTIN7P2_2	0.49924863
SEPTIN7P2_1	0.54808743
MBNL2_1	0.5102459
ISLR2_1	0.4954918
ZNF382_1	0.49214481

PEDS1_1	0.57903006
SEPTIN11_2	0.52260929
KCNIP1_1	0.53387978
CAMK2B_3	0.40969945
PTPRN2_2	0.4880806
PHF2_2	0.63934426
NADSYN1_2	0.50614754
ITGA7_2	0.52827869
CEP290_1	0.52653689
CEP290_2	0.48101093
DTX1_1	0.49378415
MED13L_1	0.54060792
ISL2_1	0.47903006
LINGO1_3	0.51434426
CORO7_1	0.54866803
MYO1C_1	0.48681694
KIAA0753_2	0.51618853
KIAA0753_1	0.51639344
PRELID3A_2	0.53483607
ZNF527_1	0.50423497
KIAA1841_1	0.54836066
SHQ1_1	0.51229508
PRKG2_1	0.50362022
MTRR_1	0.53688525
PTPRN2_1	0.50157104
MED13L_2	0.50252732
MYO9B_1	0.55935792
ZNF529_1	0.5795082
NECAB2_2	0.5306694
CCDC57_1	0.40983607
ZNF826P_1	0.52459016
RANBP17_1	0.51844262

TCTE1_1	0.4835724
LINC00963_1	0.52295082
EVL_1	0.45143443
LOXL1-AS1_1	0.48968579
GRAMD1A_1	0.48265027
CENPBD1P1_1	0.47704918
PXDN_2	0.47278006
SLC24A3_1	0.49781421
PAOX_1	0.52506831
ZNF423_1	0.5170082
ZDHHC1_1	0.50819672
AARS1_2	0.61625683
USP10_1	0.4670082
PRELID3A_1	0.51639344
GRAMD1A_2	0.48941257
ATG4B_2	0.56147541
NPEPL1_1	0.50204918
FRMD4B_1	0.57657104
CDK7_1	0.53647541
IQCE_1	0.49675546
LINC01503_1	0.52694672
MACF1_1	0.46680328
EML6_1	0.49193989
RBPMS_1	0.52202869
USP10_2	0.5170765
USP36_1	0.49337432
ELAVL3_1	0.55870902
PREX1_1	0.49334016
ADCY8_1	0.51639344
PTPRD_2	0.50833333
IGSF21_1	0.51434426
TSPAN18_1	0.50204918

NTRK3_1	0.50416667
ZDHHC1_2	0.52479508
ITGA3_1	0.5045082
NPLOC4_1	0.49904372
KALRN_1	0.51437842
IFT122_1	0.51639344
IFT122_2	0.50409836
SCFD2_1	0.50819672
SEPTIN11_1	0.50081967
SYNE1_2	0.50819672
WASL_1	0.51625683
STKLD1_1	0.51229508
RAI2_1	0.50614754
SYT7_2	0.53360656
DENND2B_1	0.48958333
LINC01503_2	0.5204918
INTS8_1	0.50409836
RALGAPA2_2	0.5204918
IQCE_3	0.5204918
ATP6V1B2_1	0.50409836
USP36_2	0.51236339
TBL1X_1	0.50409836
KCNIP2_2	0.51065574
MADD_1	0.51434426
SYT7_1	0.52035519
SIPA1L3_1	0.5102459
ETV5_1	0.53278689
POU2F2_1	0.50614754
LINGO1_2	0.50614754
RSF1_1	0.52459016
SDAD1_1	0.51229508
GNB1L_1	0.5102459

ACTR1A_1	0.50409836
RNFT2_1	0.5102459
PHF2_1	0.5102459
ARMH1_1	0.50614754
LRFN1_2	0.50614754
LRFN1_1	0.50204918
IGLON5_1	0.50409836
NKD1_2	0.50614754
PSD_2	0.51229508
FBN3_2	0.50204918
VWCE_1	0.50409836
TFAP2E_2	0.50409836
ADGRB1_1	0.49791667
SEMA6D_2	0.49375
AACSP1_1	0.49166667
LIPE-AS1_1	0.50409836
LINC02506_1	0.50204918
GRIP2_1	0.49166667
ADCY7_1	0.50409836
CNGA3_1	0.5102459
ADARB1_1	0.49778006
PSD_1	0.5102459
RALGAPA2_1	0.50819672
FRMD4B_2	0.50812842
ZGPAT_1	0.50409836
RIN2_1	0.50204918
ISL2_2	0.49375
NKD1_1	0.50204918
PXDN_1	0.47708333
ADARB2_1	0.50204918
SLC1A6_2	0.50204918
CNGA3_2	0.50614754

FBN3_4	0.49166667
CAMTA1_1	0.50204918
All cryptic	0.71010929
Predictive cryptics	0.72814208
Predictive cryptics w/o STMN2	0.71967213

Table S4M. QRTPCR primer sequences for cryptic exons validated in FTLD-TDP frontal cortex

Gene name	Primer pair tested	Forward primer	Reverse primer
ACTL6B	ACTL6B Ex4 to CE	ATCCTGGATCACACCTACAGC	AGGAGGATTGCTTGAACCC
ARHGAP32	ARHGAP32 Ex10-CE	CACCTTCTAAATTCTGGTTTTGAAG	CAGATACAGACGAAAAAGCTGAGTT
CDK7	CDK7 CE to Ex8	GCAGTGTGGACATGACTGATA	GTCCACACCTACACCATACATC
SYT7	hSYT7 Ex3-CE	GCAGTGAGAAGAAGGCTATCAA	CGGCAGACTGGAGCCT
DNM1	DNM1 Ex20 to CE ver2	TGACCCTTTCGGCCCT	CACGAAATCAACATGGCAGT
MYO18A	hMYO18A_ex2_F+cryptic_R	AAGTCCAGGGATGAGATTGTG	GCAGAGTTTTGTCCTCCTCTTTA
CAMK2B	CAMK2B_CE_F2+Ex18R	GAGTGCAGAGACTTCCCCC	CTGCTCCGTGGTCTTAATGAT
HDGFL2	HDGFL2 Ex5 to CE	TCACACCTGAGAAGAAAGCAG	TCCTCTCTTCTGTGTCCCTCT

Table S5A. Quantification of HDGFL2 cryptic peptide in HEK293 cells after TDP-43 knockdown with re-expression of si-resistant GFP-TDP-43 transgene

			Subtracting background	**% cryptic over total**
SuControl-1	Native	**18,990.13**	17793.23	2.9
	Cryptic	**1,721.90**	525.00	
	Background	**1,196.90**		
	Total		18318.23	
TDP-1	Native	**10,879.30**	9535.10	12.9
	Cryptic	**2,751.40**	1,407.20	
	Background	**1,344.20**		
	Total		10942.30	
Dox-1	Native	**11,260.10**	10016.10	3.2
	Cryptic	**1,578.90**	334.90	
	Background	**1,244.00**		
	Total		10351.00	
Control-2	Native	**12,839.41**	11628.81	2.6
	Cryptic	**1,527.10**	316.50	
	Background	**1,210.60**		
	Total		11945.31	
TDP-2	Native	**9,943.71**	8720.71	12.0
	Cryptic	**2,406.70**	1,183.70	
	Background	**1,223.00**		
	Total		9904.41	
Dox-2	Native	**9,682.61**	8495.91	2.7
	Cryptic	**1,426.20**	239.50	
	Background	**1,186.70**		
	Total		8735.41	

Control-3	Native	**17,329.10**	16129.90	2.6
	Cryptic	**1,635.10**	435.90	
	Background	**1,199.20**		
	Total		16565.80	
TDP-3	Native	**10,890.95**	9782.94	12.9
	Cryptic	**2,552.90**	1,444.89	
	Background	**1,108.01**		
	Total		11227.83	
Dox-3	Native	**10,787.72**	9608.72	2.7
	Cryptic	**1,450.00**	271.00	
	Background	**1,179.00**		
	Total		9879.72	

Table S5B. List of co-immunoprecipitated proteins using anti-HDGFL2 antibody vs control IgG

Genes	Comparison (group1/group2)	AVG Log2 Ratio	Pvalue	Qvalue	NegLog 10 Qvalue
DCTN2	HDGFL2 / IgG	2.344	1.56E-12	1.10E-10	9.960
MYO18A	HDGFL2 / IgG	4.509	1.62E-12	1.10E-10	9.960
DCTN4	HDGFL2 / IgG	3.119	5.47E-12	2.48E-10	9.610
ARPC5	HDGFL2 / IgG	3.335	1.53E-11	4.79E-10	9.320
ACTG1	HDGFL2 / IgG	2.188	1.76E-11	4.79E-10	9.320
MYH9	HDGFL2 / IgG	2.601	3.04E-11	6.89E-10	9.160
FASN	HDGFL2 / IgG	1.531	5.14E-11	7.77E-10	9.110
ACTR1A	HDGFL2 / IgG	4.803	4.51E-11	7.77E-10	9.110
SPTAN1	HDGFL2 / IgG	2.275	5.10E-11	7.77E-10	9.110
MYL6	HDGFL2 / IgG	3.411	5.78E-11	7.86E-10	9.100
HDGFL2	HDGFL2 / IgG	4.451	7.40E-11	9.15E-10	9.040
MYH10	HDGFL2 / IgG	2.942	8.29E-11	9.39E-10	9.030
CAPZA1	HDGFL2 / IgG	3.598	1.57E-10	1.64E-09	8.790
XRCC6	HDGFL2 / IgG	2.436	2.23E-10	2.03E-09	8.690
DBN1	HDGFL2 / IgG	3.051	2.24E-10	2.03E-09	8.690
CAPZA2	HDGFL2 / IgG	2.070	4.17E-10	3.55E-09	8.450
CAPZB	HDGFL2 / IgG	3.322	4.72E-10	3.78E-09	8.420
CSNK2A2	HDGFL2 / IgG	1.851	7.52E-10	5.40E-09	8.270

DCTN1	HDGFL2 / IgG	0.175	7.55E-10	5.40E-09	8.270
RUVBL1	HDGFL2 / IgG	3.728	8.11E-10	5.51E-09	8.260
SPECC1L	HDGFL2 / IgG	1.498	1.33E-09	8.60E-09	8.070
ACTR2	HDGFL2 / IgG	1.906	1.59E-09	9.84E-09	8.010
DCTN6	HDGFL2 / IgG	0.926	1.68E-09	9.94E-09	8.000
SPTBN2	HDGFL2 / IgG	2.679	2.05E-09	1.08E-08	7.970
ARPC4	HDGFL2 / IgG	2.469	2.07E-09	1.08E-08	7.970
ACTC1	HDGFL2 / IgG	2.715	2.37E-09	1.19E-08	7.920
MYO1B	HDGFL2 / IgG	2.103	2.67E-09	1.25E-08	7.900
RUVBL2	HDGFL2 / IgG	3.035	2.64E-09	1.25E-08	7.900
H2AC11;H2AC7;H2AC20;H2AC18;H2AC12;H2AC14;H2AJ	HDGFL2 / IgG	2.904	3.29E-09	1.49E-08	7.830
SPTBN1	HDGFL2 / IgG	1.466	3.55E-09	1.56E-08	7.810
MYL12B;MYL12A	HDGFL2 / IgG	3.385	4.26E-09	1.81E-08	7.740
MACF1	HDGFL2 / IgG	1.542	5.27E-09	2.17E-08	7.660
PARP1	HDGFL2 / IgG	2.016	8.42E-09	3.37E-08	7.470
CSNK2B	HDGFL2 / IgG	10.152	1.68E-08	6.55E-08	7.180
ARPC3	HDGFL2 / IgG	1.944	2.10E-08	7.95E-08	7.100
CSNK2A1	HDGFL2 / IgG	3.419	2.70E-08	9.92E-08	7.000
IMMT	HDGFL2 / IgG	1.401	2.93E-08	1.05E-07	6.980
MYL6B	HDGFL2 / IgG	4.146	4.74E-08	1.65E-07	6.780
MPRIP	HDGFL2 / IgG	2.592	1.11E-07	3.76E-07	6.420

H2BC12;H2BS1;H2BC5;H2BC4;H2BC18;H2BC9;H2BC15;H2BC14;H2BC13	HDGFL2 / IgG	2.791	1.42E-07	4.70E-07	6.330
XRCC5	HDGFL2 / IgG	2.370	2.23E-07	7.22E-07	6.140
H3C1;H3-3A;H3-4;H3C15	HDGFL2 / IgG	3.313	2.70E-07	8.35E-07	6.080
RPL14	HDGFL2 / IgG	1.035	3.19E-07	9.64E-07	6.020
TOP1	HDGFL2 / IgG	1.093	3.91E-07	1.16E-06	5.940
H2AZ1;H2AZ2	HDGFL2 / IgG	2.131	4.06E-07	1.17E-06	5.930
BCLAF1	HDGFL2 / IgG	0.870	8.35E-07	2.37E-06	5.630
CALM1;CALM2;CALM3	HDGFL2 / IgG	2.361	1.50E-06	4.16E-06	5.380
RPL10A	HDGFL2 / IgG	1.245	1.89E-06	5.14E-06	5.290
VDAC3	HDGFL2 / IgG	2.000	2.22E-06	5.91E-06	5.230
INA	HDGFL2 / IgG	1.340	2.37E-06	6.20E-06	5.210
CLTA	HDGFL2 / IgG	1.889	2.97E-06	7.35E-06	5.130
PABPC1	HDGFL2 / IgG	1.413	3.69E-06	8.96E-06	5.050
SRP14	HDGFL2 / IgG	1.518	4.15E-06	9.73E-06	5.010
YWHAG	HDGFL2 / IgG	1.258	5.05E-06	1.16E-05	4.940
H4C1	HDGFL2 / IgG	2.649	6.04E-06	1.37E-05	4.860
PRPF19	HDGFL2 / IgG	1.364	6.24E-06	1.39E-05	4.860
VDAC1	HDGFL2 / IgG	1.289	6.66E-06	1.46E-05	4.840
ERH	HDGFL2 / IgG	0.969	7.43E-06	1.60E-05	4.800
NPM1	HDGFL2 / IgG	1.285	1.02E-05	2.18E-05	4.660
IGKV1-27;IGKV1-8;IGKV1-9	HDGFL2 / IgG	3.593	1.12E-05	2.33E-05	4.630
CLTC	HDGFL2 / IgG	1.388	1.16E-05	2.39E-05	4.620

DYNC1H1	HDGFL2 / IgG	1.243	1.31E-05	2.67E-05	4.570
THRAP3	HDGFL2 / IgG	0.961	1.44E-05	2.87E-05	4.540
FUS	HDGFL2 / IgG	1.563	1.70E-05	3.36E-05	4.470
CLSTN3	HDGFL2 / IgG	11.045	1.94E-05	3.74E-05	4.430
GNB1;GNB2	HDGFL2 / IgG	0.814	2.19E-05	4.14E-05	4.380
VDAC2	HDGFL2 / IgG	1.963	5.75E-05	1.00E-04	4.000
COX4I1	HDGFL2 / IgG	0.781	7.45E-05	1.27E-04	3.900
NEFM	HDGFL2 / IgG	1.125	9.58E-05	1.61E-04	3.790
TAF15	HDGFL2 / IgG	1.614	1.10E-04	1.80E-04	3.740
EPB41L3	HDGFL2 / IgG	1.201	1.14E-04	1.85E-04	3.730
FXR1	HDGFL2 / IgG	1.550	1.42E-04	2.25E-04	3.650
RPL7A	HDGFL2 / IgG	0.677	1.49E-04	2.32E-04	3.630
RPL7	HDGFL2 / IgG	0.698	1.60E-04	2.47E-04	3.610
PPP1CA	HDGFL2 / IgG	2.024	1.73E-04	2.64E-04	3.580
G3BP2	HDGFL2 / IgG	0.885	1.80E-04	2.72E-04	3.560
ARPC1A	HDGFL2 / IgG	1.397	2.94E-04	4.25E-04	3.370
PRPF8	HDGFL2 / IgG	0.559	3.57E-04	5.11E-04	3.290
RPL12	HDGFL2 / IgG	1.012	4.28E-04	5.93E-04	3.230
NEFL	HDGFL2 / IgG	1.088	4.66E-04	6.40E-04	3.190
SRSF7	HDGFL2 / IgG	0.702	5.33E-04	7.25E-04	3.140
ACTR3	HDGFL2 / IgG	1.661	5.98E-04	7.97E-04	3.100
RPL27	HDGFL2 / IgG	0.764	6.08E-04	8.03E-04	3.100

RPS26	HDGFL2 / IgG	0.699	6.81E-04	8.82E-04	3.050
PGAM5	HDGFL2 / IgG	1.660	7.68E-04	9.66E-04	3.010
CHCHD3	HDGFL2 / IgG	1.012	8.53E-04	1.05E-03	2.980
HNRNPUL1	HDGFL2 / IgG	1.029	8.71E-04	1.07E-03	2.970
RPS16	HDGFL2 / IgG	0.780	9.48E-04	1.13E-03	2.950
SLC25A5	HDGFL2 / IgG	0.793	1.00E-03	1.15E-03	2.940
EIF2S3;EIF2S3B	HDGFL2 / IgG	0.758	9.86E-04	1.15E-03	2.940
TMPO	HDGFL2 / IgG	0.723	9.91E-04	1.15E-03	2.940
RPS20	HDGFL2 / IgG	0.741	1.12E-03	1.28E-03	2.890
RPS6	HDGFL2 / IgG	1.005	1.15E-03	1.29E-03	2.890
RPL13A;RPL13AP3	HDGFL2 / IgG	0.676	1.17E-03	1.31E-03	2.880
YWHAQ	HDGFL2 / IgG	1.016	1.22E-03	1.35E-03	2.870
SART1	HDGFL2 / IgG	0.796	1.26E-03	1.36E-03	2.860
PABPC4	HDGFL2 / IgG	0.748	1.26E-03	1.36E-03	2.860
PIP4K2B	HDGFL2 / IgG	0.620	1.39E-03	1.49E-03	2.830
PPIB	HDGFL2 / IgG	2.447	1.54E-03	1.64E-03	2.790
SRSF1	HDGFL2 / IgG	0.416	1.62E-03	1.71E-03	2.770
RPLP0;RPLP0P6	HDGFL2 / IgG	1.049	1.65E-03	1.73E-03	2.760
TFAM	HDGFL2 / IgG	1.485	1.68E-03	1.73E-03	2.760
RPL13	HDGFL2 / IgG	0.515	1.89E-03	1.89E-03	2.720
CORO2B	HDGFL2 / IgG	2.211	2.03E-03	2.01E-03	2.700
DDX5	HDGFL2 / IgG	0.558	2.19E-03	2.16E-03	2.670
TUBA1A	HDGFL2 / IgG	0.881	2.37E-03	2.32E-03	2.640

RPL18A	HDGFL2 / IgG	0.876	2.71E-03	2.63E-03	2.580
PLEC	HDGFL2 / IgG	0.457	2.75E-03	2.65E-03	2.580
SYT1	HDGFL2 / IgG	0.739	3.28E-03	3.09E-03	2.510
SLC25A11	HDGFL2 / IgG	2.555	3.59E-03	3.34E-03	2.480
HNRNPM	HDGFL2 / IgG	0.515	3.74E-03	3.46E-03	2.460
DLAT	HDGFL2 / IgG	2.184	4.33E-03	3.95E-03	2.400
PCBP2	HDGFL2 / IgG	1.035	5.13E-03	4.53E-03	2.340
CEP170	HDGFL2 / IgG	0.840	5.16E-03	4.53E-03	2.340
COX7A2	HDGFL2 / IgG	0.904	5.60E-03	4.85E-03	2.310
ADD1	HDGFL2 / IgG	0.886	5.78E-03	4.95E-03	2.310
DDX23	HDGFL2 / IgG	1.202	6.16E-03	5.22E-03	2.280
PPP1R12A	HDGFL2 / IgG	1.734	7.00E-03	5.73E-03	2.240
TRA2A	HDGFL2 / IgG	0.273	7.08E-03	5.76E-03	2.240
RPL11	HDGFL2 / IgG	0.968	7.34E-03	5.90E-03	2.230
RAN	HDGFL2 / IgG	0.741	7.80E-03	6.17E-03	2.210
SLC25A3	HDGFL2 / IgG	0.787	8.34E-03	6.56E-03	2.180
RPL8	HDGFL2 / IgG	0.585	8.76E-03	6.85E-03	2.160
ATP5MF	HDGFL2 / IgG	0.750	9.03E-03	7.02E-03	2.150
IGHG1	HDGFL2 / IgG	0.650	1.09E-02	8.24E-03	2.080
EEF1A1;EEF1A1P5	HDGFL2 / IgG	0.555	1.11E-02	8.33E-03	2.080
CFL1	HDGFL2 / IgG	0.976	1.14E-02	8.46E-03	2.070
TUBB	HDGFL2 / IgG	0.981	1.15E-02	8.48E-03	2.070
RBM14	HDGFL2 / IgG	0.209	1.32E-02	9.61E-03	2.020

RPL34	HDGFL2 / IgG	0.582	1.33E-02	9.63E-03	2.020
ATP5F1C	HDGFL2 / IgG	0.615	1.45E-02	1.04E-02	1.980
H1-10	HDGFL2 / IgG	0.449	1.47E-02	1.04E-02	1.980
HSPA8	HDGFL2 / IgG	0.553	1.67E-02	1.16E-02	1.930
DDX1	HDGFL2 / IgG	0.533	1.74E-02	1.21E-02	1.920
SLC25A6	HDGFL2 / IgG	0.669	2.02E-02	1.36E-02	1.860
RAC2;RAC3;RAC1	HDGFL2 / IgG	0.939	2.08E-02	1.39E-02	1.860
HMGB2	HDGFL2 / IgG	1.145	2.21E-02	1.46E-02	1.840
RPS14	HDGFL2 / IgG	0.458	2.21E-02	1.46E-02	1.840
RTCB	HDGFL2 / IgG	0.277	2.27E-02	1.49E-02	1.830
DYNLL1;DYNLL2	HDGFL2 / IgG	2.182	2.40E-02	1.56E-02	1.810
KRT18	HDGFL2 / IgG	0.701	2.55E-02	1.64E-02	1.790
TUBB2A	HDGFL2 / IgG	0.747	2.76E-02	1.75E-02	1.760
RBM25	HDGFL2 / IgG	1.205	2.80E-02	1.76E-02	1.750
DDX17	HDGFL2 / IgG	0.393	2.80E-02	1.76E-02	1.750
BASP1	HDGFL2 / IgG	0.621	3.07E-02	1.92E-02	1.720
RPL23	HDGFL2 / IgG	0.382	3.09E-02	1.92E-02	1.720
POLDIP3	HDGFL2 / IgG	0.250	3.36E-02	2.07E-02	1.680
YWHAE	HDGFL2 / IgG	0.108	3.40E-02	2.09E-02	1.680
RPS5	HDGFL2 / IgG	0.687	3.57E-02	2.17E-02	1.660
SFPQ	HDGFL2 / IgG	0.409	3.74E-02	2.26E-02	1.650
TUBB2B	HDGFL2 / IgG	0.940	4.07E-02	2.43E-02	1.610
TUBB4B	HDGFL2 / IgG	0.712	4.64E-02	2.71E-02	1.570

NONO	HDGFL2 / IgG	0.506	4.63E-02	2.71E-02	1.570
RPL21	HDGFL2 / IgG	1.230	4.78E-02	2.78E-02	1.560
VAT1	HDGFL2 / IgG	0.612	4.98E-02	2.85E-02	1.550
RPS9	HDGFL2 / IgG	0.435	5.11E-02	2.90E-02	1.540
RBMX	HDGFL2 / IgG	0.393	5.33E-02	2.98E-02	1.530
RPS11	HDGFL2 / IgG	0.563	5.40E-02	3.01E-02	1.520
RPL35A	HDGFL2 / IgG	1.063	5.93E-02	3.24E-02	1.490
SNRPD3	HDGFL2 / IgG	0.202	6.02E-02	3.27E-02	1.480
RPL6	HDGFL2 / IgG	0.345	6.33E-02	3.38E-02	1.470
HSPA5	HDGFL2 / IgG	0.556	6.51E-02	3.45E-02	1.460
RPL22	HDGFL2 / IgG	0.404	6.83E-02	3.58E-02	1.450
DEK	HDGFL2 / IgG	0.354	6.84E-02	3.58E-02	1.450
IGF2BP3	HDGFL2 / IgG	0.964	6.97E-02	3.59E-02	1.440
SRP9	HDGFL2 / IgG	0.783	7.09E-02	3.62E-02	1.440
COPA	HDGFL2 / IgG	0.989	7.61E-02	3.83E-02	1.420
RPL36	HDGFL2 / IgG	0.688	7.76E-02	3.89E-02	1.410
COPB1	HDGFL2 / IgG	0.249	7.94E-02	3.97E-02	1.400
PTGES3	HDGFL2 / IgG	0.044	8.72E-02	4.27E-02	1.370
RPL15	HDGFL2 / IgG	0.653	9.14E-02	4.45E-02	1.350
PRDX1	HDGFL2 / IgG	0.375	9.21E-02	4.46E-02	1.350
PHB2	HDGFL2 / IgG	0.347	9.19E-02	4.46E-02	1.350
SNRPD2	HDGFL2 / IgG	0.192	9.58E-02	4.58E-02	1.340
RPS3	HDGFL2 / IgG	0.652	9.77E-02	4.64E-02	1.330

LIMA1	HDGFL2 / IgG	0.583	9.97E-02	4.73E-02	1.330

Table S5C. Affinity purification mass spectrometry analysis of protein-protein interactions in TDP-43 KD vs control iPSC-derived neurons

Genes	AVGLog2Ratio	Pvalue	Qvalue	NegLog10Qval
ACTC1	-0.398	0.110	0.065	1.188
ACTG1	-0.299	0.082	0.052	1.286
ACTR1A	-0.179	0.727	0.260	0.585
ACTR2	-0.678	0.034	0.027	1.563
ACTR3	-1.760	0.031	0.025	1.599
ADD1	0.133	0.208	0.104	0.981
ARPC1A	-0.869	0.061	0.042	1.382
ARPC3	-0.481	0.277	0.128	0.891
ARPC4	-0.568	0.022	0.019	1.714
ARPC5	-0.237	0.076	0.049	1.308
ATP5F1C	0.257	0.786	0.277	0.558
ATP5MF	-0.151	0.846	0.292	0.535
BASP1	1.337	0.197	0.100	0.999
BCLAF1	-0.047	0.771	0.272	0.565
CALM1;CALM2;CALM3	0.430	0.503	0.198	0.704

CAPZA1	-0.201	0.779	0.274	0.561
CAPZA2	-0.039	0.771	0.272	0.565
CAPZB	-0.344	0.228	0.111	0.956
CEP170	-0.545	0.003	0.004	2.364
CFL1	-1.144	0.142	0.079	1.104
CHCHD3	0.573	0.279	0.129	0.888
CLSTN3	-0.117	0.077	0.049	1.308
CLTA	0.167	0.411	0.169	0.773
CLTC	0.362	0.967	0.321	0.493
COPA	0.173	0.571	0.217	0.664
COPB1	0.273	0.682	0.248	0.606
CORO2B	-0.379	0.302	0.137	0.864
COX4I1	0.036	0.939	0.315	0.502
COX7A2	0.807	0.252	0.119	0.924
CSNK2A1	1.194	0.012	0.013	1.898
CSNK2A2	0.035	0.640	0.237	0.626
CSNK2B	-1.010	0.302	0.137	0.864
DBN1	-0.397	0.130	0.073	1.134
DCTN1	-0.329	0.144	0.079	1.102
DCTN2	-0.117	0.594	0.223	0.653
DCTN4	0.235	0.935	0.313	0.504
DCTN6	-0.320	0.014	0.014	1.849
DDX1	0.527	0.047	0.034	1.472

DDX17	0.741	0.012	0.013	1.887
DDX23	0.465	0.820	0.286	0.544
DDX5	0.358	0.136	0.076	1.119
DEK	0.121	0.777	0.274	0.562
DLAT	-0.662	0.070	0.046	1.336
DYNC1H1	-0.094	0.364	0.156	0.808
DYNLL1;DYNLL2	-0.964	0.222	0.109	0.963
EEF1A1;EEF1A1P5	-0.322	0.142	0.078	1.106
EIF2S3;EIF2S3B	-0.060	0.688	0.249	0.603
EPB41L3	0.111	0.955	0.318	0.497
ERH	0.039	0.658	0.242	0.617
FASN	-0.486	0.032	0.026	1.583
FUS	0.308	0.485	0.193	0.715
FXR1	0.347	0.486	0.193	0.715
G3BP2	0.182	0.303	0.137	0.863
GNB1;GNB2	-0.012	0.997	0.328	0.484
H1-10	-0.094	0.143	0.079	1.103
H2AC11;H2AC7;H2AC20;H2AC18;H2AC12;H2AC14;H2AJ	0.168	0.578	0.218	0.661
H2AZ1;H2AZ2	-0.067	0.831	0.288	0.541
H2BC12;H2BS1;H2BC5;H2BC4;H2BC18;H2BC9;H2BC15;H2BC14;H2BC13	-0.317	0.402	0.167	0.778
H3C1;H3-3A;H3-4;H3C15	-0.581	0.344	0.150	0.824
H4C1	-0.479	0.363	0.156	0.808

HDGFL2	0.654	0.095	0.058	1.237
HMGB2	0.835	0.121	0.069	1.158
HNRNPM	0.420	0.240	0.115	0.939
HNRNPUL1	0.612	0.131	0.074	1.132
HSPA5	0.152	0.874	0.298	0.526
HSPA8	-0.506	0.102	0.061	1.214
IGF2BP3	-0.759	0.669	0.244	0.612
IGHG1	-0.198	0.219	0.108	0.968
IGKV1-27;IGKV1-8;IGKV1-9	0.109	0.069	0.046	1.337
IMMT	0.544	0.172	0.091	1.042
INA	-0.607	0.042	0.031	1.507
KRT18	0.416	0.267	0.125	0.904
LIMA1	-1.864	0.001	0.001	2.863
MACF1	-0.279	0.487	0.193	0.714
MPRIP	0.690	0.030	0.025	1.605
MYH10	0.338	0.225	0.110	0.960
MYH9	0.008	0.922	0.311	0.507
MYL12B;MYL12A	0.027	0.975	0.323	0.491
MYL6	0.481	0.140	0.078	1.110
MYL6B	0.534	0.291	0.133	0.876
MYO18A	0.181	0.710	0.256	0.592
MYO1B	0.109	0.525	0.204	0.691
NEFL	-0.941	0.086	0.054	1.268

NEFM	-0.632	0.068	0.046	1.342
NONO	0.507	0.064	0.043	1.363
NPM1	-0.016	0.754	0.268	0.573
PABPC1	-0.217	0.164	0.088	1.057
PABPC4	0.561	0.301	0.137	0.864
PARP1	-0.073	0.545	0.209	0.680
PCBP2	-0.018	0.549	0.210	0.678
PGAM5	0.394	0.379	0.160	0.795
PHB2	-0.030	0.308	0.138	0.859
PIP4K2B	-0.128	0.131	0.074	1.132
PLEC	0.654	0.042	0.031	1.507
POLDIP3	1.091	0.006	0.007	2.128
PPIB	1.919	0.137	0.076	1.118
PPP1CA	0.662	0.036	0.028	1.548
PPP1R12A	0.595	0.050	0.036	1.447
PRDX1	-0.194	0.212	0.106	0.976
PRPF19	0.106	0.654	0.240	0.619
PRPF8	0.968	0.037	0.028	1.547
PTGES3	1.118	0.003	0.004	2.369
RAC2;RAC3;RAC1	-0.120	0.222	0.109	0.963
RAN	0.198	0.932	0.313	0.504
RBM14	0.496	0.147	0.081	1.093
RBM25	-0.470	0.715	0.257	0.590

RBMX	0.384	0.064	0.043	1.366
RPL10A	-0.132	0.866	0.297	0.528
RPL11	-0.131	0.344	0.150	0.823
RPL12	0.034	0.944	0.316	0.501
RPL13	-0.213	0.240	0.115	0.939
RPL13A;RPL13AP3	0.399	0.589	0.221	0.655
RPL14	-0.011	0.846	0.292	0.535
RPL15	0.137	0.852	0.293	0.533
RPL18A	0.196	0.961	0.320	0.495
RPL21	-1.337	0.624	0.231	0.636
RPL22	0.099	0.650	0.239	0.621
RPL23	0.018	0.181	0.094	1.026
RPL27	-0.260	0.205	0.103	0.986
RPL34	-0.478	0.083	0.052	1.281
RPL35A	0.081	0.611	0.228	0.643
RPL36	0.505	0.180	0.094	1.027
RPL6	0.359	0.129	0.073	1.138
RPL7	-0.176	0.319	0.141	0.849
RPL7A	0.258	0.642	0.237	0.625
RPL8	0.100	0.826	0.287	0.543
RPLP0;RPLP0P6	-1.920	NA	NA	#VALUE!
RPS11	-0.402	0.172	0.091	1.042
RPS14	-0.439	0.089	0.055	1.257

RPS16	0.080	0.940	0.315	0.502
RPS20	0.516	0.089	0.055	1.257
RPS26	0.308	0.979	0.324	0.490
RPS3	-0.100	0.535	0.206	0.686
RPS5	0.607	0.041	0.031	1.513
RPS6	0.219	0.868	0.297	0.527
RPS9	-0.063	0.181	0.094	1.026
RTCB	0.432	0.328	0.145	0.840
RUVBL1	0.193	0.326	0.144	0.841
RUVBL2	0.487	0.458	0.184	0.735
SART1	0.052	0.281	0.130	0.886
SFPQ	0.590	0.031	0.025	1.600
SLC25A11	-0.252	0.463	0.186	0.731
SLC25A3	-0.268	0.545	0.209	0.680
SLC25A5	-0.102	0.514	0.200	0.698
SLC25A6	-0.029	0.449	0.181	0.742
SNRPD2	0.784	0.399	0.166	0.780
SNRPD3	0.226	0.034	0.027	1.565
SPECC1L	-0.001	0.849	0.293	0.534
SPTAN1	0.079	0.504	0.198	0.704
SPTBN1	-0.013	0.613	0.228	0.642
SPTBN2	0.555	0.044	0.032	1.494
SRP14	0.006	0.546	0.209	0.680

SRP9	-0.347	0.088	0.055	1.260
SRSF1	0.236	0.372	0.158	0.800
SRSF7	0.072	0.691	0.250	0.602
SYT1	0.490	0.681	0.248	0.606
TAF15	0.788	0.251	0.119	0.924
TFAM	1.339	0.478	0.190	0.721
THRAP3	0.454	0.145	0.080	1.099
TMPO	-0.585	0.116	0.067	1.173
TOP1	-0.111	0.449	0.181	0.742
TRA2A	0.358	0.260	0.122	0.912
TUBA1A	-0.100	0.595	0.223	0.652
TUBB	-0.426	0.231	0.112	0.952
TUBB2A	-0.134	0.636	0.235	0.628
TUBB2B	0.096	0.792	0.278	0.556
TUBB4B	-0.006	0.680	0.248	0.606
VAT1	0.048	0.208	0.104	0.982
VDAC1	-0.451	0.317	0.141	0.850
VDAC2	-0.265	0.358	0.154	0.811
VDAC3	0.287	0.925	0.312	0.506
XRCC5	0.181	0.794	0.278	0.555
XRCC6	0.113	0.993	0.327	0.486
YWHAE	-0.377	0.985	0.325	0.488
YWHAG	-0.423	0.211	0.106	0.977

YWHAQ	0.033	0.289	0.133	0.877

Table S5D. Inclusion list of co-immunoprecipitated proteins in CE-HDGFL2-myc-flag or FL-HDGFL2-myc-flag HEK-293 cells

ProteinGroups	Genes
A0JLT2	MED19
O00139	KIF2A
O00425	IGF2BP3
O00757	FBP2
O14646	CHD1
O15143	ARPC1B
O15381	NVL
O43159	RRP8
O43166	SIPA1L1
O60573	EIF4E2
O75151	PHF2
O75175	CNOT3
O75439	PMPCB
O75691	UTP20
O75794	CDC123
O95125	ZNF202
P05412	JUN
P05976	MYL1

P06746	POLB
P07585	DCN
P0DMU7;P0DMU8;P0DMU9;P0DMV0;P0DMV1;P0DMV2;Q5DJT8;Q5HYN5;Q8NHU0	CT45A6;CT45A5;CT45A10;CT45A7;CT45A8;CT45A9;CT45A2;CT45A1;CT45A3
P10301	RRAS
P17028	ZNF24
P19387	POLR2C
P20142	PGC
P22492	H1-6
P28370	SMARCA1
P29536	LMOD1
P32121	ARRB2
P34741	SDC2
P35052	GPC1
P38432	COIL
P41743	PRKCI
P45973	CBX5
P49407	ARRB1
P49916	LIG3
P50579	METAP2
P51153	RAB13
P53803	POLR2K
P54652	HSPA2

P55081	MFAP1
P57772	EEFSEC
P59780	AP3S2
P61218	POLR2F
P61244	MAX
P78356	PIP4K2B
P82663	MRPS25
P82675	MRPS5
Q00577	PURA
Q01831	XPC
Q03188	CENPC
Q09161	NCBP1
Q10589	BST2
Q12789	GTF3C1
Q13144	EIF2B5
Q13268	DHRS2
Q14160;Q9BTT6	SCRIB;LRRC1
Q14554	PDIA5
Q14571	ITPR2
Q14676	MDC1
Q14C87	TMEM132D
Q15014	MORF4L2
Q15555	MAPRE2

Q15847	ADIRF
Q2TBE0	CWF19L2
Q3B726	POLR1F
Q53HL2	CDCA8
Q5F1R6	DNAJC21
Q5QJE6	DNTTIP2
Q5SNT2	TMEM201
Q5T280	SPOUT1
Q5VSY0	GKAP1
Q5VUY2	AADACL4
Q5VZL5	ZMYM4
Q68CQ4	DIEXF
Q6AI12	ANKRD40
Q6NZY4	ZCCHC8
Q6P1X5	TAF2
Q6P5R6	RPL22L1
Q6PJT7	ZC3H14
Q6Q0C0	TRAF7
Q6RFH5	WDR74
Q6WKZ4	RAB11FIP1
Q6ZQX7	LIAT1
Q702N8	XIRP1
Q7Z5H4	VN1R5

Q86VF2	IGFN1
Q86W42	THOC6
Q86X95	CIR1
Q8IUE6	H2AC21
Q8IUF8	RIOX2
Q8IWA0	WDR75
Q8IXM2	BAP18
Q8N257	H2BU1
Q8N5C6	SRBD1
Q8N5I9	C12orf45
Q8N7H5	PAF1
Q8NDD1	C1orf131
Q8TAA9	VANGL1
Q8TAD8	SNIP1
Q8TAQ2	SMARCC2
Q8TBB5	KLHDC4
Q8WUA4	GTF3C2
Q8WVV9	HNRNPLL
Q8WXA9	SREK1
Q8WY36	BBX
Q8WYH8	ING5
Q8WYL5	SSH1
Q8WZ60	KLHL6

Q92504	SLC39A7
Q92552	MRPS27
Q92614	MYO18A
Q92784	DPF3
Q93052	LPP
Q969X6	UTP4
Q96A35	MRPL24
Q96B97	SH3KBP1
Q96BK5	PINX1
Q96C57	CUSTOS
Q96DI7	SNRNP40
Q96HR8	NAF1
Q96JN8	NEURL4
Q96K17	BTF3L4
Q96KM6	ZNF512B
Q96MG7	NSMCE3
Q96QE5	TEFM
Q96T23	RSF1
Q99442	SEC62
Q99549	MPHOSPH8
Q9BRU9	UTP23
Q9BUL5	PHF23
Q9BVA1	TUBB2B

Q9BVC6	TMEM109
Q9BWE0	REPIN1
Q9C086	INO80B
Q9C0J8	WDR33
Q9GZR2	REXO4
Q9H7N4	SCAF1
Q9H8G2	CAAP1
Q9H8M2	BRD9
Q9H9Y2	RPF1
Q9H9Y6	POLR1B
Q9HAF1	MEAF6
Q9HAU5	UPF2
Q9HCE1	MOV10
Q9HCS7	XAB2
Q9NNW5	WDR6
Q9NR12	PDLIM7
Q9NS86	LANCL2
Q9NSB2	KRT84
Q9NXF1	TEX10
Q9NY61	AATF
Q9NYV4	CDK12
Q9P003	CNIH4
Q9P2D1	CHD7

Q9UER7	DAXX
Q9UGI8	TES
Q9UGN5	PARP2
Q9UGU5	HMGXB4
Q9UI10	EIF2B4
Q9UIF9	BAZ2A
Q9UKE5	TNIK
Q9ULW0	TPX2
Q9ULW3	ABT1
Q9UMY1	NOL7
Q9UN81	L1RE1
Q9UNX4	WDR3
Q9UPW5	AGTPBP1
Q9Y2P8	RCL1
Q9Y324	FCF1
Q9Y3A2	UTP11
Q9Y3D3	MRPS16
Q9Y421	FAM32A
Q9Y450	HBS1L
Q9Y5Q9	GTF3C3
Q9Y608	LRRFIP2
Q9Y676	MRPS18B
Q9Y678	COPG1

P49588	AARS1
Q9NRN7	AASDHPPT
P08183	ABCB1
P24752	ACAT1
Q9UKV3	ACIN1
P68032	ACTC1
P63261	ACTG1
P12814	ACTN1
O43707	ACTN4
P11766	ADH5
Q09666	AHNAK
O95831	AIFM1
P54819	AK2
P54886	ALDH18A1
P49189	ALDH9A1
P04075	ALDOA
Q4VCS5	AMOT
P07355	ANXA2
P27695	APEX1
Q9BZZ5	API5
O60306	AQR
Q9NWB6	ARGLU1
P31939	ATIC

P06576	ATP5F1B
P36542	ATP5F1C
P56385	ATP5ME
P56134	ATP5MF
P24539	ATP5PB
Q8TDN6	BRIX1
Q9Y6E2	BZW2
P00918	CA2
P27708	CAD
P0DP23;P0DP24;P0DP25	CALM1;CALM2;CALM3
Q9NZT1	CALML5
P27797	CALR
P27824	CANX
P52907	CAPZA1
P47755	CAPZA2
P47756	CAPZB
O75828	CBR3
P0DN79;P35520	CBSL;CBS
P83916	CBX1
Q96CT7	CCDC124
Q7Z3E2	CCDC186
P48643	CCT5
P40227	CCT6A

P50990	CCT8
O00311	CDC7
P42771	CDKN2A
Q7Z7K6	CENPV
P23528	CFL1
Q96JM3	CHAMP1
Q9UHD1	CHORDC1
P12532	CKMT1A
O00299	CLIC1
Q9C0A0	CNTNAP4
P02461	COL3A1
P21964	COMT
P61923	COPZ1
P09669	COX6C
P14406	COX7A2
Q16630	CPSF6
P68400	CSNK2A1
P19784	CSNK2A2
P67870	CSNK2B
P07339	CTSD
P00387	CYB5R3
Q16643	DBN1
P81605	DCD

P39656	DDOST
A6NHG4;P30046	DDTL;DDT
Q96GQ7	DDX27
Q13838	DDX39B
Q7L014	DDX46
O00273	DFFA
Q96N67	DOCK7
Q8IZU8	DSEL
P63167;Q96FJ2	DYNLL1;DYNLL2
P42126	ECI1
Q15075	EEA1
P24534	EEF1B2
Q9BUP0	EFHD1
Q96C19	EFHD2
Q14152	EIF3A
P60228	EIF3E
O75822	EIF3J
Q9UBQ5	EIF3K
P38919	EIF4A3
P23588	EIF4B
Q04637	EIF4G1
P63241	EIF5A
Q14241	ELOA

P50402	EMD
P06733	ENO1
P62495	ETF1
P13804	ETFA
P38117	ETFB
Q01469	FABP5
P22087	FBL
Q02790	FKBP4
Q5D862	FLG2
P21333	FLNA
O75369	FLNB
O75955	FLOT1
Q14254	FLOT2
Q8IY81	FTSJ3
Q96AE4	FUBP1
Q9UN86	G3BP2
Q14697	GANAB
Q9NY12	GAR1
P41250	GARS1
Q8WXI9	GATAD2B
Q92616	GCN1
Q04760	GLO1
Q9HC38	GLOD4

O76003	GLRX3
P08754	GNAI3
P16520;P62873;P62879	GNB3;GNB1;GNB2
Q9BVP2	GNL3
P06744	GPI
P28799	GRN
P15170	GSPT1
P09211	GSTP1
Q9BZE4	GTPBP4
P07305	H1-0
P0C0S8;Q96KK5;Q99878;Q9BTM1	H2AC11;H2AC12;H2AC14;H2AJ
P0C0S5;Q71UI9	H2AZ1;H2AZ2
P06899;Q16778	H2BC11;H2BC21
P58876;Q5QNW6;Q93079;Q99877;Q99879	H2BC5;H2BC18;H2BC9;H2BC15;H2BC14
Q5TEC6	H3-2
P68431;P84243;Q71DI3	H3C1;H3-3A;H3C15
P62805	H4C1
P12081	HARS1
P69905	HBA1
Q7Z4V5	HDGFL2
Q9H583	HEATR1
Q13151	HNRNPA0
P22626	HNRNPA2B1

Q99729	HNRNPAB
Q14103	HNRNPD
P52597	HNRNPF
P31943	HNRNPH1
P31942	HNRNPH3
P61978	HNRNPK
P52272	HNRNPM
P49639	HOXA1
P00492	HPRT1
Q99714	HSD17B10
P07900	HSP90AA1
Q58FF8	HSP90AB2P
P14625	HSP90B1
P34932	HSPA4
P38646	HSPA9
P10809	HSPD1
P50213	IDH3A
P01857	IGHG1
P01859	IGHG2
P01834	IGKC
A0A075B6S2;A0A0A0MRZ7;A2NJV5	IGKV2D-29;IGKV2D-26;IGKV2-29
A0A075B6H7;A0A0C4DH55;P01624	IGKV3-7;IGKV3D-7;IGKV3-15
A0A0A0MRZ8;P04433	IGKV3D-11;IGKV3-11

B9A064	IGLL5
P01700	IGLV1-47
P01714	IGLV3-19
O95373	IPO7
P46940	IQGAP1
O14654	IRS4
Q14573	ITPR3
P28290	ITPRID2
Q92945	KHSRP
P33176	KIF5B
Q5T749	KPRP
P08779	KRT16
P08727	KRT19
P19013	KRT4
P02538	KRT6A
P04259	KRT6B
Q7Z794	KRT77
P05787	KRT8
O15230	LAMA5
P11047	LAMC1
Q9UHB6	LIMA1
Q03252	LMNB2
Q9H9A6	LRRC40

O75367	MACROH2A1
Q9P0M6	MACROH2A2
P61326;Q96A72	MAGOH;MAGOHB
P49006	MARCKSL1
P33993	MCM7
P40925	MDH1
P40926	MDH2
Q6WCQ1	MPRIP
Q9UKD2	MRTO4
P26038	MSN
P13995	MTHFD2
O75570	MTRF1
P35580	MYH10
Q7Z406	MYH14
P35579	MYH9
O14950;P19105	MYL12B;MYL12A
P60660	MYL6
P14649	MYL6B
O43795	MYO1B
O00159	MYO1C
O94832	MYO1D
Q9Y4I1	MYO5A
Q9UM54	MYO6

Q9H0A0	NAT10
Q6ZVX7	NCCRP1
P28331	NDUFS1
P07197	NEFM
Q9BYG3	NIFK
P59045	NLRP11
Q86W28	NLRP8
P15531	NME1
P22392	NME2
Q15233	NONO
O00567	NOP56
Q9Y2X3	NOP58
P06748	NPM1
Q9Y266	NUDC
P04181	OAT
Q9NTK5	OLA1
P07237	P4HB
P22234	PAICS
P22061	PCMT1
P30101	PDIA3
Q15084	PDIA6
O00151	PDLIM1
P30086	PEBP1

Q16875	PFKFB3
Q96HS1	PGAM5
P52209	PGD
P00558	PGK1
P35232	PHB
Q8IWS0	PHF6
Q15149	PLEC
Q9H8W4	PLEKHF2
P13797	PLS3
Q9H307	PNN
Q7Z3K3	POGZ
Q13427	PPIG
P36873	PPP1CC
Q96SB3	PPP1R9B
P30153	PPP2R1A
P30044	PRDX5
P30041	PRDX6
P07477	PRSS1
P35030	PRSS3
P25786	PSMA1
P25788	PSMA3
P25789	PSMA4
P28066	PSMA5

P60900	PSMA6
O14818	PSMA7
P28072	PSMB6
P62191	PSMC1
P35998	PSMC2
Q15008	PSMD6
Q8WXF1	PSPC1
P59190	RAB15
Q9H0U4	RAB1B
P51148	RAB5C
P43487	RANBP1
P98175	RBM10
Q96PK6	RBM14
Q14257	RCN2
P35241	RDX
Q15287	RNPS1
P10155	RO60
Q9HCK4	ROBO2
P35244	RPA3
P27635	RPL10
P62906	RPL10A
P62913	RPL11
P50914	RPL14

P61313	RPL15
P18621	RPL17
Q07020	RPL18
Q02543	RPL18A
P62829	RPL23
P83731	RPL24
P61353	RPL27
P39023	RPL3
P62888	RPL30
P49207	RPL34
P18077	RPL35A
Q9Y3U8	RPL36
P83881	RPL36A
Q969Q0	RPL36AL
P61513	RPL37A
P36578	RPL4
Q02878	RPL6
P18124	RPL7
P62424	RPL7A
P62917	RPL8
P32969	RPL9
P05388	RPLP0
P04844	RPN2

P46783	RPS10
P62280	RPS11
P62263	RPS14
P62249	RPS16
P39019	RPS19
P15880	RPS2
P62854	RPS26
P42677	RPS27
P23396	RPS3
P61247	RPS3A
P62753	RPS6
P62241	RPS8
P46781	RPS9
P08865	RPSA
Q15050	RRS1
O76021	RSL1D1
Q9Y3I0	RTCB
P31151	S100A7
P06702	S100A9
O00422	SAP18
P21912	SDHB
P04279	SEMG1
Q15019	SEPTIN2

Q8NC51	SERBP1
P50454	SERPINH1
Q12874	SF3A3
P23246	SFPQ
P34897	SHMT2
Q6NUK1	SLC25A24
Q92922	SMARCC1
Q9NTJ3	SMC4
Q8TEV9	SMCR8
P62318	SNRPD3
P62304	SNRPE
P62306	SNRPF
A8MWD9;P62308	SNRPGP15;SNRPG
Q9P0W8	SPATA7
Q13813	SPTAN1
Q01082	SPTBN1
Q8N9Q2	SREK1IP1
Q8IYB3	SRRM1
Q9BXP5	SRRT
Q08170	SRSF4
Q16629	SRSF7
Q13242	SRSF9
Q08945	SSRP1

P46977	STT3A
O75683	SURF6
Q16563	SYPL1
P26639	TARS1
P29401	TKT
Q9NYK1	TLR7
P49755	TMED10
Q6UW68	TMEM205
P28289	TMOD1
Q9NYL9	TMOD3
P11388	TOP2A
Q02880	TOP2B
P04637	TP53
P06753	TPM3
Q12931	TRAP1
Q2NL82	TSR1
P49411	TUFM
P22314	UBA1
P0CG47;P0CG48;P62979;P62987	UBB;UBC;RPS27A;UBA52
A0A1B0GUS4;P68036	UBE2L5;UBE2L3
P31930	UQCRC1
O14949	UQCRQ
Q9Y5J1	UTP18

Q99536	VAT1
P55072	VCP
P21796	VDAC1
Q9UN37	VPS4A
P61964	WDR5
P13010	XRCC5
P12956	XRCC6
P54577	YARS1
P67809	YBX1
P62258	YWHAE
P63104	YWHAZ
O75152	ZC3H11A
Q9NP64	ZCCHC17
Q96ME7	ZNF512

Table S5E. Affinity purification mass spectrometry analysis of protein-protein interactions in CE-HDGFL2-myc-flag versus FL-HDGFL2-myc-flag HEK-293 cells

Genes	Log2FoldChange	NegLog10Qvalue
CBX5	1.627003871	5.387216143
CBX1	1.01981707	4.328827157
H2BC5;H2BC18;H2BC9;H2BC15;H2BC14	0.568516921	4.236572006
MACROH2A2	0.764806162	4.236572006
RPS2	0.189143976	4.057991947
H2AZ1;H2AZ2	1.001827122	3.904074344
FCF1	0.484659926	3.887760415
MACROH2A1	0.696968255	3.765356192
CDCA8	0.637665077	3.765356192
EMD	1.046087568	3.753427566
RRS1	0.674314151	3.607281948
YWHAE	0.125466291	3.505270903
AMOT	-1.062550296	3.403145702
GCN1	0.498964097	3.335284708
NEFM	-0.781509596	3.088465811
H3C1;H3-3A;H3C15	0.418040622	3.019662509
RPL10A	0.392059063	2.908268694
H4C1	0.535018469	2.885272619
RPL17	0.549129754	2.869777876
DNTTIP2	1.215609824	2.866920537
XRCC6	0.437320111	2.811736819
EEF1B2	0.555315549	2.811736819
NLRP8	-0.738907022	2.811736819
H2AC11;H2AC12;H2AC14;H2AJ	0.462738495	2.773419684

MRPS5	0.890527006	2.741251883
H2BU1	0.681738796	2.741251883
MRTO4	0.909625976	2.727047372
POGZ	0.76575854	2.697110866
SPTBN1	-0.873949391	2.663862204
HSD17B10	0.746762631	2.663862204
FTSJ3	0.628080264	2.650695464
VCP	0.826960883	2.629896047
SPTAN1	-0.851354712	2.617781715
CHAMP1	0.640547838	2.617781715
EFHD1	-0.809860833	2.598744938
BRIX1	0.527635094	2.596161513
PPP1R9B	-0.831927581	2.596161513
XRCC5	0.405937184	2.556102858
MYO5A	-0.905777837	2.546515008
ACTG1	-0.679286906	2.509750261
H3-2	0.53502827	2.509750261
MYL6B	-0.832521206	2.49428811
UQCRQ	-0.843956718	2.479293678
PRDX6	0.302588599	2.470930167
MYL12B;MYL12A	-0.649939394	2.463996774
RSL1D1	0.586228189	2.450510086
GNL3	0.721118196	2.449465058
FBL	0.511927486	2.423640564
RPS11	0.095680157	2.423640564
ACTC1	-0.656865957	2.423640564
RPS9	0.145134617	2.416368055
DOCK7	-0.665325603	2.403568298
DDX39B	0.389576431	2.393791097
NPM1	0.271044909	2.388850573
EIF3A	0.458817101	2.388850573
CAPZA2	-0.557504699	2.386076188

RPL23	0.137831472	2.328614229
TUBB2B	0.648136412	2.328614229
LIMA1	-0.974018896	2.328614229
UBA1	0.700155693	2.328338504
CALM1;CALM2;CALM3	-0.771613667	2.322293518
TOP2A	0.912143031	2.322293518
MYH10	-0.683753457	2.322293518
RPS27	0.205720603	2.322293518
TMOD3	-0.702501776	2.322293518
MYO6	-0.759909513	2.322293518
DBN1	-0.616619987	2.312326239
XIRP1	0.866223999	2.312067698
ACTN4	-0.694054412	2.307286825
RPSA	0.409036375	2.306998418
MYH9	-0.664268243	2.302151923
UTP18	0.350792545	2.280551287
SEMG1	-4.080126428	2.264165815
RPL3	0.388595331	2.259883033
HSP90B1	0.668701486	2.252111429
MYH14	-0.792463949	2.237504419
TOP2B	1.088146846	2.233627907
HNRNPK	0.184940179	2.222318838
MYL6	-0.625161276	2.211433237
HEATR1	0.386199555	2.186824342
MYO1D	-0.720428772	2.174509619
CDC7	0.41034046	2.159638425
FLNB	-0.588036308	2.159638425
RPL36AL	0.496199764	2.159638425
RPL10	0.187693416	2.156993463
HNRNPD	0.629555823	2.156993463
EFHD2	-0.646814835	2.156993463
CHD1	0.33782592	2.154446562

PDIA6	0.837382854	2.142577216
CHD7	1.899999439	2.137796026
CCT8	0.326560832	2.136089218
MPRIP	-0.659546345	2.12774085
CAPZA1	-0.512189021	2.114660608
GANAB	0.47881106	2.114660608
RAB1B	1.295702671	2.114660608
ACTN1	-0.685568536	2.11179455
H2BC11;H2BC21	0.426797007	2.105567846
TARS1	0.505096184	2.091765067
EIF3E	0.551714297	2.065067219
RPS26	0.225410313	2.040258431
ITPR2	-2.005210168	2.034402956
RSF1	0.704318874	2.034402956
GTPBP4	0.718229229	2.031077889
GNB3;GNB1;GNB2	0.826998458	2.029642569
CENPV	1.335301624	2.011498477
RPL18	0.285246394	1.99936288
SURF6	0.995272911	1.996871692
YWHAZ	0.523123919	1.992679858
ZNF512	0.323992241	1.992679858
RPL7A	0.302376032	1.987960459
MRPS27	0.589343396	1.987960459
RPL4	0.267970909	1.986094209
PPIG	1.272342507	1.981060705
NME2	0.27888679	1.977319704
RPS14	0.353395179	1.977319704
KHSRP	0.471753288	1.977319704
LRRFIP2	-1.531898676	1.977319704
MYO1C	-0.611050532	1.975319149
CLIC1	0.655082856	1.975319149
GNAI3	-0.301508497	1.975319149

UBB;UBC;RPS27A;UBA52	0.536050168	1.960373069
DPF3	0.826861678	1.949007791
TMOD1	-0.504205225	1.935705389
MPHOSPH8	1.074658638	1.921999068
RPL34	0.049974038	1.91727662
RPL36	0.32969024	1.914482734
ATP5ME	-0.304875856	1.878602743
SSRP1	1.646368541	1.857725381
ALDH18A1	0.454941007	1.845777852
NME1	0.462199212	1.837550783
KRT77	-0.407468275	1.83060939
RPS6	0.213046617	1.817209968
EIF5A	0.189278036	1.812101128
L1RE1	1.523690969	1.812101128
IGLV3-19	-1.097757275	1.796143714
DDX27	1.049242281	1.794177612
EIF4B	0.696785131	1.766710015
RDX	0.478463975	1.759409022
CAD	-0.214399305	1.756760411
RPL24	0.129640861	1.752428138
CAAP1	1.498807543	1.738204858
MYO1B	-0.505994221	1.723817498
HNRNPH1	0.162458561	1.721356107
NOP58	0.924426166	1.72042695
APEX1	1.832609092	1.710582369
RPL14	0.199673173	1.710582369
PSMC1	0.59994744	1.706741799
TRAP1	0.609438933	1.706107708
AHNAK	-0.6594889	1.705713327
YARS1	0.183094379	1.704566023
CKMT1A	1.281284875	1.700027626
RPS10	0.389740161	1.699470513

NOP56	0.978708159	1.696387241
ARRB2	1.613694688	1.696387241
RPL6	0.243661136	1.6911544
FLNA	-1.318979244	1.687014153
ZCCHC17	0.214303685	1.685654708
CAPZB	-0.429671055	1.676838275
NIFK	1.177805633	1.674384846
PGK1	3.009691268	1.670577305
SMARCC1	0.571332399	1.670577305
SRRM1	2.707184896	1.663760191
PHF6	1.334867241	1.647396305
ALDOA	0.679801714	1.640708143
LMNB2	-0.711406935	1.639835963
H1-0	1.58706661	1.639503168
RPL30	0.29391943	1.637880909
ZMYM4	0.471249393	1.63411708
SERBP1	-0.102265757	1.633854146
GAR1	1.832337704	1.629443021
PEBP1	2.009553209	1.62785843
HNRNPA0	0.265609821	1.615967218
RPS3A	1.249082601	1.60957784
IGKV3-7;IGKV3D-7;IGKV3-15	-0.726970932	1.608685722
HOXA1	0.155306793	1.602162775
FLG2	-0.364014521	1.597105577
PPP1CC	-0.474685977	1.592337742
IQGAP1	0.88347834	1.584668323
RPL35A	0.20512073	1.580509906
WDR33	-0.911579279	1.574023364
RPL8	0.2871888	1.569496927
KRT6B	-0.383965922	1.567150774
GLO1	0.927963889	1.562078273
HNRNPA2B1	0.314973933	1.530480992

WDR3	0.688821905	1.529234941
SFPQ	-2.414813241	1.517503459
RPL11	0.170954028	1.512401417
NAT10	0.891405825	1.512401417
DHRS2	0.425858251	1.508904274
NSMCE3	-2.264707328	1.502956454
SDHB	0.675651394	1.501239819
PRSS1	0.76204265	1.501225413
HSP90AA1	0.450691064	1.501044261
SDC2	0.141952033	1.498428381
CANX	0.237900152	1.495238699
SRBD1	1.227389452	1.478465437
RBM14	-0.208991469	1.478465437
CCT6A	0.538997008	1.47355392
AARS1	1.041243906	1.471416717
CSNK2B	0.241248551	1.467595312
NONO	-1.710929981	1.458125449
ETFB	-0.007833176	1.451714727
RPL36A	0.12758623	1.451714727
NVL	2.802306859	1.440287272
RPS8	0.279694616	1.43879781
MTHFD2	-2.555869414	1.438556053
PLEC	-0.318538346	1.434297281
KRT8	-0.350759515	1.427090405
RPLP0	0.131418968	1.415228654
IGKV2D-29;IGKV2D-26;IGKV2-29	-0.184425523	1.408074162
PMPCB	-1.607678028	1.38931626
AIFM1	0.701546313	1.383548591
ATIC	0.767679908	1.383548591
COPG1	0.779811862	1.376730567
RPF1	0.716492446	1.376674766
RPL27	0.852214453	1.375698119

YBX1	0.212356793	1.374034232
RTCB	0.349760474	1.365242071
KRT6A	-0.327725767	1.362315572
GTF3C2	0.853906778	1.350247893
SREK1IP1	0.31178353	1.349809713
NOL7	0.43899555	1.342976759
REXO4	0.399964831	1.330885006
PSMA7	0.673799404	1.314324754
LAMC1	0.935349907	1.302476675
TES	0.112909953	1.292585857
HBA1	0.2034357	1.286190766
SPOUT1	1.106521912	1.256247623
MFAP1	-1.269690331	1.251145703
KRT16	-0.393517474	1.249916256
SRSF9	0.170567948	1.249916256
RPL7	0.132079146	1.239084797
IGHG2	0.201561861	1.226052647
CA2	0.329166205	1.220028143
RPL15	0.222329413	1.210878691
STT3A	-0.027690601	1.209833822
SLC39A7	4.243291307	1.209833822
CSNK2A1	0.920876885	1.178909076
ITPRID2	-0.452786221	1.163623671
SHMT2	0.390605256	1.163623671
HNRNPM	0.087416181	1.163287162
TMED10	1.156595116	1.162161864
SMC4	0.763477465	1.162161864
CDK12	2.160157334	1.162161864
TUFM	0.094901178	1.159470386
SIPA1L1	-0.607096133	1.155483876
PINX1	1.253244158	1.152289918
PRSS3	-1.853433722	1.152165344

ATP5PB	0.906784916	1.148324886
HSPA9	0.071386026	1.148324886
EIF3J	-0.172804373	1.147988498
HBS1L	0.198796802	1.144980407
ITPR3	-0.608171259	1.142562743
ATP5F1B	0.080673988	1.130592749
PSMA4	0.302945881	1.125263351
RAB15	0.423306278	1.125179234
TPX2	-0.586745574	1.099710877
HPRT1	0.003125903	1.071994487
RIOX2	0.659494647	1.071994487
LRRC40	0.494584647	1.071994487
KLHL6	0.189899972	1.05816781
ZNF24	0.215971638	1.049597546
CFL1	0.239695234	1.044150004
GSTP1	-0.214020155	1.041280019
PSPC1	-2.140594965	1.041280019
GPI	0.147075482	1.037636423
PNN	-0.695182848	1.030284728
UBE2L5;UBE2L3	-1.197851893	1.029377592
ENO1	0.141782027	1.027085798
PDIA3	0.112372443	1.022184233
EIF4A3	-0.624221329	0.996746971
AATF	-0.63796186	0.996746971
IRS4	-0.111869824	0.996521614
TAF2	-1.46467386	0.991422548
ROBO2	0.392517382	0.989623234
TKT	1.076619742	0.986537963
PSMA5	0.61869486	0.977910742
RRP8	0.5428593	0.975070647
EIF4G1	0.322846143	0.975070647
PHB	0.255100028	0.967554262

SNRPD3	0.090749556	0.955153661
CIR1	2.090711275	0.954058803
EIF2B4	1.032725663	0.952594202
RPS3	0.038502159	0.946509357
PDLIM1	-0.713562831	0.942089304
VANGL1	0.120632368	0.933047808
RO60	-0.860720669	0.931020976
ELOA	0.309485347	0.931020976
CBSL;CBS	0.51505555	0.930229671
PGAM5	0.037358187	0.9108334
IGKC	0.197927122	0.910648193
DAXX	0.060690902	0.910648193
RPN2	0.325656935	0.908204953
G3BP2	-0.183895489	0.904516574
PSMB6	0.132408295	0.904056704
HNRNPH3	0.097158249	0.904056704
FLOT1	-0.332742601	0.904032351
SNRPF	-0.409438856	0.899927935
MORF4L2	-0.395119729	0.899927935
GATAD2B	-0.14883363	0.894776807
SRSF7	0.175940015	0.890812808
IPO7	-1.223414534	0.890549047
AK2	0.17498807	0.890549047
BAP18	-2.008607303	0.886032431
HNRNPF	0.165404606	0.885430246
CCDC124	-0.798125516	0.882289083
MRPS25	0.239197247	0.877439154
PLEKHF2	0.315760244	0.875056568
OAT	-0.097236988	0.868182497
SMARCC2	-0.963814955	0.868182497
RCL1	-1.88615309	0.855257322
IGLL5	0.080911735	0.853630526

VDAC1	0.100789137	0.852383619
COX7A2	0.032980694	0.848084012
SYPL1	0.7303889	0.847053254
PCMT1	0.305428023	0.844368397
SCAF1	1.451580734	0.844368397
WDR5	-0.924382907	0.84240186
RPL22L1	0.669127938	0.83401741
MDH1	0.491999758	0.823700567
ING5	-0.40416516	0.818960844
DDX46	-0.717731394	0.814755488
THOC6	0.201072006	0.805359237
CYB5R3	-0.146345114	0.804389086
RPS19	0.106378169	0.783027332
NUDC	-0.034543487	0.775555771
SNRPGP15;SNRPG	0.115577418	0.769845456
DYNLL1;DYNLL2	-0.68861499	0.763485071
SLC25A24	0.222042378	0.762392284
UTP20	-2.211597939	0.758591589
POLR2C	-0.905158422	0.756444177
PAF1	0.923792599	0.754805495
LAMA5	-0.22886406	0.752620213
SNRPE	0.3558658	0.752606037
ACAT1	-0.093863232	0.749457493
IGHG1	0.182536521	0.744392238
ZC3H11A	0.620372	0.737187713
PSMA1	-0.182537854	0.735798897
IGF2BP3	-0.402733699	0.734987888
ANXA2	0.016209401	0.734987888
MAGOH;MAGOHB	-0.356191201	0.726841891
S100A7	-0.23956804	0.715000672
MOV10	-0.417403688	0.714572006
KIF2A	1.349832153	0.712323446

SNIP1	1.604535276	0.707657796
RPL9	0.119067602	0.704686871
MDH2	0.368310825	0.690969095
GTF3C3	-0.012495708	0.688672578
H2AC21	-0.198138273	0.688226852
ATP5F1C	-0.057108682	0.687253913
UTP11	0.970081313	0.683271715
ETFA	0.200474518	0.681585419
RCN2	0.103443025	0.678578322
HSPD1	-0.094455853	0.678250674
RNPS1	-0.286987613	0.677083567
RPS16	-0.09530912	0.675793629
COPZ1	-0.471737658	0.6729335
SRRT	0.19238193	0.668080288
ACIN1	-0.070366574	0.654273176
PHF2	2.862239734	0.651958206
POLR2F	-0.554219386	0.651761178
PIP4K2B	0.069937862	0.651761178
CTSD	-0.093284317	0.648189874
TEX10	-0.563599122	0.633524217
FLOT2	-0.187234494	0.630799499
BZW2	0.417521233	0.62245703
DCD	-0.015119622	0.619651215
WDR6	-0.119946296	0.619522706
KRT84	0.119691389	0.619522706
IGLV1-47	0.015854686	0.609291124
MCM7	-0.08097218	0.609291124
UQCRC1	0.314887074	0.609179066
WDR74	-0.107017245	0.607584015
ZNF202	0.471847659	0.601457987
KIF5B	0.373397209	0.595325702
AQR	-0.047527444	0.593155198

HNRNPAB	0.32896284	0.593137708
FABP5	0.140367404	0.586143428
HDGFL2	0.019362292	0.581331964
SERPINH1	-0.369717159	0.573384257
VN1R5	0.071238925	0.569922533
RPL37A	-0.444062383	0.561051269
MSN	-0.940217908	0.554583613
CCDC186	-0.962614706	0.554583613
CALML5	0.169256806	0.553369566
HNRNPLL	0.096266136	0.552960581
AASDHPPT	-0.141647558	0.552960581
S100A9	0.025878002	0.55274404
TSR1	-0.034214238	0.545342096
PPP2R1A	0.047115211	0.542636591
API5	-0.478609527	0.539101975
ALDH9A1	0.289990501	0.53903962
SAP18	0.203637442	0.537931995
CCT5	-0.081100641	0.524078644
IGKV3D-11;IGKV3-11	-0.217735312	0.522563769
SH3KBP1	0.441572878	0.522563769
GTF3C1	0.222766302	0.522204714
TPM3	0.139427726	0.519509899
PSMC2	0.405934989	0.512463074
PAICS	-0.074716054	0.511144985
ATP5MF	-0.01581497	0.510023958
RPL18A	-0.152618537	0.507999165
KRT4	-0.457499708	0.507023149
NDUFS1	-0.261973839	0.504826633
RAB13	0.334194186	0.498770278
KPRP	0.050534349	0.494412351
ARGLU1	0.150105548	0.492568149
MARCKSL1	1.049335274	0.486064827

NCCRP1	-0.17769766	0.484321763
RANBP1	0.595615327	0.479929985
SNRNP40	0.203289112	0.477264282
EEA1	0.330916468	0.473936206
XPC	0.152496134	0.472187108
TMEM132D	0.027925481	0.469472479
PSMA6	-0.131916799	0.468803118
RAB5C	-0.581364216	0.468275374
TP53	0.02463237	0.468077944
VPS4A	0.185317088	0.466329675
KRT19	0.05582646	0.46550542
CSNK2A2	-0.020107702	0.46550542
MTRF1	-0.640016423	0.46252065
PGD	0.023510129	0.460848347
SRSF4	0.136583884	0.460848347
SREK1	-1.634698881	0.460057886
HSPA4	0.398015708	0.458166979
POLR1B	-0.621414161	0.457695997
TRAF7	1.312789221	0.452950316

Table S5F. Lookup table of cryptic peptide amino acid sequences and corresponding symbols

Symbol	peptide sequence	sample
ADGRB1_α	EILQLIAMGKPRPQP(R)	CSF
ADGRB1_β	AGQPSPHPLG(R)	CSF
AGRN_α	MLTSSDVCFSIC(K)	CSF
AGRN_β	MLTSSDVCFSICKEA(R)	CSF

CAMK2B_α	VPRNLLPVHFWGFEFFP(R)	CSF
CAMK2B_β	MVSCRAGSCLRAGVPGAACSSL(R)	i3N, CSF
CAMK2B_γ	AGSCLRAGVPGAACSSLRVTE(R)	i3N, CSF
CAMK2B_δ	VTERSAGSAETSPTG(R)	CSF
CAMK2B_ε	MSLHSSPGDRV(R)	CSF
CAMK2B_ζ	VTERSAGSAETSPTGRVP(R)	CSF
CAMK2B_η	AEIMSLHSSPGD(R)	CSF
CAMK2B_Θ	AGVPGAACSSL(R)	CSF
CAMK2B_ι	SAGSAETSPTG(R)	CSF
CAMK2B_κ	NLLPVHFWGFEFFP(R)	CSF
CAMK2B_λ	TNYFEKPLLLVCIA(R)	CSF
CAMK2B_μ	AGSCLRAGVPGAACSSL(R)	i3N
CDH4_α	LLQALELLAEPS(R)	CSF
CDH4_β	EPEALATGAAHAW(R)	CSF
CDO1_α	GLQFVVGGGSGGGWLWYT(R)	CSF
DNM1_α	APPGVPRPAPPV(R)	i3N, CSF
DNM1_β	VNCHVDFVLSF(R)	CSF
EPB41L4A_α	EEITSDIESPY(K)	CSF
HDGFL2_α	GHSGMLASEGREAVLT(R)	CSF
HDGFL2_β	EPTIWFG(K)	CSF
HDGFL2_γ	GHSGMLASEG(R)	CSF
IGLON5_α	SSSRPSSLSAWCQLH(R)	CSF
IGLON5_β	MPSPHSLALVQPAGHGLQ(R)	CSF
IGLON5_γ	HALANLSTQCACVDVCVC(K)	CSF
ISLR2_α	ECVYACA(R)	CSF
ISLR2_β	HNTCVYLAWAIFPALP(R)	CSF
ITGA7_α	SSQSSSFPTNYH(R)	CSF
KALRN_α	MDKPPSVSARLCSGKPEGTGS(R)VS	CSF
KALRN_β	MDKPPSVSARLCSGKPEGTGS(R)	CSF

KALRN_γ	MDKPPSVSA(R)	CSF
KALRN_δ	LCSGKPEGTGS(R)	CSF
KCNQ2_α	LLGSVVYAHSKITLTTIGYGD(K)	CSF
LRFN1_α	AAAGGIPAG(R)	CSF
MADD_α	FMHNQDMLLLGGFAL(R)	CSF
MYO18A_α	EEDKTLPKPGSPG(K)	i3N, CSF
MYO18A_β	TLPKPGSPGKEEGAA(K)	CSF
MYO18A_γ	EPSDVKEED(K)	CSF
MYO18A_δ	EEGAAKTEEQIAAEEAWNETE(K)	i3N, CSF
MYO18A_ε	TLPKPGSPG(K)	i3N, CSF
MYO1C_α	EVATQF(K)	CSF
NECAB2_α	LLCAGHSA(R)	CSF
PTPRN2_α	ATEVQHNSL(R)	CSF
PTPRN2_β	AFLWLTT(K)	CSF
PTPRN2_γ	AFLWVSLTT(K)	CSF
PTPRZ1_δ	QFQGLTLSP(R)	CSF
PXDN_α	WAGETLE(K)	CSF
RSF1_α	GAGGGSSPKLNHSNEPQH(K)	CSF
RSF1_β	VLQAPPPDVGNGEGSRGG(R)	i3N, CSF
RSF1_γ	VLQAPPPDVGNGEGS(R)	i3N, CSF
RSF1_δ	LLLLTHYCSLSP(R)	i3N, CSF
RSF1_ε	KPCSSYGFEGY(R)	CSF
RSF1_ζ	LNHSNEPQH(K)	CSF
SEPTIN11_α	DSDYSDSSSED(R)	CSF
SLC24A3_α	EEWMDGWIANFH(R)	CSF
SYN3_α	FPLVEQTFFPNHKPMNLGL(K)	CSF
SYNE1_α	LANVFEQPVAEQIE(R)	CSF
SYT7_α	AINFPGA(R)LQSAA	i3N, CSF
SYT7_β	AINFPGA(R)	i3N, CSF
SYT7_γ	AINFPGARLQSAAC(R)	i3N

SYT7_δ	INFPGA(R)	i3N
TRRAP_α	YLQFVAALTDVNTQ(K)	CSF
UNC13A_α	ELLSPGTSLLN(K)	CSF
ZNF423_α	ETTDGDDDPQLSWVASSPSS(K)	CSF
ZNF423_β	CPGVLGSAWDS(R)	CSF

Table S5G. PRM intensity values of cryptic peptides in TDP-43 KD and control iPSC-derived neurons

Peptide	Replicate	Heavy peptide intensity	Light peptide intensity
AGSCLRAGVPGAACSSL(R)	CT1	7.23E+06	1.77E+03
AGSCLRAGVPGAACSSL(R)	CT2	1.17E+07	3.47E+04
AGSCLRAGVPGAACSSL(R)	CT3	1.58E+07	0.00E+00
AGSCLRAGVPGAACSSL(R)	CT4	1.38E+07	0.00E+00
AGSCLRAGVPGAACSSL(R)	KD1	3.28E+07	2.65E+06
AGSCLRAGVPGAACSSL(R)	KD2	4.77E+07	3.38E+06
AGSCLRAGVPGAACSSL(R)	KD3	4.92E+07	3.59E+06
AGSCLRAGVPGAACSSL(R)	KD4	6.17E+07	3.87E+06
MVSCRAGSCLRAGVPGAACSSL(R)	CT1	2.94E+04	0.00E+00
MVSCRAGSCLRAGVPGAACSSL(R)	CT2	2.99E+04	0.00E+00
MVSCRAGSCLRAGVPGAACSSL(R)	CT3	2.67E+04	0.00E+00
MVSCRAGSCLRAGVPGAACSSL(R)	CT4	3.90E+04	0.00E+00
MVSCRAGSCLRAGVPGAACSSL(R)	KD1	7.29E+04	0.00E+00
MVSCRAGSCLRAGVPGAACSSL(R)	KD2	3.11E+04	0.00E+00
MVSCRAGSCLRAGVPGAACSSL(R)	KD3	2.09E+05	0.00E+00
MVSCRAGSCLRAGVPGAACSSL(R)	KD4	2.60E+04	2.04E+06
AGSCLRAGVPGAACSSLRVTE(R)	KD4	0.00E+00	0.00E+00
AGSCLRAGVPGAACSSLRVTE(R)	CT1	0.00E+00	0.00E+00
AGSCLRAGVPGAACSSLRVTE(R)	CT2	0.00E+00	0.00E+00
AGSCLRAGVPGAACSSLRVTE(R)	CT3	0.00E+00	0.00E+00
AGSCLRAGVPGAACSSLRVTE(R)	CT4	0.00E+00	0.00E+00
AGSCLRAGVPGAACSSLRVTE(R)	KD1	3.81E+08	1.55E+05
AGSCLRAGVPGAACSSLRVTE(R)	KD2	4.56E+08	2.69E+05
AGSCLRAGVPGAACSSLRVTE(R)	KD3	1.04E+08	4.98E+04
AGSCLRAGVPGAACSSLRVTE(R)	KD4	1.14E+08	4.15E+04
APPGVPRPAPPV(R)	CT1	0.00E+00	0.00E+00
APPGVPRPAPPV(R)	CT2	0.00E+00	0.00E+00

APPGVPRPAPPV(R)	CT3	0.00E+00	0.00E+00
APPGVPRPAPPV(R)	CT4	0.00E+00	0.00E+00
APPGVPRPAPPV(R)	KD1	2.84E+05	0.00E+00
APPGVPRPAPPV(R)	KD2	2.71E+05	0.00E+00
APPGVPRPAPPV(R)	KD3	1.95E+05	0.00E+00
APPGVPRPAPPV(R)	KD4	1.92E+05	0.00E+00
TLPKPGSPGK	CT1	3.34E+07	0.00E+00
TLPKPGSPGK	CT2	2.89E+07	0.00E+00
TLPKPGSPGK	CT3	2.76E+07	0.00E+00
TLPKPGSPGK	CT4	2.99E+07	5.93E+03
TLPKPGSPGK	KD1	5.29E+07	1.98E+06
TLPKPGSPGK	KD2	5.69E+07	2.27E+06
TLPKPGSPGK	KD3	5.69E+07	2.35E+06
TLPKPGSPGK	KD4	7.05E+07	2.89E+06
EEGAAKTEEQIAAEEAWNETE(K)	CT1	0.00E+00	0.00E+00
EEGAAKTEEQIAAEEAWNETE(K)	CT2	1.58E+04	0.00E+00
EEGAAKTEEQIAAEEAWNETE(K)	CT3	0.00E+00	0.00E+00
EEGAAKTEEQIAAEEAWNETE(K)	CT4	2.67E+04	0.00E+00
EEGAAKTEEQIAAEEAWNETE(K)	KD1	2.27E+06	0.00E+00
EEGAAKTEEQIAAEEAWNETE(K)	KD2	2.53E+06	0.00E+00
EEGAAKTEEQIAAEEAWNETE(K)	KD3	1.49E+06	0.00E+00
EEGAAKTEEQIAAEEAWNETE(K)	KD4	2.55E+06	5.42E+04
EEDKTLPKPGSPG(K)	CT1	1.57E+05	0.00E+00
EEDKTLPKPGSPG(K)	CT2	4.87E+06	0.00E+00

EEDKTLPKPGSPG(K)	CT3	1.15E+05	0.00E+00
EEDKTLPKPGSPG(K)	CT4	0.00E+00	0.00E+00
EEDKTLPKPGSPG(K)	KD1	1.71E+08	4.89E+06
EEDKTLPKPGSPG(K)	KD2	2.49E+08	6.30E+06
EEDKTLPKPGSPG(K)	KD3	2.83E+08	7.20E+06
EEDKTLPKPGSPG(K)	KD4	3.02E+08	7.75E+06
VLQAPPPDVGNGEGS(R)	CT1	9.60E+07	0.00E+00
VLQAPPPDVGNGEGS(R)	CT2	1.12E+08	0.00E+00
VLQAPPPDVGNGEGS(R)	CT3	1.02E+08	0.00E+00
VLQAPPPDVGNGEGS(R)	CT4	1.13E+08	0.00E+00
VLQAPPPDVGNGEGS(R)	KD1	4.64E+08	1.01E+08
VLQAPPPDVGNGEGS(R)	KD2	5.32E+08	1.22E+08
VLQAPPPDVGNGEGS(R)	KD3	3.17E+08	7.66E+07
VLQAPPPDVGNGEGS(R)	KD4	3.12E+08	7.24E+07
LLLLTHYCSLSP(R)	CT1	2.28E+08	0.00E+00
LLLLTHYCSLSP(R)	CT2	3.29E+08	0.00E+00
LLLLTHYCSLSP(R)	CT3	2.50E+08	0.00E+00
LLLLTHYCSLSP(R)	CT4	2.84E+08	0.00E+00
LLLLTHYCSLSP(R)	KD1	1.11E+09	1.05E+05
LLLLTHYCSLSP(R)	KD2	1.29E+09	3.88E+04
LLLLTHYCSLSP(R)	KD3	3.67E+08	6.91E+04
LLLLTHYCSLSP(R)	KD4	4.09E+08	3.36E+04
VLQAPPPDVGNGEGSRGG(R)	CT1	1.67E+07	0.00E+00
VLQAPPPDVGNGEGSRGG(R)	CT2	1.57E+07	0.00E+00
VLQAPPPDVGNGEGSRGG(R)	CT3	1.52E+07	0.00E+00
VLQAPPPDVGNGEGSRGG(R)	CT4	1.26E+07	0.00E+00
VLQAPPPDVGNGEGSRGG(R)	KD1	2.43E+07	7.12E+04
VLQAPPPDVGNGEGSRGG(R)	KD2	2.43E+07	5.99E+04
VLQAPPPDVGNGEGSRGG(R)	KD3	1.60E+07	0.00E+00
VLQAPPPDVGNGEGSRGG(R)	KD4	1.57E+07	4.03E+04
AINFPGA(R)LQSAA	CT1	1.36E+08	2.14E+05
AINFPGA(R)LQSAA	CT2	1.36E+08	1.65E+05

AINFPGA(R)LQSAA	CT3	1.31E+08	3.65E+05
AINFPGA(R)LQSAA	CT4	1.36E+08	5.23E+05
AINFPGA(R)LQSAA	KD1	7.43E+08	9.10E+07
AINFPGA(R)LQSAA	KD2	8.30E+08	1.06E+08
AINFPGA(R)LQSAA	KD3	4.20E+08	5.43E+07
AINFPGA(R)LQSAA	KD4	4.07E+08	5.49E+07
INFPGA(R)	CT1	8.06E+08	0.00E+00
INFPGA(R)	CT2	7.85E+08	3.20E+04
INFPGA(R)	CT3	7.01E+08	0.00E+00
INFPGA(R)	CT4	5.22E+08	0.00E+00
INFPGA(R)	KD1	1.52E+09	3.54E+04
INFPGA(R)	KD2	1.60E+09	8.24E+04
INFPGA(R)	KD3	8.21E+08	8.00E+04
INFPGA(R)	KD4	8.64E+08	4.13E+04
AINFPGARLQSAAC(R)	CT1	2.03E+06	0.00E+00
AINFPGARLQSAAC(R)	CT2	1.60E+06	0.00E+00
AINFPGARLQSAAC(R)	CT3	1.61E+06	0.00E+00
AINFPGARLQSAAC(R)	CT4	1.56E+06	0.00E+00
AINFPGARLQSAAC(R)	KD1	3.41E+06	4.26E+04
AINFPGARLQSAAC(R)	KD2	2.73E+06	5.41E+04
AINFPGARLQSAAC(R)	KD3	1.86E+06	5.39E+04
AINFPGARLQSAAC(R)	KD4	2.05E+06	0.00E+00

Table S6A. Trait file for ALS CSF (TMT-MS) samples

CRIALS_ID	C9orf72 genotype	TMT batch channel	gender	ethnic category	race	age at sample collection
791013	C9+	b1.127N	Female	Non-Hispanic or Latino	Caucasian	56.08
844007	C9-	b1.127C	Male	Non-Hispanic or Latino	Asian	49.83
711022	C9-	b1.128N	Female	Non-Hispanic or Latino	Caucasian	67.34
701021	C9-	b1.128C	Male	Non-Hispanic or Latino	Caucasian	57.11
715122	C9+	b1.129N	Male	Non Hispanic/Latino	Caucasian	56.73
718017	C9+	b1.129C	Male	Non-Hispanic or Latino	Caucasian	49.91
701019	C9+	b1.130N	Male	Non-Hispanic or Latino	Caucasian	54.81
791009	C9+	b1.130C	Male	Non-Hispanic or Latino	Caucasian	65.09
844002	C9+	b2.127N	Male	Non-Hispanic or Latino	Caucasian	62.93
701027	C9-	b2.127C	Female	Hispanic/Latino	Hispanic/Latino	39.04
844006	C9+	b2.128N	Male	Non-Hispanic or Latino	Caucasian	60.09
715189	C9+	b2.128C	Female	Non Hispanic/Latino	Caucasian	37.85
783010	C9+	b2.129N	Female	Non-Hispanic or Latino	Caucasian	54.42
701026	C9-	b2.129C	Male	Non-Hispanic or Latino	Caucasian	55.39
170053	C9-	b2.130N	Male	Non Hispanic/Latino	Caucasian	47.25
701022	C9-	b2.130C	Male	Non-Hispanic or Latino	Caucasian	48.52
844003	C9+	b3.127N	Male	Non-Hispanic or Latino	Caucasian	57.42
701017	C9+	b3.127C	Male	Non-Hispanic or Latino	Caucasian	50.34

701030	C9-	b3.128N	Male	Non-Hispanic or Latino	Caucasian	25.94
701024	C9+	b3.128C	Male	Non-Hispanic or Latino	Caucasian	56.7
170066	C9-	b3.129N	Male	Non Hispanic/Latino	Caucasian	47.25
701025	C9-	b3.129C	Male	Non-Hispanic or Latino	Caucasian	49.08
711010	C9-	b3.130N	Male	Non-Hispanic or Latino	Caucasian	62.77
718020	C9-	b3.130C	Female	Non-Hispanic or Latino	Caucasian	51.41

Table S6B. Trait file for ALS CSF (2D-LC-MS/MS) samples

sampleID	gender	race	age at sample	diagnosis	C9orf72
713420	Female	Caucasian	51	ALS	Negative
714711	Female	Caucasian	68	ALS	Negative
713354	Male	Caucasian	56	ALS	Negative
714399	Male	Caucasian	72	ALS	Negative
712205	Female	Caucasian	50	ALS	Positive
711170	Male	Caucasian	40	ALS	Negative
883101	Female	Caucasian	43	ALS	Negative
712016	Male	Caucasian	55	ALS	Negative
712219	Female	Caucasian	61	ALS	Negative
712228	Female	African- American	54	ALS	Negative
712292	Female	Caucasian	52	ALS	Negative
712508	Male	Caucasian	64	ALS	Negative
712522	Female	African-American	58	ALS	Negative
715045	Male	African-American	58	ALS	Not tested
160001	Male	Caucasian	37	ALS	Negative
715122	Male	Caucasian	56	ALS	Positive
715107	Female	Caucasian	49	ALS	Negative
200069	Male	Caucasian	70	ALS	Positive
200144	Male	Caucasian	74	ALS	Negative
200140	Male	Caucasian	63	ALS	Positive
713160	Male	Caucasian	57	ALS	Negative
712549	Male	Caucasian	77	ALS	Negative
713245	Male	Caucasian	50	ALS	Negative
713380	Male	Caucasian	39	ALS	Negative
51443900	Male	Caucasian	52	ALS	Not tested
51510020	Male	Caucasian	40	ALS	Not tested
51112906	Male	Caucasian	55	ALS	Not tested
712025	Male	Caucasian	62	ALS	Negative

Table S6C. Ranked protein intensities for ALS CSF (TMT-MS) samples

Protein	Rank	Log10_med_intensity
MADD	56	10.3
TRRAP	106	9.9825
PTPRZ1	114	9.924
HYOU1	338	9.335
DNM1	370	9.28
RNASET2	428	9.17333333
SYNE1	433	9.15333333
ADGRB1	443	9.14
PTPRN2	453	9.13
IGSF21	491	9.08
SEMA6D	552	9.02
ADGRL1	599	8.97
CDH4	627	8.93
LINGO1	711	8.83
LRP8	845	8.684
MACF1	846	8.68333333
CELSR3	856	8.67
ATP6V1B2	881	8.65
PTPRT	972	8.56833333
KIF21A	1028	8.515
IGLON5	1051	8.5
NECAB2	1054	8.5
CAMK2B	1242	8.37
PXDN	1318	8.32
ITGA7	1450	8.22
NTRK3	1455	8.22

SEMA3D	1459	8.22
AGRN	1463	8.215
CHID1	1508	8.18
INSR	1574	8.12
PKD1	1713	8
CSGALNACT1	1733	7.97333333
SEPTIN11	1761	7.95
ISLR2	1773	7.94
CBLN2	1891	7.83
SYT7	1975	7.76
PFKP	2050	7.69
PTPRD	2092	7.66666667
CYFIP2	2108	7.645
AK3	2115	7.63
ACTR1A	2168	7.58
ELAVL3	2238	7.52
DLGAP3	2343	7.41
RAP1GAP	2493	7.248
BCL2L13	2572	7.15666667
STMN2	2673	7.03
SYN3	3019	6.365

Table S6D. Ranked protein intensities for ALS CSF (2D-LC-MS/MS) samples

Protein	Rank	Log10_med_intensity
PTPRZ1	126	3.25219746
RNASET2	180	2.92762696
HYOU1	419	2.10890313
CDH4	449	2.03402652
ARHGAP32	465	2.00625205
PTPRN2	471	1.99409709
SEMA6D	505	1.89569873
CAMK2B	610	1.68574174
AGRN	670	1.58035466
SIPA1L3	706	1.50242712
LINGO1	732	1.45024911
IGLON5	773	1.34242268
PTPRD	787	1.28555731

Table S6E. Ranked protein intensities from a published ALS CSF dataset *(Higginbotham et al, Sci Adv, 2020)*

Protein	Rank	Log10_sum_intensity
PTPRZ1	109	9.09360297
RNASET2	235	8.45582797
PTPRN2	265	8.35757124
ADGRL1	370	8.0915936
HYOU1	375	8.07566523
SEMA6D	385	8.05405071
LINGO1	417	7.97696682
CDH4	424	7.95735765
IGLON5	459	7.87662667
IGSF21	491	7.82091444
CAMK2B	733	7.39872256
NTRK3	739	7.39416246
CHID1	752	7.37383831
PTPRT	753	7.37354232
ISLR2	801	7.30944513
AGRN	819	7.29575583
CBLN2	868	7.23180589
LRP8	1096	6.87998879
DNM1	1199	6.75000214
ITGA7	1297	6.63003103
PTPRD	1329	6.58113436
ADGRB1	1540	6.25732332
PXDN	1746	5.89114982
SEMA3D	1768	5.83507515
AARS1	1932	5.55888849

CSGALNACT1	1965	5.50369537
PKD1	2034	5.36180336
LRFN1	2072	5.27116758
NECAB2	2134	5.02909957

Table S6F. Parent proteins of iPSC neuron-predicted cryptic exons are present in ALS CSF

ALS_CSF_TMT_MS	ALS_CSF_2D_LC_MSMS	ALS_CSF_Higginbotham_etal
MADD	PTPRZ1	PTPRZ1
TRRAP	RNASET2	RNASET2
PTPRZ1	HYOU1	PTPRN2
HYOU1	CDH4	ADGRL1
DNM1	ARHGAP32	HYOU1
RNASET2	PTPRN2	SEMA6D
SYNE1	SEMA6D	LINGO1
ADGRB1	CAMK2B	CDH4
PTPRN2	AGRN	IGLON5
IGSF21	SIPA1L3	IGSF21
SEMA6D	LINGO1	CAMK2B
ADGRL1	IGLON5	NTRK3
CDH4	PTPRD	CHID1
LINGO1		PTPRT
LRP8		ISLR2
MACF1		AGRN
CELSR3		CBLN2
ATP6V1B2		LRP8
PTPRT		DNM1
KIF21A		ITGA7
IGLON5		PTPRD
NECAB2		ADGRB1
CAMK2B		PXDN
PXDN		SEMA3D
ITGA7		AARS1
NTRK3		CSGALNACT1
SEMA3D		PKD1

AGRN	LRFN1
CHID1	NECAB2
INSR	
PKD1	
CSGALNACT1	
SEPTIN11	
ISLR2	
CBLN2	
SYT7	
PFKP	
PTPRD	
CYFIP2	
AK3	
ACTR1A	
ELAVL3	
DLGAP3	
RAP1GAP	
BCL2L13	
STMN2	
SYN3	
DLGAP3	
RAP1GAP	
BCL2L13	
STMN2	
SYN3	

Table S6G. Trait file for ALS/FTD CSF (DIA) samples

CSF ID	Symptoms at collection	Age at collection (yrs)	Sex	ALS gene status	Time from symptom onset to collection (yrs)	Time from symptom onset to death (yrs)
1	ALS	70	F	C9orf72	1.3	NA
2	ALS	78	M	C9orf72	1.51	NA
3	ALS	57	F	C9orf72	1.37	NA
4	ALS	59	M	C9orf72	3.17	NA
5	ALS	64	M	C9orf72	2.01	2.95
6	ALS	65	F	C9orf72	2.48	4.74
7	ALS and mild cognitive impairment	67	M	C9orf72	5.54	6.41
8	ALS	61	M	C9orf72	3.76	3.94
9	ALS	65	M	C9orf72	5.29	NA
10	ALS	57	M	C9orf72	1.02	1.83
11	ALS	67	M	C9orf72	2.45	6.22
12	FTD/ALS	77	F	C9orf72	1.1	3.92
13	ALS	53	F	C9orf72	4.3	NA
14	ALS	56	F	C9orf72	1.82	NA
15	ALS	50	M	C9orf72	1.08	1.77

Table S6H. Heatmap intensity values for cryptic peptides detected in ALS/FTD CSF

Peptide symbol	Peptide sequence	CSF #	Intensity
HDGFL2_Y	GHSGMLASEG(R)	1	0
HDGFL2_Y	GHSGMLASEG(R)	2	0
HDGFL2_Y	GHSGMLASEG(R)	3	8869106
HDGFL2_Y	GHSGMLASEG(R)	4	31375.3848
HDGFL2_Y	GHSGMLASEG(R)	5	14883899
HDGFL2_Y	GHSGMLASEG(R)	6	2549979
HDGFL2_Y	GHSGMLASEG(R)	7	90810616
HDGFL2_Y	GHSGMLASEG(R)	8	73432512
HDGFL2_Y	GHSGMLASEG(R)	9	16021315
HDGFL2_Y	GHSGMLASEG(R)	10	0
HDGFL2_Y	GHSGMLASEG(R)	11	18943290
HDGFL2_Y	GHSGMLASEG(R)	12	81758.125
HDGFL2_Y	GHSGMLASEG(R)	13	13645602
HDGFL2_Y	GHSGMLASEG(R)	14	292269.344
HDGFL2_Y	GHSGMLASEG(R)	15	67297.2344
KALRN_Y	MDKPPSVSA(R)	1	172606.75
KALRN_Y	MDKPPSVSA(R)	2	21914.8242
KALRN_Y	MDKPPSVSA(R)	3	651072.688
KALRN_Y	MDKPPSVSA(R)	4	0
KALRN_Y	MDKPPSVSA(R)	5	314043.969
KALRN_Y	MDKPPSVSA(R)	6	39151.9883
KALRN_Y	MDKPPSVSA(R)	7	3563059.25
KALRN_Y	MDKPPSVSA(R)	8	1551809.13
KALRN_Y	MDKPPSVSA(R)	9	0
KALRN_Y	MDKPPSVSA(R)	10	0
KALRN_Y	MDKPPSVSA(R)	11	51000.6289
KALRN_Y	MDKPPSVSA(R)	12	0
KALRN_Y	MDKPPSVSA(R)	13	47180.0234

KALRN_γ	MDKPPSVSA(R)	14	30248.1641
KALRN_γ	MDKPPSVSA(R)	15	0
KCNQ2_α	LLGSVVYAHSKITLTTIGYGD(K)	1	0
KCNQ2_α	LLGSVVYAHSKITLTTIGYGD(K)	2	0
KCNQ2_α	LLGSVVYAHSKITLTTIGYGD(K)	3	0
KCNQ2_α	LLGSVVYAHSKITLTTIGYGD(K)	4	4139415.75
KCNQ2_α	LLGSVVYAHSKITLTTIGYGD(K)	5	0
KCNQ2_α	LLGSVVYAHSKITLTTIGYGD(K)	6	1240545.75
KCNQ2_α	LLGSVVYAHSKITLTTIGYGD(K)	7	28349.5391
KCNQ2_α	LLGSVVYAHSKITLTTIGYGD(K)	8	0
KCNQ2_α	LLGSVVYAHSKITLTTIGYGD(K)	9	0
KCNQ2_α	LLGSVVYAHSKITLTTIGYGD(K)	10	3257245.75
KCNQ2_α	LLGSVVYAHSKITLTTIGYGD(K)	11	0
KCNQ2_α	LLGSVVYAHSKITLTTIGYGD(K)	12	2932168.5
KCNQ2_α	LLGSVVYAHSKITLTTIGYGD(K)	13	2170360
KCNQ2_α	LLGSVVYAHSKITLTTIGYGD(K)	14	2448221.75
KCNQ2_α	LLGSVVYAHSKITLTTIGYGD(K)	15	3874099.25
MYO18A_ε	TLPKPGSPG(K)	1	521736.156
MYO18A_ε	TLPKPGSPG(K)	2	1030383.75
MYO18A_ε	TLPKPGSPG(K)	3	69741.3906
MYO18A_ε	TLPKPGSPG(K)	4	1838934.63
MYO18A_ε	TLPKPGSPG(K)	5	84122.1328
MYO18A_ε	TLPKPGSPG(K)	6	1777008.88
MYO18A_ε	TLPKPGSPG(K)	7	161050.969
MYO18A_ε	TLPKPGSPG(K)	8	543539.875
MYO18A_ε	TLPKPGSPG(K)	9	775771.313
MYO18A_ε	TLPKPGSPG(K)	10	1304095.38
MYO18A_ε	TLPKPGSPG(K)	11	275538.375
MYO18A_ε	TLPKPGSPG(K)	12	1735961.13
MYO18A_ε	TLPKPGSPG(K)	13	1984925.25

MYO18A_ε	TLPKPGSPG(K)	14	446540.719
MYO18A_ε	TLPKPGSPG(K)	15	2008996.75
MYO18A_α	EEDKTLPKPGSPG(K)	1	926971.75
MYO18A_α	EEDKTLPKPGSPG(K)	2	0
MYO18A_α	EEDKTLPKPGSPG(K)	3	0
MYO18A_α	EEDKTLPKPGSPG(K)	4	0
MYO18A_α	EEDKTLPKPGSPG(K)	5	0
MYO18A_α	EEDKTLPKPGSPG(K)	6	0
MYO18A_α	EEDKTLPKPGSPG(K)	7	0
MYO18A_α	EEDKTLPKPGSPG(K)	8	0
MYO18A_α	EEDKTLPKPGSPG(K)	9	0
MYO18A_α	EEDKTLPKPGSPG(K)	10	0
MYO18A_α	EEDKTLPKPGSPG(K)	11	0
MYO18A_α	EEDKTLPKPGSPG(K)	12	0
MYO18A_α	EEDKTLPKPGSPG(K)	13	0
MYO18A_α	EEDKTLPKPGSPG(K)	14	0
MYO18A_α	EEDKTLPKPGSPG(K)	15	0
RSF1_γ	VLQAPPPDVGNGEGS(R)	1	1336771.13
RSF1_γ	VLQAPPPDVGNGEGS(R)	2	1755109.25
RSF1_γ	VLQAPPPDVGNGEGS(R)	3	396274016
RSF1_γ	VLQAPPPDVGNGEGS(R)	4	3617483.5
RSF1_γ	VLQAPPPDVGNGEGS(R)	5	2232740096
RSF1_γ	VLQAPPPDVGNGEGS(R)	6	11909423
RSF1_γ	VLQAPPPDVGNGEGS(R)	7	221247680
RSF1_γ	VLQAPPPDVGNGEGS(R)	8	128941752
RSF1_γ	VLQAPPPDVGNGEGS(R)	9	137168608
RSF1_γ	VLQAPPPDVGNGEGS(R)	10	2960405.75
RSF1_γ	VLQAPPPDVGNGEGS(R)	11	444707360
RSF1_γ	VLQAPPPDVGNGEGS(R)	12	2467014
RSF1_γ	VLQAPPPDVGNGEGS(R)	13	36572596

RSF1_Y	VLQAPPPDVGNGEGS(R)	14	6231715.5
RSF1_Y	VLQAPPPDVGNGEGS(R)	15	4365772.5
SYT7_β	AINFPGA(R)	1	28937.6289
SYT7_β	AINFPGA(R)	2	235336
SYT7_β	AINFPGA(R)	3	1277070.63
SYT7_β	AINFPGA(R)	4	227307.656
SYT7_β	AINFPGA(R)	5	1988398.38
SYT7_β	AINFPGA(R)	6	271470.938
SYT7_β	AINFPGA(R)	7	1086827.63
SYT7_β	AINFPGA(R)	8	597841.375
SYT7_β	AINFPGA(R)	9	898979.688
SYT7_β	AINFPGA(R)	10	179104.031
SYT7_β	AINFPGA(R)	11	1686499.63
SYT7_β	AINFPGA(R)	12	95756.5313
SYT7_β	AINFPGA(R)	13	213511.297
SYT7_β	AINFPGA(R)	14	152662.734
SYT7_β	AINFPGA(R)	15	252799.891
SYNE1_α	LANVFEQPVAEQIE(R)	1	38087.2734
SYNE1_α	LANVFEQPVAEQIE(R)	2	0
SYNE1_α	LANVFEQPVAEQIE(R)	3	51821.5625
SYNE1_α	LANVFEQPVAEQIE(R)	4	58894.9727
SYNE1_α	LANVFEQPVAEQIE(R)	5	83586.6094
SYNE1_α	LANVFEQPVAEQIE(R)	6	26004.7227
SYNE1_α	LANVFEQPVAEQIE(R)	7	188636.766
SYNE1_α	LANVFEQPVAEQIE(R)	8	130190.313
SYNE1_α	LANVFEQPVAEQIE(R)	9	115065.602
SYNE1_α	LANVFEQPVAEQIE(R)	10	21669.6211
SYNE1_α	LANVFEQPVAEQIE(R)	11	113414
SYNE1_α	LANVFEQPVAEQIE(R)	12	65861.2109
SYNE1_α	LANVFEQPVAEQIE(R)	13	61423.7617
SYNE1_α	LANVFEQPVAEQIE(R)	14	79714.4844

SYNE1_α	LANVFEQPVAEQIE(R)	15	58577.7383
CAMK2B_α	VPRNLLPVHFWGFEFFP(R)	1	0
CAMK2B_α	VPRNLLPVHFWGFEFFP(R)	2	0
CAMK2B_α	VPRNLLPVHFWGFEFFP(R)	3	92414.4297
CAMK2B_α	VPRNLLPVHFWGFEFFP(R)	4	0
CAMK2B_α	VPRNLLPVHFWGFEFFP(R)	5	204809.422
CAMK2B_α	VPRNLLPVHFWGFEFFP(R)	6	0
CAMK2B_α	VPRNLLPVHFWGFEFFP(R)	7	0
CAMK2B_α	VPRNLLPVHFWGFEFFP(R)	8	0
CAMK2B_α	VPRNLLPVHFWGFEFFP(R)	9	0
CAMK2B_α	VPRNLLPVHFWGFEFFP(R)	10	70350.2969
CAMK2B_α	VPRNLLPVHFWGFEFFP(R)	11	62049.9063
CAMK2B_α	VPRNLLPVHFWGFEFFP(R)	12	0
CAMK2B_α	VPRNLLPVHFWGFEFFP(R)	13	94223.3516
CAMK2B_α	VPRNLLPVHFWGFEFFP(R)	14	37266.9727
CAMK2B_α	VPRNLLPVHFWGFEFFP(R)	15	1340.14356
CAMK2B_ζ	VTERSAGSAETSPTGRVP(R)	1	0
CAMK2B_ζ	VTERSAGSAETSPTGRVP(R)	2	212582.203
CAMK2B_ζ	VTERSAGSAETSPTGRVP(R)	3	0
CAMK2B_ζ	VTERSAGSAETSPTGRVP(R)	4	0
CAMK2B_ζ	VTERSAGSAETSPTGRVP(R)	5	0
CAMK2B_ζ	VTERSAGSAETSPTGRVP(R)	6	0
CAMK2B_ζ	VTERSAGSAETSPTGRVP(R)	7	0
CAMK2B_ζ	VTERSAGSAETSPTGRVP(R)	8	0
CAMK2B_ζ	VTERSAGSAETSPTGRVP(R)	9	0
CAMK2B_ζ	VTERSAGSAETSPTGRVP(R)	10	0
CAMK2B_ζ	VTERSAGSAETSPTGRVP(R)	11	0
CAMK2B_ζ	VTERSAGSAETSPTGRVP(R)	12	0
CAMK2B_ζ	VTERSAGSAETSPTGRVP(R)	13	0
CAMK2B_ζ	VTERSAGSAETSPTGRVP(R)	14	0

CAMK2B_ζ	VTERSAGSAETSPTGRVP(R)	15	11495.3848
MYO18A_δ	EEGAAKTEEQIAAEEAWNETE(K)	1	0
MYO18A_δ	EEGAAKTEEQIAAEEAWNETE(K)	2	0
MYO18A_δ	EEGAAKTEEQIAAEEAWNETE(K)	3	0
MYO18A_δ	EEGAAKTEEQIAAEEAWNETE(K)	4	0
MYO18A_δ	EEGAAKTEEQIAAEEAWNETE(K)	5	0
MYO18A_δ	EEGAAKTEEQIAAEEAWNETE(K)	6	0
MYO18A_δ	EEGAAKTEEQIAAEEAWNETE(K)	7	0
MYO18A_δ	EEGAAKTEEQIAAEEAWNETE(K)	8	27857.5664
MYO18A_δ	EEGAAKTEEQIAAEEAWNETE(K)	9	0
MYO18A_δ	EEGAAKTEEQIAAEEAWNETE(K)	10	0
MYO18A_δ	EEGAAKTEEQIAAEEAWNETE(K)	11	0
MYO18A_δ	EEGAAKTEEQIAAEEAWNETE(K)	12	0
MYO18A_δ	EEGAAKTEEQIAAEEAWNETE(K)	13	0
MYO18A_δ	EEGAAKTEEQIAAEEAWNETE(K)	14	0
MYO18A_δ	EEGAAKTEEQIAAEEAWNETE(K)	15	0
RSF1_ε	KPCSSYGFEGY(R)	1	1262671.25

RSF1_ε	KPCSSYGFEGY(R)	2	1963860.25
RSF1_ε	KPCSSYGFEGY(R)	3	878967
RSF1_ε	KPCSSYGFEGY(R)	4	6990920.5
RSF1_ε	KPCSSYGFEGY(R)	5	3441648.75
RSF1_ε	KPCSSYGFEGY(R)	6	5455025.5
RSF1_ε	KPCSSYGFEGY(R)	7	18688170
RSF1_ε	KPCSSYGFEGY(R)	8	15928859
RSF1_ε	KPCSSYGFEGY(R)	9	7674593
RSF1_ε	KPCSSYGFEGY(R)	10	4309779
RSF1_ε	KPCSSYGFEGY(R)	11	2380750.75
RSF1_ε	KPCSSYGFEGY(R)	12	6748761.5
RSF1_ε	KPCSSYGFEGY(R)	13	6189167
RSF1_ε	KPCSSYGFEGY(R)	14	199128.578
RSF1_ε	KPCSSYGFEGY(R)	15	7903377.5
SLC24A3_α	EEWMDGWIANFH(R)	1	0
SLC24A3_α	EEWMDGWIANFH(R)	2	432744.656
SLC24A3_α	EEWMDGWIANFH(R)	3	33102.1953
SLC24A3_α	EEWMDGWIANFH(R)	4	642005.188
SLC24A3_α	EEWMDGWIANFH(R)	5	0
SLC24A3_α	EEWMDGWIANFH(R)	6	21374.9434
SLC24A3_α	EEWMDGWIANFH(R)	7	895451.063
SLC24A3_α	EEWMDGWIANFH(R)	8	0
SLC24A3_α	EEWMDGWIANFH(R)	9	348012.406
SLC24A3_α	EEWMDGWIANFH(R)	10	458324.188
SLC24A3_α	EEWMDGWIANFH(R)	11	324101.438
SLC24A3_α	EEWMDGWIANFH(R)	12	127598.898
SLC24A3_α	EEWMDGWIANFH(R)	13	71920.0859
SLC24A3_α	EEWMDGWIANFH(R)	14	1329865.38
SLC24A3_α	EEWMDGWIANFH(R)	15	0
SYT7_α	AINFPGA(R)LQSAA	1	57350.3555

SYT7_α	AINFPGA(R)LQSAA	2	64156.8867
SYT7_α	AINFPGA(R)LQSAA	3	121802.609
SYT7_α	AINFPGA(R)LQSAA	4	439777.625
SYT7_α	AINFPGA(R)LQSAA	5	0
SYT7_α	AINFPGA(R)LQSAA	6	285084.438
SYT7_α	AINFPGA(R)LQSAA	7	321171.75
SYT7_α	AINFPGA(R)LQSAA	8	2148973.5
SYT7_α	AINFPGA(R)LQSAA	9	247017.359
SYT7_α	AINFPGA(R)LQSAA	10	327632.594
SYT7_α	AINFPGA(R)LQSAA	11	10770.499
SYT7_α	AINFPGA(R)LQSAA	12	383228.281
SYT7_α	AINFPGA(R)LQSAA	13	368814.906
SYT7_α	AINFPGA(R)LQSAA	14	716648.563
SYT7_α	AINFPGA(R)LQSAA	15	512983.313
IGLON5_β	MPSPHSLALVQPAGHGLQ(R)	1	165298.078
IGLON5_β	MPSPHSLALVQPAGHGLQ(R)	2	1063245
IGLON5_β	MPSPHSLALVQPAGHGLQ(R)	3	543500.188
IGLON5_β	MPSPHSLALVQPAGHGLQ(R)	4	210095.422
IGLON5_β	MPSPHSLALVQPAGHGLQ(R)	5	172644.656
IGLON5_β	MPSPHSLALVQPAGHGLQ(R)	6	127237.93
IGLON5_β	MPSPHSLALVQPAGHGLQ(R)	7	697200.688
IGLON5_β	MPSPHSLALVQPAGHGLQ(R)	8	445214.031
IGLON5_β	MPSPHSLALVQPAGHGLQ(R)	9	701601.125
IGLON5_β	MPSPHSLALVQPAGHGLQ(R)	10	289762.188
IGLON5_β	MPSPHSLALVQPAGHGLQ(R)	11	516579.031
IGLON5_β	MPSPHSLALVQPAGHGLQ(R)	12	336855.406
IGLON5_β	MPSPHSLALVQPAGHGLQ(R)	13	260658.781
IGLON5_β	MPSPHSLALVQPAGHGLQ(R)	14	343538.938
IGLON5_β	MPSPHSLALVQPAGHGLQ(R)	15	180593.953
PXDN_α	WAGETLE(K)	1	0

PXDN_α	WAGETLE(K)	2	0
PXDN_α	WAGETLE(K)	3	0
PXDN_α	WAGETLE(K)	4	0
PXDN_α	WAGETLE(K)	5	0
PXDN_α	WAGETLE(K)	6	89239.5781
PXDN_α	WAGETLE(K)	7	0
PXDN_α	WAGETLE(K)	8	0
PXDN_α	WAGETLE(K)	9	0
PXDN_α	WAGETLE(K)	10	0
PXDN_α	WAGETLE(K)	11	0
PXDN_α	WAGETLE(K)	12	0
PXDN_α	WAGETLE(K)	13	0
PXDN_α	WAGETLE(K)	14	0
PXDN_α	WAGETLE(K)	15	0
SYN3_α	FPLVEQTFFPNHKPMNLGL(K)	1	2264390.75
SYN3_α	FPLVEQTFFPNHKPMNLGL(K)	2	3274986
SYN3_α	FPLVEQTFFPNHKPMNLGL(K)	3	1437872.13
SYN3_α	FPLVEQTFFPNHKPMNLGL(K)	4	1825987.38
SYN3_α	FPLVEQTFFPNHKPMNLGL(K)	5	2084189
SYN3_α	FPLVEQTFFPNHKPMNLGL(K)	6	1788972.38
SYN3_α	FPLVEQTFFPNHKPMNLGL(K)	7	2503068.5
SYN3_α	FPLVEQTFFPNHKPMNLGL(K)	8	1660122.5
SYN3_α	FPLVEQTFFPNHKPMNLGL(K)	9	2963981.25
SYN3_α	FPLVEQTFFPNHKPMNLGL(K)	10	1507707
SYN3_α	FPLVEQTFFPNHKPMNLGL(K)	11	3475215.25
SYN3_α	FPLVEQTFFPNHKPMNLGL(K)	12	1405993.88
SYN3_α	FPLVEQTFFPNHKPMNLGL(K)	13	2160299.5
SYN3_α	FPLVEQTFFPNHKPMNLGL(K)	14	2683112
SYN3_α	FPLVEQTFFPNHKPMNLGL(K)	15	2162461.25
TRRAP_α	YLQFVAALTDVNTQ(K)	1	0

TRRAP_α	YLQFVAALTDVNTQ(K)	2	0
TRRAP_α	YLQFVAALTDVNTQ(K)	3	117533.672
TRRAP_α	YLQFVAALTDVNTQ(K)	4	197186.172
TRRAP_α	YLQFVAALTDVNTQ(K)	5	0
TRRAP_α	YLQFVAALTDVNTQ(K)	6	183486.047
TRRAP_α	YLQFVAALTDVNTQ(K)	7	951372
TRRAP_α	YLQFVAALTDVNTQ(K)	8	708689.188
TRRAP_α	YLQFVAALTDVNTQ(K)	9	218040.516
TRRAP_α	YLQFVAALTDVNTQ(K)	10	178308.734
TRRAP_α	YLQFVAALTDVNTQ(K)	11	196166.25
TRRAP_α	YLQFVAALTDVNTQ(K)	12	217429.844
TRRAP_α	YLQFVAALTDVNTQ(K)	13	130060.039
TRRAP_α	YLQFVAALTDVNTQ(K)	14	235117.906
TRRAP_α	YLQFVAALTDVNTQ(K)	15	177235.641

Table S6I. DIA-targeted proteomics intensity values for all cryptic peptides detected in ALS/FTD CSF

Peptide symbol	Peptide sequence	CSF #	Heavy peptide intensity	Light peptide intensity
HDGFL2_Y	GHSGMLASEG(R)	1	4093018.297	483642.6583
HDGFL2_Y	GHSGMLASEG(R)	2	4386209.281	114684.793
HDGFL2_Y	GHSGMLASEG(R)	3	5702898.813	166098.0625
HDGFL2_Y	GHSGMLASEG(R)	4	8490831.188	1417.138672
HDGFL2_Y	GHSGMLASEG(R)	5	5425666.031	16277720.31
HDGFL2_Y	GHSGMLASEG(R)	6	4217374.188	0
HDGFL2_Y	GHSGMLASEG(R)	7	7583762.313	26466599.75
HDGFL2_Y	GHSGMLASEG(R)	8	7473173.375	4518154.344
HDGFL2_Y	GHSGMLASEG(R)	9	45957503.25	158708302.5
HDGFL2_Y	GHSGMLASEG(R)	10	5822709.626	167427.3632
HDGFL2_Y	GHSGMLASEG(R)	11	7391087.34	28466162.63
HDGFL2_Y	GHSGMLASEG(R)	12	2351984.121	0
HDGFL2_Y	GHSGMLASEG(R)	13	8548878.461	35234307
HDGFL2_Y	GHSGMLASEG(R)	14	10079097.5	202604.8457
HDGFL2_Y	GHSGMLASEG(R)	15	14173337.44	25718387.25
KALRN_Y	MDKPPSVSA(R)	1	10218359.57	30248.16406
KALRN_Y	MDKPPSVSA(R)	2	11835162.7	0
KALRN_Y	MDKPPSVSA(R)	3	2032352260	504051.0449

KALRN_γ	MDKPPSVSA(R)	4	443606468	21914.82422
KALRN_γ	MDKPPSVSA(R)	5	3492107.422	1463115.309
KALRN_γ	MDKPPSVSA(R)	6	2167879.113	0
KALRN_γ	MDKPPSVSA(R)	7	11128634.86	397004.7422
KALRN_γ	MDKPPSVSA(R)	8	11052779.84	39151.98828
KALRN_γ	MDKPPSVSA(R)	9	30088733.69	12017056.03
KALRN_γ	MDKPPSVSA(R)	10	27382653	4971703.711
KALRN_γ	MDKPPSVSA(R)	11	20689375.89	0
KALRN_γ	MDKPPSVSA(R)	12	6470966.602	0
KALRN_γ	MDKPPSVSA(R)	13	11069267.14	51000.62891
KALRN_γ	MDKPPSVSA(R)	14	13324421.47	0
KALRN_γ	MDKPPSVSA(R)	15	8715135.859	47180.02344
KCNQ2_α	LLGSVVYAHSKITLTTIGYGD(K)	1	153235484	4180059.438
KCNQ2_α	LLGSVVYAHSKITLTTIGYGD(K)	2	188994508	5930400.063
KCNQ2_α	LLGSVVYAHSKITLTTIGYGD(K)	3	80250072	2164597.087
KCNQ2_α	LLGSVVYAHSKITLTTIGYGD(K)	4	94314296	776960.8125
KCNQ2_α	LLGSVVYAHSKITLTTIGYGD(K)	5	562080.7891	0
KCNQ2_α	LLGSVVYAHSKITLTTIGYGD(K)	6	152666864	6531275.969
KCNQ2_α	LLGSVVYAHSKITLTTIGYGD(K)	7	899716.6094	0
KCNQ2_α	LLGSVVYAHSKITLTTIGYGD(K)	8	154045304	5441239.375
KCNQ2_α	LLGSVVYAHSKITLTTIGYGD(K)	9	5841458.75	28349.53906
KCNQ2_α	LLGSVVYAHSKITLTTIGYGD(K)	10	3048322.875	0

KCNQ2_α	LLGSVVYAHSKITLTTIGYGD(K)	11	1111652.766	0
KCNQ2_α	LLGSVVYAHSKITLTTIGYGD(K)	12	145046996	4169974.375
KCNQ2_α	LLGSVVYAHSKITLTTIGYGD(K)	13	2055902	0
KCNQ2_α	LLGSVVYAHSKITLTTIGYGD(K)	14	150737528	3470988.883
KCNQ2_α	LLGSVVYAHSKITLTTIGYGD(K)	15	146660208	5133430.25
MYO18A_ε	TLPKPGSPG(K)	1	64211014	477444.0879
MYO18A_ε	TLPKPGSPG(K)	2	373897376	2266475.156
MYO18A_ε	TLPKPGSPG(K)	3	133861220	789461.7188
MYO18A_ε	TLPKPGSPG(K)	4	227982448	938724.7969
MYO18A_ε	TLPKPGSPG(K)	5	9997823	1469345.063
MYO18A_ε	TLPKPGSPG(K)	6	362943480	2308775.969
MYO18A_ε	TLPKPGSPG(K)	7	49352570	750141.9063
MYO18A_ε	TLPKPGSPG(K)	8	290800840	1975785.078
MYO18A_ε	TLPKPGSPG(K)	9	139162744	42446014.5
MYO18A_ε	TLPKPGSPG(K)	10	147170696	32446422.5
MYO18A_ε	TLPKPGSPG(K)	11	19638687	7339179.75
MYO18A_ε	TLPKPGSPG(K)	12	251741088	1304095.375
MYO18A_ε	TLPKPGSPG(K)	13	18973615	12842862.25
MYO18A_ε	TLPKPGSPG(K)	14	429365248	1813155.16
MYO18A_ε	TLPKPGSPG(K)	15	355699104	2275334.531
MYO18A_α	EEDKTLPKPGSPG(K)	1	26565215.03	401731.3399
MYO18A_α	EEDKTLPKPGSPG(K)	2	120731264.6	17427.00781

MYO18A_α	EEDKTLPKPGSPG(K)	3	8710332148	4608189.957
MYO18A_α	EEDKTLPKPGSPG(K)	4	5694652354	2111822.938
MYO18A_α	EEDKTLPKPGSPG(K)	5	14691189.2	11784953.91
MYO18A_α	EEDKTLPKPGSPG(K)	6	112736625.4	30569.73633
MYO18A_α	EEDKTLPKPGSPG(K)	7	10751899.17	29804369.29
MYO18A_α	EEDKTLPKPGSPG(K)	8	99198971.81	18803.4043
MYO18A_α	EEDKTLPKPGSPG(K)	9	68601671	58554237.64
MYO18A_α	EEDKTLPKPGSPG(K)	10	150811399.4	40084631.2
MYO18A_α	EEDKTLPKPGSPG(K)	11	8012562.055	12476464.88
MYO18A_α	EEDKTLPKPGSPG(K)	12	153030439.9	98083.28906
MYO18A_α	EEDKTLPKPGSPG(K)	13	15042642.63	1011493.379
MYO18A_α	EEDKTLPKPGSPG(K)	14	610700234.5	205626.5547
MYO18A_α	EEDKTLPKPGSPG(K)	15	86884306.94	272705.289
RSF1_Y	VLQAPPPDVGNGEGS(R)	1	5320145306	15033631.89
RSF1_Y	VLQAPPPDVGNGEGS(R)	2	4457322754	12373101.75
RSF1_Y	VLQAPPPDVGNGEGS(R)	3	2937643182	4595743.219
RSF1_Y	VLQAPPPDVGNGEGS(R)	4	5387143264	7294046.156
RSF1_Y	VLQAPPPDVGNGEGS(R)	5	4548515704	1050866276
RSF1_Y	VLQAPPPDVGNGEGS(R)	6	3710162682	9535008.984
RSF1_Y	VLQAPPPDVGNGEGS(R)	7	4618874400	6217676716
RSF1_Y	VLQAPPPDVGNGEGS(R)	8	3697011695	33640890.83
RSF1_Y	VLQAPPPDVGNGEGS(R)	9	10308377512	465790396.3

RSF1_ɣ	VLQAPPPDVGNGEGS(R)	10	6864275768	273184201.8
RSF1_ɣ	VLQAPPPDVGNGEGS(R)	11	5071832354	370555630.5
RSF1_ɣ	VLQAPPPDVGNGEGS(R)	12	3491287647	8690738.262
RSF1_ɣ	VLQAPPPDVGNGEGS(R)	13	6067742620	1227706678
RSF1_ɣ	VLQAPPPDVGNGEGS(R)	14	4078908328	7638865.221
RSF1_ɣ	VLQAPPPDVGNGEGS(R)	15	3942566414	96110194.81
SYT7_β	AINFPGA(R)	1	2055876480	327612.3047
SYT7_β	AINFPGA(R)	2	2999592608	696641.7344
SYT7_β	AINFPGA(R)	3	2749867552	28937.62891
SYT7_β	AINFPGA(R)	4	3860329824	274552.1328
SYT7_β	AINFPGA(R)	5	17487356160	2169456.406
SYT7_β	AINFPGA(R)	6	2711459488	355506.959
SYT7_β	AINFPGA(R)	7	18383530496	3222915.938
SYT7_β	AINFPGA(R)	8	2722003328	663008.8907
SYT7_β	AINFPGA(R)	9	25098592512	4161365.375
SYT7_β	AINFPGA(R)	10	13496340352	1974670
SYT7_β	AINFPGA(R)	11	8705376640	1496319.109
SYT7_β	AINFPGA(R)	12	2699004192	416487.1641
SYT7_β	AINFPGA(R)	13	19905187072	2925316.625
SYT7_β	AINFPGA(R)	14	2613812544	240034.0938
SYT7_β	AINFPGA(R)	15	3449214272	758645.0782
SYNE1_α	LANVFEQPVAEQIE(R)	1	5518445952	79714.48438

SYNE1_α	LANVFEQPVAEQIE(R)	2	4831304320	58577.73828
SYNE1_α	LANVFEQPVAEQIE(R)	3	4181415360	38087.27344
SYNE1_α	LANVFEQPVAEQIE(R)	4	3556168224	0
SYNE1_α	LANVFEQPVAEQIE(R)	5	5550064640	100118.5
SYNE1_α	LANVFEQPVAEQIE(R)	6	5569269504	58894.97266
SYNE1_α	LANVFEQPVAEQIE(R)	7	5469914112	148691.0664
SYNE1_α	LANVFEQPVAEQIE(R)	8	3391178304	26004.72266
SYNE1_α	LANVFEQPVAEQIE(R)	9	13738519296	249613.5156
SYNE1_α	LANVFEQPVAEQIE(R)	10	10612709504	243309.7188
SYNE1_α	LANVFEQPVAEQIE(R)	11	7551763200	220619.5508
SYNE1_α	LANVFEQPVAEQIE(R)	12	4223848896	21669.62109
SYNE1_α	LANVFEQPVAEQIE(R)	13	7926394112	113414
SYNE1_α	LANVFEQPVAEQIE(R)	14	5024624256	65861.21094
SYNE1_α	LANVFEQPVAEQIE(R)	15	4008403840	61423.76172
CAMK2B_α	VPRNLLPVHFWGFEFFP(R)	1	374438912	37266.97266
CAMK2B_α	VPRNLLPVHFWGFEFFP(R)	2	334947152	1340.143555
CAMK2B_α	VPRNLLPVHFWGFEFFP(R)	3	340554264	0
CAMK2B_α	VPRNLLPVHFWGFEFFP(R)	4	362887376	0
CAMK2B_α	VPRNLLPVHFWGFEFFP(R)	5	191042760	89791.32813
CAMK2B_α	VPRNLLPVHFWGFEFFP(R)	6	273969568	0
CAMK2B_α	VPRNLLPVHFWGFEFFP(R)	7	33336432	204809.4219

CAMK2B_α	VPRNLLPVHFWGFEFFP(R)	8	293660240	0
CAMK2B_α	VPRNLLPVHFWGFEFFP(R)	9	847144704	0
CAMK2B_α	VPRNLLPVHFWGFEFFP(R)	10	898396864	0
CAMK2B_α	VPRNLLPVHFWGFEFFP(R)	11	305808472	0
CAMK2B_α	VPRNLLPVHFWGFEFFP(R)	12	237605440	72242.95312
CAMK2B_α	VPRNLLPVHFWGFEFFP(R)	13	254877080	31859.67773
CAMK2B_α	VPRNLLPVHFWGFEFFP(R)	14	258331904	0
CAMK2B_α	VPRNLLPVHFWGFEFFP(R)	15	345631216	94223.35156
CAMK2B_ζ	VTERSAGSAETSPTGRVP(R)	1	3549386.5	25353.9375
CAMK2B_ζ	VTERSAGSAETSPTGRVP(R)	2	2933829	87501.07422
CAMK2B_ζ	VTERSAGSAETSPTGRVP(R)	3	10703424.75	0
CAMK2B_ζ	VTERSAGSAETSPTGRVP(R)	4	16747865.75	212582.2031
CAMK2B_ζ	VTERSAGSAETSPTGRVP(R)	5	2667178	50406.19922
CAMK2B_ζ	VTERSAGSAETSPTGRVP(R)	6	520156.086	0
CAMK2B_ζ	VTERSAGSAETSPTGRVP(R)	7	1807932.625	0
CAMK2B_ζ	VTERSAGSAETSPTGRVP(R)	8	5575465.5	44430.88672
CAMK2B_ζ	VTERSAGSAETSPTGRVP(R)	9	1001534.656	0
CAMK2B_ζ	VTERSAGSAETSPTGRVP(R)	10	11287486.88	0
CAMK2B_ζ	VTERSAGSAETSPTGRVP(R)	11	3932153.75	40170.00391
CAMK2B_ζ	VTERSAGSAETSPTGRVP(R)	12	3625626.5	29968.67383
CAMK2B_ζ	VTERSAGSAETSPTGRVP(R)	13	4106024.75	110377.0781
CAMK2B_ζ	VTERSAGSAETSPTGRVP(R)	14	7624208.5	0

CAMK2B_ζ	VTERSAGSAETSPTGRVP(R)	15	3219319	16542.71875
MYO18A_δ	EEGAAKTEEQIAAEEAWNETE(K)	1	208421968	0
MYO18A_δ	EEGAAKTEEQIAAEEAWNETE(K)	2	140178796	0
MYO18A_δ	EEGAAKTEEQIAAEEAWNETE(K)	3	4899804.125	0
MYO18A_δ	EEGAAKTEEQIAAEEAWNETE(K)	4	9349349.75	0
MYO18A_δ	EEGAAKTEEQIAAEEAWNETE(K)	5	3981789.875	203319.2109
MYO18A_δ	EEGAAKTEEQIAAEEAWNETE(K)	6	139913448	0
MYO18A_δ	EEGAAKTEEQIAAEEAWNETE(K)	7	4538810	0
MYO18A_δ	EEGAAKTEEQIAAEEAWNETE(K)	8	130794240	0
MYO18A_δ	EEGAAKTEEQIAAEEAWNETE(K)	9	23826802	56134.69922
MYO18A_δ	EEGAAKTEEQIAAEEAWNETE(K)	10	23140427	825806.7813
MYO18A_δ	EEGAAKTEEQIAAEEAWNETE(K)	11	4240249.125	198932.5313
MYO18A_δ	EEGAAKTEEQIAAEEAWNETE(K)	12	89391848	0
MYO18A_δ	EEGAAKTEEQIAAEEAWNETE(K)	13	4165410.5	164491.0938
MYO18A_δ	EEGAAKTEEQIAAEEAWNETE(K)	14	139240504	0
MYO18A_δ	EEGAAKTEEQIAAEEAWNETE(K)	15	85981984	576596.375
RSF1_ε	KPCSSYGFEGY(R)	1	7203825.703	431468.9531
RSF1_ε	KPCSSYGFEGY(R)	2	894948198	7862891.5
RSF1_ε	KPCSSYGFEGY(R)	3	174844260.3	1323772.422
RSF1_ε	KPCSSYGFEGY(R)	4	393693469.5	1990673.76
RSF1_ε	KPCSSYGFEGY(R)	5	84473421.88	1186511.906
RSF1_ε	KPCSSYGFEGY(R)	6	752274517	6990920.5
RSF1_ε	KPCSSYGFEGY(R)	7	364932329	3485158.531

RSF1_ε	KPCSSYGFEGY(R)	8	509342675	5749226.5
RSF1_ε	KPCSSYGFEGY(R)	9	2298332012	18688170
RSF1_ε	KPCSSYGFEGY(R)	10	1929620664	15928859
RSF1_ε	KPCSSYGFEGY(R)	11	868823000	8271177.375
RSF1_ε	KPCSSYGFEGY(R)	12	477263196	4715366.219
RSF1_ε	KPCSSYGFEGY(R)	13	216735127.5	3644575.25
RSF1_ε	KPCSSYGFEGY(R)	14	709885160	6886967.246
RSF1_ε	KPCSSYGFEGY(R)	15	636367630	7427521.125
SLC24A3_α	EEWMDGWIANFH(R)	1	2113965248	1329865.375
SLC24A3_α	EEWMDGWIANFH(R)	2	1860860960	0
SLC24A3_α	EEWMDGWIANFH(R)	3	1728083840	514295.4063
SLC24A3_α	EEWMDGWIANFH(R)	4	2951553280	3494681.906
SLC24A3_α	EEWMDGWIANFH(R)	5	2004377088	68180.03906
SLC24A3_α	EEWMDGWIANFH(R)	6	1398952672	642005.1875
SLC24A3_α	EEWMDGWIANFH(R)	7	2211462592	1511001
SLC24A3_α	EEWMDGWIANFH(R)	8	1801729568	21374.94336
SLC24A3_α	EEWMDGWIANFH(R)	9	4277069440	4143553.563
SLC24A3_α	EEWMDGWIANFH(R)	10	3483360064	132750.0938
SLC24A3_α	EEWMDGWIANFH(R)	11	2484656832	960762.9063
SLC24A3_α	EEWMDGWIANFH(R)	12	1170191360	458324.1875
SLC24A3_α	EEWMDGWIANFH(R)	13	2946354816	324101.4375
SLC24A3_α	EEWMDGWIANFH(R)	14	1538490272	297056.1484

SLC24A3_α	EEWMDGWIANFH(R)	15	2157097216	71920.08594
SYT7_α	AINFPGA(R)LQSAA	1	6123068192	461652380
SYT7_α	AINFPGA(R)LQSAA	2	5103393728	428432284.6
SYT7_α	AINFPGA(R)LQSAA	3	3275404896	318063344
SYT7_α	AINFPGA(R)LQSAA	4	3609444544	397409032
SYT7_α	AINFPGA(R)LQSAA	5	1351993064	119557326.4
SYT7_α	AINFPGA(R)LQSAA	6	5280753120	424726810.5
SYT7_α	AINFPGA(R)LQSAA	7	5209798.438	185394.0938
SYT7_α	AINFPGA(R)LQSAA	8	3914842496	323739971.3
SYT7_α	AINFPGA(R)LQSAA	9	6527650848	489544222.5
SYT7_α	AINFPGA(R)LQSAA	10	6185511040	436834736
SYT7_α	AINFPGA(R)LQSAA	11	4051182432	360003030.3
SYT7_α	AINFPGA(R)LQSAA	12	3807138752	328218416
SYT7_α	AINFPGA(R)LQSAA	13	904238952	126323624
SYT7_α	AINFPGA(R)LQSAA	14	4890650560	421822564
SYT7_α	AINFPGA(R)LQSAA	15	3922264288	320609704
IGLON5_β	MPSPHSLALVQPAGHGLQ(R)	1	286909376	416523.1719
IGLON5_β	MPSPHSLALVQPAGHGLQ(R)	2	282968612	329546.9219
IGLON5_β	MPSPHSLALVQPAGHGLQ(R)	3	254987104	165298.0781
IGLON5_β	MPSPHSLALVQPAGHGLQ(R)	4	230652032	1063245
IGLON5_β	MPSPHSLALVQPAGHGLQ(R)	5	249945620	606516.6055
IGLON5_β	MPSPHSLALVQPAGHGLQ(R)	6	208589248	259518.8282

IGLON5_β	MPSPHSLALVQPAGHGLQ(R)	7	290114700	172644.6563
IGLON5_β	MPSPHSLALVQPAGHGLQ(R)	8	258066564	127237.9297
IGLON5_β	MPSPHSLALVQPAGHGLQ(R)	9	790013768	735477.4219
IGLON5_β	MPSPHSLALVQPAGHGLQ(R)	10	611158328	445214.0313
IGLON5_β	MPSPHSLALVQPAGHGLQ(R)	11	309466712	701601.125
IGLON5_β	MPSPHSLALVQPAGHGLQ(R)	12	227622768	468636.0938
IGLON5_β	MPSPHSLALVQPAGHGLQ(R)	13	349339752	516579.0313
IGLON5_β	MPSPHSLALVQPAGHGLQ(R)	14	238339916	539234.9844
IGLON5_β	MPSPHSLALVQPAGHGLQ(R)	15	227219188	260658.7813
PXDN_α	WAGETLE(K)	1	1740139.828	0
PXDN_α	WAGETLE(K)	2	39718290	119957.9688
PXDN_α	WAGETLE(K)	3	234865314	0
PXDN_α	WAGETLE(K)	4	414809214	0
PXDN_α	WAGETLE(K)	5	2680153.609	0
PXDN_α	WAGETLE(K)	6	83311078.5	0
PXDN_α	WAGETLE(K)	7	12865674.31	0
PXDN_α	WAGETLE(K)	8	18451574.5	0
PXDN_α	WAGETLE(K)	9	2051294784	1261524.395
PXDN_α	WAGETLE(K)	10	2781908400	19420.9043
PXDN_α	WAGETLE(K)	11	52009136	0
PXDN_α	WAGETLE(K)	12	10407568.44	0
PXDN_α	WAGETLE(K)	13	12158176.81	71960.99219

PXDN_α	WAGETLE(K)	14	662501068	574896.1875
PXDN_α	WAGETLE(K)	15	22009366.88	214195.75
SYN3_α	FPLVEQTFFPNHKPMNLGL(K)	1	195306952	2683112
SYN3_α	FPLVEQTFFPNHKPMNLGL(K)	2	153483031	2162461.25
SYN3_α	FPLVEQTFFPNHKPMNLGL(K)	3	141159486.5	2264390.75
SYN3_α	FPLVEQTFFPNHKPMNLGL(K)	4	207997367	3274986
SYN3_α	FPLVEQTFFPNHKPMNLGL(K)	5	185023245	1437872.125
SYN3_α	FPLVEQTFFPNHKPMNLGL(K)	6	154829033	1825987.375
SYN3_α	FPLVEQTFFPNHKPMNLGL(K)	7	186971556	2084189
SYN3_α	FPLVEQTFFPNHKPMNLGL(K)	8	144254501	1788972.375
SYN3_α	FPLVEQTFFPNHKPMNLGL(K)	9	439385324	2543355.805
SYN3_α	FPLVEQTFFPNHKPMNLGL(K)	10	242799106	1660122.5
SYN3_α	FPLVEQTFFPNHKPMNLGL(K)	11	212231946	2963981.25
SYN3_α	FPLVEQTFFPNHKPMNLGL(K)	12	114864808	1507707
SYN3_α	FPLVEQTFFPNHKPMNLGL(K)	13	262384414	3475215.25
SYN3_α	FPLVEQTFFPNHKPMNLGL(K)	14	155780590	1405993.875
SYN3_α	FPLVEQTFFPNHKPMNLGL(K)	15	177819403	2160299.5
TRRAP_α	YLQFVAALTDVNTQ(K)	1	208954.3594	285011.1133
TRRAP_α	YLQFVAALTDVNTQ(K)	2	137868.8281	248075.4844
TRRAP_α	YLQFVAALTDVNTQ(K)	3	51780.21094	476700.4063
TRRAP_α	YLQFVAALTDVNTQ(K)	4	0	533173.4942

TRRAP_α	YLQFVAALTDVNTQ(K)	5	138914.5039	164179.3399
TRRAP_α	YLQFVAALTDVNTQ(K)	6	102588.1172	264930.5157
TRRAP_α	YLQFVAALTDVNTQ(K)	7	171644.1641	0
TRRAP_α	YLQFVAALTDVNTQ(K)	8	193314.5391	281039.125
TRRAP_α	YLQFVAALTDVNTQ(K)	9	750165.3438	1141658.688
TRRAP_α	YLQFVAALTDVNTQ(K)	10	470026.7501	826294.4688
TRRAP_α	YLQFVAALTDVNTQ(K)	11	256367.9219	295316.1094
TRRAP_α	YLQFVAALTDVNTQ(K)	12	76230.10938	213288.2891
TRRAP_α	YLQFVAALTDVNTQ(K)	13	456490.1759	196166.25
TRRAP_α	YLQFVAALTDVNTQ(K)	14	121078.8672	249771.5928
TRRAP_α	YLQFVAALTDVNTQ(K)	15	218696.8125	181856.3907

Table S6J. DIA-targeted proteomics intensity values for all cryptic peptides detected in a larger control and ALS/FTD CSF cohort

Protein	Peptide sequence	CSF #	Condition	Heavy	Light
HDGFL2	GHSGMLASEGR	1	ALS	9616495	20631.5313
HDGFL2	GHSGMLASEGR	2	ALS	14420914	300389.219
HDGFL2	GHSGMLASEGR	3	ALS	10639940	386304.434
HDGFL2	GHSGMLASEGR	4	ALS	1320500259	4885660791
HDGFL2	GHSGMLASEGR	5	ALS	8987027.75	8002087.5
HDGFL2	GHSGMLASEGR	6	ALS	6811841.56	1127409.25
HDGFL2	GHSGMLASEGR	7	ALS	33186406.3	80743719
HDGFL2	GHSGMLASEGR	8	ALS	142397133	33408989.9
HDGFL2	GHSGMLASEGR	9	ALS	7178214.88	5942737.88
HDGFL2	GHSGMLASEGR	10	ALS	4361007.5	14347751.5
HDGFL2	GHSGMLASEGR	11	ALS	11434341.3	9295179.34
HDGFL2	GHSGMLASEGR	12	ALS	6534053.75	15120694
HDGFL2	GHSGMLASEGR	13	ALS	11068091.5	2679879.27
HDGFL2	GHSGMLASEGR	14	ALS	33518661.5	91450505.4
HDGFL2	GHSGMLASEGR	15	ALS	74957128	134092908
HDGFL2	GHSGMLASEGR	16	ALS	11799981.8	16071549.8
HDGFL2	GHSGMLASEGR	17	ALS	2069107.45	165621.297
HDGFL2	GHSGMLASEGR	18	ALS	11182263	19030291.2

HDGFL2	GHSGMLASEGR	19	ALS	10845287.5	81758.125
HDGFL2	GHSGMLASEGR	20	ALS	14407162	13645602
HDGFL2	GHSGMLASEGR	21	ALS	8590251.25	507826.281
HDGFL2	GHSGMLASEGR	22	ALS	9601176.5	67297.2344
HDGFL2	GHSGMLASEGR	23	ALSFTD	7293905	177675.4
HDGFL2	GHSGMLASEGR	24	C9ALS	6985087.5	9553320
HDGFL2	GHSGMLASEGR	25	C9ALS	1259626565	22052034.4
HDGFL2	GHSGMLASEGR	26	C9ALS	7860664.75	164846.605
HDGFL2	GHSGMLASEGR	27	C9ALS	16234409	33230515.8
HDGFL2	GHSGMLASEGR	28	C9ALS	7403270.38	47363.1719
HDGFL2	GHSGMLASEGR	29	C9ALS	12419385.3	327590.617
HDGFL2	GHSGMLASEGR	30	C9ALS	10539258.8	9061809
HDGFL2	GHSGMLASEGR	31	C9ALS	17099093	30466913.9
HDGFL2	GHSGMLASEGR	32	C9ALS	7763538.25	72727.2036
HDGFL2	GHSGMLASEGR	33	C9ALS	15459256	22122272
HDGFL2	GHSGMLASEGR	34	C9ALS	26456691	37950758.8
HDGFL2	GHSGMLASEGR	35	C9ALS	88456522	288455910
HDGFL2	GHSGMLASEGR	36	C9ALS	6388099.75	8081626
HDGFL2	GHSGMLASEGR	37	C9ALSFTD	20088212	577062.875
HDGFL2	GHSGMLASEGR	38	C9ALSFTD	17007578.3	41941751.9
HDGFL2	GHSGMLASEGR	39	C9ALSFTD	42827190	116681761
HDGFL2	GHSGMLASEGR	40	C9ALSFTD	14643324	6480328
HDGFL2	GHSGMLASEGR	41	C9ALSFTD	83964920	47688404

HDGFL2	GHSGMLASEGR	42	C9ASYMPTOMATIC	6723060.81	0
HDGFL2	GHSGMLASEGR	43	C9ASYMPTOMATIC	7588270.63	628227.357
HDGFL2	GHSGMLASEGR	44	C9ASYMPTOMATIC	4240191.63	0
HDGFL2	GHSGMLASEGR	45	C9ASYMPTOMATIC	23168406	388864.969
HDGFL2	GHSGMLASEGR	46	C9ASYMPTOMATIC	1000163.19	0
HDGFL2	GHSGMLASEGR	47	C9ASYMPTOMATIC	9911679	300213.266
HDGFL2	GHSGMLASEGR	48	C9FTD	8872822.5	9096246
HDGFL2	GHSGMLASEGR	49	C9FTD	25790037.5	60920749.3
HDGFL2	GHSGMLASEGR	50	Healthy control	20407634	299627.844
HDGFL2	GHSGMLASEGR	51	Healthy control	17043143.5	22323633.3
HDGFL2	GHSGMLASEGR	52	Healthy control	23601093	386245.813
HDGFL2	GHSGMLASEGR	53	Healthy control	20834575.5	173001.188
HDGFL2	GHSGMLASEGR	54	Healthy control	20678461	323643.438
HDGFL2	GHSGMLASEGR	55	Healthy control	93263924	1660901.45
HDGFL2	GHSGMLASEGR	56	Healthy control	13429275.5	145090.828
HDGFL2	GHSGMLASEGR	57	Healthy control	11146179	28083202
HDGFL2	GHSGMLASEGR	58	Healthy control	17143423.5	374245.953

HDGFL2	GHSGMLASEGR	59	Healthy control	20349461.5	47831600.3
HDGFL2	GHSGMLASEGR	60	Healthy control	50286629	176967827
HDGFL2	GHSGMLASEGR	61	Healthy control	8218119.13	57228.8242
HDGFL2	GHSGMLASEGR	62	Healthy control	8512557.38	213673.906
HDGFL2	GHSGMLASEGR	63	Healthy control	66766761.5	239853840
HDGFL2	GHSGMLASEGR	64	Healthy control	8778058.75	6040063
HDGFL2	GHSGMLASEGR	65	Healthy control	42550977	136315088
HDGFL2	GHSGMLASEGR	66	Healthy control	31465039.5	71323518.3
HDGFL2	GHSGMLASEGR	67	Healthy control	28614345.5	42378740
HDGFL2	GHSGMLASEGR	68	Healthy control	13865182	29304036.4
HDGFL2	GHSGMLASEGR	69	Healthy control	11521305	5227471.72
HDGFL2	GHSGMLASEGR	70	Healthy spouse	2062266.56	4714025.94
HDGFL2	GHSGMLASEGR	71	Healthy spouse	16375490	394895.063
HDGFL2	GHSGMLASEGR	72	Healthy spouse	2021675	3565144
HDGFL2	GHSGMLASEGR	73	Multiple Sclerosis	10397487	472131
HDGFL2	GHSGMLASEGR	74	Multiple Sclerosis	12024987	259986.703
HDGFL2	GHSGMLASEGR	75	Multiple Sclerosis	184267.313	0
HDGFL2	GHSGMLASEGR	76	Multiple Sclerosis	10178515	335403.188
HDGFL2	GHSGMLASEGR	77	Multiple Sclerosis	1588321.38	0
HDGFL2	GHSGMLASEGR	78	Multiple Sclerosis	9412910	22855426
HDGFL2	GHSGMLASEGR	79	Multiple Sclerosis	9243371	195632.328
HDGFL2	GHSGMLASEGR	80	Multiple Sclerosis	15361697.5	228535.203
HDGFL2	GHSGMLASEGR	81	Multiple Sclerosis	1888213.75	0

HDGFL2	GHSGMLASEGR	82	Multiple Sclerosis	21660571.5	43024380.9
KALRN	MDKPPSVSAR	1	ALS	3584725.38	0
KALRN	MDKPPSVSAR	2	ALS	4036785	0
KALRN	MDKPPSVSAR	3	ALS	6433924.25	62594.582
KALRN	MDKPPSVSAR	4	ALS	938770278	462165355
KALRN	MDKPPSVSAR	5	ALS	6384297.25	7580000.63
KALRN	MDKPPSVSAR	6	ALS	6963994	2503706.13
KALRN	MDKPPSVSAR	7	ALS	3323110.25	64158.5195
KALRN	MDKPPSVSAR	8	ALS	11713732.9	3111419.06
KALRN	MDKPPSVSAR	9	ALS	3018690.63	87641.9297
KALRN	MDKPPSVSAR	10	ALS	6307007.56	11052592
KALRN	MDKPPSVSAR	11	ALS	4052891.13	703882.715
KALRN	MDKPPSVSAR	12	ALS	5371621.69	332503.418
KALRN	MDKPPSVSAR	13	ALS	10321025.5	417744.77
KALRN	MDKPPSVSAR	14	ALS	11590715	3563059.25
KALRN	MDKPPSVSAR	15	ALS	10185008.4	1551809.13
KALRN	MDKPPSVSAR	16	ALS	9612078	0
KALRN	MDKPPSVSAR	17	ALS	4462969.63	0
KALRN	MDKPPSVSAR	18	ALS	6377441.5	299344.457
KALRN	MDKPPSVSAR	19	ALS	8902109.75	0
KALRN	MDKPPSVSAR	20	ALS	8096013.25	336220.18
KALRN	MDKPPSVSAR	21	ALS	6497183.75	945032.539
KALRN	MDKPPSVSAR	22	ALS	6787335	0

KALRN	MDKPPSVSAR	23	ALSFTD	3806117.63	235288.109
KALRN	MDKPPSVSAR	24	C9ALS	7279631.97	1364993.5
KALRN	MDKPPSVSAR	25	C9ALS	1068633649	0
KALRN	MDKPPSVSAR	26	C9ALS	3264739.19	210992.203
KALRN	MDKPPSVSAR	27	C9ALS	1168002129	1226965504
KALRN	MDKPPSVSAR	28	C9ALS	4708285.5	203148.141
KALRN	MDKPPSVSAR	29	C9ALS	3989750.13	88150.8203
KALRN	MDKPPSVSAR	30	C9ALS	5066304.38	0
KALRN	MDKPPSVSAR	31	C9ALS	5588679	0
KALRN	MDKPPSVSAR	32	C9ALS	4490662.25	47772.625
KALRN	MDKPPSVSAR	33	C9ALS	3638562	323610.289
KALRN	MDKPPSVSAR	34	C9ALS	8245616.5	233542.141
KALRN	MDKPPSVSAR	35	C9ALS	219178622	164720472
KALRN	MDKPPSVSAR	36	C9ALS	4102315.25	506332.313
KALRN	MDKPPSVSAR	37	C9ALSFTD	905757.313	0
KALRN	MDKPPSVSAR	38	C9ALSFTD	5301448.13	10029015
KALRN	MDKPPSVSAR	39	C9ALSFTD	10812100.6	13065146.1
KALRN	MDKPPSVSAR	40	C9ALSFTD	4215408.75	1615856.38
KALRN	MDKPPSVSAR	41	C9ALSFTD	9090116	0
KALRN	MDKPPSVSAR	42	C9ASYMPTOMATIC	4892687.63	0
KALRN	MDKPPSVSAR	43	C9ASYMPTOMATIC	6459259.75	77474.4219

KALRN	MDKPPSVSAR	44	C9ASYMPTOMATIC	15777077.6	0
KALRN	MDKPPSVSAR	45	C9ASYMPTOMATIC	10926985.3	93091.832
KALRN	MDKPPSVSAR	46	C9ASYMPTOMATIC	879777.938	0
KALRN	MDKPPSVSAR	47	C9ASYMPTOMATIC	5456325.5	326786.844
KALRN	MDKPPSVSAR	48	C9FTD	4986837.38	56762.3984
KALRN	MDKPPSVSAR	49	C9FTD	21939028.5	5426747.5
KALRN	MDKPPSVSAR	50	Healthy control	14071138.8	218867.469
KALRN	MDKPPSVSAR	51	Healthy control	4750698.63	338747.656
KALRN	MDKPPSVSAR	52	Healthy control	9388504	294811
KALRN	MDKPPSVSAR	53	Healthy control	7879312.25	0
KALRN	MDKPPSVSAR	54	Healthy control	6605033.5	0
KALRN	MDKPPSVSAR	55	Healthy control	4320438.25	390220.305
KALRN	MDKPPSVSAR	56	Healthy control	3980238.44	0
KALRN	MDKPPSVSAR	57	Healthy control	3187701.75	421717.063
KALRN	MDKPPSVSAR	58	Healthy control	5015090	0
KALRN	MDKPPSVSAR	59	Healthy control	4244986	5934802.02
KALRN	MDKPPSVSAR	60	Healthy control	13484190.4	26091639.4
KALRN	MDKPPSVSAR	61	Healthy control	9103633.75	173825.922
KALRN	MDKPPSVSAR	62	Healthy control	2044249.56	79748.625

KALRN	MDKPPSVSAR	63	Healthy control	9559329.5	155316779
KALRN	MDKPPSVSAR	64	Healthy control	5867563.75	1705091.52
KALRN	MDKPPSVSAR	65	Healthy control	8486859.75	627277.672
KALRN	MDKPPSVSAR	66	Healthy control	39314620.3	26571156.8
KALRN	MDKPPSVSAR	67	Healthy control	7287352.94	188691.672
KALRN	MDKPPSVSAR	68	Healthy control	6228508.75	868.664368
KALRN	MDKPPSVSAR	69	Healthy control	4464826.75	74842.9141
KALRN	MDKPPSVSAR	70	Healthy spouse	7365300	303064.219
KALRN	MDKPPSVSAR	71	Healthy spouse	3344538.88	0
KALRN	MDKPPSVSAR	72	Healthy spouse	3551979.75	0
KALRN	MDKPPSVSAR	73	Multiple Sclerosis	5042547.75	114090.953
KALRN	MDKPPSVSAR	74	Multiple Sclerosis	2063457.13	0
KALRN	MDKPPSVSAR	75	Multiple Sclerosis	3103991	27033.4023
KALRN	MDKPPSVSAR	76	Multiple Sclerosis	2775992.63	226987.453
KALRN	MDKPPSVSAR	77	Multiple Sclerosis	1260071.5	0
KALRN	MDKPPSVSAR	78	Multiple Sclerosis	5260948	775885.563
KALRN	MDKPPSVSAR	79	Multiple Sclerosis	8637761	0
KALRN	MDKPPSVSAR	80	Multiple Sclerosis	6277833.25	174667.641
KALRN	MDKPPSVSAR	81	Multiple Sclerosis	2816248	28668.7754
KALRN	MDKPPSVSAR	82	Multiple Sclerosis	15063130.5	4126972.25
KCNQ2	LLGSVVYAHSKITLTTIGYGDK	1	ALS	17841682.4	1257153.88
KCNQ3	LLGSVVYAHSKITLTTIGYGDK	2	ALS	37769024.6	1319311.88
KCNQ4	LLGSVVYAHSKITLTTIGYGDK	3	ALS	41804454.9	3146573

KCNQ5	LLGSVVYAHSKITLTTIGYGDK	4	ALS	7639467	340419.125
KCNQ6	LLGSVVYAHSKITLTTIGYGDK	5	ALS	757897.625	0
KCNQ7	LLGSVVYAHSKITLTTIGYGDK	6	ALS	5932316.63	288517.359
KCNQ8	LLGSVVYAHSKITLTTIGYGDK	7	ALS	819895.188	3286.68604
KCNQ9	LLGSVVYAHSKITLTTIGYGDK	8	ALS	3289673.56	58905.0781
KCNQ10	LLGSVVYAHSKITLTTIGYGDK	9	ALS	1924026.63	26386.0781
KCNQ11	LLGSVVYAHSKITLTTIGYGDK	10	ALS	6003555.47	0
KCNQ12	LLGSVVYAHSKITLTTIGYGDK	11	ALS	196972.359	0
KCNQ13	LLGSVVYAHSKITLTTIGYGDK	12	ALS	536459.156	0
KCNQ14	LLGSVVYAHSKITLTTIGYGDK	13	ALS	50512950.7	1240545.75
KCNQ15	LLGSVVYAHSKITLTTIGYGDK	14	ALS	2480073.88	28349.5391
KCNQ16	LLGSVVYAHSKITLTTIGYGDK	15	ALS	1520135.25	0
KCNQ17	LLGSVVYAHSKITLTTIGYGDK	16	ALS	570687.297	0
KCNQ18	LLGSVVYAHSKITLTTIGYGDK	17	ALS	48100268.1	3257245.75
KCNQ19	LLGSVVYAHSKITLTTIGYGDK	18	ALS	9969102.38	0
KCNQ20	LLGSVVYAHSKITLTTIGYGDK	19	ALS	48552620	2932168.5
KCNQ21	LLGSVVYAHSKITLTTIGYGDK	20	ALS	47928940	2170360
KCNQ22	LLGSVVYAHSKITLTTIGYGDK	21	ALS	51629162.1	2448221.75
KCNQ23	LLGSVVYAHSKITLTTIGYGDK	22	ALS	62399416.6	3926491.16
KCNQ24	LLGSVVYAHSKITLTTIGYGDK	23	ALSFTD	53778996	4175731.93
KCNQ25	LLGSVVYAHSKITLTTIGYGDK	24	C9ALS	825692.875	0
KCNQ26	LLGSVVYAHSKITLTTIGYGDK	25	C9ALS	309704145	11630814
KCNQ27	LLGSVVYAHSKITLTTIGYGDK	26	C9ALS	57621200.5	2661454.75

KCNQ28	LLGSVVYAHSKITLTTIGYGDK	27	C9ALS	93045.2344	195968.359
KCNQ29	LLGSVVYAHSKITLTTIGYGDK	28	C9ALS	47943992	1766217
KCNQ30	LLGSVVYAHSKITLTTIGYGDK	29	C9ALS	255166716	5849763
KCNQ31	LLGSVVYAHSKITLTTIGYGDK	30	C9ALS	6172750.5	105842.602
KCNQ32	LLGSVVYAHSKITLTTIGYGDK	31	C9ALS	578808.375	0
KCNQ33	LLGSVVYAHSKITLTTIGYGDK	32	C9ALS	63582060	2851321.25
KCNQ34	LLGSVVYAHSKITLTTIGYGDK	33	C9ALS	2127967	111893.211
KCNQ35	LLGSVVYAHSKITLTTIGYGDK	34	C9ALS	36768310.3	1413654.63
KCNQ36	LLGSVVYAHSKITLTTIGYGDK	35	C9ALS	2904428.61	25971.9512
KCNQ37	LLGSVVYAHSKITLTTIGYGDK	36	C9ALS	5288656.5	126511.891
KCNQ38	LLGSVVYAHSKITLTTIGYGDK	37	C9ALSFTD	261372352	5806225
KCNQ39	LLGSVVYAHSKITLTTIGYGDK	38	C9ALSFTD	6250890	0
KCNQ40	LLGSVVYAHSKITLTTIGYGDK	39	C9ALSFTD	7902846.13	283296
KCNQ41	LLGSVVYAHSKITLTTIGYGDK	40	C9ALSFTD	199234857	4460839
KCNQ42	LLGSVVYAHSKITLTTIGYGDK	41	C9ALSFTD	87457756.1	1889221.88
KCNQ43	LLGSVVYAHSKITLTTIGYGDK	42	C9ASYMPTOMATIC	60811030.5	2580013.75
KCNQ44	LLGSVVYAHSKITLTTIGYGDK	43	C9ASYMPTOMATIC	53830634.9	4126789
KCNQ45	LLGSVVYAHSKITLTTIGYGDK	44	C9ASYMPTOMATIC	52854291	3960329.19
KCNQ46	LLGSVVYAHSKITLTTIGYGDK	45	C9ASYMPTOMATIC	270476769	11007157

KCNQ47	LLGSVVYAHSKITLTTIGYGDK	46	C9ASYMPTOMATIC	59877408	3837914
KCNQ48	LLGSVVYAHSKITLTTIGYGDK	47	C9ASYMPTOMATIC	44495122.8	430555.906
KCNQ49	LLGSVVYAHSKITLTTIGYGDK	48	C9FTD	11679361	189183.094
KCNQ50	LLGSVVYAHSKITLTTIGYGDK	49	C9FTD	25869586.2	604581.438
KCNQ51	LLGSVVYAHSKITLTTIGYGDK	50	Healthy control	242303325	8454612.41
KCNQ52	LLGSVVYAHSKITLTTIGYGDK	51	Healthy control	238923.016	44919.0469
KCNQ53	LLGSVVYAHSKITLTTIGYGDK	52	Healthy control	200833011	3263903.52
KCNQ54	LLGSVVYAHSKITLTTIGYGDK	53	Healthy control	234261945	11613034
KCNQ55	LLGSVVYAHSKITLTTIGYGDK	54	Healthy control	225105323	5731822
KCNQ56	LLGSVVYAHSKITLTTIGYGDK	55	Healthy control	267564250	7514565
KCNQ57	LLGSVVYAHSKITLTTIGYGDK	56	Healthy control	10607452.5	0
KCNQ58	LLGSVVYAHSKITLTTIGYGDK	57	Healthy control	289200.094	0
KCNQ59	LLGSVVYAHSKITLTTIGYGDK	58	Healthy control	232539904	11831178.3
KCNQ60	LLGSVVYAHSKITLTTIGYGDK	59	Healthy control	25632328.3	940456.277
KCNQ61	LLGSVVYAHSKITLTTIGYGDK	60	Healthy control	2168110.63	0
KCNQ62	LLGSVVYAHSKITLTTIGYGDK	61	Healthy control	53596503.5	1190620.38
KCNQ63	LLGSVVYAHSKITLTTIGYGDK	62	Healthy control	60947540	3347257.5
KCNQ64	LLGSVVYAHSKITLTTIGYGDK	63	Healthy control	5094475.5	256113.797
KCNQ65	LLGSVVYAHSKITLTTIGYGDK	64	Healthy control	42281835.1	1713954.38
KCNQ66	LLGSVVYAHSKITLTTIGYGDK	65	Healthy control	8169495.75	268892.035
KCNQ67	LLGSVVYAHSKITLTTIGYGDK	66	Healthy control	6339220.5	31482.8691

KCNQ68	LLGSVVYAHSKITLTTIGYGDK	67	Healthy control	31112216.8	555673.5
KCNQ69	LLGSVVYAHSKITLTTIGYGDK	68	Healthy control	2722024.97	86375.7578
KCNQ70	LLGSVVYAHSKITLTTIGYGDK	69	Healthy control	161329216	6478847.5
KCNQ71	LLGSVVYAHSKITLTTIGYGDK	70	Healthy spouse	5974695.5	227990.234
KCNQ72	LLGSVVYAHSKITLTTIGYGDK	71	Healthy spouse	54682689.3	4187280.97
KCNQ73	LLGSVVYAHSKITLTTIGYGDK	72	Healthy spouse	9520803	458443.656
KCNQ74	LLGSVVYAHSKITLTTIGYGDK	73	Multiple Sclerosis	207334332	9767418
KCNQ75	LLGSVVYAHSKITLTTIGYGDK	74	Multiple Sclerosis	203720336	10005152
KCNQ76	LLGSVVYAHSKITLTTIGYGDK	75	Multiple Sclerosis	54274072	2750672.25
KCNQ77	LLGSVVYAHSKITLTTIGYGDK	76	Multiple Sclerosis	45233607.1	2544211.2
KCNQ78	LLGSVVYAHSKITLTTIGYGDK	77	Multiple Sclerosis	111372112	4380524.5
KCNQ79	LLGSVVYAHSKITLTTIGYGDK	78	Multiple Sclerosis	17811950	43432.7969
KCNQ80	LLGSVVYAHSKITLTTIGYGDK	79	Multiple Sclerosis	63219008	6913868.5
KCNQ81	LLGSVVYAHSKITLTTIGYGDK	80	Multiple Sclerosis	230163281	7420674.5
KCNQ82	LLGSVVYAHSKITLTTIGYGDK	81	Multiple Sclerosis	47428508	1970931
KCNQ83	LLGSVVYAHSKITLTTIGYGDK	82	Multiple Sclerosis	6353641.81	339469.281
MYO18A	TLPKPGSPGK	1	ALS	135268746	9363231.5
MYO18A	TLPKPGSPGK	2	ALS	164015695	1944674.06
MYO18A	TLPKPGSPGK	3	ALS	83887042.5	2128279.38
MYO18A	TLPKPGSPGK	4	ALS	1765348425	562636799
MYO18A	TLPKPGSPGK	5	ALS	37309955	19548296.3
MYO18A	TLPKPGSPGK	6	ALS	136137118	5155705
MYO18A	TLPKPGSPGK	7	ALS	130362204	248299434

MYO18A	TLPKPGSPGK	8	ALS	42634854	127492525
MYO18A	TLPKPGSPGK	9	ALS	14838191.3	291112.063
MYO18A	TLPKPGSPGK	10	ALS	12399686.8	410275.875
MYO18A	TLPKPGSPGK	11	ALS	14036156.5	136438.453
MYO18A	TLPKPGSPGK	12	ALS	40314695.5	98582370.1
MYO18A	TLPKPGSPGK	13	ALS	111604366	2337729.75
MYO18A	TLPKPGSPGK	14	ALS	26785335.5	433864.469
MYO18A	TLPKPGSPGK	15	ALS	71294082.8	604074.703
MYO18A	TLPKPGSPGK	16	ALS	14295854.5	796606.525
MYO18A	TLPKPGSPGK	17	ALS	99365923.3	1356142.11
MYO18A	TLPKPGSPGK	18	ALS	15169127.5	6522272.88
MYO18A	TLPKPGSPGK	19	ALS	152680505	1802855.91
MYO18A	TLPKPGSPGK	20	ALS	132857615	2049546.5
MYO18A	TLPKPGSPGK	21	ALS	37275998	2103742.59
MYO18A	TLPKPGSPGK	22	ALS	140113496	2104045.16
MYO18A	TLPKPGSPGK	23	ALSFTD	134105478	2100122.94
MYO18A	TLPKPGSPGK	24	C9ALS	13142124	1506045.53
MYO18A	TLPKPGSPGK	25	C9ALS	1689924240	227927023
MYO18A	TLPKPGSPGK	26	C9ALS	190188929	2424441.25
MYO18A	TLPKPGSPGK	27	C9ALS	267104408	228919360
MYO18A	TLPKPGSPGK	28	C9ALS	111312289	1926467.91
MYO18A	TLPKPGSPGK	29	C9ALS	257256548	2955599.38
MYO18A	TLPKPGSPGK	30	C9ALS	13531615.5	297893.016

MYO18A	TLPKPGSPGK	31	C9ALS	9906223.5	2204658.39
MYO18A	TLPKPGSPGK	32	C9ALS	134164343	2022738.5
MYO18A	TLPKPGSPGK	33	C9ALS	54230529.8	623731.078
MYO18A	TLPKPGSPGK	34	C9ALS	32962180.8	129727.941
MYO18A	TLPKPGSPGK	35	C9ALS	19668693.8	1855086.25
MYO18A	TLPKPGSPGK	36	C9ALS	5085422.75	9643404.5
MYO18A	TLPKPGSPGK	37	C9ALSFTD	264720432	2696334.25
MYO18A	TLPKPGSPGK	38	C9ALSFTD	128834420	357626710
MYO18A	TLPKPGSPGK	39	C9ALSFTD	21790085	20907128.3
MYO18A	TLPKPGSPGK	40	C9ALSFTD	97773694	1081379
MYO18A	TLPKPGSPGK	41	C9ALSFTD	207877817	6014807.25
MYO18A	TLPKPGSPGK	42	C9ASYMPTOMATIC	137755486	1952534.25
MYO18A	TLPKPGSPGK	43	C9ASYMPTOMATIC	163243110	3250010.13
MYO18A	TLPKPGSPGK	44	C9ASYMPTOMATIC	160114675	2219323.5
MYO18A	TLPKPGSPGK	45	C9ASYMPTOMATIC	342499506	3349992.16
MYO18A	TLPKPGSPGK	46	C9ASYMPTOMATIC	162717680	2662589.5
MYO18A	TLPKPGSPGK	47	C9ASYMPTOMATIC	96790053	1688053.84

MYO18A	TLPKPGSPGK	48	C9FTD	38639928.3	480766.75
MYO18A	TLPKPGSPGK	49	C9FTD	8005584.88	2542703.08
MYO18A	TLPKPGSPGK	50	Healthy control	262013850	2994021.47
MYO18A	TLPKPGSPGK	51	Healthy control	140640792	15126844.1
MYO18A	TLPKPGSPGK	52	Healthy control	260257142	2647453.47
MYO18A	TLPKPGSPGK	53	Healthy control	302977373	3078427.45
MYO18A	TLPKPGSPGK	54	Healthy control	245327262	2525390.08
MYO18A	TLPKPGSPGK	55	Healthy control	356912072	16923157
MYO18A	TLPKPGSPGK	56	Healthy control	133849432	1422473.65
MYO18A	TLPKPGSPGK	57	Healthy control	54829344	513691.813
MYO18A	TLPKPGSPGK	58	Healthy control	177019305	2218756.48
MYO18A	TLPKPGSPGK	59	Healthy control	2908197.56	666400.188
MYO18A	TLPKPGSPGK	60	Healthy control	9244552.5	4786888.38
MYO18A	TLPKPGSPGK	61	Healthy control	98138256	1245183.02
MYO18A	TLPKPGSPGK	62	Healthy control	154186835	2563127.66
MYO18A	TLPKPGSPGK	63	Healthy control	2925228.25	349376.008
MYO18A	TLPKPGSPGK	64	Healthy control	163015518	5464351
MYO18A	TLPKPGSPGK	65	Healthy control	138348305	298079891
MYO18A	TLPKPGSPGK	66	Healthy control	3790972.5	124927.688
MYO18A	TLPKPGSPGK	67	Healthy control	245578599	2585419.75
MYO18A	TLPKPGSPGK	68	Healthy control	16457587	516888.797
MYO18A	TLPKPGSPGK	69	Healthy control	272507961	2638931.75
MYO18A	TLPKPGSPGK	70	Healthy spouse	8461399	707325.938

MYO18A	TLPKPGSPGK	71	Healthy spouse	150429368	4863653.88
MYO18A	TLPKPGSPGK	72	Healthy spouse	127223984	1913003.5
MYO18A	TLPKPGSPGK	73	Multiple Sclerosis	115874887	927469.121
MYO18A	TLPKPGSPGK	74	Multiple Sclerosis	260384272	2666785.25
MYO18A	TLPKPGSPGK	75	Multiple Sclerosis	130995720	2257056.25
MYO18A	TLPKPGSPGK	76	Multiple Sclerosis	136694554	2325307.5
MYO18A	TLPKPGSPGK	77	Multiple Sclerosis	132754424	1255542.13
MYO18A	TLPKPGSPGK	78	Multiple Sclerosis	25353422	286665.75
MYO18A	TLPKPGSPGK	79	Multiple Sclerosis	175191488	2803706
MYO18A	TLPKPGSPGK	80	Multiple Sclerosis	61385740	4811934.25
MYO18A	TLPKPGSPGK	81	Multiple Sclerosis	21278872	287349.094
MYO18A	TLPKPGSPGK	82	Multiple Sclerosis	2925393.25	313458.598
MYO18A	TLPKPGSPGK	1	ALS	2146597.75	19510.3535
MYO18A	TLPKPGSPGK	2	ALS	3116950.99	0
MYO18A	TLPKPGSPGK	3	ALS	1498649.88	67482.7109
MYO18A	EEDKTLPKPGSPGK	4	ALS	32983684.5	100989.109
MYO18A	EEDKTLPKPGSPGK	5	ALS	4493096.13	0
MYO18A	EEDKTLPKPGSPGK	6	ALS	2447825.5	0
MYO18A	EEDKTLPKPGSPGK	7	ALS	1454024.13	0
MYO18A	EEDKTLPKPGSPGK	8	ALS	4877010.5	0
MYO18A	EEDKTLPKPGSPGK	9	ALS	910717.813	18551.7305
MYO18A	EEDKTLPKPGSPGK	10	ALS	2599135.75	0
MYO18A	EEDKTLPKPGSPGK	11	ALS	13825909.1	0

MYO18A	EEDKTLPKPGSPGK	12	ALS	65616.043	0
MYO18A	EEDKTLPKPGSPGK	13	ALS	3153352.23	19450.1465
MYO18A	EEDKTLPKPGSPGK	14	ALS	1228788.88	53932.1328
MYO18A	EEDKTLPKPGSPGK	15	ALS	261676.594	9174.54883
MYO18A	EEDKTLPKPGSPGK	16	ALS	138232.887	0
MYO18A	EEDKTLPKPGSPGK	17	ALS	1037004	21540.2402
MYO18A	EEDKTLPKPGSPGK	18	ALS	1794432.13	0
MYO18A	EEDKTLPKPGSPGK	19	ALS	24880177	0
MYO18A	EEDKTLPKPGSPGK	20	ALS	1617755.38	0
MYO18A	EEDKTLPKPGSPGK	21	ALS	440002	27703.9609
MYO18A	EEDKTLPKPGSPGK	22	ALS	4117114.65	0
MYO18A	EEDKTLPKPGSPGK	23	ALSFTD	4000723	0
MYO18A	EEDKTLPKPGSPGK	24	C9ALS	79267.4805	0
MYO18A	EEDKTLPKPGSPGK	25	C9ALS	22098691.3	44645044
MYO18A	EEDKTLPKPGSPGK	26	C9ALS	538776.25	0
MYO18A	EEDKTLPKPGSPGK	27	C9ALS	2609623.25	0
MYO18A	EEDKTLPKPGSPGK	28	C9ALS	11529067.9	0
MYO18A	EEDKTLPKPGSPGK	29	C9ALS	1397925.44	0
MYO18A	EEDKTLPKPGSPGK	30	C9ALS	11779745.2	0
MYO18A	EEDKTLPKPGSPGK	31	C9ALS	54892.3972	0
MYO18A	EEDKTLPKPGSPGK	32	C9ALS	2024205.56	0
MYO18A	EEDKTLPKPGSPGK	33	C9ALS	820481.025	4521.86133
MYO18A	EEDKTLPKPGSPGK	34	C9ALS	1071358.15	88881.3828

MYO18A	EEDKTLPKPGSPGK	35	C9ALS	11506805	0
MYO18A	EEDKTLPKPGSPGK	36	C9ALS	0	0
MYO18A	EEDKTLPKPGSPGK	37	C9ALSFTD	3786114.5	0
MYO18A	EEDKTLPKPGSPGK	38	C9ALSFTD	20809.8457	0
MYO18A	EEDKTLPKPGSPGK	39	C9ALSFTD	5810140.81	38118.2383
MYO18A	EEDKTLPKPGSPGK	40	C9ALSFTD	13946734.9	0
MYO18A	EEDKTLPKPGSPGK	41	C9ALSFTD	6849501.34	23047.3496
MYO18A	EEDKTLPKPGSPGK	42	C9ASYMPTOMATIC	458873.578	0
MYO18A	EEDKTLPKPGSPGK	43	C9ASYMPTOMATIC	2324698.5	0
MYO18A	EEDKTLPKPGSPGK	44	C9ASYMPTOMATIC	14485103.3	78546.8828
MYO18A	EEDKTLPKPGSPGK	45	C9ASYMPTOMATIC	6123832.64	27381.4199
MYO18A	EEDKTLPKPGSPGK	46	C9ASYMPTOMATIC	2006852.75	0
MYO18A	EEDKTLPKPGSPGK	47	C9ASYMPTOMATIC	556141.25	0
MYO18A	EEDKTLPKPGSPGK	48	C9FTD	367958.094	0
MYO18A	EEDKTLPKPGSPGK	49	C9FTD	2874538.81	0
MYO18A	EEDKTLPKPGSPGK	50	Healthy control	6548169.5	0
MYO18A	EEDKTLPKPGSPGK	51	Healthy control	378125.813	268542.844

MYO18A	EEDKTLPKPGSPGK	52	Healthy control	1551802.75	0
MYO18A	EEDKTLPKPGSPGK	53	Healthy control	343129.613	0
MYO18A	EEDKTLPKPGSPGK	54	Healthy control	931034	87585.7188
MYO18A	EEDKTLPKPGSPGK	55	Healthy control	4556142.38	90953.9922
MYO18A	EEDKTLPKPGSPGK	56	Healthy control	1244047.1	138705.281
MYO18A	EEDKTLPKPGSPGK	57	Healthy control	401992.344	0
MYO18A	EEDKTLPKPGSPGK	58	Healthy control	13143752.9	0
MYO18A	EEDKTLPKPGSPGK	59	Healthy control	51434.9609	0
MYO18A	EEDKTLPKPGSPGK	60	Healthy control	1595308.22	30797.0117
MYO18A	EEDKTLPKPGSPGK	61	Healthy control	3181104.25	0
MYO18A	EEDKTLPKPGSPGK	62	Healthy control	2933987.25	0
MYO18A	EEDKTLPKPGSPGK	63	Healthy control	517425.957	350164.031
MYO18A	EEDKTLPKPGSPGK	64	Healthy control	2103755.83	37100.4883
MYO18A	EEDKTLPKPGSPGK	65	Healthy control	62887.5547	0
MYO18A	EEDKTLPKPGSPGK	66	Healthy control	669468.375	0
MYO18A	EEDKTLPKPGSPGK	67	Healthy control	5238353.18	0
MYO18A	EEDKTLPKPGSPGK	68	Healthy control	14149922.9	0
MYO18A	EEDKTLPKPGSPGK	69	Healthy control	1578397.63	0
MYO18A	EEDKTLPKPGSPGK	70	Healthy spouse	80797.9121	26103.1719
MYO18A	EEDKTLPKPGSPGK	71	Healthy spouse	1626563.75	0
MYO18A	EEDKTLPKPGSPGK	72	Healthy spouse	2676206	0
MYO18A	EEDKTLPKPGSPGK	73	Multiple Sclerosis	11172302.6	0
MYO18A	EEDKTLPKPGSPGK	74	Multiple Sclerosis	2121435.25	0

MYO18A	EEDKTLPKPGSPGK	75	Multiple Sclerosis	403291.031	0
MYO18A	EEDKTLPKPGSPGK	76	Multiple Sclerosis	2960306.25	0
MYO18A	EEDKTLPKPGSPGK	77	Multiple Sclerosis	548728.063	0
MYO18A	EEDKTLPKPGSPGK	78	Multiple Sclerosis	382913.656	0
MYO18A	EEDKTLPKPGSPGK	79	Multiple Sclerosis	4175971.5	0
MYO18A	EEDKTLPKPGSPGK	80	Multiple Sclerosis	297025.469	37923.0313
MYO18A	EEDKTLPKPGSPGK	81	Multiple Sclerosis	364950.75	0
MYO18A	EEDKTLPKPGSPGK	82	Multiple Sclerosis	3161387.01	0
RSF1	VLQAPPPDVGNGEGSR	1	ALS	1904628640	872317912
RSF1	VLQAPPPDVGNGEGSR	2	ALS	1938635488	927072177
RSF1	VLQAPPPDVGNGEGSR	3	ALS	985636137	32738421.1
RSF1	VLQAPPPDVGNGEGSR	4	ALS	1104267404	104217916
RSF1	VLQAPPPDVGNGEGSR	5	ALS	2114838976	4534841472
RSF1	VLQAPPPDVGNGEGSR	6	ALS	2099294016	923237094
RSF1	VLQAPPPDVGNGEGSR	7	ALS	1411962972	3968063488
RSF1	VLQAPPPDVGNGEGSR	8	ALS	1878382848	8983963136
RSF1	VLQAPPPDVGNGEGSR	9	ALS	1865435264	3512031936
RSF1	VLQAPPPDVGNGEGSR	10	ALS	1719991520	6670373632
RSF1	VLQAPPPDVGNGEGSR	11	ALS	2189840256	1509523936
RSF1	VLQAPPPDVGNGEGSR	12	ALS	1799398080	2742111744
RSF1	VLQAPPPDVGNGEGSR	13	ALS	1729144992	907820399
RSF1	VLQAPPPDVGNGEGSR	14	ALS	4937716836	255209084
RSF1	VLQAPPPDVGNGEGSR	15	ALS	3238245529	159206590

RSF1	VLQAPPPDVGNGEGSR	16	ALS	2198584928	1022895840
RSF1	VLQAPPPDVGNGEGSR	17	ALS	1208040409	19797097.8
RSF1	VLQAPPPDVGNGEGSR	18	ALS	2403060160	1022892192
RSF1	VLQAPPPDVGNGEGSR	19	ALS	1955455232	808760134
RSF1	VLQAPPPDVGNGEGSR	20	ALS	1632198768	350335476
RSF1	VLQAPPPDVGNGEGSR	21	ALS	2024987244	64365899.5
RSF1	VLQAPPPDVGNGEGSR	22	ALS	1935809120	982829517
RSF1	VLQAPPPDVGNGEGSR	23	ALSFTD	1718722208	663645516
RSF1	VLQAPPPDVGNGEGSR	24	C9ALS	1869888736	748863608
RSF1	VLQAPPPDVGNGEGSR	25	C9ALS	4070236832	649120205
RSF1	VLQAPPPDVGNGEGSR	26	C9ALS	1990756128	621682844
RSF1	VLQAPPPDVGNGEGSR	27	C9ALS	1392469760	1020835488
RSF1	VLQAPPPDVGNGEGSR	28	C9ALS	1591955584	803233585
RSF1	VLQAPPPDVGNGEGSR	29	C9ALS	3674897536	451596551
RSF1	VLQAPPPDVGNGEGSR	30	C9ALS	2009894592	807769868
RSF1	VLQAPPPDVGNGEGSR	31	C9ALS	2032102880	849836416
RSF1	VLQAPPPDVGNGEGSR	32	C9ALS	1831520224	494158462
RSF1	VLQAPPPDVGNGEGSR	33	C9ALS	1603082464	537133360
RSF1	VLQAPPPDVGNGEGSR	34	C9ALS	3963765344	786919848
RSF1	VLQAPPPDVGNGEGSR	35	C9ALS	4096524928	1132262432
RSF1	VLQAPPPDVGNGEGSR	36	C9ALS	1848120704	2834579840
RSF1	VLQAPPPDVGNGEGSR	37	C9ALSFTD	3120928512	7666377.5
RSF1	VLQAPPPDVGNGEGSR	38	C9ALSFTD	3662083318	2047293056

RSF1	VLQAPPPDVGNGEGSR	39	C9ALSFTD	4792126720	1883409920
RSF1	VLQAPPPDVGNGEGSR	40	C9ALSFTD	4476526464	854321516
RSF1	VLQAPPPDVGNGEGSR	41	C9ALSFTD	3217520955	60540292
RSF1	VLQAPPPDVGNGEGSR	42	C9ASYMPTOMATIC	1653420896	663555776
RSF1	VLQAPPPDVGNGEGSR	43	C9ASYMPTOMATIC	1745953920	578139156
RSF1	VLQAPPPDVGNGEGSR	44	C9ASYMPTOMATIC	1787460672	511603478
RSF1	VLQAPPPDVGNGEGSR	45	C9ASYMPTOMATIC	5737024640	790631047
RSF1	VLQAPPPDVGNGEGSR	46	C9ASYMPTOMATIC	1722238976	4504400.5
RSF1	VLQAPPPDVGNGEGSR	47	C9ASYMPTOMATIC	2267256448	1123673844
RSF1	VLQAPPPDVGNGEGSR	48	C9FTD	4513263648	588582400
RSF1	VLQAPPPDVGNGEGSR	49	C9FTD	3098972196	512795968
RSF1	VLQAPPPDVGNGEGSR	50	Healthy control	5060723456	962704330
RSF1	VLQAPPPDVGNGEGSR	51	Healthy control	5018945120	825653760
RSF1	VLQAPPPDVGNGEGSR	52	Healthy control	4830461360	311293581
RSF1	VLQAPPPDVGNGEGSR	53	Healthy control	5911785536	1017636063
RSF1	VLQAPPPDVGNGEGSR	54	Healthy control	5814016352	49246011
RSF1	VLQAPPPDVGNGEGSR	55	Healthy control	4325129504	641471548

RSF1	VLQAPPPDVGNGEGSR	56	Healthy control	3430245616	496177420
RSF1	VLQAPPPDVGNGEGSR	57	Healthy control	5522825216	185850576
RSF1	VLQAPPPDVGNGEGSR	58	Healthy control	4370224256	880963326
RSF1	VLQAPPPDVGNGEGSR	59	Healthy control	4175169024	7410537472
RSF1	VLQAPPPDVGNGEGSR	60	Healthy control	3919026976	1520498048
RSF1	VLQAPPPDVGNGEGSR	61	Healthy control	1638186368	684791138
RSF1	VLQAPPPDVGNGEGSR	62	Healthy control	1808276832	426702969
RSF1	VLQAPPPDVGNGEGSR	63	Healthy control	1398737376	1229082720
RSF1	VLQAPPPDVGNGEGSR	64	Healthy control	1749740672	489627180
RSF1	VLQAPPPDVGNGEGSR	65	Healthy control	1961544800	3919878912
RSF1	VLQAPPPDVGNGEGSR	66	Healthy control	1774871072	1270925216
RSF1	VLQAPPPDVGNGEGSR	67	Healthy control	5292498768	585898776
RSF1	VLQAPPPDVGNGEGSR	68	Healthy control	1788720605	1495008384
RSF1	VLQAPPPDVGNGEGSR	69	Healthy control	3808977873	102403740
RSF1	VLQAPPPDVGNGEGSR	70	Healthy spouse	2167301216	4628826112
RSF1	VLQAPPPDVGNGEGSR	71	Healthy spouse	1499613332	26274416.5
RSF1	VLQAPPPDVGNGEGSR	72	Healthy spouse	1916580992	22253918
RSF1	VLQAPPPDVGNGEGSR	73	Multiple Sclerosis	5023745184	804391422
RSF1	VLQAPPPDVGNGEGSR	74	Multiple Sclerosis	4179435776	9642244
RSF1	VLQAPPPDVGNGEGSR	75	Multiple Sclerosis	1465866368	5016671.5
RSF1	VLQAPPPDVGNGEGSR	76	Multiple Sclerosis	1367619897	28040395.5
RSF1	VLQAPPPDVGNGEGSR	77	Multiple Sclerosis	2373098240	4316122
RSF1	VLQAPPPDVGNGEGSR	78	Multiple Sclerosis	4621235200	206012240

RSF1	VLQAPPPDVGNGEGSR	79	Multiple Sclerosis	2247469824	5602643.5
RSF1	VLQAPPPDVGNGEGSR	80	Multiple Sclerosis	4203034958	52705853
RSF1	VLQAPPPDVGNGEGSR	81	Multiple Sclerosis	1443477248	3049750.75
RSF1	VLQAPPPDVGNGEGSR	82	Multiple Sclerosis	1303091529	247454972
SYT7	AINFPGAR	1	ALS	1236566698	211666.195
SYT7	AINFPGAR	2	ALS	1420528114	226154.967
SYT7	AINFPGAR	3	ALS	854433151	65466
SYT7	AINFPGAR	4	ALS	3362980335	448446.156
SYT7	AINFPGAR	5	ALS	8698208896	26311512.4
SYT7	AINFPGAR	6	ALS	1428482633	219977.391
SYT7	AINFPGAR	7	ALS	7940757616	7844314.13
SYT7	AINFPGAR	8	ALS	8531957248	12019579.3
SYT7	AINFPGAR	9	ALS	7738270000	4930006
SYT7	AINFPGAR	10	ALS	8331481536	26533391.4
SYT7	AINFPGAR	11	ALS	1.1427E+10	45408966.6
SYT7	AINFPGAR	12	ALS	1.0846E+10	31156004.4
SYT7	AINFPGAR	13	ALS	1341242059	291983.785
SYT7	AINFPGAR	14	ALS	1.0524E+10	1301238.41
SYT7	AINFPGAR	15	ALS	5628508160	721113.508
SYT7	AINFPGAR	16	ALS	4586323638	936739.309

SYT7	AINFPGAR	17	ALS	1334692413	230052.637
SYT7	AINFPGAR	18	ALS	1.0787E+10	1775783.97
SYT7	AINFPGAR	19	ALS	1616530272	3905733.53
SYT7	AINFPGAR	20	ALS	1751949548	290471.563
SYT7	AINFPGAR	21	ALS	1029335617	173158.223
SYT7	AINFPGAR	22	ALS	1513169985	252799.891
SYT7	AINFPGAR	23	ALSFTD	1375994112	227307.656
SYT7	AINFPGAR	24	C9ALS	4074712519	766715.75
SYT7	AINFPGAR	25	C9ALS	2722113408	3713566.44
SYT7	AINFPGAR	26	C9ALS	1403060544	170859.047
SYT7	AINFPGAR	27	C9ALS	8895443552	1725476.25
SYT7	AINFPGAR	28	C9ALS	1202775200	5987011.03
SYT7	AINFPGAR	29	C9ALS	2700465482	600626.617
SYT7	AINFPGAR	30	C9ALS	4010486656	20494112.8
SYT7	AINFPGAR	31	C9ALS	6160461604	1352655.72
SYT7	AINFPGAR	32	C9ALS	1417179008	161692.063
SYT7	AINFPGAR	33	C9ALS	1592457662	180533.469
SYT7	AINFPGAR	34	C9ALS	4429476381	1039246.78
SYT7	AINFPGAR	35	C9ALS	9337794097	1389003.11
SYT7	AINFPGAR	36	C9ALS	7981795136	2687983
SYT7	AINFPGAR	37	C9ALSFTD	3083936512	359670.313

SYT7	AINFPGAR	38	C9ALSFTD	1.5645E+10	6656850.25
SYT7	AINFPGAR	39	C9ALSFTD	2.0546E+10	96894075.8
SYT7	AINFPGAR	40	C9ALSFTD	3265513312	5916481.25
SYT7	AINFPGAR	41	C9ALSFTD	2920289680	551731.531
SYT7	AINFPGAR	42	C9ASYMPTOMATIC	1255186171	144908.141
SYT7	AINFPGAR	43	C9ASYMPTOMATIC	1321990274	275353.125
SYT7	AINFPGAR	44	C9ASYMPTOMATIC	1630703692	276246.438
SYT7	AINFPGAR	45	C9ASYMPTOMATIC	3007575746	476702.707
SYT7	AINFPGAR	46	C9ASYMPTOMATIC	1575942144	243585.797
SYT7	AINFPGAR	47	C9ASYMPTOMATIC	1723437824	212880.703
SYT7	AINFPGAR	48	C9FTD	5265911325	868470.625
SYT7	AINFPGAR	49	C9FTD	1.6631E+10	2810362.25
SYT7	AINFPGAR	50	Healthy control	2719539736	450972.602
SYT7	AINFPGAR	51	Healthy control	1027992564	26200211.3

SYT7	AINFPGAR	52	Healthy control	22656556.5	1549839.75
SYT7	AINFPGAR	53	Healthy control	2838509278	467794.031
SYT7	AINFPGAR	54	Healthy control	12213525.3	1209525.07
SYT7	AINFPGAR	55	Healthy control	2004886688	455329.188
SYT7	AINFPGAR	56	Healthy control	2827944901	380086.625
SYT7	AINFPGAR	57	Healthy control	10216966	2691153.5
SYT7	AINFPGAR	58	Healthy control	271681065	7939600.75
SYT7	AINFPGAR	59	Healthy control	1.7822E+10	4259694.13
SYT7	AINFPGAR	60	Healthy control	1.6338E+10	3680932.13
SYT7	AINFPGAR	61	Healthy control	1276456328	349222.711
SYT7	AINFPGAR	62	Healthy control	1273958538	367091.543
SYT7	AINFPGAR	63	Healthy control	1.1827E+10	139774572
SYT7	AINFPGAR	64	Healthy control	1726539494	237739.25
SYT7	AINFPGAR	65	Healthy control	8899924556	3605631.5
SYT7	AINFPGAR	66	Healthy control	5960217562	880705.73
SYT7	AINFPGAR	67	Healthy control	5895584032	11128807.7
SYT7	AINFPGAR	68	Healthy control	1.1035E+10	42608355.5
SYT7	AINFPGAR	69	Healthy control	3237943133	403134
SYT7	AINFPGAR	70	Healthy spouse	5269901384	4799333.69

SYT7	AINFPGAR	71	Healthy spouse	1163872774	87899.3672
SYT7	AINFPGAR	72	Healthy spouse	2150664960	378152.25
SYT7	AINFPGAR	73	Multiple Sclerosis	312906566	5656247
SYT7	AINFPGAR	74	Multiple Sclerosis	14276656	1669715.38
SYT7	AINFPGAR	75	Multiple Sclerosis	1263158144	107623.203
SYT7	AINFPGAR	76	Multiple Sclerosis	1303991227	114228.734
SYT7	AINFPGAR	77	Multiple Sclerosis	5949099.5	1942844.75
SYT7	AINFPGAR	78	Multiple Sclerosis	7185075712	914378.813
SYT7	AINFPGAR	79	Multiple Sclerosis	1985311104	320401.344
SYT7	AINFPGAR	80	Multiple Sclerosis	6508564.5	2194621.27
SYT7	AINFPGAR	81	Multiple Sclerosis	1495801984	141069.688
SYT7	AINFPGAR	82	Multiple Sclerosis	2370433636	1115828.56
SYNE1	LANVFEQPVAEQIER	1	ALS	2726758756	44564.7656
SYNE1	LANVFEQPVAEQIER	2	ALS	2920014960	59037.8281
SYNE1	LANVFEQPVAEQIER	3	ALS	1494812624	0
SYNE1	LANVFEQPVAEQIER	4	ALS	3050462330	62182.6406
SYNE1	LANVFEQPVAEQIER	5	ALS	2592792328	43253.1406
SYNE1	LANVFEQPVAEQIER	6	ALS	3298117360	55343.3203
SYNE1	LANVFEQPVAEQIER	7	ALS	2932410850	48402.2031
SYNE1	LANVFEQPVAEQIER	8	ALS	2835867840	87792.2969
SYNE1	LANVFEQPVAEQIER	9	ALS	2453322368	34151.1563
SYNE1	LANVFEQPVAEQIER	10	ALS	2947549812	52711.8711
SYNE1	LANVFEQPVAEQIER	11	ALS	3288958728	51821.5625

SYNE1	LANVFEQPVAEQIER	12	ALS	3235646814	83586.6094
SYNE1	LANVFEQPVAEQIER	13	ALS	2070139048	26004.7227
SYNE1	LANVFEQPVAEQIER	14	ALS	7575931544	188636.766
SYNE1	LANVFEQPVAEQIER	15	ALS	5859955784	130190.313
SYNE1	LANVFEQPVAEQIER	16	ALS	4486065788	115065.602
SYNE1	LANVFEQPVAEQIER	17	ALS	2504330784	21669.6211
SYNE1	LANVFEQPVAEQIER	18	ALS	4738315932	113414
SYNE1	LANVFEQPVAEQIER	19	ALS	3031790392	65861.2109
SYNE1	LANVFEQPVAEQIER	20	ALS	2413160964	61423.7617
SYNE1	LANVFEQPVAEQIER	21	ALS	3327343072	79714.4844
SYNE1	LANVFEQPVAEQIER	22	ALS	2890556284	58577.7383
SYNE1	LANVFEQPVAEQIER	23	ALSFTD	3282221806	58894.9727
SYNE1	LANVFEQPVAEQIER	24	C9ALS	2814101156	53406.9609
SYNE1	LANVFEQPVAEQIER	25	C9ALS	5356633560	121249.898
SYNE1	LANVFEQPVAEQIER	26	C9ALS	3852956816	26310.7051
SYNE1	LANVFEQPVAEQIER	27	C9ALS	4402817144	25519.0527
SYNE1	LANVFEQPVAEQIER	28	C9ALS	2657372736	71600.4297
SYNE1	LANVFEQPVAEQIER	29	C9ALS	5957223458	193835.5
SYNE1	LANVFEQPVAEQIER	30	C9ALS	946046608	51454.582
SYNE1	LANVFEQPVAEQIER	31	C9ALS	3336678582	55788.543
SYNE1	LANVFEQPVAEQIER	32	C9ALS	2919345522	56617.9297
SYNE1	LANVFEQPVAEQIER	33	C9ALS	2058529978	29444.9063
SYNE1	LANVFEQPVAEQIER	34	C9ALS	6782216928	152864.344

SYNE1	LANVFEQPVAEQIER	35	C9ALS	5260871212	107644.727
SYNE1	LANVFEQPVAEQIER	36	C9ALS	3035317768	51786.082
SYNE1	LANVFEQPVAEQIER	37	C9ALSFTD	5205036032	114663.922
SYNE1	LANVFEQPVAEQIER	38	C9ALSFTD	6086882232	131617.094
SYNE1	LANVFEQPVAEQIER	39	C9ALSFTD	8447906924	195800.328
SYNE1	LANVFEQPVAEQIER	40	C9ALSFTD	6633382420	102197.172
SYNE1	LANVFEQPVAEQIER	41	C9ALSFTD	5586328360	90981.5703
SYNE1	LANVFEQPVAEQIER	42	C9ASYMPTOMATIC	2638212862	57474.2305
SYNE1	LANVFEQPVAEQIER	43	C9ASYMPTOMATIC	2728261436	54104.0781
SYNE1	LANVFEQPVAEQIER	44	C9ASYMPTOMATIC	3799751272	73242.8438
SYNE1	LANVFEQPVAEQIER	45	C9ASYMPTOMATIC	7526135532	192709.078
SYNE1	LANVFEQPVAEQIER	46	C9ASYMPTOMATIC	3248995840	45899.8164
SYNE1	LANVFEQPVAEQIER	47	C9ASYMPTOMATIC	3120359728	77138.2031
SYNE1	LANVFEQPVAEQIER	48	C9FTD	6767803300	139059.453
SYNE1	LANVFEQPVAEQIER	49	C9FTD	6421460116	94098.9063
SYNE1	LANVFEQPVAEQIER	50	Healthy control	7117151064	190608.391
SYNE1	LANVFEQPVAEQIER	51	Healthy control	6840793356	128316.758

SYNE1	LANVFEQPVAEQIER	52	Healthy control	5683446992	96032.2266
SYNE1	LANVFEQPVAEQIER	53	Healthy control	5344841180	181699.563
SYNE1	LANVFEQPVAEQIER	54	Healthy control	5945721824	167696.859
SYNE1	LANVFEQPVAEQIER	55	Healthy control	4450640128	145628.047
SYNE1	LANVFEQPVAEQIER	56	Healthy control	5998455776	99112.5547
SYNE1	LANVFEQPVAEQIER	57	Healthy control	5946445824	70058.1484
SYNE1	LANVFEQPVAEQIER	58	Healthy control	5758964348	92631.5
SYNE1	LANVFEQPVAEQIER	59	Healthy control	8585859800	149622.219
SYNE1	LANVFEQPVAEQIER	60	Healthy control	5849304902	151655.563
SYNE1	LANVFEQPVAEQIER	61	Healthy control	2887157918	59113.6797
SYNE1	LANVFEQPVAEQIER	62	Healthy control	2828424946	78297.2344
SYNE1	LANVFEQPVAEQIER	63	Healthy control	3211565376	92336.6016
SYNE1	LANVFEQPVAEQIER	64	Healthy control	2573526788	53957.6602
SYNE1	LANVFEQPVAEQIER	65	Healthy control	3352298022	35244.2773
SYNE1	LANVFEQPVAEQIER	66	Healthy control	3181508544	60777.1328
SYNE1	LANVFEQPVAEQIER	67	Healthy control	6534635320	177951.656
SYNE1	LANVFEQPVAEQIER	68	Healthy control	2792690060	66702.8281
SYNE1	LANVFEQPVAEQIER	69	Healthy control	4389911086	146766.047
SYNE1	LANVFEQPVAEQIER	70	Healthy spouse	3875752616	85978.5859
SYNE1	LANVFEQPVAEQIER	71	Healthy spouse	2901211640	66672.4219
SYNE1	LANVFEQPVAEQIER	72	Healthy spouse	3739020544	78897.5938
SYNE1	LANVFEQPVAEQIER	73	Multiple Sclerosis	7170773536	171639.766
SYNE1	LANVFEQPVAEQIER	74	Multiple Sclerosis	6434611200	104534.758

SYNE1	LANVFEQPVAEQIER	75	Multiple Sclerosis	2529570304	96555.6328
SYNE1	LANVFEQPVAEQIER	76	Multiple Sclerosis	2537443162	65646.7813
SYNE1	LANVFEQPVAEQIER	77	Multiple Sclerosis	2765132288	43686.6563
SYNE1	LANVFEQPVAEQIER	78	Multiple Sclerosis	7282222592	158778.453
SYNE1	LANVFEQPVAEQIER	79	Multiple Sclerosis	3855362816	100710.828
SYNE1	LANVFEQPVAEQIER	80	Multiple Sclerosis	6710488024	117101.633
SYNE1	LANVFEQPVAEQIER	81	Multiple Sclerosis	2980333312	84702.5469
SYNE1	LANVFEQPVAEQIER	82	Multiple Sclerosis	2903721936	93978.22
CAMK2B	VPRNLLPVHFWGFEFFPR	1	ALS	4321667.77	17240.3789
CAMK2B	VPRNLLPVHFWGFEFFPR	2	ALS	49528630.5	0
CAMK2B	VPRNLLPVHFWGFEFFPR	3	ALS	135555411	55588.1016
CAMK2B	VPRNLLPVHFWGFEFFPR	4	ALS	151625527	95358.1641
CAMK2B	VPRNLLPVHFWGFEFFPR	5	ALS	1163928.47	0
CAMK2B	VPRNLLPVHFWGFEFFPR	6	ALS	62648786.3	7176.84131
CAMK2B	VPRNLLPVHFWGFEFFPR	7	ALS	7400238.38	0
CAMK2B	VPRNLLPVHFWGFEFFPR	8	ALS	1163756.38	0
CAMK2B	VPRNLLPVHFWGFEFFPR	9	ALS	725522.078	0
CAMK2B	VPRNLLPVHFWGFEFFPR	10	ALS	126729349	99251.1192
CAMK2B	VPRNLLPVHFWGFEFFPR	11	ALS	117893781	92414.4297
CAMK2B	VPRNLLPVHFWGFEFFPR	12	ALS	21736574	204809.422
CAMK2B	VPRNLLPVHFWGFEFFPR	13	ALS	176656132	28689.0195
CAMK2B	VPRNLLPVHFWGFEFFPR	14	ALS	494619557	0
CAMK2B	VPRNLLPVHFWGFEFFPR	15	ALS	518548896	0

CAMK2B	VPRNLLPVHFWGFEFFPR	16	ALS	183809067	4657.08594
CAMK2B	VPRNLLPVHFWGFEFFPR	17	ALS	149487336	85899.9551
CAMK2B	VPRNLLPVHFWGFEFFPR	18	ALS	151931493	62049.9063
CAMK2B	VPRNLLPVHFWGFEFFPR	19	ALS	156319782	234771.422
CAMK2B	VPRNLLPVHFWGFEFFPR	20	ALS	206467184	94223.3516
CAMK2B	VPRNLLPVHFWGFEFFPR	21	ALS	224873606	37266.9727
CAMK2B	VPRNLLPVHFWGFEFFPR	22	ALS	201054419	1340.14356
CAMK2B	VPRNLLPVHFWGFEFFPR	23	ALSFTD	166232128	0
CAMK2B	VPRNLLPVHFWGFEFFPR	24	C9ALS	164182006	0
CAMK2B	VPRNLLPVHFWGFEFFPR	25	C9ALS	624585466	14180.4981
CAMK2B	VPRNLLPVHFWGFEFFPR	26	C9ALS	180190245	0
CAMK2B	VPRNLLPVHFWGFEFFPR	27	C9ALS	282330819	0
CAMK2B	VPRNLLPVHFWGFEFFPR	28	C9ALS	158188540	0
CAMK2B	VPRNLLPVHFWGFEFFPR	29	C9ALS	560364865	0
CAMK2B	VPRNLLPVHFWGFEFFPR	30	C9ALS	198289801	111110.457
CAMK2B	VPRNLLPVHFWGFEFFPR	31	C9ALS	173038993	27537.2402
CAMK2B	VPRNLLPVHFWGFEFFPR	32	C9ALS	204357130	66654.9453
CAMK2B	VPRNLLPVHFWGFEFFPR	33	C9ALS	172369330	60740.9805
CAMK2B	VPRNLLPVHFWGFEFFPR	34	C9ALS	563330320	211476.516
CAMK2B	VPRNLLPVHFWGFEFFPR	35	C9ALS	172610706	549.99707
CAMK2B	VPRNLLPVHFWGFEFFPR	36	C9ALS	28103254.5	150342.875
CAMK2B	VPRNLLPVHFWGFEFFPR	37	C9ALSFTD	627701312	5468.60547
CAMK2B	VPRNLLPVHFWGFEFFPR	38	C9ALSFTD	226127902	0

CAMK2B	VPRNLLPVHFWGFEFFPR	39	C9ALSFTD	493809970	0
CAMK2B	VPRNLLPVHFWGFEFFPR	40	C9ALSFTD	642936040	7631.86768
CAMK2B	VPRNLLPVHFWGFEFFPR	41	C9ALSFTD	568071015	23824.7285
CAMK2B	VPRNLLPVHFWGFEFFPR	42	C9ASYMPTOMATIC	201471448	0
CAMK2B	VPRNLLPVHFWGFEFFPR	43	C9ASYMPTOMATIC	189297168	0
CAMK2B	VPRNLLPVHFWGFEFFPR	44	C9ASYMPTOMATIC	222804363	64872.4023
CAMK2B	VPRNLLPVHFWGFEFFPR	45	C9ASYMPTOMATIC	563320167	0
CAMK2B	VPRNLLPVHFWGFEFFPR	46	C9ASYMPTOMATIC	190006944	36346.8984
CAMK2B	VPRNLLPVHFWGFEFFPR	47	C9ASYMPTOMATIC	194291354	59714.7813
CAMK2B	VPRNLLPVHFWGFEFFPR	48	C9FTD	584569789	6567.36035
CAMK2B	VPRNLLPVHFWGFEFFPR	49	C9FTD	169738687	0
CAMK2B	VPRNLLPVHFWGFEFFPR	50	Healthy control	478413318	7449.58398
CAMK2B	VPRNLLPVHFWGFEFFPR	51	Healthy control	383177614	52043.7148
CAMK2B	VPRNLLPVHFWGFEFFPR	52	Healthy control	512929867	364103.469
CAMK2B	VPRNLLPVHFWGFEFFPR	53	Healthy control	407439386	0
CAMK2B	VPRNLLPVHFWGFEFFPR	54	Healthy control	549324343	254848.344
CAMK2B	VPRNLLPVHFWGFEFFPR	55	Healthy control	516891514	0

CAMK2B	VPRNLLPVHFWGFEFFPR	56	Healthy control	463154402	28964.0547
CAMK2B	VPRNLLPVHFWGFEFFPR	57	Healthy control	441652736	92326.2109
CAMK2B	VPRNLLPVHFWGFEFFPR	58	Healthy control	537049804	41361.5938
CAMK2B	VPRNLLPVHFWGFEFFPR	59	Healthy control	8433233.19	175669.188
CAMK2B	VPRNLLPVHFWGFEFFPR	60	Healthy control	368040390	0
CAMK2B	VPRNLLPVHFWGFEFFPR	61	Healthy control	164145948	83504.3438
CAMK2B	VPRNLLPVHFWGFEFFPR	62	Healthy control	155026513	22354.3594
CAMK2B	VPRNLLPVHFWGFEFFPR	63	Healthy control	156004066	141455.938
CAMK2B	VPRNLLPVHFWGFEFFPR	64	Healthy control	192746335	64820.6973
CAMK2B	VPRNLLPVHFWGFEFFPR	65	Healthy control	2735415.63	0
CAMK2B	VPRNLLPVHFWGFEFFPR	66	Healthy control	146446237	293396.594
CAMK2B	VPRNLLPVHFWGFEFFPR	67	Healthy control	604153545	779901.063
CAMK2B	VPRNLLPVHFWGFEFFPR	68	Healthy control	147014710	104191.945
CAMK2B	VPRNLLPVHFWGFEFFPR	69	Healthy control	553637098	128681.719
CAMK2B	VPRNLLPVHFWGFEFFPR	70	Healthy spouse	5087939	54303.875
CAMK2B	VPRNLLPVHFWGFEFFPR	71	Healthy spouse	201213795	103885.117
CAMK2B	VPRNLLPVHFWGFEFFPR	72	Healthy spouse	117357176	0
CAMK2B	VPRNLLPVHFWGFEFFPR	73	Multiple Sclerosis	448570684	106864.352
CAMK2B	VPRNLLPVHFWGFEFFPR	74	Multiple Sclerosis	421786144	16941.5684
CAMK2B	VPRNLLPVHFWGFEFFPR	75	Multiple Sclerosis	193753408	0
CAMK2B	VPRNLLPVHFWGFEFFPR	76	Multiple Sclerosis	218357214	0
CAMK2B	VPRNLLPVHFWGFEFFPR	77	Multiple Sclerosis	327201280	0
CAMK2B	VPRNLLPVHFWGFEFFPR	78	Multiple Sclerosis	487622368	20296.6231

CAMK2B	VPRNLLPVHFWGFEFFPR	79	Multiple Sclerosis	277904832	0
CAMK2B	VPRNLLPVHFWGFEFFPR	80	Multiple Sclerosis	411852325	467771.375
CAMK2B	VPRNLLPVHFWGFEFFPR	81	Multiple Sclerosis	173765664	20384.7109
CAMK2B	VPRNLLPVHFWGFEFFPR	82	Multiple Sclerosis	63292409.8	0
CAMK2B	VTERSAGSAETSPTGRVPR	1	ALS	264507.875	0
CAMK2B	VTERSAGSAETSPTGRVPR	2	ALS	270974.734	0
CAMK2B	VTERSAGSAETSPTGRVPR	3	ALS	306378.328	0
CAMK2B	VTERSAGSAETSPTGRVPR	4	ALS	1705294.93	0
CAMK2B	VTERSAGSAETSPTGRVPR	5	ALS	116929.43	0
CAMK2B	VTERSAGSAETSPTGRVPR	6	ALS	529232.785	0
CAMK2B	VTERSAGSAETSPTGRVPR	7	ALS	242132.438	0
CAMK2B	VTERSAGSAETSPTGRVPR	8	ALS	365232.789	0
CAMK2B	VTERSAGSAETSPTGRVPR	9	ALS	0	127340.945
CAMK2B	VTERSAGSAETSPTGRVPR	10	ALS	0	0
CAMK2B	VTERSAGSAETSPTGRVPR	11	ALS	3229926.06	0
CAMK2B	VTERSAGSAETSPTGRVPR	12	ALS	2087516.25	0
CAMK2B	VTERSAGSAETSPTGRVPR	13	ALS	20822.2402	51189.5195
CAMK2B	VTERSAGSAETSPTGRVPR	14	ALS	220458.5	0
CAMK2B	VTERSAGSAETSPTGRVPR	15	ALS	1848406.66	0
CAMK2B	VTERSAGSAETSPTGRVPR	16	ALS	24816.3574	0
CAMK2B	VTERSAGSAETSPTGRVPR	17	ALS	19851.8398	0
CAMK2B	VTERSAGSAETSPTGRVPR	18	ALS	22848.2461	25710.7734
CAMK2B	VTERSAGSAETSPTGRVPR	19	ALS	2225758	0

CAMK2B	VTERSAGSAETSPTGRVPR	20	ALS	6794019.25	0
CAMK2B	VTERSAGSAETSPTGRVPR	21	ALS	20445.916	0
CAMK2B	VTERSAGSAETSPTGRVPR	22	ALS	44952.2617	11495.3848
CAMK2B	VTERSAGSAETSPTGRVPR	23	ALSFTD	112996.305	0
CAMK2B	VTERSAGSAETSPTGRVPR	24	C9ALS	83103.2617	0
CAMK2B	VTERSAGSAETSPTGRVPR	25	C9ALS	25421953	26956.3457
CAMK2B	VTERSAGSAETSPTGRVPR	26	C9ALS	0	0
CAMK2B	VTERSAGSAETSPTGRVPR	27	C9ALS	2788126.25	23457.0156
CAMK2B	VTERSAGSAETSPTGRVPR	28	C9ALS	853446.375	40355.3906
CAMK2B	VTERSAGSAETSPTGRVPR	29	C9ALS	0	0
CAMK2B	VTERSAGSAETSPTGRVPR	30	C9ALS	1049304.7	0
CAMK2B	VTERSAGSAETSPTGRVPR	31	C9ALS	43776.2656	0
CAMK2B	VTERSAGSAETSPTGRVPR	32	C9ALS	269476.438	0
CAMK2B	VTERSAGSAETSPTGRVPR	33	C9ALS	4337493.5	0
CAMK2B	VTERSAGSAETSPTGRVPR	34	C9ALS	5760195.63	0
CAMK2B	VTERSAGSAETSPTGRVPR	35	C9ALS	4622936.75	0
CAMK2B	VTERSAGSAETSPTGRVPR	36	C9ALS	42902.7031	56427.7656
CAMK2B	VTERSAGSAETSPTGRVPR	37	C9ALSFTD	32405.7598	0
CAMK2B	VTERSAGSAETSPTGRVPR	38	C9ALSFTD	1105111.97	0
CAMK2B	VTERSAGSAETSPTGRVPR	39	C9ALSFTD	1036157.8	0
CAMK2B	VTERSAGSAETSPTGRVPR	40	C9ALSFTD	245658.75	0
CAMK2B	VTERSAGSAETSPTGRVPR	41	C9ALSFTD	331261.578	0

CAMK2B	VTERSAGSAETSPTGRVPR	42	C9ASYMPTOMATIC	35585.8008	0
CAMK2B	VTERSAGSAETSPTGRVPR	43	C9ASYMPTOMATIC	307329.273	0
CAMK2B	VTERSAGSAETSPTGRVPR	44	C9ASYMPTOMATIC	230862.469	0
CAMK2B	VTERSAGSAETSPTGRVPR	45	C9ASYMPTOMATIC	90777.5313	0
CAMK2B	VTERSAGSAETSPTGRVPR	46	C9ASYMPTOMATIC	45319.5664	0
CAMK2B	VTERSAGSAETSPTGRVPR	47	C9ASYMPTOMATIC	0	0
CAMK2B	VTERSAGSAETSPTGRVPR	48	C9FTD	4277330.94	0
CAMK2B	VTERSAGSAETSPTGRVPR	49	C9FTD	325092.781	0
CAMK2B	VTERSAGSAETSPTGRVPR	50	Healthy control	0	0
CAMK2B	VTERSAGSAETSPTGRVPR	51	Healthy control	1037630.85	0
CAMK2B	VTERSAGSAETSPTGRVPR	52	Healthy control	0	0
CAMK2B	VTERSAGSAETSPTGRVPR	53	Healthy control	0	0
CAMK2B	VTERSAGSAETSPTGRVPR	54	Healthy control	69082.9922	0
CAMK2B	VTERSAGSAETSPTGRVPR	55	Healthy control	44306.1211	0
CAMK2B	VTERSAGSAETSPTGRVPR	56	Healthy control	0	0
CAMK2B	VTERSAGSAETSPTGRVPR	57	Healthy control	10905166	0
CAMK2B	VTERSAGSAETSPTGRVPR	58	Healthy control	540742.25	227811.875

CAMK2B	VTERSAGSAETSPTGRVPR	59	Healthy control	0	0
CAMK2B	VTERSAGSAETSPTGRVPR	60	Healthy control	1062351.88	0
CAMK2B	VTERSAGSAETSPTGRVPR	61	Healthy control	120571.064	0
CAMK2B	VTERSAGSAETSPTGRVPR	62	Healthy control	82702.4063	0
CAMK2B	VTERSAGSAETSPTGRVPR	63	Healthy control	278765.094	0
CAMK2B	VTERSAGSAETSPTGRVPR	64	Healthy control	3493683.75	0
CAMK2B	VTERSAGSAETSPTGRVPR	65	Healthy control	1776097.87	0
CAMK2B	VTERSAGSAETSPTGRVPR	66	Healthy control	5770160	0
CAMK2B	VTERSAGSAETSPTGRVPR	67	Healthy control	513008.969	0
CAMK2B	VTERSAGSAETSPTGRVPR	68	Healthy control	616677.563	0
CAMK2B	VTERSAGSAETSPTGRVPR	69	Healthy control	83378.1719	0
CAMK2B	VTERSAGSAETSPTGRVPR	70	Healthy spouse	7860808.75	0
CAMK2B	VTERSAGSAETSPTGRVPR	71	Healthy spouse	0	0
CAMK2B	VTERSAGSAETSPTGRVPR	72	Healthy spouse	23635.2988	0
CAMK2B	VTERSAGSAETSPTGRVPR	73	Multiple Sclerosis	815356.875	0
CAMK2B	VTERSAGSAETSPTGRVPR	74	Multiple Sclerosis	0	0
CAMK2B	VTERSAGSAETSPTGRVPR	75	Multiple Sclerosis	69868.3203	0
CAMK2B	VTERSAGSAETSPTGRVPR	76	Multiple Sclerosis	1057877.79	0
CAMK2B	VTERSAGSAETSPTGRVPR	77	Multiple Sclerosis	0	0
CAMK2B	VTERSAGSAETSPTGRVPR	78	Multiple Sclerosis	22094.4746	0
CAMK2B	VTERSAGSAETSPTGRVPR	79	Multiple Sclerosis	338711.594	0
CAMK2B	VTERSAGSAETSPTGRVPR	80	Multiple Sclerosis	0	0
CAMK2B	VTERSAGSAETSPTGRVPR	81	Multiple Sclerosis	0	0

CAMK2B	VTERSAGSAETSPTGRVPR	82	Multiple Sclerosis	31273.5352	0
MYO18A	EEGAAKTEEQIAAEEAWNETEK	1	ALS	114342576	0
MYO18A	EEGAAKTEEQIAAEEAWNETEK	2	ALS	125339651	0
MYO18A	EEGAAKTEEQIAAEEAWNETEK	3	ALS	80938572	0
MYO18A	EEGAAKTEEQIAAEEAWNETEK	4	ALS	10802486.7	0
MYO18A	EEGAAKTEEQIAAEEAWNETEK	5	ALS	2127337.5	0
MYO18A	EEGAAKTEEQIAAEEAWNETEK	6	ALS	81725163	0
MYO18A	EEGAAKTEEQIAAEEAWNETEK	7	ALS	12492211	0
MYO18A	EEGAAKTEEQIAAEEAWNETEK	8	ALS	2380593.15	0
MYO18A	EEGAAKTEEQIAAEEAWNETEK	9	ALS	1978979.59	0
MYO18A	EEGAAKTEEQIAAEEAWNETEK	10	ALS	268273.125	0
MYO18A	EEGAAKTEEQIAAEEAWNETEK	11	ALS	3749981.13	0

MYO18A	EEGAAKTEEQIAAEEAWNETEK	12	ALS	3176147.05	0
MYO18A	EEGAAKTEEQIAAEEAWNETEK	13	ALS	101700564	0
MYO18A	EEGAAKTEEQIAAEEAWNETEK	14	ALS	14900588.4	0
MYO18A	EEGAAKTEEQIAAEEAWNETEK	15	ALS	15920985.3	27857.5664
MYO18A	EEGAAKTEEQIAAEEAWNETEK	16	ALS	8108750	0
MYO18A	EEGAAKTEEQIAAEEAWNETEK	17	ALS	75916281.5	0
MYO18A	EEGAAKTEEQIAAEEAWNETEK	18	ALS	3529077.61	0
MYO18A	EEGAAKTEEQIAAEEAWNETEK	19	ALS	103544079	0
MYO18A	EEGAAKTEEQIAAEEAWNETEK	20	ALS	70100171.5	0
MYO18A	EEGAAKTEEQIAAEEAWNETEK	21	ALS	159057414	0
MYO18A	EEGAAKTEEQIAAEEAWNETEK	22	ALS	107479509	0

MYO18A	EEGAAKTEEQIAAEEAWNETEK	23	ALSFTD	94800900	0
MYO18A	EEGAAKTEEQIAAEEAWNETEK	24	C9ALS	7028543.75	0
MYO18A	EEGAAKTEEQIAAEEAWNETEK	25	C9ALS	432752997	0
MYO18A	EEGAAKTEEQIAAEEAWNETEK	26	C9ALS	93960713	0
MYO18A	EEGAAKTEEQIAAEEAWNETEK	27	C9ALS	6460483.41	0
MYO18A	EEGAAKTEEQIAAEEAWNETEK	28	C9ALS	97349807	0
MYO18A	EEGAAKTEEQIAAEEAWNETEK	29	C9ALS	491513633	0
MYO18A	EEGAAKTEEQIAAEEAWNETEK	30	C9ALS	12016654	0
MYO18A	EEGAAKTEEQIAAEEAWNETEK	31	C9ALS	1771878.38	0
MYO18A	EEGAAKTEEQIAAEEAWNETEK	32	C9ALS	96000574	14016.7481
MYO18A	EEGAAKTEEQIAAEEAWNETEK	33	C9ALS	6461667.75	0

MYO18A	EEGAAKTEEQIAAEEAWNETEK	34	C9ALS	87659439.5	1536.97974
MYO18A	EEGAAKTEEQIAAEEAWNETEK	35	C9ALS	13440984.1	9638.88184
MYO18A	EEGAAKTEEQIAAEEAWNETEK	36	C9ALS	4486777.77	0
MYO18A	EEGAAKTEEQIAAEEAWNETEK	37	C9ALSFTD	432419488	0
MYO18A	EEGAAKTEEQIAAEEAWNETEK	38	C9ALSFTD	9742280	805.838562
MYO18A	EEGAAKTEEQIAAEEAWNETEK	39	C9ALSFTD	22309589.1	17678.8457
MYO18A	EEGAAKTEEQIAAEEAWNETEK	40	C9ALSFTD	307450017	0
MYO18A	EEGAAKTEEQIAAEEAWNETEK	41	C9ALSFTD	263856355	26868.5488
MYO18A	EEGAAKTEEQIAAEEAWNETEK	42	C9ASYMPTOMATIC	71224097.3	0
MYO18A	EEGAAKTEEQIAAEEAWNETEK	43	C9ASYMPTOMATIC	99313151	0
MYO18A	EEGAAKTEEQIAAEEAWNETEK	44	C9ASYMPTOMATIC	136492892	0

MYO18A	EEGAAKTEEQIAAEEAWNETEK	45	C9ASYMPTOMATIC	521026438	0
MYO18A	EEGAAKTEEQIAAEEAWNETEK	46	C9ASYMPTOMATIC	104745448	0
MYO18A	EEGAAKTEEQIAAEEAWNETEK	47	C9ASYMPTOMATIC	92418896.5	0
MYO18A	EEGAAKTEEQIAAEEAWNETEK	48	C9FTD	41994870	0
MYO18A	EEGAAKTEEQIAAEEAWNETEK	49	C9FTD	48870400.3	0
MYO18A	EEGAAKTEEQIAAEEAWNETEK	50	Healthy control	487343377	0
MYO18A	EEGAAKTEEQIAAEEAWNETEK	51	Healthy control	33381636.3	0
MYO18A	EEGAAKTEEQIAAEEAWNETEK	52	Healthy control	633922126	0
MYO18A	EEGAAKTEEQIAAEEAWNETEK	53	Healthy control	578141095	43428.2148
MYO18A	EEGAAKTEEQIAAEEAWNETEK	54	Healthy control	729513083	0
MYO18A	EEGAAKTEEQIAAEEAWNETEK	55	Healthy control	521811461	0

MYO18A	EEGAAKTEEQIAAEEAWNETEK	56	Healthy control	504125672	0
MYO18A	EEGAAKTEEQIAAEEAWNETEK	57	Healthy control	15440142	0
MYO18A	EEGAAKTEEQIAAEEAWNETEK	58	Healthy control	541029108	0
MYO18A	EEGAAKTEEQIAAEEAWNETEK	59	Healthy control	72881203.1	0
MYO18A	EEGAAKTEEQIAAEEAWNETEK	60	Healthy control	12537859	0
MYO18A	EEGAAKTEEQIAAEEAWNETEK	61	Healthy control	83982024.5	0
MYO18A	EEGAAKTEEQIAAEEAWNETEK	62	Healthy control	109874939	0
MYO18A	EEGAAKTEEQIAAEEAWNETEK	63	Healthy control	12773867.9	0
MYO18A	EEGAAKTEEQIAAEEAWNETEK	64	Healthy control	67972681.5	0
MYO18A	EEGAAKTEEQIAAEEAWNETEK	65	Healthy control	12512623.9	0
MYO18A	EEGAAKTEEQIAAEEAWNETEK	66	Healthy control	16456612	0

MYO18A	EEGAAKTEEQIAAEEAWNETEK	67	Healthy control	105734236	0
MYO18A	EEGAAKTEEQIAAEEAWNETEK	68	Healthy control	4421683.94	0
MYO18A	EEGAAKTEEQIAAEEAWNETEK	69	Healthy control	453354041	0
MYO18A	EEGAAKTEEQIAAEEAWNETEK	70	Healthy spouse	2000631.47	0
MYO18A	EEGAAKTEEQIAAEEAWNETEK	71	Healthy spouse	110960941	0
MYO18A	EEGAAKTEEQIAAEEAWNETEK	72	Healthy spouse	37983320	0
MYO18A	EEGAAKTEEQIAAEEAWNETEK	73	Multiple Sclerosis	568411112	0
MYO18A	EEGAAKTEEQIAAEEAWNETEK	74	Multiple Sclerosis	617688192	0
MYO18A	EEGAAKTEEQIAAEEAWNETEK	75	Multiple Sclerosis	117953440	0
MYO18A	EEGAAKTEEQIAAEEAWNETEK	76	Multiple Sclerosis	82953127	0
MYO18A	EEGAAKTEEQIAAEEAWNETEK	77	Multiple Sclerosis	369069472	0

MYO18A	EEGAAKTEEQIAAEEAWNETEK	78	Multiple Sclerosis	48326424	0
MYO18A	EEGAAKTEEQIAAEEAWNETEK	79	Multiple Sclerosis	137564688	0
MYO18A	EEGAAKTEEQIAAEEAWNETEK	80	Multiple Sclerosis	538143528	70140.7734
MYO18A	EEGAAKTEEQIAAEEAWNETEK	81	Multiple Sclerosis	109419072	0
MYO18A	EEGAAKTEEQIAAEEAWNETEK	82	Multiple Sclerosis	4283788.48	0
RSF1	KPCSSYGFEGYR	1	ALS	101529095	5912336
RSF1	KPCSSYGFEGYR	2	ALS	120159426	7136006.5
RSF1	KPCSSYGFEGYR	3	ALS	63809930	3633272.63
RSF1	KPCSSYGFEGYR	4	ALS	57630196	4271570.69
RSF1	KPCSSYGFEGYR	5	ALS	138195501	7973453.31
RSF1	KPCSSYGFEGYR	6	ALS	136216693	6989574
RSF1	KPCSSYGFEGYR	7	ALS	151151955	8725303
RSF1	KPCSSYGFEGYR	8	ALS	119264136	7169287.91
RSF1	KPCSSYGFEGYR	9	ALS	144584972	7002755.64
RSF1	KPCSSYGFEGYR	10	ALS	149681793	8505933
RSF1	KPCSSYGFEGYR	11	ALS	20038679	1052688.78
RSF1	KPCSSYGFEGYR	12	ALS	65277702.1	3441648.75
RSF1	KPCSSYGFEGYR	13	ALS	92423635.6	5505275.6

RSF1	KPCSSYGFEGYR	14	ALS	437676384	18957513.3
RSF1	KPCSSYGFEGYR	15	ALS	370767808	16273804.3
RSF1	KPCSSYGFEGYR	16	ALS	146090336	7697706.5
RSF1	KPCSSYGFEGYR	17	ALS	87499433	4393031.41
RSF1	KPCSSYGFEGYR	18	ALS	36998689.1	2461621.41
RSF1	KPCSSYGFEGYR	19	ALS	128068408	6948004.11
RSF1	KPCSSYGFEGYR	20	ALS	114911784	6571301.38
RSF1	KPCSSYGFEGYR	21	ALS	1280597.88	199128.578
RSF1	KPCSSYGFEGYR	22	ALS	158855040	8672317.06
RSF1	KPCSSYGFEGYR	23	ALSFTD	131055080	6990920.5
RSF1	KPCSSYGFEGYR	24	C9ALS	60400569.2	4146381
RSF1	KPCSSYGFEGYR	25	C9ALS	216671054	11862372.1
RSF1	KPCSSYGFEGYR	26	C9ALS	119142505	6621707.5
RSF1	KPCSSYGFEGYR	27	C9ALS	44977996	3510734.44
RSF1	KPCSSYGFEGYR	28	C9ALS	76864076	4333785.27
RSF1	KPCSSYGFEGYR	29	C9ALS	264188089	11737149
RSF1	KPCSSYGFEGYR	30	C9ALS	74087768.5	4711568.5
RSF1	KPCSSYGFEGYR	31	C9ALS	123952888	6903858
RSF1	KPCSSYGFEGYR	32	C9ALS	94631860.1	5454490
RSF1	KPCSSYGFEGYR	33	C9ALS	81157134.7	4409157.5
RSF1	KPCSSYGFEGYR	34	C9ALS	356396512	16654392.1
RSF1	KPCSSYGFEGYR	35	C9ALS	207040114	10246140
RSF1	KPCSSYGFEGYR	36	C9ALS	99485980.4	5985979.64

RSF1	KPCSSYGFEGYR	37	C9ALSFTD	388740480	15909715
RSF1	KPCSSYGFEGYR	38	C9ALSFTD	367758336	18666571.6
RSF1	KPCSSYGFEGYR	39	C9ALSFTD	485317172	24089876.8
RSF1	KPCSSYGFEGYR	40	C9ALSFTD	56125041	2331407
RSF1	KPCSSYGFEGYR	41	C9ALSFTD	320717920	15568762.8
RSF1	KPCSSYGFEGYR	42	C9ASYMPTOMATIC	95257871.2	4900254.5
RSF1	KPCSSYGFEGYR	43	C9ASYMPTOMATIC	103557294	6103991.48
RSF1	KPCSSYGFEGYR	44	C9ASYMPTOMATIC	105392032	5712383.5
RSF1	KPCSSYGFEGYR	45	C9ASYMPTOMATIC	408588279	19822362
RSF1	KPCSSYGFEGYR	46	C9ASYMPTOMATIC	117871832	6062255
RSF1	KPCSSYGFEGYR	47	C9ASYMPTOMATIC	26895567	1400607.75
RSF1	KPCSSYGFEGYR	48	C9FTD	42165371	1830995.25
RSF1	KPCSSYGFEGYR	49	C9FTD	456479764	20747560
RSF1	KPCSSYGFEGYR	50	Healthy control	362097664	14356750.9
RSF1	KPCSSYGFEGYR	51	Healthy control	315924630	15336107.6
RSF1	KPCSSYGFEGYR	52	Healthy control	313380416	15998830.1
RSF1	KPCSSYGFEGYR	53	Healthy control	435678691	21805708

RSF1	KPCSSYGFEGYR	54	Healthy control	211796152	9128144
RSF1	KPCSSYGFEGYR	55	Healthy control	297781824	13827867.6
RSF1	KPCSSYGFEGYR	56	Healthy control	98683484	5015636.5
RSF1	KPCSSYGFEGYR	57	Healthy control	204075440	9216749
RSF1	KPCSSYGFEGYR	58	Healthy control	119222607	5583760.27
RSF1	KPCSSYGFEGYR	59	Healthy control	80108046.3	3305448.6
RSF1	KPCSSYGFEGYR	60	Healthy control	316132071	16727959
RSF1	KPCSSYGFEGYR	61	Healthy control	54795726.4	3012950.25
RSF1	KPCSSYGFEGYR	62	Healthy control	158044576	9887064
RSF1	KPCSSYGFEGYR	63	Healthy control	91453544	6575899.64
RSF1	KPCSSYGFEGYR	64	Healthy control	163747232	7784356.16
RSF1	KPCSSYGFEGYR	65	Healthy control	135979745	6669003.48
RSF1	KPCSSYGFEGYR	66	Healthy control	64451885	5739216
RSF1	KPCSSYGFEGYR	67	Healthy control	559770937	27087732.5
RSF1	KPCSSYGFEGYR	68	Healthy control	170800302	8942548
RSF1	KPCSSYGFEGYR	69	Healthy control	332935904	16317297.2
RSF1	KPCSSYGFEGYR	70	Healthy spouse	801379.813	278258.606
RSF1	KPCSSYGFEGYR	71	Healthy spouse	124647736	6842708.42
RSF1	KPCSSYGFEGYR	72	Healthy spouse	152095968	8260791.5
RSF1	KPCSSYGFEGYR	73	Multiple Sclerosis	34851819	1496297.88
RSF1	KPCSSYGFEGYR	74	Multiple Sclerosis	290149024	13620383
RSF1	KPCSSYGFEGYR	75	Multiple Sclerosis	103435424	6470748.5
RSF1	KPCSSYGFEGYR	76	Multiple Sclerosis	88223435.4	5464214.5

RSF1	KPCSSYGFEGYR	77	Multiple Sclerosis	155925728	7776097
RSF1	KPCSSYGFEGYR	78	Multiple Sclerosis	152580192	7074840.5
RSF1	KPCSSYGFEGYR	79	Multiple Sclerosis	115022936	5522257.5
RSF1	KPCSSYGFEGYR	80	Multiple Sclerosis	20688074	655510.778
RSF1	KPCSSYGFEGYR	81	Multiple Sclerosis	4782734	390731.156
RSF1	KPCSSYGFEGYR	82	Multiple Sclerosis	2130764.99	358787.195
SLC24A3	EEWMDGWIANFHR	1	ALS	861748161	36447.0508
SLC24A3	EEWMDGWIANFHR	2	ALS	1091177322	0
SLC24A3	EEWMDGWIANFHR	3	ALS	639644571	0
SLC24A3	EEWMDGWIANFHR	4	ALS	1932291584	454098.781
SLC24A3	EEWMDGWIANFHR	5	ALS	1129336440	81585.3359
SLC24A3	EEWMDGWIANFHR	6	ALS	1309913319	526948.625
SLC24A3	EEWMDGWIANFHR	7	ALS	1527937855	0
SLC24A3	EEWMDGWIANFHR	8	ALS	1258596152	27031.8145
SLC24A3	EEWMDGWIANFHR	9	ALS	1347652655	0
SLC24A3	EEWMDGWIANFHR	10	ALS	1169823858	37954.5
SLC24A3	EEWMDGWIANFHR	11	ALS	1499270803	33102.1953
SLC24A3	EEWMDGWIANFHR	12	ALS	1626020901	23114.1563
SLC24A3	EEWMDGWIANFHR	13	ALS	1339455258	21374.9434
SLC24A3	EEWMDGWIANFHR	14	ALS	3185491959	897563.219
SLC24A3	EEWMDGWIANFHR	15	ALS	2610242274	0
SLC24A3	EEWMDGWIANFHR	16	ALS	1843699917	348012.406
SLC24A3	EEWMDGWIANFHR	17	ALS	880907109	501549.188

SLC24A3	EEWMDGWIANFHR	18	ALS	2208370904	349921.887
SLC24A3	EEWMDGWIANFHR	19	ALS	1155093976	171239.242
SLC24A3	EEWMDGWIANFHR	20	ALS	1602249088	71920.0859
SLC24A3	EEWMDGWIANFHR	21	ALS	1574514610	1329865.38
SLC24A3	EEWMDGWIANFHR	22	ALS	1393636396	7322.59668
SLC24A3	EEWMDGWIANFHR	23	ALSFTD	1033499884	642005.188
SLC24A3	EEWMDGWIANFHR	24	C9ALS	1241010788	672404.625
SLC24A3	EEWMDGWIANFHR	25	C9ALS	2356756292	919836.813
SLC24A3	EEWMDGWIANFHR	26	C9ALS	1268972087	0
SLC24A3	EEWMDGWIANFHR	27	C9ALS	2337275106	330228.281
SLC24A3	EEWMDGWIANFHR	28	C9ALS	1003618162	364678.125
SLC24A3	EEWMDGWIANFHR	29	C9ALS	2739971328	0
SLC24A3	EEWMDGWIANFHR	30	C9ALS	1670334726	329309.688
SLC24A3	EEWMDGWIANFHR	31	C9ALS	1509510944	1598421.63
SLC24A3	EEWMDGWIANFHR	32	C9ALS	1442491941	1337943.06
SLC24A3	EEWMDGWIANFHR	33	C9ALS	1074569088	136581.422
SLC24A3	EEWMDGWIANFHR	34	C9ALS	2524100235	0
SLC24A3	EEWMDGWIANFHR	35	C9ALS	1689413251	0
SLC24A3	EEWMDGWIANFHR	36	C9ALS	1531840937	29273.1016
SLC24A3	EEWMDGWIANFHR	37	C9ALSFTD	2554100224	85499.8516
SLC24A3	EEWMDGWIANFHR	38	C9ALSFTD	2886035579	0
SLC24A3	EEWMDGWIANFHR	39	C9ALSFTD	3044444737	1399518.88
SLC24A3	EEWMDGWIANFHR	40	C9ALSFTD	1570536965	24724.5762

SLC24A3	EEWMDGWIANFHR	41	C9ALSFTD	2991743695	0
SLC24A3	EEWMDGWIANFHR	42	C9ASYMPTOMATIC	1159842932	2274698.5
SLC24A3	EEWMDGWIANFHR	43	C9ASYMPTOMATIC	1185442549	57210.293
SLC24A3	EEWMDGWIANFHR	44	C9ASYMPTOMATIC	1703962251	176327.078
SLC24A3	EEWMDGWIANFHR	45	C9ASYMPTOMATIC	2906887005	77743.0313
SLC24A3	EEWMDGWIANFHR	46	C9ASYMPTOMATIC	1184011392	1577106.88
SLC24A3	EEWMDGWIANFHR	47	C9ASYMPTOMATIC	1364090822	576852.938
SLC24A3	EEWMDGWIANFHR	48	C9FTD	3320898160	42914.4336
SLC24A3	EEWMDGWIANFHR	49	C9FTD	2294469520	0
SLC24A3	EEWMDGWIANFHR	50	Healthy control	2466557879	0
SLC24A3	EEWMDGWIANFHR	51	Healthy control	2689974394	0
SLC24A3	EEWMDGWIANFHR	52	Healthy control	2278958332	184245.094
SLC24A3	EEWMDGWIANFHR	53	Healthy control	2774923916	0
SLC24A3	EEWMDGWIANFHR	54	Healthy control	2978649369	23161.5195
SLC24A3	EEWMDGWIANFHR	55	Healthy control	2442324480	0
SLC24A3	EEWMDGWIANFHR	56	Healthy control	2414529001	0
SLC24A3	EEWMDGWIANFHR	57	Healthy control	2919698176	0

SLC24A3	EEWMDGWIANFHR	58	Healthy control	2516281950	2203093
SLC24A3	EEWMDGWIANFHR	59	Healthy control	3164723773	1276291.69
SLC24A3	EEWMDGWIANFHR	60	Healthy control	3116588288	51126.2031
SLC24A3	EEWMDGWIANFHR	61	Healthy control	1332856832	365654.375
SLC24A3	EEWMDGWIANFHR	62	Healthy control	1492515296	0
SLC24A3	EEWMDGWIANFHR	63	Healthy control	1455610608	327524.813
SLC24A3	EEWMDGWIANFHR	64	Healthy control	1786182215	42890.3438
SLC24A3	EEWMDGWIANFHR	65	Healthy control	1672934083	886940.188
SLC24A3	EEWMDGWIANFHR	66	Healthy control	1298970394	2371618.75
SLC24A3	EEWMDGWIANFHR	67	Healthy control	3356211438	81813.6016
SLC24A3	EEWMDGWIANFHR	68	Healthy control	1437664768	176476.172
SLC24A3	EEWMDGWIANFHR	69	Healthy control	2493570101	0
SLC24A3	EEWMDGWIANFHR	70	Healthy spouse	2010927495	642187.625
SLC24A3	EEWMDGWIANFHR	71	Healthy spouse	1265571252	1844998.63
SLC24A3	EEWMDGWIANFHR	72	Healthy spouse	1306388096	0
SLC24A3	EEWMDGWIANFHR	73	Multiple Sclerosis	2719276882	751186.25
SLC24A3	EEWMDGWIANFHR	74	Multiple Sclerosis	2794760192	0
SLC24A3	EEWMDGWIANFHR	75	Multiple Sclerosis	1177950464	0
SLC24A3	EEWMDGWIANFHR	76	Multiple Sclerosis	1227375608	0
SLC24A3	EEWMDGWIANFHR	77	Multiple Sclerosis	1346186624	0
SLC24A3	EEWMDGWIANFHR	78	Multiple Sclerosis	3087630080	814556.063
SLC24A3	EEWMDGWIANFHR	79	Multiple Sclerosis	1894068224	0
SLC24A3	EEWMDGWIANFHR	80	Multiple Sclerosis	2865463607	196315.016

SLC24A3	EEWMDGWIANFHR	81	Multiple Sclerosis	1082850304	311278.281
SLC24A3	EEWMDGWIANFHR	82	Multiple Sclerosis	1136151634	0
SYT7	AINFPGARLQSAA	1	ALS	3562051.69	857682.25
SYT7	AINFPGARLQSAA	2	ALS	4183987.38	761013.031
SYT7	AINFPGARLQSAA	3	ALS	3838528.94	879453.813
SYT7	AINFPGARLQSAA	4	ALS	4952563.69	433159.839
SYT7	AINFPGARLQSAA	5	ALS	312857.781	3278956.75
SYT7	AINFPGARLQSAA	6	ALS	4483786	1909995.41
SYT7	AINFPGARLQSAA	7	ALS	2087700	955920.828
SYT7	AINFPGARLQSAA	8	ALS	0	1356951.87
SYT7	AINFPGARLQSAA	9	ALS	1628115.38	809506
SYT7	AINFPGARLQSAA	10	ALS	95448.7891	2139826.77
SYT7	AINFPGARLQSAA	11	ALS	3068285.86	933179.172
SYT7	AINFPGARLQSAA	12	ALS	716026.563	584912.563
SYT7	AINFPGARLQSAA	13	ALS	4001028.25	1863094.56
SYT7	AINFPGARLQSAA	14	ALS	7129805	400307.703
SYT7	AINFPGARLQSAA	15	ALS	7235331.75	2188628.79
SYT7	AINFPGARLQSAA	16	ALS	3804136.5	876729.734
SYT7	AINFPGARLQSAA	17	ALS	3917586	1060263.84
SYT7	AINFPGARLQSAA	18	ALS	2075939.5	483784.687
SYT7	AINFPGARLQSAA	19	ALS	3783424.88	1171011.84
SYT7	AINFPGARLQSAA	20	ALS	4947473.5	1077418.97
SYT7	AINFPGARLQSAA	21	ALS	4262493	759650.488

SYT7	AINFPGARLQSAA	22	ALS	3682720.88	2232116.69
SYT7	AINFPGARLQSAA	23	ALSFTD	3393962.25	789062.031
SYT7	AINFPGARLQSAA	24	C9ALS	3034589.13	459643.672
SYT7	AINFPGARLQSAA	25	C9ALS	6575684.88	133552.029
SYT7	AINFPGARLQSAA	26	C9ALS	3965082.75	580088.906
SYT7	AINFPGARLQSAA	27	C9ALS	5449191.25	976964.156
SYT7	AINFPGARLQSAA	28	C9ALS	4447360.5	832839.563
SYT7	AINFPGARLQSAA	29	C9ALS	6918207.75	3061783.13
SYT7	AINFPGARLQSAA	30	C9ALS	4635408.13	694000.875
SYT7	AINFPGARLQSAA	31	C9ALS	2575575.81	368189.918
SYT7	AINFPGARLQSAA	32	C9ALS	2757749.5	697789.406
SYT7	AINFPGARLQSAA	33	C9ALS	3021402.5	293379.511
SYT7	AINFPGARLQSAA	34	C9ALS	8474611.5	3252520.56
SYT7	AINFPGARLQSAA	35	C9ALS	4020737.5	1099079.37
SYT7	AINFPGARLQSAA	36	C9ALS	844477.688	376680.844
SYT7	AINFPGARLQSAA	37	C9ALSFTD	5406120.5	476731.938
SYT7	AINFPGARLQSAA	38	C9ALSFTD	1993616.25	165677.102
SYT7	AINFPGARLQSAA	39	C9ALSFTD	2894293.56	1321074.06
SYT7	AINFPGARLQSAA	40	C9ALSFTD	7618323	1073733.97
SYT7	AINFPGARLQSAA	41	C9ALSFTD	6614905.75	1214413.84
SYT7	AINFPGARLQSAA	42	C9ASYMPTOMATIC	2657966.13	521544.188

SYT7	AINFPGARLQSAA	43	C9ASYMPTOMATIC	3007539.13	657587.75
SYT7	AINFPGARLQSAA	44	C9ASYMPTOMATIC	3515810.38	982223.625
SYT7	AINFPGARLQSAA	45	C9ASYMPTOMATIC	9639187.75	537563.689
SYT7	AINFPGARLQSAA	46	C9ASYMPTOMATIC	1318467.75	674237.25
SYT7	AINFPGARLQSAA	47	C9ASYMPTOMATIC	4297217.5	1306706.72
SYT7	AINFPGARLQSAA	48	C9FTD	7938788	1742793.72
SYT7	AINFPGARLQSAA	49	C9FTD	2739125.19	758508.477
SYT7	AINFPGARLQSAA	50	Healthy control	8795928.25	4309692
SYT7	AINFPGARLQSAA	51	Healthy control	7987702.25	376277.148
SYT7	AINFPGARLQSAA	52	Healthy control	6553840.38	512769.32
SYT7	AINFPGARLQSAA	53	Healthy control	7131189.75	1056242.35
SYT7	AINFPGARLQSAA	54	Healthy control	7188387.5	212172.602
SYT7	AINFPGARLQSAA	55	Healthy control	7097512.25	1457882.12
SYT7	AINFPGARLQSAA	56	Healthy control	7194940.5	898458.965
SYT7	AINFPGARLQSAA	57	Healthy control	5173217.5	115860.883
SYT7	AINFPGARLQSAA	58	Healthy control	9242709	1074557.23
SYT7	AINFPGARLQSAA	59	Healthy control	1408908.25	211429.731
SYT7	AINFPGARLQSAA	60	Healthy control	1457085.57	2916077.95

SYT7	AINFPGARLQSAA	61	Healthy control	5062335.5	1472321.03
SYT7	AINFPGARLQSAA	62	Healthy control	2384806	1167214.94
SYT7	AINFPGARLQSAA	63	Healthy control	1199732.63	703755.531
SYT7	AINFPGARLQSAA	64	Healthy control	3347608.75	546321.641
SYT7	AINFPGARLQSAA	65	Healthy control	2125678.25	108182.074
SYT7	AINFPGARLQSAA	66	Healthy control	3373115.63	557365
SYT7	AINFPGARLQSAA	67	Healthy control	7223877.88	2821837.83
SYT7	AINFPGARLQSAA	68	Healthy control	2447272.34	867771.906
SYT7	AINFPGARLQSAA	69	Healthy control	6093427.75	994902.719
SYT7	AINFPGARLQSAA	70	Healthy spouse	53302.6797	2809097.32
SYT7	AINFPGARLQSAA	71	Healthy spouse	4148641	747406.625
SYT7	AINFPGARLQSAA	72	Healthy spouse	956146.938	248866.219
SYT7	AINFPGARLQSAA	73	Multiple Sclerosis	6994199	1086662
SYT7	AINFPGARLQSAA	74	Multiple Sclerosis	4311444.5	293115.125
SYT7	AINFPGARLQSAA	75	Multiple Sclerosis	1191472.75	528212.75
SYT7	AINFPGARLQSAA	76	Multiple Sclerosis	3679765.5	887241.406
SYT7	AINFPGARLQSAA	77	Multiple Sclerosis	2998794.25	20999.0078
SYT7	AINFPGARLQSAA	78	Multiple Sclerosis	3550097	183078.828
SYT7	AINFPGARLQSAA	79	Multiple Sclerosis	1724114.63	663505.938
SYT7	AINFPGARLQSAA	80	Multiple Sclerosis	7267675.75	668019.563
SYT7	AINFPGARLQSAA	81	Multiple Sclerosis	1091602.88	443559.156
SYT7	AINFPGARLQSAA	82	Multiple Sclerosis	2227045.56	200648.128
IGLON5	MPSPHSLALVQPAGHGLQR	1	ALS	54001982.9	314502.219

IGLON5	MPSPHSLALVQPAGHGLQR	2	ALS	79349489.3	377702.188
IGLON5	MPSPHSLALVQPAGHGLQR	3	ALS	29635213.5	319180.852
IGLON5	MPSPHSLALVQPAGHGLQR	4	ALS	71965855.7	462933.625
IGLON5	MPSPHSLALVQPAGHGLQR	5	ALS	67157310.9	815088.219
IGLON5	MPSPHSLALVQPAGHGLQR	6	ALS	68710513.5	116860.805
IGLON5	MPSPHSLALVQPAGHGLQR	7	ALS	57125138.3	537980.805
IGLON5	MPSPHSLALVQPAGHGLQR	8	ALS	68599060.6	811010.922
IGLON5	MPSPHSLALVQPAGHGLQR	9	ALS	78989022.2	509468.117
IGLON5	MPSPHSLALVQPAGHGLQR	10	ALS	78718832	277234.805
IGLON5	MPSPHSLALVQPAGHGLQR	11	ALS	47012646.3	985040.469
IGLON5	MPSPHSLALVQPAGHGLQR	12	ALS	52808823	177305.27
IGLON5	MPSPHSLALVQPAGHGLQR	13	ALS	47264669.4	150220.072
IGLON5	MPSPHSLALVQPAGHGLQR	14	ALS	127204046	798509.148
IGLON5	MPSPHSLALVQPAGHGLQR	15	ALS	94779969.1	517767.297
IGLON5	MPSPHSLALVQPAGHGLQR	16	ALS	59637463.8	834685.875
IGLON5	MPSPHSLALVQPAGHGLQR	17	ALS	41515491.3	289762.188
IGLON5	MPSPHSLALVQPAGHGLQR	18	ALS	68582676.1	651171.453
IGLON5	MPSPHSLALVQPAGHGLQR	19	ALS	46348963.6	659456.563
IGLON5	MPSPHSLALVQPAGHGLQR	20	ALS	41884533.9	456750.75
IGLON5	MPSPHSLALVQPAGHGLQR	21	ALS	57074147.3	343538.938
IGLON5	MPSPHSLALVQPAGHGLQR	22	ALS	51127659.6	248918.437
IGLON5	MPSPHSLALVQPAGHGLQR	23	ALSFTD	37479656.3	211508.668
IGLON5	MPSPHSLALVQPAGHGLQR	24	C9ALS	47021022.3	48170.1289

IGLON5	MPSPHSLALVQPAGHGLQR	25	C9ALS	80500593.5	1465807.5
IGLON5	MPSPHSLALVQPAGHGLQR	26	C9ALS	46656336.2	619726.639
IGLON5	MPSPHSLALVQPAGHGLQR	27	C9ALS	110637018	182063.484
IGLON5	MPSPHSLALVQPAGHGLQR	28	C9ALS	38495072.1	814918.125
IGLON5	MPSPHSLALVQPAGHGLQR	29	C9ALS	80882208.9	643044.962
IGLON5	MPSPHSLALVQPAGHGLQR	30	C9ALS	46387709.9	746965.047
IGLON5	MPSPHSLALVQPAGHGLQR	31	C9ALS	50068303.2	647403.371
IGLON5	MPSPHSLALVQPAGHGLQR	32	C9ALS	46499366.6	286399.473
IGLON5	MPSPHSLALVQPAGHGLQR	33	C9ALS	35861956.3	769879.209
IGLON5	MPSPHSLALVQPAGHGLQR	34	C9ALS	73048176.6	1376024.93
IGLON5	MPSPHSLALVQPAGHGLQR	35	C9ALS	64568832.9	57563.3125
IGLON5	MPSPHSLALVQPAGHGLQR	36	C9ALS	47645971.3	991693.773
IGLON5	MPSPHSLALVQPAGHGLQR	37	C9ALSFTD	73634936	603146.75
IGLON5	MPSPHSLALVQPAGHGLQR	38	C9ALSFTD	71490389.9	1845440
IGLON5	MPSPHSLALVQPAGHGLQR	39	C9ALSFTD	117406464	1432963.59
IGLON5	MPSPHSLALVQPAGHGLQR	40	C9ALSFTD	85899913.3	151167.063
IGLON5	MPSPHSLALVQPAGHGLQR	41	C9ALSFTD	88465519.8	283344.727
IGLON5	MPSPHSLALVQPAGHGLQR	42	C9ASYMPTOMATIC	42651856	381455.375
IGLON5	MPSPHSLALVQPAGHGLQR	43	C9ASYMPTOMATIC	45753618.8	751187.543
IGLON5	MPSPHSLALVQPAGHGLQR	44	C9ASYMPTOMATIC	56124411.3	19199.6816

IGLON5	MPSPHSLALVQPAGHGLQR	45	C9ASYMPTOMATIC	88092580.9	898399.367
IGLON5	MPSPHSLALVQPAGHGLQR	46	C9ASYMPTOMATIC	46912564	199530.625
IGLON5	MPSPHSLALVQPAGHGLQR	47	C9ASYMPTOMATIC	49561207	71842.584
IGLON5	MPSPHSLALVQPAGHGLQR	48	C9FTD	107764857	378927.852
IGLON5	MPSPHSLALVQPAGHGLQR	49	C9FTD	74368218	1006304.21
IGLON5	MPSPHSLALVQPAGHGLQR	50	Healthy control	84238868.8	187249.828
IGLON5	MPSPHSLALVQPAGHGLQR	51	Healthy control	83720369	1696810.14
IGLON5	MPSPHSLALVQPAGHGLQR	52	Healthy control	79193017.1	550906.297
IGLON5	MPSPHSLALVQPAGHGLQR	53	Healthy control	87329281.6	719500.719
IGLON5	MPSPHSLALVQPAGHGLQR	54	Healthy control	98931269	94477.7617
IGLON5	MPSPHSLALVQPAGHGLQR	55	Healthy control	72730003.4	149057.105
IGLON5	MPSPHSLALVQPAGHGLQR	56	Healthy control	83819077.5	299291.125
IGLON5	MPSPHSLALVQPAGHGLQR	57	Healthy control	88790112	78266.9375
IGLON5	MPSPHSLALVQPAGHGLQR	58	Healthy control	66681912.2	222178.316
IGLON5	MPSPHSLALVQPAGHGLQR	59	Healthy control	85402328	369437.703
IGLON5	MPSPHSLALVQPAGHGLQR	60	Healthy control	107055054	660059.477
IGLON5	MPSPHSLALVQPAGHGLQR	61	Healthy control	43640236.4	413038.906
IGLON5	MPSPHSLALVQPAGHGLQR	62	Healthy control	43987652.2	166851.063
IGLON5	MPSPHSLALVQPAGHGLQR	63	Healthy control	69986004.6	1116580.21
IGLON5	MPSPHSLALVQPAGHGLQR	64	Healthy control	51242342.3	897819.105

IGLON5	MPSPHSLALVQPAGHGLQR	65	Healthy control	52793116.9	638892.232
IGLON5	MPSPHSLALVQPAGHGLQR	66	Healthy control	77464037	989118.953
IGLON5	MPSPHSLALVQPAGHGLQR	67	Healthy control	115133247	1057119.84
IGLON5	MPSPHSLALVQPAGHGLQR	68	Healthy control	51916616.9	677435.875
IGLON5	MPSPHSLALVQPAGHGLQR	69	Healthy control	96145910.6	730079.887
IGLON5	MPSPHSLALVQPAGHGLQR	70	Healthy spouse	45669284.7	205330.812
IGLON5	MPSPHSLALVQPAGHGLQR	71	Healthy spouse	43716215.6	460445.25
IGLON5	MPSPHSLALVQPAGHGLQR	72	Healthy spouse	58422896	204076.25
IGLON5	MPSPHSLALVQPAGHGLQR	73	Multiple Sclerosis	76655108	483474.344
IGLON5	MPSPHSLALVQPAGHGLQR	74	Multiple Sclerosis	70846128	237904.203
IGLON5	MPSPHSLALVQPAGHGLQR	75	Multiple Sclerosis	42067408	36640.3672
IGLON5	MPSPHSLALVQPAGHGLQR	76	Multiple Sclerosis	42313826.7	153029.453
IGLON5	MPSPHSLALVQPAGHGLQR	77	Multiple Sclerosis	36296376	338618.406
IGLON5	MPSPHSLALVQPAGHGLQR	78	Multiple Sclerosis	90553216	551825
IGLON5	MPSPHSLALVQPAGHGLQR	79	Multiple Sclerosis	59206504	114642.141
IGLON5	MPSPHSLALVQPAGHGLQR	80	Multiple Sclerosis	78364167.4	64868.4883
IGLON5	MPSPHSLALVQPAGHGLQR	81	Multiple Sclerosis	49152536	56265.4688
IGLON5	MPSPHSLALVQPAGHGLQR	82	Multiple Sclerosis	50597374.2	517423.109
PXDN	WAGETLEK	1	ALS	133051919	5372504.5
PXDN	WAGETLEK	2	ALS	145101889	5791270.5
PXDN	WAGETLEK	3	ALS	124189269	3751032.94
PXDN	WAGETLEK	4	ALS	208350710	4330660.43
PXDN	WAGETLEK	5	ALS	118446739	3902834.75

PXDN	WAGETLEK	6	ALS	70611043.8	1622299
PXDN	WAGETLEK	7	ALS	243881475	10473540.8
PXDN	WAGETLEK	8	ALS	204707986	35117051
PXDN	WAGETLEK	9	ALS	138113089	1409936.25
PXDN	WAGETLEK	10	ALS	297987983	7056387.5
PXDN	WAGETLEK	11	ALS	8658483.25	4958125.5
PXDN	WAGETLEK	12	ALS	6215057.81	842854.375
PXDN	WAGETLEK	13	ALS	8390108	355561.609
PXDN	WAGETLEK	14	ALS	967393499	4477836.5
PXDN	WAGETLEK	15	ALS	1259628126	3971436
PXDN	WAGETLEK	16	ALS	22435472	0
PXDN	WAGETLEK	17	ALS	5257997.19	489427.344
PXDN	WAGETLEK	18	ALS	6611180.13	1264188.88
PXDN	WAGETLEK	19	ALS	284469018	6228812.5
PXDN	WAGETLEK	20	ALS	12945701.3	2163214
PXDN	WAGETLEK	21	ALS	8810958.63	5037429
PXDN	WAGETLEK	22	ALS	16349233	465424.875
PXDN	WAGETLEK	23	ALSFTD	33181363.3	250271.672
PXDN	WAGETLEK	24	C9ALS	76016884.8	913690.75
PXDN	WAGETLEK	25	C9ALS	128446438	57703052
PXDN	WAGETLEK	26	C9ALS	7460689	160741.844
PXDN	WAGETLEK	27	C9ALS	116346756	1014774.66
PXDN	WAGETLEK	28	C9ALS	5003234.05	0

PXDN	WAGETLEK	29	C9ALS	12895433	1109745.38
PXDN	WAGETLEK	30	C9ALS	51513082.5	0
PXDN	WAGETLEK	31	C9ALS	216998538	1783979.5
PXDN	WAGETLEK	32	C9ALS	19790445.8	0
PXDN	WAGETLEK	33	C9ALS	122908198	240115.984
PXDN	WAGETLEK	34	C9ALS	476382455	3063265.56
PXDN	WAGETLEK	35	C9ALS	1180129311	366613.781
PXDN	WAGETLEK	36	C9ALS	84679440.8	2369418.06
PXDN	WAGETLEK	37	C9ALSFTD	148884864	0
PXDN	WAGETLEK	38	C9ALSFTD	66772250	14620145
PXDN	WAGETLEK	39	C9ALSFTD	1331764248	34965062.8
PXDN	WAGETLEK	40	C9ALSFTD	174872884	98944528
PXDN	WAGETLEK	41	C9ALSFTD	834134569	3363828.75
PXDN	WAGETLEK	42	C9ASYMPTOMATIC	5397172	682038.563
PXDN	WAGETLEK	43	C9ASYMPTOMATIC	169553186	6009.54785
PXDN	WAGETLEK	44	C9ASYMPTOMATIC	252159837	1301900.56
PXDN	WAGETLEK	45	C9ASYMPTOMATIC	172523659	670304.078
PXDN	WAGETLEK	46	C9ASYMPTOMATIC	8578743	0

PXDN	WAGETLEK	47	C9ASYMPTOMATIC	4641468.88	256970.141
PXDN	WAGETLEK	48	C9FTD	24519511.6	494652.281
PXDN	WAGETLEK	49	C9FTD	1057173540	10557574.5
PXDN	WAGETLEK	50	Healthy control	37875027.6	0
PXDN	WAGETLEK	51	Healthy control	284263954	199697424
PXDN	WAGETLEK	52	Healthy control	15957244	9135998
PXDN	WAGETLEK	53	Healthy control	47654162	1157602.13
PXDN	WAGETLEK	54	Healthy control	8465061	4027498.25
PXDN	WAGETLEK	55	Healthy control	23312796	5212685.5
PXDN	WAGETLEK	56	Healthy control	10028911.3	5716642
PXDN	WAGETLEK	57	Healthy control	3753259	0
PXDN	WAGETLEK	58	Healthy control	46833096	5285186
PXDN	WAGETLEK	59	Healthy control	45682152.4	560132.875
PXDN	WAGETLEK	60	Healthy control	1574718166	12456137.5
PXDN	WAGETLEK	61	Healthy control	9604452.5	3740972.5
PXDN	WAGETLEK	62	Healthy control	174106482	1862287.25
PXDN	WAGETLEK	63	Healthy control	249770598	4370323.31
PXDN	WAGETLEK	64	Healthy control	5104644.5	1435821.25
PXDN	WAGETLEK	65	Healthy control	312961283	11556356
PXDN	WAGETLEK	66	Healthy control	296266464	1417537.89
PXDN	WAGETLEK	67	Healthy control	393779635	3686525.5
PXDN	WAGETLEK	68	Healthy control	22306858	0

PXDN	WAGETLEK	69	Healthy control	73723302	2337148
PXDN	WAGETLEK	70	Healthy spouse	1976986.38	2345634.75
PXDN	WAGETLEK	71	Healthy spouse	23614115.8	2307036.85
PXDN	WAGETLEK	72	Healthy spouse	22381810	0
PXDN	WAGETLEK	73	Multiple Sclerosis	30792078.8	20006720
PXDN	WAGETLEK	74	Multiple Sclerosis	20526670	0
PXDN	WAGETLEK	75	Multiple Sclerosis	3241134.25	0
PXDN	WAGETLEK	76	Multiple Sclerosis	188824909	3691072.19
PXDN	WAGETLEK	77	Multiple Sclerosis	4246908.5	0
PXDN	WAGETLEK	78	Multiple Sclerosis	9808866	0
PXDN	WAGETLEK	79	Multiple Sclerosis	298483968	12531.0596
PXDN	WAGETLEK	80	Multiple Sclerosis	13986180.8	7371304
PXDN	WAGETLEK	81	Multiple Sclerosis	3118630.25	48257.6563
PXDN	WAGETLEK	82	Multiple Sclerosis	4324524.13	3139014
SYN3	FPLVEQTFFPNHKPMNLGLK	1	ALS	108685466	1235379.38
SYN3	FPLVEQTFFPNHKPMNLGLK	2	ALS	142276301	1899895.38
SYN3	FPLVEQTFFPNHKPMNLGLK	3	ALS	94097964.8	1493275.25
SYN3	FPLVEQTFFPNHKPMNLGLK	4	ALS	164478377	1983196.88
SYN3	FPLVEQTFFPNHKPMNLGLK	5	ALS	128923995	1467829.75
SYN3	FPLVEQTFFPNHKPMNLGLK	6	ALS	129708652	1812546.38
SYN3	FPLVEQTFFPNHKPMNLGLK	7	ALS	154189210	1854019.5
SYN3	FPLVEQTFFPNHKPMNLGLK	8	ALS	143215079	1333088.38
SYN3	FPLVEQTFFPNHKPMNLGLK	9	ALS	136835476	1446028.88

SYN3	FPLVEQTFFPNHKPMNLGLK	10	ALS	114624565	1023605.88
SYN3	FPLVEQTFFPNHKPMNLGLK	11	ALS	177679307	1437872.13
SYN3	FPLVEQTFFPNHKPMNLGLK	12	ALS	178237826	2084189
SYN3	FPLVEQTFFPNHKPMNLGLK	13	ALS	139436843	1788972.38
SYN3	FPLVEQTFFPNHKPMNLGLK	14	ALS	415170296	2503068.5
SYN3	FPLVEQTFFPNHKPMNLGLK	15	ALS	229652140	1660122.5
SYN3	FPLVEQTFFPNHKPMNLGLK	16	ALS	205898465	2963981.25
SYN3	FPLVEQTFFPNHKPMNLGLK	17	ALS	112838144	1507707
SYN3	FPLVEQTFFPNHKPMNLGLK	18	ALS	247676616	3475215.25
SYN3	FPLVEQTFFPNHKPMNLGLK	19	ALS	154090630	1405993.88
SYN3	FPLVEQTFFPNHKPMNLGLK	20	ALS	168826430	2160299.5
SYN3	FPLVEQTFFPNHKPMNLGLK	21	ALS	191375929	2690453.88
SYN3	FPLVEQTFFPNHKPMNLGLK	22	ALS	148187759	2162461.25
SYN3	FPLVEQTFFPNHKPMNLGLK	23	ALSFTD	143758400	1825987.38
SYN3	FPLVEQTFFPNHKPMNLGLK	24	C9ALS	191989742	1843069.88
SYN3	FPLVEQTFFPNHKPMNLGLK	25	C9ALS	309837662	3089790.84
SYN3	FPLVEQTFFPNHKPMNLGLK	26	C9ALS	173581239	2160388.5
SYN3	FPLVEQTFFPNHKPMNLGLK	27	C9ALS	171254475	2796624.25
SYN3	FPLVEQTFFPNHKPMNLGLK	28	C9ALS	130521548	1676217.13
SYN3	FPLVEQTFFPNHKPMNLGLK	29	C9ALS	349050210	2994206.75
SYN3	FPLVEQTFFPNHKPMNLGLK	30	C9ALS	166209372	2019932.25
SYN3	FPLVEQTFFPNHKPMNLGLK	31	C9ALS	182477660	2662933.5
SYN3	FPLVEQTFFPNHKPMNLGLK	32	C9ALS	191535921	2832587.5

SYN3	FPLVEQTFFPNHKPMNLGLK	33	C9ALS	116289135	1291068.75
SYN3	FPLVEQTFFPNHKPMNLGLK	34	C9ALS	244663199	1221324.19
SYN3	FPLVEQTFFPNHKPMNLGLK	35	C9ALS	302656032	2651071
SYN3	FPLVEQTFFPNHKPMNLGLK	36	C9ALS	186679987	2178095.25
SYN3	FPLVEQTFFPNHKPMNLGLK	37	C9ALSFTD	285365312	2934923.75
SYN3	FPLVEQTFFPNHKPMNLGLK	38	C9ALSFTD	280857794	1162392
SYN3	FPLVEQTFFPNHKPMNLGLK	39	C9ALSFTD	239963927	1236237.63
SYN3	FPLVEQTFFPNHKPMNLGLK	40	C9ALSFTD	328564043	1911667.25
SYN3	FPLVEQTFFPNHKPMNLGLK	41	C9ALSFTD	290447887	3152245.25
SYN3	FPLVEQTFFPNHKPMNLGLK	42	C9ASYMPTOMATIC	139708589	1710888
SYN3	FPLVEQTFFPNHKPMNLGLK	43	C9ASYMPTOMATIC	89222714.5	1524339
SYN3	FPLVEQTFFPNHKPMNLGLK	44	C9ASYMPTOMATIC	186695139	2177174
SYN3	FPLVEQTFFPNHKPMNLGLK	45	C9ASYMPTOMATIC	375479890	3390753.25
SYN3	FPLVEQTFFPNHKPMNLGLK	46	C9ASYMPTOMATIC	171384928	1784937.38
SYN3	FPLVEQTFFPNHKPMNLGLK	47	C9ASYMPTOMATIC	173281865	2330310.5
SYN3	FPLVEQTFFPNHKPMNLGLK	48	C9FTD	418418440	4193938.5
SYN3	FPLVEQTFFPNHKPMNLGLK	49	C9FTD	259224737	1991748.38

SYN3	FPLVEQTFFPNHKPMNLGLK	50	Healthy control	307446648	2273808.75
SYN3	FPLVEQTFFPNHKPMNLGLK	51	Healthy control	322370812	750607.25
SYN3	FPLVEQTFFPNHKPMNLGLK	52	Healthy control	342300880	2091885.25
SYN3	FPLVEQTFFPNHKPMNLGLK	53	Healthy control	277357871	1465547.5
SYN3	FPLVEQTFFPNHKPMNLGLK	54	Healthy control	430834809	2933358
SYN3	FPLVEQTFFPNHKPMNLGLK	55	Healthy control	267060335	2514881.75
SYN3	FPLVEQTFFPNHKPMNLGLK	56	Healthy control	279300641	2403173.07
SYN3	FPLVEQTFFPNHKPMNLGLK	57	Healthy control	348232160	1972325.38
SYN3	FPLVEQTFFPNHKPMNLGLK	58	Healthy control	349359786	2229392
SYN3	FPLVEQTFFPNHKPMNLGLK	59	Healthy control	325665068	1972334.13
SYN3	FPLVEQTFFPNHKPMNLGLK	60	Healthy control	281669906	492755.094
SYN3	FPLVEQTFFPNHKPMNLGLK	61	Healthy control	161658904	1876793.75
SYN3	FPLVEQTFFPNHKPMNLGLK	62	Healthy control	147130329	1704194.38
SYN3	FPLVEQTFFPNHKPMNLGLK	63	Healthy control	141912698	1791496.5
SYN3	FPLVEQTFFPNHKPMNLGLK	64	Healthy control	199167488	2349491.75
SYN3	FPLVEQTFFPNHKPMNLGLK	65	Healthy control	175547597	2237071.75
SYN3	FPLVEQTFFPNHKPMNLGLK	66	Healthy control	146482830	54451.5859
SYN3	FPLVEQTFFPNHKPMNLGLK	67	Healthy control	382557424	630446.375
SYN3	FPLVEQTFFPNHKPMNLGLK	68	Healthy control	170020985	436021.156
SYN3	FPLVEQTFFPNHKPMNLGLK	69	Healthy control	263985492	2570408.25
SYN3	FPLVEQTFFPNHKPMNLGLK	70	Healthy spouse	205267756	3037064.5
SYN3	FPLVEQTFFPNHKPMNLGLK	71	Healthy spouse	152836566	1543520.38
SYN3	FPLVEQTFFPNHKPMNLGLK	72	Healthy spouse	175840480	2415874.75

SYN3	FPLVEQTFFPNHKPMNLGLK	73	Multiple Sclerosis	365369025	2613846.38
SYN3	FPLVEQTFFPNHKPMNLGLK	74	Multiple Sclerosis	379089440	3562363.5
SYN3	FPLVEQTFFPNHKPMNLGLK	75	Multiple Sclerosis	173793520	2564245.25
SYN3	FPLVEQTFFPNHKPMNLGLK	76	Multiple Sclerosis	147155598	1435484.75
SYN3	FPLVEQTFFPNHKPMNLGLK	77	Multiple Sclerosis	149560272	1554145.25
SYN3	FPLVEQTFFPNHKPMNLGLK	78	Multiple Sclerosis	382323040	1223388.88
SYN3	FPLVEQTFFPNHKPMNLGLK	79	Multiple Sclerosis	198756256	2201368.25
SYN3	FPLVEQTFFPNHKPMNLGLK	80	Multiple Sclerosis	338340617	2872987.75
SYN3	FPLVEQTFFPNHKPMNLGLK	81	Multiple Sclerosis	167420896	2411748.75
SYN3	FPLVEQTFFPNHKPMNLGLK	82	Multiple Sclerosis	136669707	1386992.38
TRRAP	YLQFVAALTDVNTQK	1	ALS	28917.5039	0
TRRAP	YLQFVAALTDVNTQK	2	ALS	50700.5078	119176.055
TRRAP	YLQFVAALTDVNTQK	3	ALS	164820.266	192752.656
TRRAP	YLQFVAALTDVNTQK	4	ALS	232265.609	125064.43
TRRAP	YLQFVAALTDVNTQK	5	ALS	360645.852	302358.625
TRRAP	YLQFVAALTDVNTQK	6	ALS	372112.578	170208.25
TRRAP	YLQFVAALTDVNTQK	7	ALS	268680.352	334135.313
TRRAP	YLQFVAALTDVNTQK	8	ALS	61467.7324	0
TRRAP	YLQFVAALTDVNTQK	9	ALS	166956.844	3000.92896
TRRAP	YLQFVAALTDVNTQK	10	ALS	0	0
TRRAP	YLQFVAALTDVNTQK	11	ALS	73928.6563	117914.353
TRRAP	YLQFVAALTDVNTQK	12	ALS	114290.172	0
TRRAP	YLQFVAALTDVNTQK	13	ALS	1045428.74	287788.609

TRRAP	YLQFVAALTDVNTQK	14	ALS	486519.906	951372
TRRAP	YLQFVAALTDVNTQK	15	ALS	285831.21	708689.188
TRRAP	YLQFVAALTDVNTQK	16	ALS	135680.922	218040.516
TRRAP	YLQFVAALTDVNTQK	17	ALS	84542.9443	244388.992
TRRAP	YLQFVAALTDVNTQK	18	ALS	187274.969	222913.004
TRRAP	YLQFVAALTDVNTQK	19	ALS	146775.365	217429.844
TRRAP	YLQFVAALTDVNTQK	20	ALS	335737.797	130060.039
TRRAP	YLQFVAALTDVNTQK	21	ALS	105138.631	235117.906
TRRAP	YLQFVAALTDVNTQK	22	ALS	65397.5859	177235.641
TRRAP	YLQFVAALTDVNTQK	23	ALSFTD	57592.7813	262256.832
TRRAP	YLQFVAALTDVNTQK	24	C9ALS	87271.0703	131556.016
TRRAP	YLQFVAALTDVNTQK	25	C9ALS	405315.242	944631.766
TRRAP	YLQFVAALTDVNTQK	26	C9ALS	137623.805	225972.254
TRRAP	YLQFVAALTDVNTQK	27	C9ALS	65550.2871	7315.92432
TRRAP	YLQFVAALTDVNTQK	28	C9ALS	110921.957	130590.492
TRRAP	YLQFVAALTDVNTQK	29	C9ALS	403065.063	1119861.75
TRRAP	YLQFVAALTDVNTQK	30	C9ALS	134232.516	1800394.53
TRRAP	YLQFVAALTDVNTQK	31	C9ALS	61169.8223	668777.859
TRRAP	YLQFVAALTDVNTQK	32	C9ALS	352865.969	474581.938
TRRAP	YLQFVAALTDVNTQK	33	C9ALS	179529.301	913137.578
TRRAP	YLQFVAALTDVNTQK	34	C9ALS	274860.281	864888.688
TRRAP	YLQFVAALTDVNTQK	35	C9ALS	268181.031	488529.906
TRRAP	YLQFVAALTDVNTQK	36	C9ALS	1090733.63	241019.328

TRRAP	YLQFVAALTDVNTQK	37	C9ALSFTD	406237.875	988400.813
TRRAP	YLQFVAALTDVNTQK	38	C9ALSFTD	303051.594	135960.266
TRRAP	YLQFVAALTDVNTQK	39	C9ALSFTD	369516.406	605262.313
TRRAP	YLQFVAALTDVNTQK	40	C9ALSFTD	333306.125	2529956.75
TRRAP	YLQFVAALTDVNTQK	41	C9ALSFTD	398314.524	1131302.88
TRRAP	YLQFVAALTDVNTQK	42	C9ASYMPTOMATIC	1350952.68	516727.813
TRRAP	YLQFVAALTDVNTQK	43	C9ASYMPTOMATIC	345555.977	409300.063
TRRAP	YLQFVAALTDVNTQK	44	C9ASYMPTOMATIC	242613	329682.406
TRRAP	YLQFVAALTDVNTQK	45	C9ASYMPTOMATIC	1728283.25	1079805
TRRAP	YLQFVAALTDVNTQK	46	C9ASYMPTOMATIC	66924.2344	176135.391
TRRAP	YLQFVAALTDVNTQK	47	C9ASYMPTOMATIC	111688.836	138710.297
TRRAP	YLQFVAALTDVNTQK	48	C9FTD	778626.25	1596766.19
TRRAP	YLQFVAALTDVNTQK	49	C9FTD	195293.51	514421.625
TRRAP	YLQFVAALTDVNTQK	50	Healthy control	487530.281	1464440.19
TRRAP	YLQFVAALTDVNTQK	51	Healthy control	499001.992	129992.25
TRRAP	YLQFVAALTDVNTQK	52	Healthy control	449054.625	900276.563
TRRAP	YLQFVAALTDVNTQK	53	Healthy control	420681.039	723195.063

TRRAP	YLQFVAALTDVNTQK	54	Healthy control	423103.188	783300.875
TRRAP	YLQFVAALTDVNTQK	55	Healthy control	412556.902	1084761.48
TRRAP	YLQFVAALTDVNTQK	56	Healthy control	395050.645	987559.37
TRRAP	YLQFVAALTDVNTQK	57	Healthy control	452129.531	430101.656
TRRAP	YLQFVAALTDVNTQK	58	Healthy control	366972.57	515812.813
TRRAP	YLQFVAALTDVNTQK	59	Healthy control	373093.195	0
TRRAP	YLQFVAALTDVNTQK	60	Healthy control	479876.836	864279.188
TRRAP	YLQFVAALTDVNTQK	61	Healthy control	1634838.35	6693656.97
TRRAP	YLQFVAALTDVNTQK	62	Healthy control	231244.555	411978.047
TRRAP	YLQFVAALTDVNTQK	63	Healthy control	150626.539	889032.688
TRRAP	YLQFVAALTDVNTQK	64	Healthy control	1049246.94	578685.766
TRRAP	YLQFVAALTDVNTQK	65	Healthy control	2173135.13	107983.273
TRRAP	YLQFVAALTDVNTQK	66	Healthy control	143263.414	164970
TRRAP	YLQFVAALTDVNTQK	67	Healthy control	322286.125	1813172.13
TRRAP	YLQFVAALTDVNTQK	68	Healthy control	316974.617	569017.016
TRRAP	YLQFVAALTDVNTQK	69	Healthy control	280132.916	1790309.06
TRRAP	YLQFVAALTDVNTQK	70	Healthy spouse	187204.527	780298.455
TRRAP	YLQFVAALTDVNTQK	71	Healthy spouse	64910.2773	163156.531
TRRAP	YLQFVAALTDVNTQK	72	Healthy spouse	76739.1563	171525.063
TRRAP	YLQFVAALTDVNTQK	73	Multiple Sclerosis	493612.5	1077331.25
TRRAP	YLQFVAALTDVNTQK	74	Multiple Sclerosis	310870.344	788360.938
TRRAP	YLQFVAALTDVNTQK	75	Multiple Sclerosis	127574.438	143439.094
TRRAP	YLQFVAALTDVNTQK	76	Multiple Sclerosis	244877.953	194185.988

TRRAP	YLQFVAALTDVNTQK	77	Multiple Sclerosis	129042.313	641060.063
TRRAP	YLQFVAALTDVNTQK	78	Multiple Sclerosis	350214.406	938673.5
TRRAP	YLQFVAALTDVNTQK	79	Multiple Sclerosis	209177.797	361495.531
TRRAP	YLQFVAALTDVNTQK	80	Multiple Sclerosis	441496.99	1142884.88
TRRAP	YLQFVAALTDVNTQK	81	Multiple Sclerosis	22067.9805	195945.781
TRRAP	YLQFVAALTDVNTQK	82	Multiple Sclerosis	75800.6875	65528.125